MCEER
MULTIDISCIPLINARY CENTER FOR EARTHQUAKE ENGINEERING RESEARCH
A National Center of Excellence in Advanced Technology Applications

ISSN 1520-295X

PB2002-100534

Experimental Investigation of P-Delta Effects to Collapse During Earthquakes

by

Darren Vian and Michel Bruneau
University at Buffalo
Department of Civil, Structural and
Environmental Engineering
Ketter Hall
Buffalo, NY 14260

Technical Report MCEER-01-0001

June 25, 2001

This research was conducted at the University at Buffalo and was supported primarily by the Earthquake Engineering Research Centers Program of the National Science Foundation under award number EEC-9701471.

NOTICE

This report was prepared by the University at Buffalo as a result of research sponsored by the Multidisciplinary Center for Earthquake Engineering Research (MCEER) through a grant from the Earthquake Engineering Research Centers Program of the National Science Foundation and other sponsors. Neither MCEER, associates of MCEER, its sponsors, the University at Buffalo, nor any person acting on their behalf:

a. makes any warranty, express or implied, with respect to the use of any information, apparatus, method, or process disclosed in this report or that such use may not infringe upon privately owned rights; or

b. assumes any liabilities of whatsoever kind with respect to the use of, or the damage resulting from the use of, any information, apparatus, method, or process disclosed in this report.

Any opinions, findings, and conclusions or recommendations expressed in this publication are those of the author(s) and do not necessarily reflect the views of MCEER, the National Science Foundation, or other sponsors.

Report Doumentation Page 50272-101	1. Report No. MCEER-01-0001	2.	3. Recipient's Accession No.

4. Title and Subtitle
Experimental Investigation of P-Delta Effects to Collapse During Earthquakes

5. Report Date
6/25/01

6.

7. Authors
D. Vian and M. Bruneau

8. Perfoming Organization Report No.

10. Project / Task / Work Unit No
00-2023

9. Performing Organization Name and Address
Department of Civil, Structural and Environmental Engineering
University at Buffalo, State University of New York
Buffalo, NY 14260

11.Contract (C) or Grant (G) No.
(C)
(G) EEC-9701471

12. Sponsoring Organization Name and Address
Multidisciplinary Center for Earthquake Engineering Research
State University of New York at Buffalo
Red Jacket Quadrangle
Buffalo, NY 14261

13. Type of Report / Period Covered
Technical Report

14.

15. Supplementary Notes
This research was conducted at the University at Buffalo and was supported primarily by the Earthquake Engineering Research Centers Program of the National Science Foundation.

16. Abstract (limit 200 Words)

This report addresses structural safety and the risk of damage, by determining the collapse performance limit in engineering terms. It documents an experimental study of the P-delta effect on a Single Degree of Freedom (SDOF) test structure subjected to earthquake ground motion. Fifteen four-column frame specimens were subjected to progressive unidirectional ground shaking and structural response was measured up to collapse. An example of how to use the experimental data for analytical model verification is provided. A full series of tests with a single specimen were analyzed using a simple SDOF dynamic analysis program. The example illustrated the shortcomings/inaccuracies of a particular simplified model of structural damping. Test structure performance was compared with proposed limits for minimizing P-delta effects in highway bridge piers. The stability factor was found to have a strong relationship to the relative structural performance in this regard. Performance was also compared with currently used strength, and stability limits for axial-moment interaction. Specimens generally reached accelerations and, maximum base shear (as a fraction of the system's weight) in excess of the maximum spectral accelerations calculated considering second order effects, but less than that considering only member strength.

17. Document Analysis a. Descriptors

Earthquake Engineering. P Delta effect. Collapses performance limits. Highway bridges. Highway bridge piers. Shaking table tests.

b. Identifiers/Open-Ended Terms

c. COSATI Field/Group

18. Availability Statement	19. Security Class (This Report)	21. No. of Pages
Release Unlimited.	Unclassified	360
	20. Security Class (This Page)	22. Price
	Unclassified	

MULTIDISCIPLINARY CENTER FOR EARTHQUAKE ENGINEERING RESEARCH
A National Center of Excellence in Advanced Technology Applications

Experimental Investigation of P-Delta Effects to Collapse During Earthquakes

by

Darren Vian[1] and Michel Bruneau[2]

Publication Date: June 25, 2001
Submittal Date: September 1, 2000

Technical Report MCEER-01-0001

Task Number 00-2023

NSF Master Contract Number EEC 9701471

1 Graduate Research Assistant, Department of Civil, Structural and Environmental Engineering, University at Buffalo
2 Professor, Department of Civil, Structural and Environmental Engineering, University at Buffalo

MULTIDISCIPLINARY CENTER FOR EARTHQUAKE ENGINEERING RESEARCH
University at Buffalo, State University of New York
Red Jacket Quadrangle, Buffalo, NY 14261

Preface

The Multidisciplinary Center for Earthquake Engineering Research (MCEER) is a national center of excellence in advanced technology applications that is dedicated to the reduction of earthquake losses nationwide. Headquartered at the University at Buffalo, State University of New York, the Center was originally established by the National Science Foundation in 1986, as the National Center for Earthquake Engineering Research (NCEER).

Comprising a consortium of researchers from numerous disciplines and institutions throughout the United States, the Center's mission is to reduce earthquake losses through research and the application of advanced technologies that improve engineering, pre-earthquake planning and post-earthquake recovery strategies. Toward this end, the Center coordinates a nationwide program of multidisciplinary team research, education and outreach activities.

MCEER's research is conducted under the sponsorship of two major federal agencies: the National Science Foundation (NSF) and the Federal Highway Administration (FHWA), and the State of New York. Significant support is derived from the Federal Emergency Management Agency (FEMA), other state governments, academic institutions, foreign governments and private industry.

MCEER's NSF-sponsored research objectives are twofold: to increase resilience by developing seismic evaluation and rehabilitation strategies for the post-disaster facilities and systems (hospitals, electrical and water lifelines, and bridges and highways) that society expects to be operational following an earthquake; and to further enhance resilience by developing improved emergency management capabilities to ensure an effective response and recovery following the earthquake (see the figure below).

A cross-program activity focuses on the establishment of an effective experimental and analytical network to facilitate the exchange of information between researchers located in various institutions across the

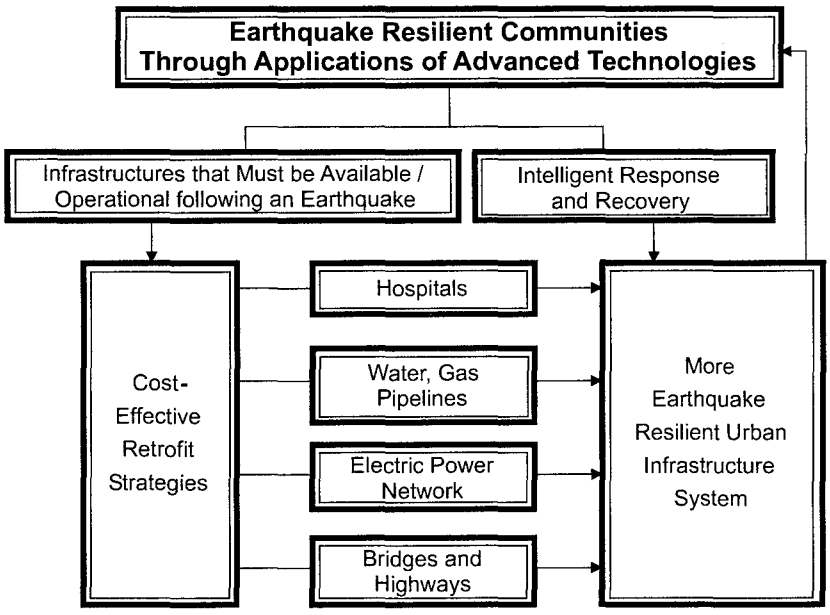

country. These are complemented by, and integrated with, other MCEER activities in education, outreach, technology transfer, and industry partnerships.

This report addresses structural safety and the risk of damage, by determining the collapse performance limit in engineering terms. It documents an experimental study of the P-delta effect on a Single Degree of Freedom (SDOF) test structure subjected to earthquake ground motion. Fifteen four-column frame specimens were subjected to progressive unidirectional ground shaking and structural response was measured up to collapse.

An example of how to use the experimental data for analytical model verification is provided. A full series of tests with a single specimen were analyzed using a simple SDOF dynamic analysis program. The example illustrated the shortcomings/inaccuracies of a particular simplified model of structural damping.

Test structure performance was compared with proposed limits for minimizing P-delta effects in highway bridge piers. The stability factor was found to have a strong relationship to the relative structural performance in this regard. Performance was also compared with currently used strength and stability limits for axial-moment interaction. Specimens generally reached accelerations and maximum base shear (as a fraction of the system's weight) in excess of the maximum spectral accelerations calculated considering second order effects, but less than that considering only member strength.

ABSTRACT

The effect of gravity on the lateral force resistance of structures, known as the P-Δ effect, has been studied for a number of years. Most of the research into this phenomenon has been performed using analytical models, with very few tests performed for verification.

This report is an experimental study of the P-Δ effect on a Single Degree of Freedom (SDOF) test structure subjected to earthquake ground motion. It involves testing columns subjected to SDOF ground shaking and measuring the displacements and accelerations of the structure for the duration of the test, up to collapse. A literature review found no other tests of a similar nature.

Fifteen four-column frame specimens were subjected to progressive unidirectional ground shaking and structural response was measured up to collapse. The specimens are subdivided into sets of three different column slenderness ratios: 100, 150, and 200. For a given slenderness ratio, column dimensions are varied from specimen to specimen, as is the mass used, such that ground motions of various magnitudes are required to collapse each specimen.

An example of how to use the experimental data for analytical model verification is presented. A full series of tests with a single specimen is analyzed using a simple SDOF dynamic analysis program. This example illustrates the shortcomings/inaccuracies of a particular simplified model of structural damping.

Test structure performance is compared with proposed limits for minimizing P-Δ effects in highway bridge piers. The stability factor is found to have a strong relation to the relative structural performance in this regard.

Performance is also compared with currently used strength and stability limits for axial-moment interaction. Specimens generally reached accelerations and maximum base shear (as a fraction of the system's weight) in excess of the maximum spectral accelerations calculated considering second order effects, but less than that considering only member strength.

ACKNOWLEDGEMENTS

The authors thank Mrs. Richard Cizdziel, Mark Pitman, and Dan Walch (technical specialists at the University at Buffalo Structural Engineering & Earthquake Simulation Laboratory) for their help in the measurement, instrumentation, and logistics of the test structure assembly, and Jeffrey Berman, Dragos Bontea, Thomas Boyle, Stephen Percassi (graduate students, University at Buffalo) and Przemyslaw Kobialka (undergraduate lab assistant, University at Buffalo) for their help during the physical assembly and instrumentation of the test structures. Also acknowledged are the contributions of Madan Makasare (University of Ottawa, engineering machine shop), Professor Jianhua Yu (Visiting Scholar from Chengdu University) and Ms. Wendy Scouten (former undergraduate student at the University of Ottawa) for their assistance in the early conceptual stages of specimens' development. The editorial assistance of Ms. Jane Stoyle (from MCEER) in producing this report is also appreciated.

This work was supported in part by the Earthquake Engineering Research Centers Program of the National Science Foundation under Award Number ECC-9701471 to the Multidisciplinary Center for Earthquake Engineering Research.

TABLE OF CONTENTS

TABLE OF CONTENTS (cont'd)

TABLE OF CONTENTS (cont'd)

LIST OF ILLUSTRATIONS

LIST OF ILLUSTRATIONS (cont'd)

LIST OF ILLUSTRATIONS (cont'd)

LIST OF ILLUSTRATIONS (cont'd)

LIST OF ILLUSTRATIONS (cont'd)

LIST OF ILLUSTRATIONS (cont'd)

LIST OF TABLES

LIST OF TABLES (cont'd)

NOTATIONS

AccEast	east side total acceleration instrumentation channel
AccTbl	table acceleration instrumentation channel
AccWest	west side total acceleration instrumentation channel
C_s*	estimated maximum base shear coefficient
E	modulus of elasticity (MPa)
f_D	damping force
f_I	inertial force in specimen mass
f_S	restoring spring force
F_y	yield stress
g	gravitational constant (=9.807m/s^2)
h	nominal width of column
HorEast	east side total displacement instrumentation channel
HorWest	west side total displacement instrumentation channel
i	index of damping estimates (=1,2,3)
I	moment of inertia of column
j	number of free vibration cycles between peaks used for estimate of ξ
K_1	elastic stiffness with P-Δ effect considered
K_2	post-elastic stiffness with P-Δ effect considered
k_i	cycle number used as first peak for ith estimate of the damping ratio
k_i+j	cycle number used as second peak for ith estimate of the damping ratio
K_o	stiffness without P-Δ
l	length of rod used on the horizontal displacement transducers
L	height of the column
l_1 l_2	length of column as shown in Fig 3-7
M	moment at ends of column
M_m	moment calculated from the strains measured at the third point of column height
M_p	plastic moment of column
P	nominal axial load on column

P-Δ

P_n	axial capacity of column (AISC notation)
P_u	axial load on column (AISC notation)
r	bilinear stiffness ratio (k_2/k_1)
$S_{a\text{-filt}}$	elastic spectral acceleration of measured & filtered ground motion
$S_{a\text{-meas}}$	elastic spectral acceleration of measured ground motion
$S_{a\text{-target}}$	elastic spectral acceleration of target ground motion
$S_{a\text{-ultim.}}$	spectral acceleration for design at ultimate strength
$S_{a\text{-yield}}$	spectral acceleration at first yield of structure
S_{RDR}	residual displacement ratio spectrum
Strain	strain at third point of column instrumentation channel
t	time, s
T_n	nominal fundamental period, s
T_{no}	predicted fundamental period ignoring P-Δ
T_{np}	predicted fundamental period including P-Δ
$T_{n\text{-spectrum}}$	calculated period from Fourier Analysis of test data
u^*_i	average of amplitude of peaks k to k+j throughout the i^{th} estimate interval (mm or g)
$u_a(t)$	actual horizontal displacement at time, t, mm
UG	instrument channel table displacement, mm
$u_g(t)$	measured ground displacement at time, t, mm
u_k	amplitude of kth peak (first peak used for the estimate)
u_{k+j}	amplitude of (k+j)th peak (last peak used for the estimate)
u_{ki} =	amplitude of first peak used for ith estimate of the damping ratio
u_{ki+j} =	amplitude of second peak used for ith estimate of the damping ratio
$u_m(t)$	measured horizontal displacement at time, t
u_o	maximum amplitude of free vibration response (mm or g)
u_r	residual displacement of test structure at end of test
$u_{rel\text{-}max}$	maximum relative displacement of the specimen during test
u_{rmax}	maximum residual displacement of the specimen from Eq. (2-7)
$\ddot{u}_{tmax}$	maximum total acceleration of the structural mass (g)

v(t)	measured vertical displacement / vertical projection of *l* at time, t
V^*_{max}	maximum experimentally estimated base shear
v_1 v_2	lateral shifts of baseplate corners as shown in Fig 3-9
Vert	vertical displacement instrument channel
V_o	base shear on structure ignoring P-Δ
V_o^*	estimated base shear from experiment (without P-Δ Effects)
V_p	base shear on structure affected by P-Δ
V_p^*	estimated base shear from experiment (including P-Δ Effects)
V_{unif}	average lateral shift of top baseplate of column (=average(v_1 and v_2))
V_{yo}	base shear on structure at plastic moment
V_{yo}'	reduced lateral yield force in analysis
V_{yp}	base shear on P- Δ affected structure at yield
w_1 w_2 w_3	width of column at bottom, middle, and top as shown in Fig 3-7
x(t)	horizontal projection of *l* at time, t
Δ	relative displacement of top of column
$\Delta_{coll.}$	residual displacement at formation of plastic mechanism
ΔF_y	change in analytical yield force due to residual displacement
ΔT_n	percent differnce in period between observed and analytical, s
Δ_u	ultimate Displacement
Δ_y	yield Displacement
ε_m	strain measured by strain gage at third point of column height
ϕ	angle of twist of column
μ	displacement ductility of structure (Δ/Δ_y)
μ_s	static stability limit
θ	stability coefficient
θ_b	angle of bow of column
ξ	damping ratio (percent of critical damping)
ξ_i	i^{th} estimate of the damping ratio

ABBREVIATIONS

NSP	Nonlinear Static Procedure
PGA	peak ground acceleration
SDOF	single-degree-of-freedom
SEESL	Structural Engineering and Earthquake Simulation Laboratory
UB	University at Buffalo

SECTION 1
INTRODUCTION

1.1 Motivation for this Study

The effect of gravity on the lateral force resistance of structures, known as the P-Δ effect, has been studied for a number of years. Modern design codes impose lateral drift limits to ensure that structural performance is minimally affected by P-Δ, especially in the elastic range. However, as inelastic behavior is relied upon to a greater extent in the dissipation of seismic input energy, the destabilizing effect of gravity becomes more significant in structural design. In addition, advances in construction technology are allowing the fabrication of more slender structures than in the past. As a result, it may be desirable to investigate the behavior of those structures in order to enhance our understanding of the condition ultimately leading to their collapse, and to ensure public safety during extreme events.

Strength and deformation capacities of elements and structures can be evaluated with reasonable confidence in the elastic range of response. However, excursions into the inelastic range of behavior complicate the process of calculating these ultimate capacities, and the maximum ductilities that can be developed. While many experimental studies and theoretical damage models support these calculated values, it remains that few experimental studies have pushed the shake table tests up to collapse.

This research attempts to provide some of that data through a program of shake-table testing of simple frames through collapse. Every effort was made to ensure that the experimental data is fully documented (geometry, material properties, initial imperfections, detailed test results, etc.) such that the tests can be used at a later time as a benchmark to which analytical models can be compared.

1.2 Research Objectives

There are two main objectives in this research: to perform dynamic testing through collapse of SDOF specimens; and, to make results available to researchers to assist in the development or validation of analytical tools to model the inelastic dynamic behavior of structures up to collapse.

Fifteen specimens having various properties were tested in an attempt to identify some of the general parameters responsible for trends in behavior due to P-Δ effects on SDOF structures.

1.3 Scope of Work

The scope of work in this research project contains the following steps:

- Set up experimental program of shake-table testing of columns to collapse
- Document the pretest condition of all specimens
- Perform testing on fifteen specimens each having four columns
- Present and summarize the test results
- Discuss the effect of material properties on the specimen dynamic properties
- Demonstrate by an example how to use the test data for analytical model verification
  - Discuss the effect of differing damping estimates on analysis accuracy
  - Compare a series of tests with a simplified SDOF analysis
- Investigate trends in the specimens behavior due to P-Δ effects
- Compare the ultimate behavior of the specimens with proposed limits for minimizing P-Δ effects in bridge piers

1.4 Outline

In Chapter 2, a brief review of past research on P-Δ effects is presented, along with some basic concepts of P-Δ analysis.

In Chapter 3, details of the experimental setup, data acquisition systems, and instrumentation used during the tests are presented and described. The preliminary design, fabrication, and properties of the specimens are documented. The SDOF shaking table and input ground motion used in these tests are also described.

In Chapter 4, the test results are presented. Material properties extracted from tension tests, dynamic properties measured from free vibration tests, and shake table test results, are presented. The peak response parameters extracted from each test are described.

In Chapter 5, the test results are discussed. An example is presented of how to use the specimen test data for the purpose of comparison with an analytical model. The effects of damping estimates on analysis results are discussed. A preliminary investigation of behavioral trends of the shake table results is presented. Peak responses are compared with limits proposed to minimize P-Δ effects in bridge piers. Specimen behavior is investigated with respect to axial-moment strength and stability interaction limits.

Conclusions and recommendations for further research are presented in Chapter 6.

SECTION 2
LITERATURE REVIEW

2.1 General

The concept of P-Δ effects under static loading can be illustrated using the Single-Degree-Of-Freedom (SDOF) structure shown in figure 2-1. In this figure, 2P represents the force due to gravity acting on the mass lumped at the top of the structure, L is the structure height, 2V is the lateral force on the mass, and Δ is the horizontal displacement of the mass. As the structure sways by Δ under the effect of the lateral force, the product of P by Δ produces an additional moment at the base of each column which can be obtained by considering static equilibrium in the deformed configuration.

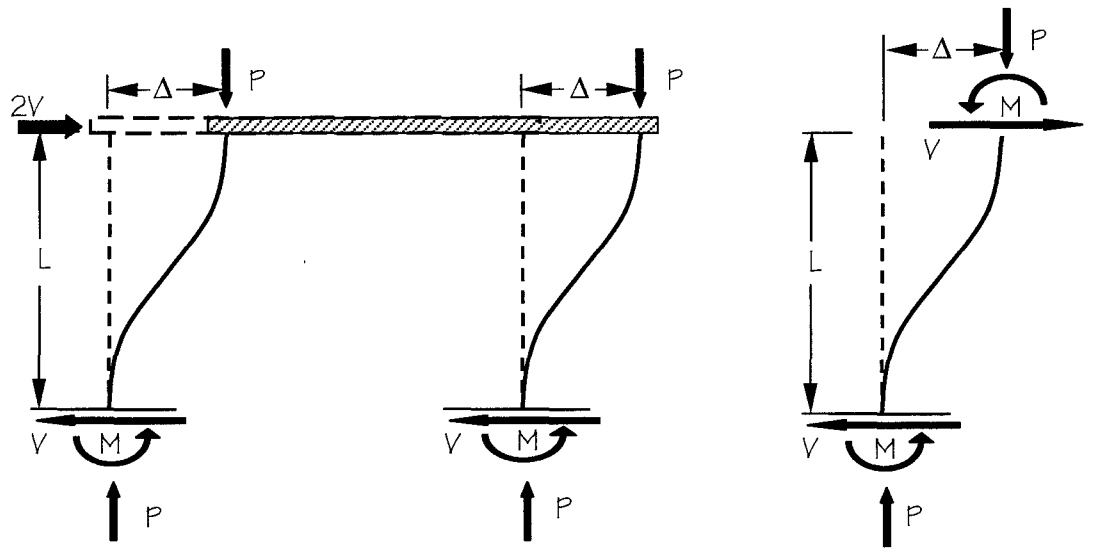

(a) Portal frame with rigid beam

(b) Single column removed from portal frame

FIGURE 2-1 Free Body Diagrams of Typical SDOF structure

Many approximate methods have been developed (using equivalent lateral loads) for elastic static analysis to allow consideration of P-Δ effects using conventional equilibrium in the undeformed configuration. However, few studies have investigated P-Δ effects on yielding structures subjected to earthquake excitations. Some key parameters proposed by other researchers for the consideration of P-Δ effects in the seismic analysis of non-linear inelastic

structures are described below, along with an overall view of the fundamental structural behavior.

2.2 Basic Theory

The relationship between the lateral force applied to the structure and its resulting displacement must be known in order to account for the P-Δ effect in design. Figure 2-2 displays a plot of the monotonically increasing lateral force, V, as a function of the lateral displacement, Δ. The solid line represents this relationship when P-Δ effects are ignored, while the dashed line represents the behavior when P-Δ effects are included.

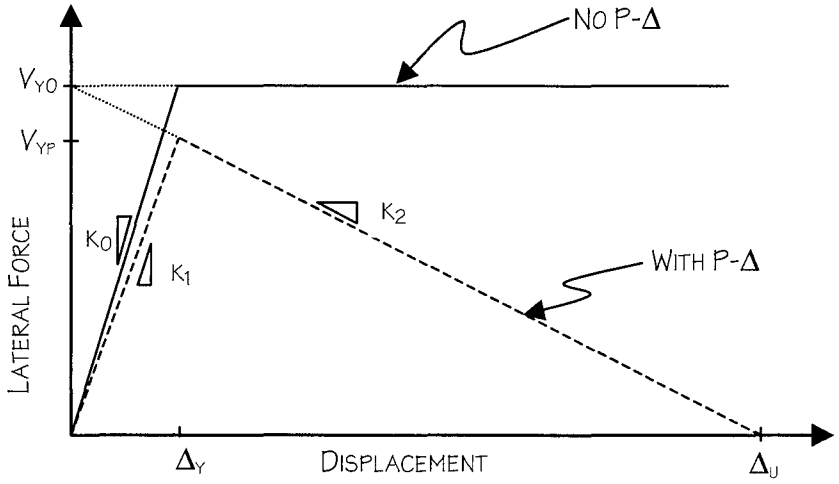

FIGURE 2-2 Bilinear Lateral Force vs. Displacement model for SDOF structure

If the typical SDOF structure considered in figure 2-1(a) is a single-bay portal frame with an infinitely rigid beam, the elastic lateral stiffness of each column within the frame, ignoring the P-Δ effect is given by:

$$K_o = 12 \cdot E \cdot I / L^3 \tag{2-1}$$

where:

E = Elastic Modulus of the material

I = Moment of inertia of the column section

L = Height of the column

For the bilinear elastic-perfectly plastic model shown, the ultimate lateral force, ignoring the P-Δ effect, that can be applied to that frame is reached when the plastic moment of the column, M_p, develops at the top and bottom of the column, and is given by:

$$V_{yo} = {}^{2 \cdot M_p}\!/_{L} \tag{2-2}$$

The corresponding yield displacement is:

$$\Delta_y = {}^{V_{yo}}\!/_{K_o} \tag{2-3}$$

Now, as shown in figure 2-1(b), considering P-Δ effects for a single column in the same frame, moment equilibrium gives:

$$2 \cdot M = VL + P\Delta \tag{2-4}$$

where V is the lateral force at the top of the column

Rearranging (2-4), the lateral force, V, can be expressed as:

$$V = \frac{(2 \cdot M - P\Delta)}{L} = \frac{2 \cdot M}{L} - \frac{P\Delta}{L} = V_o - \frac{P\Delta}{L} \tag{2-5}$$

where V_o is the lateral force that would be obtained ignoring the P-Δ effect.

Shown in figure 2-2, as a consequence of P-Δ effects seen in (2-5), V decreases relative to V_o, as the displacement, Δ, increases. This equation can also be expressed as:

$$V = V_o - \frac{P\Delta}{L} = V_o - \theta K_o \Delta \tag{2-6}$$

where θ is the P-Δ stability factor given by:

$$\theta = \frac{P}{K_o L} \tag{2-7}$$

From (2-6), the elastic stiffness considering P-Δ, K_1, is therefore[1]:

---

[1] It has been suggested (Sivaselvan and Reinhorn, UB private communication, 2001) that better results could be obtained if (2-8) was replaced by: $K_1 = K_o \cdot \left[\frac{{}^{p^3}\!/_{3}}{\tan(p) - p} \right]$ where $p = \frac{L}{2} \cdot \sqrt{\frac{P}{EI}}$. However, this potential

$$K_1 = K_o(1-\theta) \tag{2-8}$$

Similarly, the lateral force at which the system, including P-Δ effects, yields, V_{yp}, is:

$$V_{yp} = V_{yo}(1-\theta) \tag{2-9}$$

When elastic-perfectly plastic material properties are assumed for the idealized frame described earlier, lateral force V_o in (2-6) remains constant in the post-elastic region of the force-displacement graph as the plastic moment, M_p, is developed. However, when P-Δ effects are considered, the corresponding lateral force versus displacement curve exhibits a negative slope past the yield point, with a stiffness of:

$$K_2 = -\theta \cdot K_o \tag{2-10}$$

as shown in figure 2-2.

Therefore, the monotonic bilinear force-displacement response of a SDOF structure, including P-Δ effects, can be summarized as follows:

$$V = \begin{cases} K_1 \cdot \Delta & if: \Delta \le \Delta_y \\ V_{yo} + K_2 \cdot \Delta & if: \Delta > \Delta_y \end{cases} \tag{2-11}$$

Another useful term in the characterization of P-Δ effects is the ratio of post-elastic to elastic stiffness, known as the stiffness ratio, r, and given by:

$$r = \frac{K_2}{K_1} = \frac{\alpha - \theta}{1-\theta} \tag{2-12}$$

where $\alpha \cdot K_o$ is the stiffness (in absence of stability effects) of the strain hardening segment of a bilinear elastic-plastic material model. In this study, as shown in figure 2-2, the value of α=0.0 is considered.

The concept of ductility is often used when discussing inelastic structural behavior. The displacement ductility of a structure, μ, is defined as:

$$\mu = \Delta / \Delta_y \tag{2-13}$$

---

improvement has not been quantified in this study as this recent development was brought to the authors' attention shortly before the publication of this report.

The ultimate displacement of the structure is designated as Δ_u, as shown on figure 2-2, the point at which the negative-slope, post-elastic lateral strength curve intersects the displacement axis. This theoretically implies that for any additional lateral displacement, lateral instability develops (i.e. lateral strength becomes negative for any additional positive displacement). The ductility at ultimate displacement, Δ_u, is known as the static stability limit, μ_s, and derived using the relationships given in (2-3) and (2-10):

$$V = V_{yo} + K_2 \cdot \Delta_u = 0$$

$$V_{yo} - \theta \cdot K_o \cdot \Delta_u = 0$$

$$V_{yo} = K_o \cdot \Delta_y = \theta \cdot K_o \cdot \Delta_u$$

$$1/\theta = \frac{\Delta_u}{\Delta_y} = \mu_s \qquad \text{(2-14a)}$$

which can also be written in terms of the stiffness ratio using (2-12):

$$\mu_s = 1 - 1/r \qquad \text{(2-14b)}$$

2.3 Hysteresis Center Curve Concept

MacRae and Kawashima (1993) proposed the "hysteresis centre curve" (HCC) concept for analyzing the stability of general hysteresis loops. For the case of a bilinear system assumed for the analysis in this research, the HCC is a line parallel to the secondary stiffness that passes through the origin of the force-displacement space as pictured in figure 2-3.

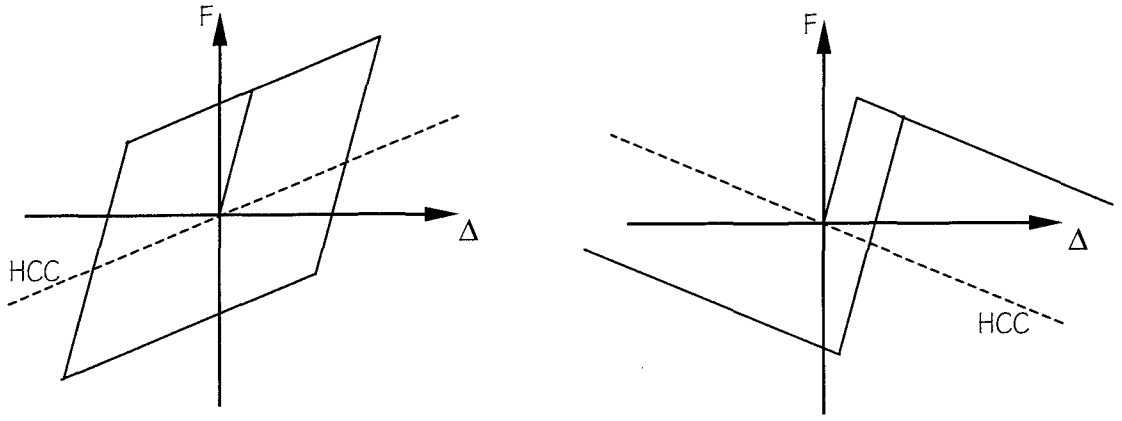

FIGURE 2-3 Force vs. Displacement Behavior for a dynamically (a) stable and (b) unstable bilinear system

The HCC characterizes a structure as follows: If the secondary stiffness, K_2, is positive as shown in figure 2-3(a) the system is considered stable and after the structure yields, will tend to return towards the point of zero displacement upon repeated reverse cyclic yielding during ground shaking. However, if K_2 is negative as shown in (b) of the same figure, the structure is deemed to be dynamically unstable.

The dynamically unstable system will tend to drift in a given direction once yielding has started. This results in large cumulative residual displacements and low cyclic energy absorption. Due to these large displacements, structures may be difficult to straighten and may perform poorly in a subsequent earthquake.

Some types of structures, such as reinforced concrete piers, will have a hysteresis loop which changes as the loading is occurring. This causes the point at which the HCC crosses the line of zero force to change from the initial location, even if the system response is stable.

2.4 Use of Amplification Factors to account for P-Δ Effects

Bernal (1987) investigated dynamic P-Δ effects in elastic and inelastic systems through the use of amplification factors. The ratio between displacement spectra with and without gravity effects represents the amplification spectrum that will amplify the elastic displacement for design.

Inelastic P-Δ effects were generated using four ground motions for a series of time history analyses. Damping was held constant at 5 percent of critical while the target displacement ductility and stability coefficient were both varied, from one to six and zero to 0.2, respectively, providing a total of 192 amplification spectra.

In the course of Bernal's parametric study, the target ductility was made to satisfy a maximum limit equal to $0.4\mu_s$, based on the requirement that the structure must remain fit to resist the factored gravity load following the inelastic response. In addition, the derivation assumed that the post-earthquake permanent deformation was equal to the maximum response ductility. Based on a statistical analysis of the 192 spectra generated in the study, the following expression for the amplification factor was proposed:

$$\alpha = \frac{1+\beta\theta}{1-\theta} \tag{2-15}$$

where regression analysis for the mean amplification yielded:

$$\beta = 1.87 \cdot (\mu - 1) \tag{2-16}$$

2.5 Residual Displacement Ratio Response Spectrum

Kawashima et al. (1996) proposed a technique for characterizing residual displacements of a structure following a seismic event, known as the residual displacement ratio, S_{RDR}. A SDOF oscillator with bilinear hysteretic restoring force was analyzed over a range of natural periods, stiffness ratios, and ductility for a number of ground motion time histories. Residual displacement ratio response spectra were designated as the plots of S_{RDR} against the above-mentioned factors.

Three parameters are necessary to calculate the maximum residual displacement of the SDOF bilinear oscillator: the stiffness factor, r, the displacement ductility, μ, and the yield displacement, Δ_y. The maximum residual displacement, illustrated in figure 2-4, is given by:

$$u_{r\,max} = \begin{cases} (\mu-1)(1-r)\Delta_y \xrightarrow{IF} r(\mu-1) < 1 \\ \left(\dfrac{1-r}{r}\right)\Delta_y \xrightarrow{IF} r(\mu-1) \geq 1 \end{cases} \tag{2-17}$$

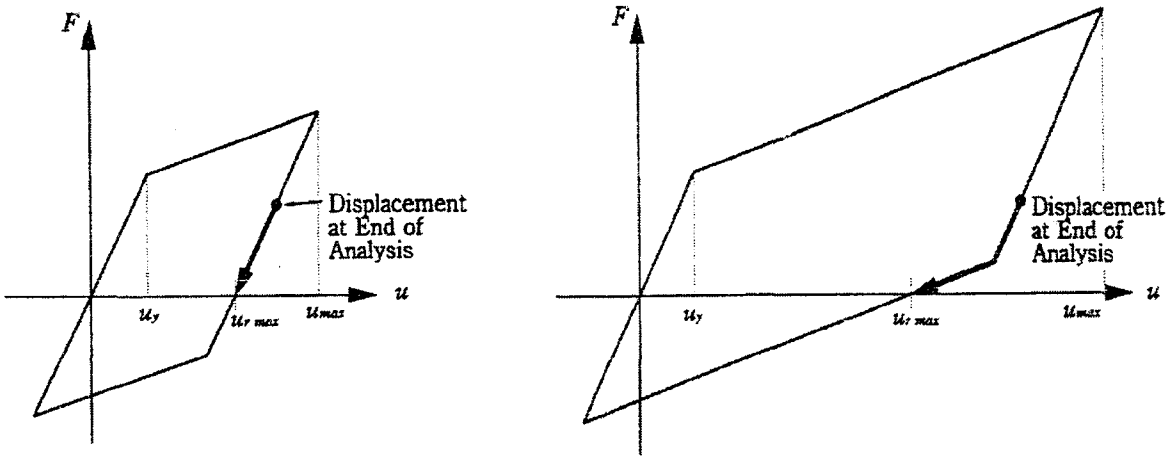

(a) r(μ-1)<1 (b) r(μ-1)≥1

FIGURE 2-4 Maximum Residual Displacement (Kawashima et al. 1996)

The authors proposed the residual displacement ratio defined as:

$$S_{RDR} = \left| u_r / u_{r\,max} \right| \tag{2-18}$$

where u_r is the residual displacement of the structure.

The stiffness ratio, r, was found to be the most significant factor controlling the residual displacement response ratio S_{RDR}. Figure 2-5 shows the mean value of S_{RDR} versus r, as proposed by the authors for use in seismic design based on analyses of 63 components of ground motion. This proposed spectrum can be used for any structures where the hysteresis loop shape may be reasonably approximated by a bilinear model.

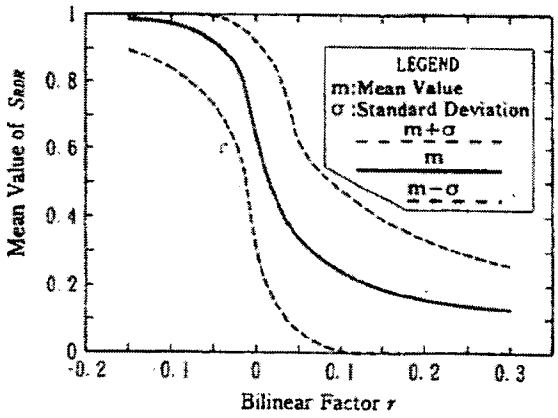

FIGURE 2-5 Residual Displacement Ratio Response Spectra S_{RDR} vs. Bilinear Factor r as Proposed for Design (Kawashima et al. 1996)

SECTION 3
EXPERIMENTAL SETUP

3.1 General

The University at Buffalo Structural Engineering and Earthquake Simulation Laboratory (UB SEESL) features two shaking tables capable of simulating earthquake ground motions: a 3.66 m x 3.66 m (12 ft x 12 ft), Five-Degree-of-Freedom Large Shaking Table and a smaller Single-Degree-of-Freedom (SDOF) Shaking Table. The latter was used for the experiments in this research and is described in Section 3.2. The test specimens are discussed in Section 3.3, followed by an overview of the test structure assembly, and the instrumentation thereof in Sections 3.4 and 3.5, respectively. Finally, the testing of the specimen, and the acquisition and reduction of the experimental data is described in Sections 3.6, 3.7, and 3.8, respectively.

3.2 Description of UB SDOF Shaking Table

3.2.1 Characteristics and Performance

The SDOF shaking table mentioned in the previous section was used to conduct the testing program in this research. The 0.91 m x 1.52 m (3 ft x 5 ft) table is driven by a displacement controlled, 24.47 kN (5.5 kip) MTS actuator with two 56.78 lpm (15 gpm) servovalves, and travels on four Teflon bearings sliding on stainless steel plates. It has a payload capacity of at least 26.7 kN (6 kips) and can achieve accelerations of 0.8g (Constantinou et al. 1999). A photograph of the SDOF shaking table is shown in figure 3-1. The direction of shaking is parallel to the longitudinal axis of the table and is in the North-South direction of the UB SEESL. This will be referenced in later discussions of the setup.

The displacement-controlled actuator accepts input from the controller in terms of voltage. This is known as the "Span" setting on the MTS controller, and indicated as such in the tables of test schedules and results. The maximum input span voltage of ±10 volts results in an actuator displacment of ±76.2 mm (±3 in).

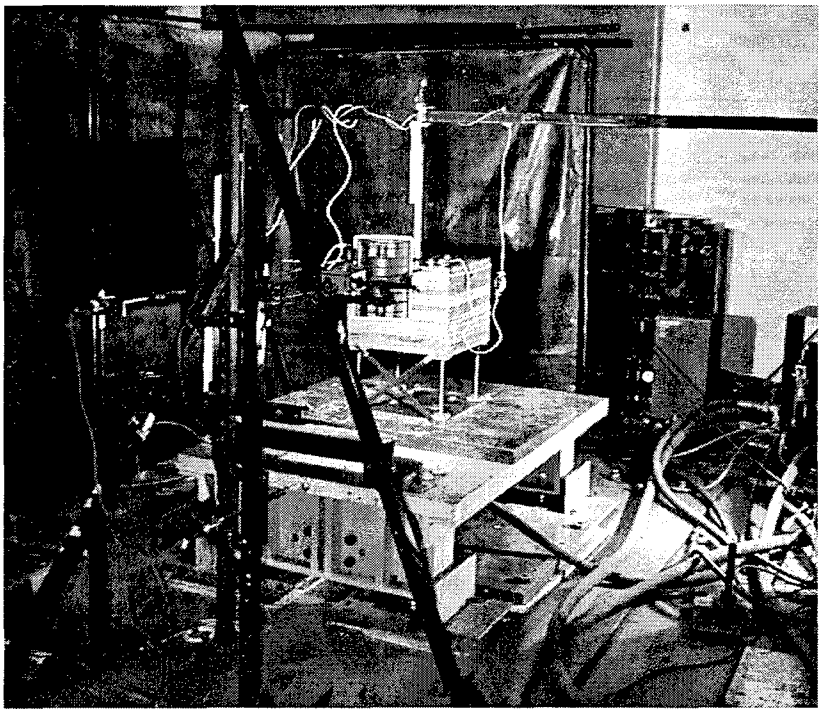

(a)

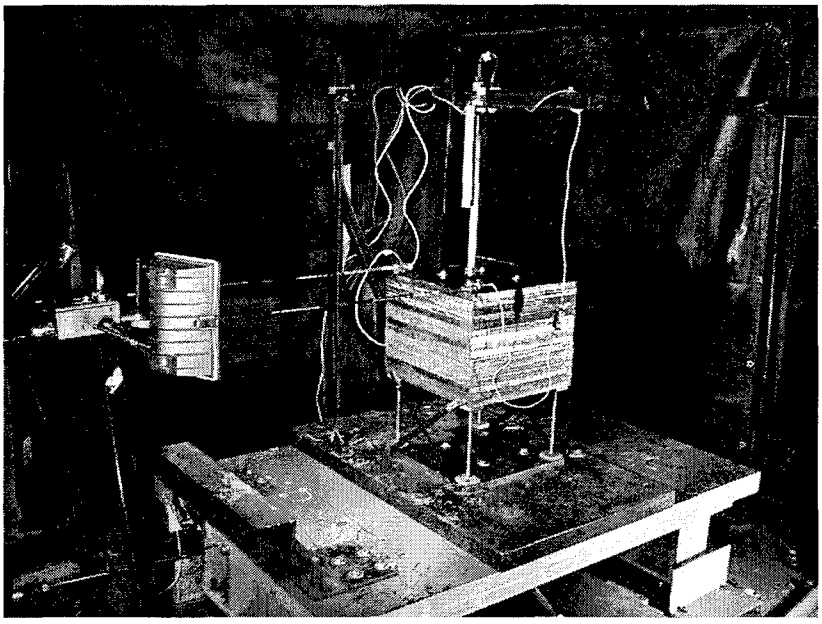

(b)

FIGURE 3-1 University at Buffalo SDOF Shaking Table (With Specimen 9 and instrumentation)

3.2.2 Selection of Ground Motion

The ground acceleration time history for the El Centro S00E-Imperial Valley Earthquake of May 1940, shown in figure 3-2, was used in this study. A displacement record was generated from this time history for use as input to the displacement-controlled actuator. The acceleration record was integrated twice with respect to time and subsequently corrected by linear regression. This integration technique resulted in an initial displacement, shown in figure 3-3, as commonly observed in the literature (Naeim 1989, Chopra 1995). This initial displacement was accommodated by slowly moving the table to this initial position at the beginning of each test. This was done over approximately twenty-four seconds at the beginning of the earthquake displacement record. Accurate reproduction of the acceleration time history was obtained with this correction. High frequency noise in the acceleration time history was obtained when this correction was not made.

The initial displacement was applied in the following manner: First, at a parabolically increasing rate, followed by a linear ramp bringing the displacement of the table past that of the initial displacement, and finally, at a parabolically decreasing rate to smoothly link into the El Centro displacement record. The slopes of the added parabolic curves were adjusted to be tangents to zero, and to the linear segment. The final parabolic segment was made tangent to the earthquake record as well, to produce an interval of constant acceleration leading into the ground motion that would be identical to that of the original record, avoiding the introduction of sudden acceleration pulses. The final input displacement, and target table acceleration time histories, at maximum actuator displacement, are shown in figures 3-4 and 3-5, respectively.

The El Centro ground motion was applied at the original time scale. However, there were a few instances where the largest peak ground acceleration (PGA) that could be produced by the table at that time scale was not sufficient to cause collapse of the specimen. In those instances, the time scale was compressed to half of the original length. These will be noted in the discussion of testing schedules.

Also, note that unscaled ground motions were used as the specimens were designed to fit actual parameters of interest, and not intended to be scaled models of actual structures.

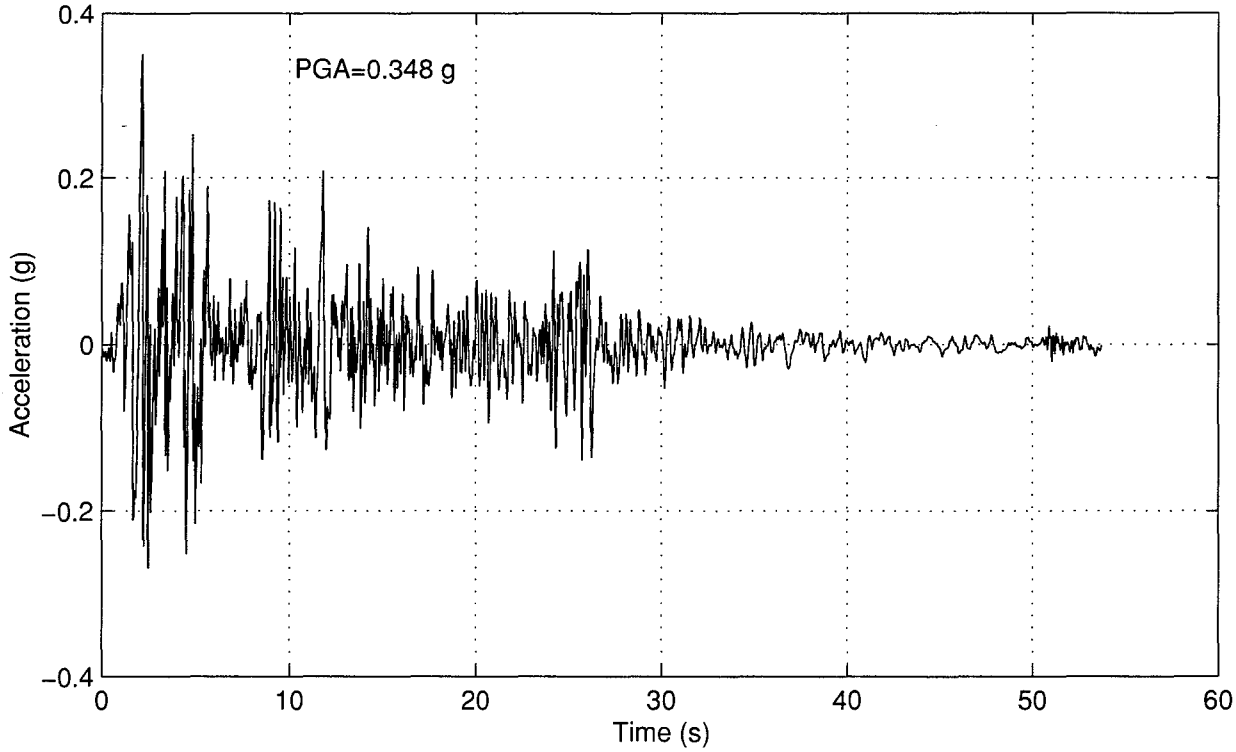

FIGURE 3–2 El Centro S00E Ground Acceleration

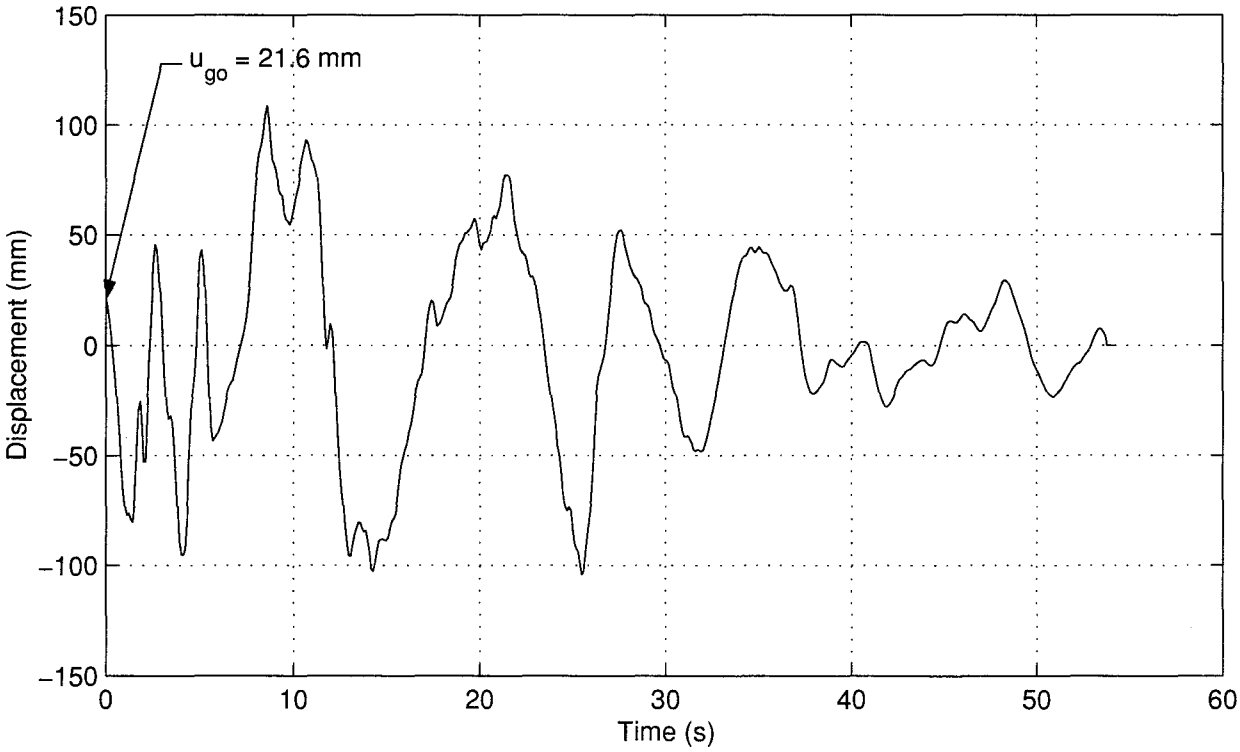

FIGURE 3–3 El Centro S00E Ground Displacement

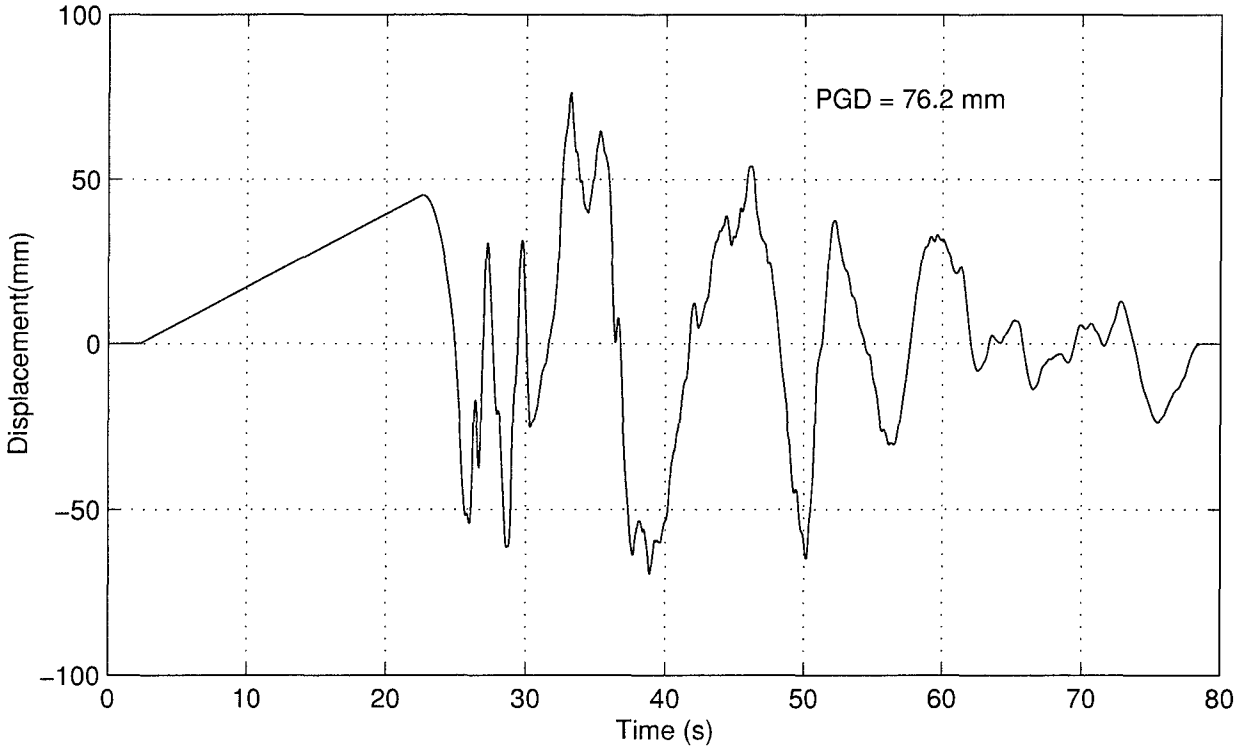

FIGURE 3–4 Shaking Table Input Displacement

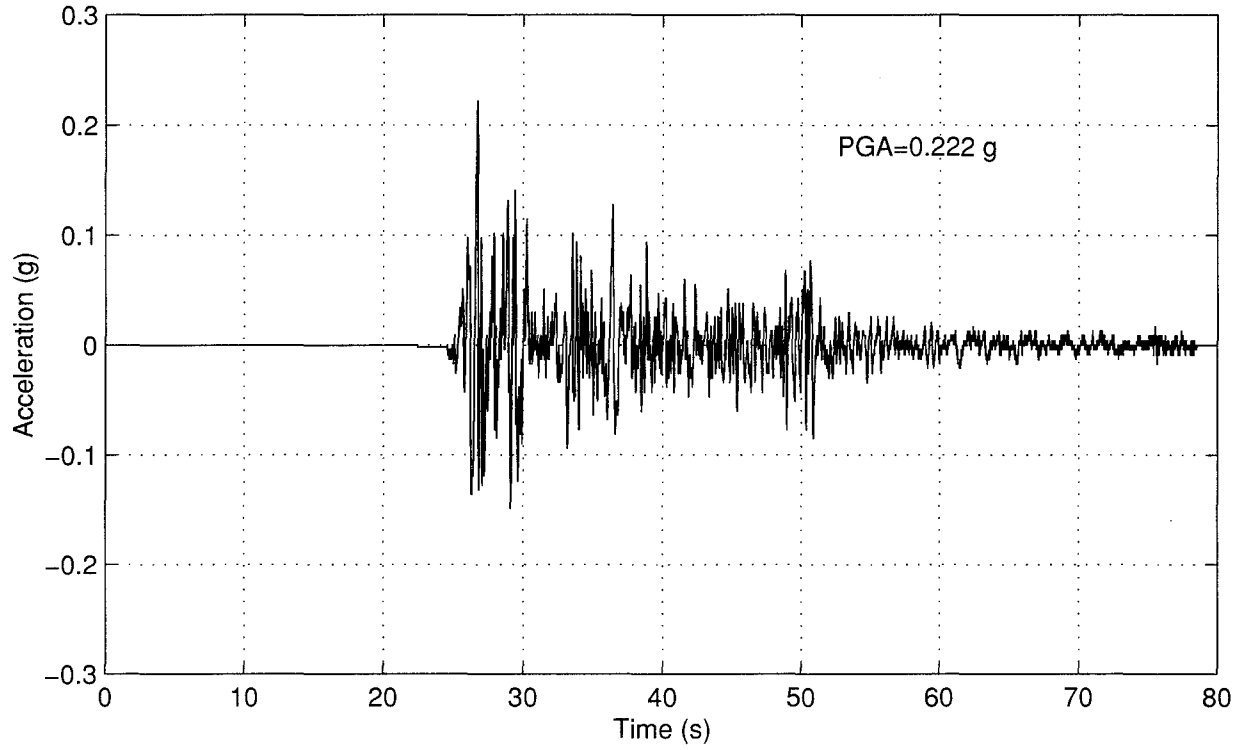

FIGURE 3–5 Target Shaking Table Acceleration

3.3 Description of Specimen

3.3.1 General

Fifteen specimens, each consisting of four columns, were tested to failure in the course of this research (An additional specimen was used for trial runs while developing the test program). These fifteen specimens were subdivided into three groups of five with slenderness ratios of 100, 150, and 200. A variety of shapes were considered in the initial stages of this research, and a square cross-section was chosen for ease of fabrication, and to avoid problems associated with local buckling. Sizes were chosen based on the preliminary hand calculations in Appendix A, with final nominal sizes of specimen and masses used listed in table 3-1. The dimensions and mass used were varied within each respective group. A range of values for axial capacity versus demand, P_u/P_n, was used for each slenderness ratio, where P_u is the weight of the mass plates used in the test, and P_n is the axial capacity of all columns in the specimen, calculated using the AISC-LRFD specifications (AISC 1994). This range of values is displayed graphically in figure 3-6.

TABLE 3-1 Specimen Nominal Dimensions

Specimen	Height (mm)	Width (mm)	Mass/column (kg)
1	137.41	4.76	35.6
2	137.41	4.76	71.2
3	91.69	3.18	71.2
4	137.41	4.76	95.0
5	91.69	2.83	95.0
KL/r = 100			
6	412.50	9.53	95.0
7	343.15	7.94	95.0
8	274.57	6.35	95.0
9	206.25	4.76	95.0
10	137.41	3.18	47.6
KL/r = 150			
11	549.91	9.53	71.2
12	457.71	7.94	71.2
13	366.52	6.35	71.2
14	275.08	4.76	71.2
15	183.39	3.18	35.6
KL/r = 200			

The specimens were fabricated at the University of Ottawa. Individual columns were cut from hot-rolled steel plate and then milled to size. A 50.8 mm (2 in) wide square by 12.7 mm (0.5 in) thick base plate was attached to the top and bottom of the column such that a rigid connection to both the shaking table and the mass plates above it could be provided. The columns were attached to base plates using silver solder and brazing to avoid loss of section as a result of welding. A sample column layout is shown in figure 3-7.

A number of methods, as described in the following subsections, were used to analyze each specimen prior to testing to estimate its response.

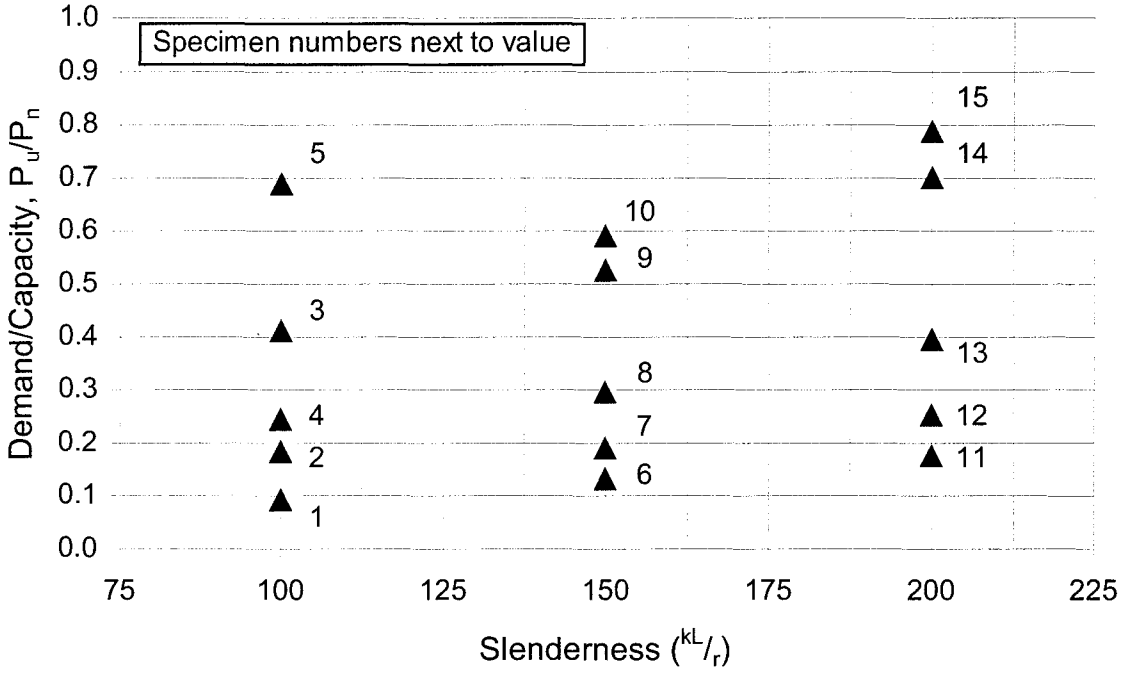

FIGURE 3-6 Specimen Axial Strength versus Slenderness

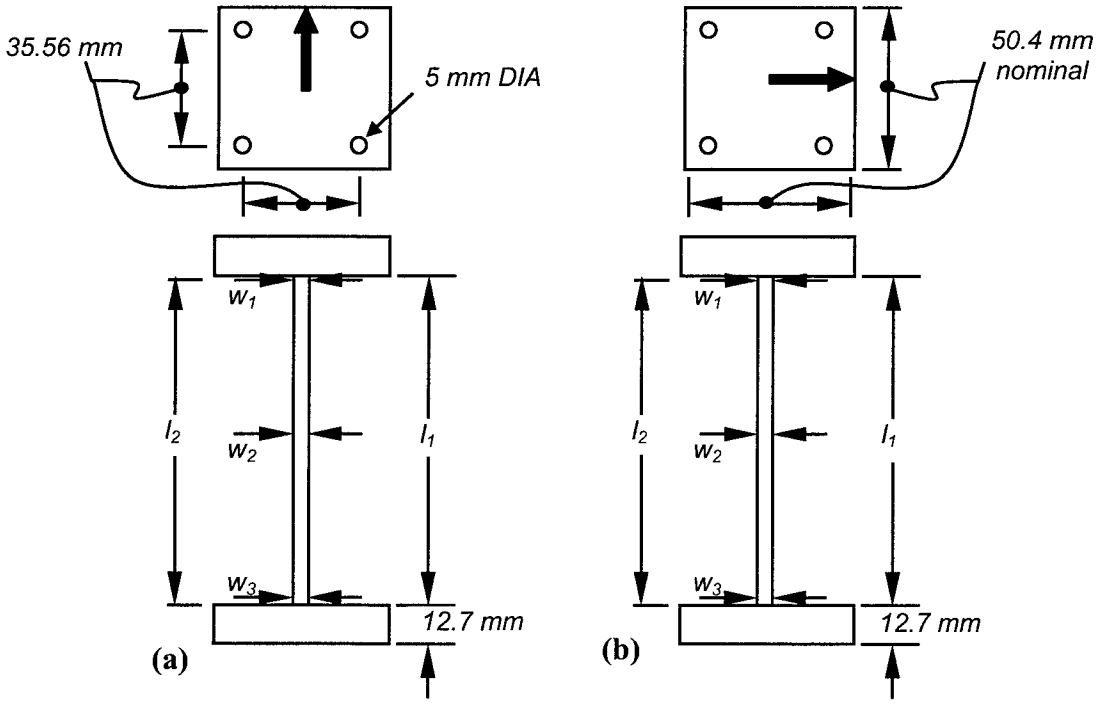

FIGURE 3-7 General Specimen Dimensions and Conventions for Imperfection Measurements in the (a) U-D and (b) L-R Orientations

3.3.2 General Specimen Properties

Bilinear behavioral properties of the specimen tested, according to the model described in the previous chapter, are listed for the nominal and average dimensions in table 3-2 on the following page. The calculated fundamental period of the structure, including and excluding the P-Δ effect is listed in table 3-3 for both nominal and average dimensions for the specimens tested.

TABLE 3-2 Specimen General Properties

Spec.	Ht (mm)		Width (mm)		mass (kg/col)	K_o (N/mm)		θ		K_1 (N/mm)		K_2 (N/mm)		r (=K_2/K_1)	
	Nom	Avg	Nom	Avg	-	Nom	Avg	Nom	Avg	Nom	Avg	Nom	Avg	Nom	Avg
1	137.4	137.2	4.8	4.8	36.63	39.64	40.27	0.066	0.065	37.03	37.65	-2.61	-2.62	-0.071	-0.070
2	137.4	137.4	4.8	4.9	72.23	39.64	41.79	0.130	0.123	34.49	36.64	-5.15	-5.16	-0.149	-0.141
4	137.4	137.5	4.8	4.8	96.03	39.64	39.12	0.173	0.175	32.79	32.27	-6.85	-6.85	-0.209	-0.212
5b	91.7	91.7	2.8	2.9	96.03	16.69	23.60	0.616	0.435	6.41	13.33	-10.27	-10.27	-1.601	-0.771
6	412.5	412.4	9.5	9.4	96.03	23.45	22.56	0.097	0.101	21.17	20.28	-2.28	-2.28	-0.108	-0.113
7	343.2	343.7	7.9	7.7	96.03	19.64	17.70	0.140	0.155	16.90	14.96	-2.74	-2.74	-0.162	-0.183
8	274.6	274.5	6.4	6.0	96.03	15.70	12.88	0.218	0.266	12.27	9.45	-3.43	-3.43	-0.279	-0.363
9	206.2	205.8	4.8	4.8	96.03	11.72	11.75	0.389	0.390	7.16	7.17	-4.57	-4.58	-0.638	-0.638
10	137.4	137.0	3.2	3.1	48.58	7.83	7.54	0.443	0.461	4.36	4.06	-3.47	-3.48	-0.795	-0.856
10b	137.4	137.4	3.2	2.8	48.58	7.83	6.88	0.443	0.504	4.36	3.41	-3.47	-3.47	-0.795	-1.017
11	549.9	549.5	9.5	9.4	72.23	9.90	9.34	0.130	0.138	8.61	8.05	-1.29	-1.29	-0.150	-0.160
12	457.7	458.2	7.9	7.7	72.23	8.28	7.21	0.187	0.214	6.73	5.67	-1.55	-1.55	-0.230	-0.273
13	366.5	366.1	6.4	6.0	72.23	6.60	5.40	0.293	0.359	4.67	3.46	-1.93	-1.93	-0.414	-0.559
14	275.1	275.2	4.8	4.7	72.23	4.94	4.84	0.521	0.532	2.37	2.26	-2.58	-2.57	-1.088	-1.137
15	183.4	182.8	3.2	3.1	36.63	3.29	3.14	0.595	0.627	1.34	1.17	-1.96	-1.97	-1.467	-1.677

TABLE 3-3 Specimen Dynamic Properties

Specimen	T_{no}[1] (s)		T_{np}[2] (s)	
	Nom	Avg	Nom	Avg
1	0.191	0.189	0.198	0.196
2	0.268	0.261	0.288	0.279
4	0.309	0.311	0.340	0.343
5b	0.477	0.401	0.769	0.533
6	0.402	0.410	0.423	0.432
7	0.439	0.463	0.474	0.503
8	0.491	0.543	0.556	0.634
9	0.569	0.568	0.728	0.727
10	0.495	0.504	0.663	0.687
10b	0.495	0.528	0.663	0.750
11	0.537	0.552	0.576	0.595
12	0.587	0.629	0.651	0.709
13	0.657	0.727	0.782	0.908
14	0.760	0.768	1.098	1.123
15	0.663	0.679	1.041	1.111

1: Excluding P-Δ Effect
2: Including P-Δ Effect

3.3.3 Predicted Elastic Limit Response

A linear-elastic dynamic analysis was performed using NONLIN (Charney 1998) to find the 1.5% damped elastic response spectrum for the El Centro ground motion discussed previously in Section 3.2.2. The maximum PGA for which the maximum displacement of the specimen is equal to the yield displacement was calculated from this analysis. This data was used to determine the scaling factors for the earthquake excitation in developing a testing schedule for each specimen.

3.3.4 Predicted Inelastic Limit Response

Specimen behavior in the inelastic range was estimated using two methods of inelastic analysis. First, a nonlinear-inelastic time history analysis was performed on each specimen using NONLIN. Each specimen was modeled as a bilinear system with negative post yielding stiffness as described in the previous chapter on P-Δ theory. The PGA of the ground motion was progressively increased until the maximum value at which the system remained stable was found. The program reports the model as being unstable when the relative displacement exceeds

the ultimate displacement, Δ_u, as defined on the force-displacement curve of figure 2-2. Alternatively, the PGA causing instability can be defined as that which causes the secant stiffness to become negative.

Second, the inelastic response of the structure was calculated using the inelastic spectrum technique (Reinhorn 1997). The elastic demand spectrum using the PGA previously found as being critical using NONLIN was used in this procedure. The capacity curve for each set was generated using the Nonlinear Static Procedure (NSP) or pushover method. In the case of the SDOF system studied, the capacity curve is the bilinear curve relating lateral force to the mass versus the resulting lateral displacement as shown on figure 2-2.

3.4 Construction of Test Structure

3.4.1 General

Researchers attempting to analytically recreate tests must have data fully describing the experimental setup. Imperfections of the fabricated specimen columns are addressed in section 3.4.2. The construction sequence for the specimen is outlined in section 3.4.3. Lateral bracing of the test structure is described in section 3.4.4.

3.4.2 Measurement of Initial Imperfections

Imperfections exist in any fabricated structure. These initial imperfections have a significant impact on the behavior and must be known if accurate analysis is to follow. Thus, each column in each specimen was measured in a variety of ways prior to testing. One base plate for each column of a specimen was designated as the top and marked with an arrow, establishing a reference point from which all measurements are related. References with respect to the direction this arrow is pointing are referred to as the "Up-Down" and "Left-Right" orientations, hereafter known as "U-D" and "L-R", as shown in figure 3-7.

A graphical description of all types of imperfections considered is also defined on figures 3-8 and 3-9 such that the values tabulated can be properly incorporated into analytical models. Sign conventions adopted for each of the major dimensions tabulated are shown on the corresponding figure.

The width of each column was measured at the top, middle, and bottom in each direction and noted as w_1, w_2, and w_3, respectively. As shown in figure 3-8, the free height between base plates, l_1 and l_2 are used to calculate the angle of bowing of the specimen given by:

$$\theta_b = 2 \times \sin^{-1}\left(\frac{\left(l_1 - l_2/2\right)}{50.8mm}\right) \tag{3-1}$$

where:

l_1, l_2 = Lengths of column shown in figure 3-7 (a) and (b)

50.8mm (2in) = Nominal base plate width.

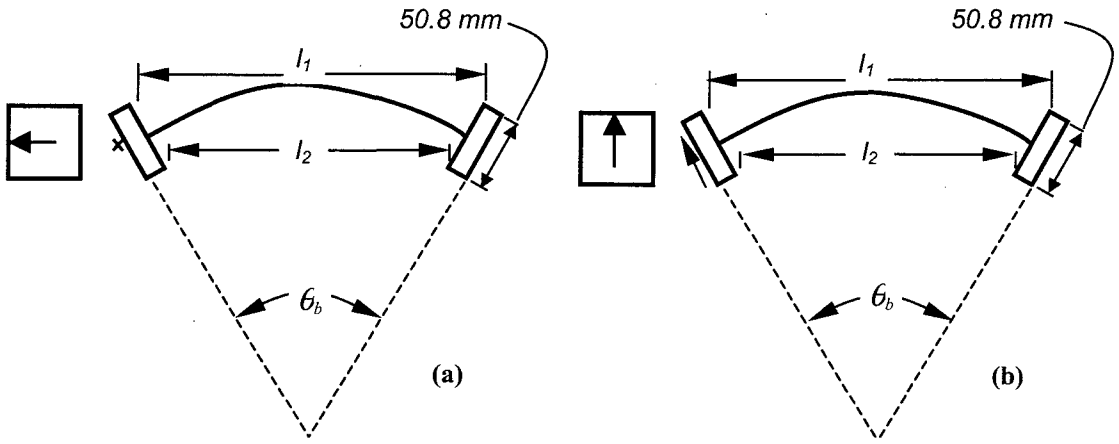

FIGURE 3-8 Angle of Bowing in (a) U-D and (b) L-R Orientations

The lateral shifts of the top of the column with respect to the bottom, v_1 and v_2, were measured at each corner of top base plates for each specimen. These measurements were made with respect to the bottom base plate, allowing two important calculations to be made: the average uniform lateral shift over the height, V_{unif}, as well as the angle of twist over the height, ϕ, which are given by the following:

$$V_{unif} = \left(\frac{v_1 + v_2}{2}\right) \tag{3-2}$$

$$\phi = \sin^{-1}\left(\frac{v_1 - v_2}{50.8mm}\right) \tag{3-3}$$

where:

v_1, v_2 = Lateral shifts of column base plate corner shown in figure 3-9 (a) and (b)

50.8mm (2in) = Nominal base plate width.

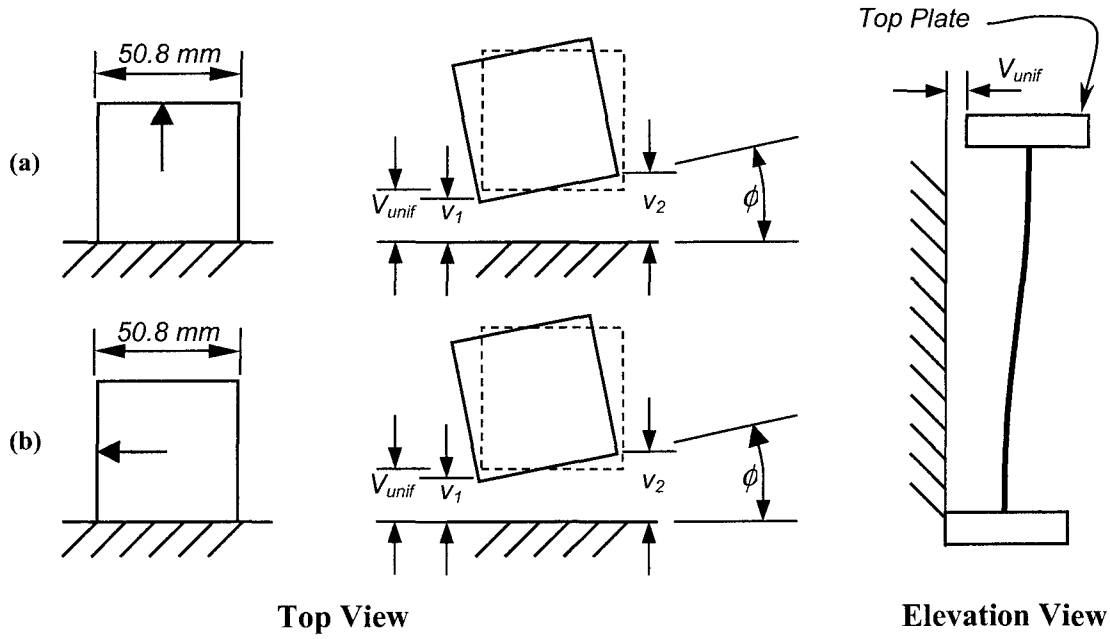

FIGURE 3-9 Lateral Shift & Angle of Twist in (a) U-D and (b) L-R Orientations

The measured quantities w_1, w_2, w_3, l_1, l_2, v_1, and v_2 for both the U-D and L-R orientations are tabulated for each column of all specimens in table 3-4. This table also includes the measured value of base plate width for each orientation so that the true value can be used in the calculation of θ_b and ϕ by (3-1) and (3-3) in place of the nominal width given above. Resulting properties calculated from those dimensions are listed in table 3-5, namely, average specimen width and height, w_{avg} and L_{avg}, respectively, as well as, imperfections θ_b, V_{unif}, and ϕ.

The uniform lateral shift, V_{unif}, was used to determine the orientation of each individual column. Orientations were chosen to minimize the net sum of lateral shifts for all of the columns parallel to or perpendicular to the direction of shaking. The locations and orientations of each column, with appropriate sign conventions, are listed in table 3-6.

TABLE 3-4 Measured Column Dimensions (mm)

Orientation	w_1	w_2	w_3	$Base_1$	$Base_2$	L_1	L_2	v_1	v_2
Specimen 1									
U-D_1	4.85	4.80	4.80	50.9	50.7	137.4	136.7	1.96	1.69
L-R_1	4.90	4.90	4.78	50.9	50.9	136.4	137.6	1.14	0.57
U-D_2	4.79	4.79	4.76	50.9	50.8	136.9	137.8	-1.31	-1.09
L-R_2	4.79	4.79	4.75	51.0	51.0	137.5	137.4	0.70	0.90
U-D_3	4.72	4.72	4.79	50.8	50.8	137.5	136.9	1.16	0.84
L-R_3	4.74	4.72	4.79	50.9	51.1	137.4	137.1	-0.75	-0.46
U-D_4	4.75	4.74	4.76	50.7	50.7	136.6	137.6	2.32	1.66
L-R_4	4.72	4.72	4.80	50.8	50.9	136.4	137.8	2.88	3.21
Specimen 2									
U-D_1	4.76	4.76	4.78	51.2	50.9	136.9	137.5	0.95	0.60
L-R_1	4.93	4.94	4.98	51.1	51.1	137.0	137.3	-0.58	-0.83
U-D_2	4.97	4.95	4.95	50.9	50.9	137.5	137.3	0.58	0.37
L-R_2	4.83	4.78	4.80	51.1	51.1	137.6	137.2	-2.08	-2.13
U-D_3	4.78	4.78	4.78	50.9	50.9	136.6	137.7	0.57	2.79
L-R_3	4.94	4.95	4.94	50.9	51.1	137.1	137.0	1.09	3.19
U-D_4	4.94	4.97	4.95	50.9	50.9	138.4	137.4	-4.15	-2.98
L-R_4	4.80	4.80	4.78	51.1	51.0	138.4	137.3	-2.01	-0.46
Specimen 3									
U-D_1	3.14	3.12	3.14	50.8	50.9	90.9	91.5	-0.98	-2.03
L-R_1	3.19	3.19	3.20	51.1	51.0	91.0	91.5	1.98	0.90
U-D_2	3.21	3.21	3.24	50.9	50.8	92.5	91.5	-1.65	-2.34
L-R_2	3.14	3.15	3.15	50.9	50.9	92.6	91.4	0.00	-0.43
U-D_3	3.15	3.16	3.18	50.8	50.9	93.1	92.0	-1.70	-1.70
L-R_3	3.19	3.21	3.23	50.8	50.9	92.8	92.3	-2.27	-1.96
U-D_4	3.16	3.18	3.18	50.8	50.8	91.5	90.9	-1.17	-1.83
L-R_4	3.14	3.14	3.18	50.7	50.9	91.9	90.6	-0.51	1.69
Specimen 4									
U-D_1	4.76	4.78	4.76	51.0	50.9	137.6	137.4	1.92	2.81
L-R_1	4.97	4.95	4.97	51.1	51.1	137.0	137.9	-3.10	-2.25
U-D_2	4.76	4.76	4.76	51.0	50.9	137.6	137.3	-1.19	0.34
L-R_2	4.93	4.93	4.93	50.9	50.9	137.6	137.2	-1.03	-3.18
U-D_3	4.78	4.78	4.78	50.8	51.0	137.4	138.0	1.51	1.33
L-R_3	4.89	4.90	4.90	50.9	51.1	137.3	138.2	2.55	2.64
U-D_4	4.52	4.50	4.62	50.9	50.9	137.6	137.3	0.25	0.43
L-R_4	4.61	4.62	4.57	51.0	50.9	137.1	137.8	-0.43	-0.38

TABLE 3-4 (cont'd) Measured Column Dimensions (mm)

Orientation	w_1	w_2	w_3	$Base_1$	$Base_2$	L_1	L_2	v_1	v_2
Specimen 5									
U-D_1	3.19	3.24	3.21	50.8	50.8	91.9	92.8	-0.75	-2.02
L-R_1	3.14	3.14	3.14	50.8	50.7	92.4	92.2	2.20	0.77
U-D_2	3.15	3.15	3.14	50.7	50.8	91.6	92.0	-0.32	-1.31
L-R_2	3.23	3.23	3.23	50.8	50.7	92.0	91.6	3.39	2.26
U-D_3	3.18	3.24	3.19	50.8	50.9	90.9	92.9	-3.35	-1.92
L-R_3	3.14	3.14	3.15	50.8	50.8	92.4	91.5	1.38	2.79
U-D_4	3.16	3.16	3.16	50.8	51.0	90.6	92.4	-3.18	-2.46
L-R_4	3.11	3.12	3.12	50.8	50.7	92.0	91.0	-1.77	-1.00
Specimen 5b									
U-D_1	2.82	2.82	2.82	51.0	50.9	91.6	91.8	-0.41	0.20
L-R_1	2.84	2.84	2.84	50.9	50.8	91.8	91.5	0.79	1.27
U-D_2	2.88	2.86	2.87	50.8	51.2	91.9	91.5	-0.25	0.30
L-R_2	2.92	2.92	2.93	50.9	50.8	92.0	91.5	-0.84	-0.36
U-D_3	2.84	2.83	2.83	50.9	50.8	91.8	91.5	0.13	0.05
L-R_3	2.84	2.84	2.84	50.8	50.9	91.5	91.7	-0.46	-0.30
U-D_4	2.82	2.92	2.88	50.9	50.9	91.6	92.0	-1.32	-0.97
L-R_4	2.83	2.86	2.86	50.9	50.9	92.1	91.4	-0.03	0.53
Specimen 6									
U-D_1	9.16	9.16	9.19	50.8	50.8	412.2	412.5	1.09	0.30
L-R_1	9.64	9.58	9.61	50.8	50.8	412.1	412.6	-5.36	-5.46
U-D_2	9.46	9.46	9.45	51.0	50.8	412.1	412.1	-5.64	-6.60
L-R_2	9.46	9.37	9.46	50.8	50.9	412.3	411.7	-0.81	-1.02
U-D_3	9.63	9.59	9.58	51.1	51.1	412.7	412.4	-2.92	-2.87
L-R_3	9.25	9.16	9.19	50.8	50.9	412.8	412.2	-5.66	-5.41
U-D_4	9.21	9.16	9.17	50.8	50.7	412.4	412.6	3.10	3.18
L-R_4	9.66	9.63	9.60	50.8	50.7	412.6	412.6	0.79	5.33
Specimen 7									
U-D_1	7.91	7.82	7.80	51.1	50.8	343.0	344.3	-0.46	1.22
L-R_1	7.66	7.54	7.61	50.7	50.8	343.7	343.7	3.30	4.78
U-D_2	7.89	7.89	7.89	51.0	51.1	343.4	343.5	-1.02	1.22
L-R_2	7.57	7.59	7.61	51.1	50.8	343.5	343.8	0.08	1.63
U-D_3	7.67	7.58	7.65	50.8	50.8	343.9	344.1	-2.46	0.28
L-R_3	7.94	7.89	7.90	50.8	50.9	344.3	343.6	-1.52	1.22
U-D_4	7.90	7.87	7.90	50.9	50.9	343.6	343.4	-4.83	3.35
L-R_4	7.62	7.61	7.61	50.7	50.9	343.6	343.6	-0.38	0.89

TABLE 3-4 (cont'd) Measured Column Dimensions (mm)

Orientation	w_1	w_2	w_3	$Base_1$	$Base_2$	L_1	L_2	v_1	v_2
Specimen 8									
U-D_1	5.74	5.82	5.75	50.7	51.0	274.8	274.4	0.40	0.79
L-R_1	6.26	6.32	6.25	50.8	50.9	274.5	274.4	0.40	0.79
U-D_2	6.27	6.27	6.32	50.7	50.7	274.1	274.6	0.00	0.00
L-R_2	5.68	5.80	5.88	50.8	51.0	274.2	274.3	3.18	3.97
U-D_3	5.82	5.78	5.85	51.1	51.1	274.6	274.8	2.78	3.18
L-R_3	6.30	6.27	6.31	50.9	50.9	274.2	275.1	0.00	0.00
U-D_4	6.29	6.29	6.34	51.0	50.8	274.4	274.2	-2.38	-1.59
L-R_4	5.78	5.75	5.72	50.9	50.8	274.3	274.3	-0.79	0.00
Specimen 9									
U-D_1	4.74	4.72	4.71	50.7	51.0	205.8	205.6	1.59	1.59
L-R_1	4.80	4.79	4.80	50.8	50.9	205.7	205.6	0.79	1.19
U-D_2	4.78	4.75	4.74	50.9	51.1	206.9	205.3	-0.40	0.00
L-R_2	4.79	4.76	4.76	50.8	50.9	206.1	206.1	-3.18	-1.98
U-D_3	4.70	4.71	4.71	50.9	50.8	205.0	206.1	0.00	0.00
L-R_3	4.76	4.78	4.76	50.7	50.7	205.4	205.7	2.38	2.38
U-D_4	4.76	4.78	4.74	50.9	50.9	205.6	206.0	-2.38	-2.78
L-R_4	4.80	4.79	4.79	51.0	50.9	206.2	205.6	-0.40	-0.79
Specimen 10									
U-D_1	3.15	3.14	3.15	51.3	51.1	136.6	137.3	-3.48	-3.48
L-R_1	3.14	3.19	3.15	51.1	50.9	137.1	137.1	-2.40	-2.31
U-D_2	3.15	3.16	3.15	50.9	50.9	137.2	137.0	2.86	2.82
L-R_2	3.12	3.16	3.14	50.8	51.2	137.0	137.2	2.31	2.41
U-D_3	3.14	3.14	3.14	51.2	50.7	136.9	137.1	1.37	1.37
L-R_3	3.11	3.12	3.15	50.7	50.8	136.9	137.1	-2.79	-2.71
U-D_4	3.11	3.11	3.16	51.0	50.8	136.7	137.2	1.24	0.76
L-R_4	3.11	3.12	3.15	50.8	50.8	136.9	137.0	3.76	3.89
Specimen 10b									
U-D_1	2.82	2.87	2.81	51.0	51.0	137.6	137.6	0.05	0.33
L-R_1	2.84	2.84	2.82	50.9	50.9	137.5	137.6	0.66	0.84
U-D_2	2.83	2.84	2.86	51.0	51.1	137.4	137.6	-0.66	-0.38
L-R_2	2.86	2.88	2.82	50.8	50.9	137.6	137.3	0.43	0.43
U-D_3	2.82	2.81	2.82	51.0	51.2	137.4	137.5	0.00	0.08
L-R_3	2.79	2.79	2.92	50.8	50.9	137.4	137.4	1.52	2.03
U-D_4	2.90	2.92	2.91	51.1	51.1	137.2	137.3	0.36	0.64
L-R_4	2.83	2.83	2.83	50.9	50.9	137.1	137.4	0.38	0.13

TABLE 3-4 (cont'd) Measured Column Dimensions (mm)

Orientation	w_1	w_2	w_3	$Base_1$	$Base_2$	L_1	L_2	v_1	v_2
Specimen 11									
U-D_1	9.14	9.18	9.22	50.9	50.9	549.3	550.1	11.07	9.22
L-R_1	9.59	9.61	9.60	51.0	51.2	549.7	550.1	5.46	3.84
U-D_2	9.27	9.23	9.39	50.9	50.8	549.3	548.9	2.31	2.41
L-R_2	9.46	9.47	9.50	50.9	51.1	548.9	549.3	-3.84	-3.78
U-D_3	9.66	9.60	9.61	51.0	50.9	549.7	550.1	1.78	2.26
L-R_3	9.21	9.19	9.23	51.0	51.1	549.7	549.7	-0.64	-1.96
U-D_4	9.17	9.18	9.23	50.8	51.1	549.3	549.3	12.62	4.19
L-R_4	9.59	9.58	9.55	50.8	51.0	549.3	549.7	4.01	-2.84
Specimen 12									
U-D_1	7.63	7.59	7.59	51.0	50.8	458.5	457.8	-2.24	0.71
L-R_1	7.90	7.89	7.90	50.8	50.9	458.0	458.1	-4.57	-3.56
U-D_2	7.59	7.59	7.59	51.0	50.8	456.4	458.5	-9.86	-11.94
L-R_2	7.87	7.87	7.90	50.9	50.9	458.5	456.7	10.44	15.37
U-D_3	7.61	7.63	7.67	50.9	50.7	458.4	458.9	4.65	5.38
L-R_3	7.87	7.94	7.92	50.7	50.9	458.5	458.9	-0.56	-0.05
U-D_4	7.61	7.57	7.59	50.8	50.8	458.1	458.6	2.03	3.89
L-R_4	7.75	7.87	7.89	50.8	50.9	458.8	458.1	4.88	7.77
Specimen 13									
U-D_1	5.79	5.77	5.73	51.0	50.7	366.2	365.9	1.27	1.57
L-R_1	6.32	6.32	6.30	50.7	50.8	366.1	366.1	-3.81	-2.67
U-D_2	6.29	6.29	6.31	50.7	51.0	366.5	365.6	0.53	0.53
L-R_2	5.65	5.65	6.02	50.8	50.9	365.9	366.1	0.46	0.56
U-D_3	6.32	6.31	6.31	50.7	50.7	366.0	366.4	-0.25	0.79
L-R_3	5.77	5.77	5.72	50.8	50.8	366.1	366.3	1.14	2.34
U-D_4	6.32	6.32	6.32	51.0	50.7	366.6	365.4	0.58	0.46
L-R_4	5.78	5.77	5.72	50.9	50.7	365.7	366.2	-3.78	-4.06
Specimen 14									
U-D_1	4.76	4.78	4.83	50.7	50.7	275.4	274.3	0.00	0.00
L-R_1	4.74	4.74	4.78	50.9	50.8	274.6	274.9	-3.18	-2.78
U-D_2	4.76	4.75	4.75	51.1	51.0	275.5	276.0	-0.79	0.79
L-R_2	4.75	4.75	4.76	50.8	50.8	276.0	275.6	-1.19	0.00
U-D_3	4.76	4.76	4.76	51.1	51.0	274.8	275.0	2.38	2.38
L-R_3	4.71	4.71	4.69	50.7	50.8	275.6	274.2	-1.59	-1.19
U-D_4	4.71	4.70	4.71	50.9	50.8	275.8	275.1	0.00	0.79
L-R_4	4.78	4.75	4.80	51.0	50.8	275.6	275.5	1.59	2.38

TABLE 3-4 (cont'd) Measured Column Dimensions (mm)

Orientation	w_1	w_2	w_3	$Base_1$	$Base_2$	L_1	L_2	v_1	v_2
Specimen 15									
U-D_1	3.15	3.12	3.12	51.1	51.1	182.9	183.0	3.40	3.47
L-R_1	3.16	3.14	3.12	51.0	50.9	182.8	183.2	2.96	2.79
U-D_2	3.12	3.12	3.12	50.7	50.7	181.5	184.0	-2.71	-3.11
L-R_2	3.11	3.11	3.16	50.8	50.8	183.0	182.4	6.71	6.44
U-D_3	3.14	3.16	3.15	50.8	51.0	183.2	182.3	1.08	-0.76
L-R_3	3.11	3.12	3.12	50.9	50.8	182.7	182.8	1.32	0.36
U-D_4	3.12	3.12	3.15	50.8	50.8	183.2	182.0	-1.37	-1.21
L-R_4	3.11	3.11	3.15	50.9	50.9	183.1	182.3	1.07	1.10

TABLE 3-5 Calculated Column Dimensions

Orientation	w_{avg} (mm)	L_{avg} (mm)	θ_b (deg)	V_{unif} (mm)	ϕ (deg)
Specimen 1					
U-D_1	4.82	137.1	0.759	1.82	0.301
L-R_1	4.86	137.0	-1.387	0.86	0.643
U-D_2	4.78	137.4	-1.016	-1.20	-0.243
L-R_2	4.78	137.4	0.143	0.80	-0.228
U-D_3	4.75	137.2	0.659	1.00	0.358
L-R_3	4.75	137.3	0.314	-0.60	-0.328
U-D_4	4.75	137.1	-1.220	1.99	0.746
L-R_4	4.75	137.1	-1.560	3.05	-0.372
Specimen 2					
U-D_1	4.77	137.2	-0.613	0.77	0.399
L-R_1	4.95	137.2	-0.356	-0.70	0.270
U-D_2	4.96	137.4	0.243	0.48	0.243
L-R_2	4.80	137.4	0.413	-2.11	0.057
U-D_3	4.78	137.1	-1.344	1.68	-2.503
L-R_3	4.94	137.1	0.043	2.14	-2.356
U-D_4	4.95	137.9	1.130	-3.57	-1.316
L-R_4	4.79	137.8	1.213	-1.23	-1.741
Specimen 3					
U-D_1	3.13	91.2	-0.701	-1.50	1.188
L-R_1	3.19	91.2	-0.584	1.44	1.212
U-D_2	3.22	92.0	1.188	-1.99	0.773
L-R_2	3.15	92.0	1.402	-0.22	0.486
U-D_3	3.16	92.5	1.274	-1.70	0.000
L-R_3	3.21	92.6	0.487	-2.11	-0.358
U-D_4	3.17	91.2	0.716	-1.50	0.745
L-R_4	3.15	91.3	1.476	0.59	-2.479
Specimen 4					
U-D_1	4.77	137.5	0.214	2.36	-1.000
L-R_1	4.96	137.5	-1.039	-2.67	-0.954
U-D_2	4.76	137.5	0.414	-0.43	-1.729
L-R_2	4.93	137.4	0.386	-2.10	2.418
U-D_3	4.78	137.7	-0.672	1.42	0.200
L-R_3	4.90	137.8	-0.970	2.60	-0.100
U-D_4	4.55	137.4	0.386	0.34	-0.200
L-R_4	4.60	137.5	-0.742	-0.41	-0.057

TABLE 3-5 (cont'd) Calculated Column Dimensions

Orientation	w_{avg} (mm)	L_{avg} (mm)	θ_b (deg)	V_{unif} (mm)	ϕ (deg)
Specimen 5					
U-D_1	3.21	92.4	-1.002	-1.38	1.431
L-R_1	3.14	92.3	0.272	1.49	1.605
U-D_2	3.15	91.8	-0.445	-0.81	1.119
L-R_2	3.23	91.8	0.358	2.83	1.276
U-D_3	3.20	91.9	-2.290	-2.64	-1.617
L-R_3	3.14	91.9	0.960	2.09	-1.590
U-D_4	3.16	91.5	-2.030	-2.82	-0.801
L-R_4	3.12	91.5	1.175	-1.38	-0.860
Specimen 5b					
U-D_1	2.82	91.7	-0.186	-0.10	-0.685
L-R_1	2.84	91.6	0.272	1.03	-0.544
U-D_2	2.87	91.7	0.414	0.03	-0.628
L-R_2	2.93	91.8	0.487	-0.60	-0.544
U-D_3	2.84	91.7	0.315	0.09	0.086
L-R_3	2.84	91.6	-0.272	-0.38	-0.172
U-D_4	2.87	91.8	-0.429	-1.14	-0.400
L-R_4	2.85	91.7	0.830	0.25	-0.629
Specimen 6					
U-D_1	9.17	412.3	-0.329	0.70	0.888
L-R_1	9.61	412.3	-0.573	-5.41	0.115
U-D_2	9.46	412.1	0.000	-6.12	1.087
L-R_2	9.43	412.0	0.644	-0.91	0.229
U-D_3	9.60	412.5	0.327	-2.90	-0.057
L-R_3	9.20	412.5	0.701	-5.54	-0.286
U-D_4	9.18	412.5	-0.143	3.14	-0.086
L-R_4	9.63	412.6	-0.029	3.06	-5.140
Specimen 7					
U-D_1	7.84	343.7	-1.457	0.38	-1.885
L-R_1	7.60	343.7	0.000	4.04	-1.663
U-D_2	7.89	343.5	-0.114	0.10	-2.511
L-R_2	7.59	343.6	-0.329	0.85	-1.743
U-D_3	7.63	344.0	-0.186	-1.09	-3.096
L-R_3	7.91	343.9	0.787	-0.15	-3.091
U-D_4	7.89	343.5	0.172	-0.74	-9.250
L-R_4	7.61	343.6	0.029	0.25	-1.433

TABLE 3-5 (cont'd) Calculated Column Dimensions

Orientation	w_{avg} (mm)	L_{avg} (mm)	θ_b (deg)	V_{unif} (mm)	ϕ (deg)
Specimen 8					
U-D_1	5.77	274.6	0.429	0.60	-0.447
L-R_1	6.28	274.5	0.072	0.60	-0.448
U-D_2	6.29	274.4	-0.545	0.00	0.000
L-R_2	5.79	274.2	-0.114	3.57	-0.893
U-D_3	5.82	274.7	-0.214	2.98	-0.445
L-R_3	6.29	274.7	-1.044	0.00	0.000
U-D_4	6.30	274.3	0.143	-1.98	-0.894
L-R_4	5.75	274.3	0.000	-0.40	-0.894
Specimen 9					
U-D_1	4.72	205.7	0.186	1.59	0.000
L-R_1	4.80	205.7	0.115	0.99	-0.447
U-D_2	4.75	206.1	1.725	-0.20	-0.446
L-R_2	4.77	206.1	-0.057	-2.58	-1.342
U-D_3	4.71	205.6	-1.202	0.00	0.000
L-R_3	4.77	205.6	-0.387	2.38	0.000
U-D_4	4.76	205.8	-0.472	-2.58	0.447
L-R_4	4.79	205.9	0.642	-0.60	0.446
Specimen 10					
U-D_1	3.15	136.9	-0.782	-3.48	0.000
L-R_1	3.16	137.1	0.043	-2.36	-0.100
U-D_2	3.15	137.1	0.243	2.84	0.043
L-R_2	3.14	137.1	-0.314	2.36	-0.114
U-D_3	3.14	137.0	-0.143	1.37	0.000
L-R_3	3.13	137.0	-0.143	-2.75	-0.100
U-D_4	3.13	137.0	-0.544	1.00	0.544
L-R_4	3.13	136.9	-0.143	3.82	-0.143
Specimen 10b					
U-D_1	2.83	137.6	0.057	0.19	-0.314
L-R_1	2.84	137.5	-0.072	0.75	-0.200
U-D_2	2.84	137.5	-0.271	-0.52	-0.314
L-R_2	2.85	137.4	0.372	0.43	0.000
U-D_3	2.82	137.4	-0.057	0.04	-0.085
L-R_3	2.84	137.4	-0.014	1.78	-0.573
U-D_4	2.91	137.2	-0.057	0.50	-0.313
L-R_4	2.83	137.3	-0.329	0.25	0.286

TABLE 3-5 (cont'd) Calculated Column Dimensions

Orientation	w_{avg} (mm)	L_{avg} (mm)	θ_b (deg)	V_{unif} (mm)	ϕ (deg)
Specimen 11					
U-D_1	9.18	549.7	-0.894	10.15	2.088
L-R_1	9.60	549.9	-0.445	4.65	1.823
U-D_2	9.30	549.1	0.447	2.36	-0.114
L-R_2	9.48	549.1	-0.446	-3.81	-0.057
U-D_3	9.63	549.9	-0.447	2.02	-0.543
L-R_3	9.21	549.7	0.000	-1.30	1.483
U-D_4	9.19	549.3	0.000	8.41	9.528
L-R_4	9.57	549.5	-0.447	0.58	7.743
Specimen 12					
U-D_1	7.61	458.2	0.729	-0.76	-3.320
L-R_1	7.90	458.1	-0.100	-4.06	-1.145
U-D_2	7.59	457.4	-2.445	-10.90	2.346
L-R_2	7.88	457.6	1.960	12.90	-5.559
U-D_3	7.64	458.6	-0.530	5.02	-0.831
L-R_3	7.91	458.7	-0.401	-0.30	-0.573
U-D_4	7.59	458.3	-0.573	2.96	-2.093
L-R_4	7.84	458.4	0.801	6.32	-3.264
Specimen 13					
U-D_1	5.76	366.1	0.386	1.42	-0.344
L-R_1	6.32	366.1	0.000	-3.24	-1.291
U-D_2	6.29	366.1	0.959	0.53	0.000
L-R_2	5.77	366.0	-0.186	0.51	-0.115
U-D_3	6.32	366.2	-0.531	0.27	-1.176
L-R_3	5.75	366.2	-0.200	1.74	-1.346
U-D_4	6.32	366.0	1.318	0.52	0.143
L-R_4	5.75	366.0	-0.573	-3.92	0.315
Specimen 14					
U-D_1	4.79	274.9	1.277	0.00	0.000
L-R_1	4.75	274.7	-0.329	-2.98	-0.447
U-D_2	4.75	275.7	-0.570	0.00	-1.782
L-R_2	4.75	275.8	0.372	-0.60	-1.343
U-D_3	4.76	274.9	-0.314	2.38	0.000
L-R_3	4.70	274.9	1.534	-1.39	-0.448
U-D_4	4.71	275.5	0.730	0.40	-0.895
L-R_4	4.78	275.5	0.114	1.98	-0.894

TABLE 3-5 (cont'd) Calculated Column Dimensions

Orientation	w_{avg} (mm)	L_{avg} (mm)	θ_b (deg)	V_{unif} (mm)	ϕ (deg)
Specimen 15					
U-D_1	3.13	182.9	-0.100	3.44	-0.071
L-R_1	3.14	183.0	-0.429	2.88	0.186
U-D_2	3.12	182.8	-2.725	-2.91	0.459
L-R_2	3.13	182.7	0.630	6.57	0.301
U-D_3	3.15	182.8	0.929	0.16	2.074
L-R_3	3.12	182.7	-0.129	0.84	1.088
U-D_4	3.13	182.6	1.332	-1.29	-0.186
L-R_4	3.12	182.7	0.930	1.09	-0.043

TABLE 3-6 Column Locations and Orientations, $^{kL}/_{r}$ =100

Column Index	Location	Orientation
Specimen 1		
1	NW	4
2	NE	1
3	SW	4
4	SE	1
Specimen 2		
1	NW	2
2	NE	1
3	SW	4
4	SE	1
Specimen 3		
1	NE	4
2	SW	1
3	NW	2
4	SE	1
Specimen 4		
1	NW	2
2	NE	4
3	SW	4
4	SE	4
Specimen 5		
1	NW	3
2	NE	4
3	SE	1
4	SW	1
Specimen 5b		
1	NW	1
2	NE	1
3	SW	1
4	SE	4

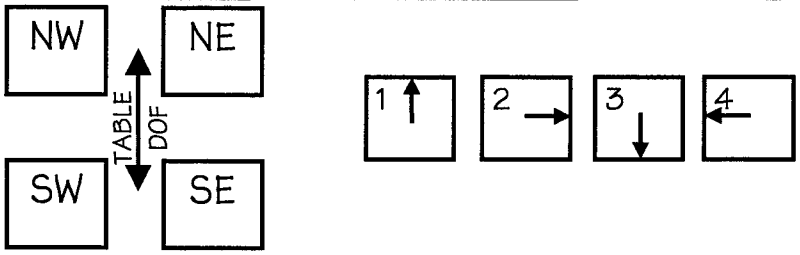

TABLE 3-6 (cont'd) Column Locations and Orientations, $^{kL}/_{r}$ =150

Column Index	Location	Orientation
Specimen 6		
1	NW	1
2	SW	3
3	NE	2
4	SE	2
Specimen 7		
1	NE	2
2	SW	3
3	NW	2
4	SE	2
Specimen 8		
1	NW	1
2	NE	1
3	SE	4
4	SW	4
Specimen 9		
1	NW	4
2	NE	1
3	SW	1
4	SE	4
Specimen 10		
1	NW	2
2	SW	3
3	NE	3
4	SE	1
Specimen 10b		
1	NW	1
2	NE	1
3	SW	1
4	SE	4

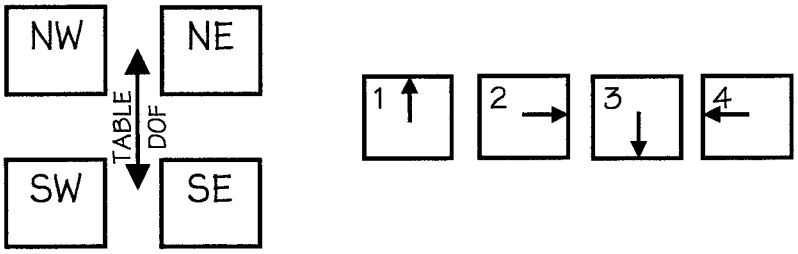

TABLE 3-6 (cont'd) Column Locations and Orientations, $^{kL}/_{r}$ =200

Column Index	Location	Orientation
Specimen 11		
1	NW	2
2	SW	1
3	SE	2
4	NE	4
Specimen 12		
1	NW	4
2	NE	4
3	SW	4
4	SE	2
Specimen 13		
1	NW	1
2	NE	2
3	SW	3
4	SE	3
Specimen 14		
1	SE	1
2	NE	3
3	SW	3
4	NW	4
Specimen 15		
1	NW	2
2	NE	4
3	SW	3
4	SE	1

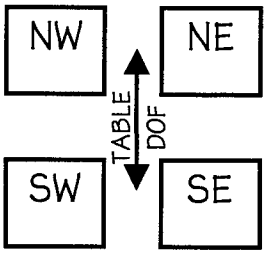

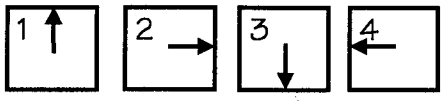

3.4.3 Construction Sequence

The assembly of the columns and mass plates into a specimen test structure on the SDOF shaking table consisted of the following steps:

1. Stack and bolt together steel mass plates for specimen.
2. Lightly bolt bottom plate of each column to the base plate on shaking table.
3. Hoist mass plates with overhead crane.
4. Ensure the mass plates are level upon hoisting, adjust as necessary.
5. Use vertical guides to center the plates in position above the specimen.
6. Lower with crane until approximately 5 mm above top plates of columns, then slowly release the turnbuckle, pictured in figure 3-10, to gently bring mass plates down onto columns in controlled manner.
7. Fasten top plate bolts as mass is lowered.
8. Attach cross bracing, then remove crane and vertical positioning guides.

Generally, this construction sequence proved adequate. However, as described later, problems were encountered in a few cases in spite of the careful procedure outlined above.

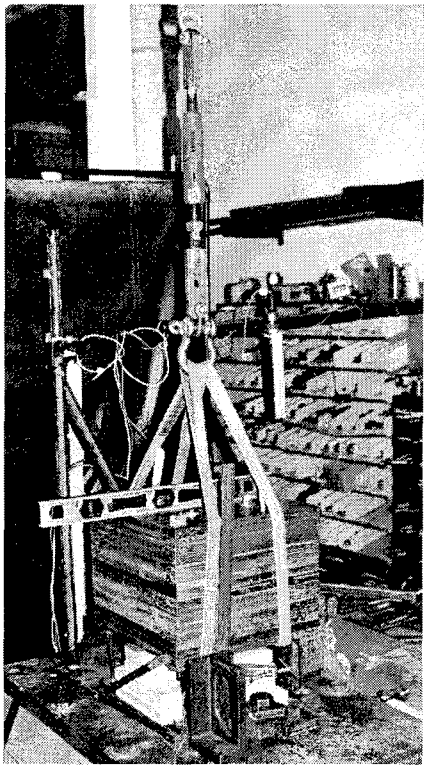

FIGURE 3-10 Construction of a Typical Test Structure

3.4.4 Lateral Bracing

Thin metal strips were used as cross bracing to prevent out-of-plane movement and torsion on the columns of the test structure during each test. The strips were sufficiently thin to add only a negligible stiffness in the direction of shaking. This was verified analytically, as well as by free vibration tests using a spare set of specimen columns which showed no change in the period of the structure with and without the addition of the metal strip bracing. Sample calculations and test results are in Appendix B.

The free vibration tests were also used to investigate the impact of the bracing strips on the damping of the structure. The damping ratio for the structure was calculated from the free vibration curves using the logarithmic decrement method (Chopra 1995). Results are presented in Appendix B for the test using the spare columns. There appears to be no significant change in damping between the bare and braced specimen.

Note that the strips were attached to the top and bottom base plates using a polyurethane material to provide additional flexibility in accommodating specimens with excessive initial imperfections. A typical cross bracing attachment is shown from various orientations and with details in figure 3-11. The gauge length along the diagonal of each specimen, assuming the absence of initial imperfections in all four columns, was calculated. Steel strips were machined such that the distance between connection holes at the ends was 50.8 mm (2 in) shorter than this value, and as such, the polyurethane band was used to bridge the remaining distance.

The polyurethane material was machined to a final size of 57.15 mm (2.25 in) long by 19.05 mm (¾ in) wide by 3.175 mm (1/8 in) thick. Holes were drilled on the longitudinal centerline axis at a gauge length of 50.4 mm (2 in). Simple single-point beam load tests were performed to estimate the elastic properties of the polyurethane material. These results are presented in Appendix B.

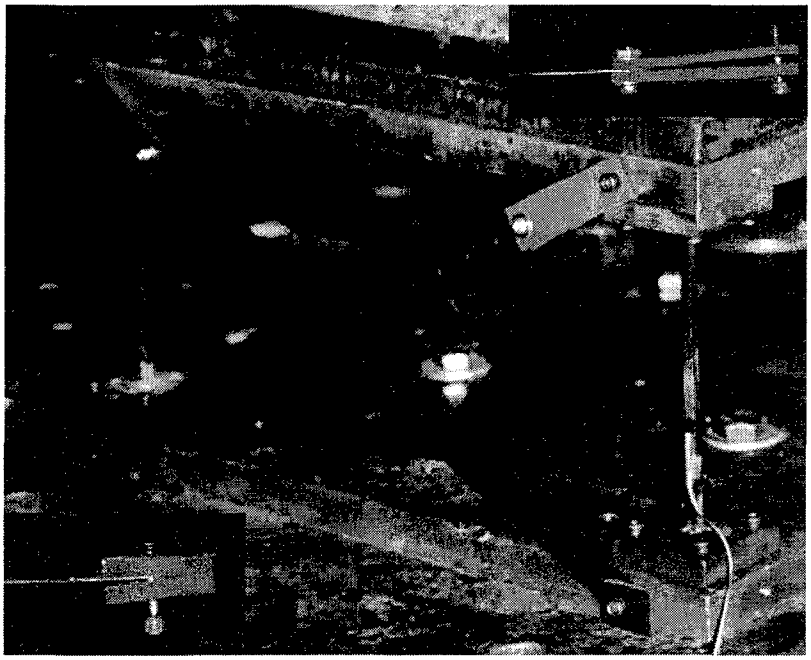

(a) Overall View (Side Details shown in insets)

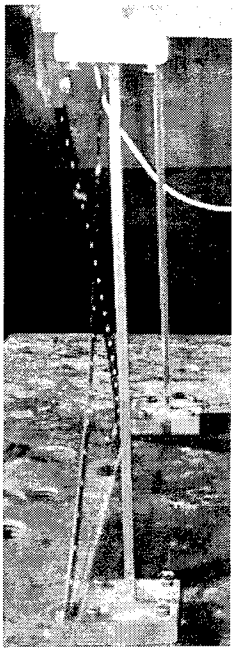

(b) Side View

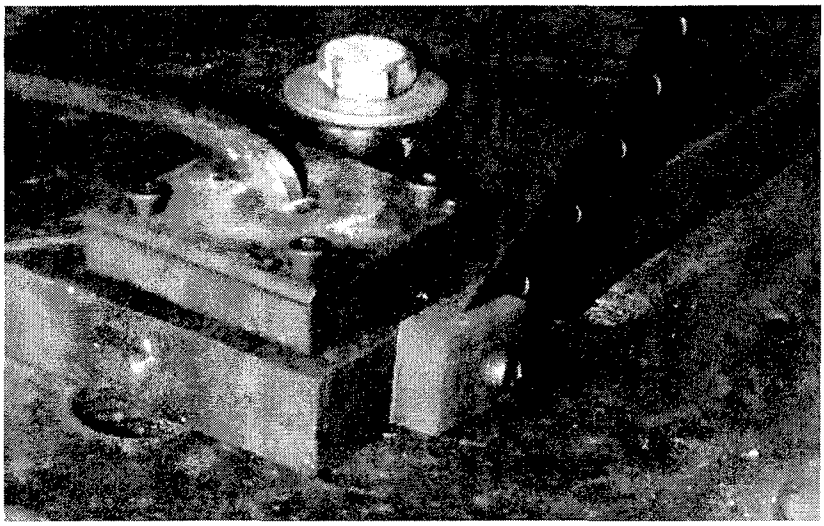

(c) Detail of Cross Bracing Attached to Lower Base Plate

FIGURE 3-11 Cross Bracing Attached to specimen

3.5 Instrumentation of Specimen

3.5.1 General

Instrumentation was designed to record structural response in a number of ways. Eight channels of data were collected for each test: four channels of displacement data, three channels of

acceleration data, and one channel of strain gage data. A schematic of the test setup and instrumentation is shown in figure 3-12.

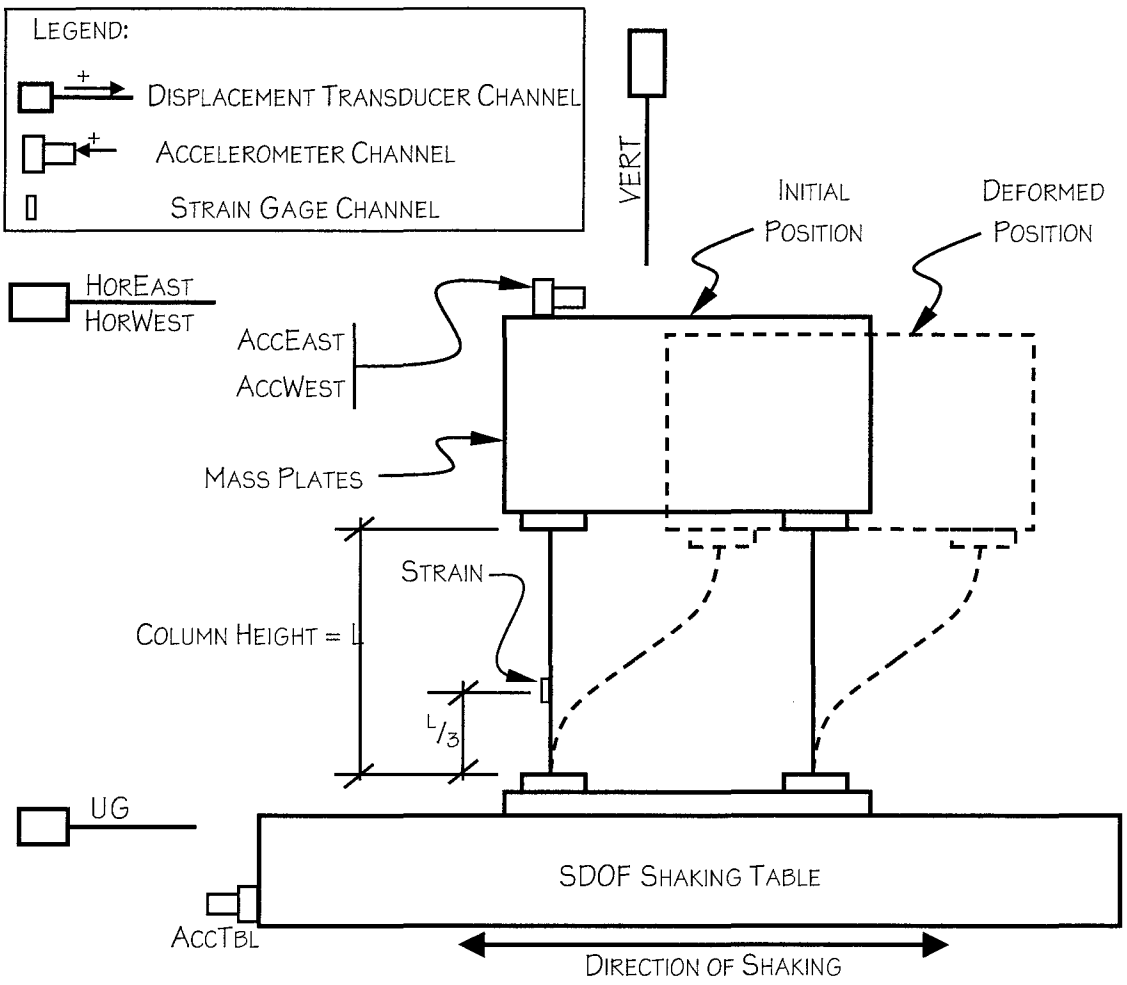

FIGURE 3-12 Schematic of Test Setup and Instrumentation (Looking West)

3.5.2 Displacement Measurements

3.5.2.1 General

MTS Temposonics® displacement transducers were used for displacement measurements during the tests. Four channels were recorded during each test: Displacement of the table (labeled UG in tables and figures), Vertical displacement of the mass (labeled Vert), and two channels of total horizontal displacement, measured at the East and West side of the mass (labeled HorEast and HorWest).

Transducers of various length were chosen on a case by case basis to appropriately capture range of data expected considering size of the specimen and availability of instrument stroke lengths in the laboratory. The transducer used in each test is listed in table 3-7.

TABLE 3-7 Displacement Transducer Properties (in) [mm]

Channel	Specimen			
	1, 2, 8, 9, 14		4, 5b[1], 6, 7, 10, 10b[1], 11, 12, 13, 15	
	Stroke	Resolution	Stroke	Resolution
HE, HW	10 [254]	0.002 [0.06]	20 [508]	0.005 [0.12]
UG	10 [254]	0.002 [0.06]	10 [254]	0.002 [0.06]
VERT	4 [101.6]	0.001 [0.02]	4 [101.6]	0.001 [0.02]

1: no HE measurement due to broken rod

Initial offsets were present in the vertical and horizontal displacement measurements prior to testing, due to the physical constraints of the SEESL and the availability of various stroke lengths of the instruments. These were eliminated from the ground displacement transducer prior to testing however. Offsets prior to the free vibration testing for channels HorEast, HorWest, and Vert, are listed in table 3-8.

TABLE 3-8 Displacement Transducer Initial Offsets (in)

Specimen	Channel		
	HorEast	HorWest	Vert
1	0.000	0.000	-0.410
2	-0.002	0.002	0.302
4	1.265	1.025	0.390
5b[1]	---	0.005	0.000
6	1.211	0.903	1.681
7	1.289	0.610	-0.638
8	-0.554	-0.957	-0.401
9	-0.662	-0.818	0.273
10[1]	1.509	1.240	-0.026
10b	---	0.005	-0.498
11	1.138	1.387	0.854
12	1.294	1.353	0.792
13	1.289	0.552	1.680
14	-0.571	-0.952	0.000
15	1.221	0.933	-0.775

1: no HE measurement due to broken rod

3.5.2.2 Horizontal Displacement

Measurement of the horizontal displacements of the structural mass during the entire structural response of the specimens, including throughout much of their collapse required special modifications to the instrument setup. Collars were machined from round PVC stock to maintain the perpendicular position of the permanent magnet with respect to the transducer tube of the Temposonics. The PVC collars were attached to a fishing rod via a ball joint end connection as pictured in figure 3-13. The rod was attached to the structural mass by an additional ball joint, allowing rigid body movement of the rod. By insuring rigid body motion, the error in horizontal displacement measurement due to the vertical displacement during collapse can be corrected as described in a subsequent section. Selection of fishing rods for this purpose was twofold: first, should the test structure collapse in the direction of the transducer, the out-of-plane flexibility of the rod would protect the instruments by bending to absorb the impact, second, the rod was selected to flex without breaking in the same collapse scenario, allowing re-use in subsequent tests.

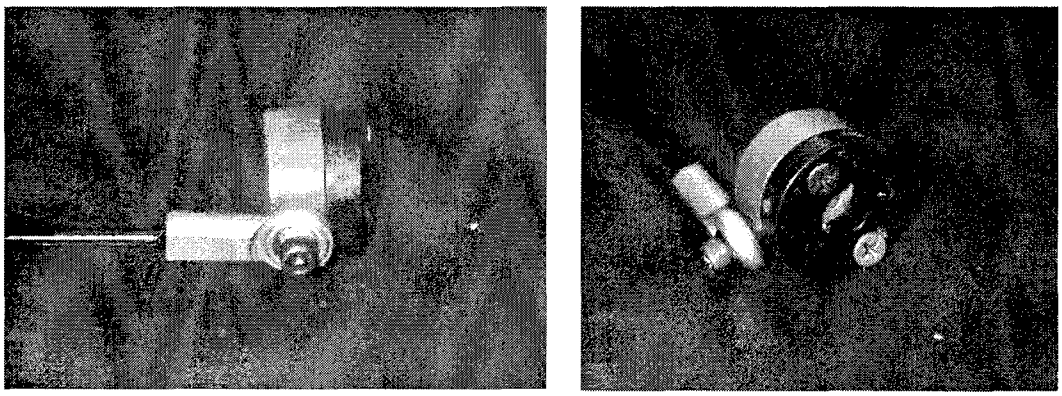

(a) Side View **(b) End View**

FIGURE 3-13 Horizontal Displacement Transducer Modification Details

3.5.2.3 Vertical Displacement

Vertical displacement of the mass was measured during the tests. In addition to providing valuable information on structural behavior, this data can be used to correct the horizontal displacements measured during large displacements, as described in the section on data reduction. Similar to the horizontal displacement instruments, special modifications were made to suit the experimental setup: PVC collars were machined in order to keep the transducer

magnet perpendicular to the transducer tube. A ball bearing roller was attached to the base of an additional PVC tube to minimize friction between the assembly and the mass plates. This roller made contact with a stainless steel plate that was attached to the top mass plate via epoxy. This assembly is pictured and shown schematically in figure 3-14 (a) and (b), respectively.

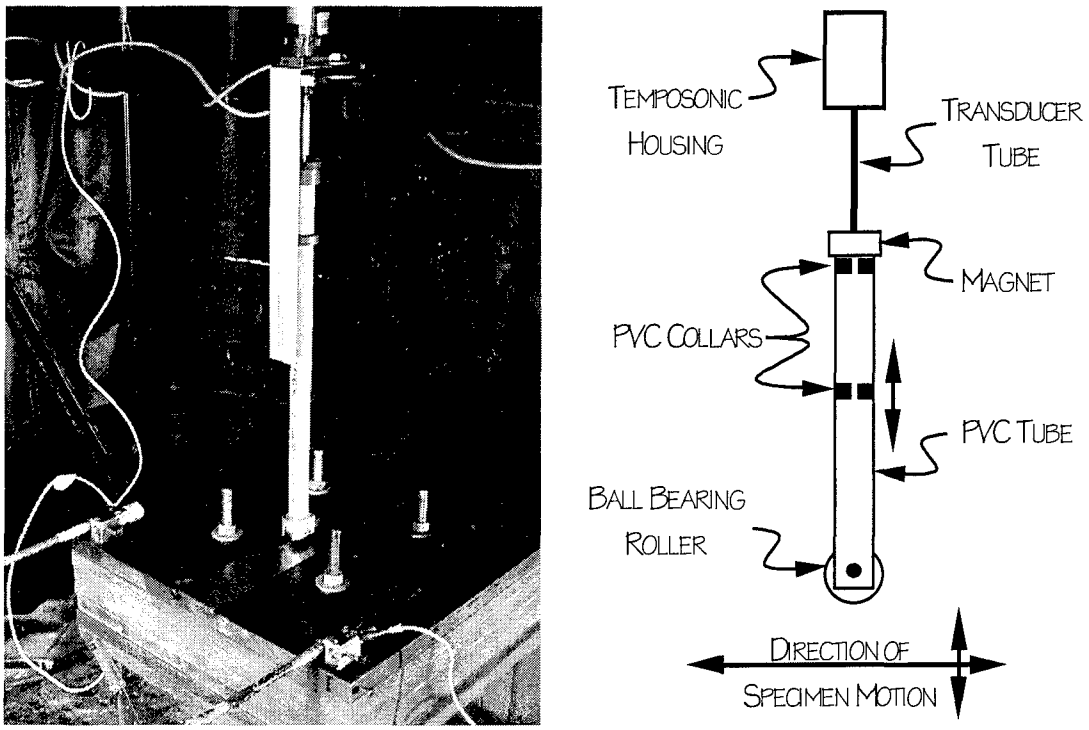

(a) Actual Device **(b) Schematic**

FIGURE 3-14 Vertical Displacement Transducer Modification Details

3.5.3 Accelerometers

One accelerometer was mounted on the shaking table to measure the ground acceleration exerted on the model structure. Two were mounted on top of the top mass plate on the test structure to measure the total acceleration, from which the inertial force on the mass can be calculated. These accelerometers were attached via a machine screw to a small aluminum block to which the ball joint ends of the horizontal displacement transducer fishing rods were attached. This mounting procedure ensured the instruments would remain undamaged at the end of each test. The location, manufacturer, and model of the accelerometers remained the same for every test, as listed table 3-9.

TABLE 3-9 Accelerometers Used During Testing

Channel	Description	Make	Model	Range
ACCTBL	Table Acceleration	Kulite	GAD-813-25	±2g
ACCEAST	Mass Acceleration-East Side	Endevco	2262-25	±2g
ACCWEST	Mass Acceleration-East Side	Kulite	GAD-813-25	±2g

3.5.4 Strain Gages

A strain gage was mounted on one column of each specimen, and located at a distance of one-third of the column height from its base. These were used for two reasons: First, the measurements can be used to calculate structural forces during testing as discussed in Section 3.8.4 below. Secondly, the gages were mounted in a region that would remain elastic throughout the shake table tests, and could then be cut out after the test and used to conduct a separate tensile test on the material to determine its stress-strain characteristics. Table 3-10 lists the type of strain gage used, number of the column to which it was attached and its location on that column for each of the specimens. A strain gage mounted on an assembled specimen is pictured in figure 3-11(a), shown previously.

TABLE 3-10 Strain Gages Used during Testing

Specimen	Column Index	Gage Type*	Location
1	3	CEA-06-240UZ-120	South
2	2	CEA-06-240UZ-120	South
3	1	CEA-06-125UN-120	North
4	4	CEA-06-240UZ-120	South
5b	2	CEA-06-125UN-120	North
6	1	CEA-06-240UZ-120	North
7	2	CEA-06-240UZ-120	North
8	2	CEA-06-240UZ-120	South
9	3	CEA-06-240UZ-120	North
10	4	CEA-06-125UN-120	South
10b	3	CEA-06-125UN-120	South
11	4	CEA-06-240UZ-120	North
12	3	CEA-06-125UN-120	South
13	3	CEA-06-240UZ-120	North
14	2	CEA-06-240UZ-120	South
15	3	CEA-06-125UN-120	North

*Note: All strain gages manufactured by Measurements Group

3.6 Testing of Specimens

3.6.1 General

Each specimen was tested in three ways: a free vibration test was performed, followed by a series of shake table tests until the structure collapsed, and finally a tension test was performed on a cutout section of one specimen column to determine material properties.

3.6.2 Free Vibration Testing

A free vibration test was performed on each specimen prior to the initiation of its respective schedule of shake table tests. This was done by manually pushing the mass of the test structure in the direction of shaking, inducing free vibration response. Though the arbitrarily applied displacement was carefully meant to keep the specimen within the elastic range, some specimen did experience yielding as will be noted in the results.

3.6.3 Shake Table Testing

Shake table test schedules were established for each specimen. These schedules, including test number, data filename, type of input signal, and magnitude of input signal, are found in table 3-11 for each test.

Input signals for the testing schedules for the shake table tests were established as follows:

1. Estimate the peak level of ground motion for elastic response as described in Section 3.3.3.
2. Estimate the peak level of ground motion for collapse of bilinear model as described in Section 3.3.4.
3. Determine the values of peak actuator displacement corresponding to the various peak response levels calculated.
4. Pre-select approximately five levels of ground motion to be applied to the specimen, progressively and proportionally increasing in magnitude from approximately two-thirds of the estimated peak elastic response to the estimated peak inelastic response.

The levels of ground motion were chosen to the nearest 0.25 volts of actuator span to simplify the execution of the test schedule.

The datafile is ASCII text, and contains the measurements recorded during the tests. Following the header describing the test at the top of the file, ten columns of data are shown:

"Time": time instance during the test (seconds)

"UG": table displacement (inches)

"HorEast": east side total displacement of specimen mass (inches)

"HorWest": west side total displacement of specimen mass (inches)

"Vert": vertical displacement of specimen mass (inches)

"AccTbl": shaking table acceleration (g)

"AccEast": east side total acceleration of specimen mass (g)

"AccWest": west side total acceleration of specimen mass (g)

"Strain": strain at third point of column specified in table 3-10 (με)

The data files are provided on MCEER's web site at *http://civil.eng.buffalo.edu/users_ntwk/*. Files are grouped, according to specimen, in winzip archives for convenience.

TABLE 3-11 Specimen Test Schedules

Test	Filename	Signal	Span	P.A.[1]	Remarks
		Specimen 1			
0	EXP01A00.DAT	FR. V.[2]	-	-	(5)
1	EXP01A01.DAT	EL-CEN-100[3]	5.25	0.114	
2	EXP01A02.DAT	EL-CEN-100	7.50	0.163	
3	EXP01A03.DAT	EL-CEN-100	10.00	0.217	
4	EXP01A04.DAT	EL-CEN-100	10.00	0.217	
5	EXP01A05.DAT	EL-CEN-200[4]	1.00		
6	EXP01A06.DAT	EL-CEN-200	3.33		
7	EXP01A07.DAT	EL-CEN-200	5.00		
8	EXP01A08.DAT	EL-CEN-200	6.00		
9	EXP01A09.DAT	EL-CEN-200	7.00		
10	EXP01A10.DAT	EL-CEN-200	8.00		
11	EXP01A11.DAT	EL-CEN-200	7.00		
12	EXP01AT3.DAT	Tension test	--	--	
		Specimen 2			
0	EXP02A00.DAT	FR. V.[2]	-	-	(5)
1	EXP02A01.DAT	EL-CEN-100[3]	2.50	0.054	
2	EXP02A02.DAT	EL-CEN-100	3.50	0.076	
3	EXP02A03.DAT	EL-CEN-100	4.50	0.098	
4	EXP02A04.DAT	EL-CEN-100	5.50	0.119	
5	EXP02A05.DAT	EL-CEN-100	6.50	0.141	
6	EXP02A06.DAT	EL-CEN-100	7.50	0.163	
7	EXP02A07.DAT	EL-CEN-100	8.50	0.184	
8	EXP02A08.DAT	EL-CEN-100	10.00	0.217	
9	EXP02A09.DAT	EL-CEN-100	10.00	0.217	
10	EXP02A10.DAT	EL-CEN-100	10.00	0.217	
11	EXP02AT2.DAT	Tension test			
		Specimen 3			
--	EXP03AT1.DAT	Tension test	--	--	

1: Target table peak acceleration
2: Free Vibration Test
3: El Centro Ground Motion without Time Scaling (100 Hz)
4: El Centro Ground Motion at compressed Time Scale (200 Hz)
5: Phase shift in displacement data of ~0.02 s since transducers were not low-pass filtered

TABLE 3-11 (cont'd) Specimen Test Schedules

Test	Filename	Signal	Span	P.A.[1]	Remarks
		Specimen 4			
0	EXP04A00.DAT	FR. V.[2]	-	-	(6)
1	EXP04A01.DAT	EL-CEN-100[3]	0.75	0.016	
2	EXP04A02.DAT	EL-CEN-100	2.00	0.043	
3	EXP04A03.DAT	EL-CEN-100	3.00	0.065	
4	EXP04A04.DAT	EL-CEN-100	4.00	0.087	
5	EXP04A05.DAT	EL-CEN-100	5.00	0.109	
6	EXP04A06.DAT	EL-CEN-100	6.00	0.130	
7	EXP04AT4.DAT	Tension test	--	--	
		Specimen 5			
	Not tested	Collapse			
		Specimen 5b			
0	EXP05B00.DAT	FR. V.[2]	-	-	(6)
1	EXP05B01.DAT	EL-CEN-100[3]	0.50	0.011	
2	EXP05B02.DAT	EL-CEN-100	1.25	0.027	
3	EXP05BT.DAT	Tension Test	--	--	
		Specimen 6			
0	EXP06A00.DAT	FR. V.[2]	-	-	
1	EXP06A01.DAT	EL-CEN-100[3]	5.25	0.114	
2	EXP06A02.DAT	EL-CEN-100	7.50	0.163	
3	EXP06A03.DAT	EL-CEN-100	10.00	0.217	
4	EXP06A04.DAT	EL-CEN-100	10.00	0.217	
5	EXP06A05.DAT	EL-CEN-200[4]	1.00		
6	EXP06A06.DAT	EL-CEN-200	3.33		
7	EXP06A07.DAT	EL-CEN-200	5.00		
8	EXP06A08.DAT	EL-CEN-200	6.00		
9	EXP06A09.DAT	EL-CEN-200	7.00		
10	EXP06A10.DAT	EL-CEN-200	8.00		
11	EXP06A11.DAT	EL-CEN-200	7.00		
12	EXP06AT1.DAT	Tension Test	--	--	
		Specimen 7			
0	EXP07A00.DAT	FR. V.[2]	-	-	
1	EXP07A01.DAT	EL-CEN-100[3]	2.00	0.043	
2	EXP07A02.DAT	EL-CEN-100	3.00	0.065	
3	EXP07A03.DAT	EL-CEN-100	4.00	0.087	
4	EXP07A04.DAT	EL-CEN-100	5.00	0.109	
5	EXP07A05.DAT	EL-CEN-100	6.00	0.130	
6	EXP07AT2.DAT	Tension Test	--	--	

1: Target table peak acceleration
2: Free Vibration Test
3: El Centro Ground Motion without Time Scaling (100 Hz)
4: El Centro Ground Motion at compressed Time Scale (200 Hz)
6: Excessive resolution data noise in displacement channels

TABLE 3-11 (cont'd) Specimen Test Schedules

Test	Filename	Signal	Span	P.A.[1]	Remarks
		Specimen 8			
0	EXP08A00.DAT	FR. V.[2]	-	-	(7)
1	EXP08A01.DAT	EL-CEN-100[3]	1.25	0.027	
2	EXP08A02.DAT	EL-CEN-100	2.50	0.054	
3	EXP08A03.DAT	EL-CEN-100	3.50	0.076	
4	EXP08A04.DAT	EL-CEN-100	4.50	0.098	
5	EXP08AT2.DAT	Tension Test	--	--	
		Specimen 9			
0	EXP09A00.DAT	FR. V.[2]	-	-	
1	EXP09A01.DAT	EL-CEN-100[3]	1.25	0.027	
2	EXP09A02.DAT	EL-CEN-100	1.50	0.033	
3	EXP09A03.DAT	EL-CEN-100	1.75	0.038	
4	EXP09A04.DAT	EL-CEN-100	2.00	0.043	
5	EXP09AT3.DAT	Tension Test	--	--	
		Specimen 10			
0	EXP10A00.DAT	FR. V.[2]	-		
1	EXP10A01.DAT	EL-CEN-200[3]	0.75	0.066	
2	EXP10AT4.DAT	Tension Test	--	--	
		Specimen 10b			
0	EXP10B00.DAT	FR. V.[2]	-	-	
1	EXP10B01.DAT	EL-CEN-100[3]	0.50	0.011	
2	EXP10B02.DAT	EL-CEN-100	0.75	0.016	
3	EXP10B03.DAT	EL-CEN-100	1.00	0.022	
4	EXP10B04.DAT	EL-CEN-100	1.25	0.027	
5	EXP10B05.DAT	EL-CEN-100	1.50	0.033	
6	EXP10B06.DAT	EL-CEN-100	1.75	0.038	
7	EXP10BT3.DAT	Tension Test	--	--	
		Specimen 11			
0	EXP11A00.DAT	FR. V.[2]	-	-	
1	EXP11A01.DAT	EL-CEN-100[3]	4.00	0.087	
2	EXP11A02.DAT	EL-CEN-100	5.25	0.114	
3	EXP11A03.DAT	EL-CEN-100	7.50	0.163	
4	EXP11A04.DAT	EL-CEN-100	10.00	0.217	
5	EXP11A05.DAT	EL-CEN-100	10.00	0.217	
6	EXP11A06.DAT	EL-CEN-100	10.00	0.217	
7	EXP11A07.DAT	EL-CEN-100	10.00	0.217	
8	EXP11AT4.DAT	Tension Test	--	--	

1: Target table peak acceleration
2: Free Vibration Test
3: El Centro Ground Motion without Time Scaling (100 Hz)
4: El Centro Ground Motion at compressed Time Scale (200 Hz)
7: Unexplained corruption of HorWest Channel

TABLE 3-11 (cont'd) Specimen Test Schedules

Test	Filename	Signal	Span	P.A.[1]	Remarks
		Specimen 12			
0	EXP12A00.DAT	FR. V.[2]	-	-	
1	EXP12A01.DAT	EL-CEN-100[3]	3.50	0.076	
2	EXP12A02.DAT	EL-CEN-100	5.00	0.109	
3	EXP12A03.DAT	EL-CEN-100	7.00	0.152	
4	EXP12AT3.DAT	Tension Test	--	--	
		Specimen 13			
0	EXP13A00.DAT	FR. V.[2]	-	-	
1	EXP13A01.DAT	EL-CEN-100[3]	2.50	0.054	
2	EXP13A02.DAT	EL-CEN-100	3.50	0.076	
3	EXP13A03.DAT	EL-CEN-100	4.50	0.098	
4	EXP13A04.DAT	EL-CEN-100	5.50	0.119	
5	EXP13A05.DAT	EL-CEN-100	6.50	0.141	
6	EXP13AT3.DAT	Tension Test	--	--	
		Specimen 14			
0	EXP14A00.DAT	FR. V.[2]	-	-	
1	EXP14A01.DAT	EL-CEN-100[3]	1.25	0.027	
2	EXP14A02.DAT	EL-CEN-100	1.50	0.033	
3	EXP14A03.DAT	EL-CEN-100	1.75	0.038	
4	EXP14A04.DAT	EL-CEN-100	2.00	0.043	
5	EXP14A05.DAT	EL-CEN-100	2.25	0.049	
6	EXP14AT2.DAT	Tension Test	--	--	
		Specimen 15			
0	EXP15A00.DAT	FR. V.[2]	-		
1	EXP15A01.DAT	EL-CEN-100[3]	0.75		
2	EXP15AT3.DAT	Tension Test	--	--	

1: Target table peak acceleration
2: Free Vibration Test
3: El Centro Ground Motion without Time Scaling (100 Hz)
4: El Centro Ground Motion at compressed Time Scale (200 Hz)

3.6.4 Tension Testing

Tension testing of specimen was performed in the Axial-Torsion MTS Machine in the UB SEESL (Constantinou et al. 1999) pictured in figure 3-15. Tests were executed in a displacement-controlled mode. Built-in load cells in the actuator grips measured the axial force exerted by the machine. Strain in the specimen was measured by the strain gage described previously.

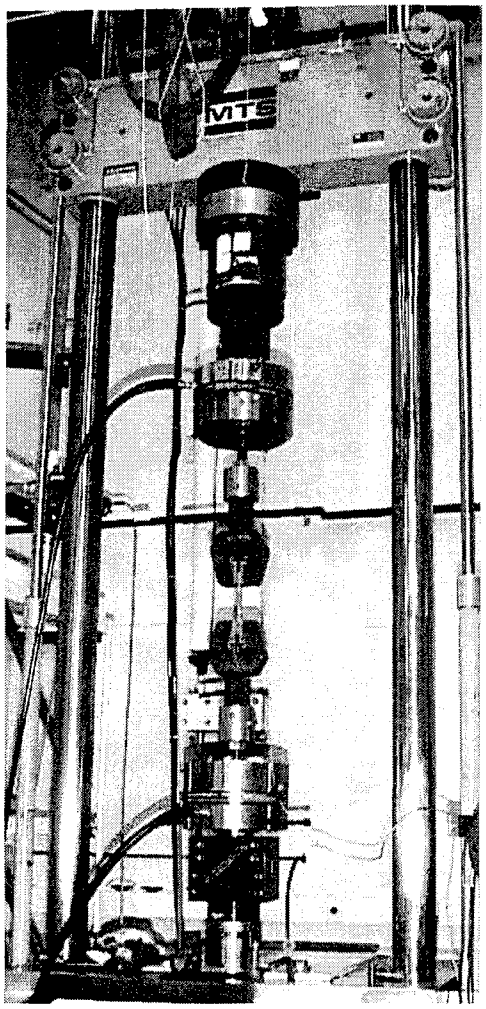

FIGURE 3-15 MTS Axial-Torsion Testing Machine

3.7 Data Acquisition

A *Cyrix* 5x86 120 MHz computer running *Microsoft* Windows 95 was used for data collection during shake tabe testing. Data was read from a *Data Translation* VDTAD.386 12-bit data acquisition board.

The SDOF shake table's data acquisition system works in the following manner. A generic potentiometer power supply built in-house provides the required 10-volt excitation voltage for the displacement transducers. The transducer output is then fed into a *Measurements Group* 2310 DC Signal Conditioning Amplifier used as a lowpass filter with a 25 Hz cutoff frequency. After lowpass filtering, the signal data is read by the data acquisition board and written to the hard disk in the form of the ASCII text file described in the previous section. Accelerometer and

strain gage measurements follow an identical path except that the Signal Conditioning Amplifiers used, simultaneously act as a lowpass filter and provide the required excitation voltage, eliminating the need for the additional power supply. The entire data acquisition system is pictured in figure 3-16.

The LABTECH NOTEBOOK PRO data acquisition software was used to input ground motion to the MTS controller. In addition, it was used to manage the recorded data from the data acquisition board and write it to the datafile.

The measurement resolution of a displacement transducer is determined by dividing the total stroke length by 2^{12} since a "True" 12-bit data acquisition board is being used. Displacement measurement resolution for each stroke length transducer is listed in table 3-7. All accelerometers have the same range of ±2 g, and therefore the same resolution of 0.001 g.

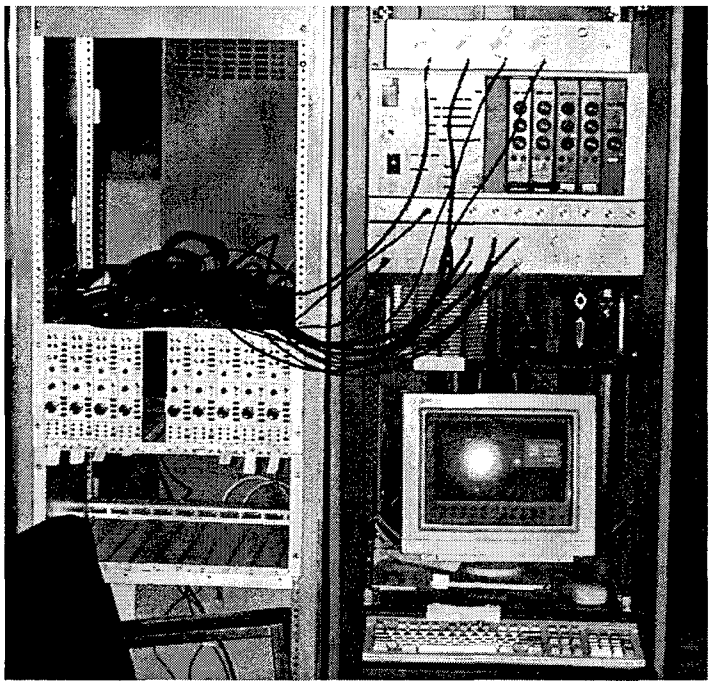

FIGURE 3-16 Data Acquisition System

At left, center:
1. Signal Conditioning Amplifiers

At right, from top:
2. Temposonics Power Supply
3. Controller for Table Actuator
4. A/D converter
5. Computer used in data collection

3.8 Data Reduction

3.8.1 Data Noise

The data noise encountered in the course of an experimental program can be dealt with in a variety of ways, depending upon the nature of the source. High frequency noises native to this experimental setup were found to be at 60 Hz, the frequency of Alternating Current (AC) voltage in the United States, and 58 Hz, which was found to be the fundamental frequency of the SDOF shake table. Both of these frequencies are well above those of the specimen as shown in table 3-3 and therefore have negligible effect on structural response. These high frequency noises were reduced by the 25 Hz lowpass filter described in the previous section.

Low frequency noise takes the form of offsets in the instrument readings. Physical constraints in the lab prevented the Temposonics from being mounted such that the initial reading was always zeroed. Therefore, displacement readings often do not start from zero in the recorded data files as discussed previously. Beyond this consideration, note that displacement and strain offsets at the end of a test that occurred due to inelastic behavior of the specimens are physically significant and are kept as the starting offset of each subsequent test, and included in the results. Accelerometer offsets, however, are due to drift of the instrument and are eliminated prior to each run by resetting at the signal conditioner level.

3.8.2 Horizontal Displacement Correction

The actual total horizontal displacement of a specimen is calculated using the measured vertical and horizontal displacements described previously. Variables shown in figure 3-17 yield the following geometric relations:

$$x(t)^2 + v(t)^2 = l^2 \tag{3-4}$$

$$u_a(t) = x(t) + u_m(t) - l \tag{3-5}$$

which can be combined, resulting in:

$$u_a(t) = \sqrt{l^2 - v(t)^2} + u_m(t) - l \tag{3-6}$$

where:

l = Length of the rod used on the horizontal displacement transducers

$x(t)$ = Horizontal projection of l at time, t

$v(t)$ = Measured vertical displacement / vertical projection of l at time, t

$u_m(t)$ = Measured horizontal displacement at time, t

$u_a(t)$ = Actual horizontal displacement at time, t

This relation describes the total horizontal displacement of the specimen at time t. The relative displacement of the specimen at time t is calculated by subtracting the ground displacement, $u_g(t)$, from $u_a(t)$ calculated in (3-6).

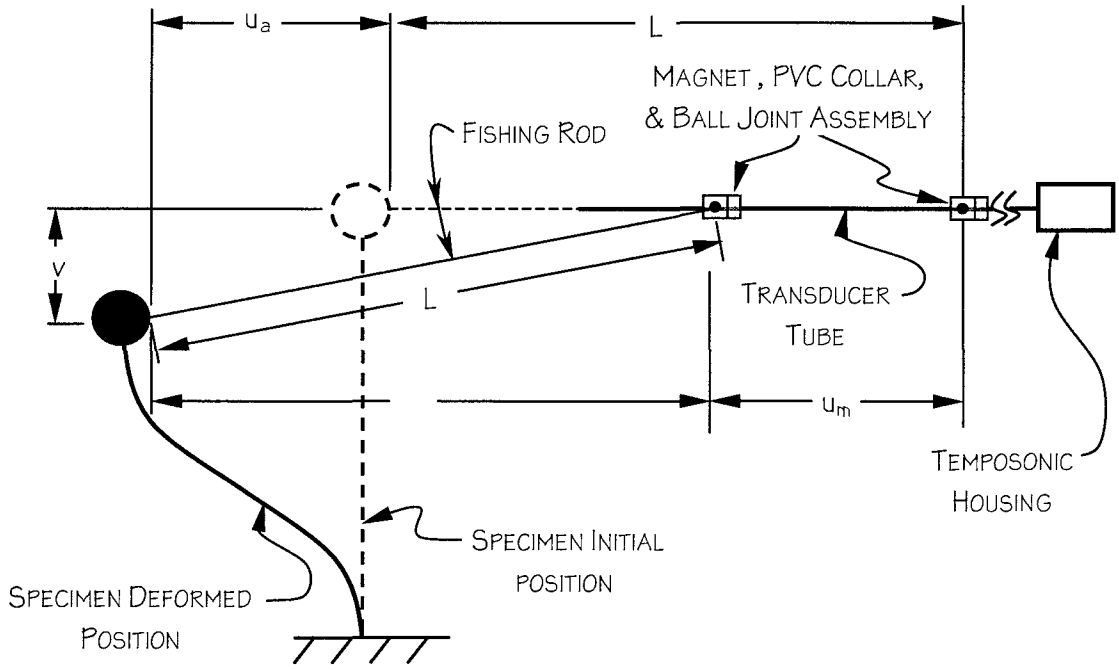

FIGURE 3-17 Definition of Variables used in Horizontal Displacement Correction

3.8.3 Sign Convention

Displacement measurements with a Temposonic become increasing positive as its magnet moves toward the tip of the transducer tube. Transducers measuring horizontal displacements were all oriented pointing to the north side of the UB SEESL as indicated schematically in figure 3-11. Therefore, a displacement towards the north is recorded as an increasingly positive reading. As the test structure collapses, and the elevation of the mass plates decreases, an increasingly positive vertical displacement will be measured by the vertical displacement channel.

The type of accelerometers used record a positive acceleration when the acceleration is in the direction from the top of the instrument (smaller diameter barrel) to the base, as indicated in figure 3-12.

Strain gages were wired to give a positive reading when subjected to tensile strains. The surface condition of the specimen dictated the side on which the gage was mounted (North or South). The sign of the calculated moment from strain gage readings will therefore vary depending on the gage location, which is listed in table 3-10. Specimens with a gage mounted on the south side of the column must have the strain data multiplied by –1 so that positive relative displacements result in postive strains, and therefore a positive estimate of base shear, as will be discussed later.

3.8.4 Estimated Base Shear Calculation

The base shear force on the test structure can be calculated using two methods: First, by equating base shear to the inertia force on the structural mass. Second, by consideration of measured strains and simple statics at an instant of time.

The advantage of the first method is that the computation is straightforward if the accelerometers are calibrated accurately and the structural mass is accurately known. The disadvantage of this method is that the effect of the damping force is ignored. The equation of dynamic equilibrium of the structural mass is given by:

$$f_I = -(f_S + f_D) \tag{3-7}$$

where f_I, f_S, and f_D are the inertia force, the restoring force and the damping force, respectively. The damping force inherent in the structure cannot be measured directly and is thusly ignored, resulting in a method that is only reliable when the damping is small, i.e. when $f_I \approx -f_S$.

In the second method, the strain gages described previously in Section 3.5.4 are used to calculate an estimate of base shear (or restoring force, f_s) on the structure due to the earthquake loading. Assuming the moment along the height of the column varies linearly from top to bottom with the point of inflection at mid-height (i.e. neglecting P-Δ and P-δ moments), the base shear on that column can be estimated by the following equation:

$$V_o^* = \frac{6M_m}{L} = \frac{6}{L} \cdot \left(\frac{\varepsilon_m \cdot E \cdot I}{h/2} \right) \tag{3-8}$$

where:

V_o^* = Estimated column base shear ignoring P-Δ effect

M_m = Moment calculated from the strains measured at the third point of column height

ε_m = Strain measured by strain gage at third point of column height

E = Elastic modulus of steel, equal to 200,000 MPa

I = Moment of inertia of column

h = Width of column

Strain gages were carefully placed on the third point of the column noted in the previously described table. A digital height gauge was used to scribe a mark on the column at the exact height desired.

The estimated base shear force is further improved by the inclusion of the P-Δ effect. The previous result is modified by an additional term:

$$V_p^* = V_o^* - \left(\frac{P}{L} \right) \cdot \Delta \tag{3-9}$$

where:

Δ = $u_a(t) - u_g(t)$: Relative displacement at time, t

This approach was deemed sufficient for the purpose of this report. However, the reader must be aware that for more accurate analytical studies, the linear variation of moment along the height assumed in (3-8) is incorrect, the inaccuracies introduced by this simplification being a function of the magnitude of axial force and of columns deformations, δ.

SECTION 4
EXPERIMENTAL RESULTS

4.1 General

Each specimen was tested according to the schedules described and presented in Chapter 3. Data was acquired for each test using the instrumentation and data acquisition system described in the same chapter. This chapter presents the key numerical and graphical results of those tests. Discussion of the results follows in the next chapter.

4.2 Summary of Test Results

4.2.1 Tension Testing

A column from each specimen was tested in the MTS testing machine described in the previous chapter. In general, the column with the strain gage mounted on it to measure moment and base shear during the shake table tests was used for this purpose. Results are presented in Table 4-1. Missing data indicates that the strain-gaged specimen column was excessively damaged during collapse of the test structure, making tension testing impossible.

Considering all specimens for which there is data, except 5b and 10b which were fabricated using an alternate grade of steel, the mean elastic modulus is 198,736 MPa (28,824 ksi), with a standard deviation of 29,906 MPa (4,338 ksi). When ignoring Specimen 14, which appears to have an unusually low elastic modulus, the mean and standard deviation become 205,584 MPa (29,817 ksi) and 20,509 MPa (2,975 ksi), respectively.

For specimens fabricated from standard steel, (i.e. all except 5b and 10b), the standard elastic modulus of 200,000 MPa (29,000 ksi) is used in the calculation of specimen properties for comparison with experimental results. However, for Specimens 5b and 10b, the experimentally obtained average value of 269,809 MPa (39,133 ksi) will be used for the same comparisons.

The yield stress of each specimen column tested was calculated using the 0.2% offset method. These experimentally obtained yield stresses are used in the calculation of theoretical strength for comparison with observed behavior. The average value of other specimens having the same

nominal cross-section is used for those specimens for which tension test data could not be obtained. In other words, the strength of Specimens 9 and 4 is computed using the average yield stress of 1, 2, and 14 and Specimen 7 using the yield stress of Specimen 12.

TABLE 4-1 Tension Test Results

Specimen	Column ID	E (ksi)	E (MPa)	F_y (ksi)	F_y (MPa)	Remarks
1	3	25773	177700	63.0	434	
2	2	30326	209093	65.5	452	
3	1	33467	230744	46.8	323	
4	4	-	-	74.0	510	
5b	-	39505	272379	150.0	1034	(1, 2)
6	1	27509	189666	52.5	362	
7	2	-	-	-	-	
8	2	27139	187116	61.0	421	
9	3	-	-	-	-	
10	4	33963	234167	42.5	293	
10b	3	38760	267240	148.0	1020	(1)
11	4	32952	227197	57.0	393	
12	3	29916	206261	42.5	293	
13	3	30440	209879	62.2	429	
14	2	18892	130256	63.5	438	
15	3	26689	184018	41.0	283	

1: AISI M1 cold-worked steel
2: Extra Piece of Material Tested (not from shake table test)

4.2.2 Free Vibration Tests

To determine the fundamental period of vibration and damping properties of the specimens, a free vibration test in the linear elastic range was first performed on each specimen before subjecting it to earthquake excitations. This was done by manually pushing the test structure at the mass level to a small distance in the direction of shaking.

4.2.2.1 Fundamental Period of Vibration

The fundamental period of vibration of each specimen is obtained via Fourier Spectrum Analysis of the time history data obtained during the free-vibration tests. Table 4-2 lists the fundamental period of vibration predicted for each structure, using average dimensions for each column making up the structure, along with the experimentally obtained period. T_{no} is the predicted

fundamental period excluding P-Δ effects, T_{np}, including P-Δ effects, and $T_{n\text{-spectrum}}$, calculated from time history data using Fourier Spectrum Analysis. The percent difference in the measured from the predicted value (including P-Δ effects), ΔT_n, is listed in the rightmost column. Predicted and experimental values are within approximately 10% of each other for all specimens except 5b.

TABLE 4-2 Free Vibration Period Comparison

Specimen	T_{no} [1] (s)	T_{np} [2] (s)	$T_{n\text{-spectrum}}$ [3] (s)	ΔT_n [4]
1	0.189	0.196	0.200	1.93%
2	0.261	0.279	0.272	-2.50%
4	0.311	0.343	0.323	-5.86%
5b	0.401	0.533	0.698	30.93%
6	0.410	0.432	0.430	-0.55%
7	0.463	0.503	0.490	-2.66%
8	0.543	0.634	0.655	3.39%
9	0.568	0.727	0.760	4.52%
10	0.504	0.687	0.662	-3.68%
10b	0.528	0.750	0.727	-3.01%
11	0.552	0.595	0.597	0.32%
12	0.629	0.709	0.682	-3.85%
13	0.727	0.908	0.959	5.61%
14	0.768	1.123	1.200	6.90%
15	0.679	1.111	1.004	-9.63%

1: Predicted Fundamental Period excluding P-Δ effect (stiffness using (2-1))
2: Predicted Fundamental Period including P-Δ effect (stiffness using (2-8))
3: Fundamental Period Calculated from Fourier Spectrum
4: Difference between 2 and 3

The fundamental period of the structure is directly proportional to the height of the columns. The "effective" height of the columns varies with the degree of fixity at the top and bottom base plates. The brazing material used in the fabrication of a number of the specimen often left a fillet around the base of the columns. This fillet was not accounted for in the measurement of column dimensions. This result of the fabrication process may then have produced columns that are effectively shorter than the tabulated value listed, resulting in a shorter natural period. This may partly account for the fact that eight of the fifteen specimens had observed periods that were less than (but within 10%) that predicted using the average dimensions. However, given that the remaining seven specimens tested had observed periods that were larger than predicted using

average dimensions, the small difference between experimentally and analytically calculated periods may not warrant extensive attempts at explaining these variations.

However, for specimen 5b fabricated of AISI M1 steel, the predicted natural period of the structure using average column dimensions is 0.533 s while the observed period obtained from Fourier Spectrum of the free vibration response is 0.698 s, a difference of 30.93%.

Many causes can be postulated for such a difference. If a good weld was not achieved to fill the space between and properly fuse the column and base plate, and if "too-soft" a brazing material was used, then the full-fixity desired at the face of the base plate may not exist.

The fabrication of specimens 5b and 10b took place in the fabrication shop of the UB SEESL. The fabrication procedures were somewhat different than that implemented by the staff at the University of Ottawa where all other specimens were prepared. Columns for Specimens 5b and 10b were fused with the base plates using a Gas Tungsten Arc Welding (GTAW) process from the underside of the column base plates to prevent section undercutting within the effective specimen height due to the imparted heat from welding. The remainder of the hole on the inside of the base plates was filled with silver solder using an oxy-acetylene torch with a brazing tip. The silver solder is quite malleable and transforms to the liquid state at a much lower temperature than steel, which was convenient as filler. However, due to this extreme malleability, the base of the column sections may not have been as well confined as intended. The resulting lack of full base fixity can be quantified by expressing it into an equivalent system having fully-fixed columns of an effective height. Knowing that the fundamental period of the structure including P-Δ effects is:

$$T_n = 2 \cdot \pi \sqrt{\frac{m}{K_1}} = 2 \cdot \pi \sqrt{\frac{m \cdot L^3}{12 \cdot E \cdot I - P \cdot L^2}} \qquad (4\text{-}1)$$

Solving (4-1) for the height, L, and using the observed period for T_n, and average measured values for all other quantities, results in an effective height of 102.3 mm (4.029 in). In other words, the average end conditions of the columns at the bottom and top plates caused the specimen to behave as if the columns were effectively 10.4 mm (0.411 in) longer than the average measured value.

4.2.2.2 Inherent Damping

The percentage of critical damping due to inherent damping in the structure, ξ, is also estimated from the free-vibration time history data, using the logarithmic decrement method (Chopra 1995) given by:

$$\xi = \frac{1}{2 \cdot \pi \cdot j} \ln \left| \frac{u_k}{u_{k+j}} \right| \tag{4-2}$$

where:

j = Number of cycles between peaks used for estimate of ξ

u_k = Amplitude of k^{th} peak (first peak used for the estimate)

u_{k+j} = Amplitude of $(k+j)^{th}$ peak (last peak used for the estimate)

To better characterize the inherent damping of each structure, the free vibration response curve obtained for each specimen was divided into three approximately equal intervals and estimates of the damping ratio were made using the first and last peaks of each interval. These estimates are summarized in Table 4-3. The following parameters, in accordance with the logarithmic decrement method shown above, are used with the time history data of each displacement and acceleration channel:

u_o = Maximum amplitude of free vibration response (mm or g)

u^*_i = Mean amplitude of peaks k to $k+j$ through i^{th} estimate interval (mm or g)

k_i = Cycle number used as first peak for i^{th} damping ratio estimate

u_{ki} = Amplitude of first peak used for i^{th} damping ratio estimate

k_i+j = Cycle number used as second peak for i^{th} damping ratio estimate

u_{ki+j} = Amplitude of second peak used for i^{th} damping ratio estimate

ξ_i = i^{th} damping ratio estimate

TABLE 4-3 Free Vibration Damping Estimates

i	u^*_i	k_i	u_{ki}	k_i+j	u_{ki+j}	ξ_i	Remarks
Specimen 1							
HorEast Channel, u_o = 0.559 mm							
1	0.448	1	0.559	14	0.381	0.469	--
2	0.315	14	0.381	25	0.254	0.587	--
3	0.186	25	0.254	42	0.127	0.649	--
HorWest Channel, u_o = 0.559 mm							
1	0.452	1	0.559	14	0.381	0.469	--
2	0.315	14	0.381	25	0.254	0.587	--
3	0.188	25	0.254	42	0.127	0.649	--
AccEast Channel, u_o = 0.053 g							
1	0.043	1	0.053	14	0.036	0.474	--
2	0.03	14	0.036	25	0.025	0.528	--
3	0.018	25	0.025	42	0.011	0.769	--
AccWest Channel, u_o = 0.050 g							
1	0.043	1	0.047	14	0.036	0.326	--
2	0.031	14	0.036	25	0.025	0.528	--
3	0.018	25	0.025	42	0.012	0.687	--
Specimen 2							
HorEast Channel, u_o = 0.508 mm							
1	0.229	3	0.254	10	0.203	0.507	(1)
2	0.171	10	0.203	20	0.127	0.748	--
3	0.099	20	0.127	29	0.076	0.903	--
HorWest Channel, u_o = 0.483 mm							
1	0.219	3	0.254	10	0.203	0.507	--
2	0.141	10	0.203	20	0.127	0.748	--
3	0.104	20	0.127	29	0.076	0.903	--
AccEast Channel, u_o = 0.015 g							
1	0.013	3	0.015	10	0.011	0.705	--
2	0.009	10	0.011	20	0.007	0.719	--
3	0.005	20	0.007	29	0.003	1.498	--
AccWest Channel, u_o = 0.014 g							
1	0.012	3	0.014	10	0.01	0.765	--
2	0.008	10	0.01	20	0.006	0.813	--
3	0.005	20	0.006	29	0.003	1.226	--

(1): Estimates based on first of 2 free vibration pushes performed

TABLE 4-3 (cont'd) Free Vibration Damping Estimates

i	u^*_i	k_i	u_{ki}	k_i+j	u_{ki+j}	ξ_i	Remarks
Specimen 4							
AccEast Channel, u_o = 0.008 g							
1	0.007	2	0.008	6	0.005	1.87	(2)
2	0.004	6	0.005	10	0.003	2.033	--
3	0.002	10	0.003	23	0.001	1.345	--
AccWest Channel, u_o = 0.008 g							
1	0.006	2	0.008	6	0.005	1.87	--
2	0.004	6	0.005	10	0.003	2.033	--
3	0.002	10	0.003	23	0.002	0.496	--
Specimen 5b							
HorWest Channel, u_o = 1.118 mm							
1	0.906	1	1.118	3	0.737	3.318	(3)
2	0.629	3	0.737	6	0.508	1.971	--
3	0.457	6	0.508	10	0.381	1.145	--
AccEast Channel, u_o = 0.009 g							
1	0.007	1	0.009	3	0.006	3.227	--
2	0.004	3	0.006	6	0.003	3.677	--
3	0.003	6	0.003	10	0.002	1.613	--
AccWest Channel, u_o = 0.008 g							
1	0.007	1	0.008	3	0.005	3.74	--
2	0.004	3	0.005	6	0.003	2.71	--
3	0.002	6	0.003	10	0.002	1.613	--

1: Estimates based on first of 2 free vibration pushes performed
2: Resolution too low to use HorEast or HorWest Signals for Estimate
3: No HorEast measurement due to broken rod

TABLE 4-3 (cont'd) Free Vibration Damping Estimates

i	u^*_i	k_i	u_{ki}	k_i+j	u_{ki+j}	ξ_i	Remarks
Specimen 6							
HorEast Channel, u_o = 0.991 mm							
1	0.800	2	0.991	11	0.737	0.524	--
2	0.563	11	0.737	22	0.381	0.954	--
3	0.314	22	0.381	38	0.254	0.403	--
HorWest Channel, u_o = 0.991 mm							
1	0.724	2	0.889	11	0.635	0.595	--
2	0.487	11	0.635	22	0.381	0.739	--
3	0.239	22	0.381	38	0.127	1.093	--
AccEast Channel, u_o = 0.019 g							
1	0.016	2	0.019	11	0.013	0.671	--
2	0.011	11	0.013	22	0.008	0.702	--
3	0.005	22	0.008	38	0.003	0.976	--
AccWest Channel, u_o = 0.017 g							
1	0.015	2	0.017	11	0.013	0.474	--
2	0.010	11	0.013	22	0.008	0.702	--
3	0.005	22	0.008	38	0.003	0.976	--
Specimen 7							
AccEast Channel, u_o = 0.018 g							
1	0.006	2	0.008	10	0.005	0.935	(1, 2, 4)
2	0.004	10	0.005	19	0.002	1.620	--
3	0.001	19	0.002	28	0.001	1.226	--
AccWest Channel, u_o = 0.02 g							
1	0.007	2	0.008	10	0.005	0.935	--
2	0.004	10	0.005	19	0.002	1.620	--
3	0.002	19	0.002	28	0.001	1.226	--

1: Estimates based on first of 2 free vibration pushes performed
2: Resolution too low to use HorEast or HorWest Signals for Estimate
4: Residual displacement offset at conclusion of test

TABLE 4-3 (cont'd) Free Vibration Damping Estimates

i	u^*_i	k_i	u_{ki}	k_i+j	u_{ki+j}	ξ_i	Remarks
Specimen 8							
HorEast Channel, u_o = 1.168 mm							
1	1.008	1	1.168	6	0.813	1.155	--
2	0.650	6	0.813	12	0.483	1.383	--
3	0.311	12	0.483	19	0.178	2.270	--
HorWest Channel, u_o = 1.118 mm							
1	0.961	1	1.118	6	0.813	1.014	--
2	0.624	6	0.813	12	0.483	1.383	--
3	0.324	12	0.483	19	0.178	2.270	--
AccEast Channel, u_o = 0.011 g							
1	0.009	1	0.011	6	0.008	1.014	--
2	0.006	6	0.008	12	0.005	1.247	--
3	0.003	12	0.005	19	0.002	2.083	--
AccWest Channel, u_o = 0.011 g							
1	0.009	1	0.011	6	0.007	1.439	--
2	0.006	6	0.007	12	0.005	0.893	--
3	0.003	12	0.005	19	0.002	2.083	--
Specimen 9							
HorEast Channel, u_o = 2.184 mm							
1	1.822	1	2.184	8	1.499	0.857	--
2	1.168	8	1.499	16	0.889	1.039	--
3	0.576	16	0.889	24	0.330	1.970	--
HorWest Channel, u_o = 2.235 mm							
1	1.797	1	2.235	8	1.422	1.028	--
2	1.112	8	1.422	16	0.813	1.113	--
3	0.550	16	0.813	24	0.305	1.951	--
AccEast Channel, u_o = 0.017 g							
1	0.013	1	0.017	8	0.011	0.990	--
2	0.009	8	0.011	16	0.006	1.206	--
3	0.005	16	0.006	24	0.003	1.379	--
AccWest Channel, u_o = 0.017 g							
1	0.013	1	0.017	8	0.011	0.990	--
2	0.008	8	0.011	16	0.006	1.206	--
3	0.004	16	0.006	24	0.003	1.379	--

TABLE 4-3 (cont'd) Free Vibration Damping Estimates

i	u^*_i	k_i	u_{ki}	k_i+j	u_{ki+j}	ξ_i	Remarks
Specimen 10							
HorEast Channel, u_o = 1.626 mm							
1	1.075	1	1.245	3	0.864	2.908	Res. Disp.
2	0.705	3	0.864	6	0.483	3.087	--
3	0.398	6	0.483	8	0.356	2.430	--
HorWest Channel, u_o = 1.473 mm							
1	1.160	1	1.372	3	0.991	2.590	Res. Disp.
2	0.813	3	0.991	6	0.635	2.359	--
3	0.508	6	0.635	8	0.381	4.065	--
AccEast Channel, u_o = 0.011 g							
1	0.009	1	0.011	3	0.007	3.597	--
2	0.006	3	0.007	6	0.004	2.969	--
3	0.003	6	0.004	8	0.002	5.516	--
AccWest Channel, u_o = 0.010 g							
1	0.008	1	0.010	3	0.007	2.838	--
2	0.005	3	0.007	6	0.003	4.495	--
3	0.003	6	0.003	8	0.002	3.227	--
Specimen 10b							
HorWest Channel, u_o = 0.864 mm							
1	0.737	1	0.864	3	0.610	2.772	(3, 4)
2	0.513	3	0.610	7	0.381	1.870	--
3	0.330	7	0.381	11	0.254	1.613	--
AccEast Channel, u_o = 0.007 g							
1	0.006	1	0.007	3	0.005	2.678	--
2	0.004	3	0.005	7	0.003	2.033	--
3	0.002	7	0.003	11	0.001	4.371	--
AccWest Channel, u_o = 0.007 g							
1	0.006	1	0.007	3	0.005	2.678	--
2	0.004	3	0.005	7	0.003	2.033	--
3	0.003	7	0.003	11	0.002	1.613	--

3: No HorEast measurement due to broken rod
4: Residual displacement offset at conclusion of test

TABLE 4-3 (cont'd) Free Vibration Damping Estimates

i	u^*_i	k_i	u_{ki}	k_i+j	u_{ki+j}	ξ_i	Remarks
Specimen 11							
HorEast Channel, u_o = 1.118 mm							
1	1.022	1	1.118	4	0.991	0.640	--
2	0.737	4	0.991	9	0.610	1.545	--
3	0.440	9	0.610	14	0.229	3.122	--
HorWest Channel, u_o = 0.991 mm							
1	0.902	1	0.991	4	0.762	1.392	--
2	0.639	4	0.762	9	0.483	1.454	--
3	0.347	9	0.483	14	0.229	2.378	--
AccEast Channel, u_o = 0.012 g							
1	0.011	1	0.012	4	0.010	0.967	--
2	0.008	4	0.010	9	0.006	1.626	--
3	0.004	9	0.006	14	0.003	2.206	--
AccWest Channel, u_o = 0.012 g							
1	0.011	1	0.012	4	0.009	1.526	--
2	0.007	4	0.009	9	0.006	1.291	--
3	0.004	9	0.006	14	0.002	3.497	--
Specimen 12							
HorEast Channel, u_o = 1.626 mm							
1	1.335	1	1.626	7	1.118	0.994	--
2	0.864	7	1.118	14	0.610	1.378	--
3	0.451	14	0.610	21	0.254	1.991	--
HorWest Channel, u_o = 1.600 mm							
1	1.317	1	1.600	7	1.092	1.013	--
2	0.848	7	1.092	14	0.610	1.326	--
3	0.441	14	0.610	21	0.254	1.991	--
AccEast Channel, u_o = 0.014 g							
1	0.012	1	0.014	7	0.010	0.893	--
2	0.007	7	0.010	14	0.005	1.576	--
3	0.004	14	0.005	21	0.003	1.161	--
AccWest Channel, u_o = 0.014 g							
1	0.012	1	0.014	7	0.010	0.893	--
2	0.007	7	0.010	14	0.006	1.161	--
3	0.004	14	0.006	21	0.003	1.576	--

TABLE 4-3 (cont'd) Free Vibration Damping Estimates

i	u^*_i	k_i	u_{ki}	k_i+j	u_{ki+j}	ξ_i	Remarks
Specimen 13							
HorEast Channel, u_o = 2.489 mm							
1	2.159	1	2.489	5	1.854	1.172	--
2	1.566	5	1.854	10	1.245	1.269	--
3	0.952	10	1.245	15	0.635	2.142	--
HorWest Channel, u_o = 2.362 mm							
1	2.134	1	2.362	5	1.854	0.963	--
2	1.516	5	1.854	10	1.245	1.269	--
3	0.936	10	1.245	15	0.635	2.142	--
AccEast Channel, u_o = 0.011 g							
1	0.010	1	0.011	5	0.009	0.798	--
2	0.008	5	0.009	10	0.007	0.800	--
3	0.006	10	0.007	15	0.005	1.071	--
AccWest Channel, u_o = 0.012 g							
1	0.010	1	0.012	5	0.009	1.145	--
2	0.007	5	0.009	10	0.006	1.291	--
3	0.005	10	0.006	15	0.004	1.291	--
Specimen 14							
HorEast Channel, u_o = 4.14 mm							
1	3.683	1	4.140	4	3.226	1.324	(4)
2	2.723	4	3.226	8	2.235	1.460	--
3	1.589	8	2.235	14	0.991	2.159	--
HorWest Channel, u_o = 4.267 mm							
1	3.746	1	4.267	4	3.277	1.401	--
2	2.738	4	3.277	8	2.235	1.522	--
3	1.618	8	2.235	14	1.041	2.026	--
AccEast Channel, u_o = 0.013 g							
1	0.011	1	0.013	4	0.009	1.951	--
2	0.007	4	0.009	8	0.006	1.613	--
3	0.004	8	0.006	14	0.003	1.839	--
AccWest Channel, u_o = 0.014 g							
1	0.011	1	0.014	4	0.009	2.344	--
2	0.007	4	0.009	8	0.006	1.613	--
3	0.004	8	0.006	14	0.003	1.839	--

4: Residual displacement offset at conclusion of test

TABLE 4-3 (cont'd) Free Vibration Damping Estimates

i	u^*_i	k_i	u_{ki}	k_i+j	u_{ki+j}	ξ_i	Remarks
Specimen 15							
HorEast Channel, u_o = 1.854 mm							
1	1.613	1	1.854	2	1.372	4.798	(4)
2	1.054	2	1.372	3	0.737	9.894	--
3	0.610	3	0.737	4	0.483	6.730	--
HorWest Channel, u_o = 1.600 mm							
1	1.359	1	1.600	2	1.118	5.713	--
2	0.927	2	1.118	3	0.737	6.635	--
3	0.559	3	0.737	4	0.381	10.492	--
AccEast Channel, u_o = 0.007 g							
1	0.006	1	0.007	2	0.005	5.355	--
2	0.005	2	0.005	3	0.004	3.551	--
3	0.004	3	0.004	4	0.003	4.579	--
AccWest Channel, u_o = 0.008 g							
1	0.007	1	0.008	2	0.005	7.480	--
2	0.005	2	0.005	3	0.004	3.551	--
3	0.004	3	0.004	4	0.003	4.579	--

4: Residual displacement offset at conclusion of test

Note that the limited resolution of the displacement transducers at the small amplitudes used in some free-vibration tests resulted in a "stepping" of descending amplitudes for some free vibration histories. The acceleration data therefore appears to be more appropriate to estimate the damping ratio for these particular experiments. However, the "stepped" data can still be reliably used to calculate damping ratios by selecting data points with peaks in the middle of the step for each subsequent estimate. Furthermore, as noted in the rightmost column of the table, a small residual displacement was measured at the end of some of the tests. Careful review of this data indicates that these values were within the resolution of the instruments, except for Specimens 14 and 15, suggesting that these two specimens may have yielded slightly during the free vibration test.

When the mean amplitude of vibration of a given interval, u^*_i, is plotted versus the estimated damping ratio for that interval, ξ_i, it is observed as a general trend that the two variables are inversely related. Considering all of the individual data channels (displacement and acceleration) used in the free vibration analyses, approximately 80% of all specimens display this

behavior. The remaining 20% display a trend indicating a direct relation of these variables for unknown reasons.

The results of the free vibration test are presented by the following series of plots, (Figures 4-1, 4-31, and 4-70), which are presented for specimen 1, 6, and 11:

1. Time history response of each recorded displacement and acceleration channel
2. Damping ratio estimates, ξ_i, versus the mean response amplitude, u^*_i.
3. Fourier Amplitude versus period displaying the observed fundamental period peak.

These plots are located preceding the shake table test plots for the respective specimen described in the next section.

4.2.3 SDOF Shake Table Tests

A summary of the shake table test results is provided in Table 4-4, following the schedules established for each specimen and described in the previous chapter. The following peak input and response parameters are defined:

Span =	Actuator span setting (Volts)
Input PGA =	Target peak table acceleration (g)
Output PGA =	Measured table PGA after filtering (g)
Max. Drift =	Maximum relative displacement of the structure, in terms of displacement (mm) and also expressed as inter-story drift, i.e. normalized by the average column height of the specimen (%)
$\ddot{u}_{Tmax}$ =	Maximum total acceleration of the structural mass (g)
V^*_{max} =	Maximum estimated base shear, not corrected for P-Δ (N)
u_r =	Residual displacement at end of test (mm)

The significance of these results is discussed in the next chapter.

TABLE 4-4 Shake Table Test Results

Test	Span (V)	Input PGA (g)	Output PGA (g)	Max. Drift (mm)	Max. Drift (%)	$\ddot{u}_{Tmax}$ (g)	V^*_{max} (N)	u_r (mm)
Specimen 1								
1	5.25	0.114	0.148	3.7	2.72	0.332	135.8	0.0
2	7.50	0.163	0.198	4.8	3.52	0.387	155.2	0.2
3	10.00	0.217	0.274	5.8	4.26	0.420	155.2	0.4
4	10.00	0.217	0.277	6.0	4.37	0.429	155.2	0.2
5	1.00	0.089	0.116	2.5	1.81	0.231	97.0	0.1
6	3.33	0.295	0.335	5.9	4.33	0.431	159.1	0.3
7	5.00	0.443	0.491	10.5	7.67	0.495	209.6	1.7
8	6.00	0.531	0.583	13.5	9.81	0.527	236.7	0.8
9	7.00	0.619	0.674	16.0	11.68	0.545	229.0	3.1
10	8.00	0.708	0.779	87.2	63.54	0.607	279.4	86.1
11	7.00	0.619	0.643	∞	∞	--	--	∞
Specimen 2								
1	2.50	0.054	0.097	3.2	2.35	0.137	94.2	0.5
2	3.50	0.076	0.112	4.1	2.98	0.169	118.8	0.9
3	4.50	0.098	0.130	4.6	3.38	0.186	131.1	0.9
4	5.50	0.119	0.177	5.0	3.62	0.203	151.6	0.9
5	6.50	0.141	0.287	5.2	3.79	0.217	155.7	0.7
6	7.50	0.163	0.192	5.8	4.20	0.227	163.9	0.7
7	8.50	0.184	0.257	6.6	4.79	0.233	168.0	1.0
8	10.00	0.217	0.252	7.4	5.42	0.246	188.4	2.7
9	10.00	0.217	0.342	11.9	8.67	0.253	221.2	8.1
10	10.00	0.217	0.325	∞	∞	--	--	∞
Specimen 4								
1	0.75	0.016	0.043	1.2	0.87	0.035	34.9	0.1
2	2.00	0.043	0.095	3.0	2.22	0.097	93.0	0.3
3	3.00	0.065	0.121	5.3	3.84	0.135	135.7	0.6
4	4.00	0.087	0.146	7.4	5.39	0.158	158.9	1.5
5	5.00	0.109	0.176	10.6	7.70	0.173	166.7	5.3
6	6.00	0.130	0.408	∞	∞	--	--	∞
Specimen 5b								
1	0.50	0.011	0.027	3.7	4.02	0.017	57.2	2.0
2	1.25	0.027	0.079	∞	∞	--	--	∞

TABLE 4-4 (cont'd) Shake Table Test Results

Test	Span (V)	Input PGA (g)	Output PGA (g)	Max. Drift (mm)	Max. Drift (%)	$\ddot{u}_{Tmax}$ (g)	V^*_{max} (N)	u_r (mm)
Specimen 6								
1	5.25	0.114	0.154	16.1	3.89	0.317	414.1	0.1
2	7.50	0.163	0.213	22.6	5.49	0.360	453.6	2.4
3	10.00	0.217	0.330	26.4	6.41	0.362	463.5	4.6
4	10.00	0.217	0.277	25.2	6.10	0.358	463.5	3.9
5	1.00	0.089	0.122	27.1	6.58	0.225	276.1	1.1
6	3.33	0.295	0.335	25.9	6.27	0.351	443.7	1.2
7	5.00	0.443	0.560	28.4	6.89	0.365	473.3	0.1
8	6.00	0.531	0.592	36.0	8.74	0.356	493.0	4.5
9	7.00	0.619	0.698	45.3	11.00	0.359	473.3	14.1
10	8.00	0.708	0.770	73.5	17.83	0.381	473.3	59.8
11	7.00	0.619	0.705	∞	∞	--	--	∞
Specimen 7								
1	2.00	0.043	0.067	8.6	2.51	0.147	132.0	0.2
2	3.00	0.065	0.095	12.2	3.56	0.197	178.2	0.2
3	4.00	0.087	0.131	16.2	4.72	0.222	231.0	2.8
4	5.00	0.109	0.147	25.1	7.29	0.208	231.0	13.4
5	6.00	0.130	0.346	∞	∞	--	--	∞
Specimen 8								
1	1.25	0.027	0.055	13.0	4.72	0.072	74.3	0.1
2	2.50	0.054	0.086	20.8	7.58	0.105	113.4	2.0
3	3.50	0.076	0.233	30.1	10.96	0.110	187.7	19.9
4	4.50	0.098	0.181	∞	∞	--	--	∞
Specimen 9								
1	1.25	0.027	0.060	7.6	3.69	0.048	86.9	0.8
2	1.50	0.033	0.064	10.1	4.89	0.055	115.0	2.4
3	1.75	0.038	0.078	17.6	8.54	0.058	138.1	13.4
4	2.00	0.043	0.147	∞	∞	--	--	∞
Specimen 10								
1	0.75	0.066	0.118	∞	∞	--	--	∞

1: 200 Hz sampling of shake table input

TABLE 4-4 (cont'd) Shake Table Test Results

Test	Span (V)	Input PGA (g)	Output PGA (g)	Max. Drift (mm)	Max. Drift (%)	$\ddot{u}_{Tmax}$ (g)	V^*_{max} (N)	u_r (mm)
Specimen 10b								
1	0.50	0.011	0.026	3.6	2.63	0.022	18.8	1.1
2	0.75	0.016	0.035	6.9	5.01	0.039	36.8	2.1
3	1.00	0.022	0.045	8.9	6.51	0.051	52.4	2.8
4	1.25	0.027	0.051	12.3	8.98	0.052	72.8	6.8
5	1.50	0.033	0.058	12.6	9.17	0.048	71.2	8.1
6	1.75	0.038	0.069	∞	∞	--	--	∞
Specimen 11								
1	4.00	0.087	0.132	23.7	4.32	0.271	184.2	0.7
2	5.25	0.114	0.166	32.2	5.86	0.324	206.3	3.1
3	7.50	0.163	0.201	45.7	8.32	0.352	206.3	12.8
4	10.00	0.217	0.262	58.1	10.57	0.346	221.0	24.3
5	10.00	0.217	0.244	63.7	11.59	0.316	221.0	35.7
6	10.00	0.217	0.248	82.4	15.00	0.303	228.4	63.2
7	10.00	0.217	0.242	∞	∞	--	--	∞
Specimen 12								
1	3.50	0.076	0.124	26.3	5.74	0.183	197.9	4.7
2	5.00	0.109	0.166	34.5	7.53	0.184	212.8	14.1
3	7.00	0.152	0.408	∞	∞	--	--	∞
Specimen 13								
1	2.50	0.054	0.085	25.3	6.91	0.100	114.4	0.8
2	3.50	0.076	0.103	28.0	7.64	0.099	123.2	2.6
3	4.50	0.098	0.122	32.1	8.78	0.103	132.0	1.0
4	5.50	0.119	0.161	45.8	12.52	0.102	158.4	28.3
5	6.50	0.141	0.222	∞	∞	--	--	∞
Specimen 14								
1	1.25	0.027	0.053	12.8	4.64	0.030	60.8	1.4
2	1.50	0.033	0.073	15.6	5.69	0.033	74.1	2.7
3	1.75	0.038	0.070	17.0	6.16	0.034	77.9	4.0
4	2.00	0.043	0.083	20.4	7.42	0.035	85.5	10.2
5	2.25	0.049	0.402	∞	∞	--	--	∞
Specimen 15								
1	0.75	0.016	0.100	∞	∞	--	--	∞

1: 200 Hz sampling of shake table input

Note that, for all tests reported here, a 20 Hz lowpass filter was used during post-processing of the measured table accelerations. These accelerations were analyzed in the frequency domain using the FFT technique, and an abrupt cut-off frequency of 20 Hz was used in the filtering procedure to eliminate all frequencies above that point before inverting back to the time domain. This was done to eliminate high frequency noise that would otherwise have caused the recorded peak ground acceleration values to appear larger than the peak ground acceleration "effectively" acting on the structure. Note that the fundamental frequencies of the specimens are well below 20 Hz, which justifies the selected filtering threshold.

The insignificance of the high frequency noise present within the recorded acceleration records on structural response is demonstrated by comparison of elastic time history analyses. Elastic response spectra were generated using the target, unfiltered, and filtered table acceleration time histories as input. Listed in Table 4-5 is the elastic spectral acceleration for the target ground motion, $S_{a\text{-target}}$, the measured ground motion, $S_{a\text{-meas.}}$, and the filtered ground motion, $S_{a\text{-filt}}$, for each specimen.

The ratios $S_{a\text{-filt}}/S_{a\text{-target}}$ and $S_{a\text{-meas}}/S_{a\text{-target}}$ are calculated over a range of periods bracketing the fundamental periods of the specimens investigated in the test program, namely from 0.15 s to 1.25 s. The ratio values calculated at the experimentally obtained period of the specimen, as well as the mean and standard deviation over the period range are reported in the table. The effect of the measured ground acceleration is closer to that of the target time history, for the range of periods under consideration, as the ratios approach unity. Good agreement is seen both at the experimentally obtained periods for each specimen (Spec.), and throughout the selected range of periods as shown by the Mean and Standard Deviation.

TABLE 4-5 Shake Table Acceleration Statistical Analysis

Test	$S_{a\text{-target}}$ (g)	$S_{a\text{-filt}}$ (g)	$S_{a\text{-filt}}/S_{a\text{-target}}$ Spec.	Mean*	Std Dev.*	$S_{a\text{-meas}}$ (g)	$S_{a\text{-meas}}/S_{a\text{-target}}$ Spec.	Mean*	Std Dev.*
Specimen 1									
1	0.326	0.335	1.030	1.005	0.047	0.337	1.035	1.005	0.047
2	0.465	0.489	1.050	1.019	0.075	0.488	1.050	1.004	0.041
3	0.620	0.633	1.021	1.017	0.074	0.489	0.788	0.753	0.030
4	0.620	0.638	1.028	1.025	0.102	0.638	1.029	0.997	0.030
5	0.234	0.188	0.802	0.948	0.075	0.188	0.803	0.953	0.054
6	0.780	0.728	0.933	0.961	0.054	0.728	0.933	0.979	0.026
7	1.172	1.103	0.941	0.976	0.051	1.103	0.941	0.980	0.029
8	1.406	1.336	0.950	0.975	0.028	1.337	0.951	0.979	0.018
9	1.641	1.530	0.933	0.971	0.040	1.529	0.932	0.981	0.025
10	1.875	1.726	0.921	0.961	0.046	1.724	0.919	0.973	0.031
11	1.641	1.605	0.978	0.982	0.022	1.604	0.978	0.986	0.011
Specimen 2									
1	0.166	0.168	1.011	1.054	0.087	0.168	1.012	1.054	0.087
2	0.233	0.228	0.979	1.049	0.073	0.228	0.978	1.049	0.073
3	0.299	0.303	1.013	1.053	0.063	0.303	1.013	1.053	0.063
4	0.366	0.379	1.037	1.069	0.064	0.379	1.038	1.069	0.063
5	0.432	0.452	1.045	1.072	0.065	0.452	1.045	1.072	0.066
6	0.499	0.493	0.989	1.059	0.060	0.493	0.989	1.059	0.061
7	0.565	0.550	0.973	1.054	0.049	0.550	0.973	1.054	0.049
8	0.665	0.658	0.990	1.058	0.047	0.658	0.990	1.058	0.048
9	0.665	0.680	1.022	1.053	0.037	0.680	1.023	1.053	0.037
10	0.665	0.675	1.015	1.058	0.054	0.675	1.015	1.058	0.054
Specimen 4									
1	0.055	0.064	1.168	1.217	0.407	0.064	1.168	1.217	0.407
2	0.147	0.156	1.061	1.127	0.226	0.156	1.061	1.126	0.226
3	0.220	0.223	1.011	1.089	0.125	0.223	1.011	1.089	0.125
4	0.294	0.309	1.050	1.073	0.090	0.309	1.050	1.073	0.089
5	0.367	0.398	1.082	1.073	0.085	0.398	1.082	1.073	0.085
6	0.441	0.474	1.074	1.075	0.085	0.474	1.074	1.076	0.086
Specimen 5b									
1	0.035	0.028	0.797	1.136	0.397	0.028	0.797	1.136	0.397
2	0.087	0.067	0.775	1.197	0.575	0.067	0.775	1.197	0.575

*Period Range: 0.15 s < T < 1.25 s

TABLE 4-5 (cont'd) Shake Table Acceleration Statistical Analysis

Test	$S_{a\text{-target}}$ (g)	$S_{a\text{-filt}}$ (g)	$S_{a\text{-filt}}/S_{a\text{-target}}$			$S_{a\text{-meas}}$ (g)	$S_{a\text{-meas}}/S_{a\text{-target}}$		
			Spec.	Mean*	Std Dev.*		Spec.	Mean*	Std Dev.*
Specimen 6									
1	0.284	0.305	1.073	1.069	0.059	0.305	1.073	1.069	0.059
2	0.406	0.427	1.051	1.061	0.060	0.427	1.052	1.061	0.060
3	0.542	0.573	1.057	1.055	0.057	0.573	1.058	1.056	0.057
4	0.542	0.564	1.042	1.059	0.048	0.564	1.042	1.059	0.048
5	0.249	0.242	0.973	0.998	0.050	0.242	0.973	0.998	0.049
6	0.828	0.850	1.026	1.037	0.037	0.850	1.026	1.037	0.037
7	1.243	1.274	1.025	1.032	0.022	1.274	1.025	1.032	0.022
8	1.492	1.536	1.029	1.038	0.021	1.536	1.030	1.038	0.021
9	1.741	1.782	1.024	1.045	0.025	1.782	1.024	1.045	0.026
10	1.990	2.078	1.044	1.046	0.019	2.078	1.044	1.046	0.019
11	1.741	1.817	1.044	1.050	0.024	1.817	1.044	1.051	0.024
Specimen 7									
1	0.134	0.135	1.011	1.077	0.106	0.135	1.011	1.077	0.106
2	0.200	0.209	1.046	1.054	0.058	0.210	1.048	1.054	0.058
3	0.267	0.279	1.044	1.061	0.061	0.279	1.044	1.061	0.061
4	0.334	0.350	1.049	1.063	0.062	0.350	1.049	1.063	0.062
5	0.401	0.421	1.051	1.073	0.068	0.421	1.052	1.073	0.068
Specimen 8									
1	0.073	0.073	1.008	1.107	0.211	0.073	1.008	1.107	0.212
2	0.145	0.151	1.043	1.060	0.093	0.151	1.043	1.060	0.092
3	0.203	0.208	1.023	1.068	0.079	0.208	1.023	1.068	0.079
4	0.261	0.274	1.048	1.054	0.099	0.274	1.048	1.055	0.100
Specimen 9									
1	0.056	0.056	0.999	1.092	0.203	0.056	0.999	1.092	0.203
2	0.068	0.068	1.005	1.085	0.158	0.068	1.005	1.085	0.157
3	0.079	0.081	1.029	1.108	0.152	0.081	1.029	1.109	0.153
4	0.090	0.093	1.026	1.125	0.184	0.093	1.026	1.127	0.186
Specimen 10									
1	0.044	0.040	0.904	1.231	0.444	0.040	0.904	1.234	0.452

*Period Range: 0.15 s < T < 1.25 s

TABLE 4-5 (cont'd) Shake Table Acceleration Statistical Analysis

Test	$S_{a\text{-target}}$ (g)	$S_{a\text{-filt}}$ (g)	$S_{a\text{-filt}}/S_{a\text{-target}}$			$S_{a\text{-meas}}$ (g)	$S_{a\text{-meas}}/S_{a\text{-target}}$		
			Spec.	Mean*	Std Dev.*		Spec.	Mean*	Std Dev.*
Specimen 10b									
1	0.024	0.020	0.854	1.095	0.384	0.020	0.854	1.095	0.384
2	0.036	0.033	0.932	1.064	0.296	0.033	0.932	1.064	0.296
3	0.047	0.045	0.939	1.045	0.215	0.045	0.939	1.045	0.214
4	0.059	0.058	0.977	1.041	0.176	0.058	0.977	1.041	0.175
5	0.071	0.067	0.943	1.021	0.147	0.067	0.943	1.021	0.147
6	0.083	0.079	0.955	1.039	0.201	0.079	0.955	1.039	0.201
Specimen 11									
1	0.261	0.266	1.021	1.057	0.078	0.266	1.021	1.057	0.078
2	0.342	0.354	1.035	1.055	0.070	0.354	1.035	1.055	0.070
3	0.489	0.505	1.032	1.051	0.061	0.505	1.032	1.051	0.060
4	0.652	0.669	1.026	1.052	0.058	0.669	1.026	1.052	0.058
5	0.652	0.673	1.032	1.049	0.050	0.673	1.032	1.049	0.050
6	0.652	0.672	1.030	1.047	0.044	0.672	1.030	1.047	0.044
7	0.652	0.672	1.030	1.047	0.044	0.672	1.030	1.047	0.044
Specimen 12									
1	0.242	0.240	0.991	1.050	0.082	0.240	0.990	1.049	0.082
2	0.345	0.350	1.012	1.054	0.073	0.350	1.012	1.054	0.073
3	0.484	0.508	1.050	1.058	0.075	0.508	1.050	1.057	0.075
Specimen 13									
1	0.131	0.134	1.025	1.065	0.096	0.134	1.024	1.065	0.096
2	0.183	0.190	1.039	1.053	0.068	0.190	1.039	1.053	0.069
3	0.235	0.242	1.027	1.041	0.056	0.241	1.027	1.041	0.056
4	0.287	0.299	1.042	1.056	0.051	0.299	1.042	1.057	0.052
5	0.340	0.352	1.035	1.063	0.054	0.352	1.035	1.063	0.054
Specimen 14									
1	0.038	0.039	1.023	1.102	0.180	0.039	1.023	1.102	0.179
2	0.046	0.046	1.000	1.084	0.159	0.046	1.000	1.084	0.159
3	0.053	0.143	2.676	2.678	0.143	0.055	1.023	1.069	0.122
4	0.061	0.061	1.000	1.077	0.122	0.061	1.000	1.077	0.122
5	0.069	0.069	1.004	1.109	0.232	0.069	1.004	1.112	0.242
Specimen 15									
1	0.048	0.047	0.987	0.996	0.090	0.047	0.987	0.996	0.091

*Period Range: 0.15 s < T < 1.25 s

The following four series of plots are sequentially provided for each specimen to demonstrate the inelastic behavior:

1. Seismic response of shake table tests including time history plots of target table acceleration, measured and filtered table acceleration, total mass acceleration, relative mass displacement, as well as a plot of estimated base shear, including P-Δ, V_p^*, versus relative displacement.
2. Time history plots of relative displacement for each test in the schedule for comparison of displacements throughout the range of progressive collapse.
3. Plots of estimated base shear, V_p^*, normalized by the plastic base shear, V_{yo}, versus displacement ductility, μ.
4. Plots of estimated base shear, V_p^*, normalized by the plastic base shear, V_{yo}, versus percent drift, γ ($=u_{rel\text{-}max}/L_{avg}$).

The first type of plot is provided for every test of Specimens 1, 6, and 11 (Figures 4-2 to 4-12, 4-32 to 4-42, and 4-71 to 4-77). For the remaining specimens, only tests resulting in large inelastic action and collapse are provided (although the entire data set is available electronically). These plots, along with the free vibration results described in the previous subsection, are found in Figures 4-1 to 4-98.

4.2.4 Exceptions

A few specimens could not be tested, as they failed during the erection procedure. Specimens 3 and 5 each had one column buckle prior to shake table testing. Initial imperfections and an unsuccessful execution during the delicate procedure of placing the mass plates on such small columns both contributed to the collapse of these specimens.

Specimen 10 collapsed early in the first run of its test schedule for a different reason: Input from the LABTECH software used to drive the table actuator was accidentally set at a 200 Hz sampling rate instead of 100 Hz. This resulted in a compressed time-scale for the input earthquake and thus a ground motion with higher frequency content. As a result, the test structure was subjected to a more severe excitation and collapsed well before what would have been expected under the correct time-scale ground motion.

Specimen 15 suffered from initial fabrication imperfections. As a result, prior to testing, the test structure had a substantial initial lean towards the south when the mass was released from the overhead crane support. This initial lean precipitated the structure's collapse early in the first test of the schedule.

Two additional specimens, labeled 5b and 10b, of same nominal dimensions as specimens 5 and 10, were fabricated in an attempt to provide some of the data lost by the premature collapses. These specimens were fabricated from 1/8" square AISI M1 cold-rolled tool steel as the steel and special machining of the original specimens was not available. However, tension tests revealed that this type of work-hardened steel has an average elastic modulus and yield strength of 269,809 MPa (39,133 ksi) and 1030 MPa (150 ksi), respectively. These differences should be kept in mind while reviewing the test results.

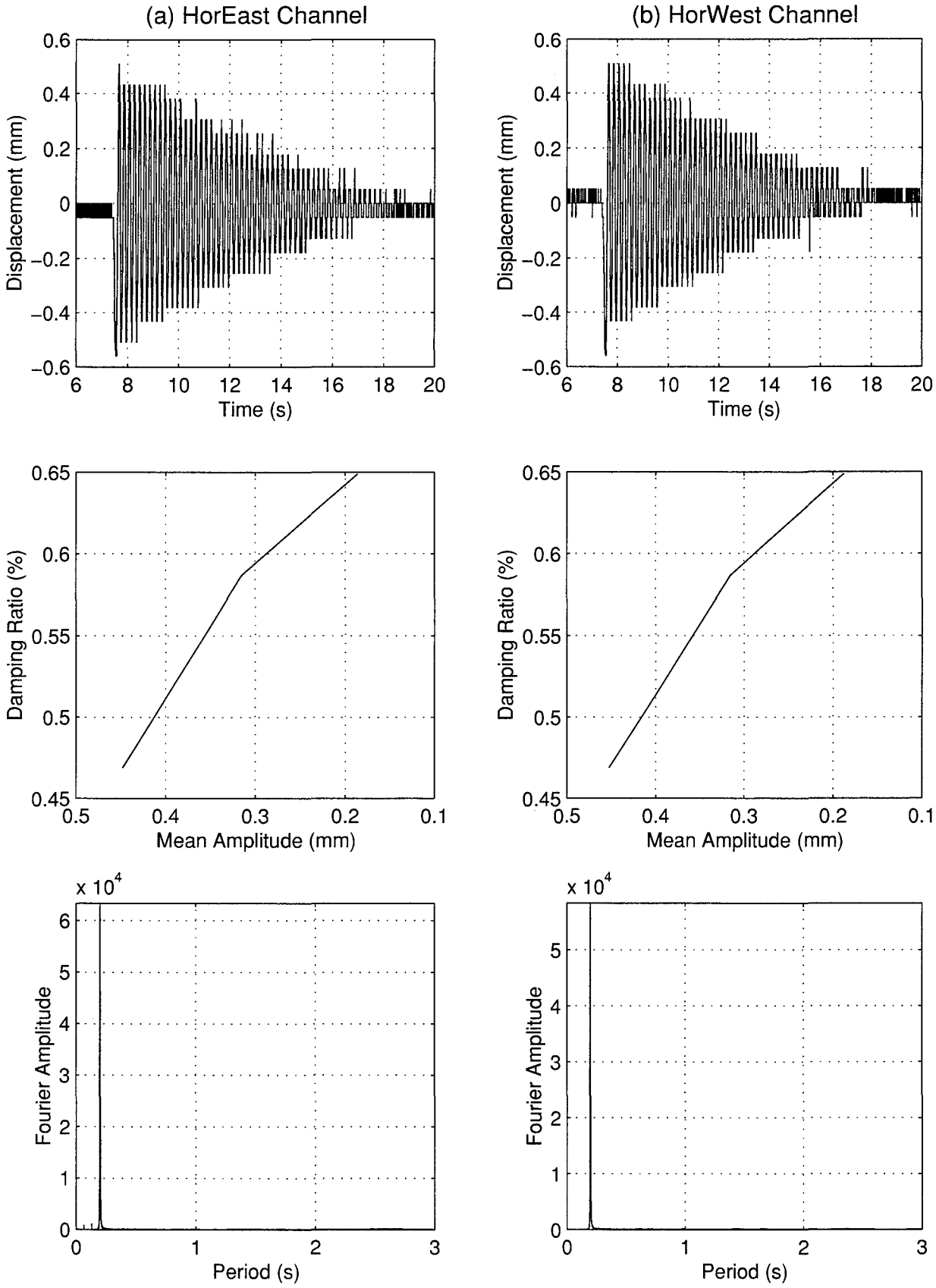

FIGURE 4–1 Free Vibration Test of Specimen1

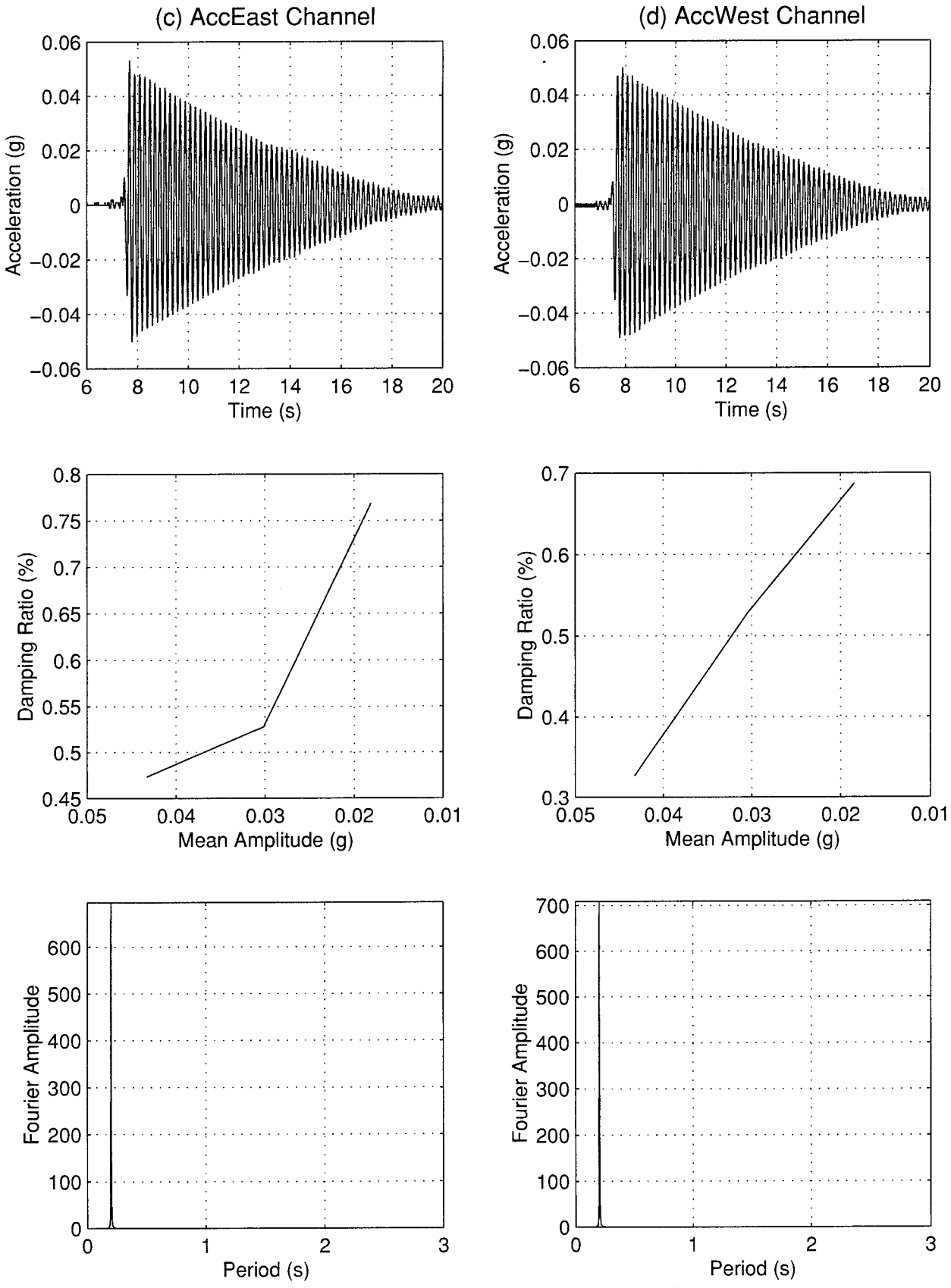

FIGURE 4–1 (cont'd) Free Vibration Test of Specimen1

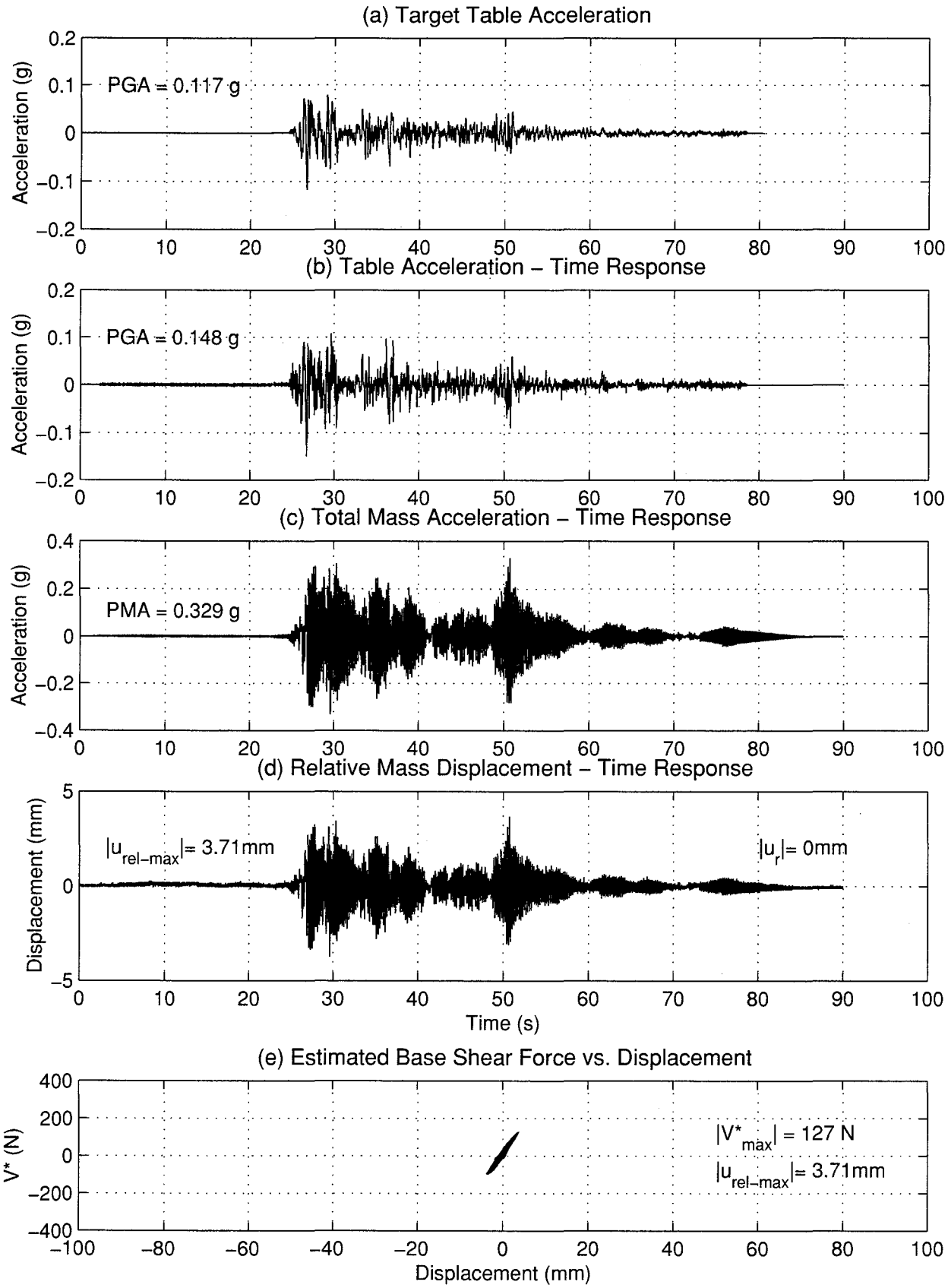

FIGURE 4–2 Seismic Response of Specimen 1 – Trial 1

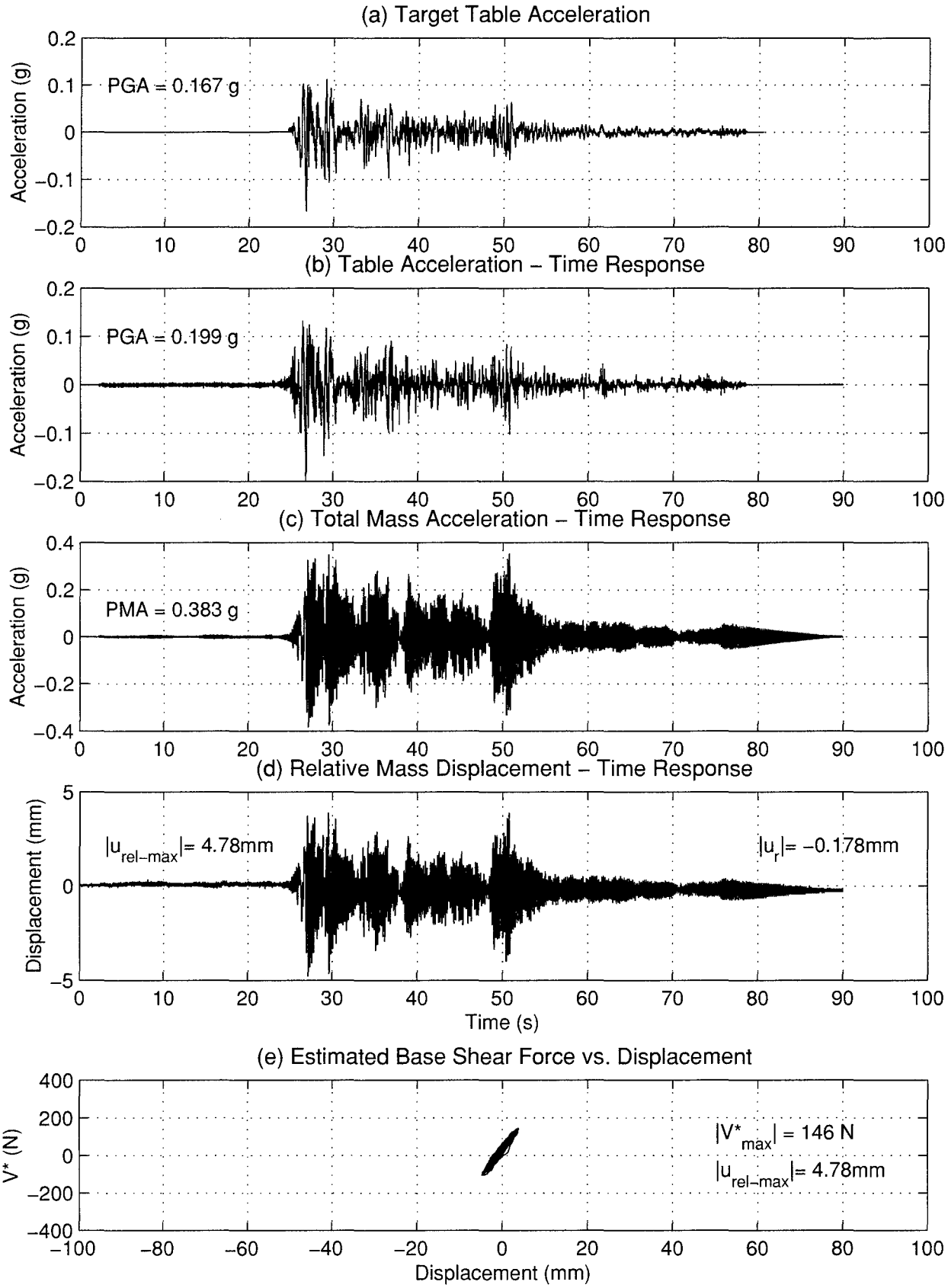

FIGURE 4–3 Seismic Response of Specimen 1 – Trial 2

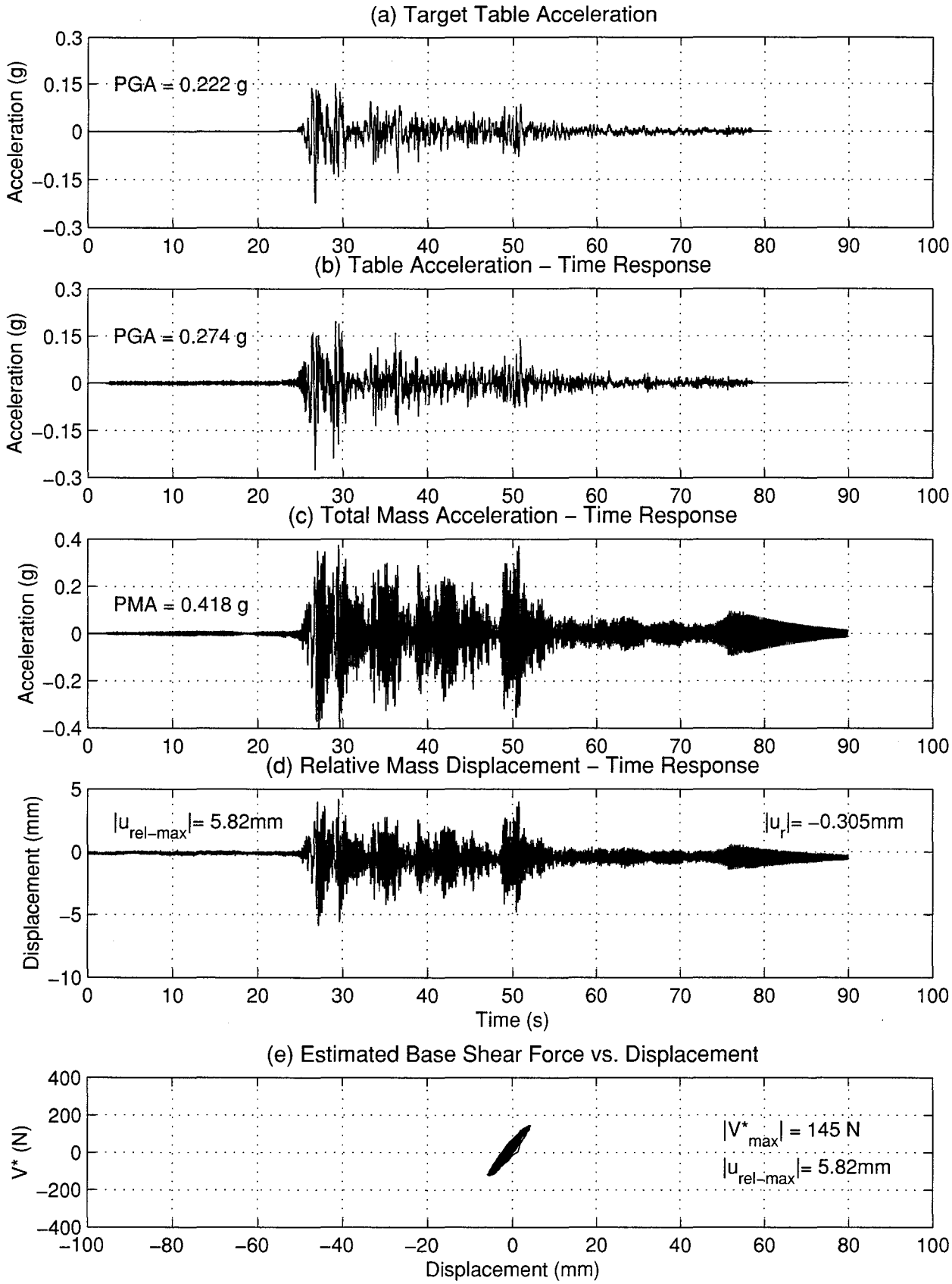

FIGURE 4–4 Seismic Response of Specimen 1 – Trial 3

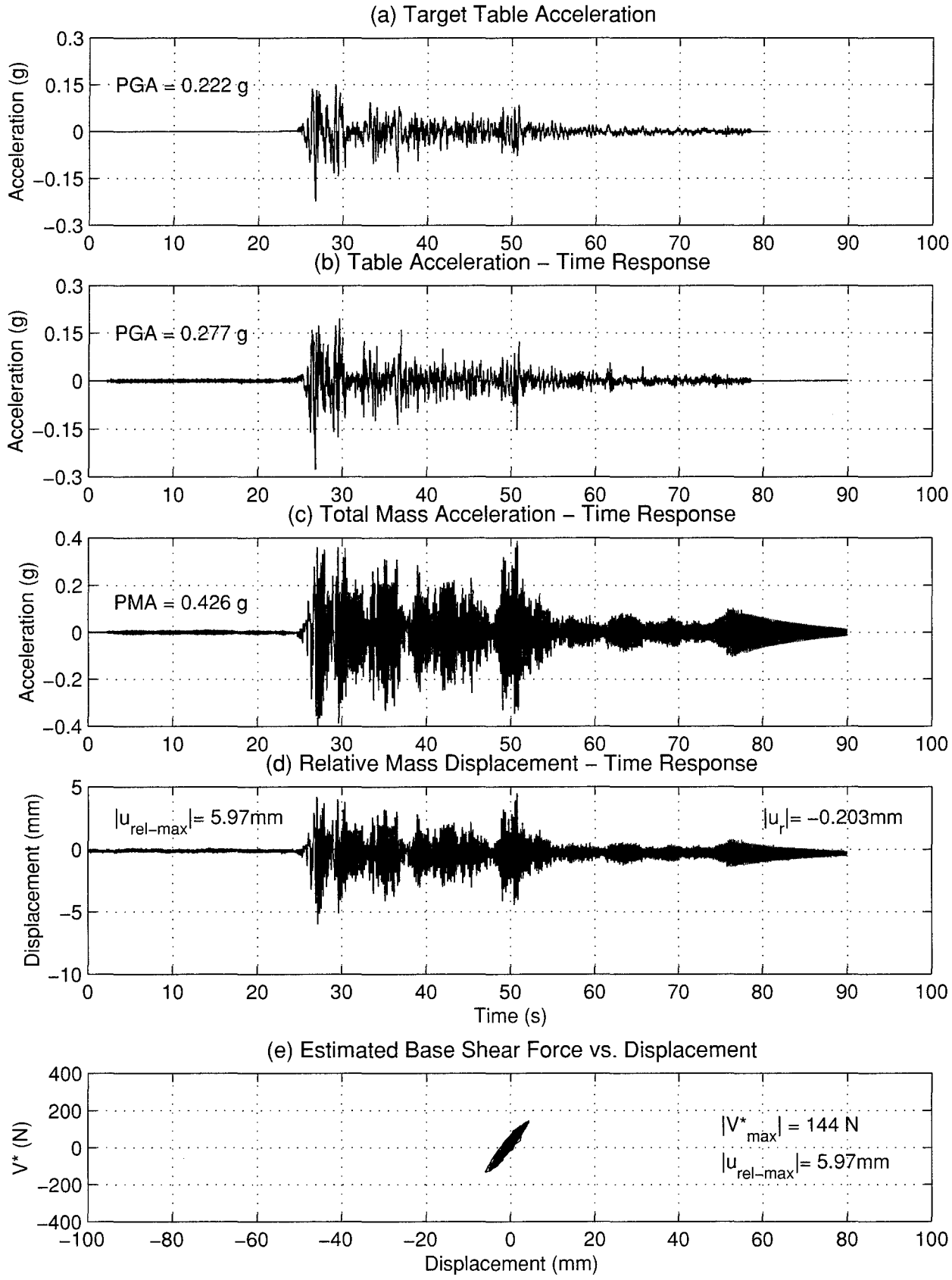

FIGURE 4-5 Seismic Response of Specimen 1 – Trial 4

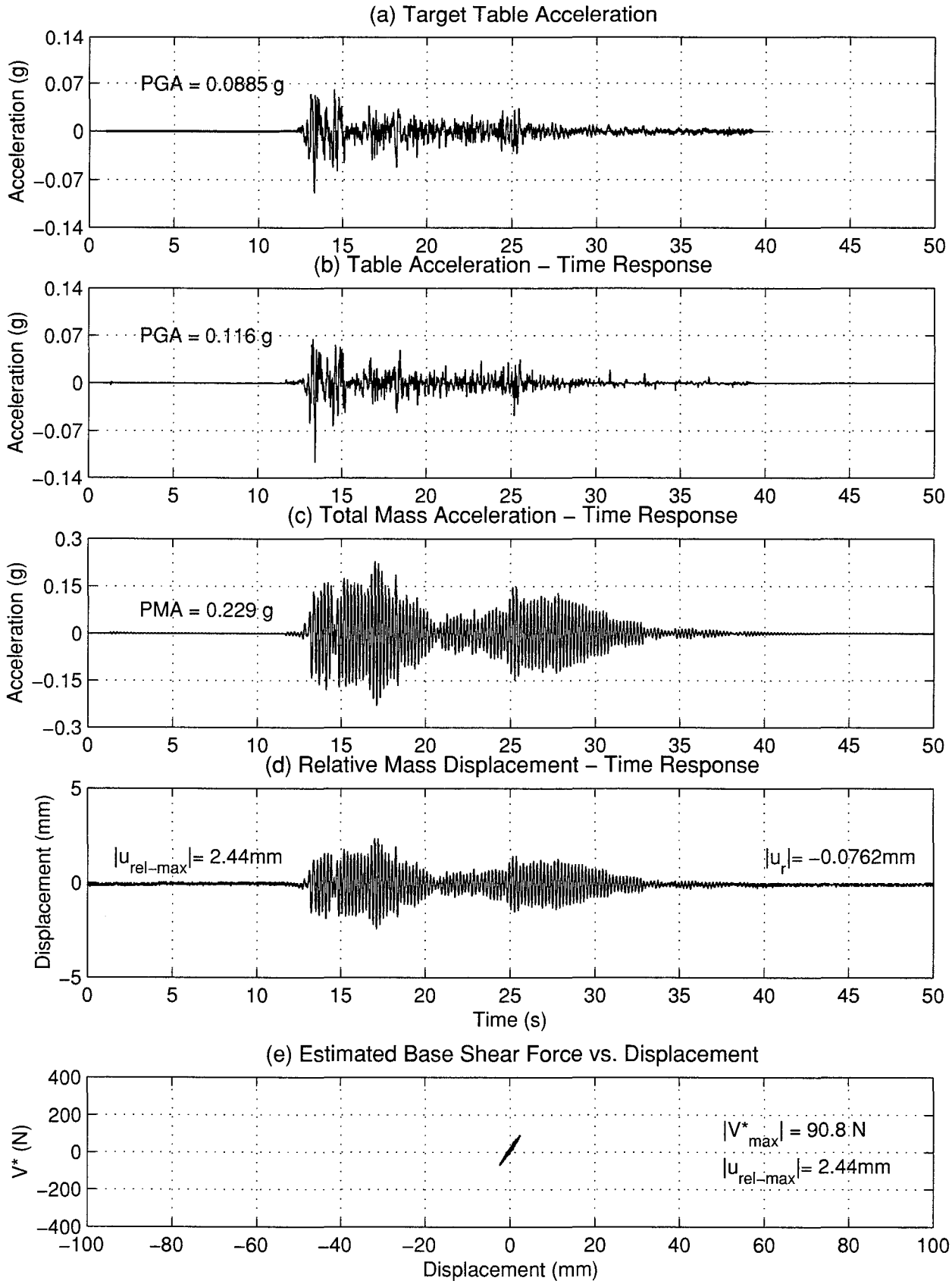

FIGURE 4–6 Seismic Response of Specimen 1 – Trial 5

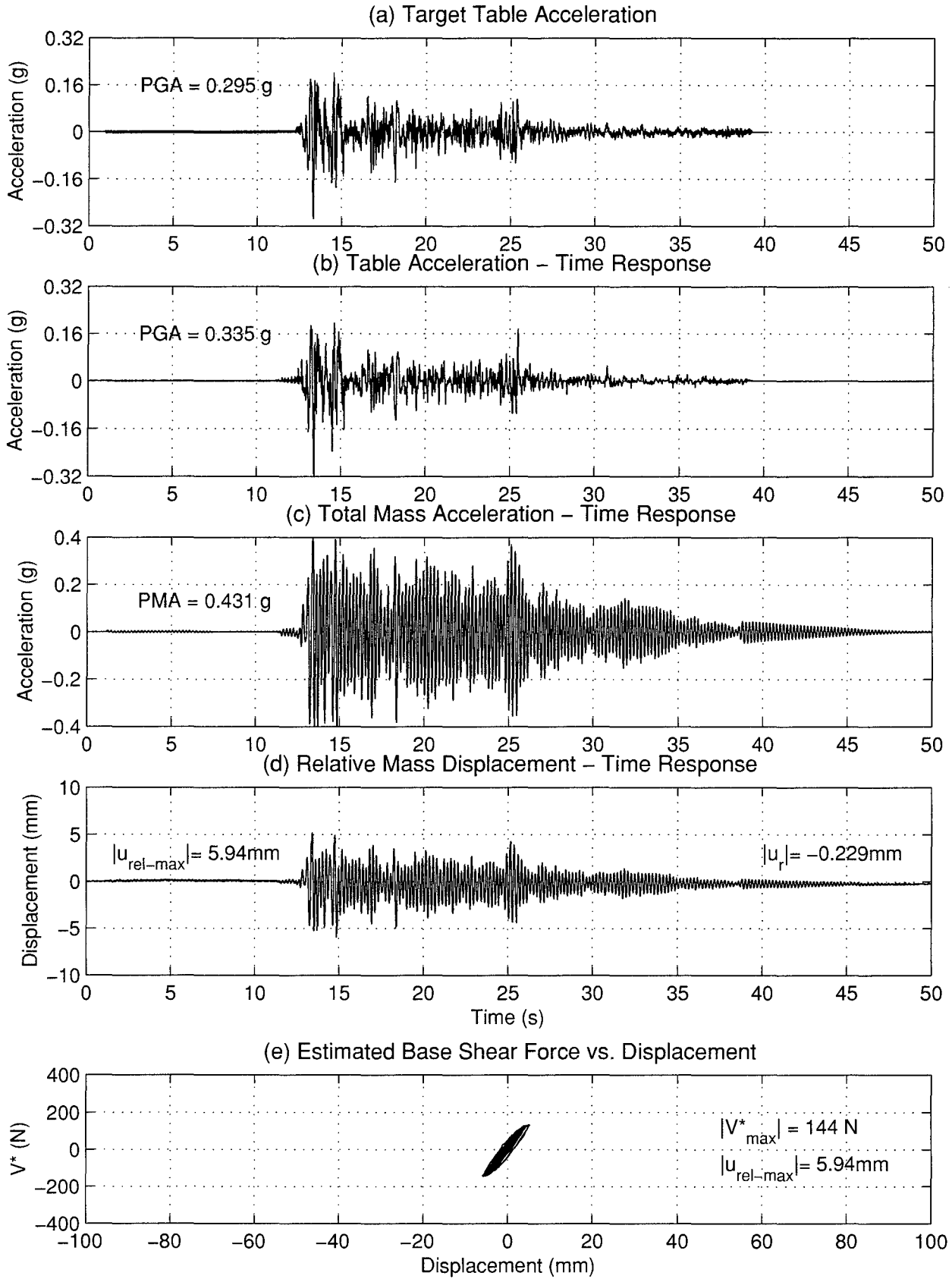

FIGURE 4–7 Seismic Response of Specimen 1 – Trial 6

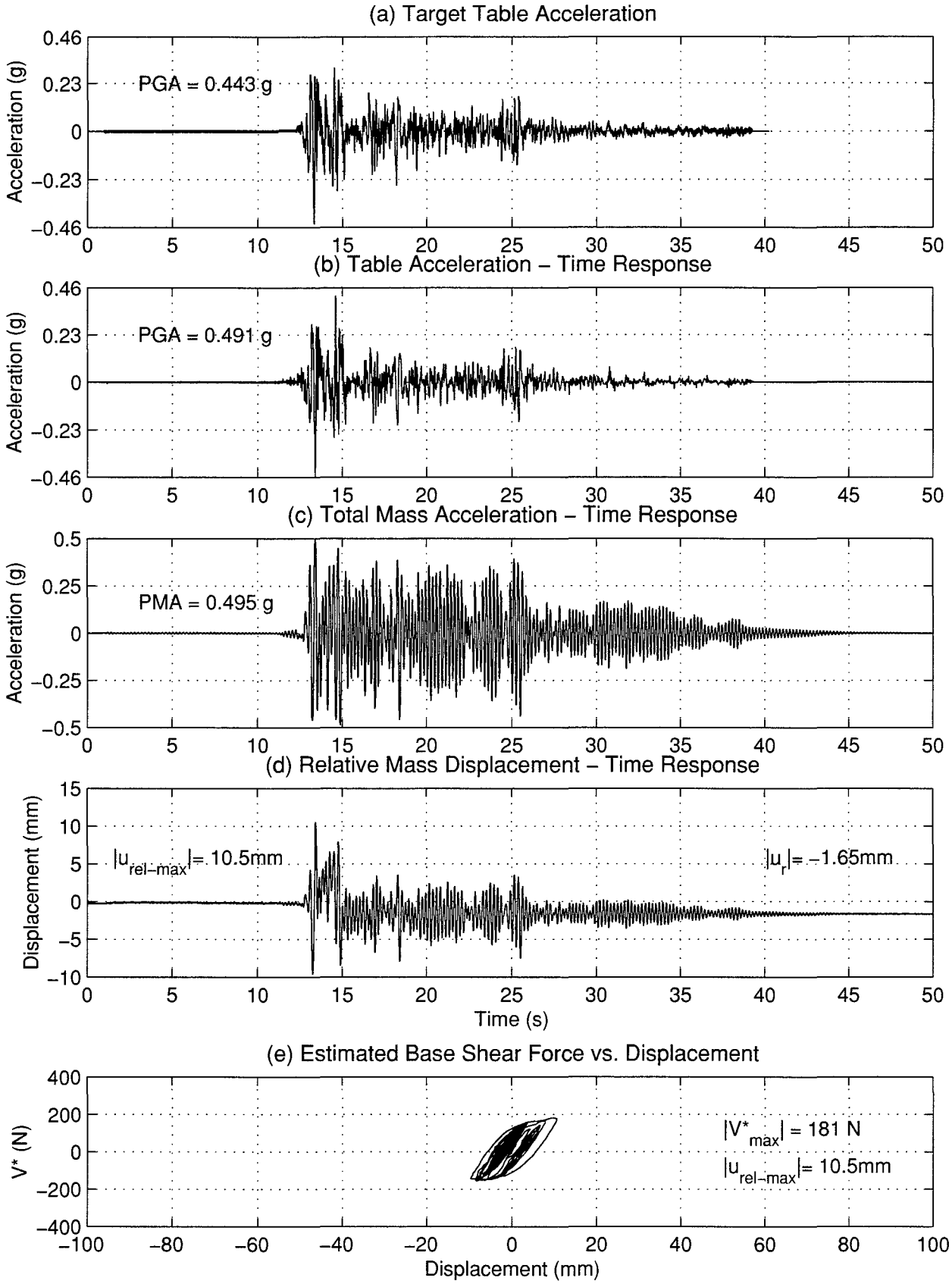

FIGURE 4–8 Seismic Response of Specimen 1 – Trial 7

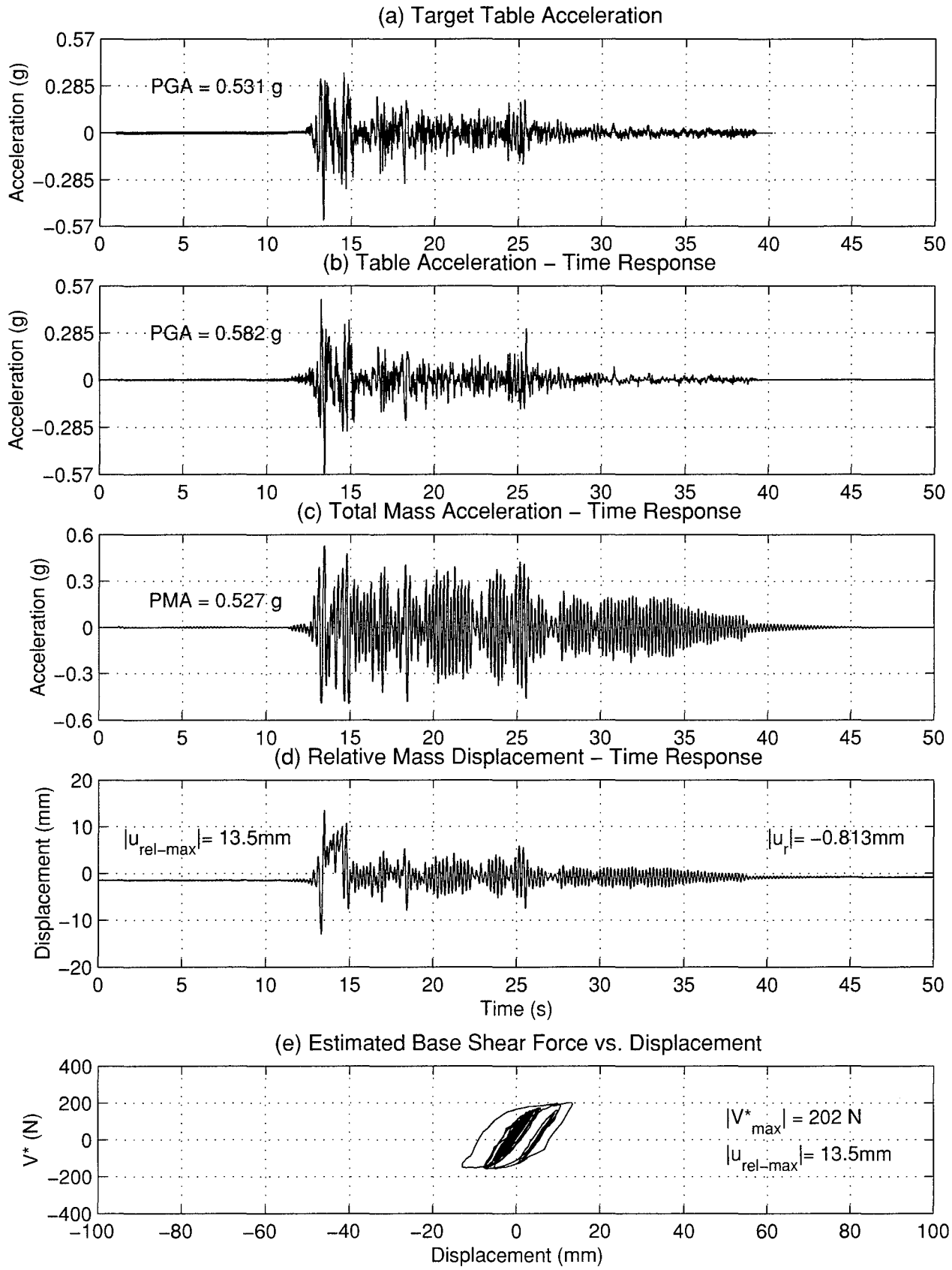

FIGURE 4–9 Seismic Response of Specimen 1 – Trial 8

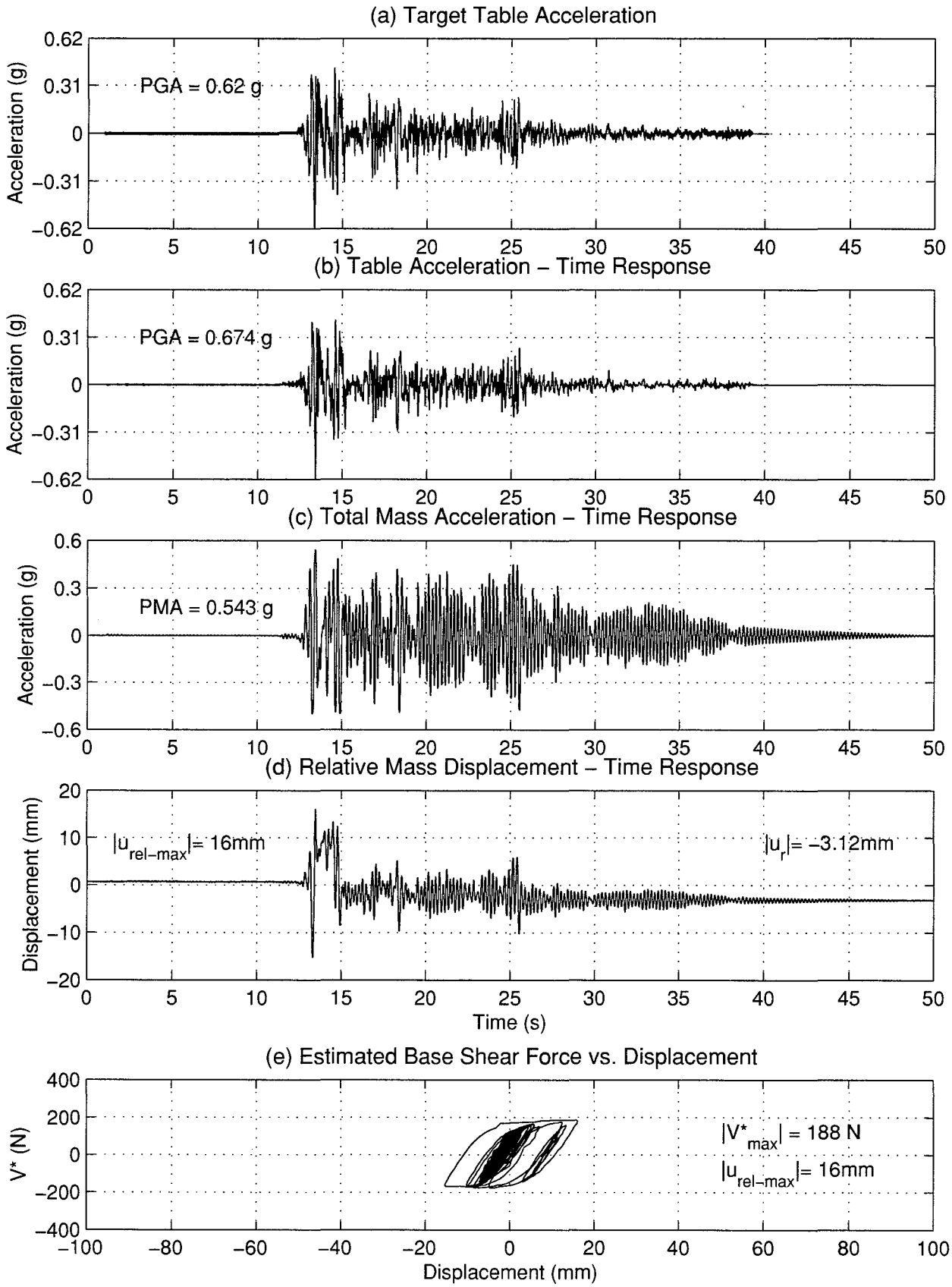

FIGURE 4–10 Seismic Response of Specimen 1 – Trial 9

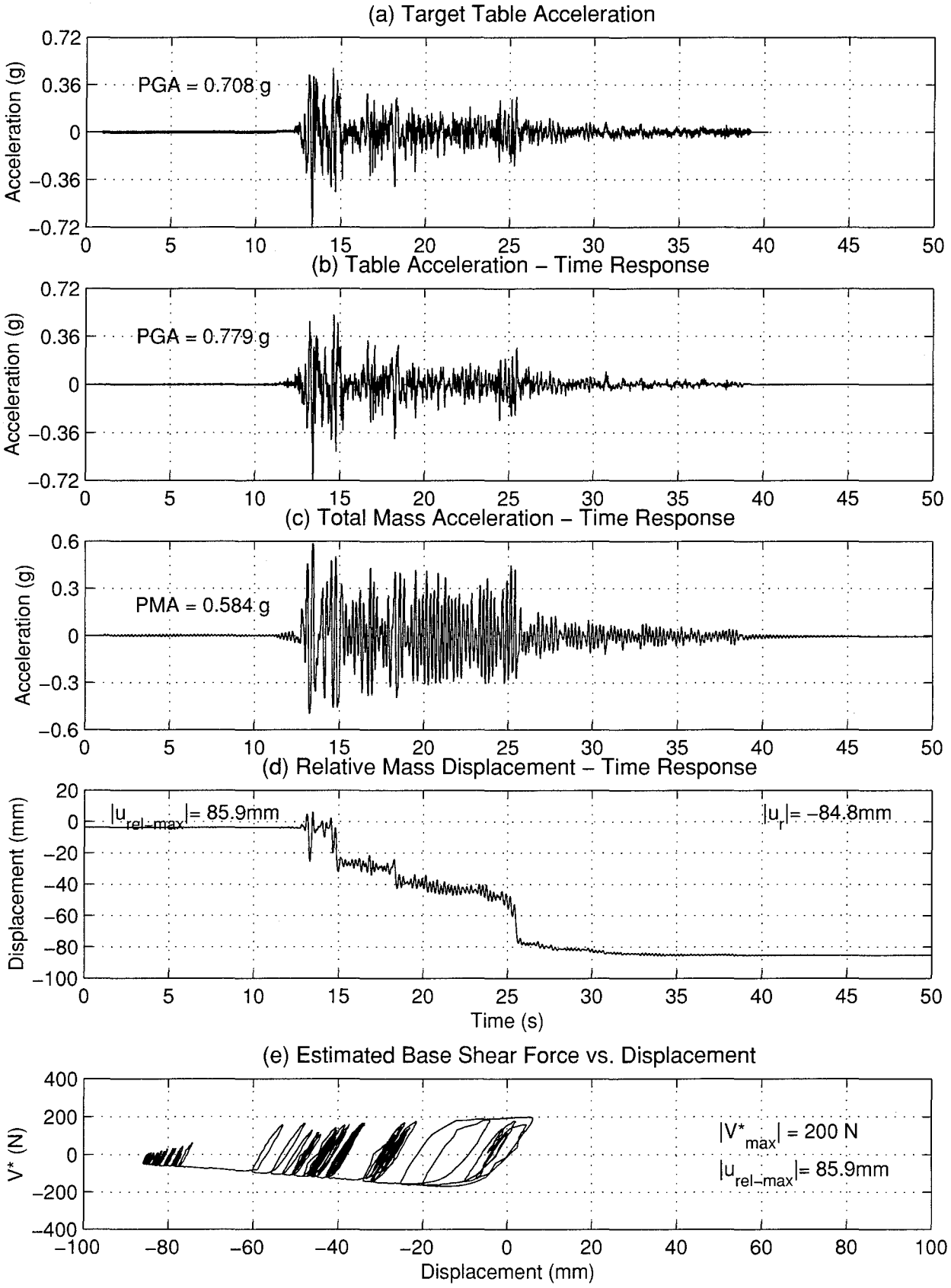

FIGURE 4–11 Seismic Response of Specimen 1 – Trial 10

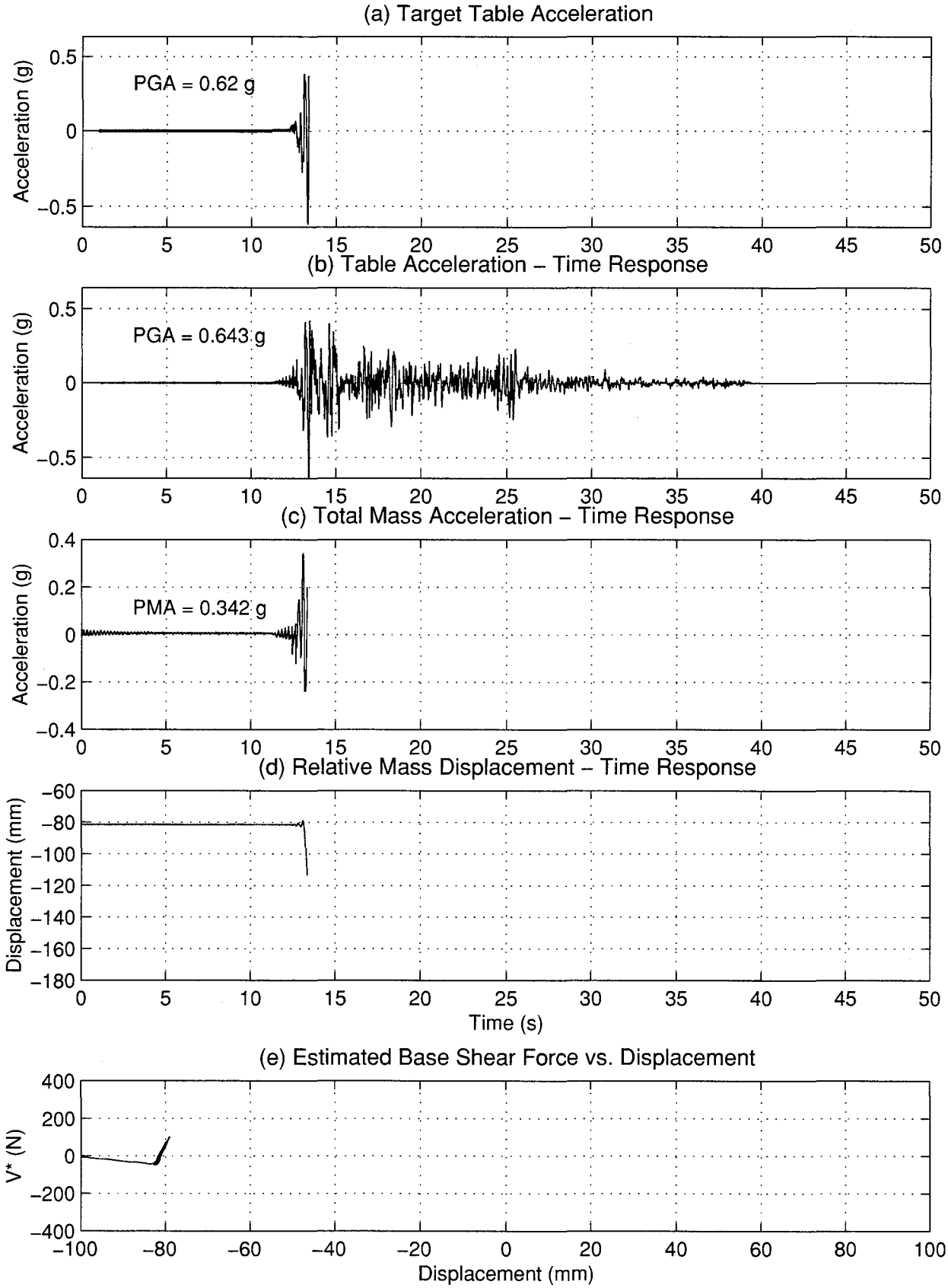

FIGURE 4–12 Seismic Response of Specimen 1 – Trial 11

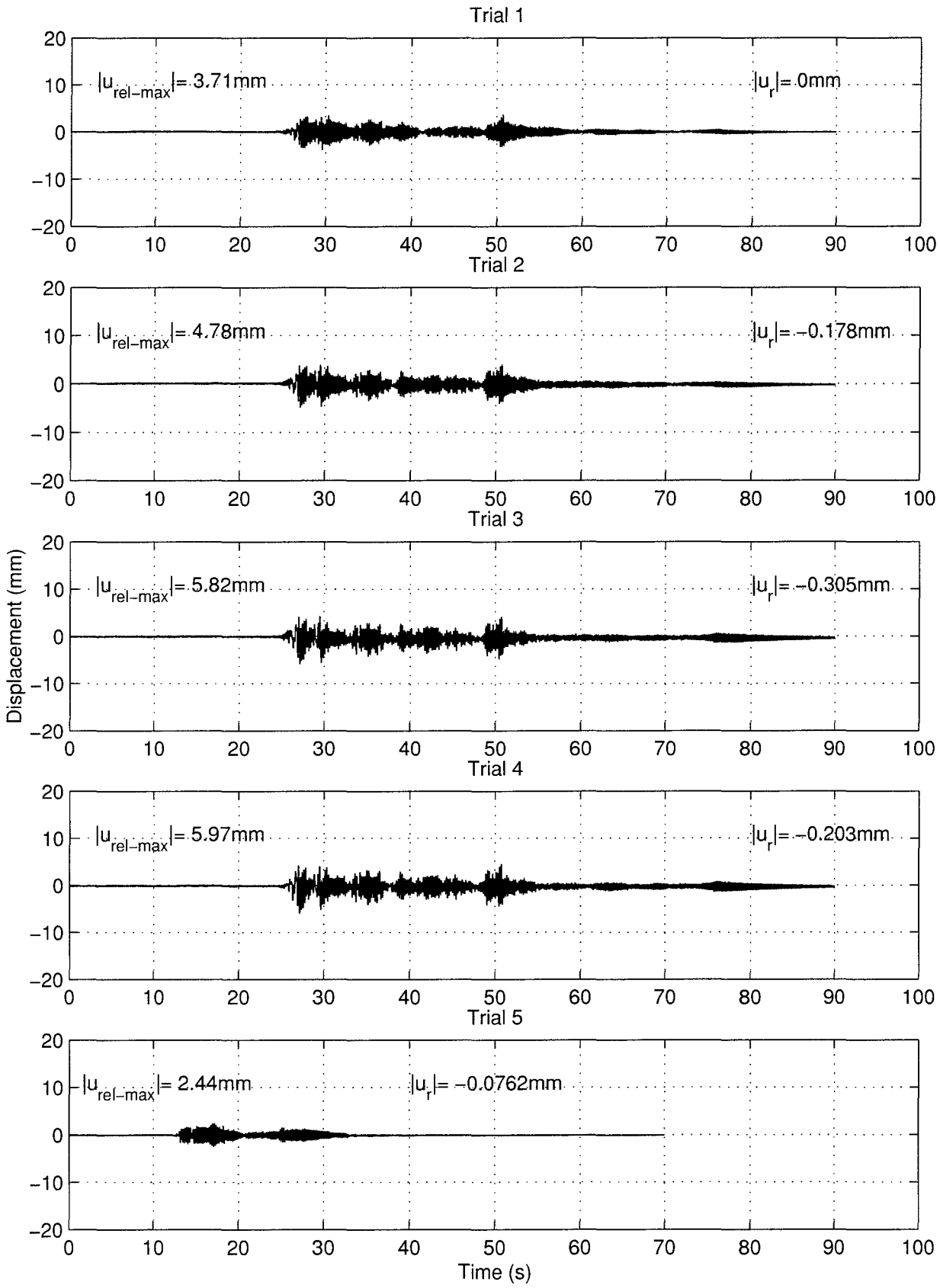

FIGURE 4–13 Specimen 1 – Progressive Displacement Time Histories

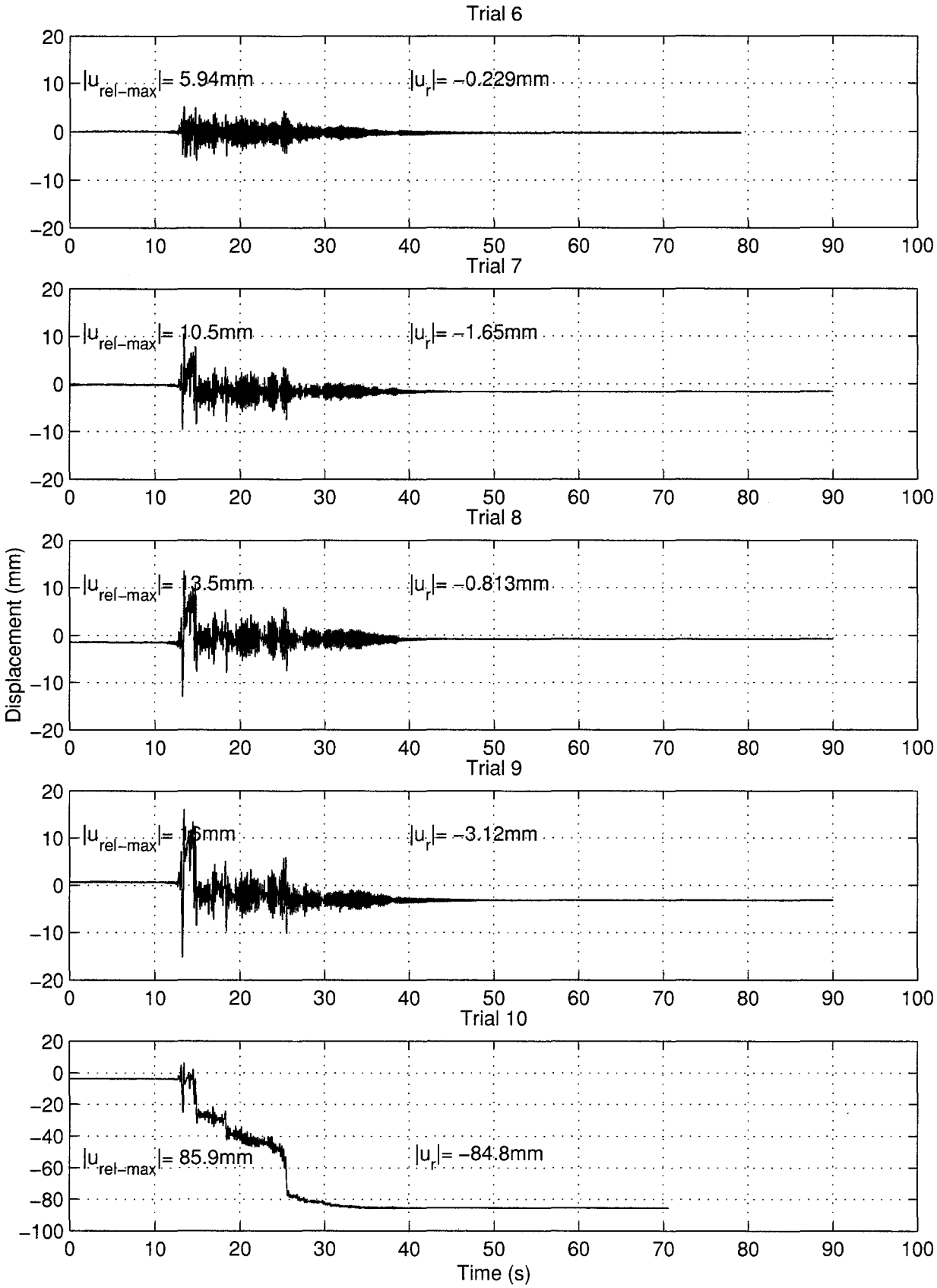

FIGURE 4–13 (cont'd) Specimen 1 – Progressive Displacement Time Histories

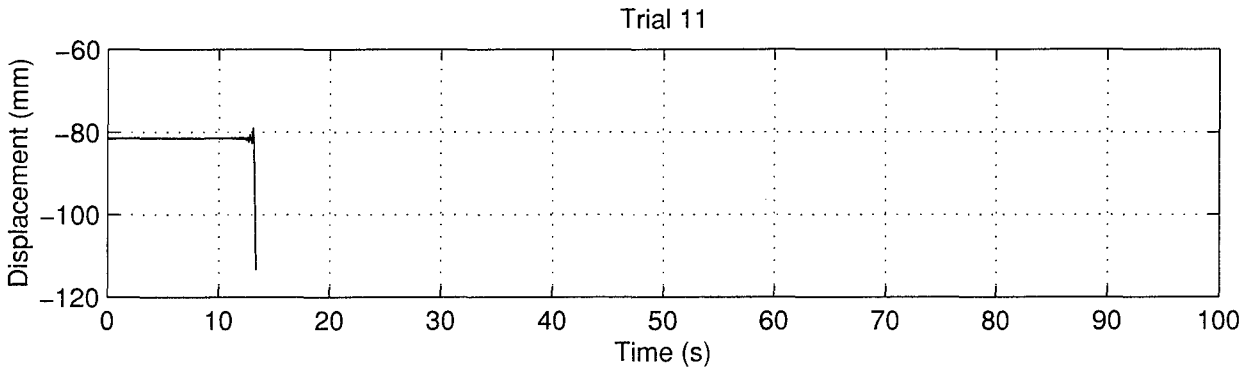

FIGURE 4–13 (cont'd) Specimen 1 – Progressive Displacement Time Histories

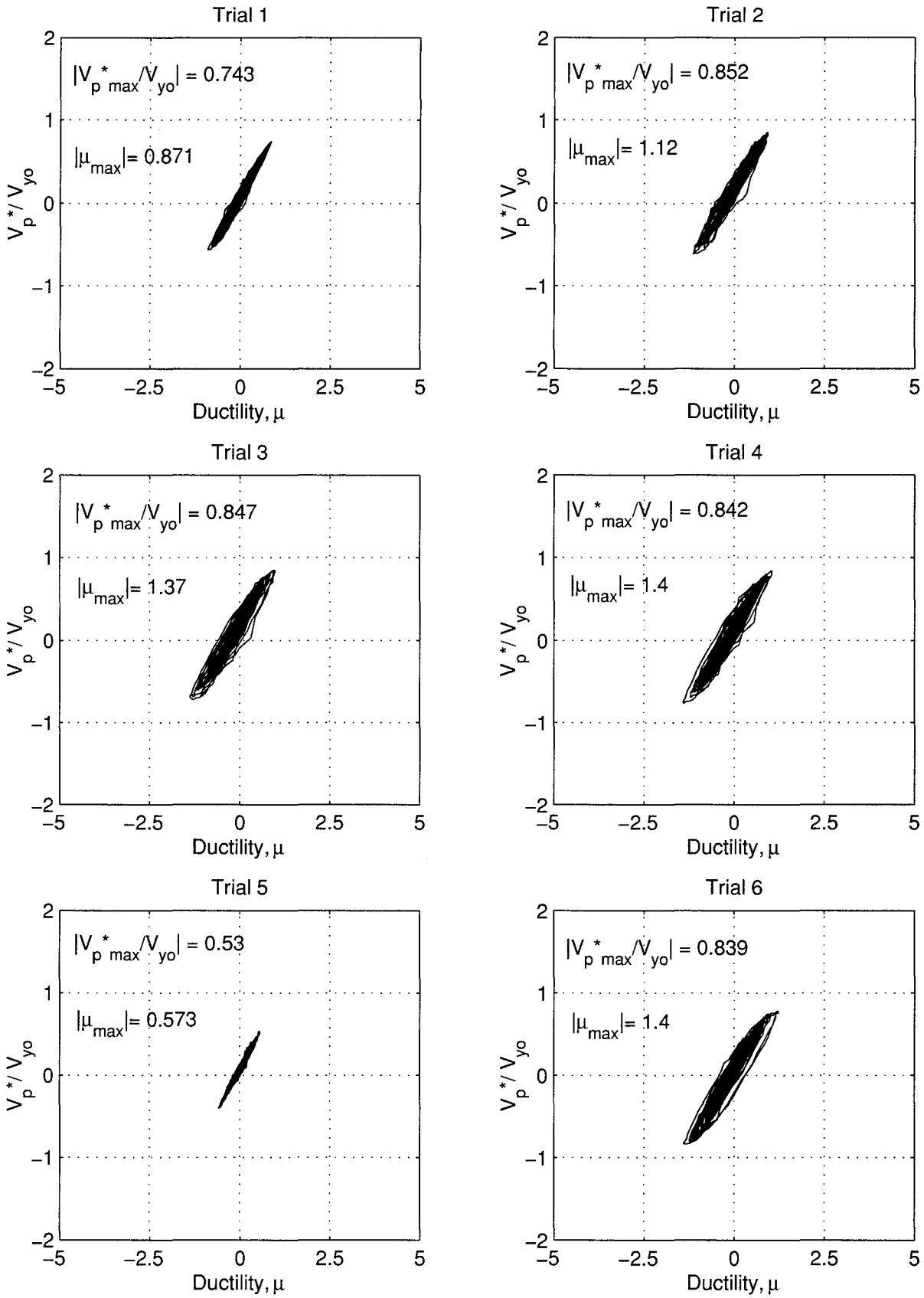

FIGURE 4-14 Specimen 1 – Normalized Base Shear vs. Ductility

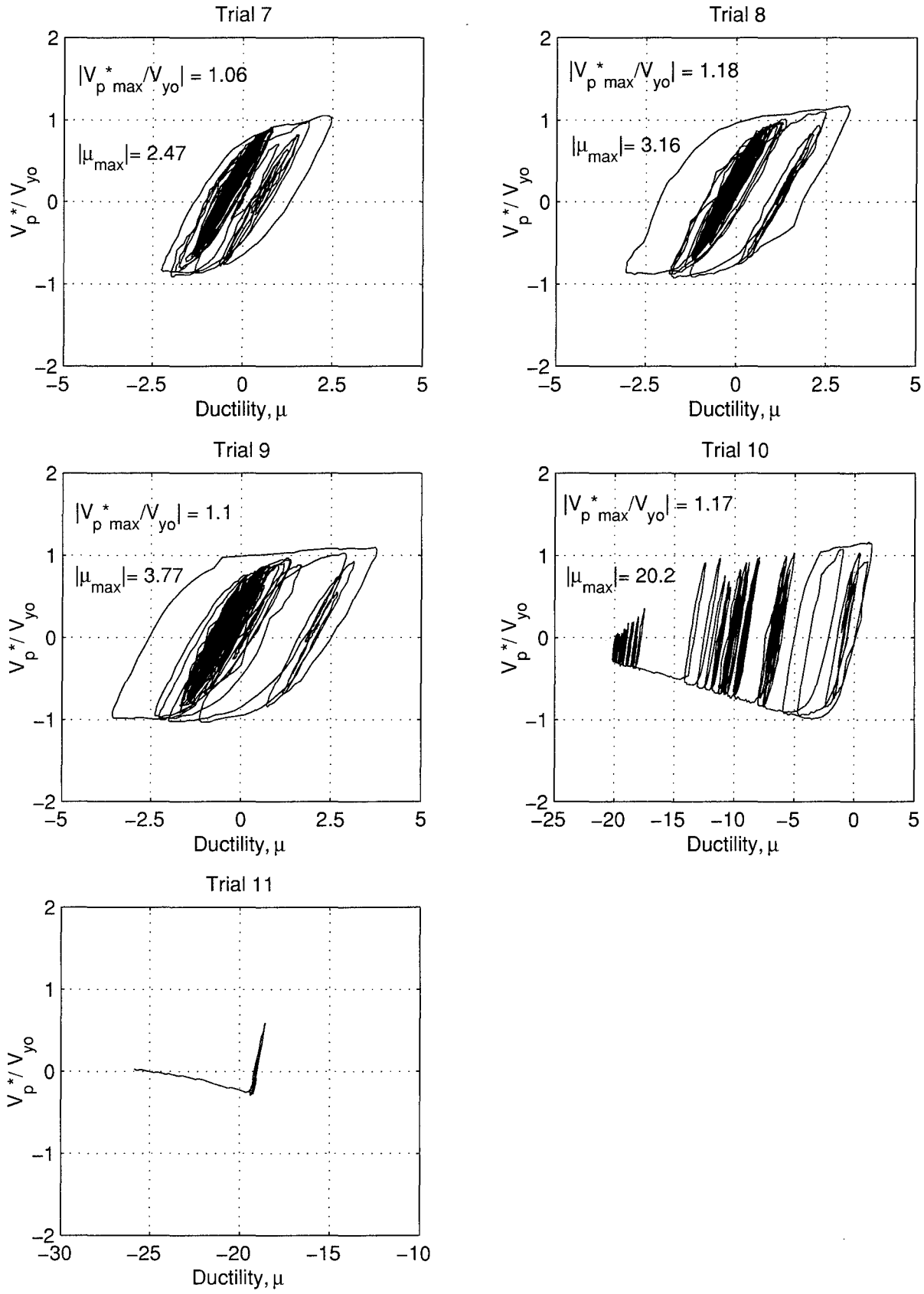

FIGURE 4–14 (cont'd) Specimen 1 – Normalized Base Shear vs. Ductility

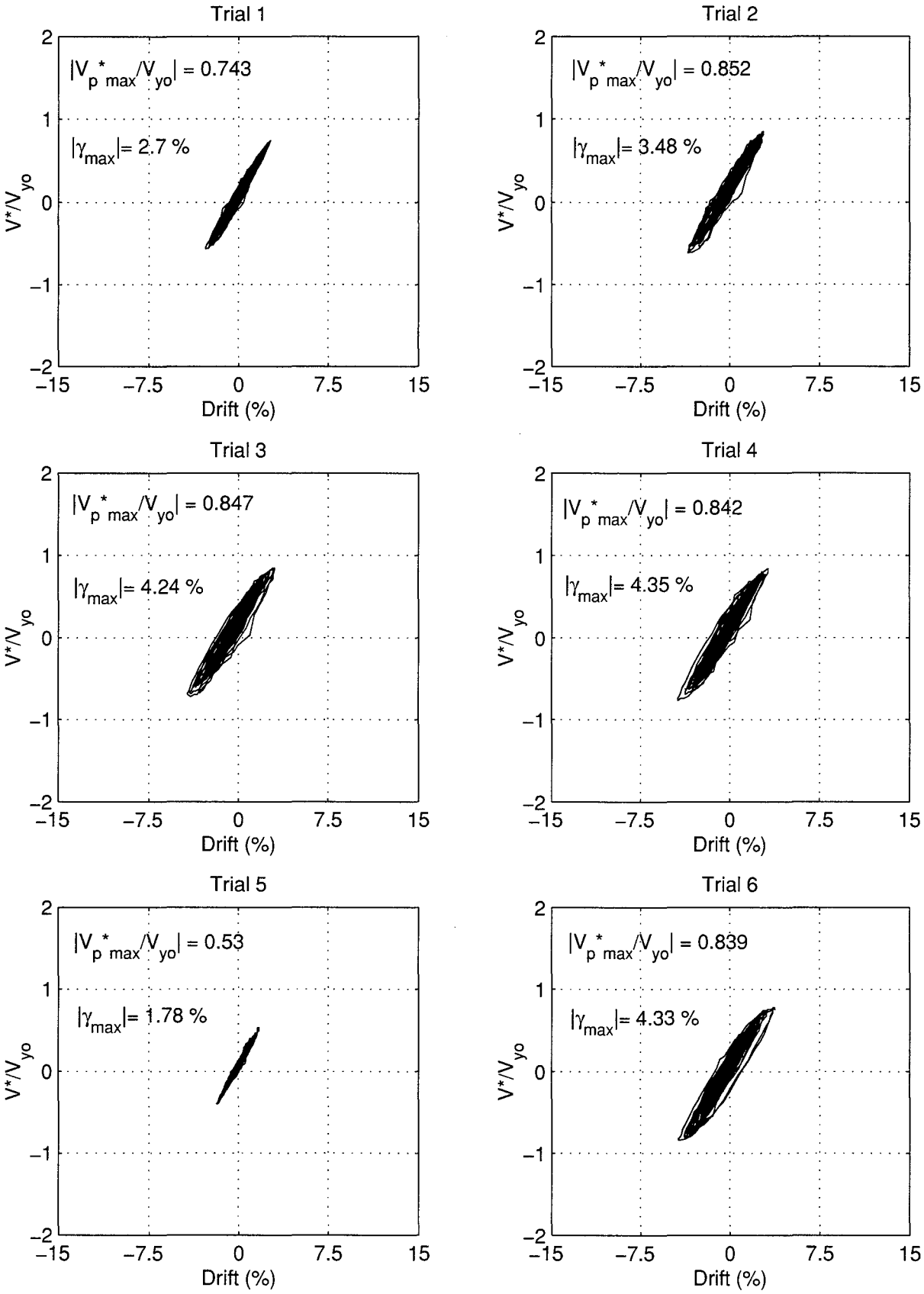

FIGURE 4–15 Specimen 1 – Normalized Base Shear vs. Drift

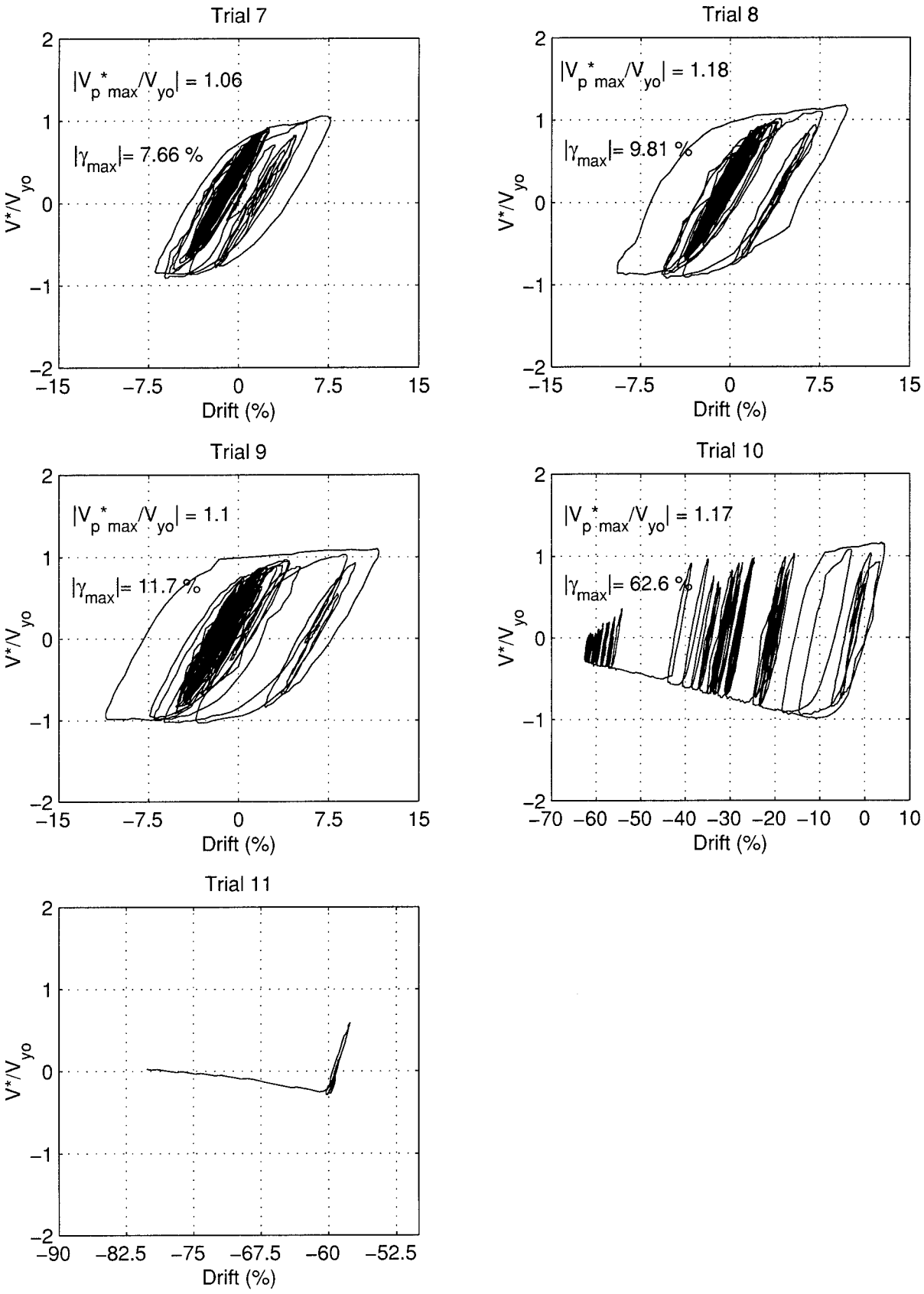

FIGURE 4–15 (cont'd) Specimen 1 – Normalized Base Shear vs. Drift

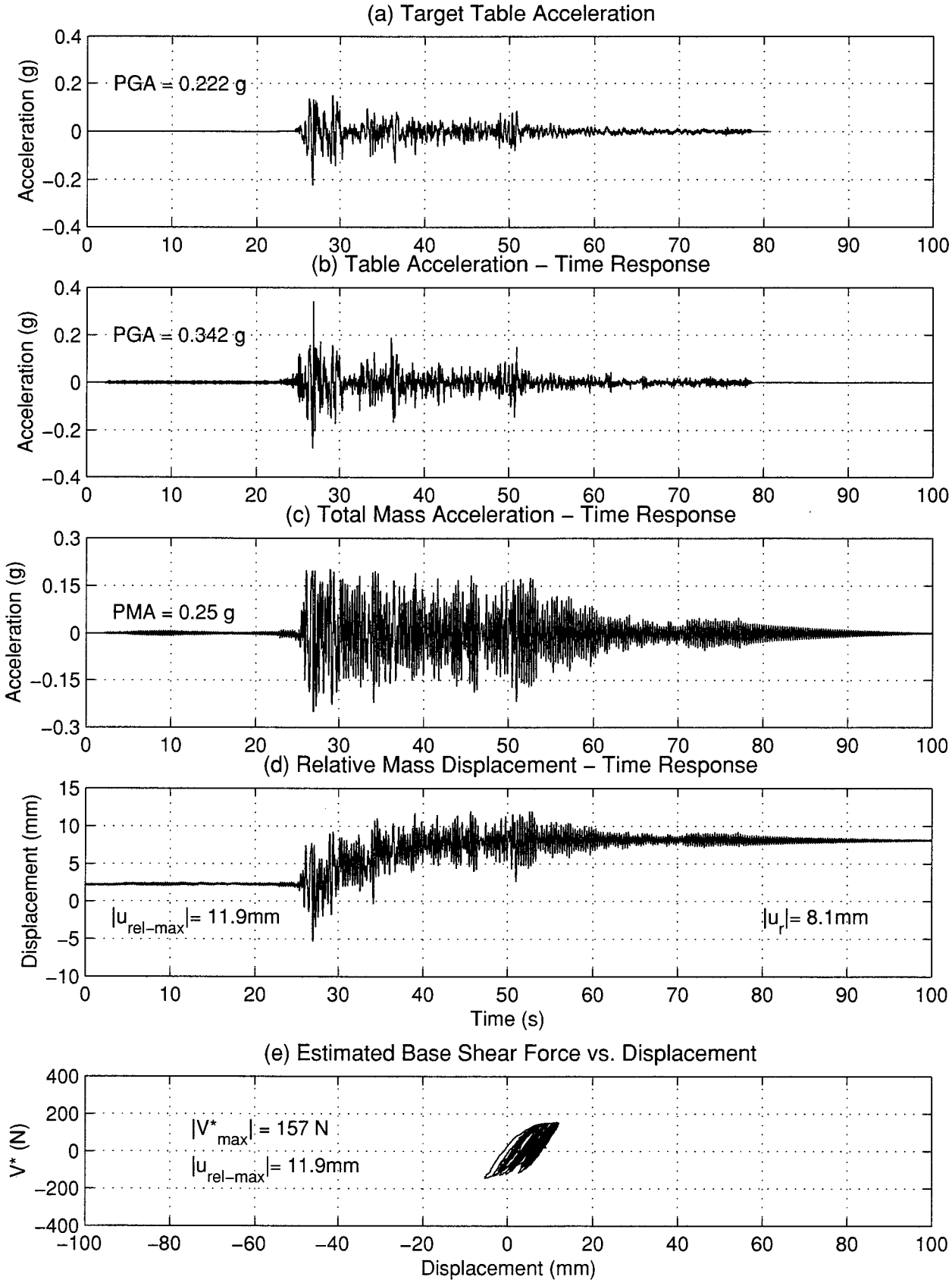

FIGURE 4–16 Seismic Response of Specimen 2 – Trial 9

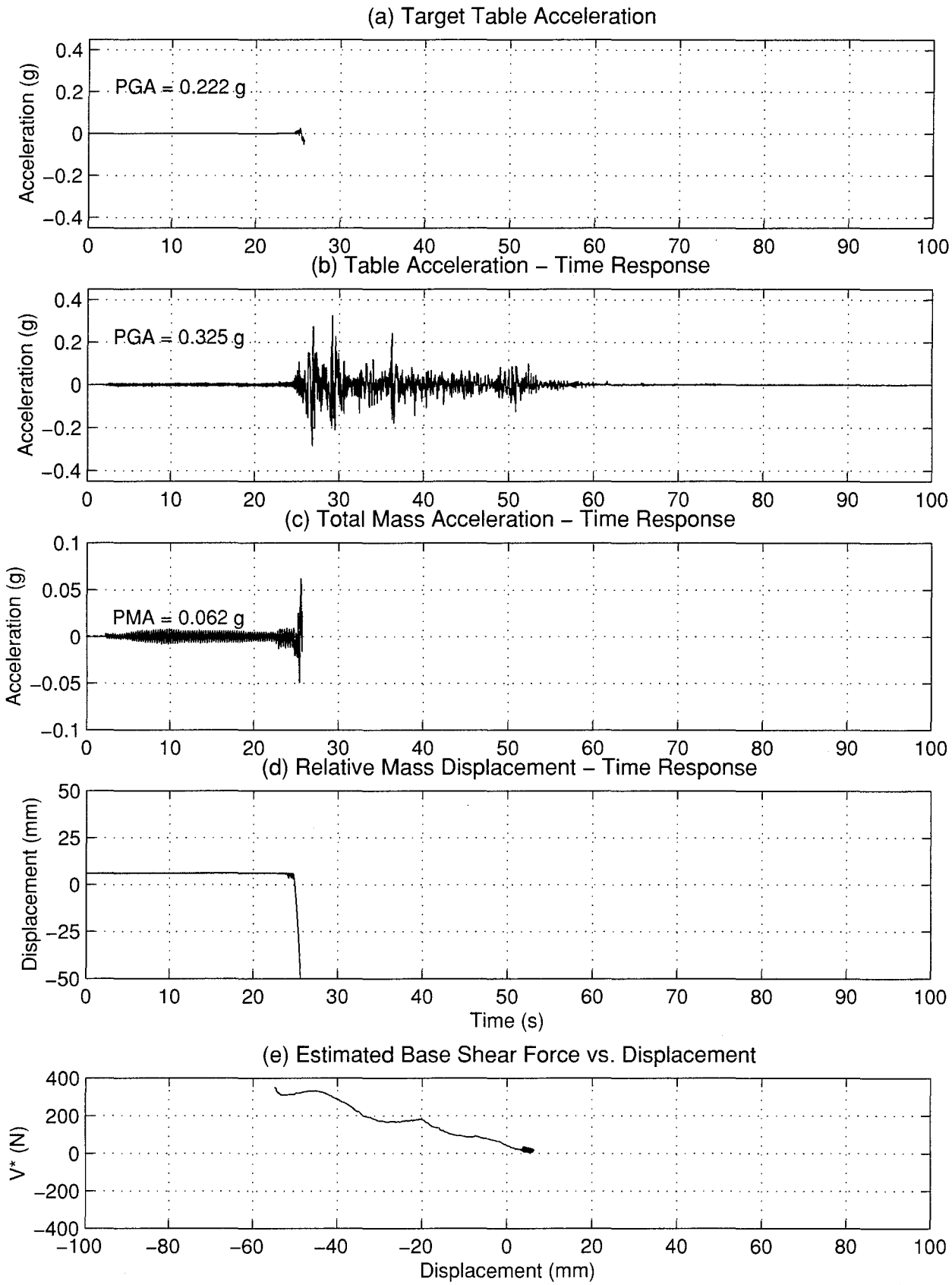

FIGURE 4–17 Seismic Response of Specimen 2 – Trial 10

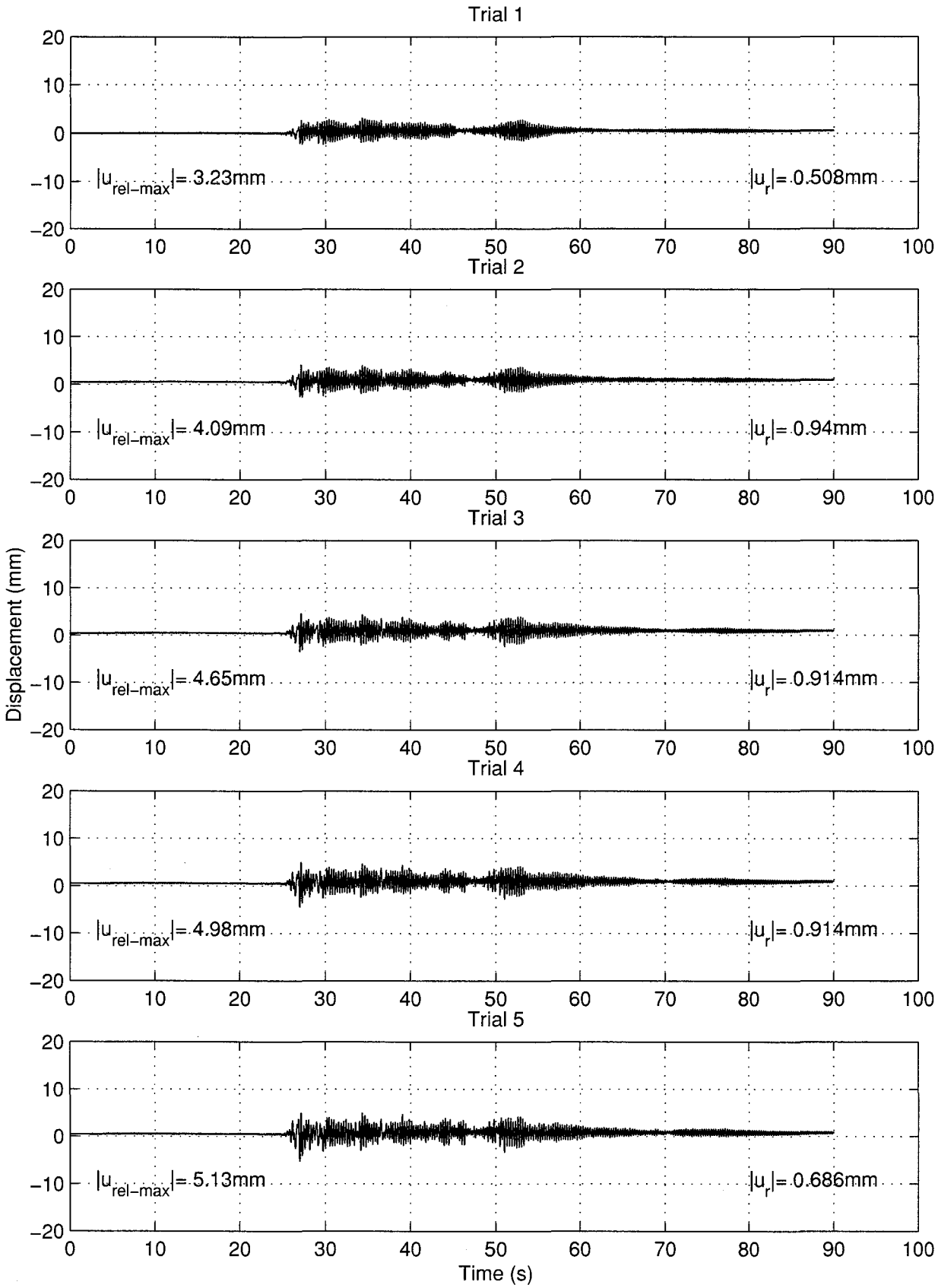

FIGURE 4–18 Specimen 2 – Progressive Displacement Time Histories

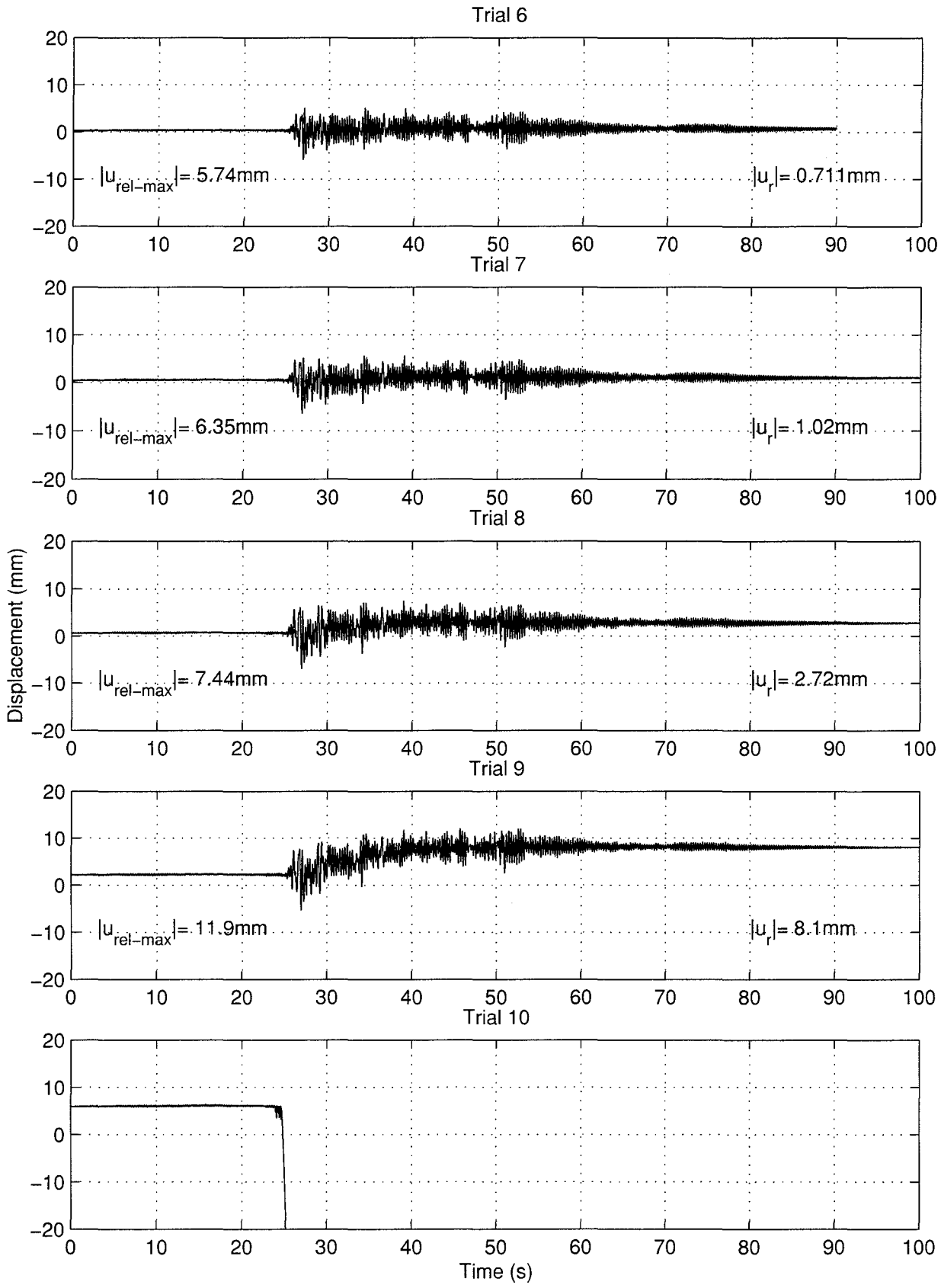

FIGURE 4–18 (cont'd) Specimen 2 – Progressive Displacement Time Histories

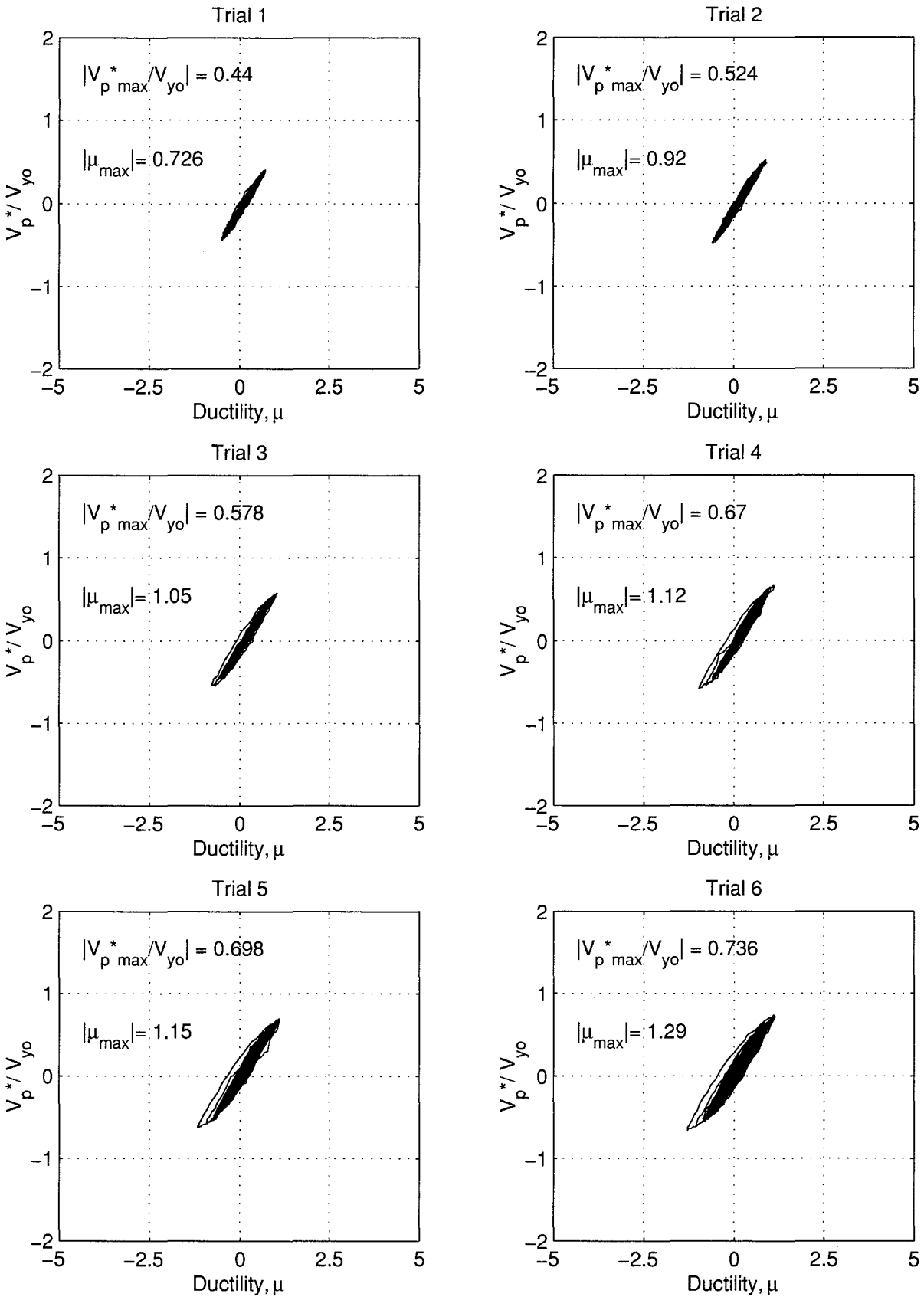

FIGURE 4–19 Specimen 2 – Normalized Base Shear vs. Ductility

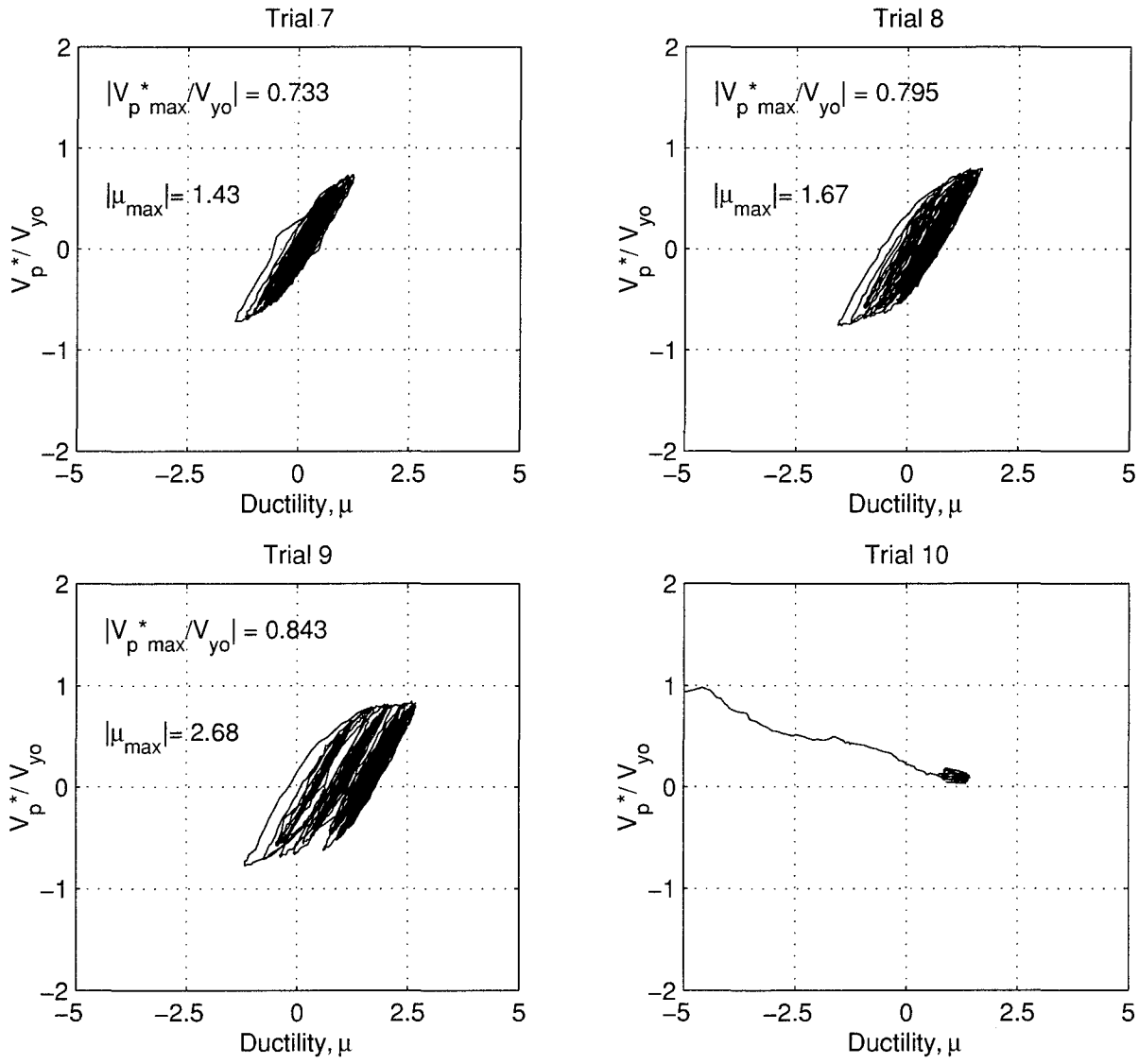

FIGURE 4–19 (cont'd) Specimen 2 – Normalized Base Shear vs. Ductility

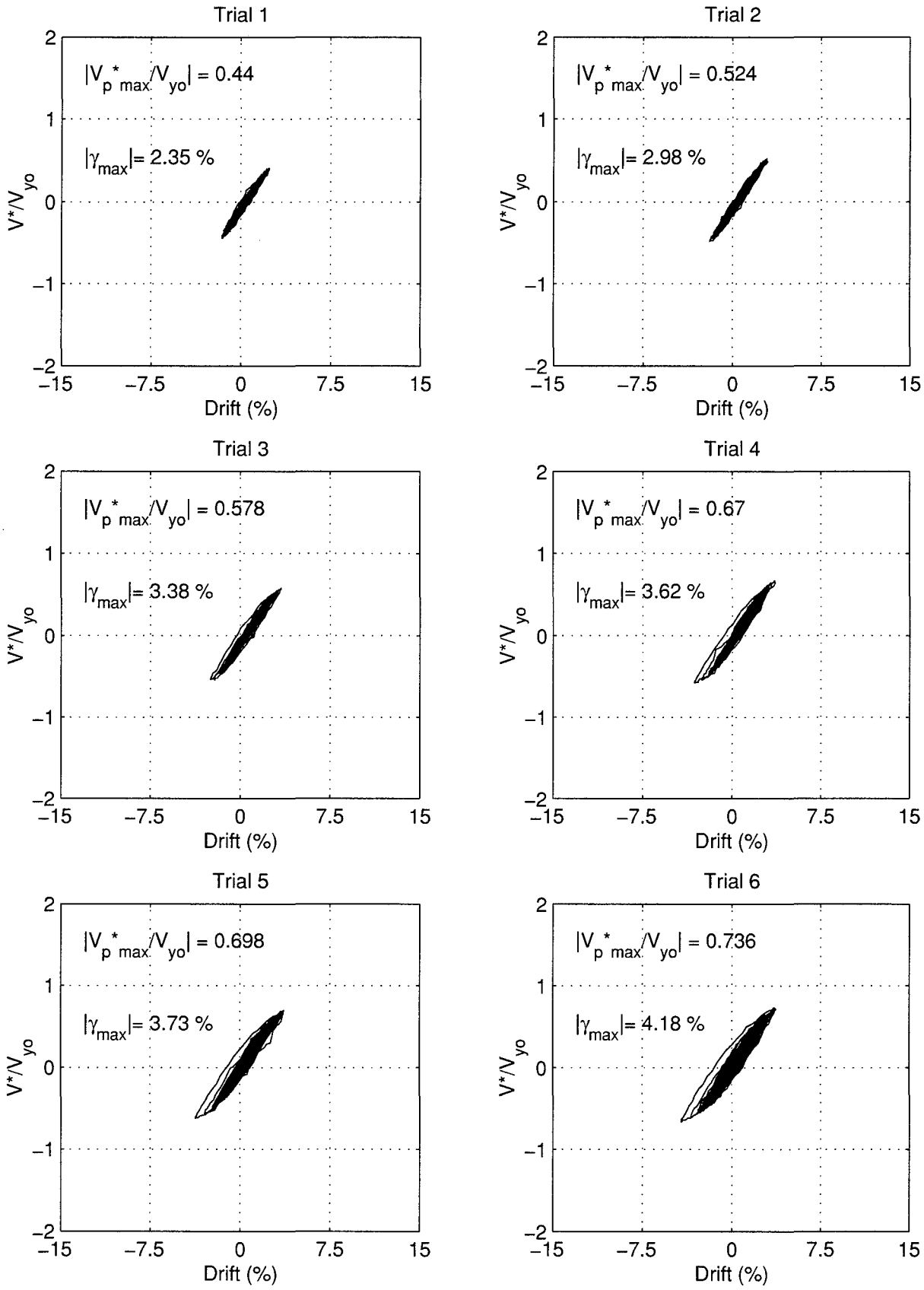

FIGURE 4–20 Specimen 2 – Normalized Base Shear vs. Drift

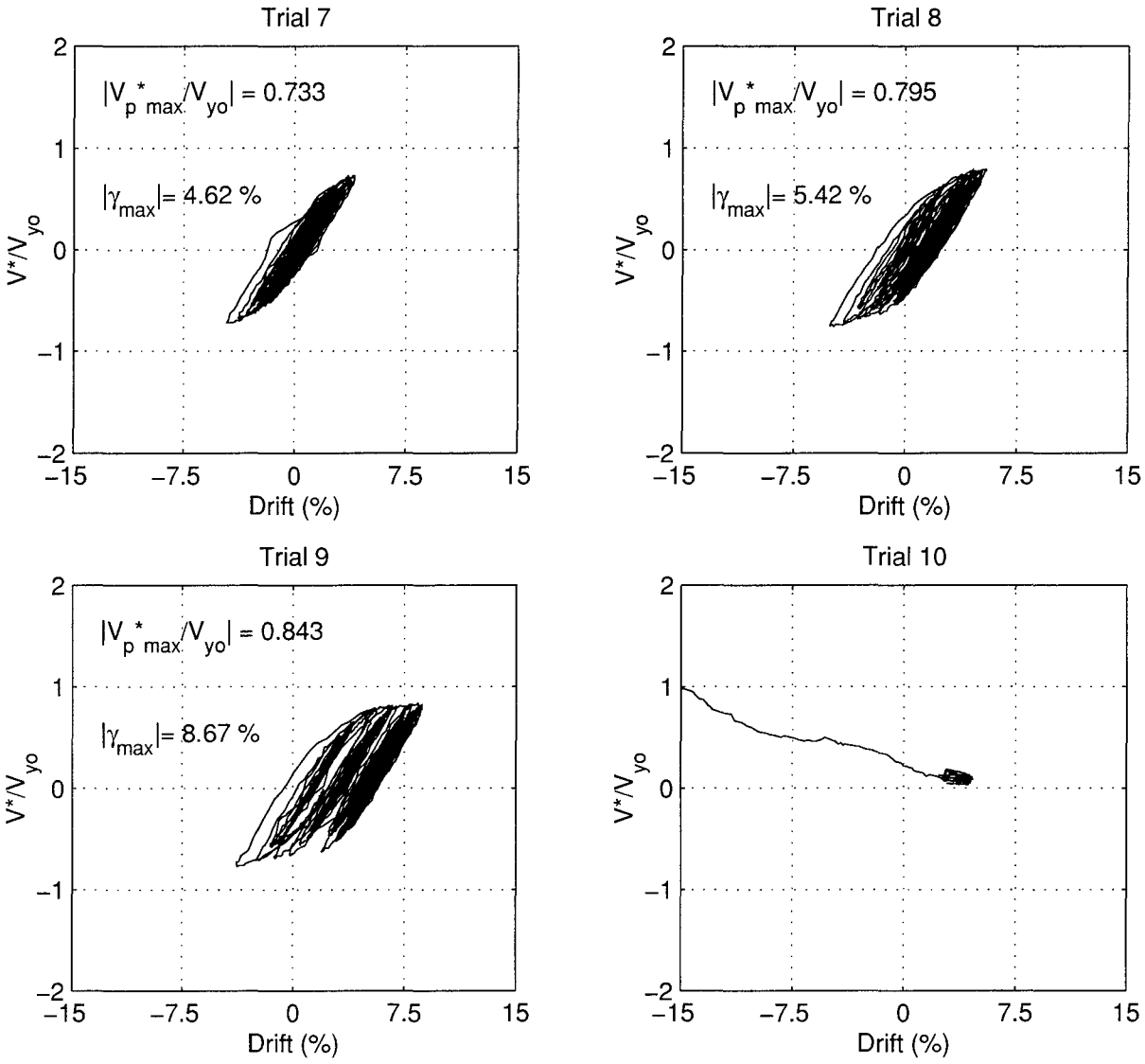

FIGURE 4–20 (cont'd) Specimen 2 – Normalized Base Shear vs. Drift

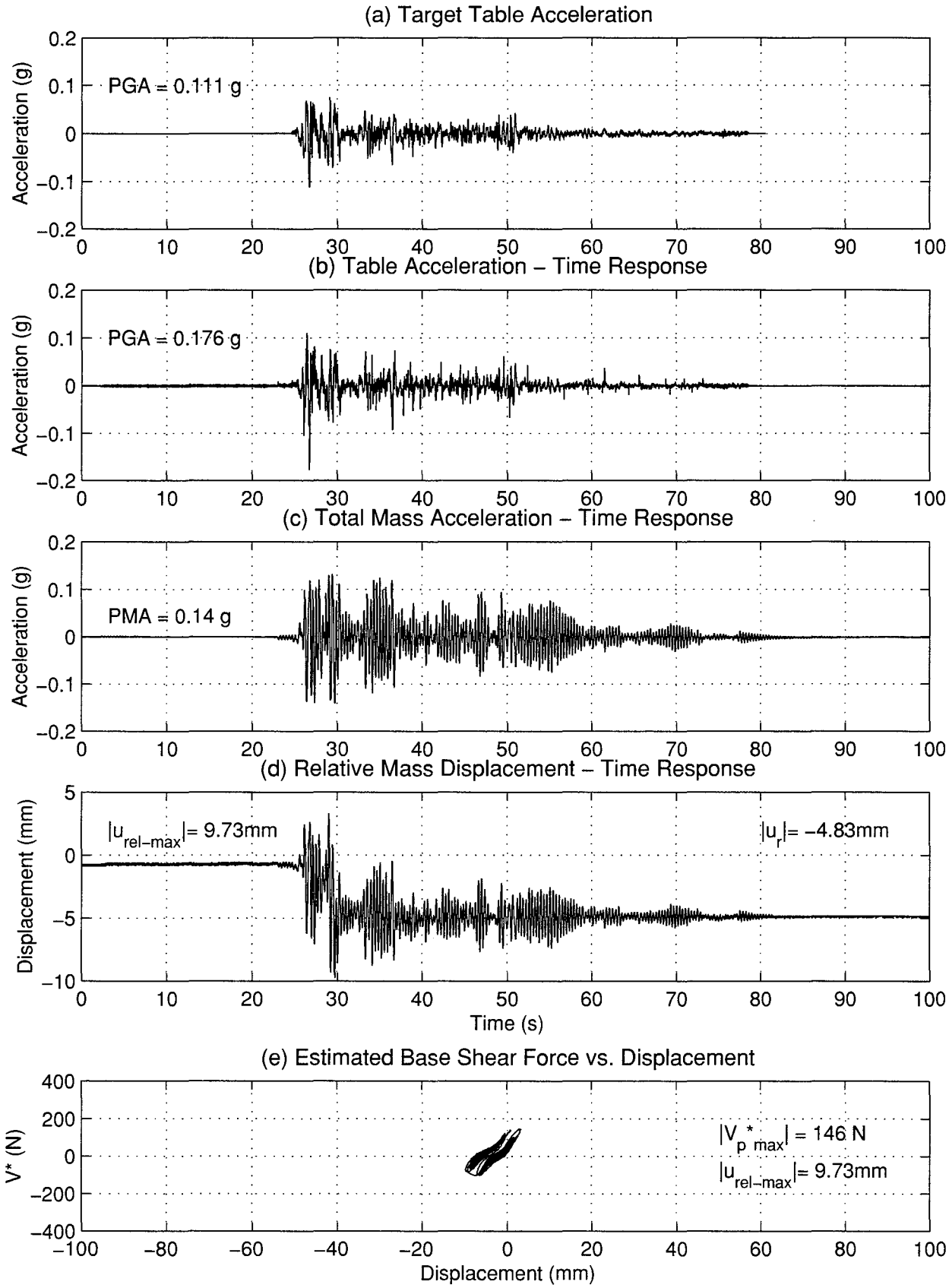

FIGURE 4–21 Seismic Response of Specimen 4 – Trial 5

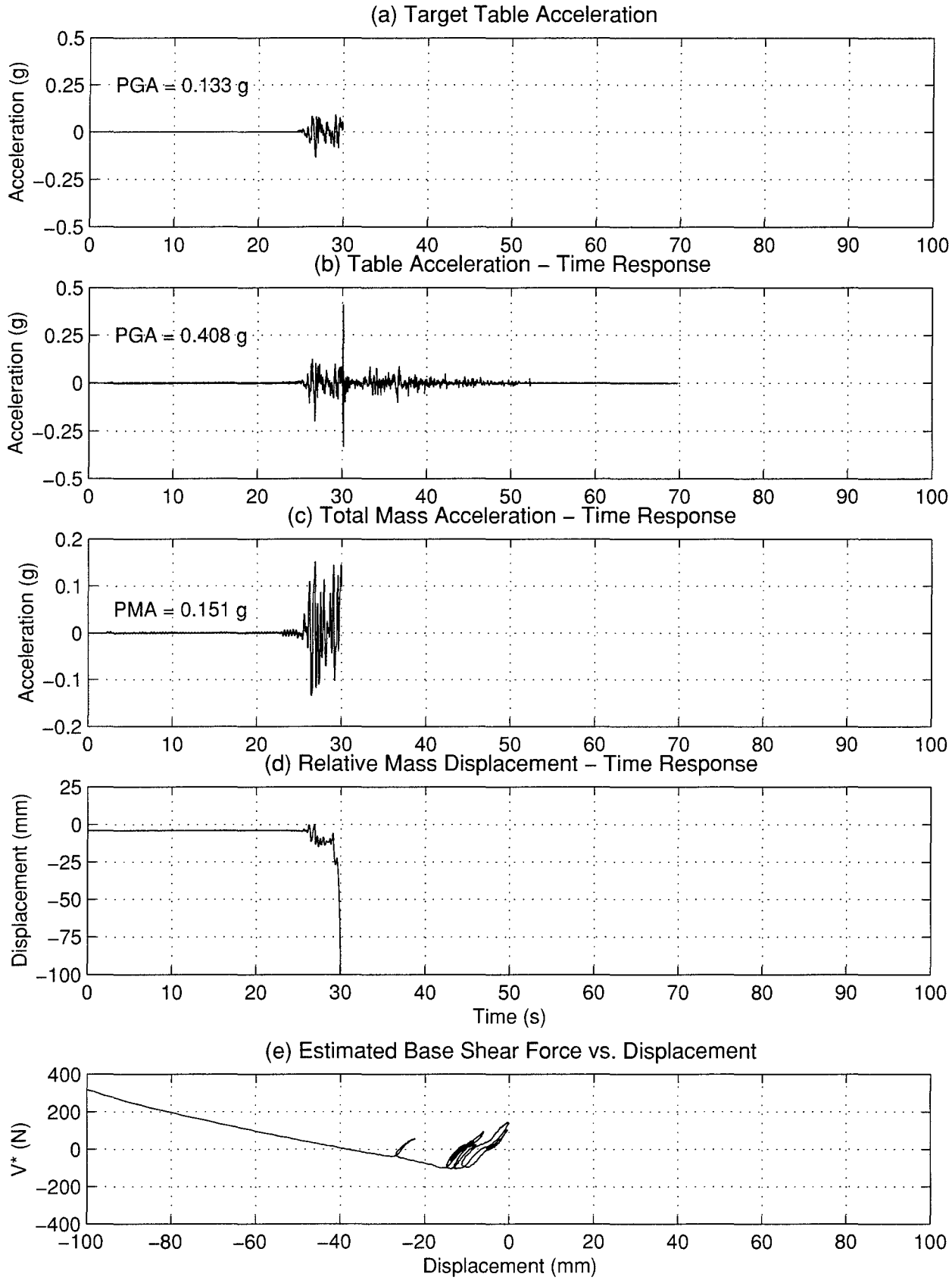

FIGURE 4–22 Seismic Response of Specimen 4 – Trial 6

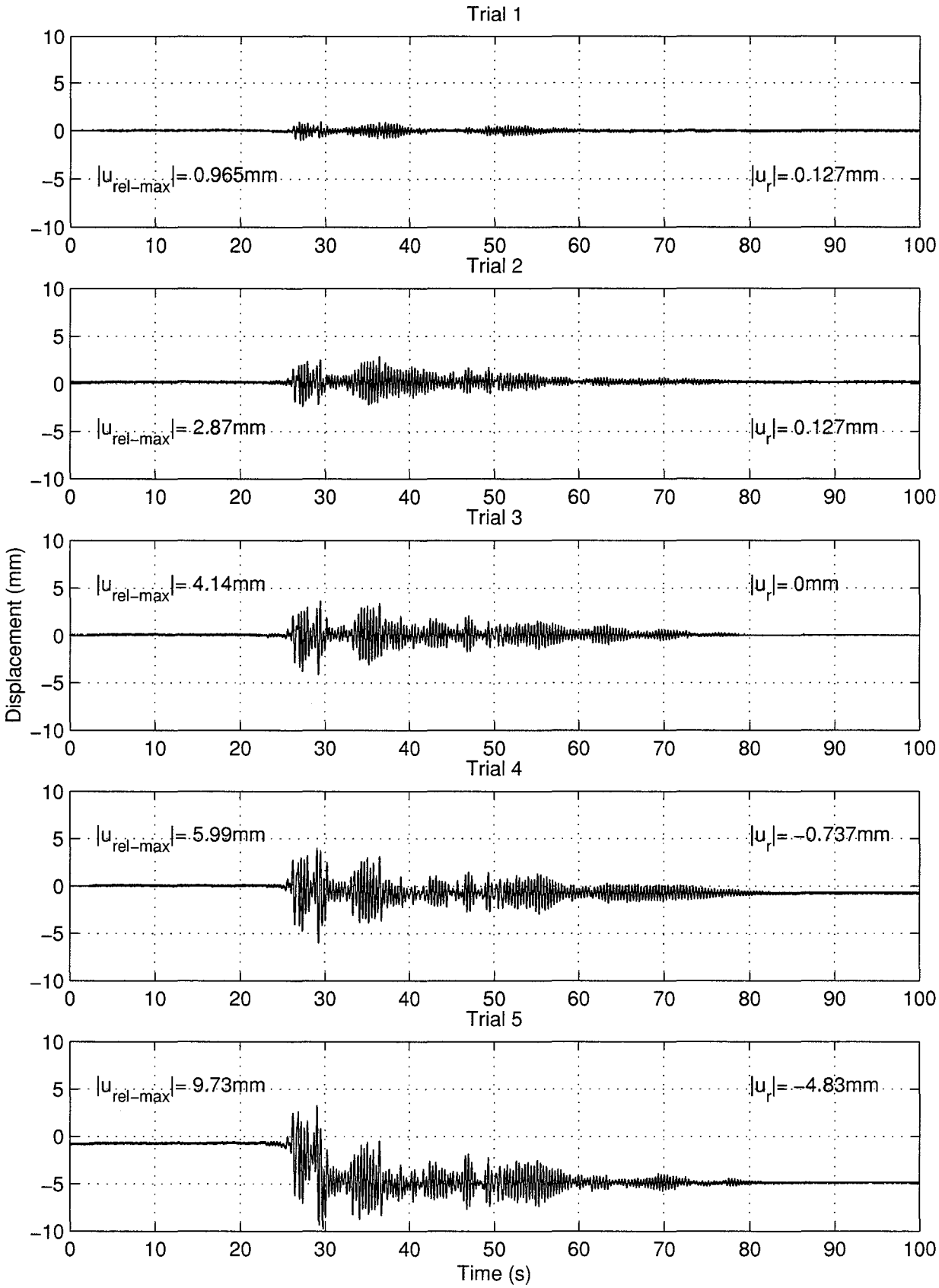

FIGURE 4–23 Specimen 4 – Progressive Displacement Time Histories

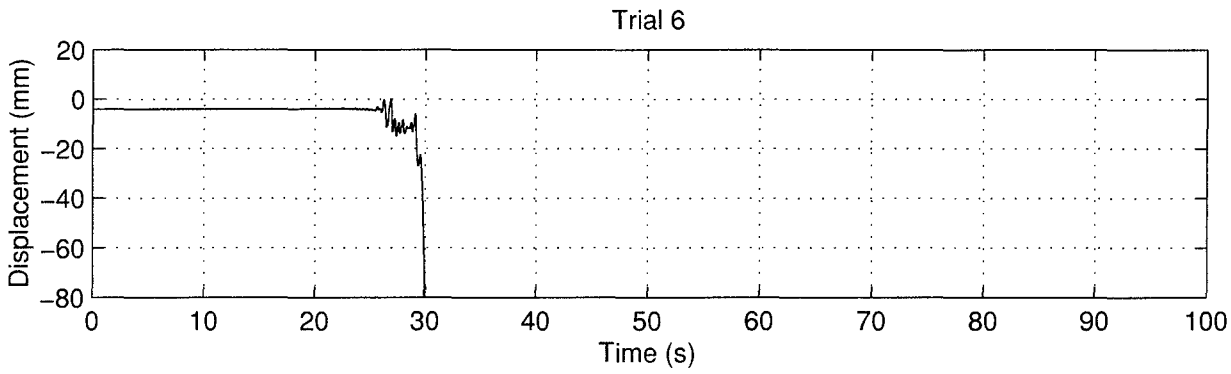

FIGURE 4–23 (cont'd) Specimen 4 – Progressive Displacement Time Histories

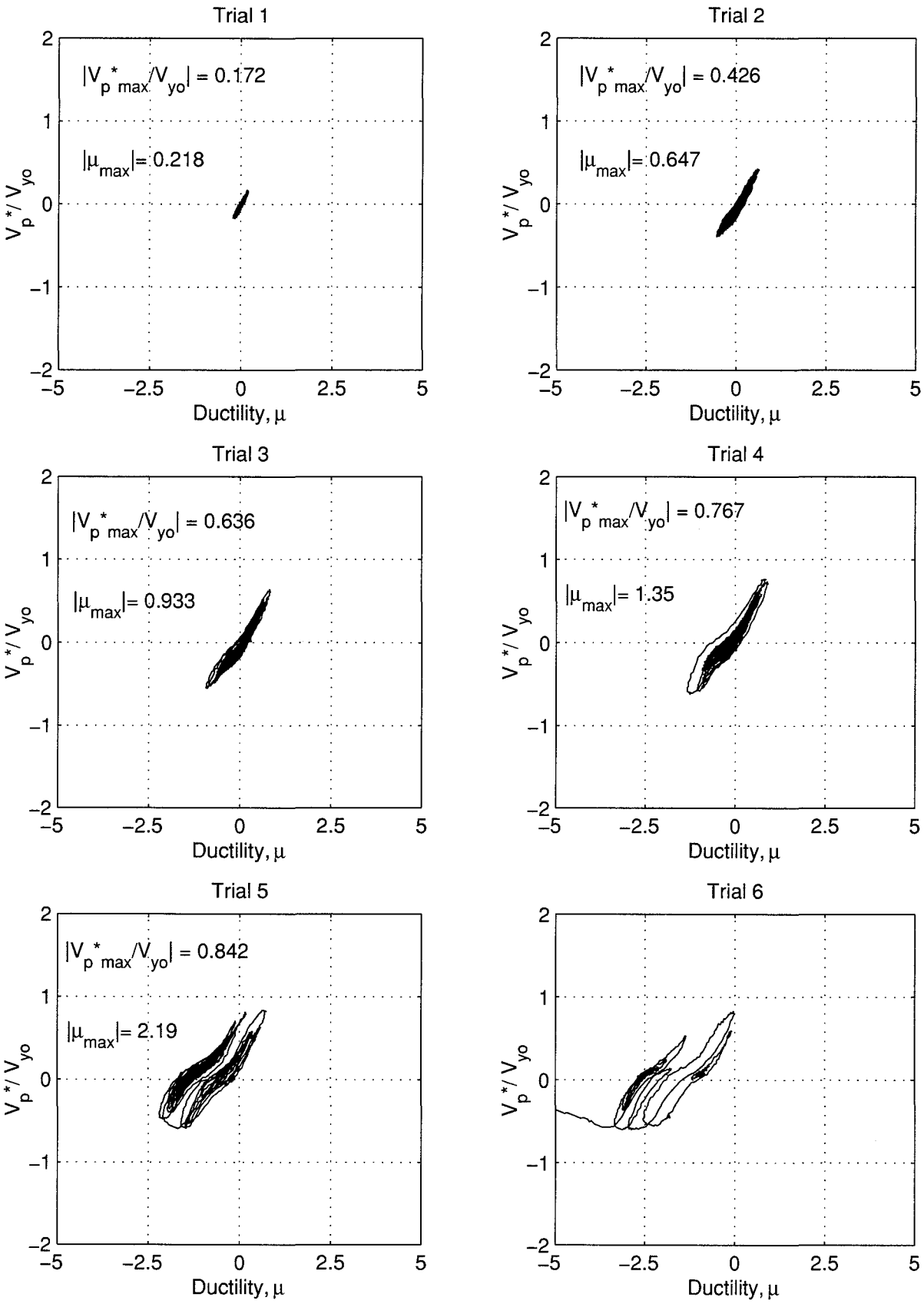

FIGURE 4–24 Specimen 4 – Normalized Base Shear vs. Ductility

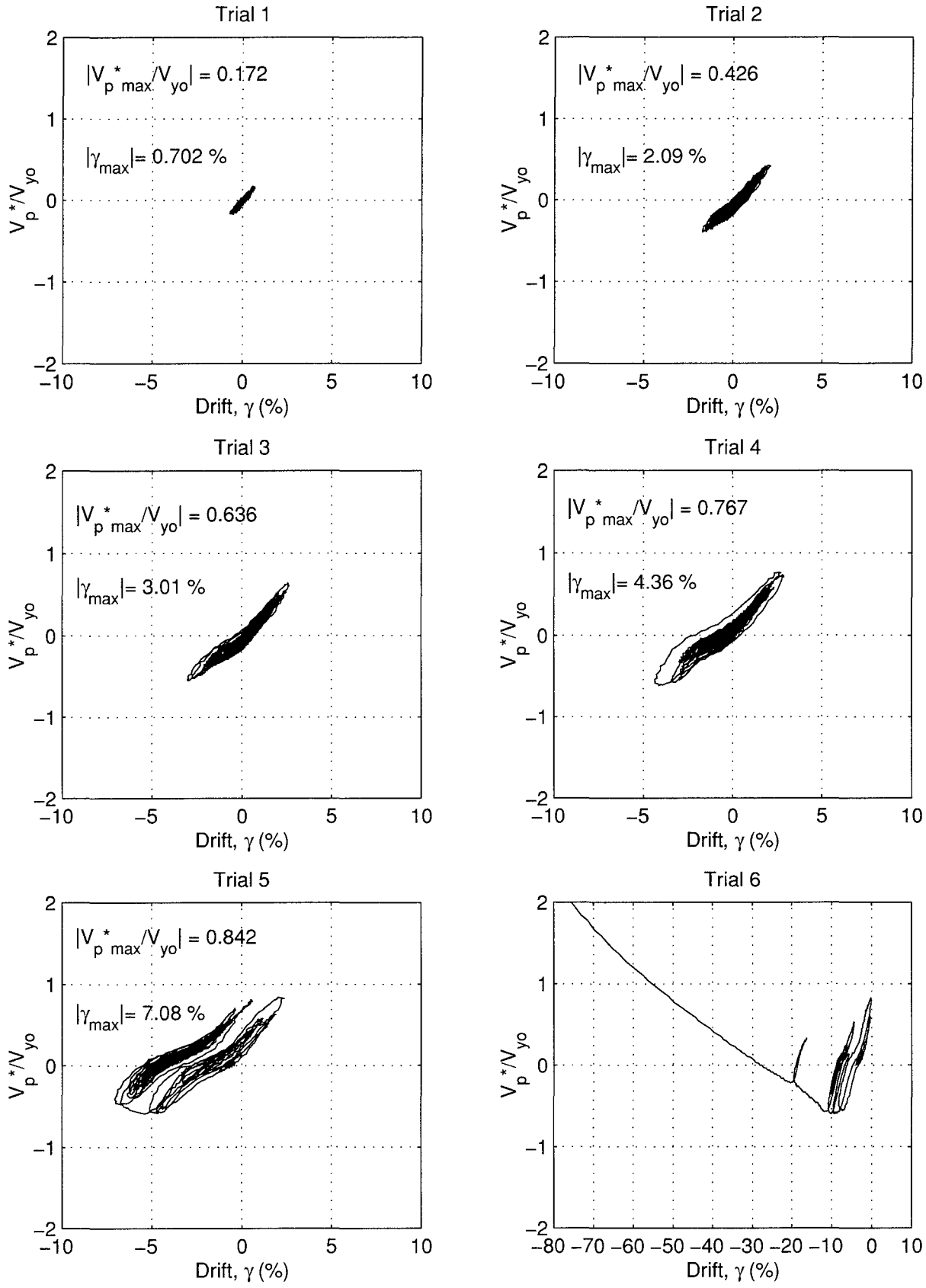

FIGURE 4–25 Specimen 4 – Normalized Base Shear vs. Drift

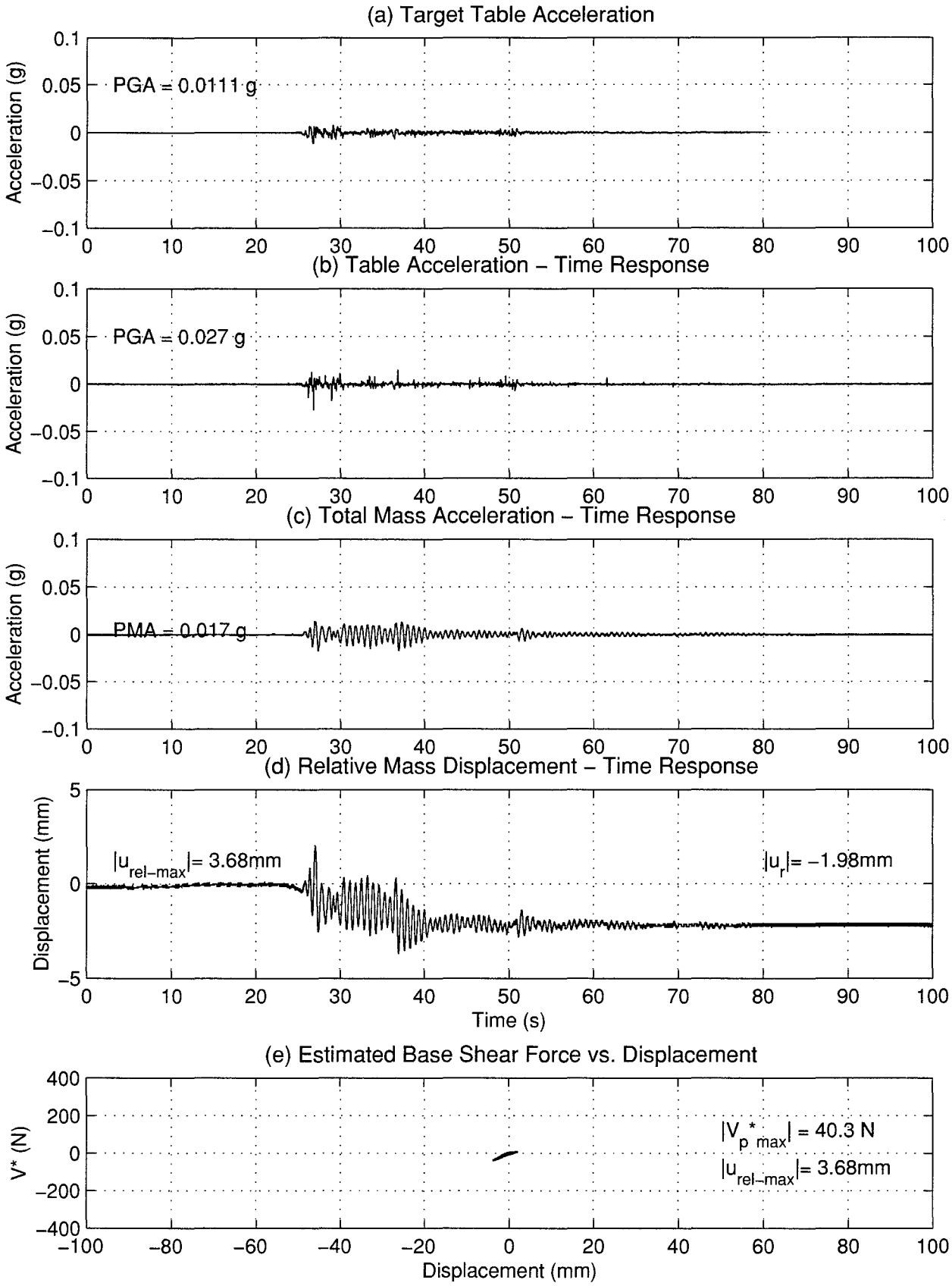

FIGURE 4–26 Seismic Response of Specimen 5b – Trial 1

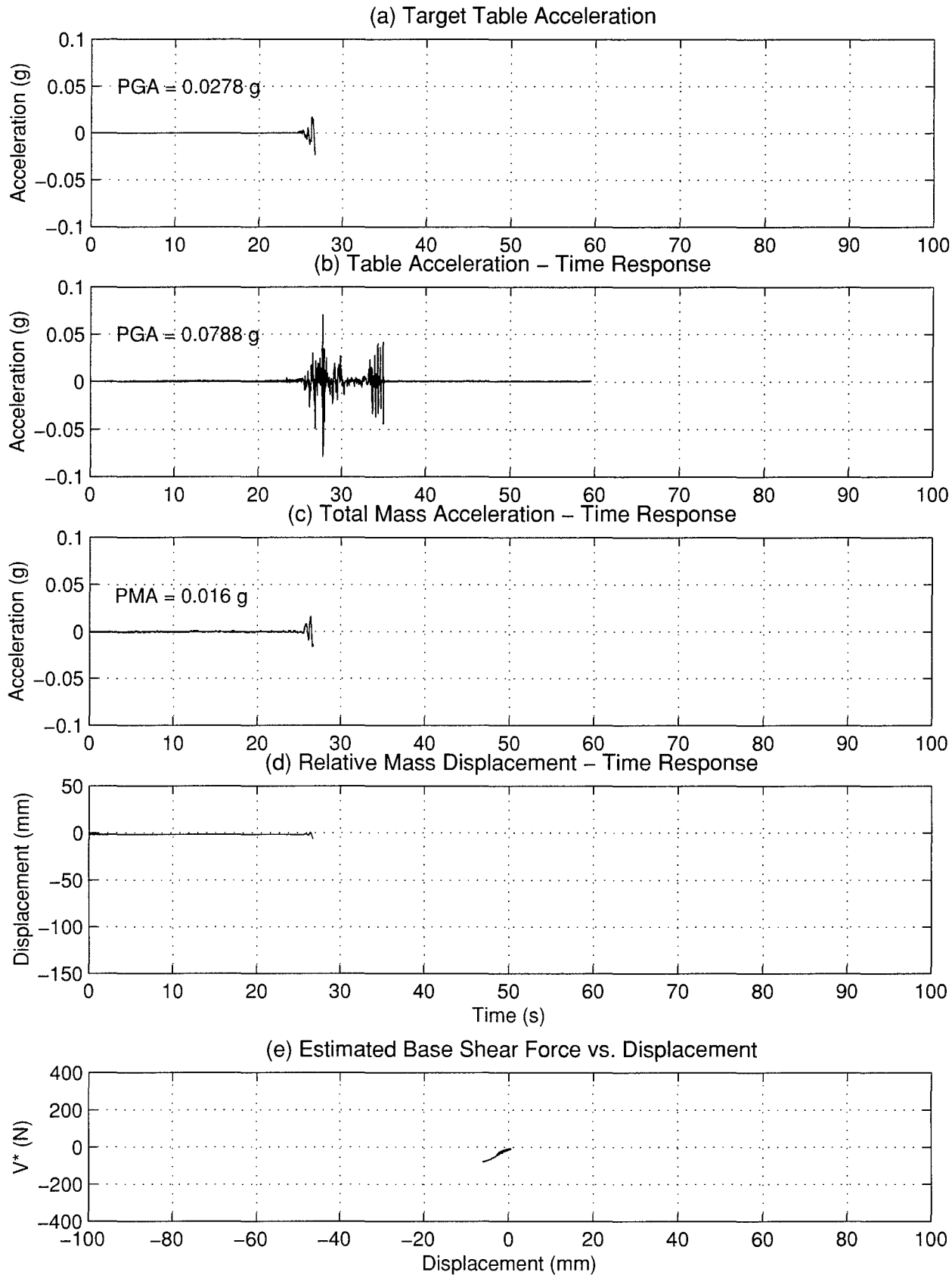

FIGURE 4–27 Seismic Response of Specimen 5b – Trial 2

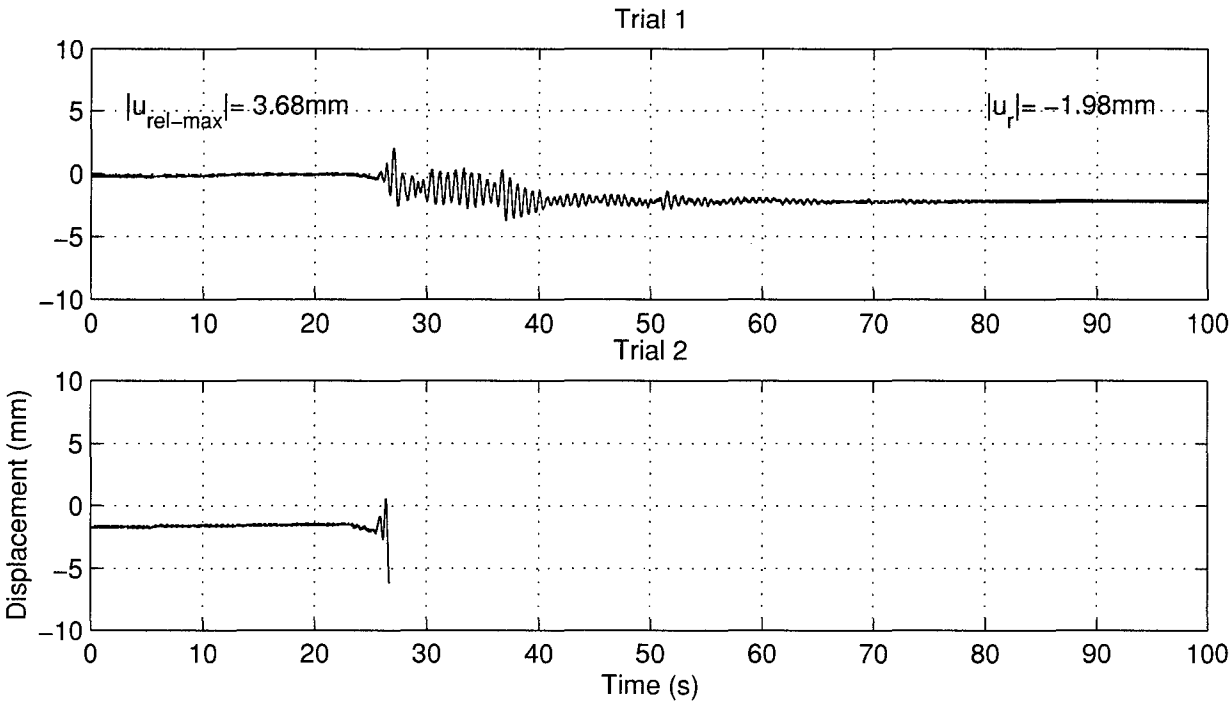

FIGURE 4–28 Specimen 5b – Progressive Displacement Time Histories

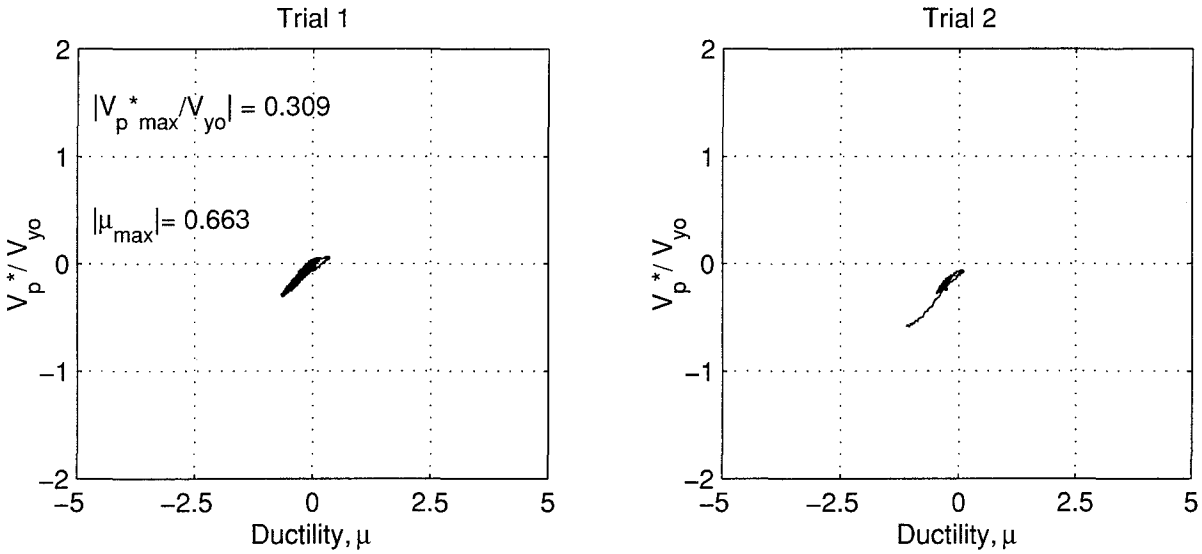

FIGURE 4–29 Specimen 5b – Normalized Base Shear vs. Ductility

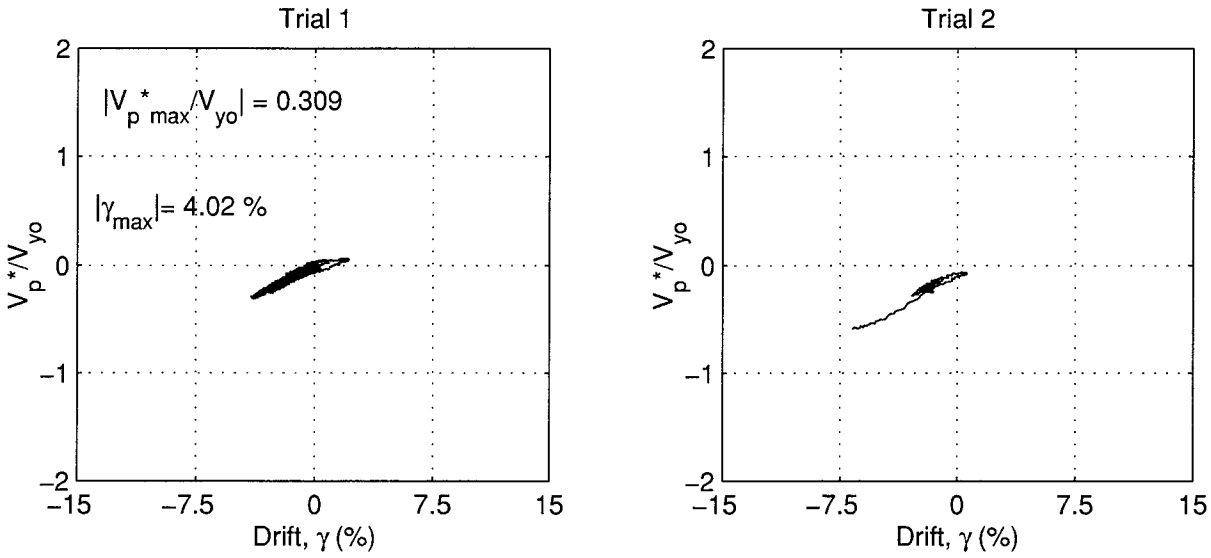

FIGURE 4–30 Specimen 5b – Normalized Base Shear vs. Drift

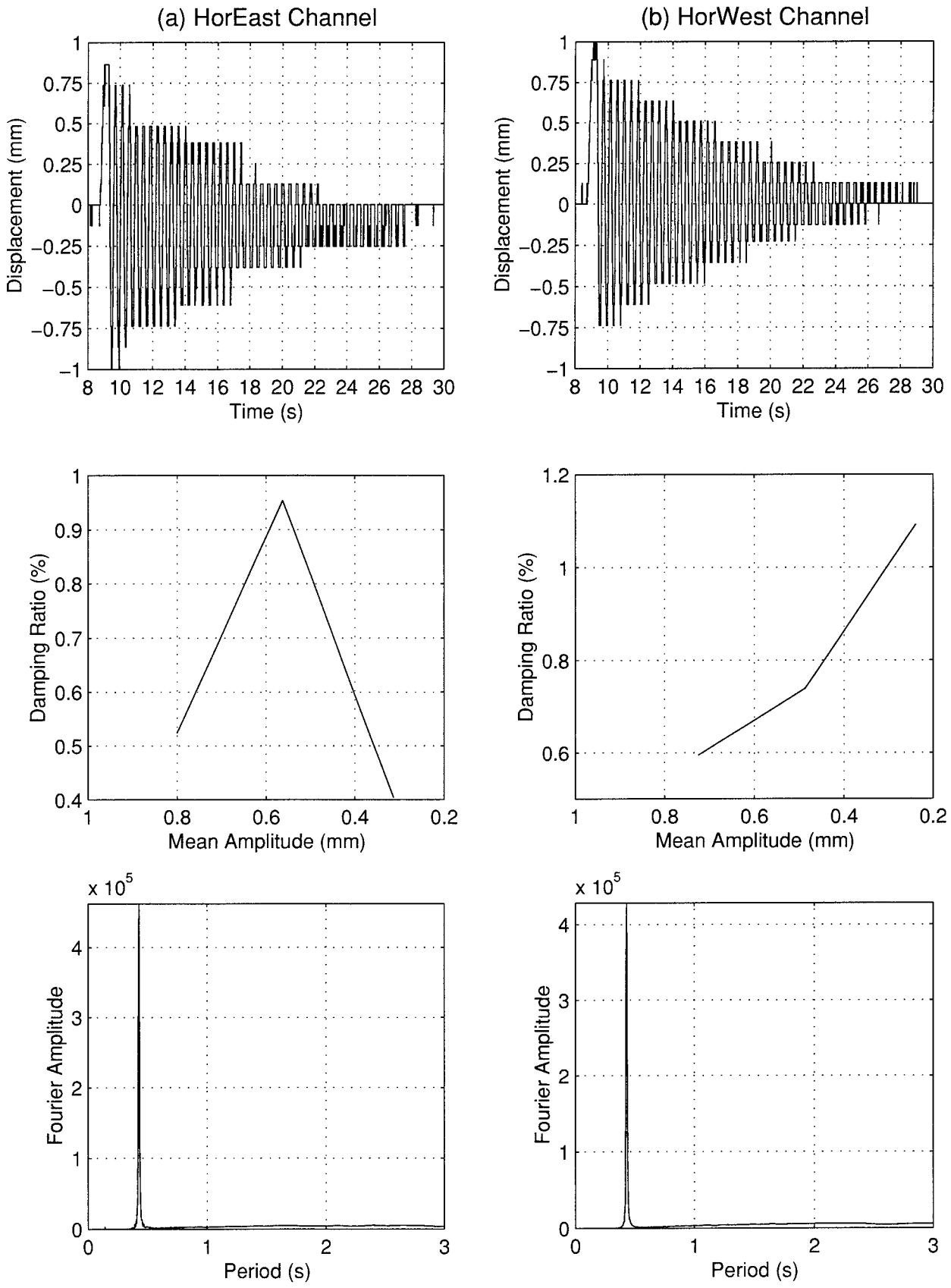

FIGURE 4-31 Free Vibration Test of Specimen6

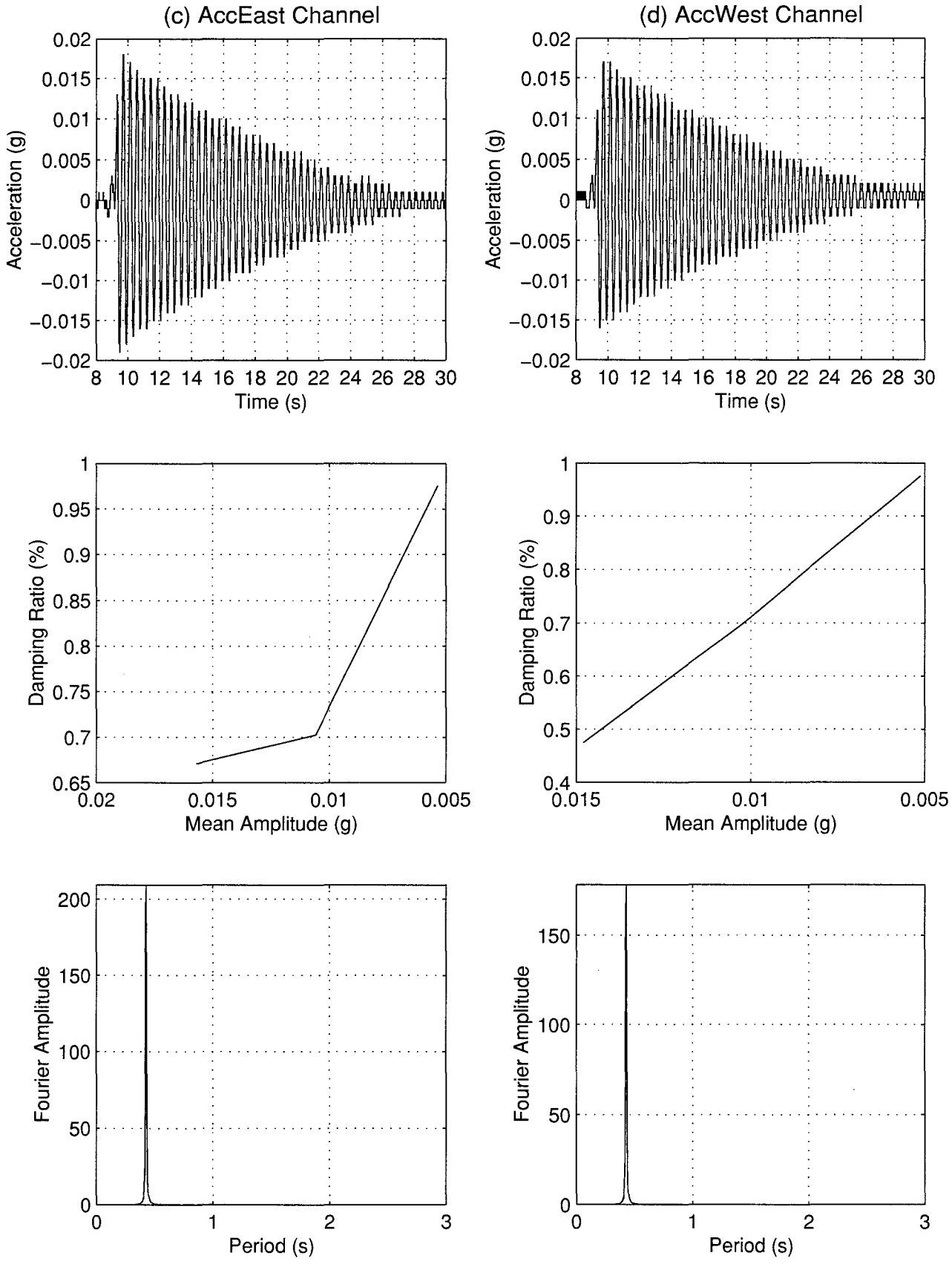

FIGURE 4–31 (cont'd) Free Vibration Test of Specimen6

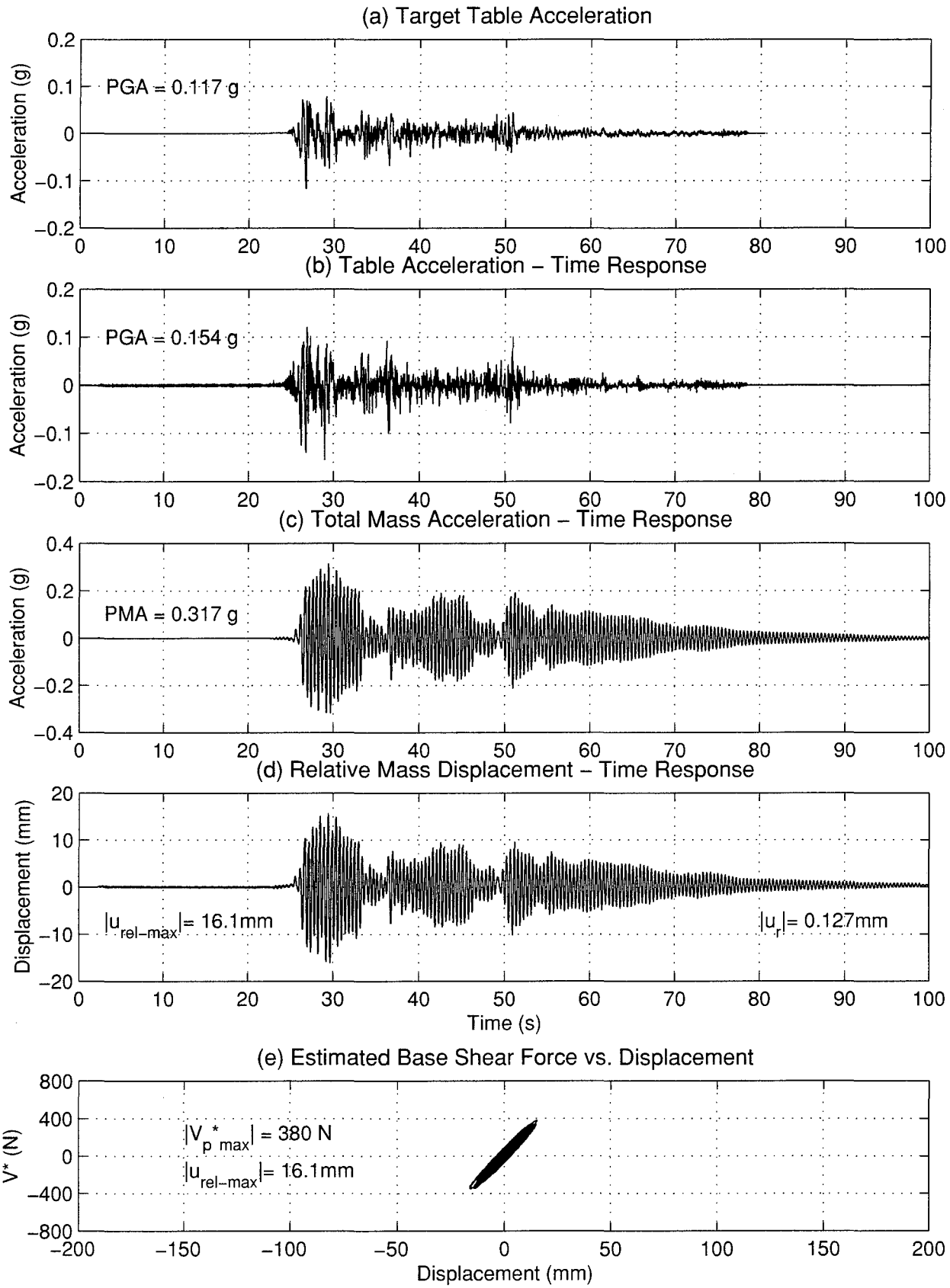

FIGURE 4–32 Seismic Response of Specimen 6 – Trial 1

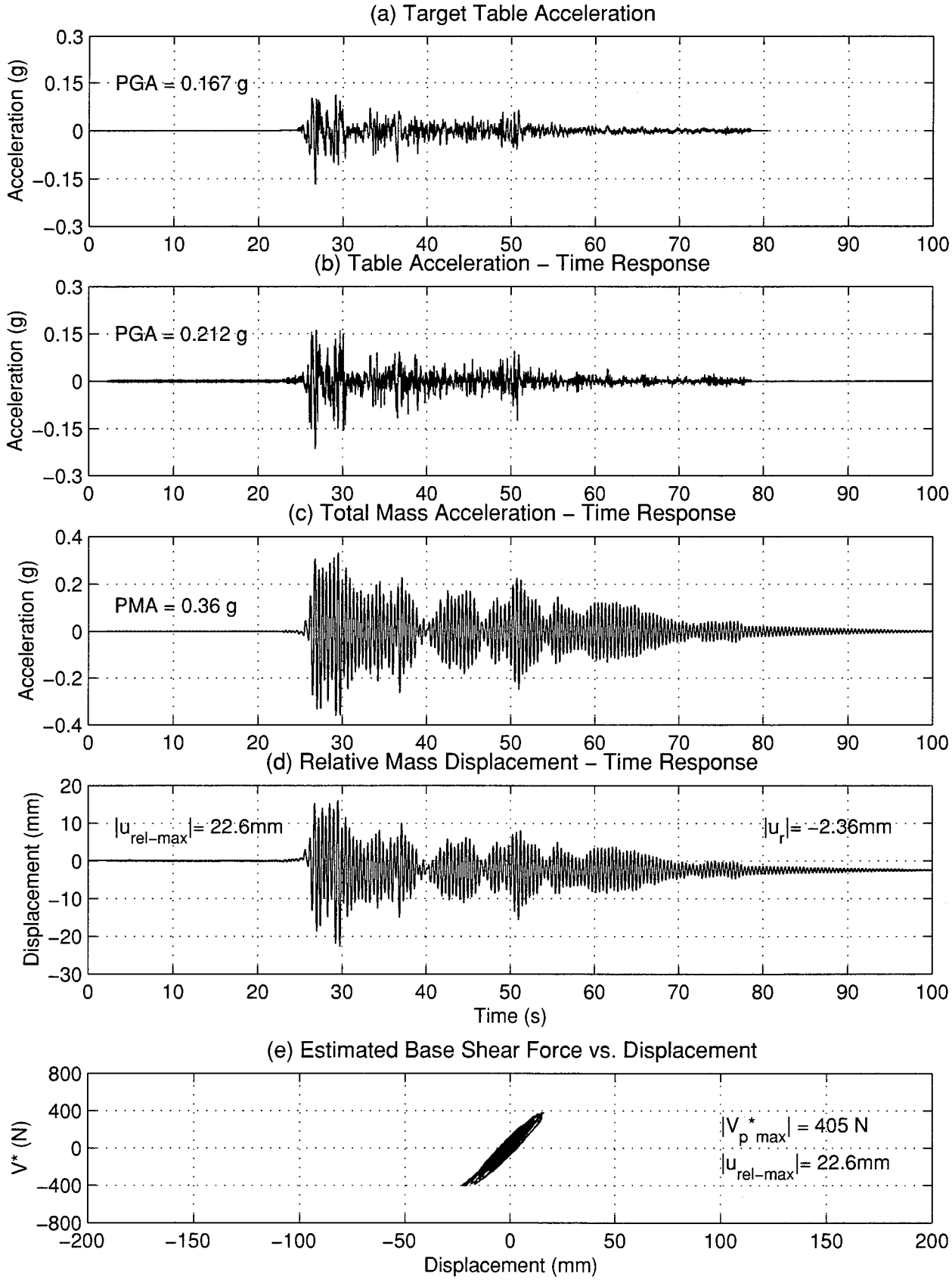

FIGURE 4–33 Seismic Response of Specimen 6 – Trial 2

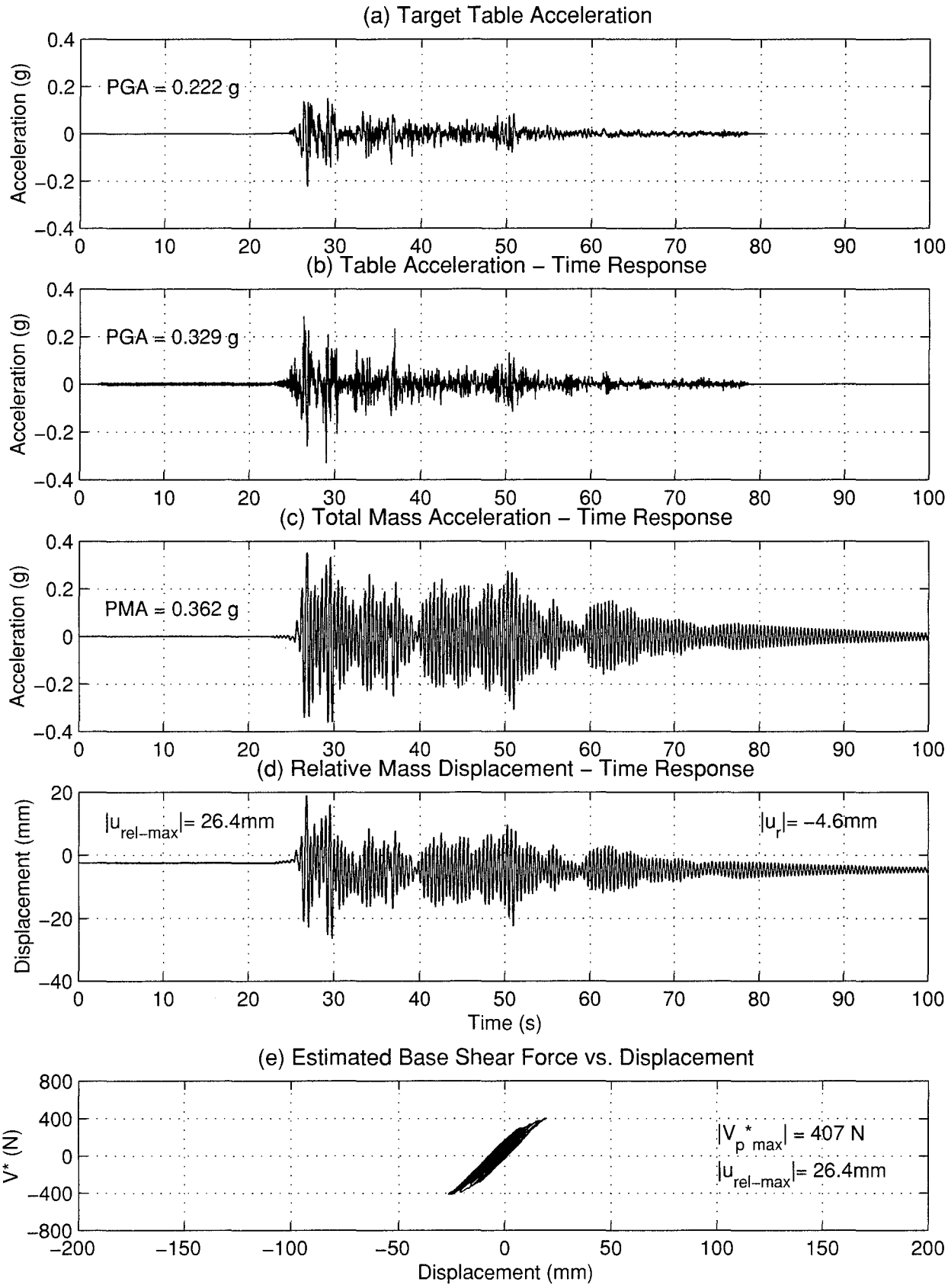

FIGURE 4–34 Seismic Response of Specimen 6 – Trial 3

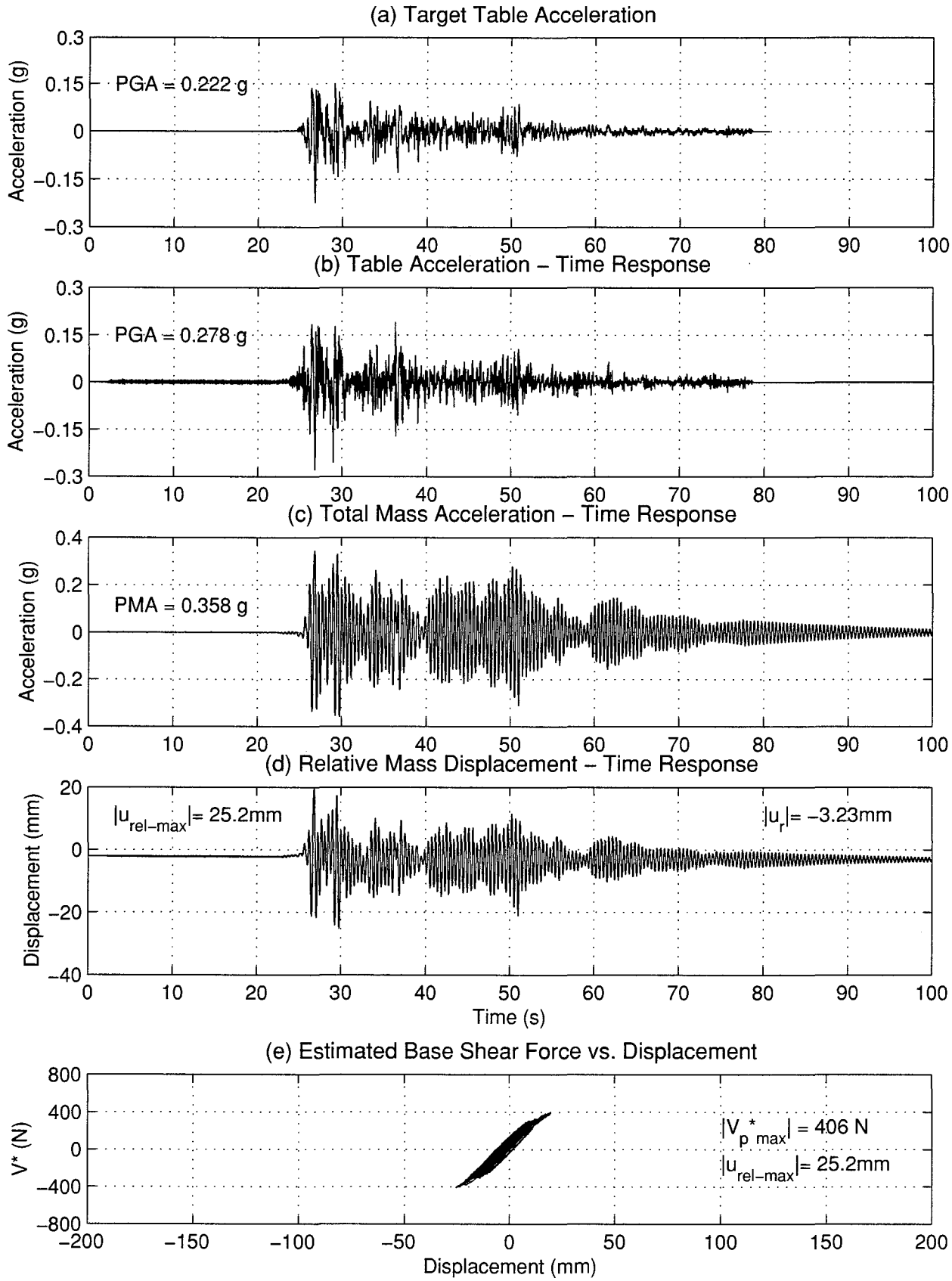

FIGURE 4–35 Seismic Response of Specimen 6 – Trial 4

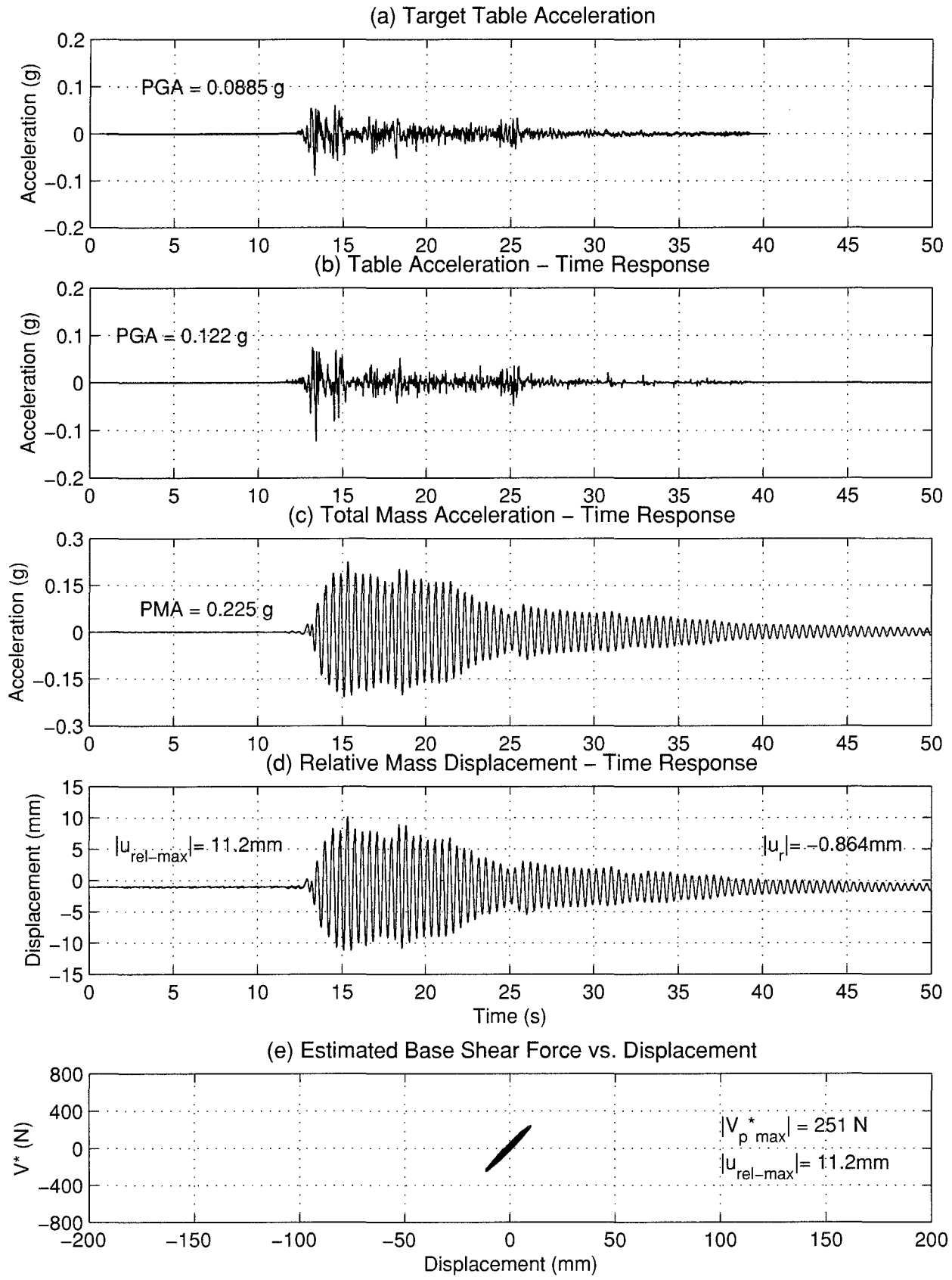

FIGURE 4–36 Seismic Response of Specimen 6 – Trial 5

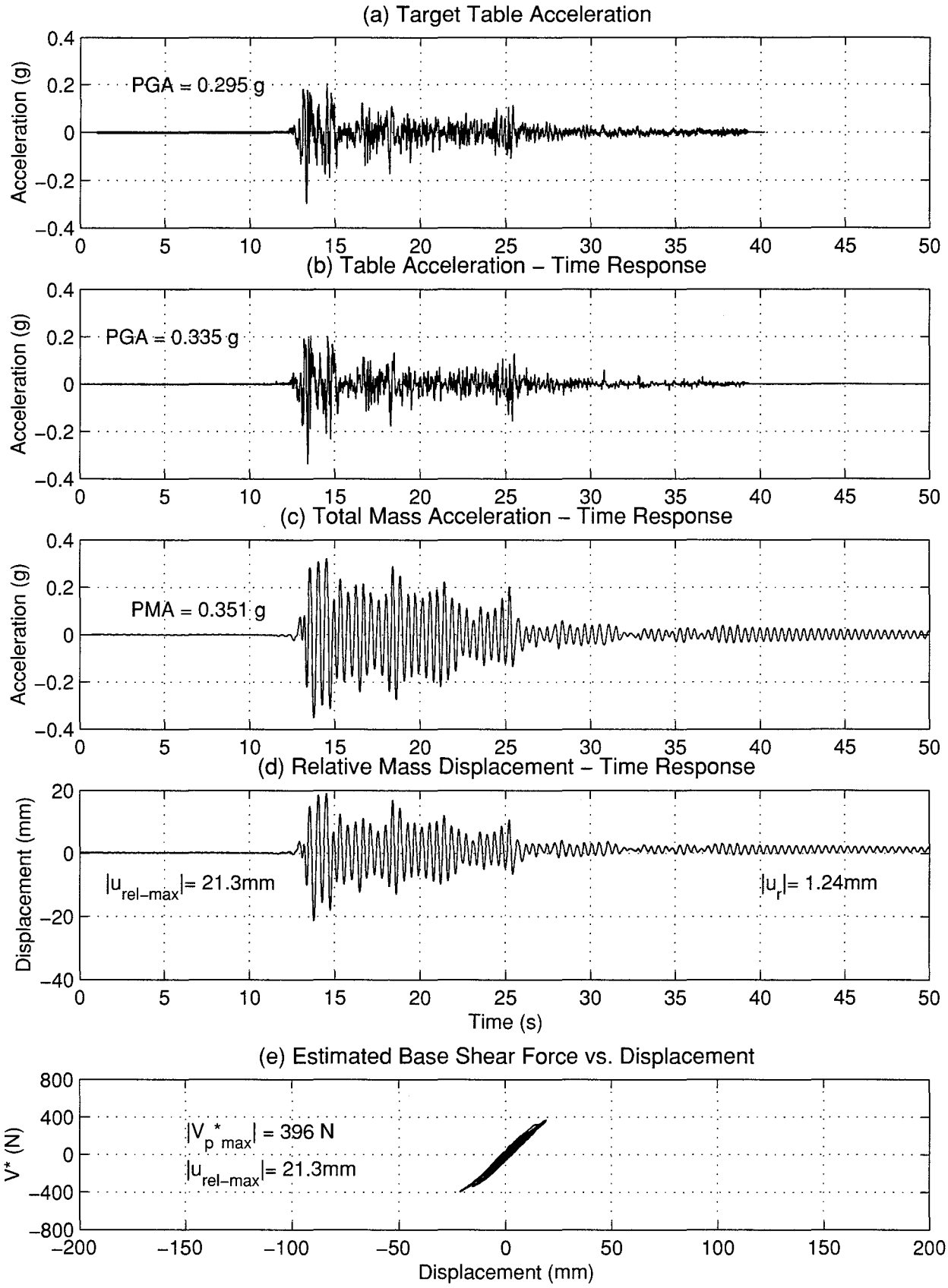

FIGURE 4–37 Seismic Response of Specimen 6 – Trial 6

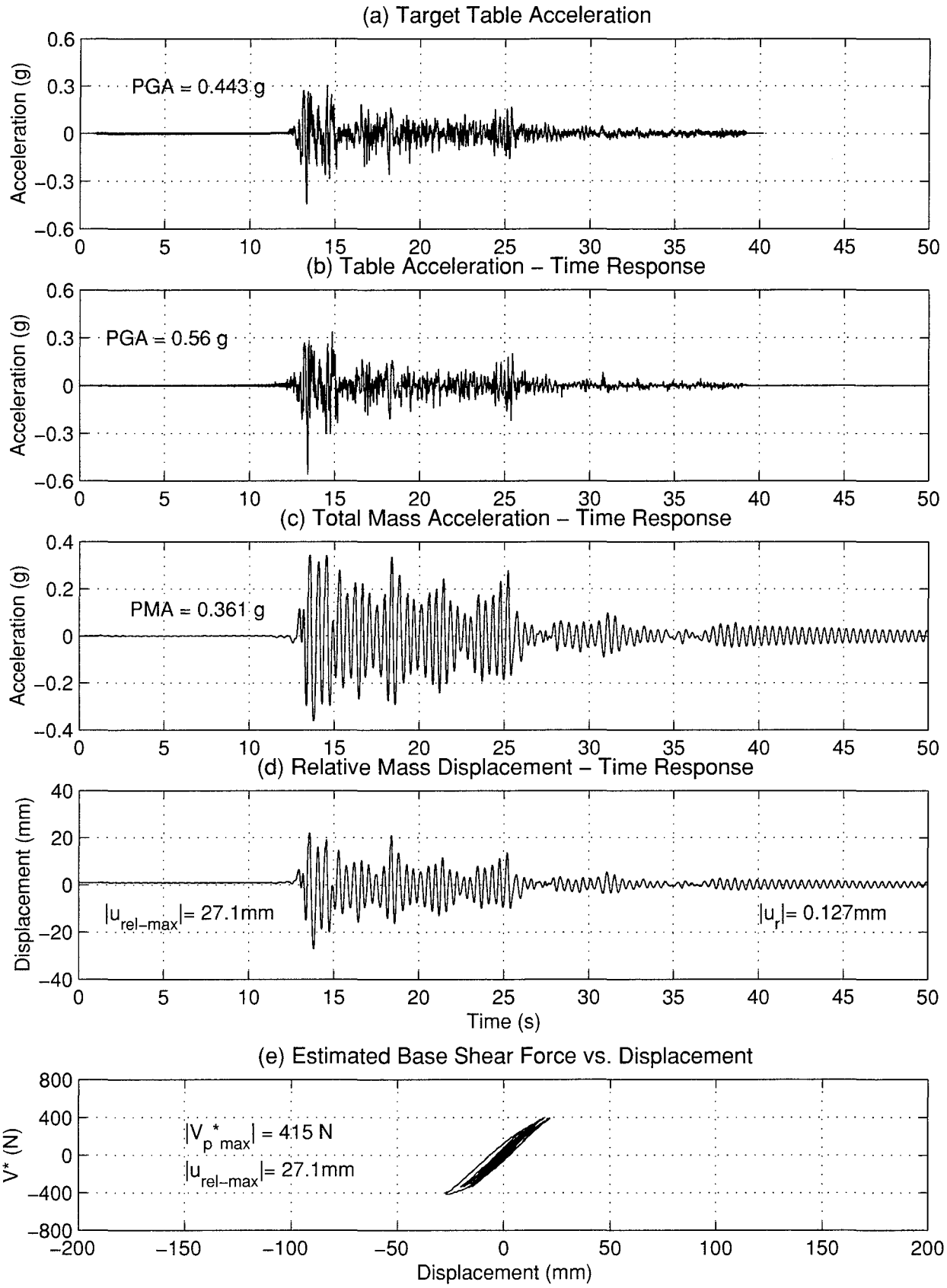

FIGURE 4–38 Seismic Response of Specimen 6 – Trial 7

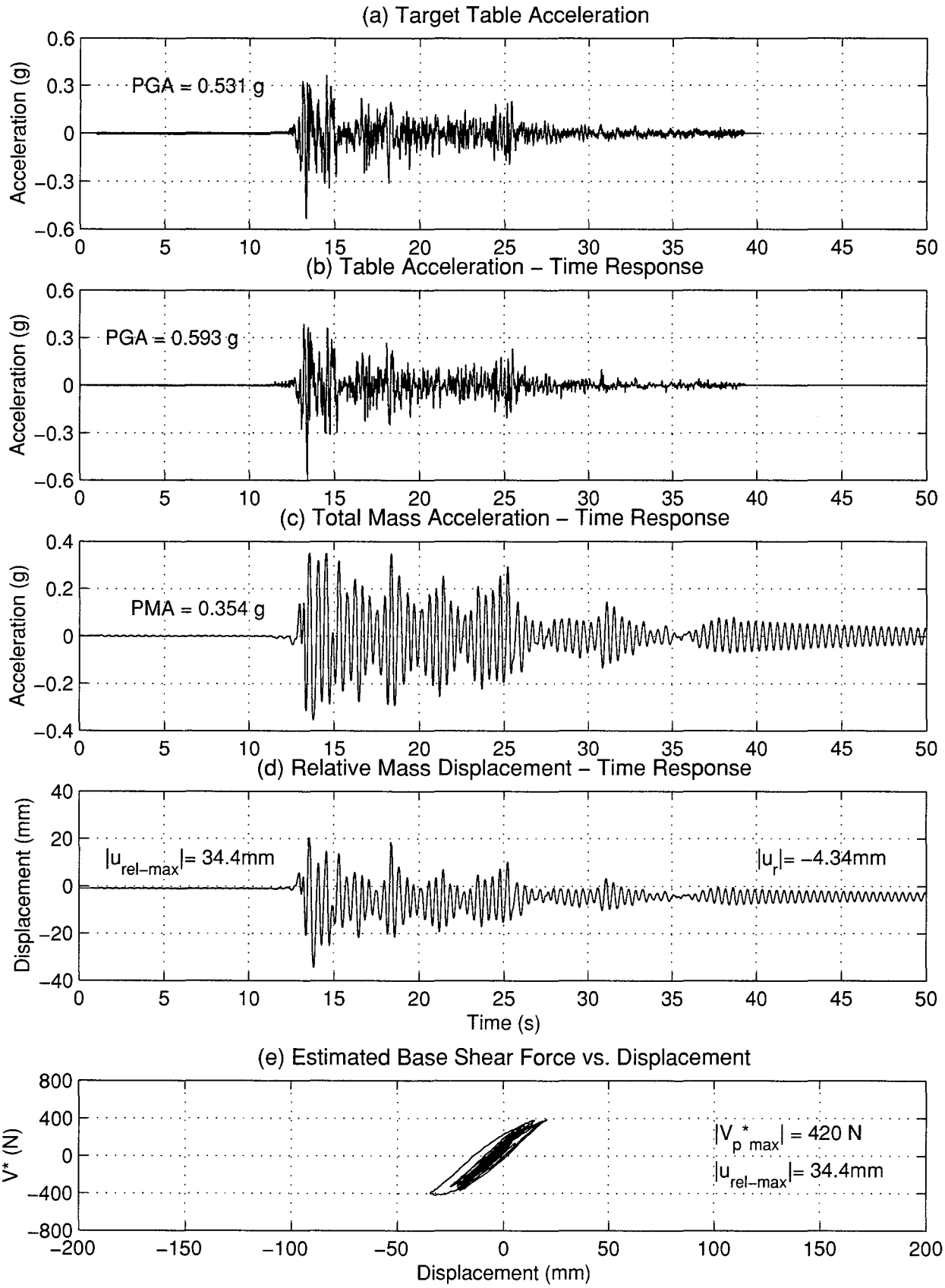

FIGURE 4–39 Seismic Response of Specimen 6 – Trial 8

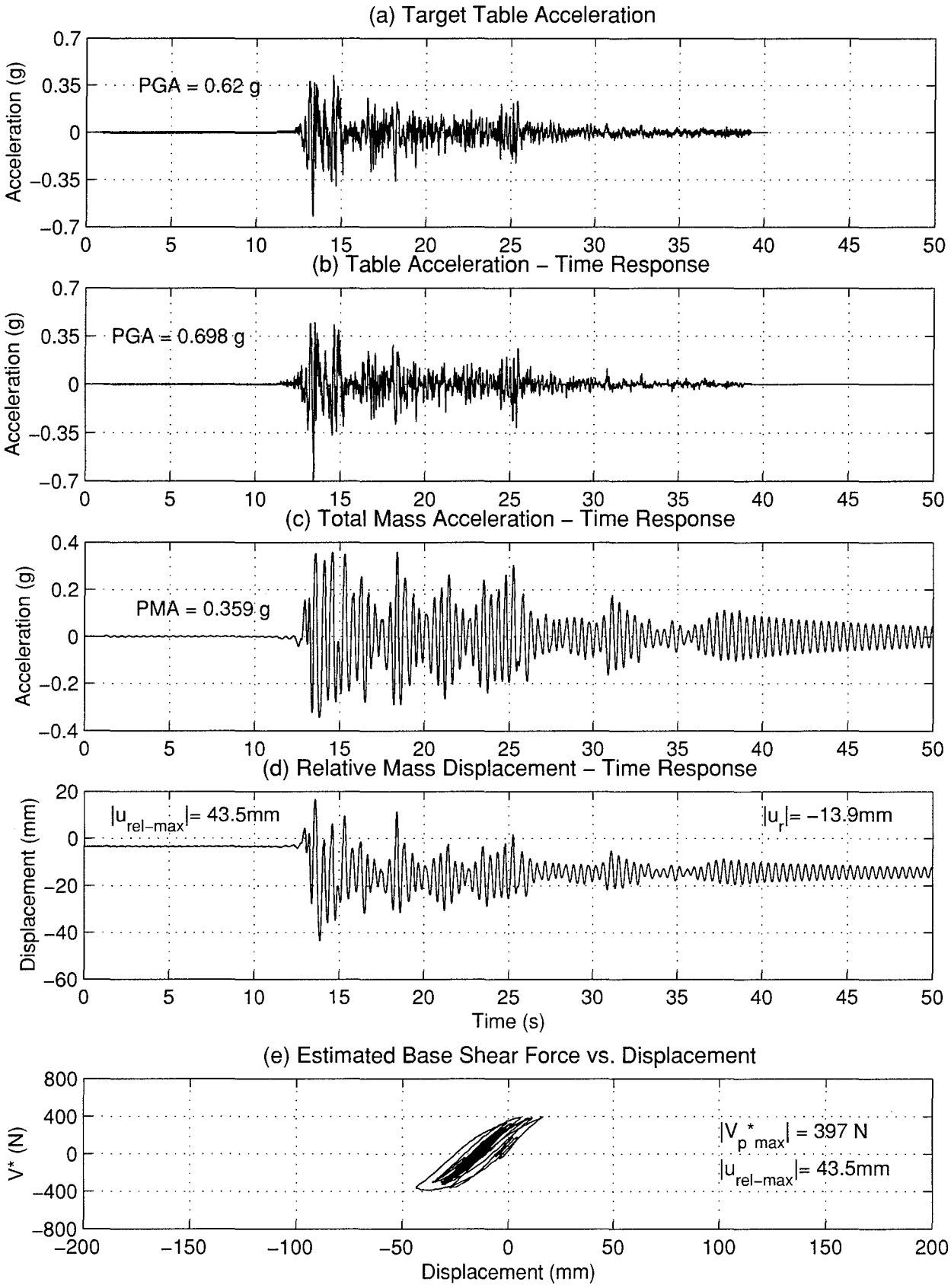

FIGURE 4–40 Seismic Response of Specimen 6 – Trial 9

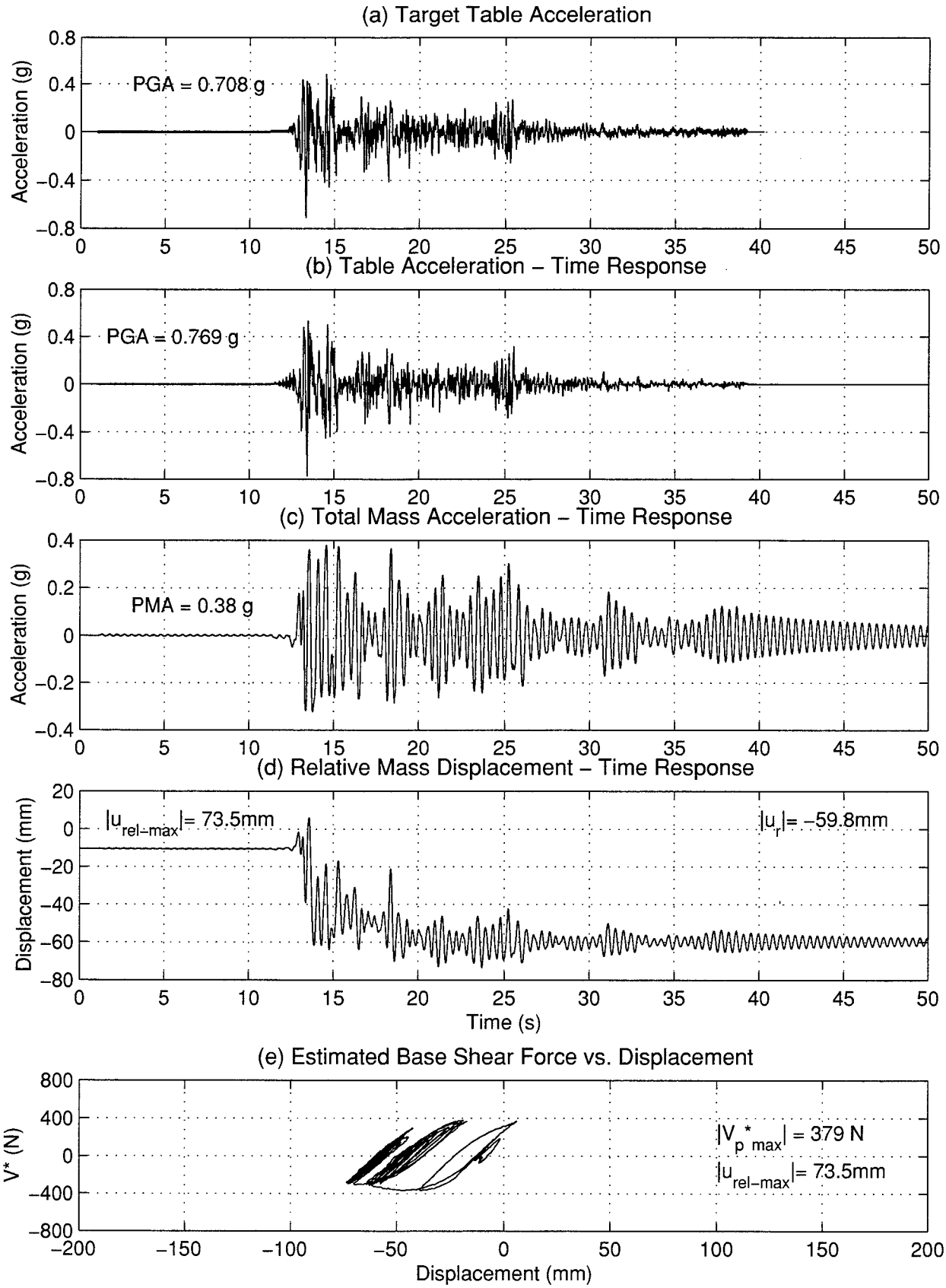

FIGURE 4–41 Seismic Response of Specimen 6 – Trial 10

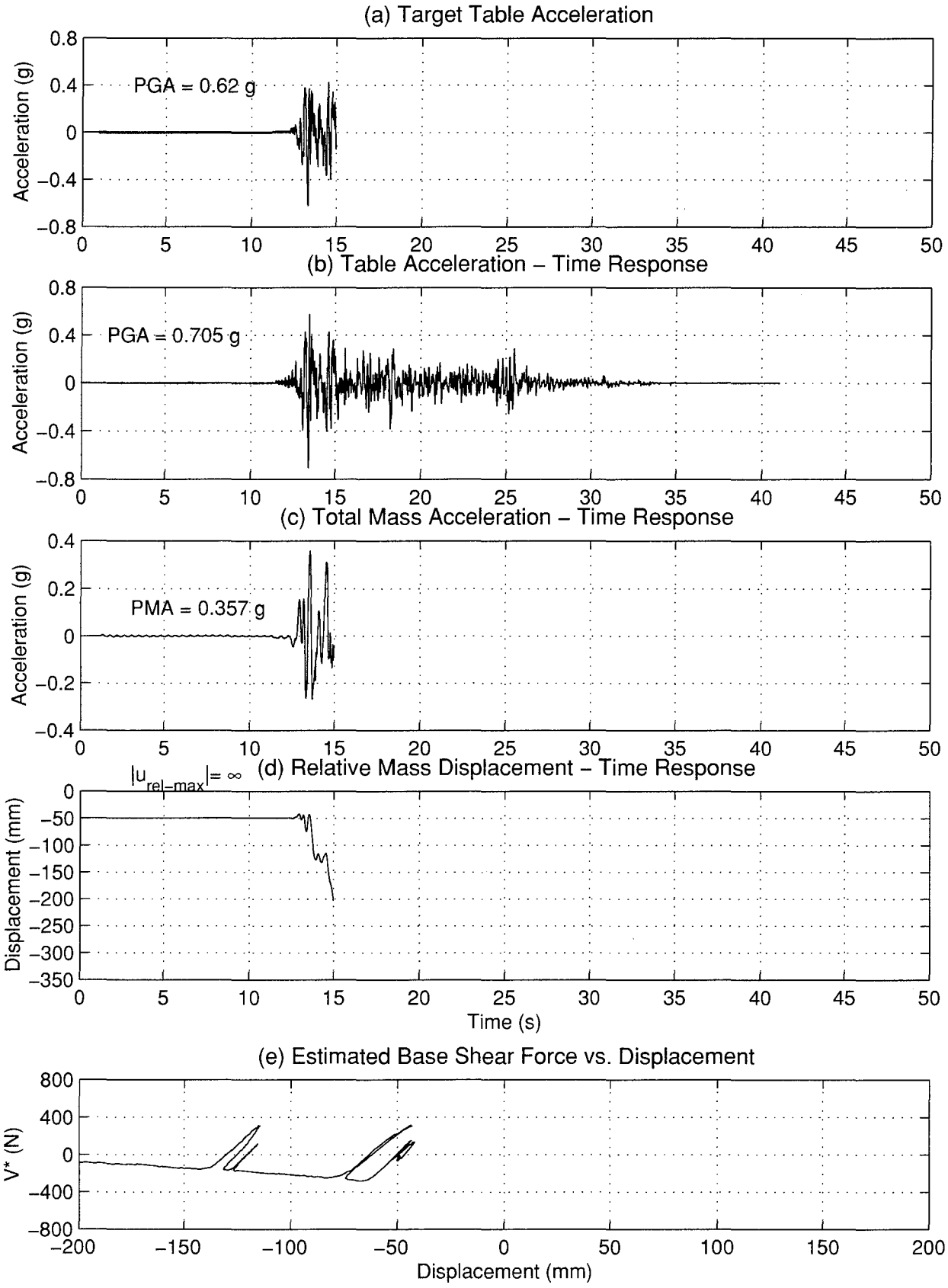

FIGURE 4–42 Seismic Response of Specimen 6 – Trial 11

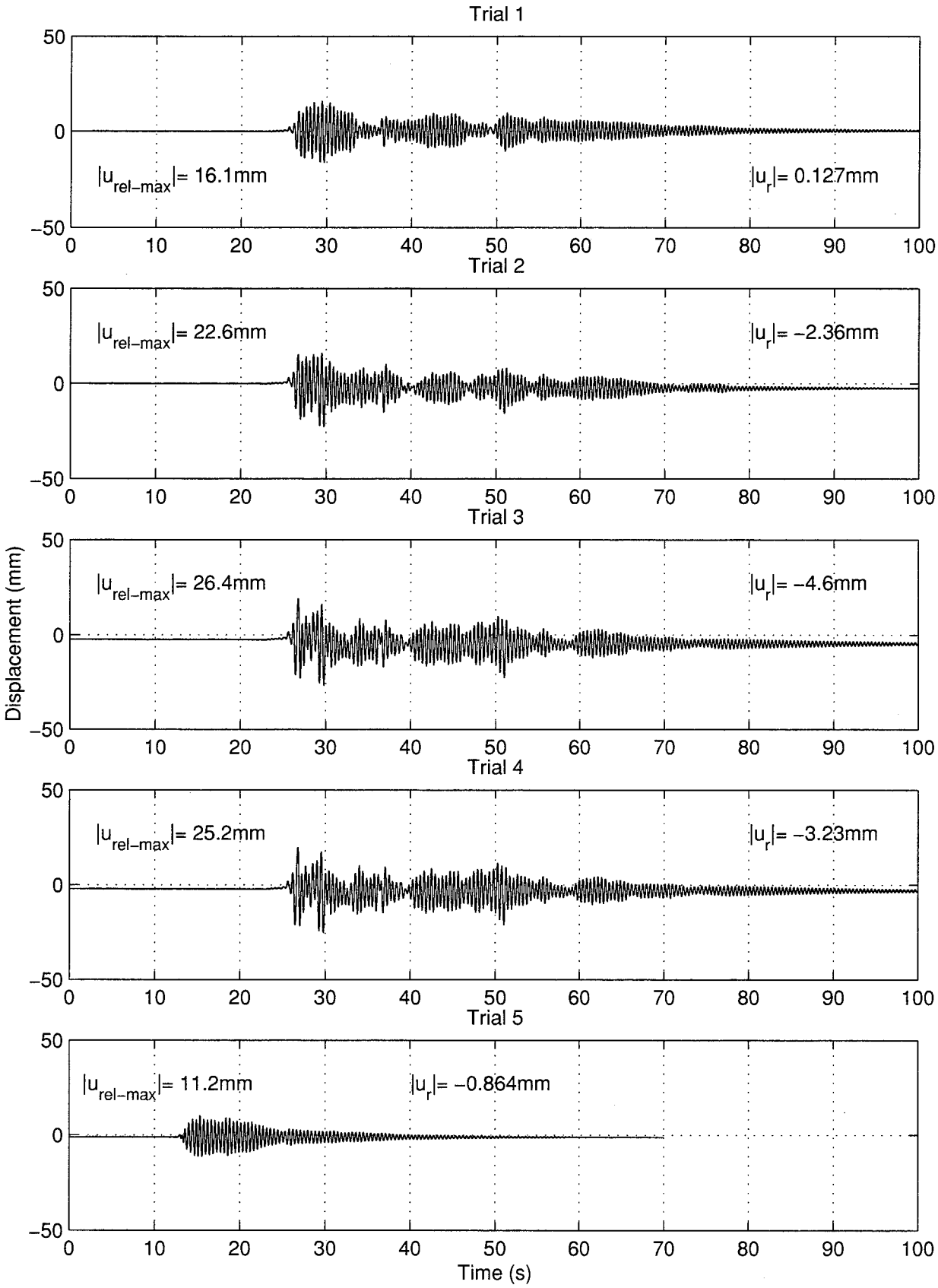

FIGURE 4–43 Specimen 6 – Progressive Displacement Time Histories

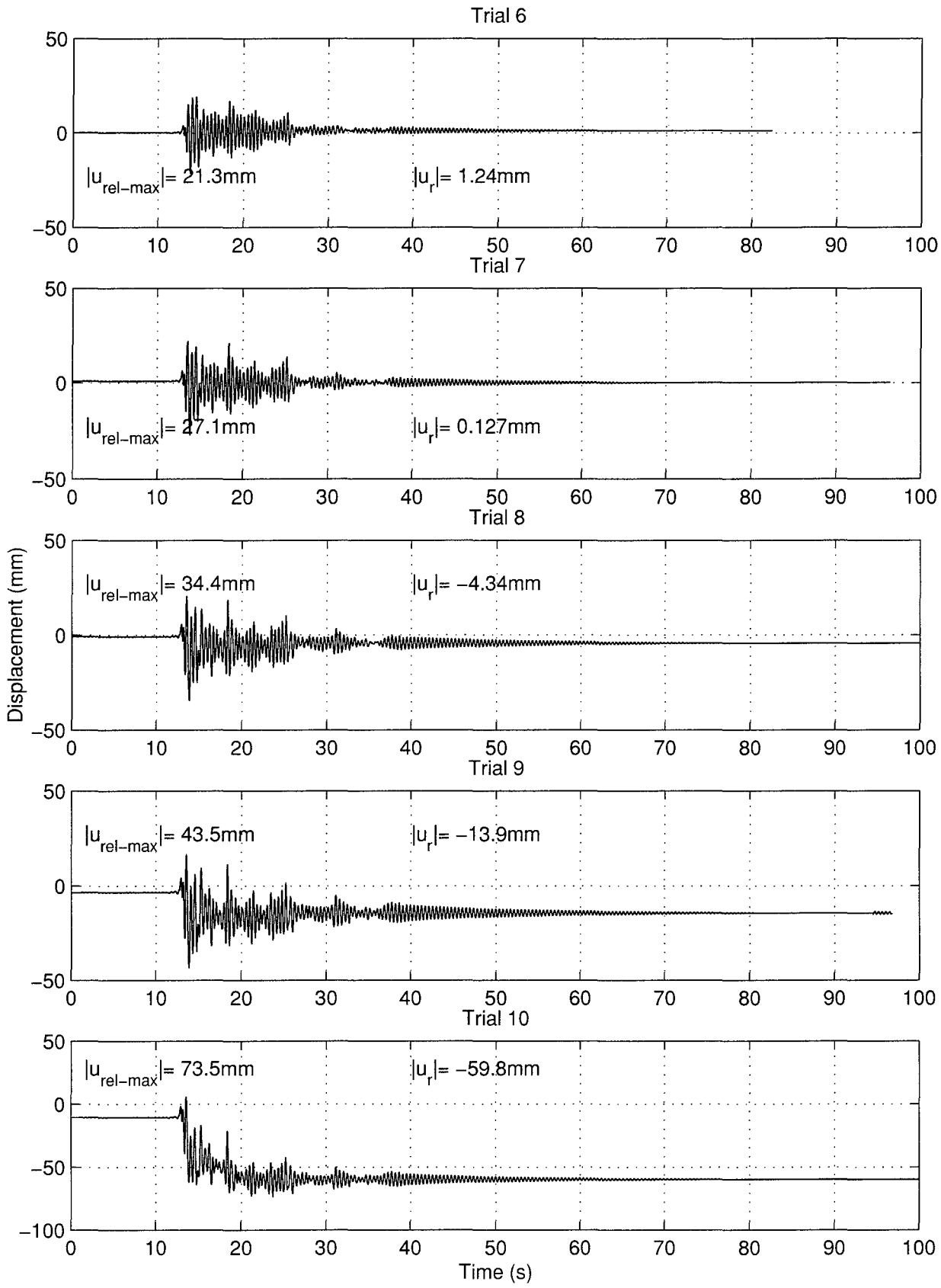

FIGURE 4–43 (cont'd) Specimen 6 – Progressive Displacement Time Histories

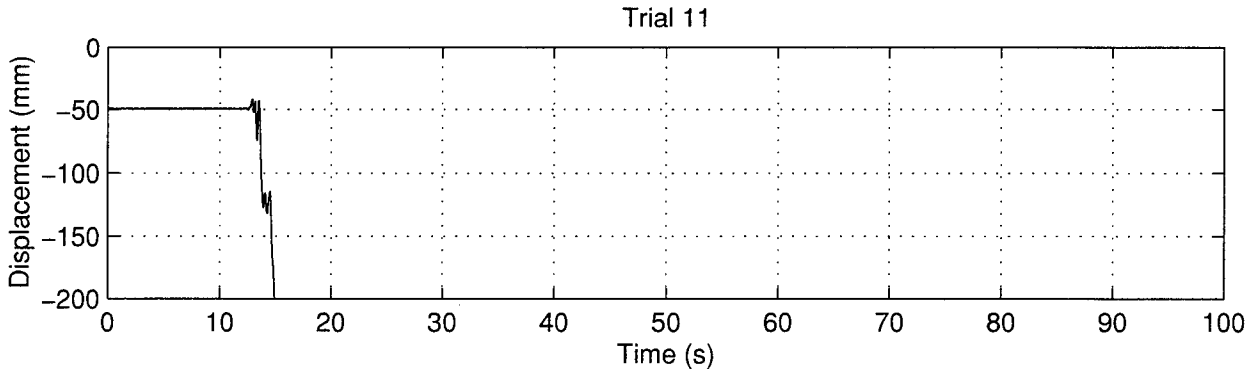

FIGURE 4–43 (cont'd) Specimen 6 – Progressive Displacement Time Histories

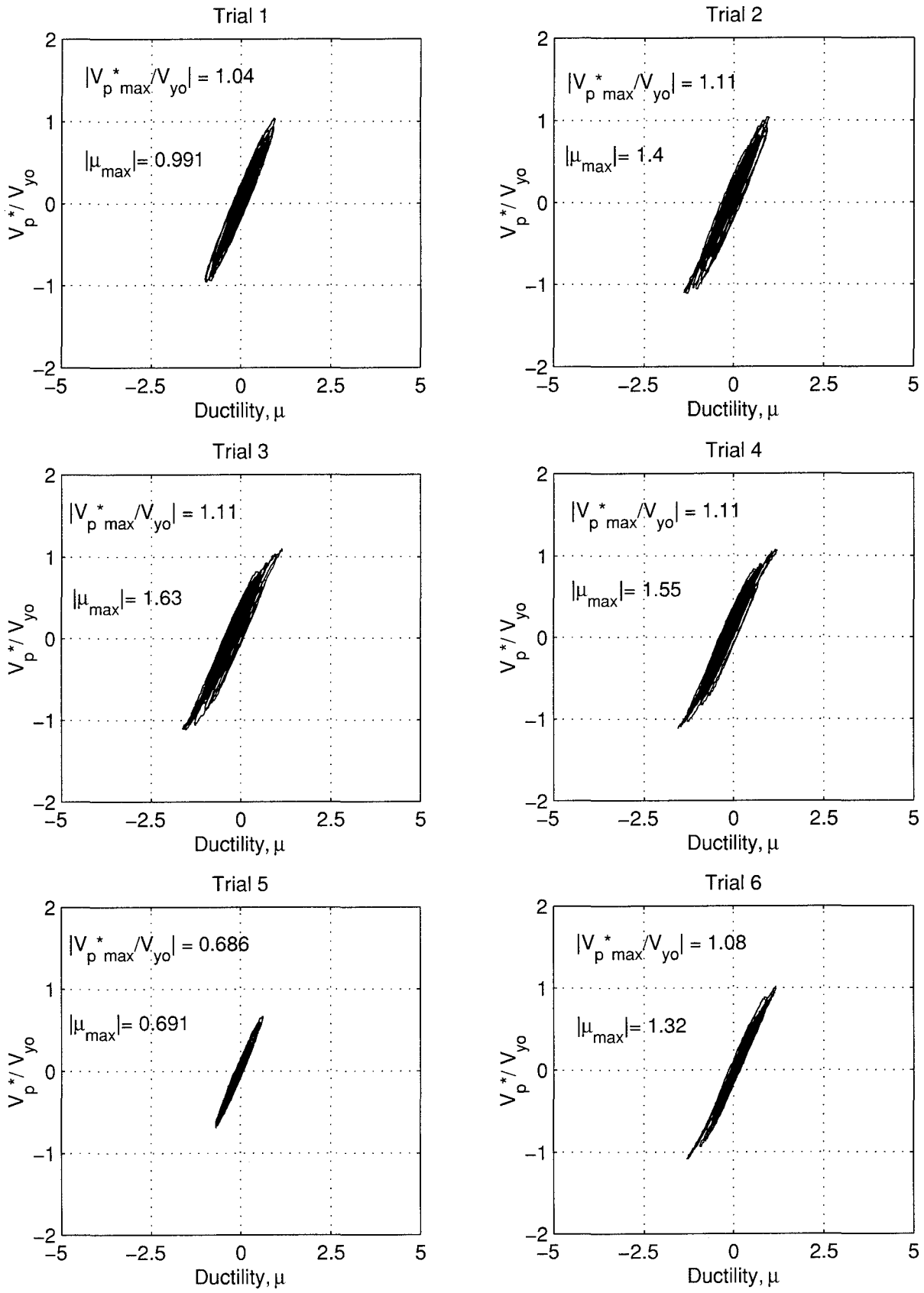

FIGURE 4–44 Specimen 6 – Normalized Base Shear vs. Ductility

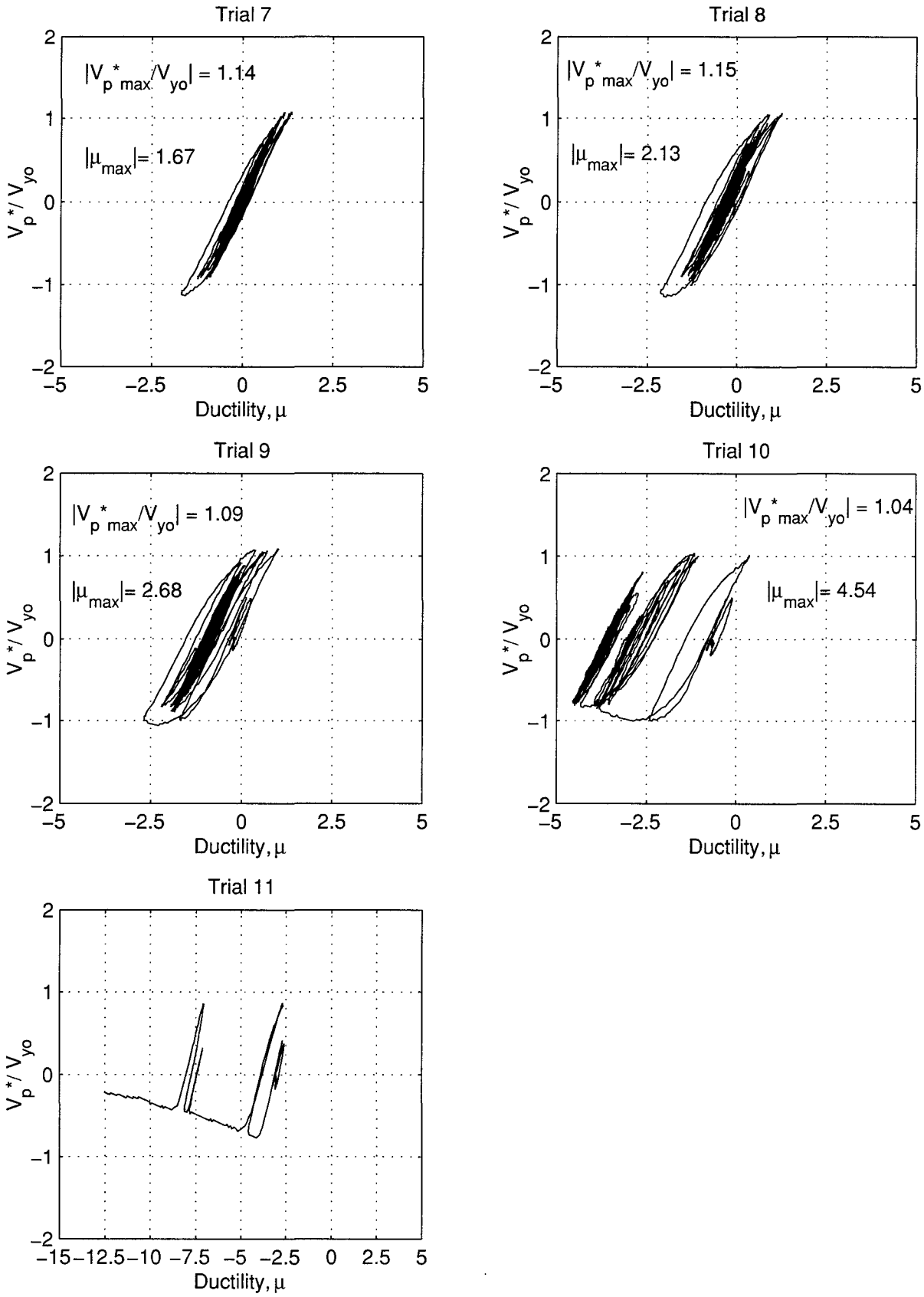

FIGURE 4–44 (cont'd) Specimen 6 – Normalized Base Shear vs. Ductility

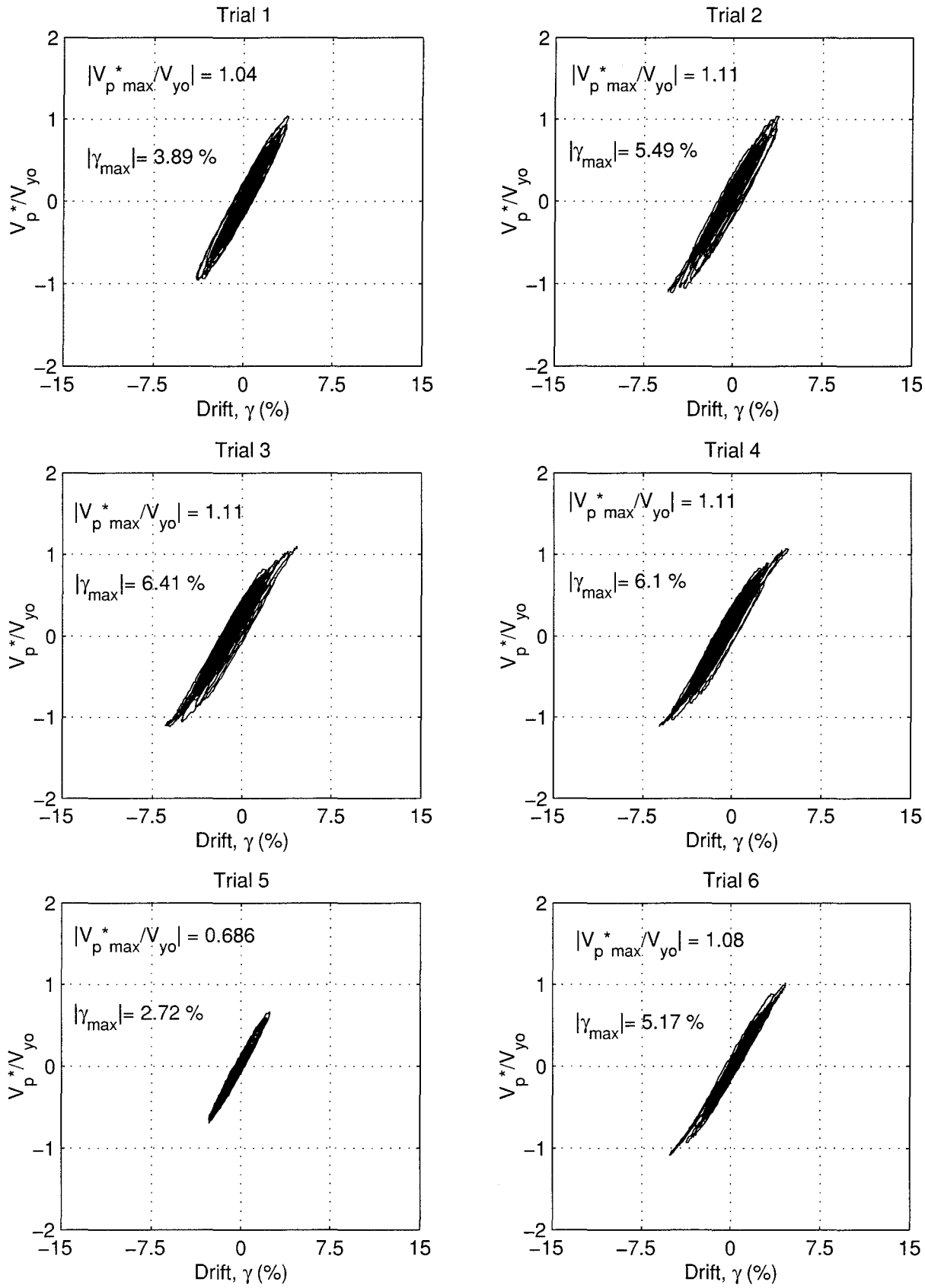

FIGURE 4–45 Specimen 6 – Normalized Base Shear vs. Drift

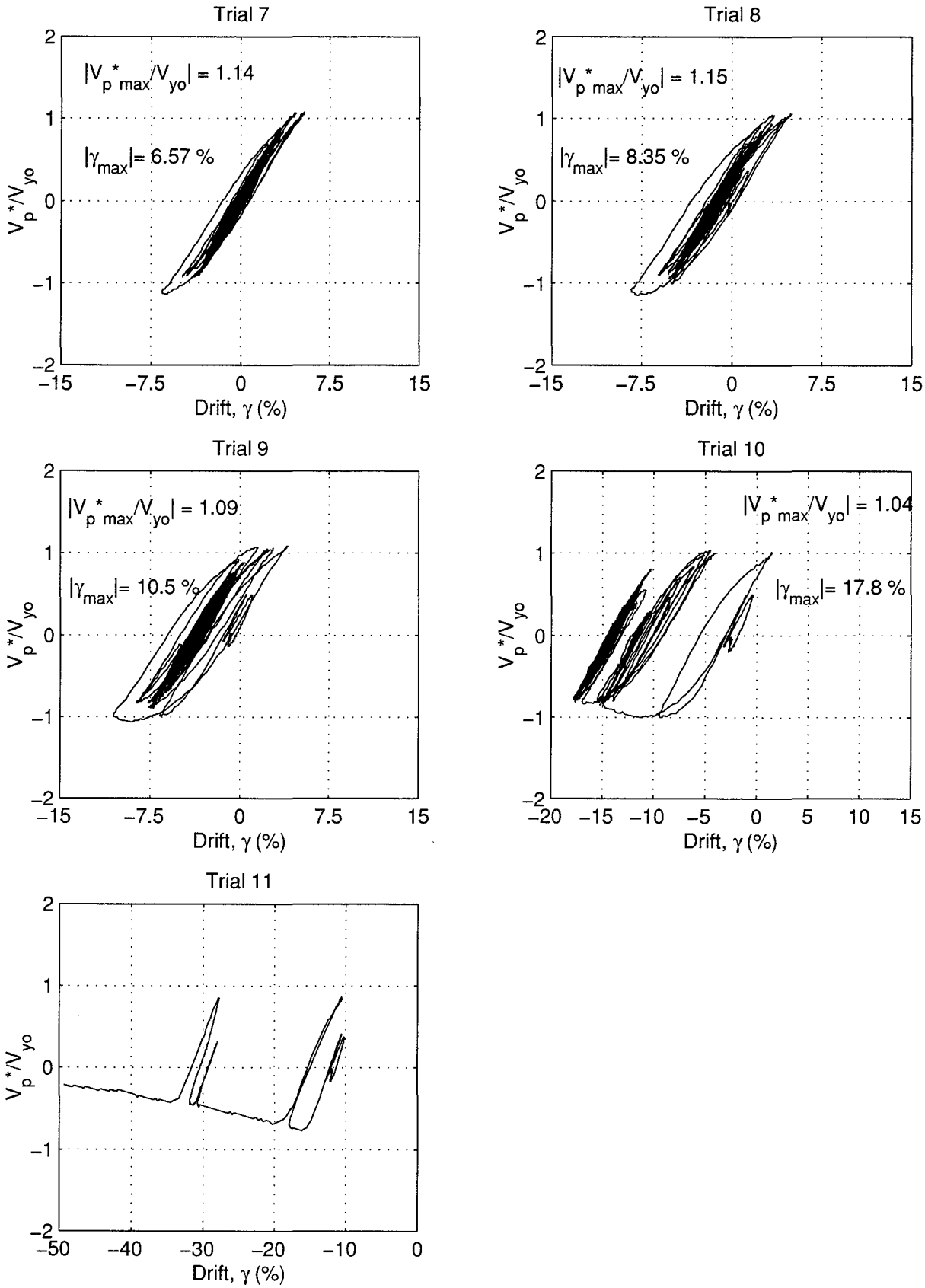

FIGURE 4–45 (cont'd) Specimen 6 – Normalized Base Shear vs. Drift

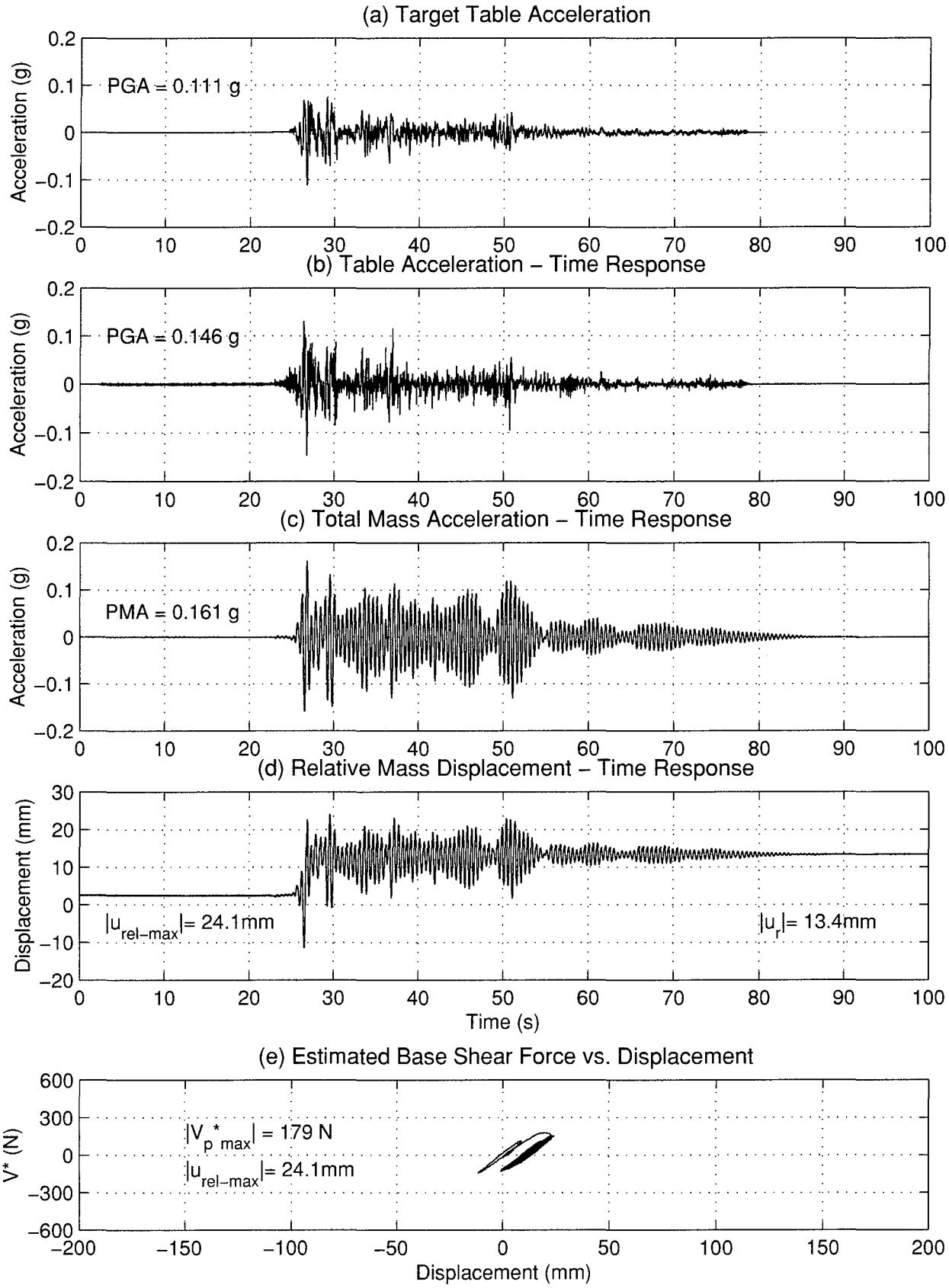

FIGURE 4–46 Seismic Response of Specimen 7 – Trial 4

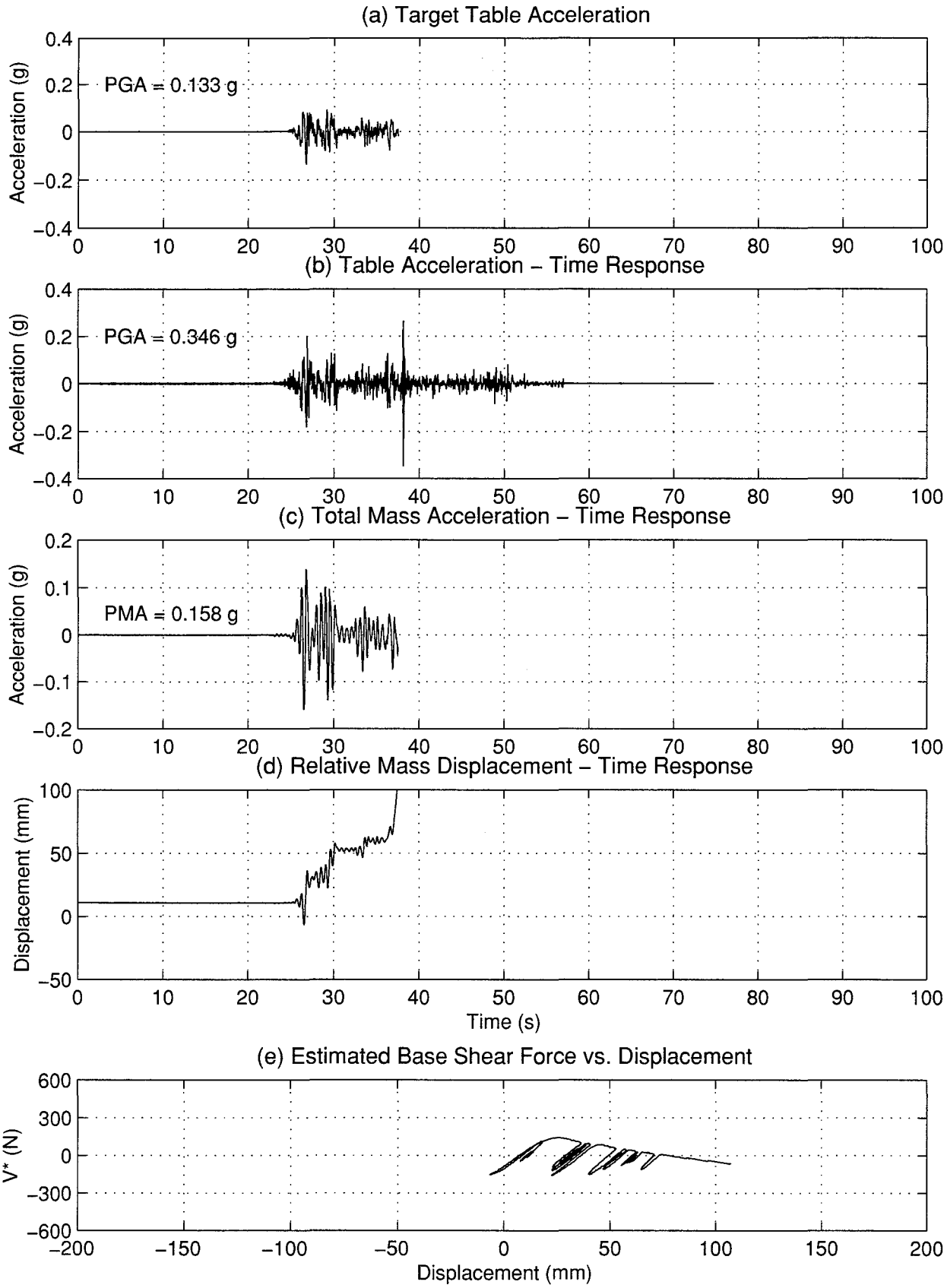

FIGURE 4–47 Seismic Response of Specimen 7 – Trial 5

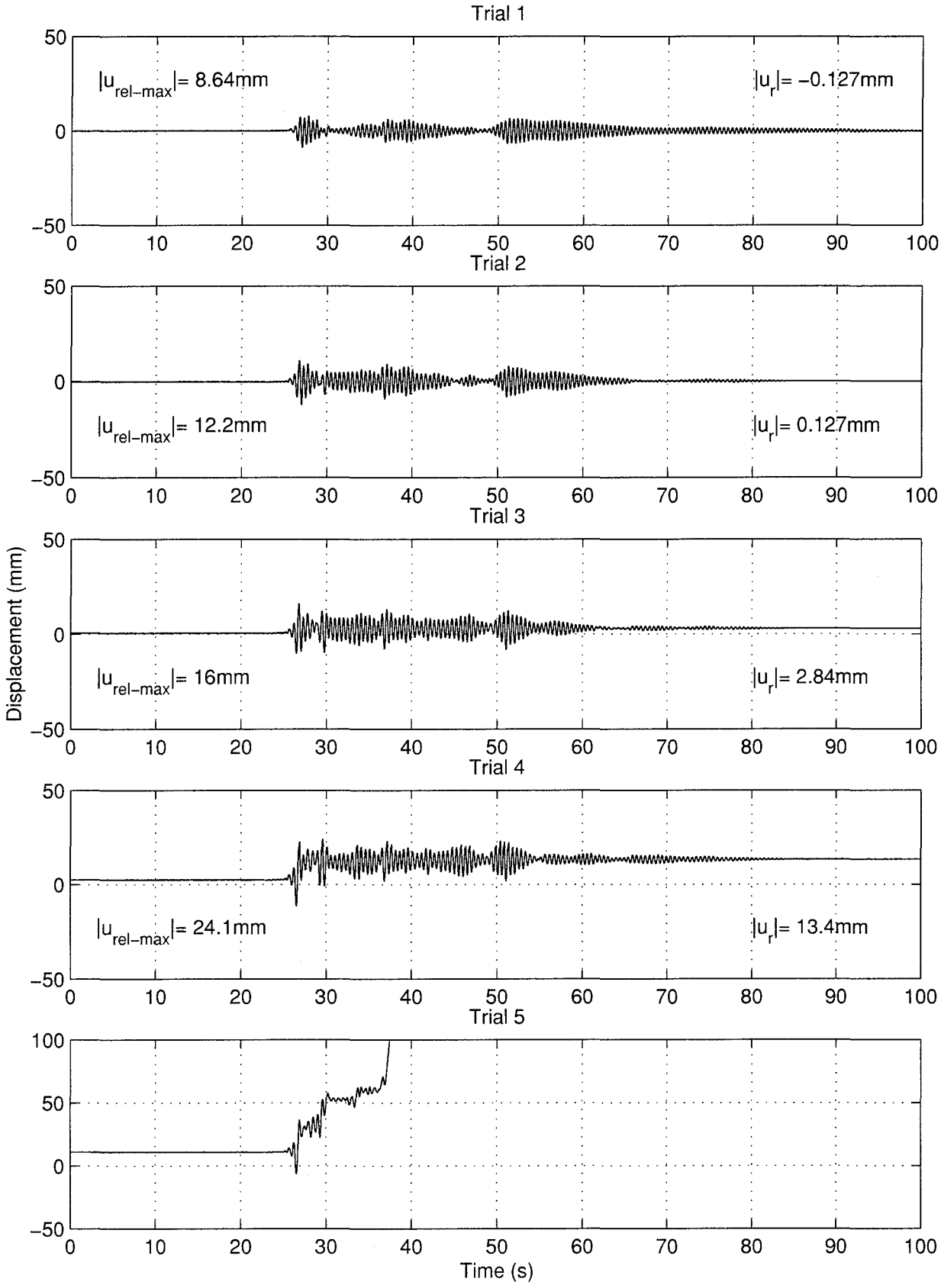

FIGURE 4–48 Specimen 7 – Progressive Displacement Time Histories

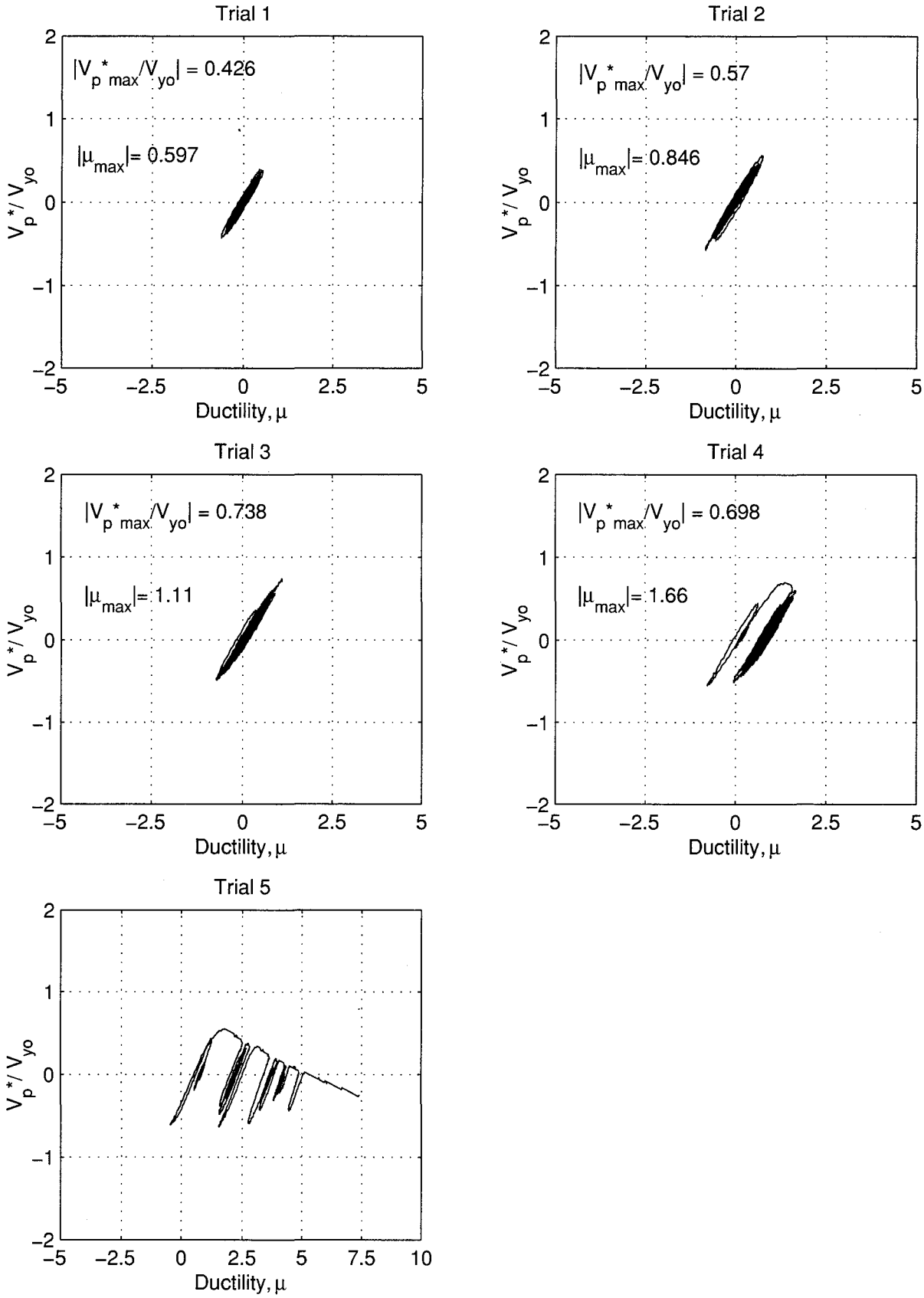

FIGURE 4–49 Specimen 7 – Normalized Base Shear vs. Ductility

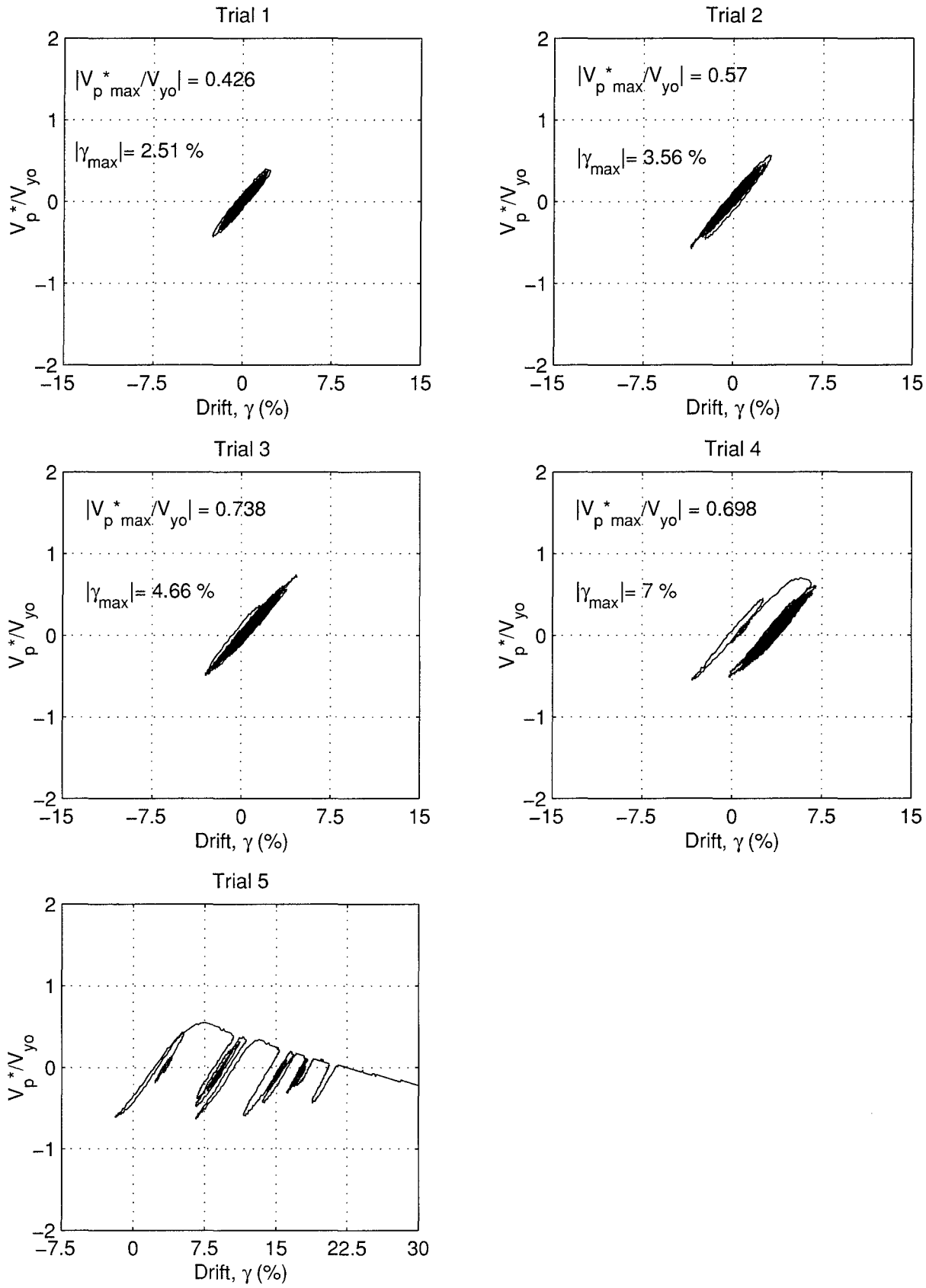

FIGURE 4–50 Specimen 7 – Normalized Base Shear vs. Drift

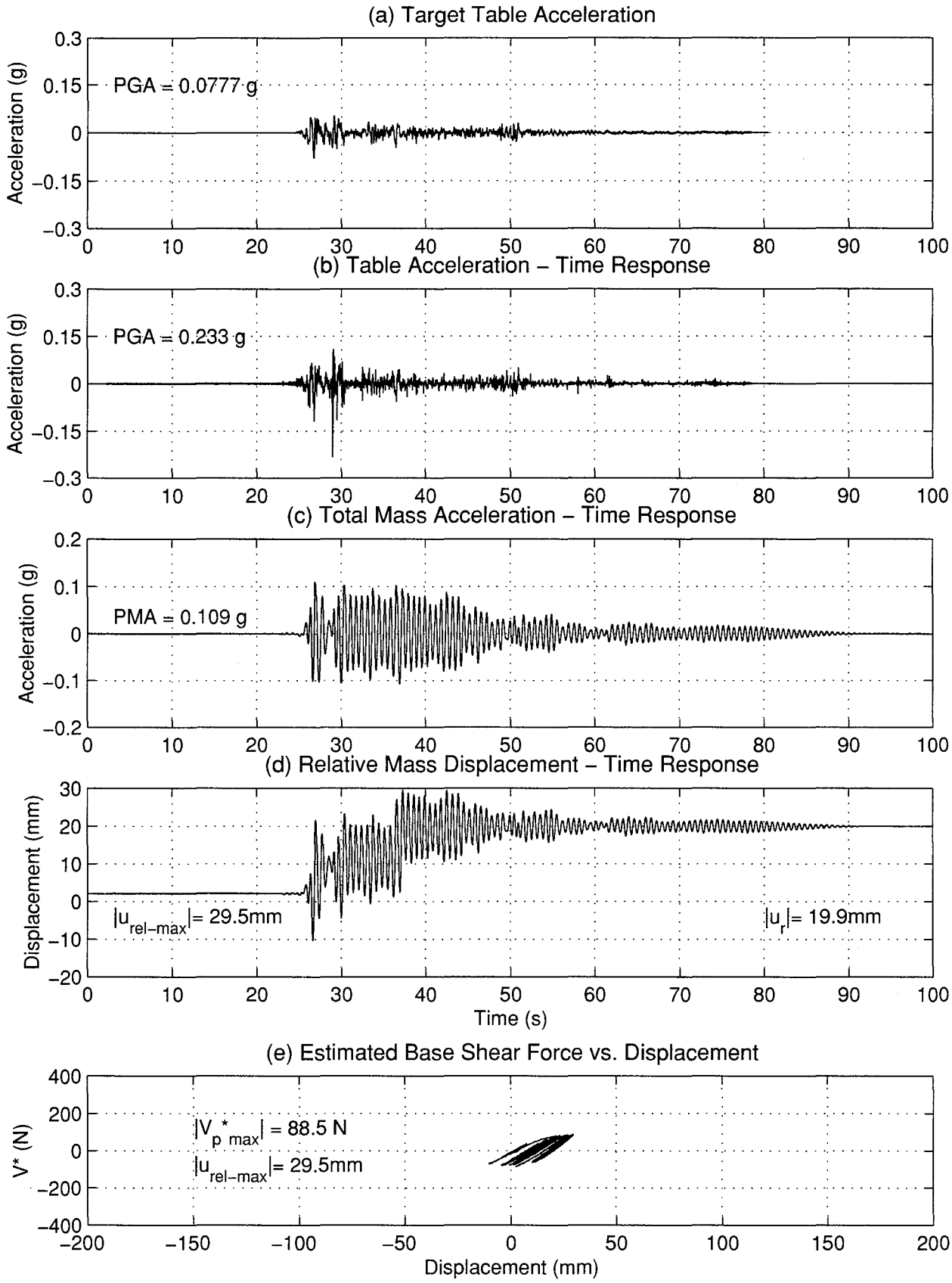

FIGURE 4–51 Seismic Response of Specimen 8 – Trial 3

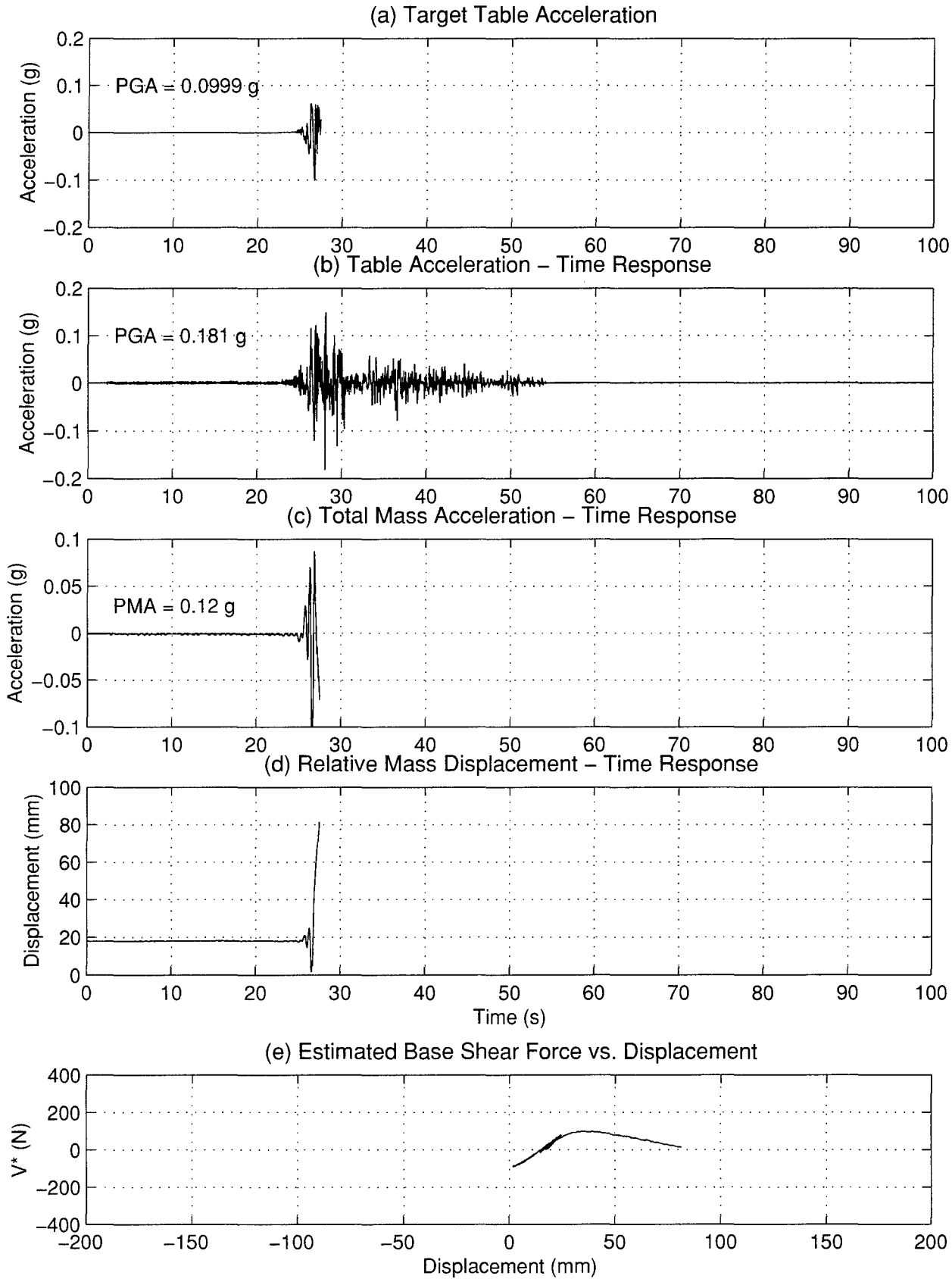

FIGURE 4–52 Seismic Response of Specimen 8 – Trial 4

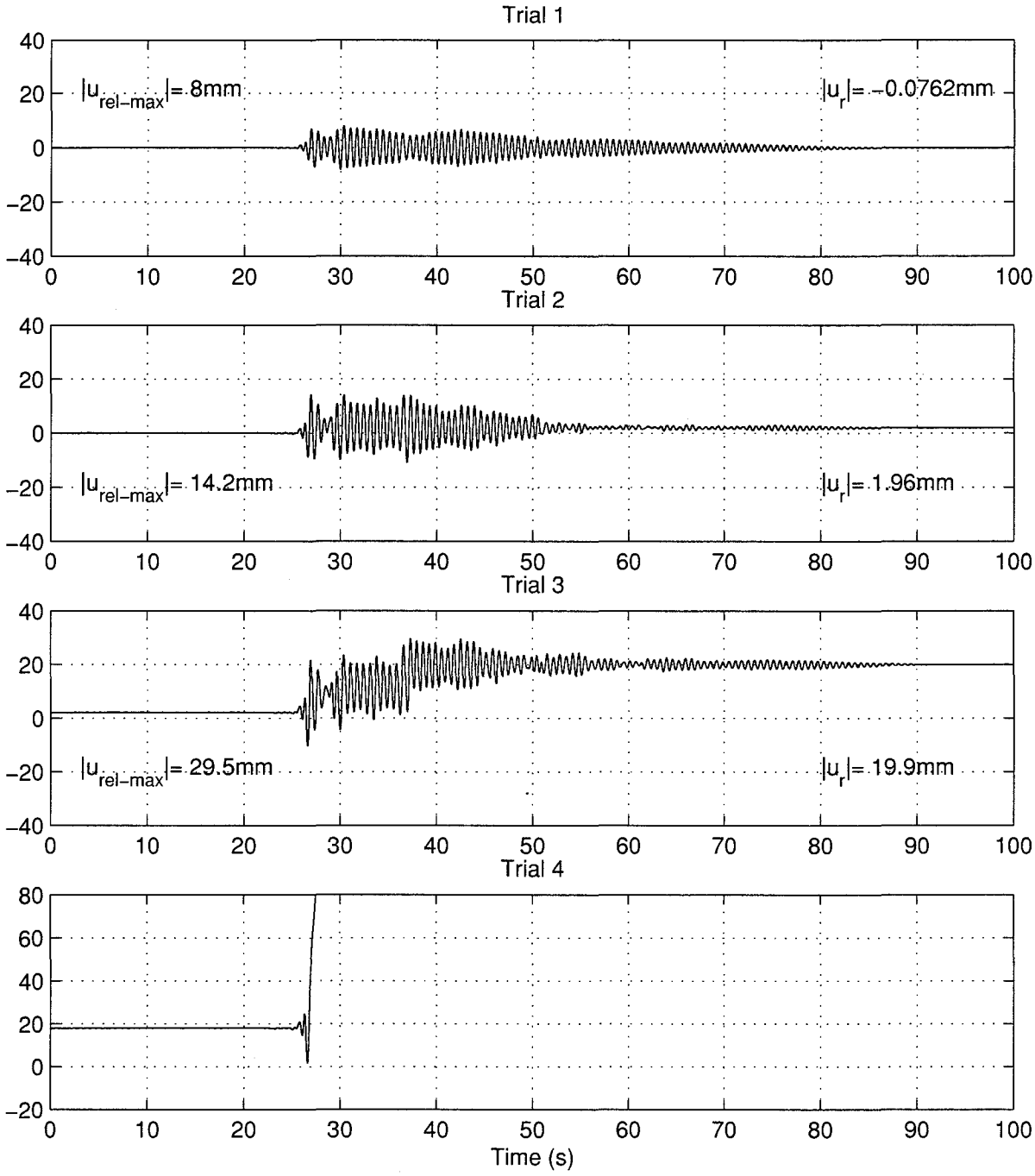

FIGURE 4–53 Specimen 8 – Progressive Displacement Time Histories

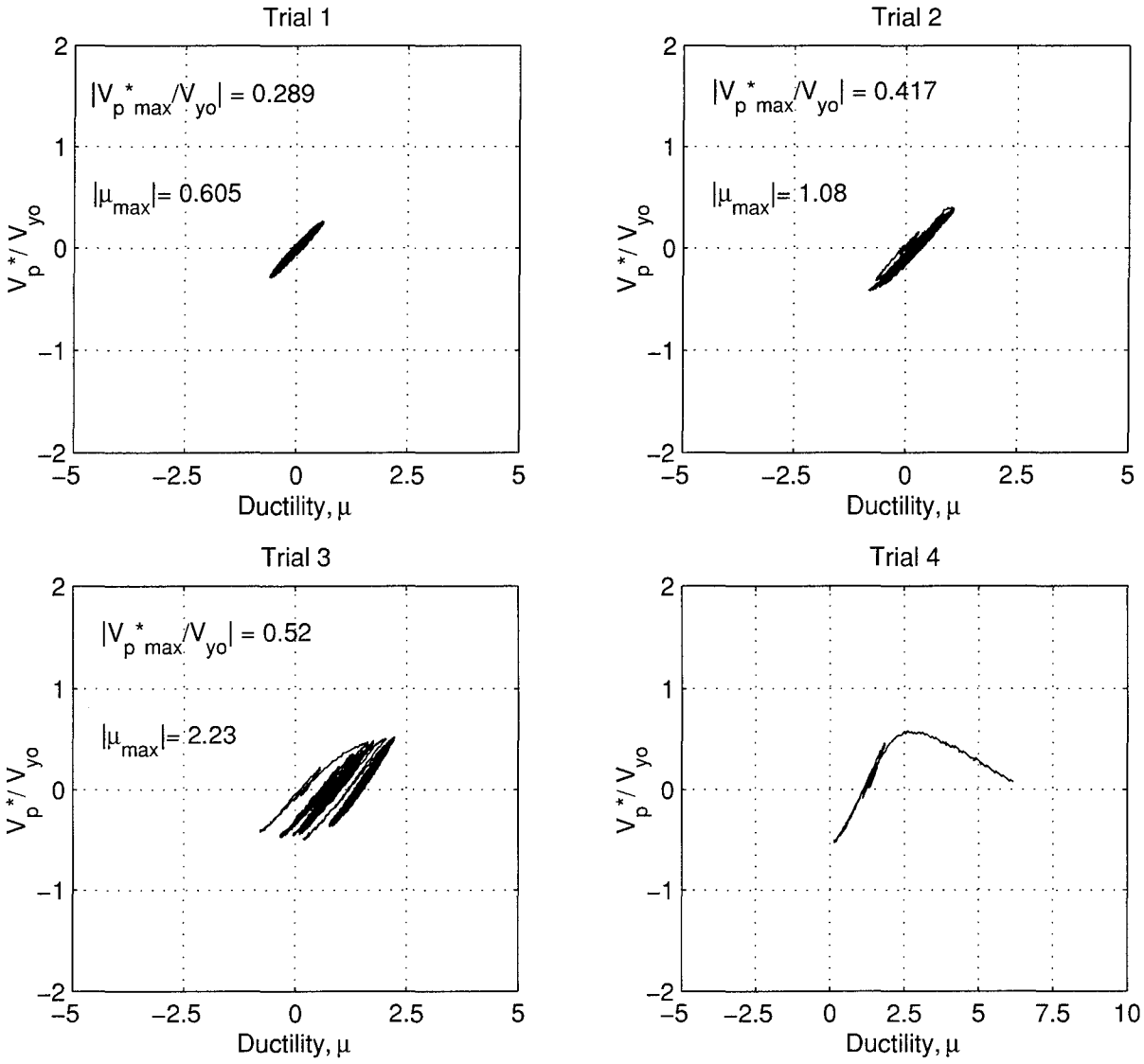

FIGURE 4–54 Specimen 8 – Normalized Base Shear vs. Ductility

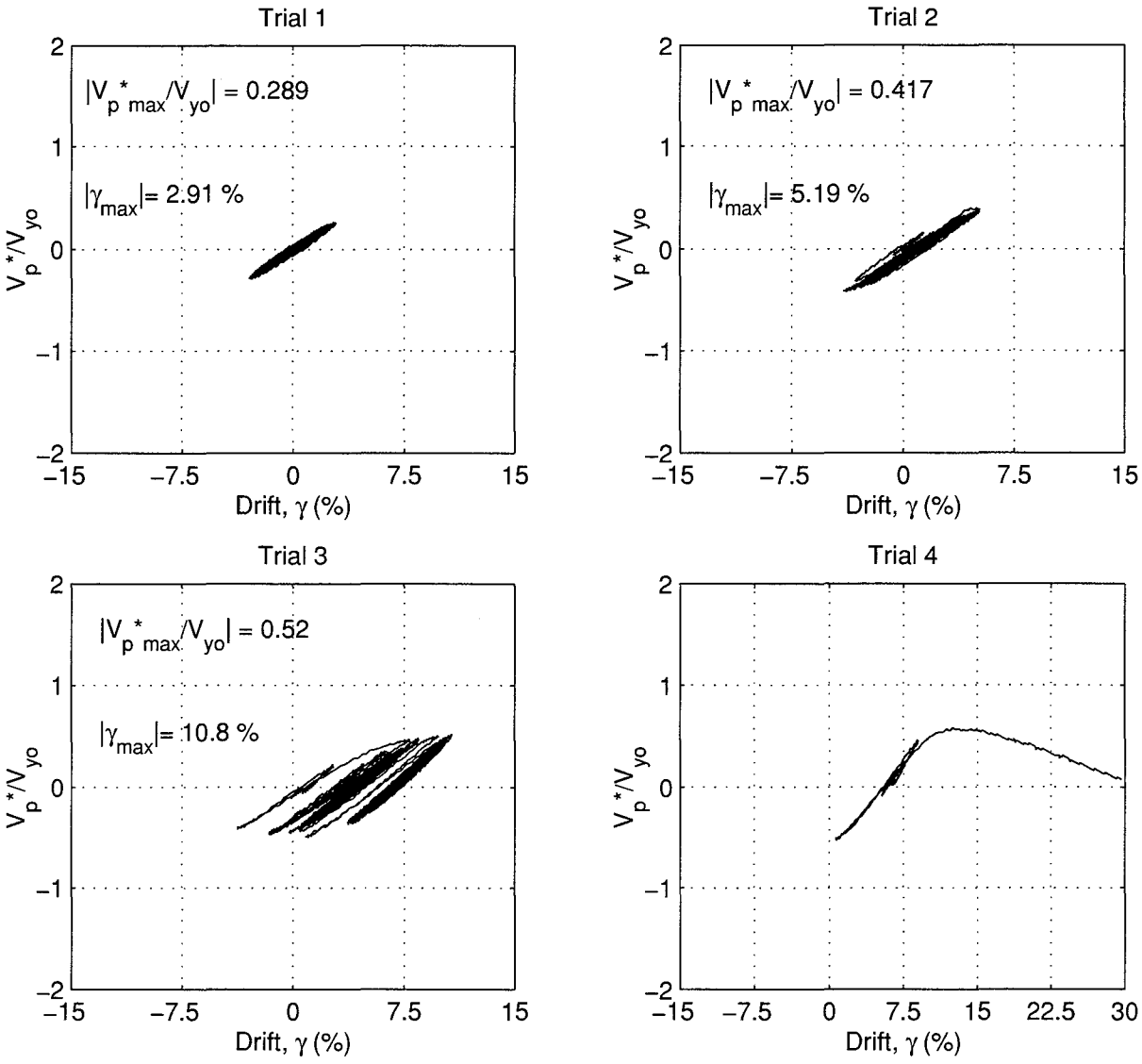

FIGURE 4–55 Specimen 8 – Normalized Base Shear vs. Drift

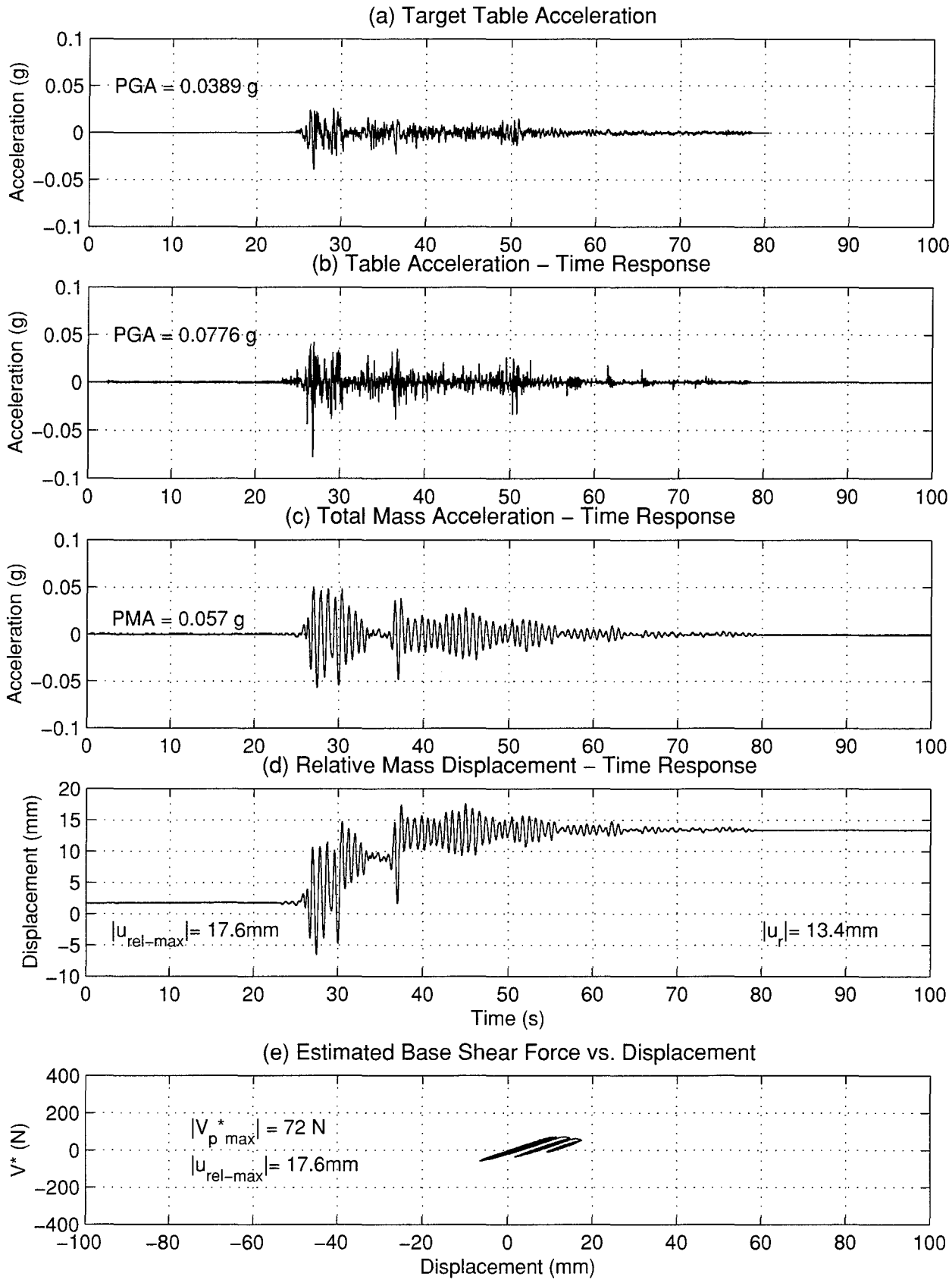

FIGURE 4-56 Seismic Response of Specimen 9 – Trial 3

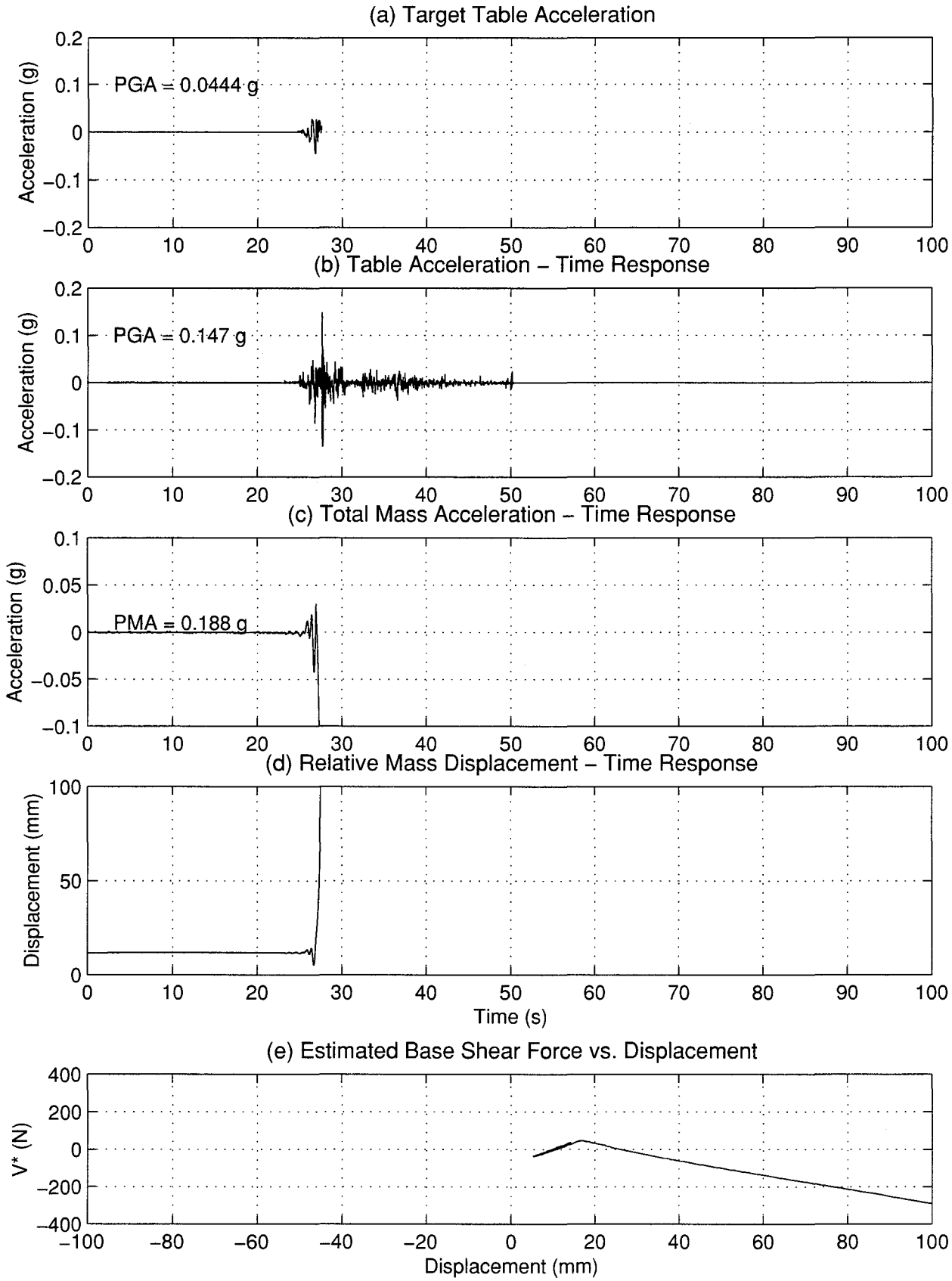

FIGURE 4–57 Seismic Response of Specimen 9 – Trial 4

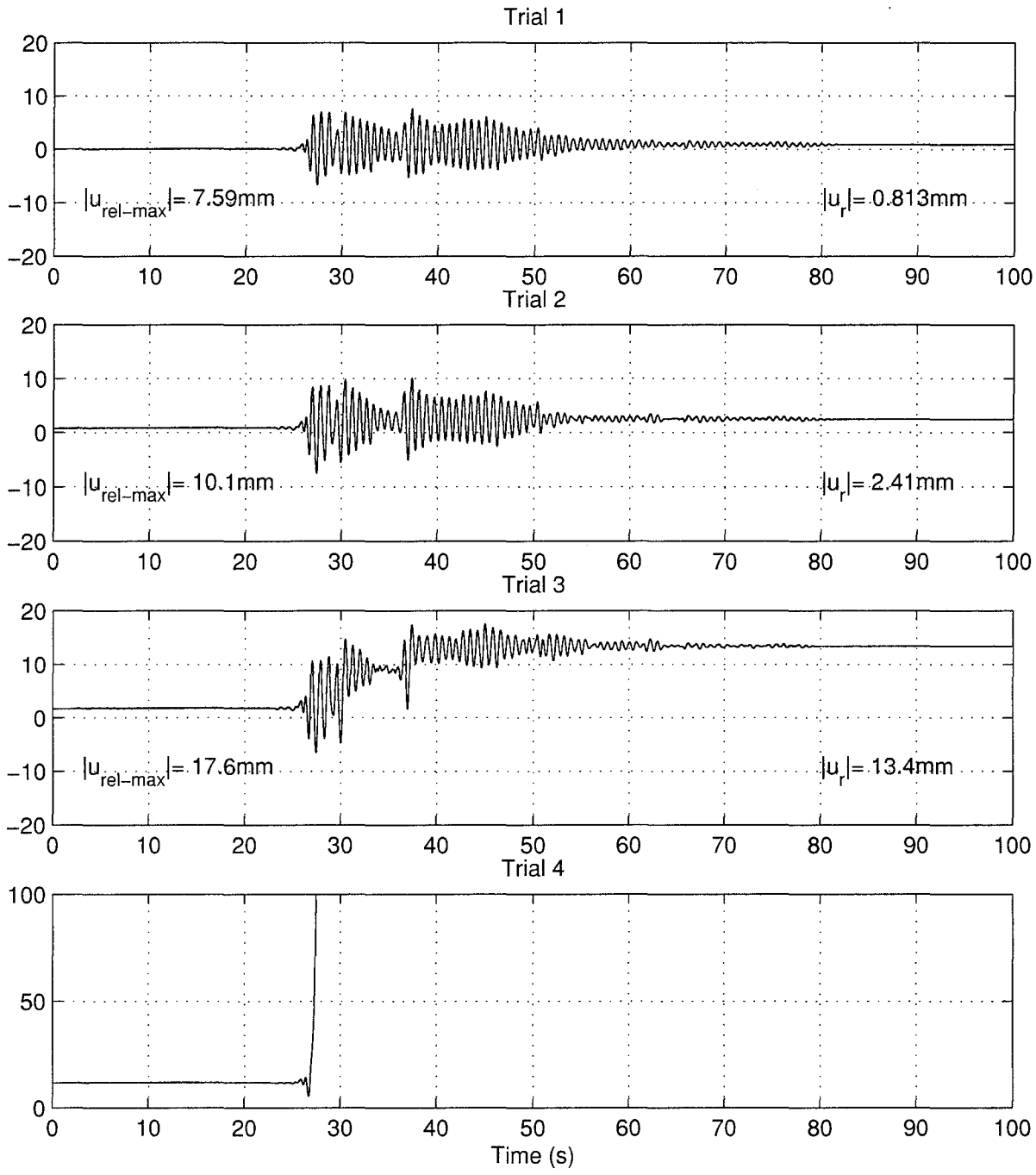

FIGURE 4–58 Specimen 9 – Progressive Displacement Time Histories

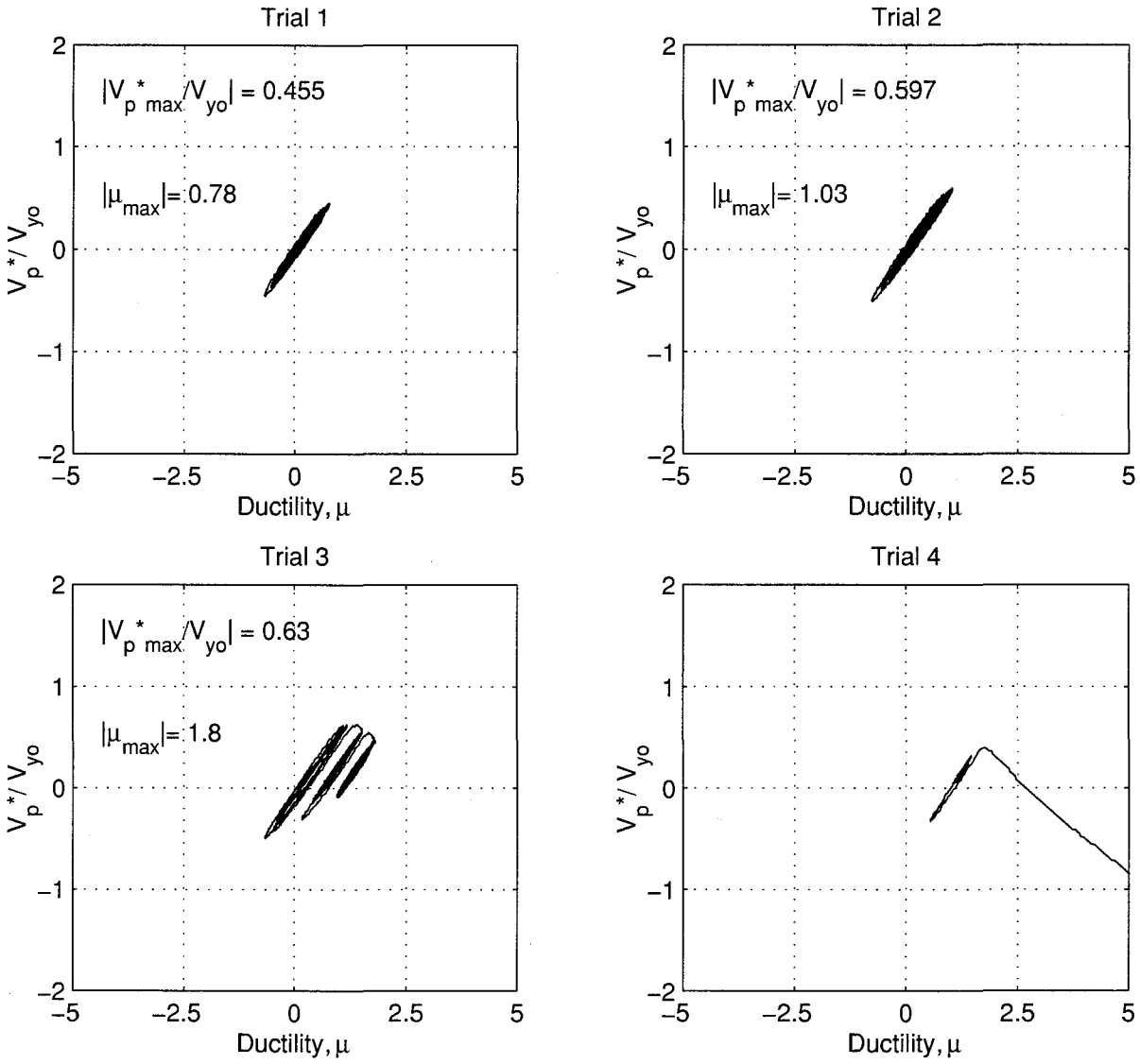

FIGURE 4–59 Specimen 9 – Normalized Base Shear vs. Ductility

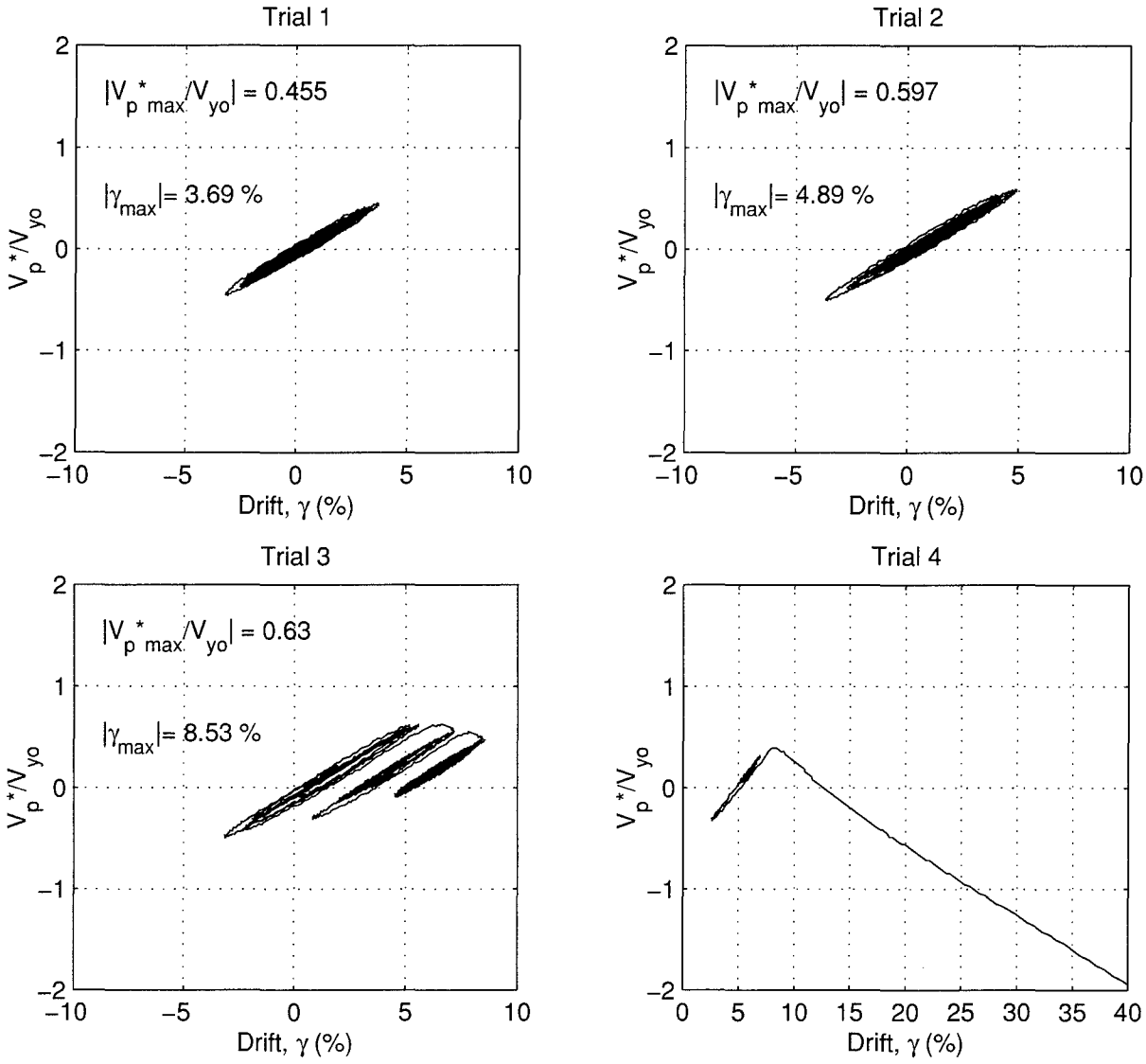

FIGURE 4-60 Specimen 9 – Normalized Base Shear vs. Drift

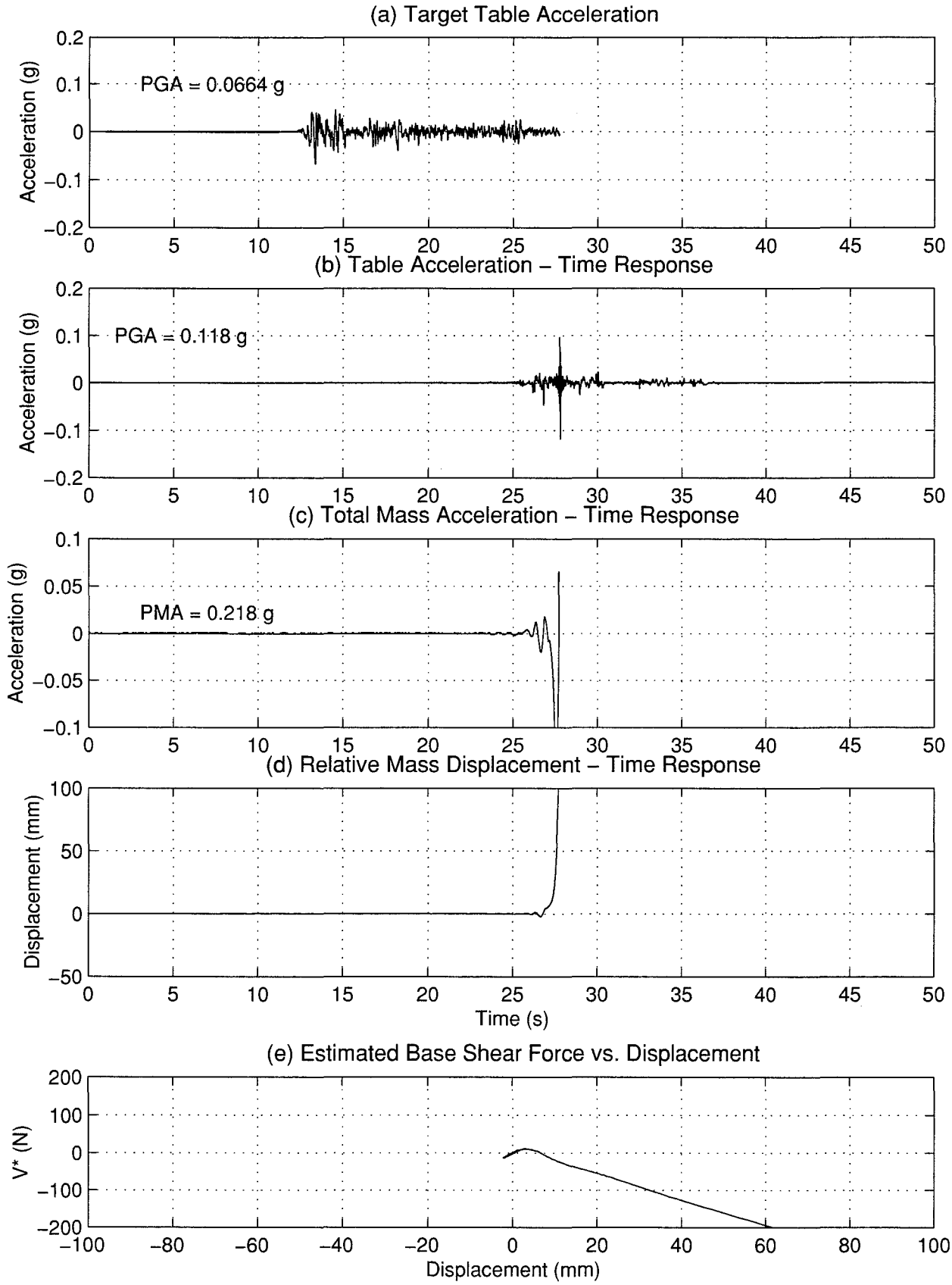

FIGURE 4–61 Seismic Response of Specimen 10 – Trial 1

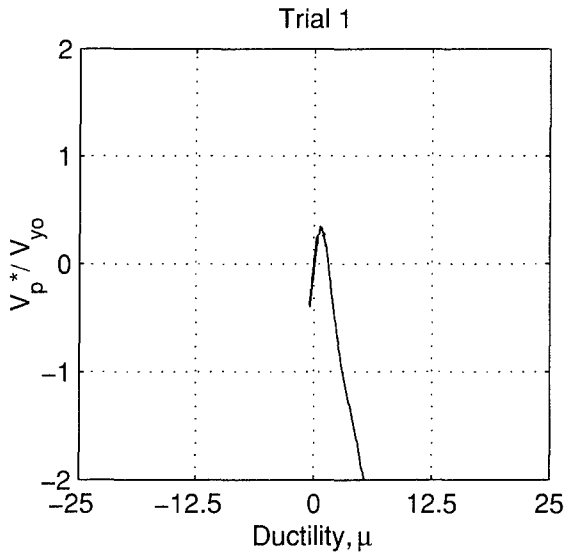

FIGURE 4–62 Specimen 10 – Normalized Base Shear vs. Ductility

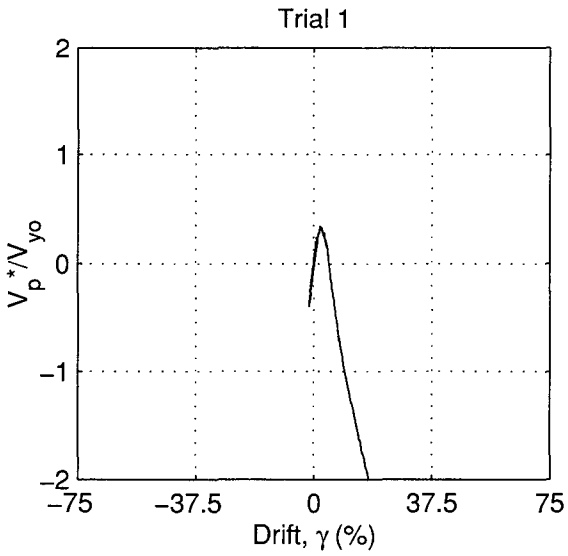

FIGURE 4–63 Specimen 10 – Normalized Base Shear vs. Drift

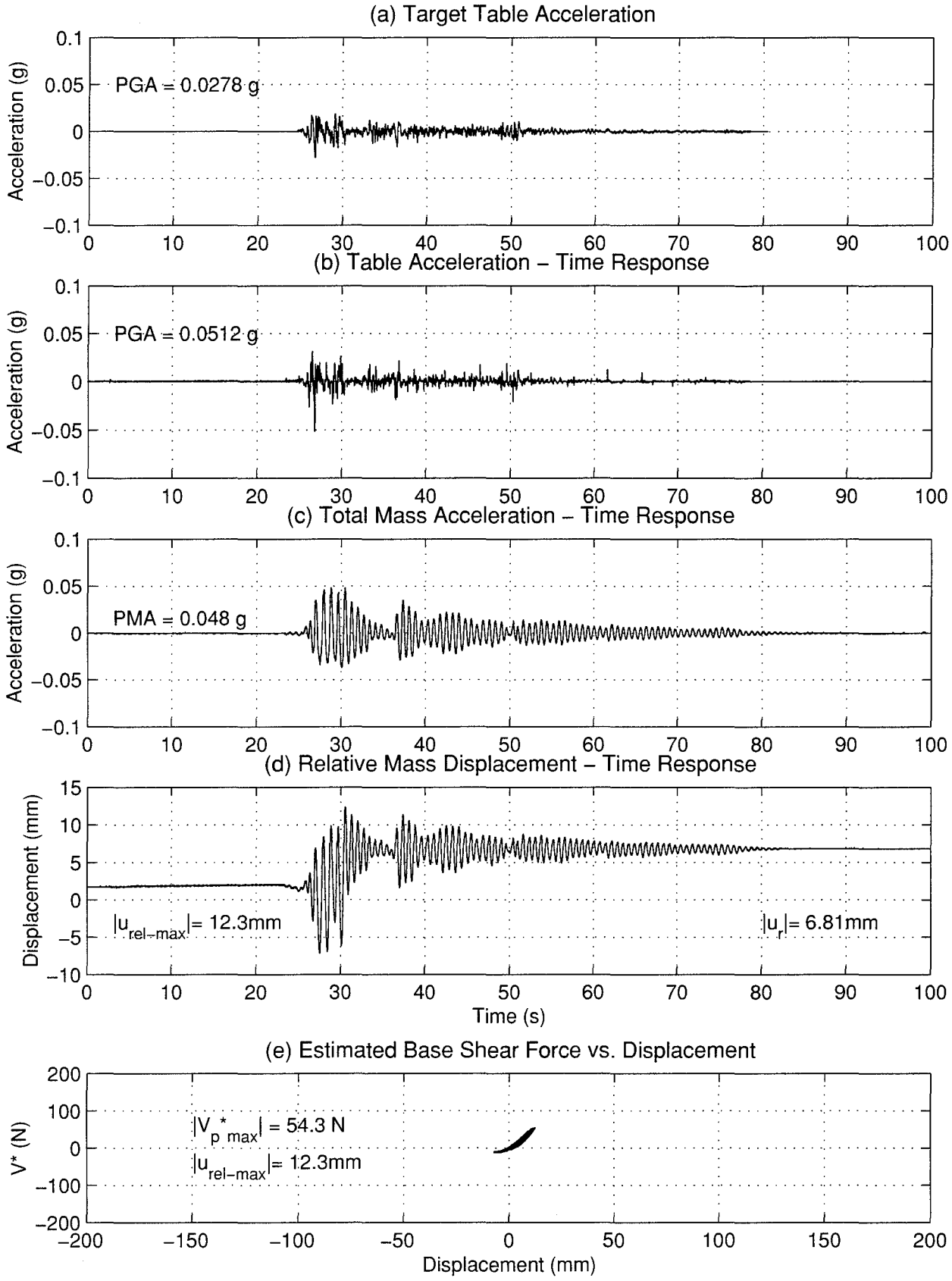

FIGURE 4–64 Seismic Response of Specimen 10b – Trial 4

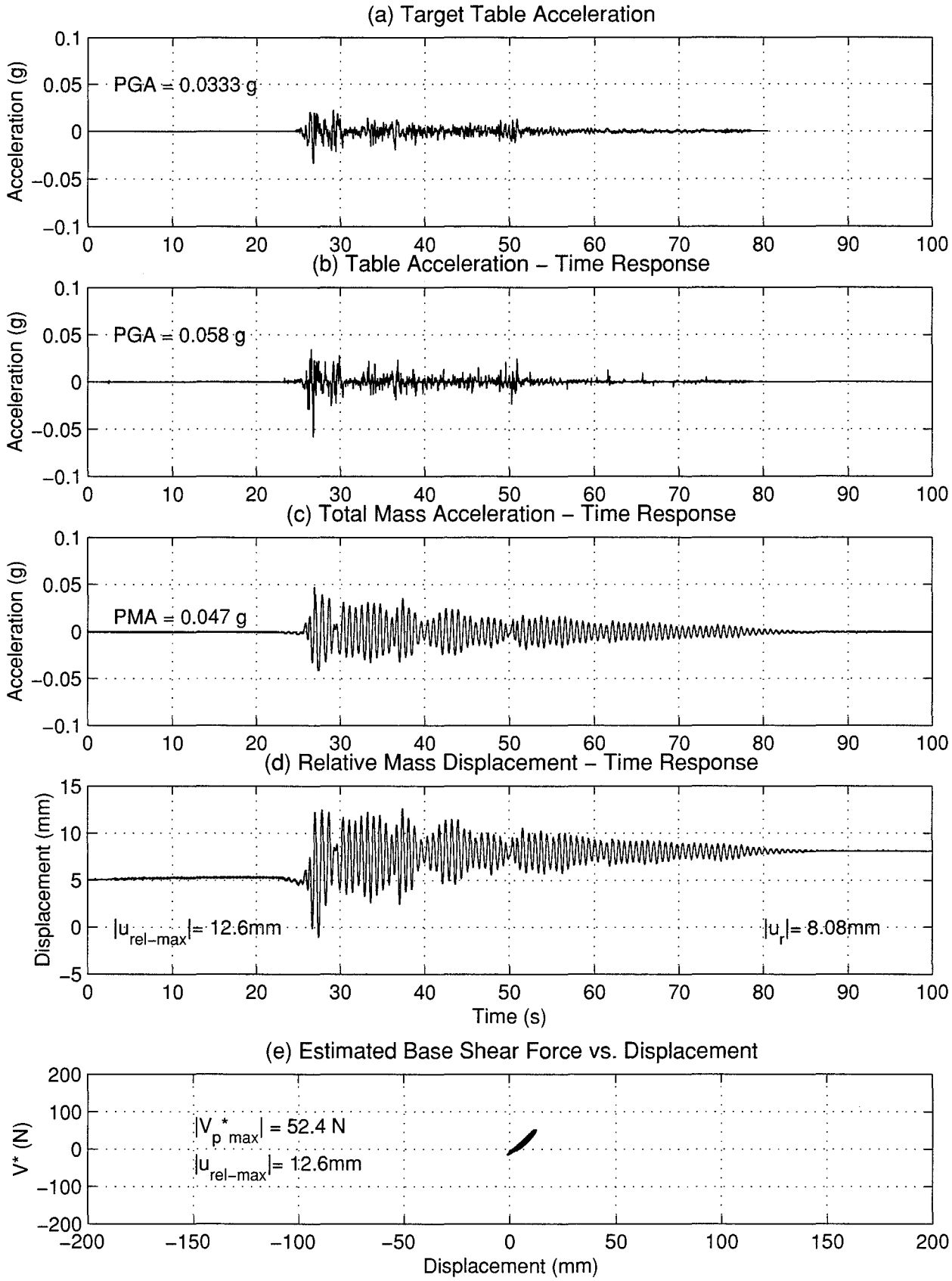

FIGURE 4–65 Seismic Response of Specimen 10b – Trial 5

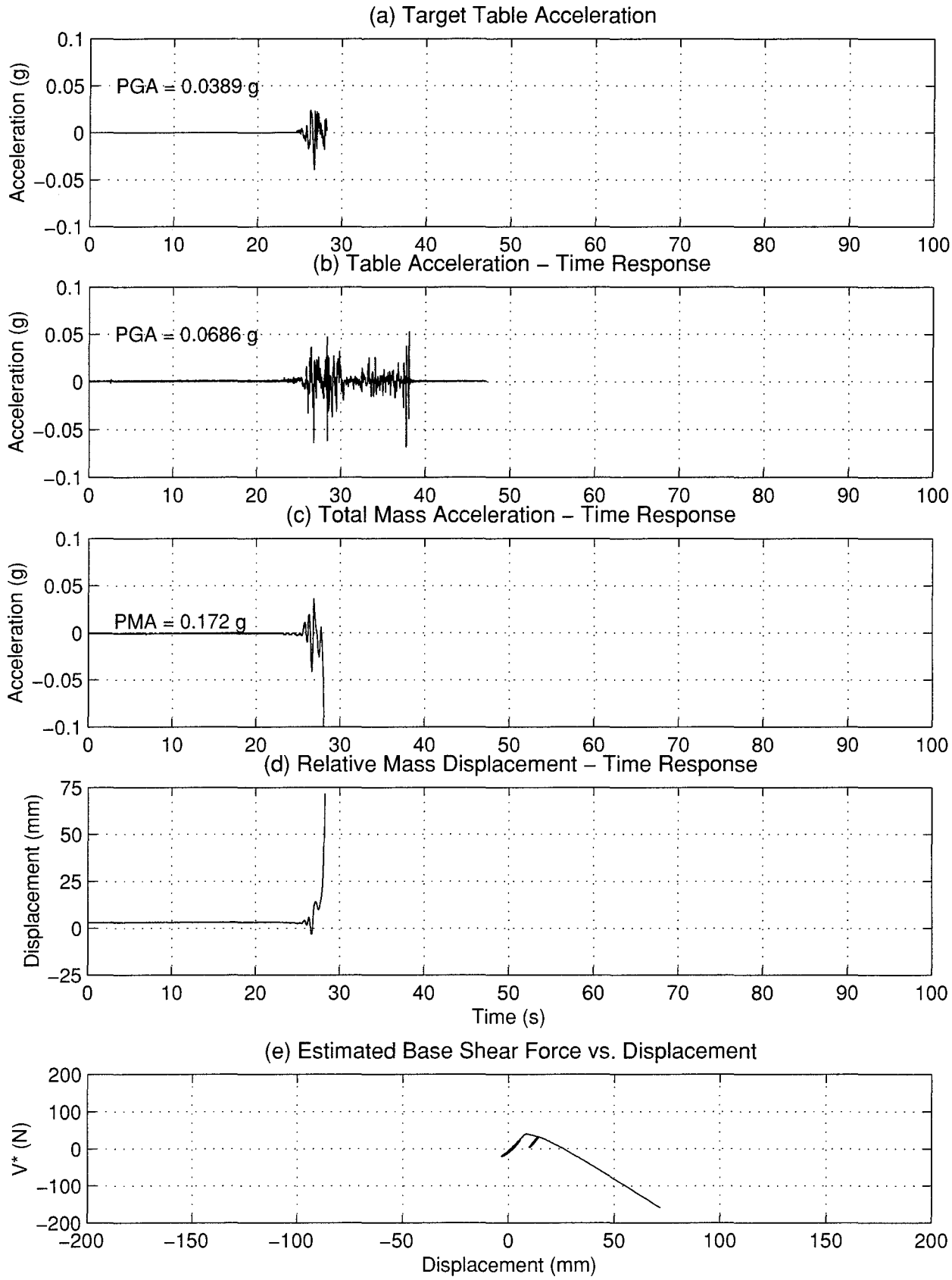

FIGURE 4–66 Seismic Response of Specimen 10b – Trial 6

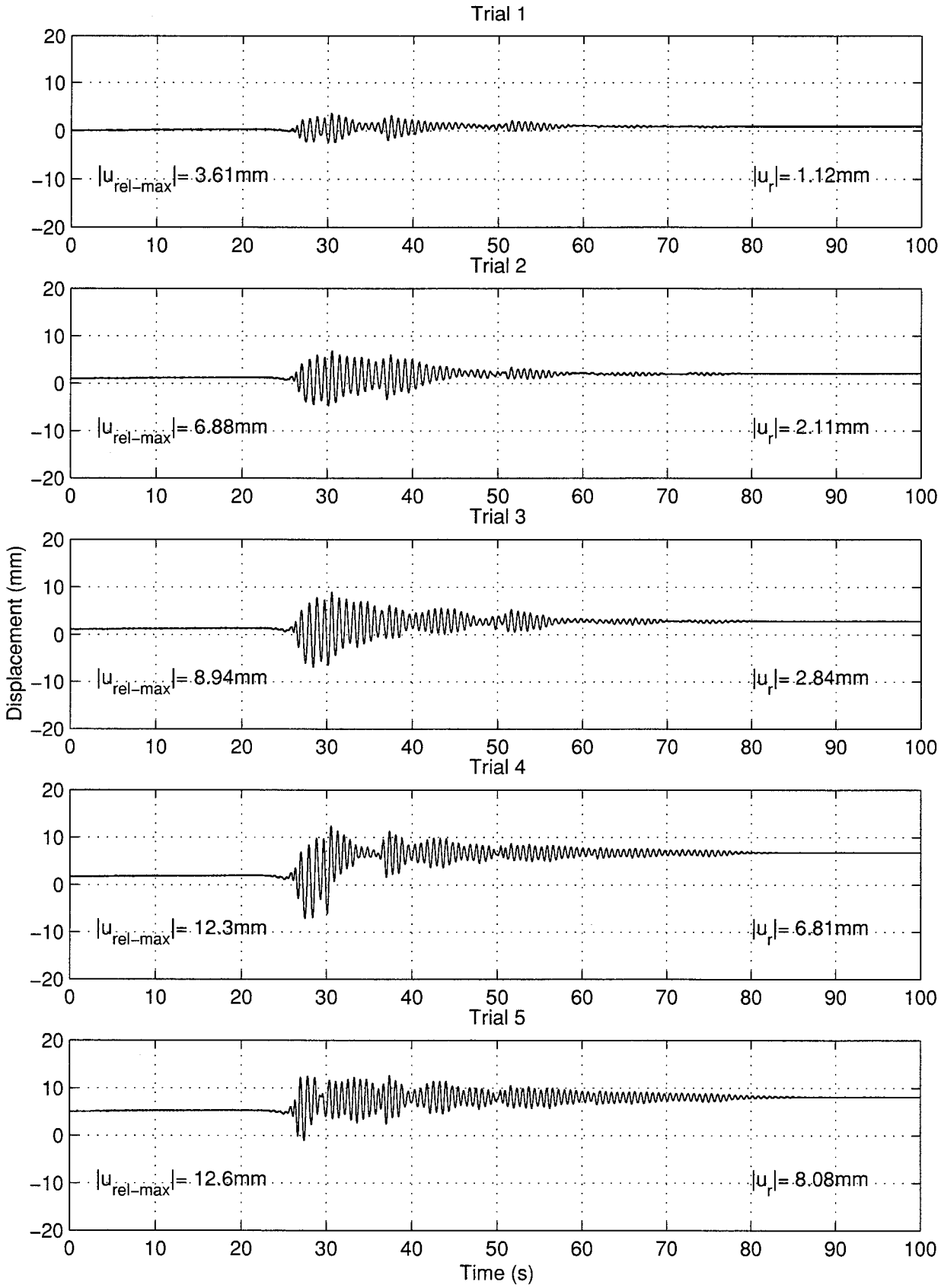

FIGURE 4–67 Specimen 10b – Progressive Displacement Time Histories

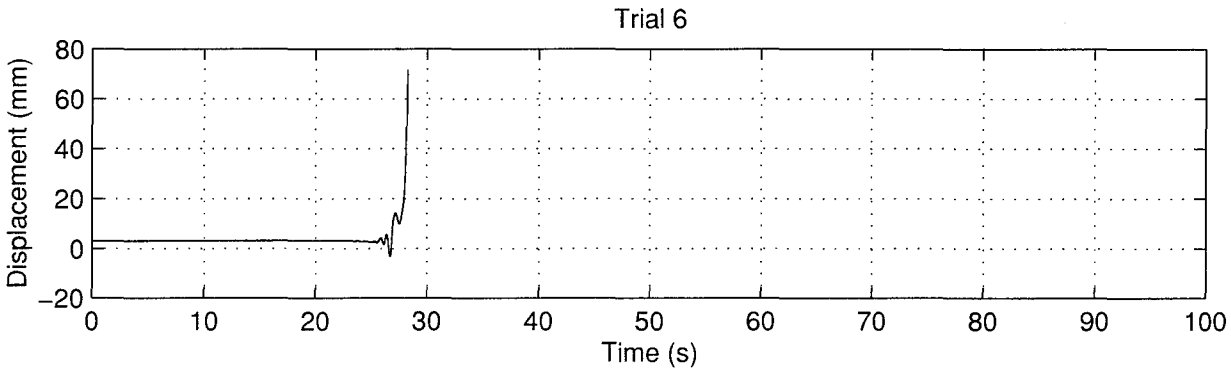

FIGURE 4–67 (cont'd) Specimen 10b – Progressive Displacement Time Histories

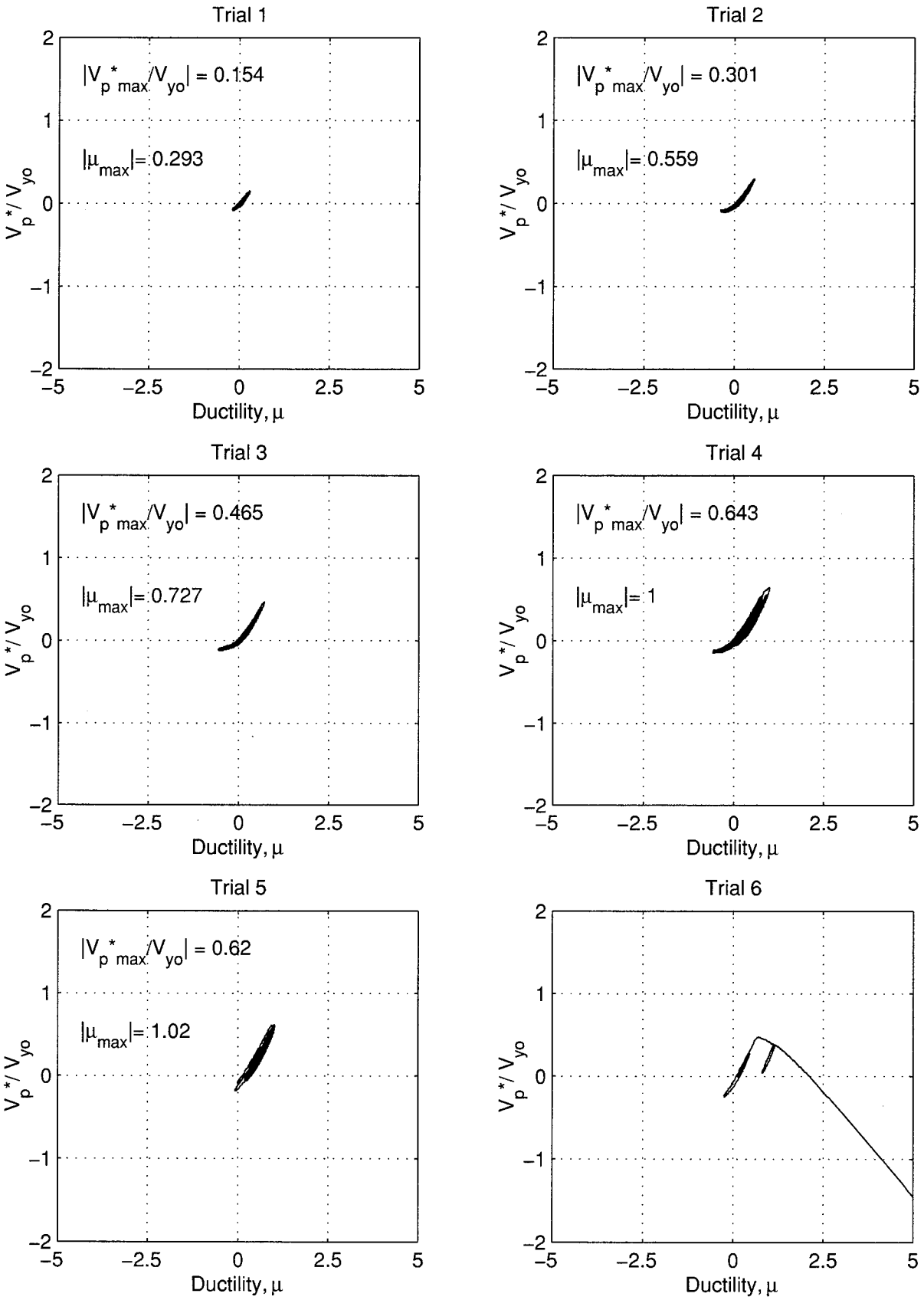

FIGURE 4–68 Specimen 10b – Normalized Base Shear vs. Ductility

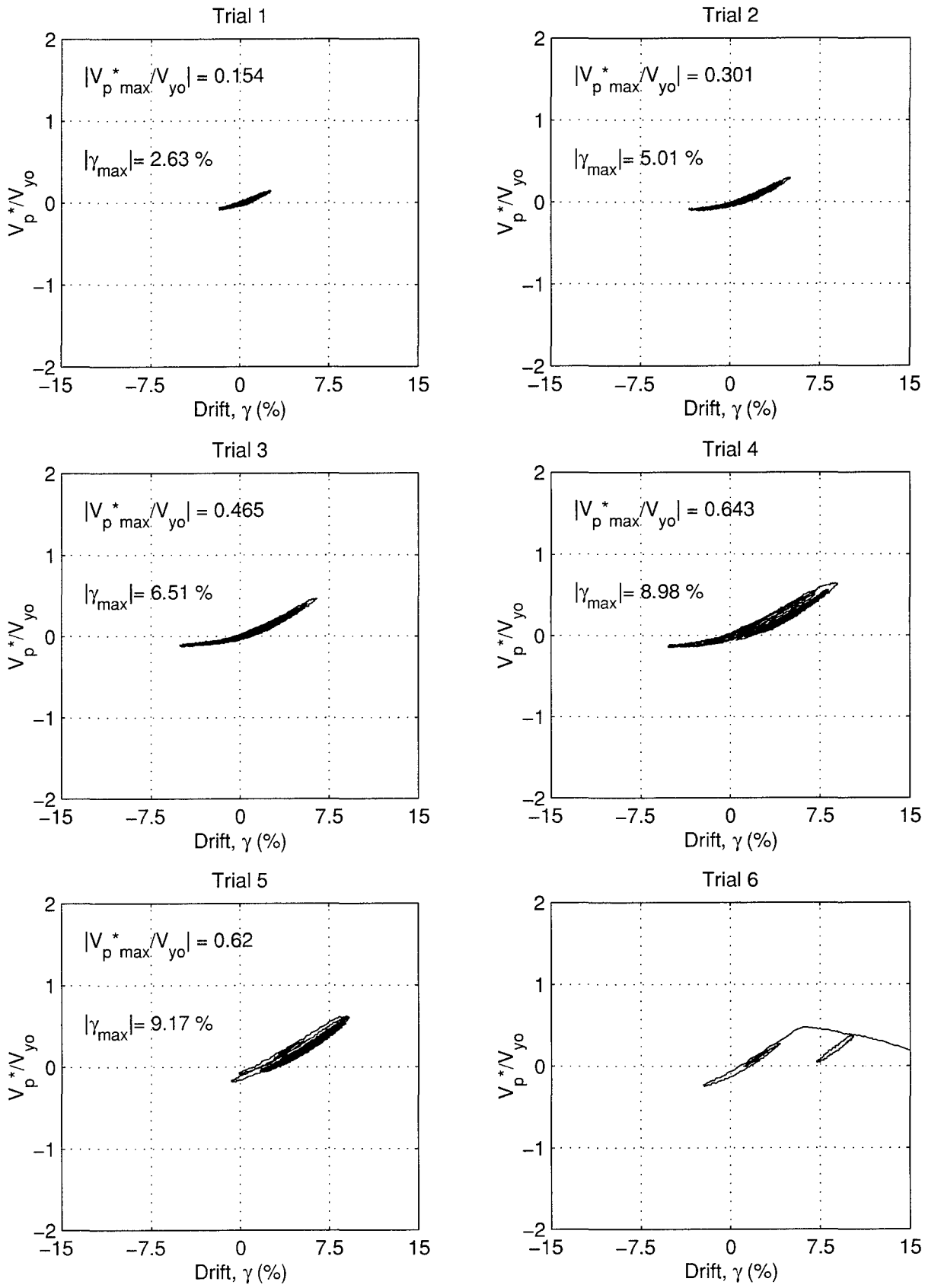

FIGURE 4-69 Specimen 10b - Normalized Base Shear vs. Drift

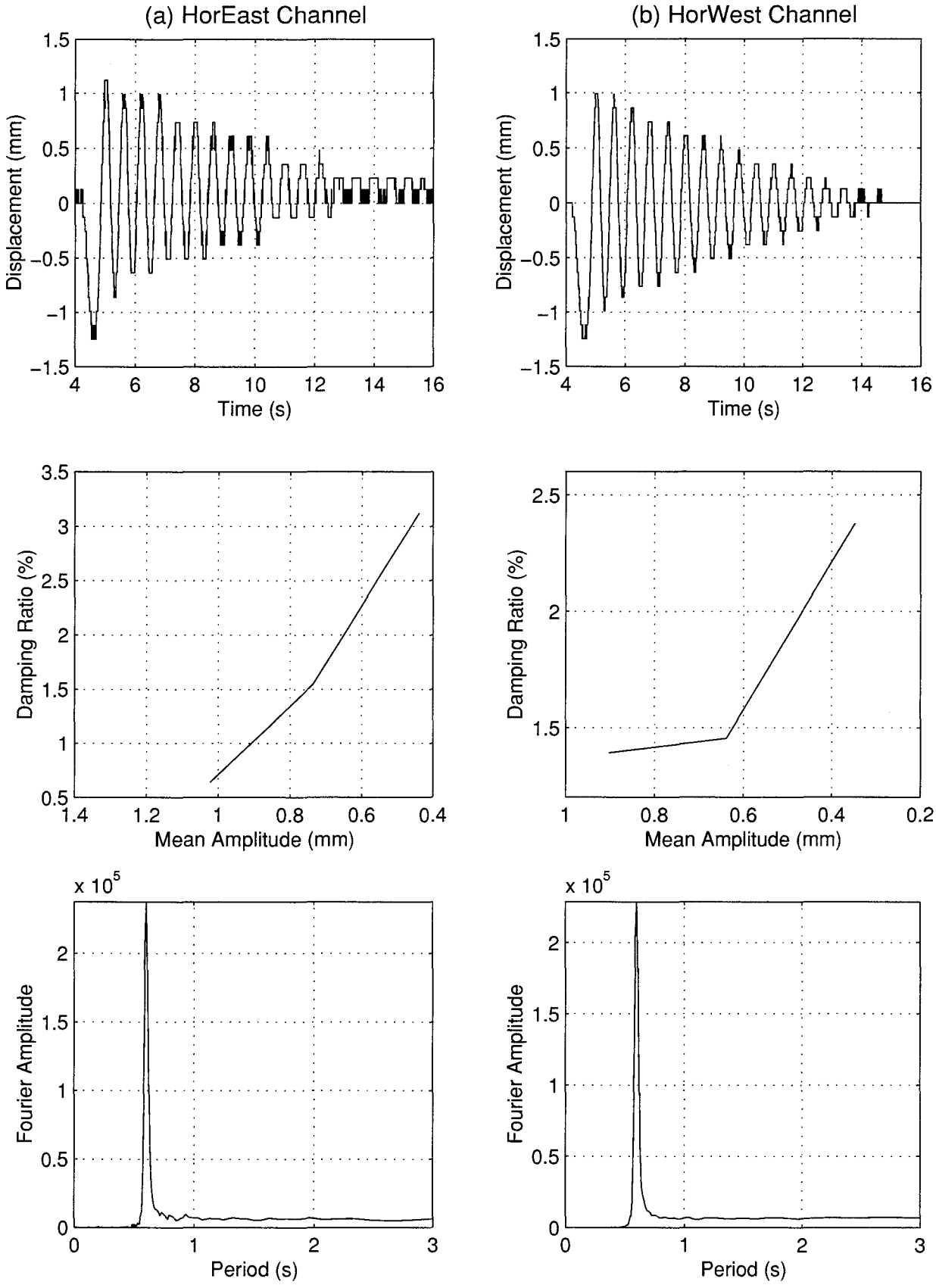

FIGURE 4–70 Free Vibration Test of Specimen11

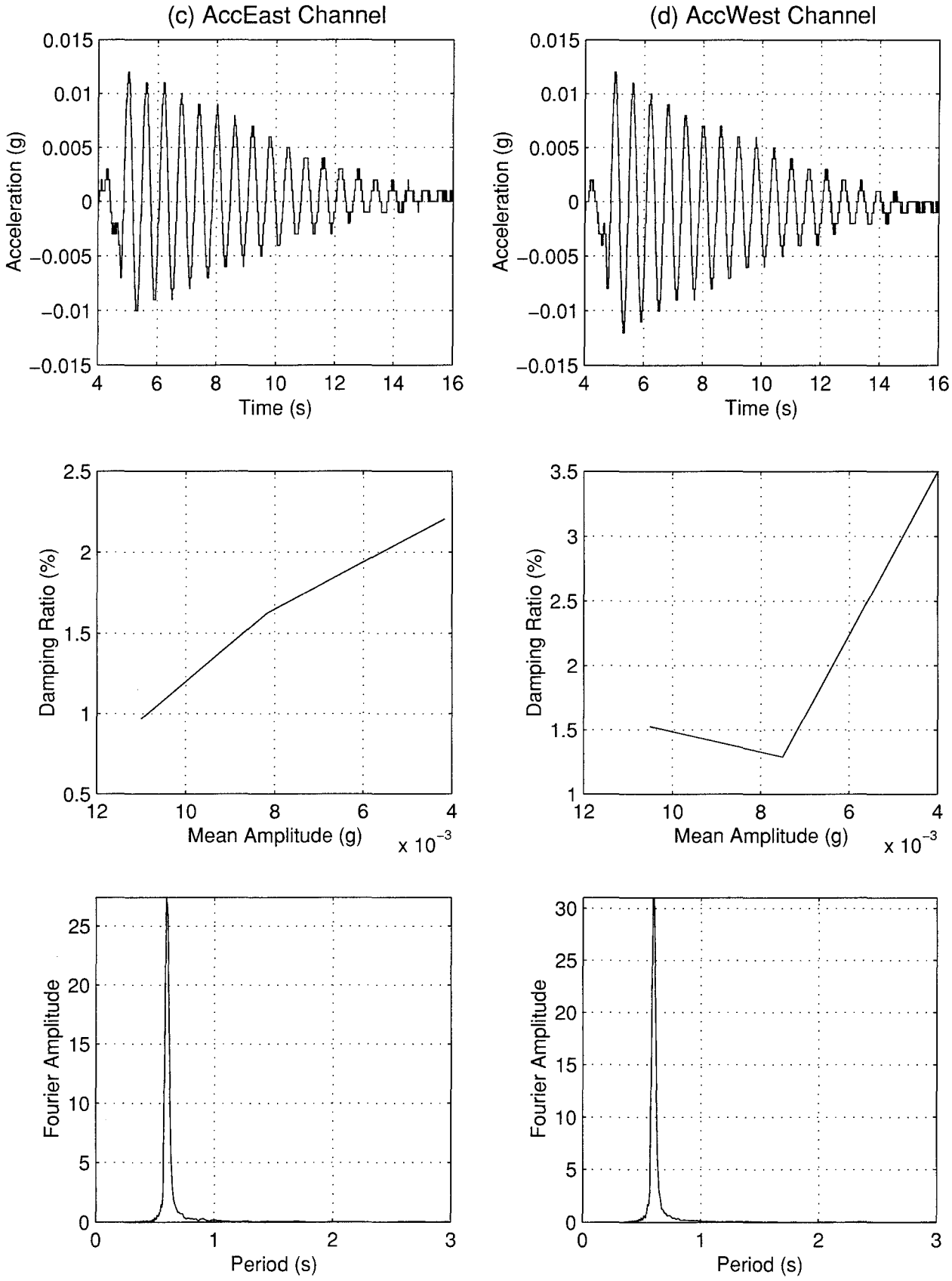

FIGURE 4-70 (cont'd) Free Vibration Test of Specimen11

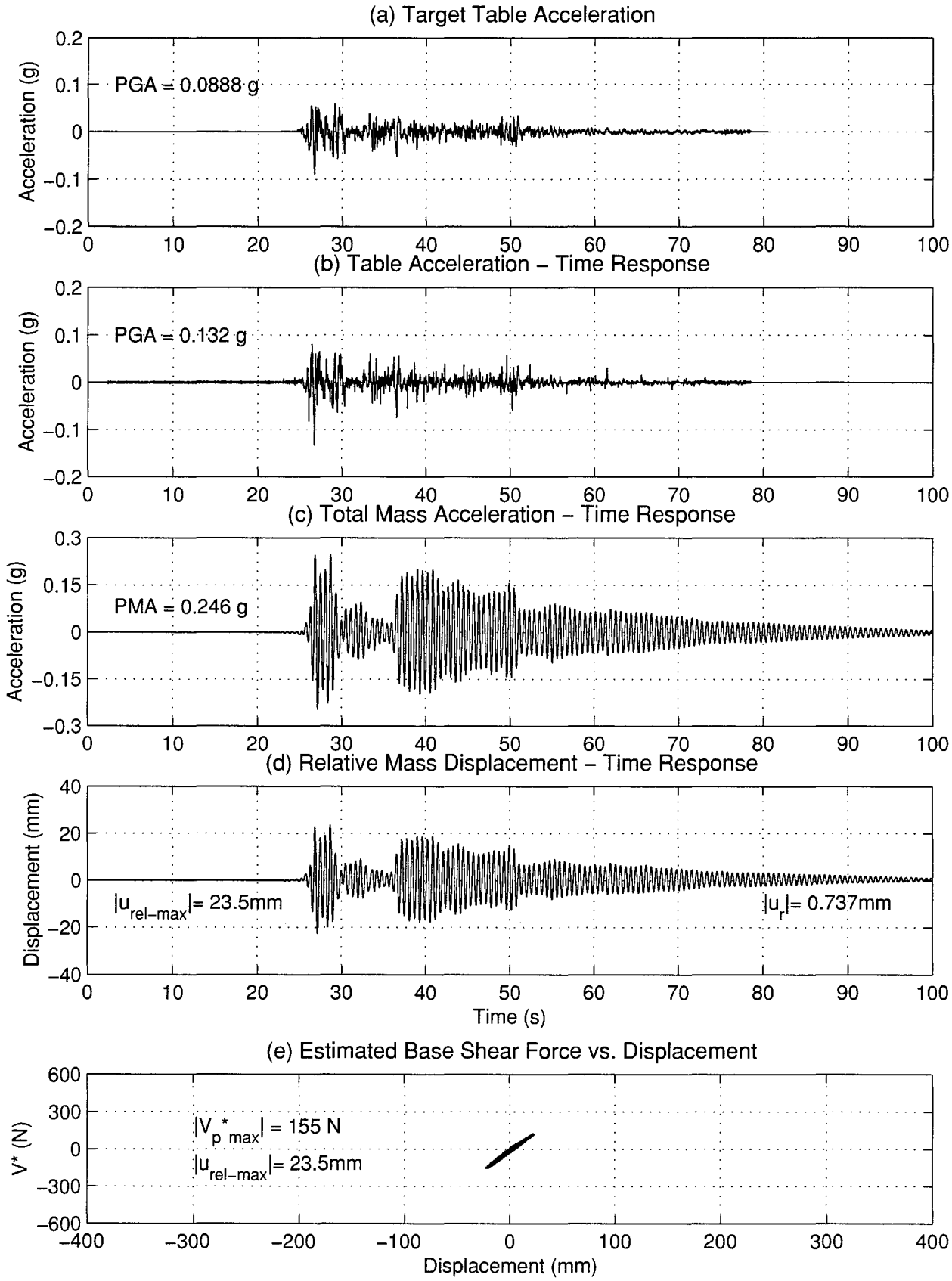

FIGURE 4–71 Seismic Response of Specimen 11 – Trial 1

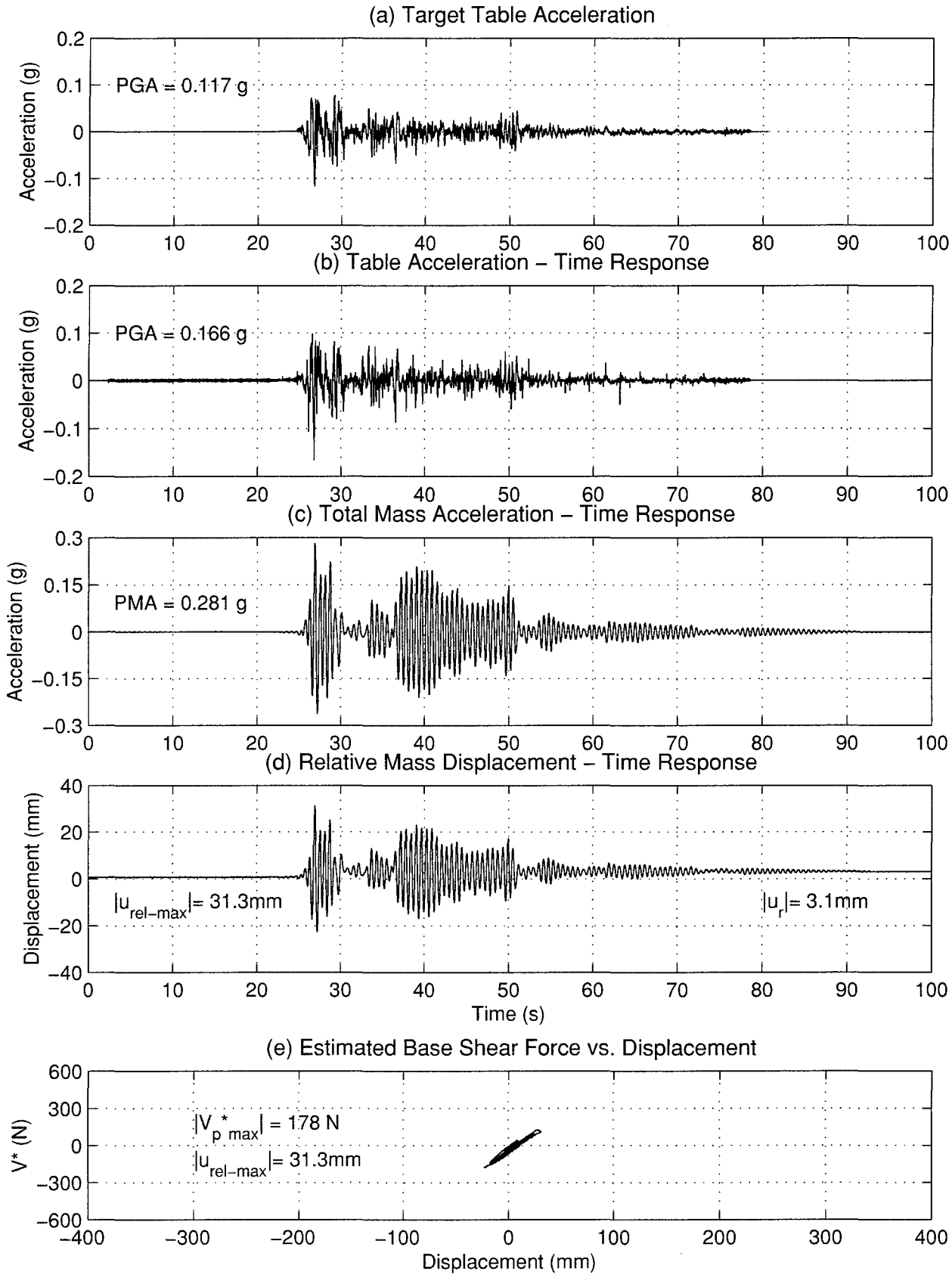

FIGURE 4–72 Seismic Response of Specimen 11 – Trial 2

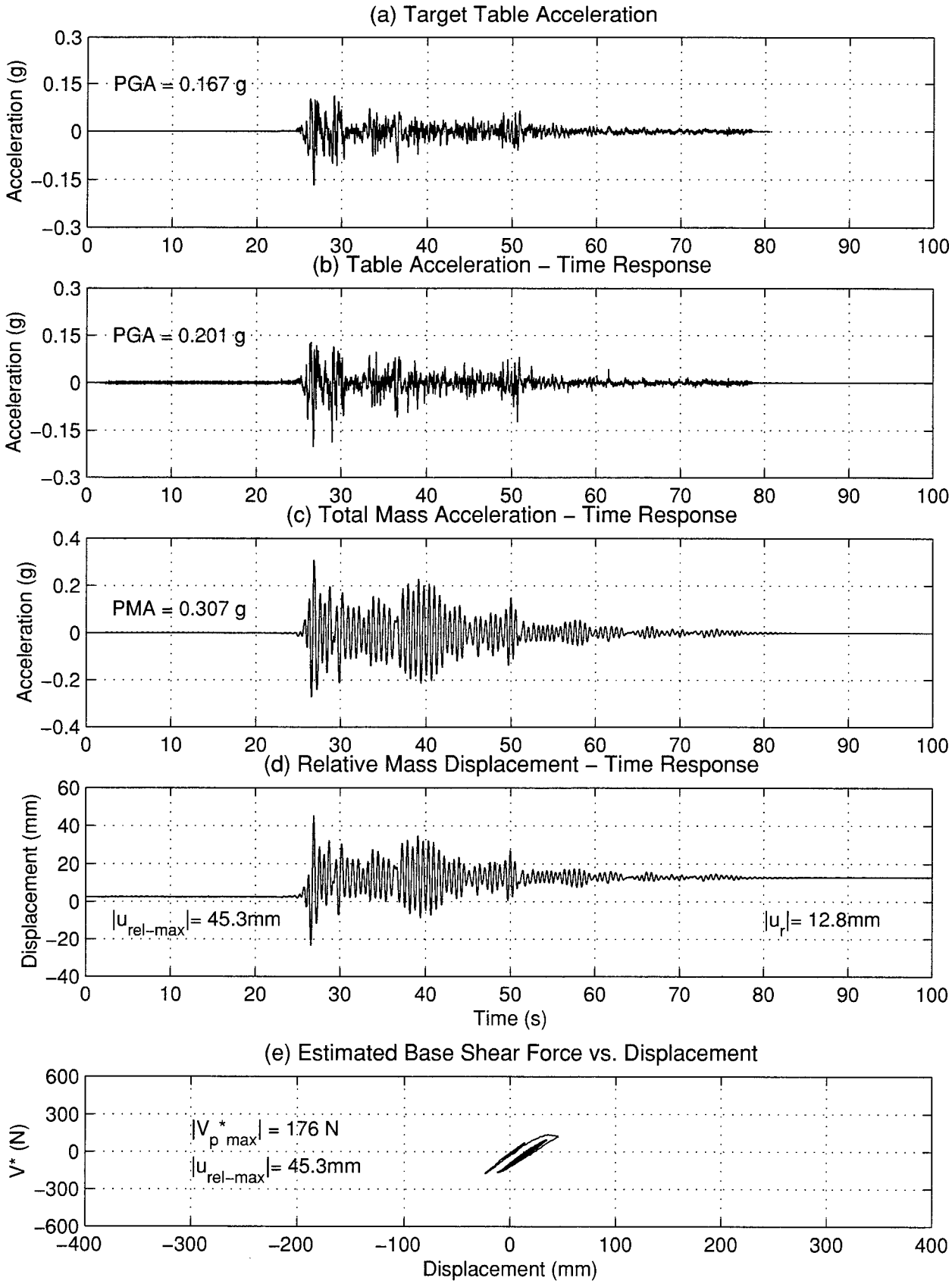

FIGURE 4–73 Seismic Response of Specimen 11 – Trial 3

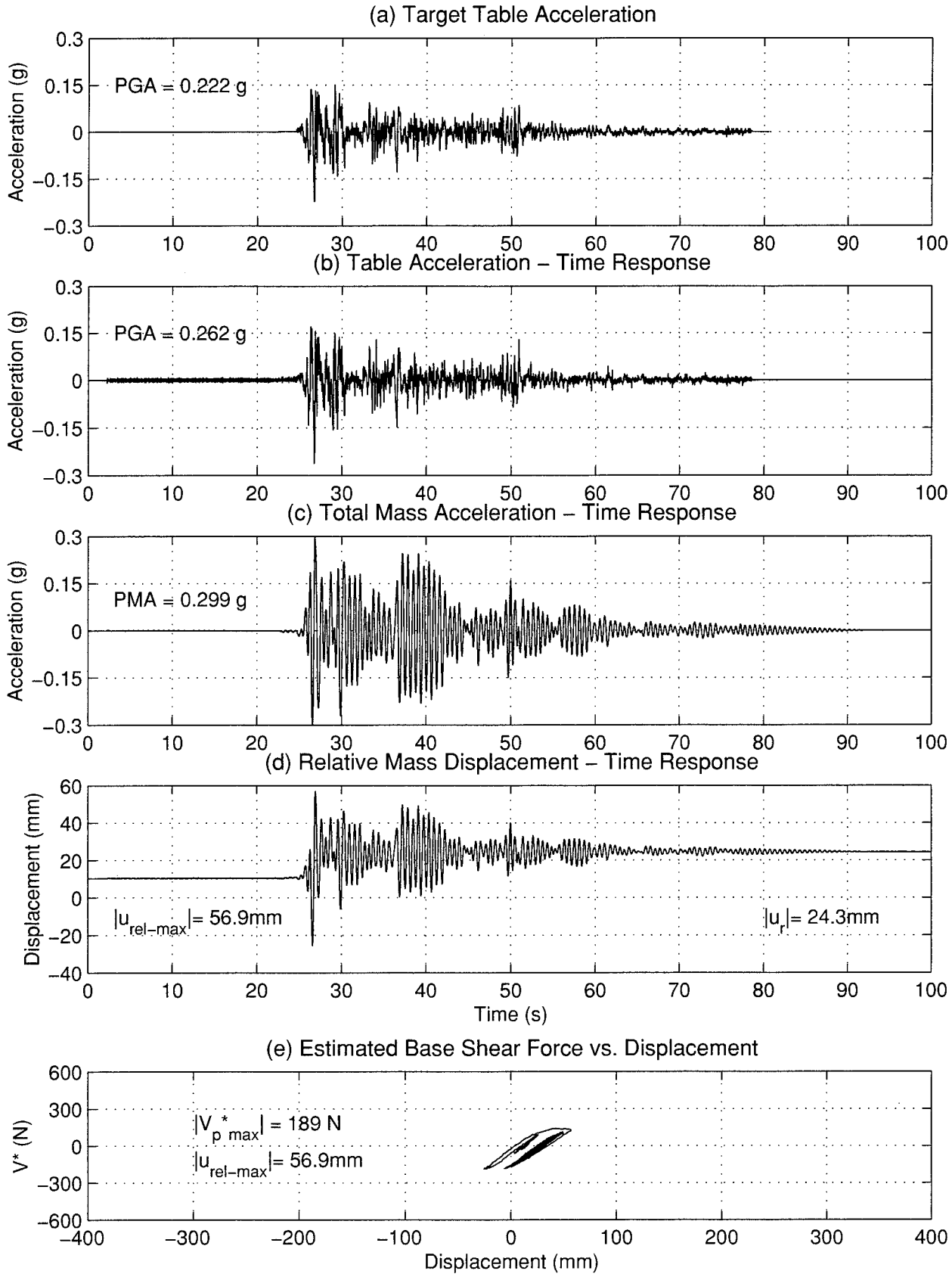

FIGURE 4–74 Seismic Response of Specimen 11 – Trial 4

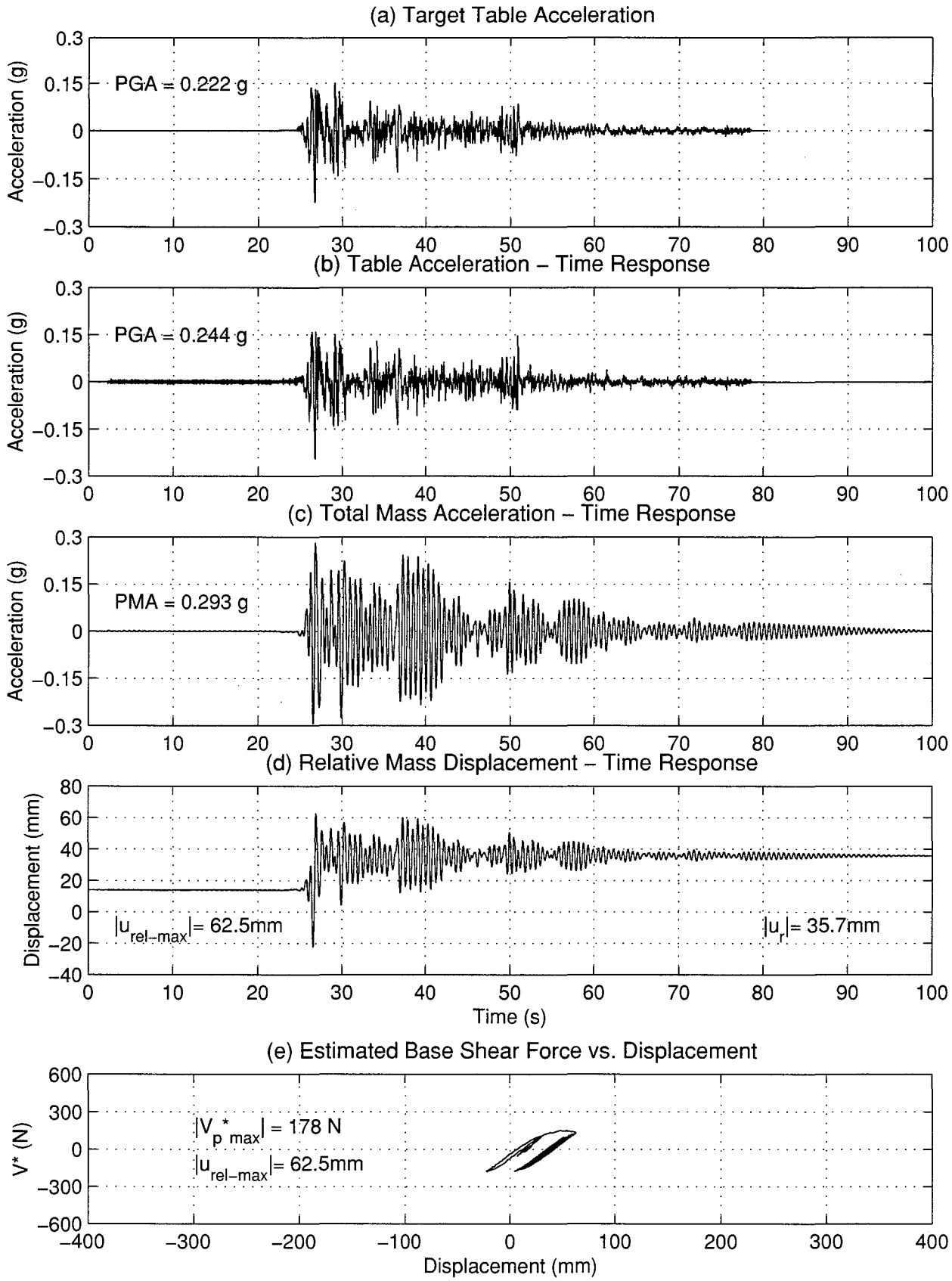

FIGURE 4–75 Seismic Response of Specimen 11 – Trial 5

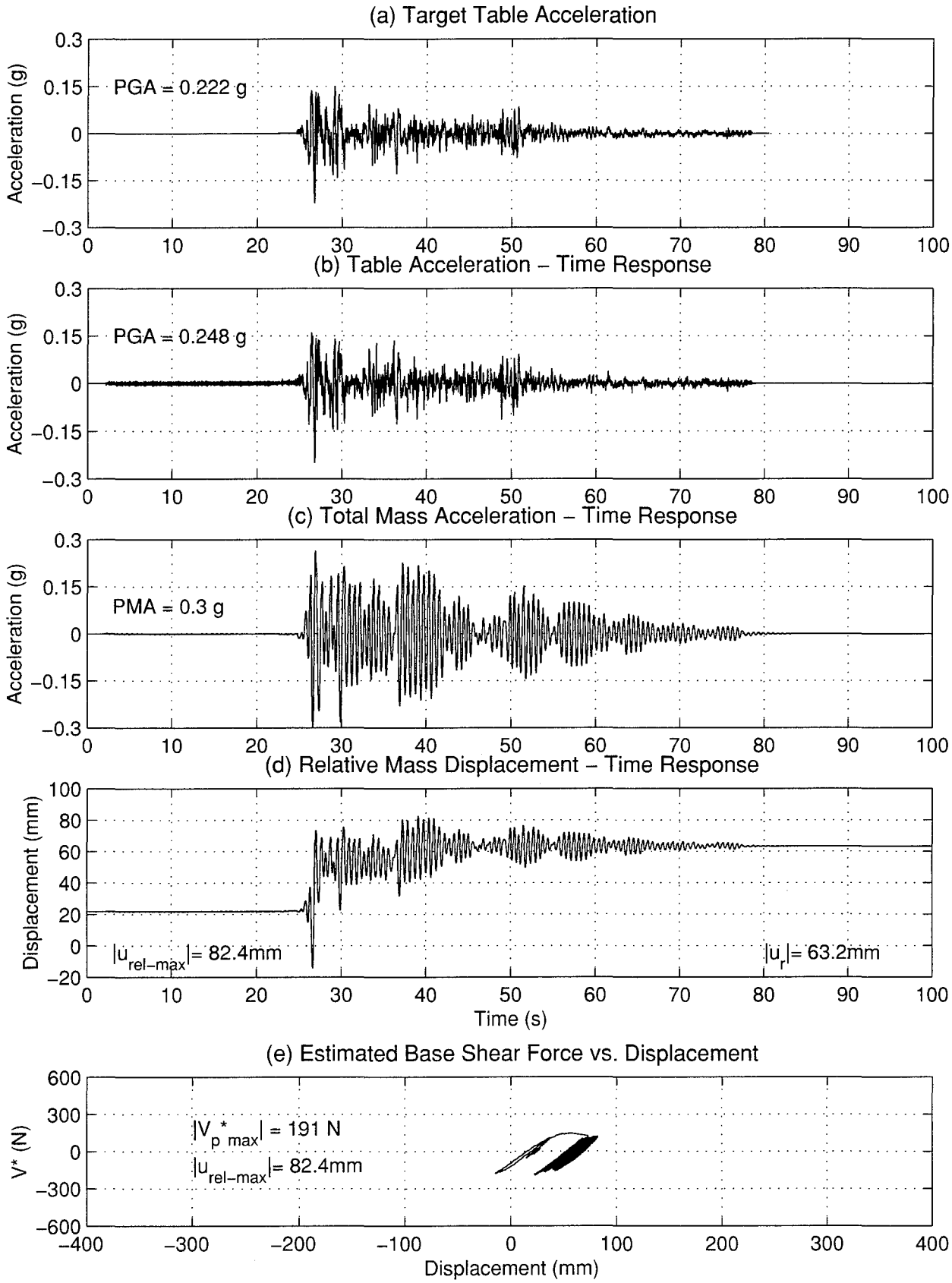

FIGURE 4–76 Seismic Response of Specimen 11 – Trial 6

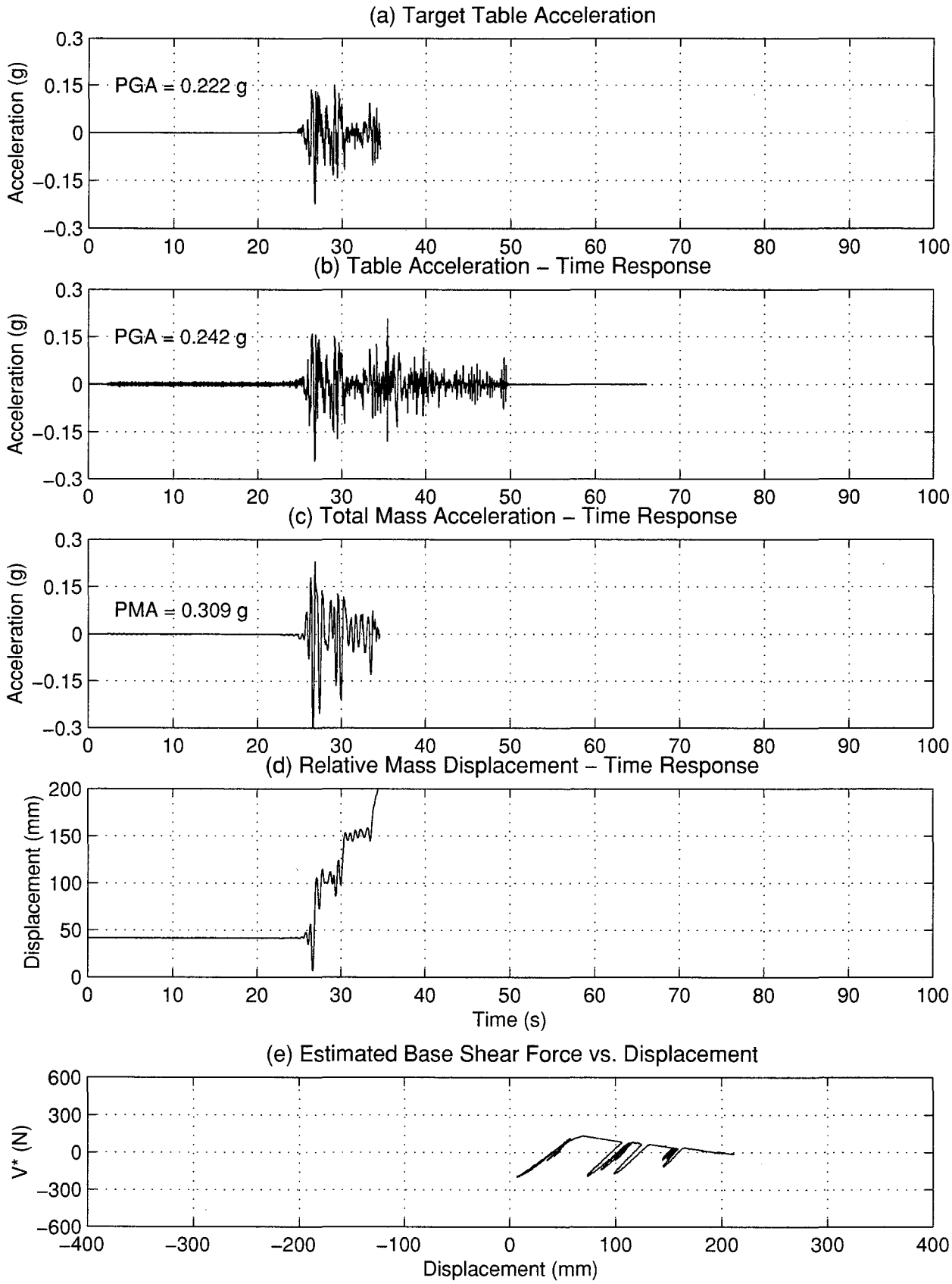

FIGURE 4–77 Seismic Response of Specimen 11 – Trial 7

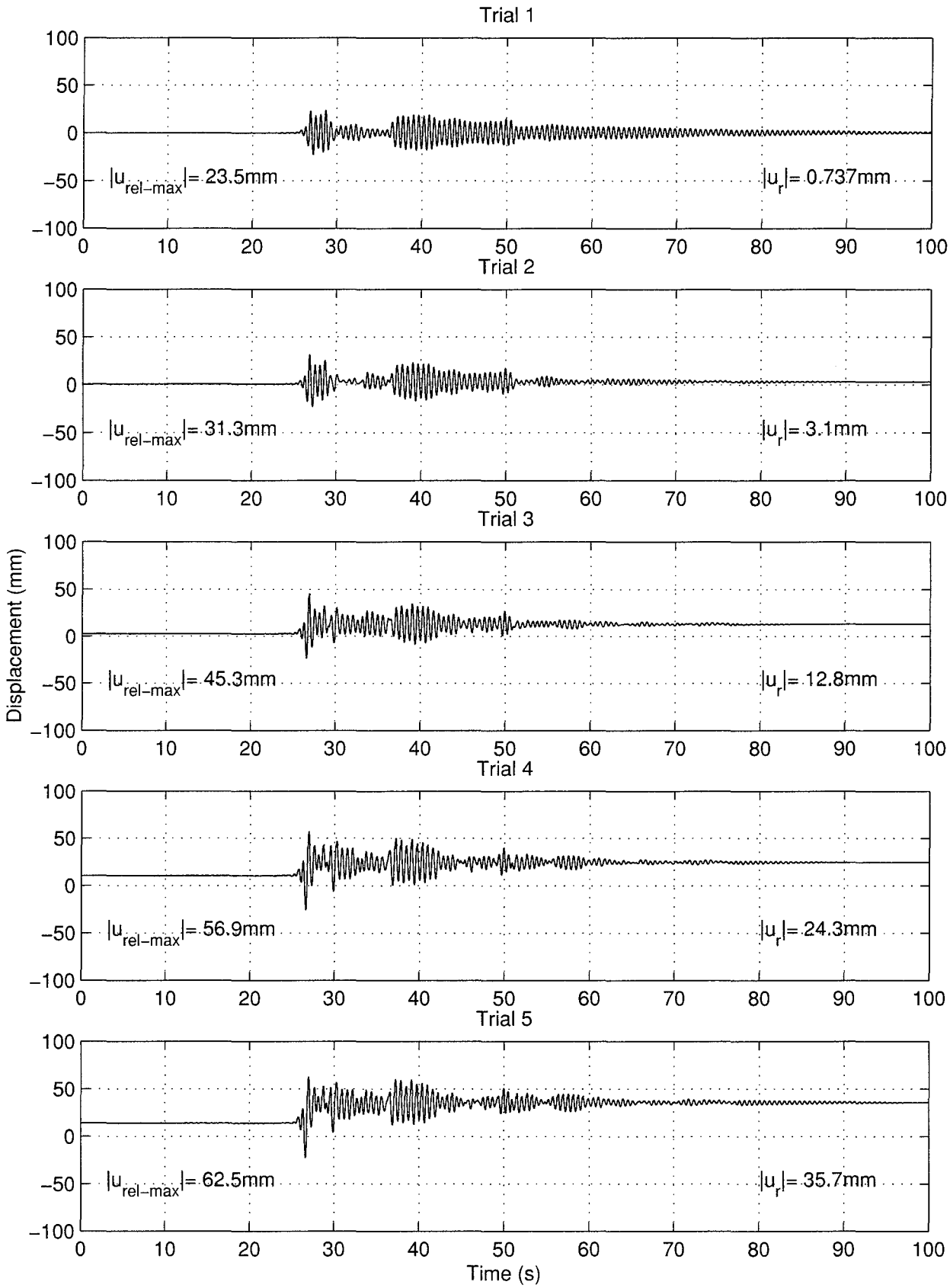

FIGURE 4–78 Specimen 11 – Progressive Displacement Time Histories

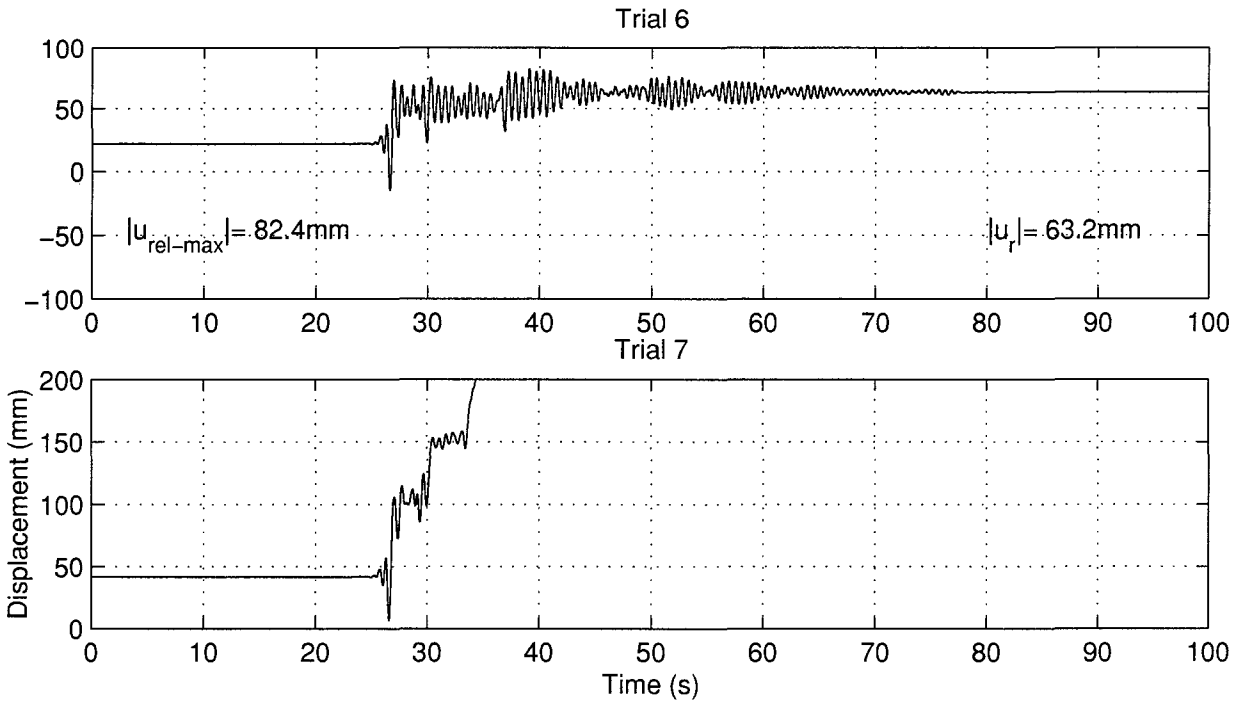

FIGURE 4–78 (cont'd) Specimen 11 – Progressive Displacement Time Histories

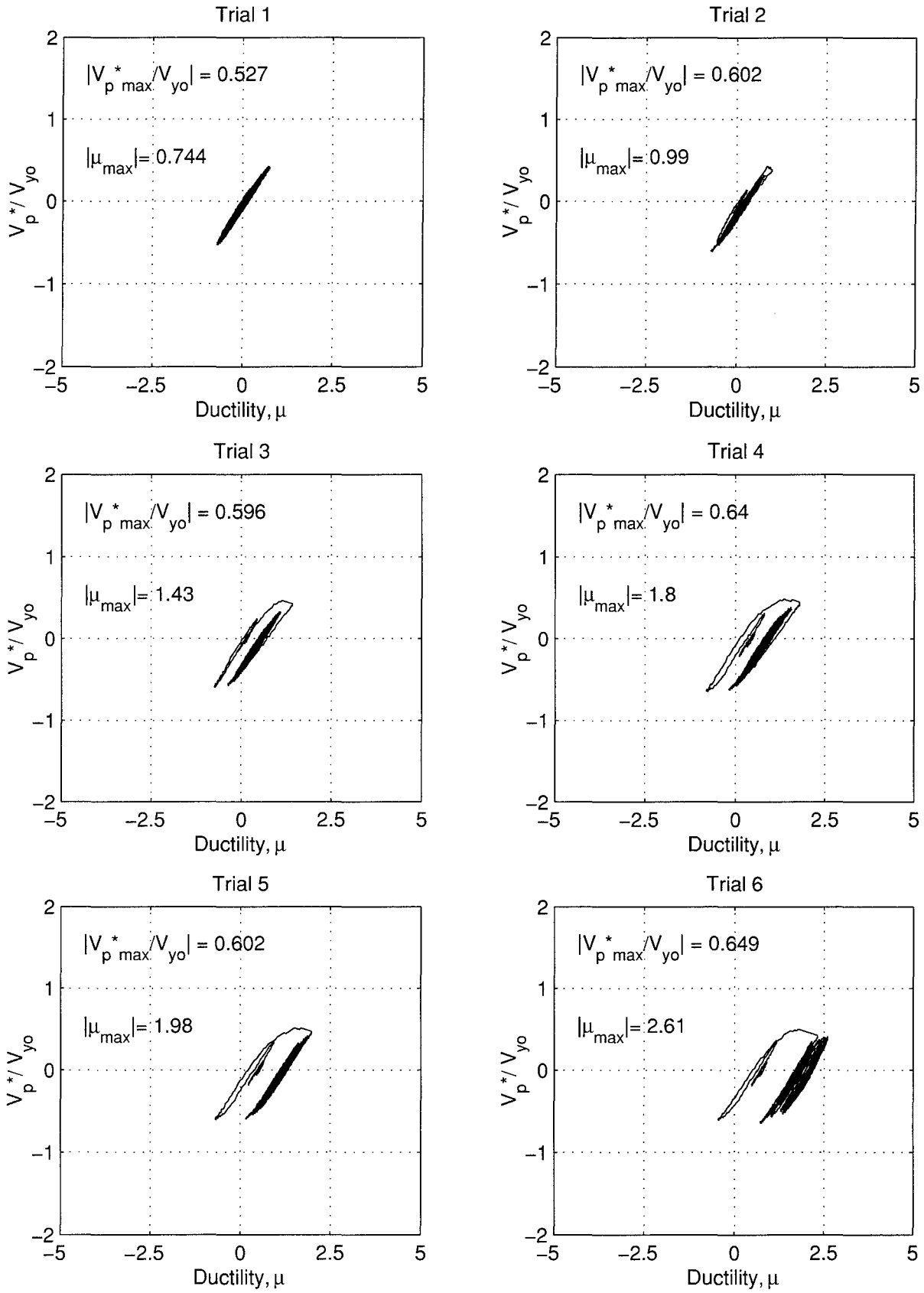

FIGURE 4–79 Specimen 11 – Normalized Base Shear vs. Ductility

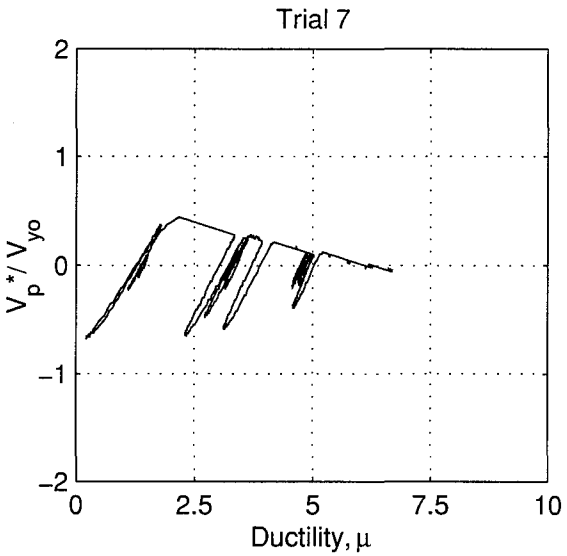

FIGURE 4–79 (cont'd) Specimen 11 – Normalized Base Shear vs. Ductility

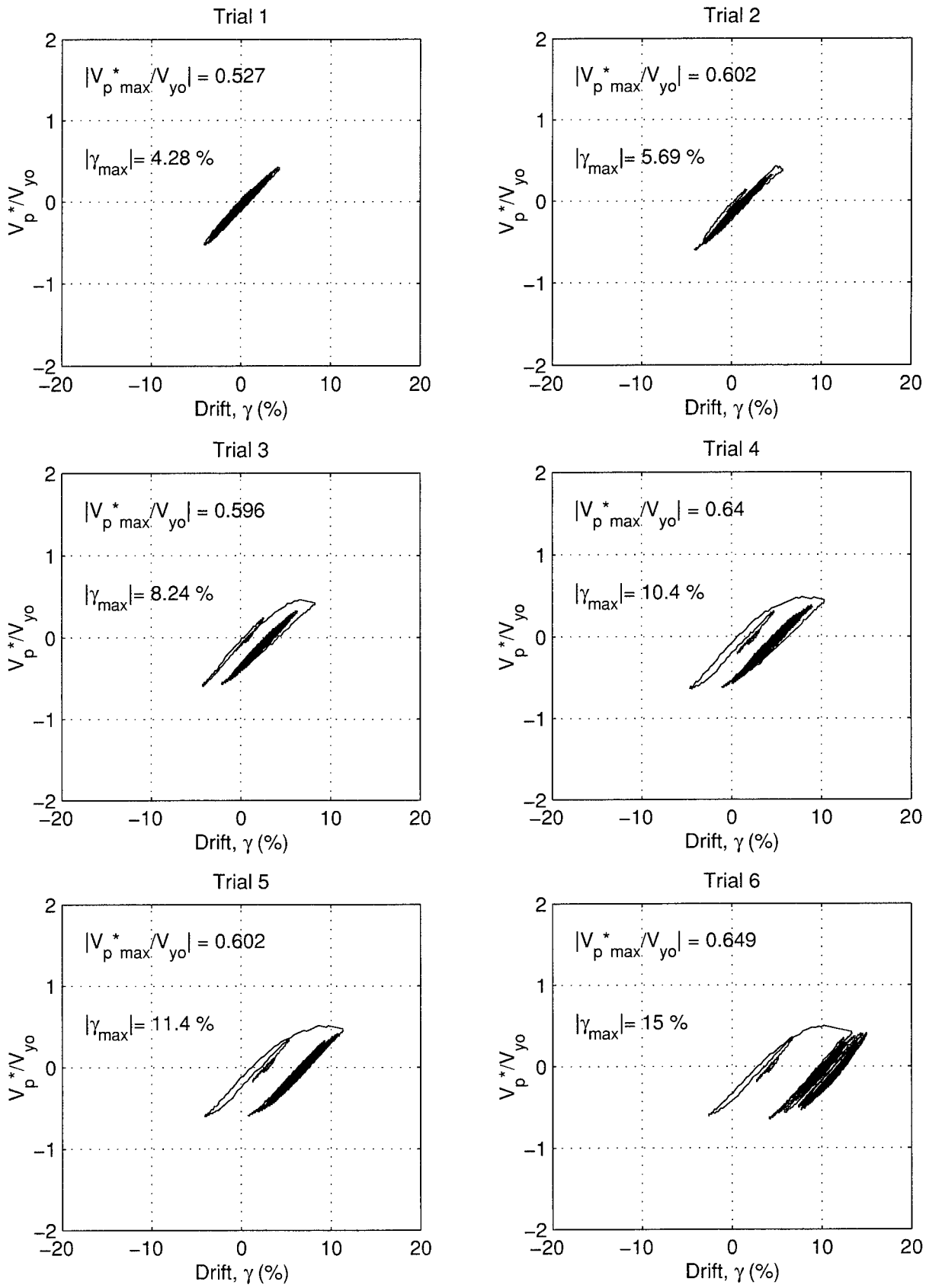

FIGURE 4–80 Specimen 11 – Normalized Base Shear vs. Drift

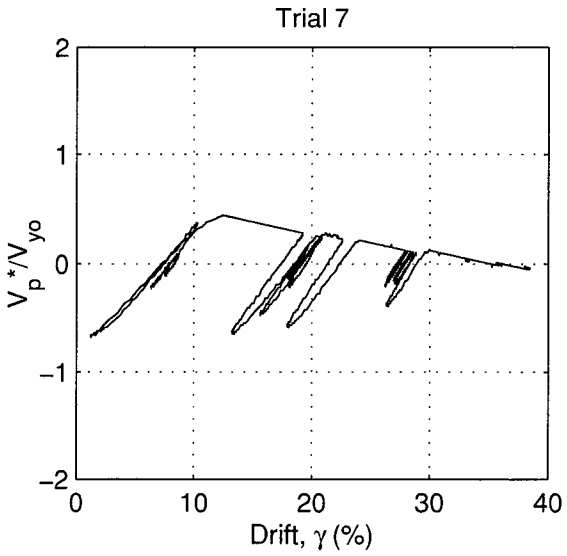

FIGURE 4–80 (cont'd) Specimen 11 – Normalized Base Shear vs. Drift

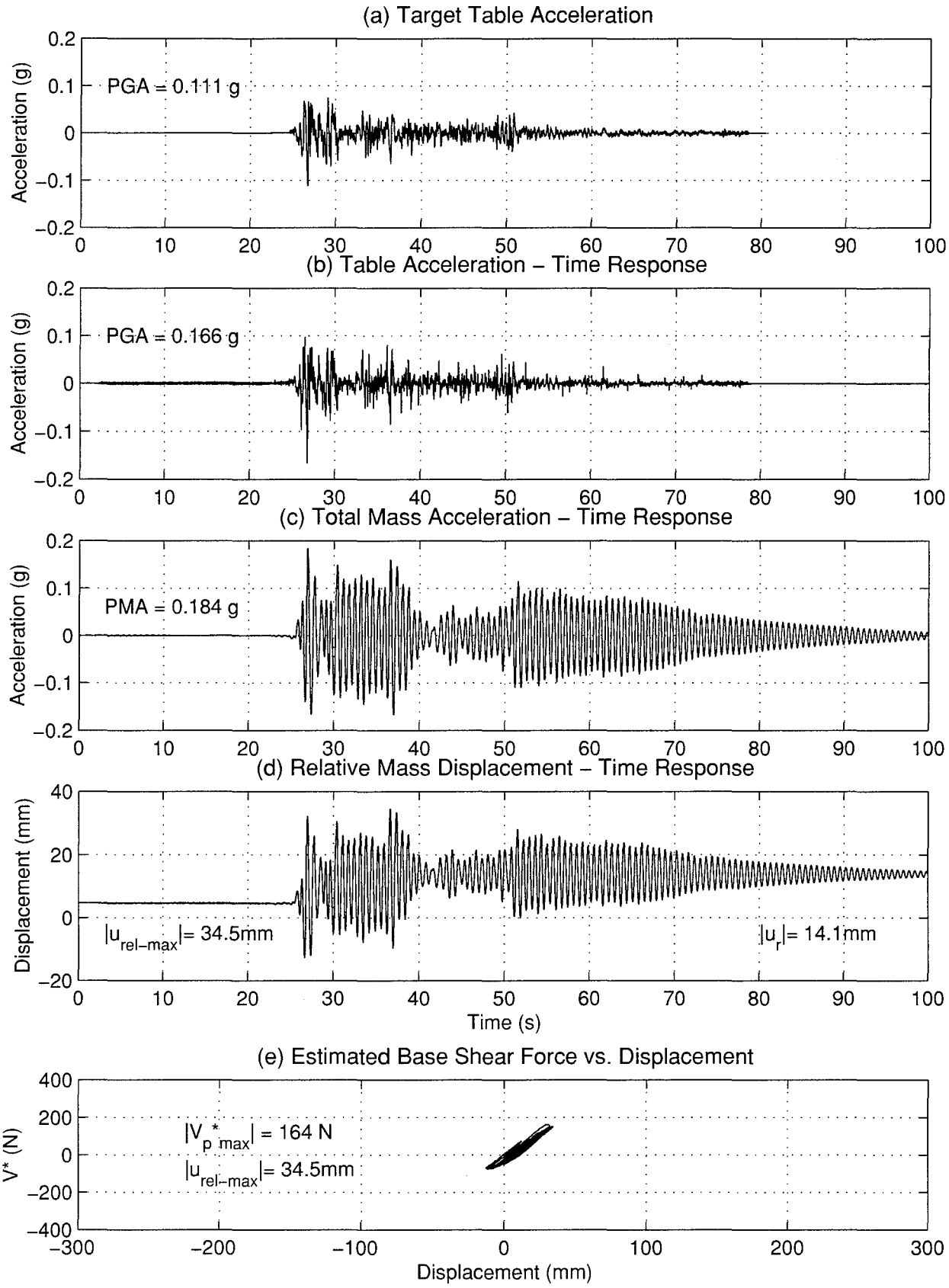

FIGURE 4–81 Seismic Response of Specimen 12 – Trial 2

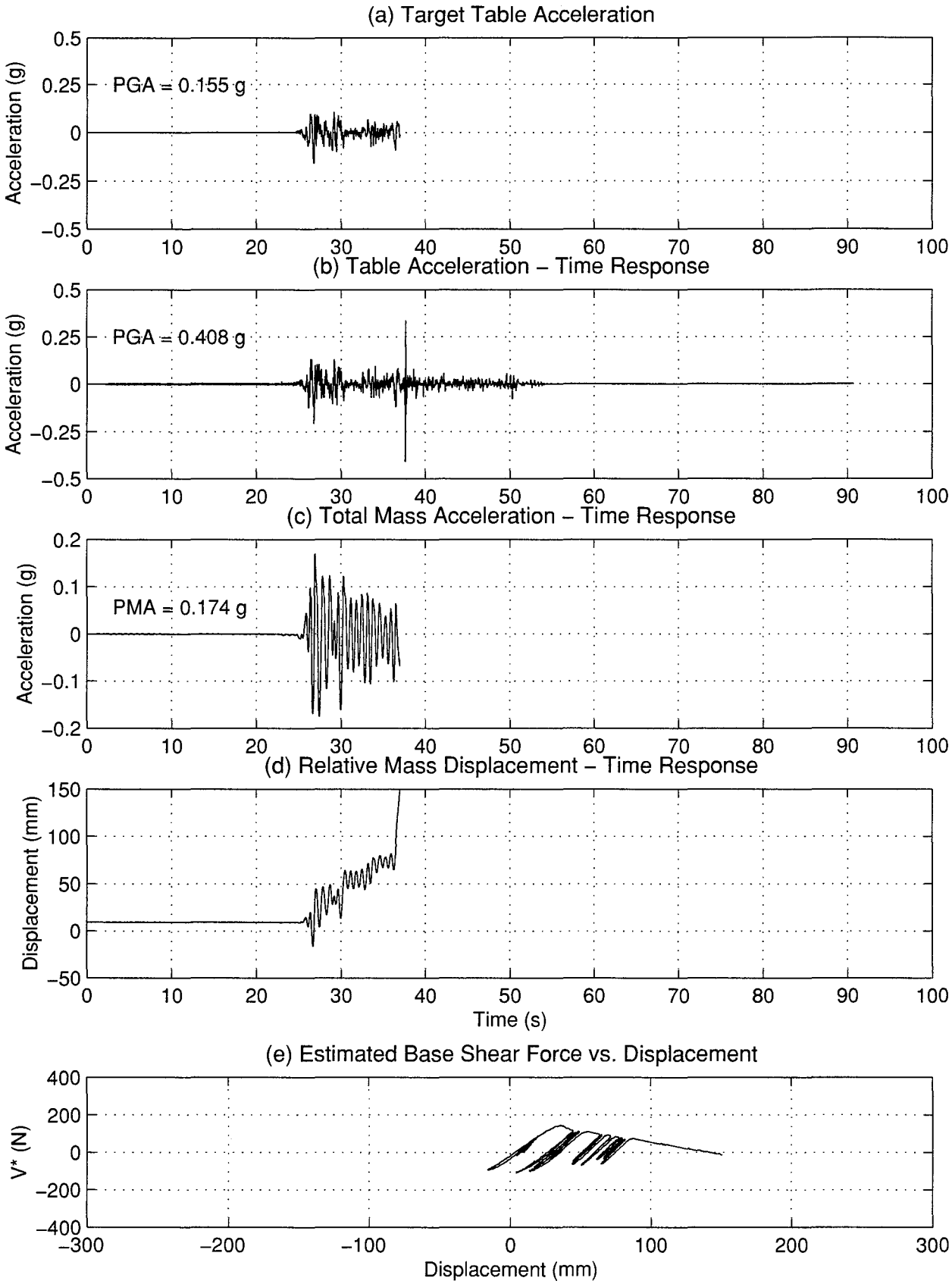

FIGURE 4–82 Seismic Response of Specimen 12 – Trial 3

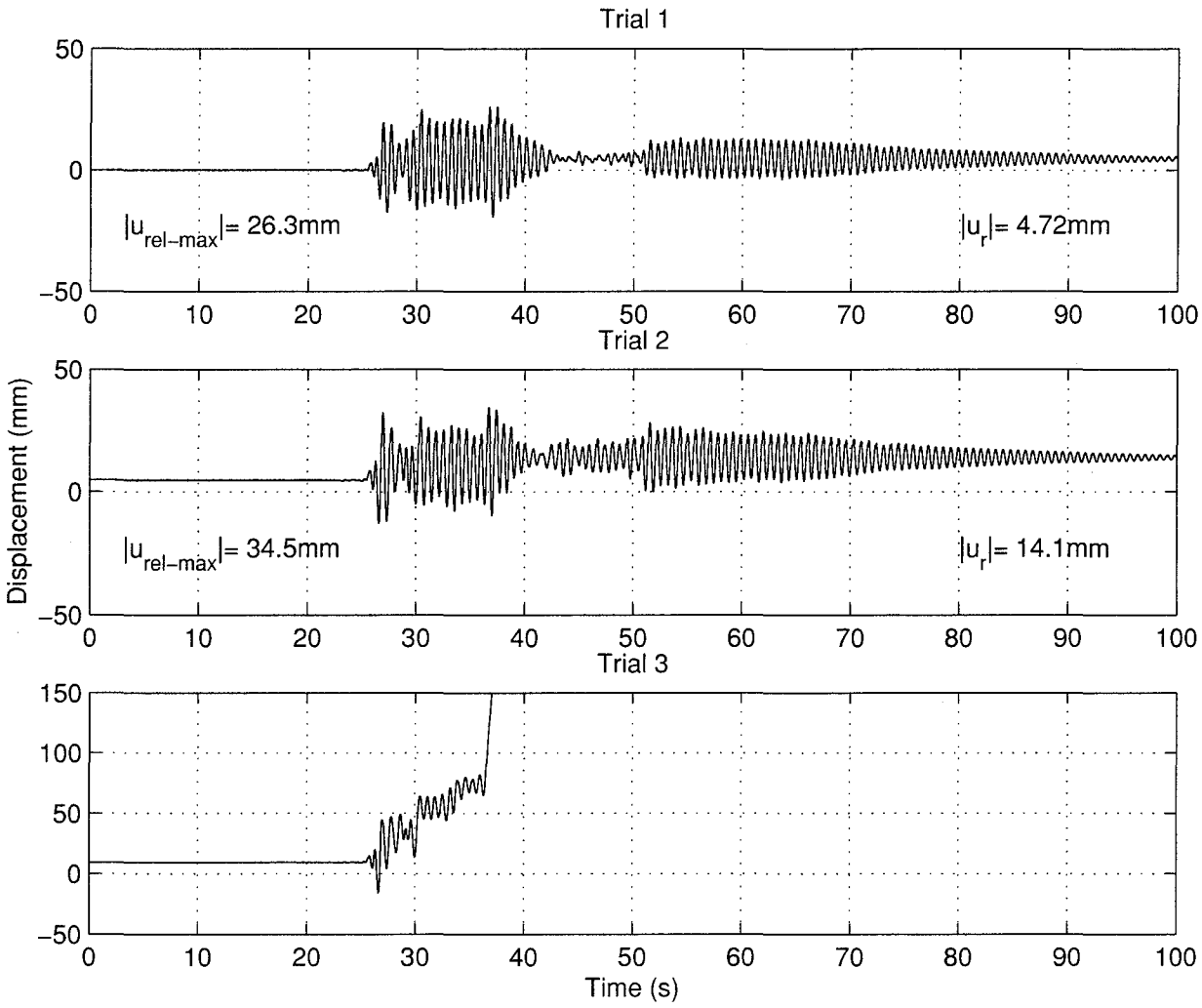

FIGURE 4-83 Specimen 12 – Progressive Displacement Time Histories

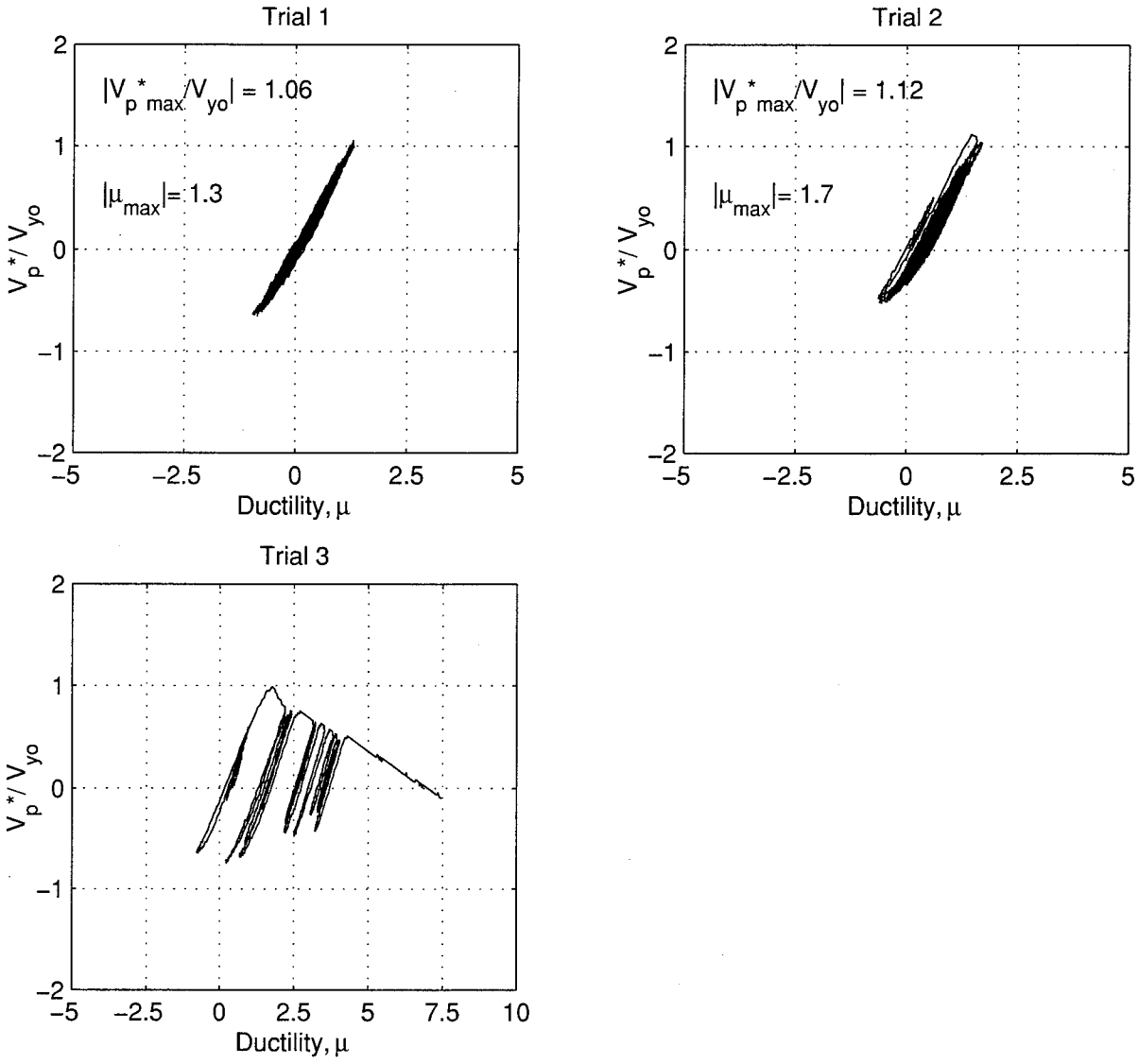

FIGURE 4–84 Specimen 12 – Normalized Base Shear vs. Ductility

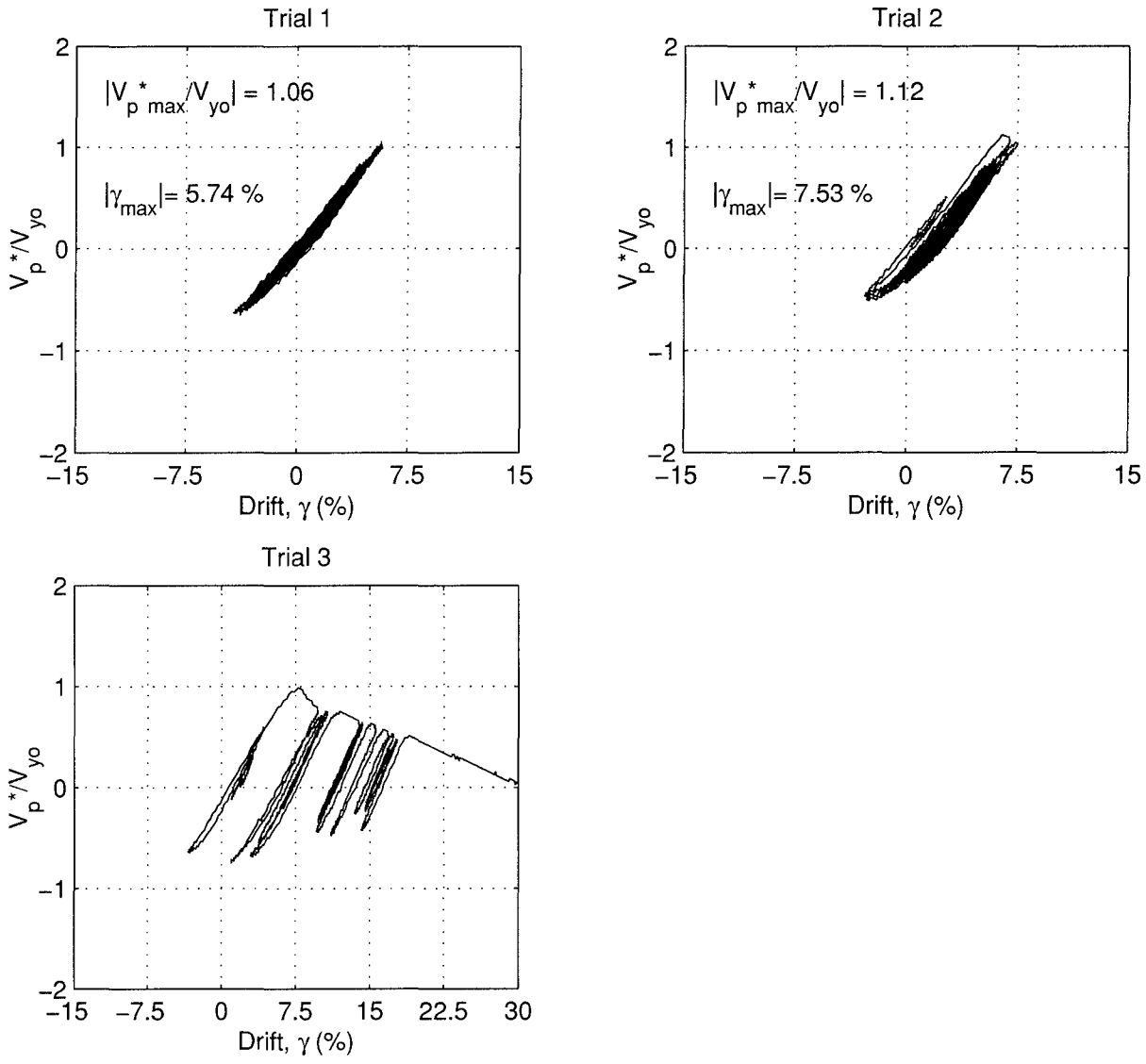

FIGURE 4–85 Specimen 12 – Normalized Base Shear vs. Drift

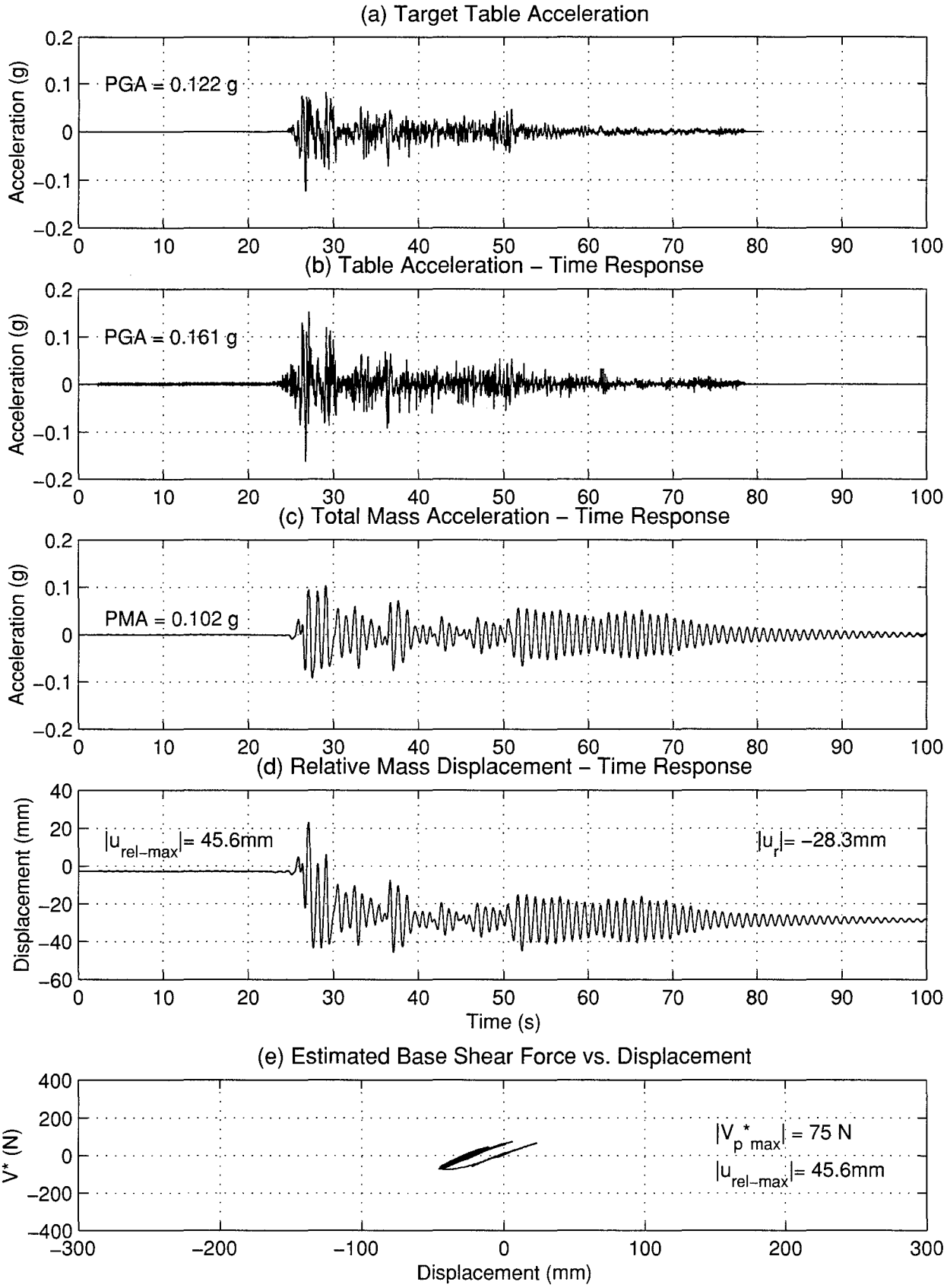

FIGURE 4–86 Seismic Response of Specimen 13 – Trial 4

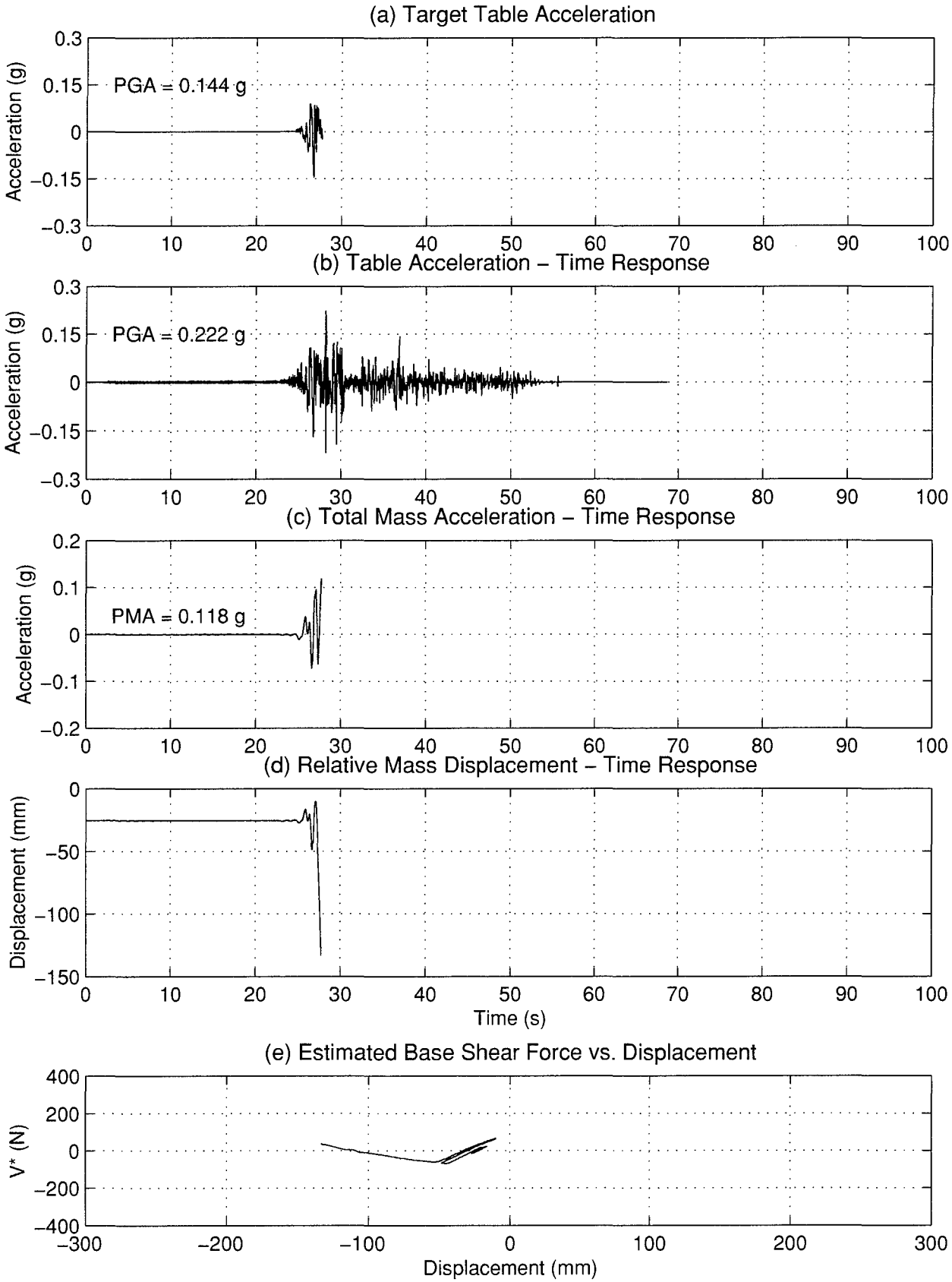

FIGURE 4–87 Seismic Response of Specimen 13 – Trial 5

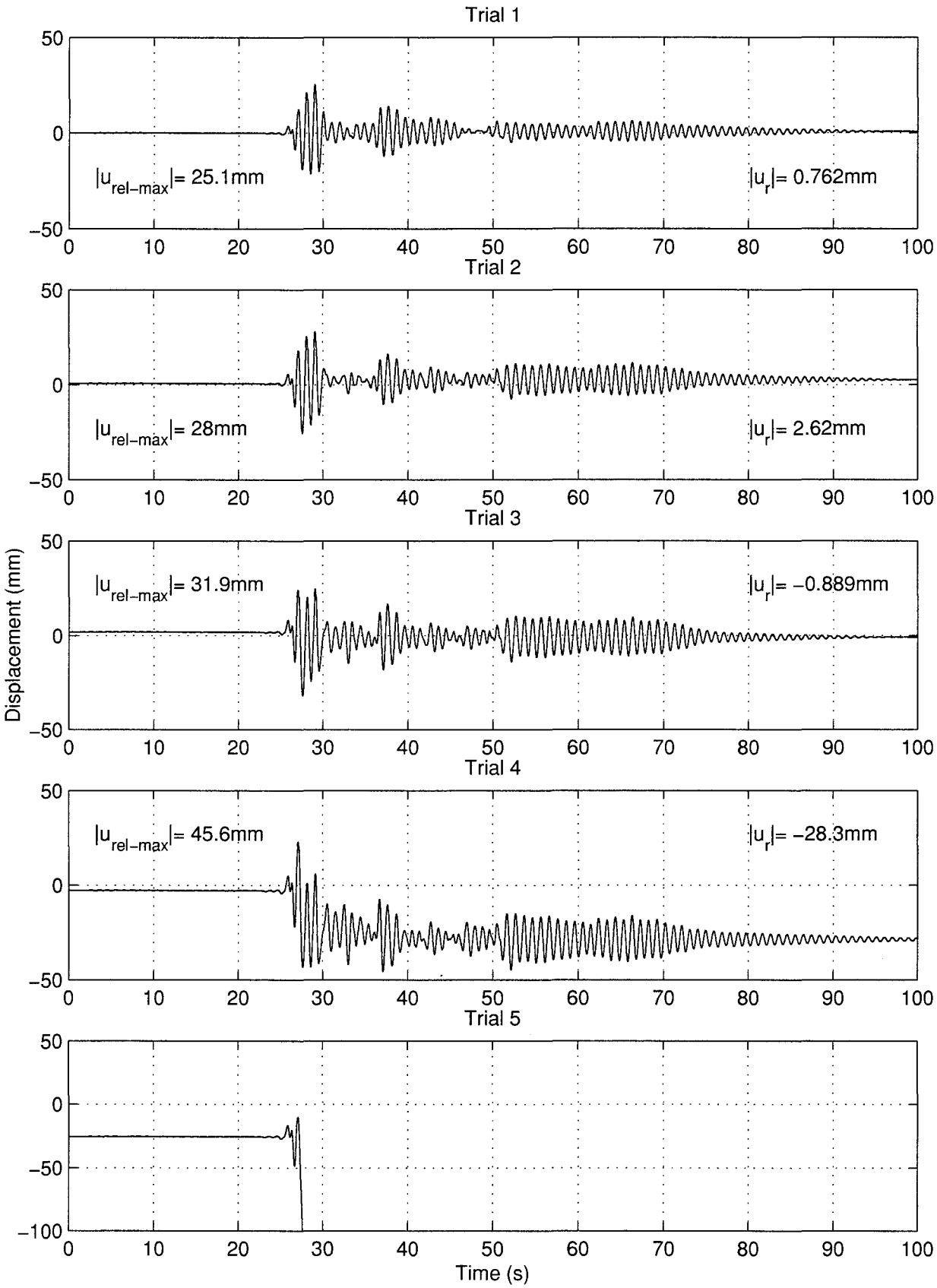

FIGURE 4–88 Specimen 13 – Progressive Displacement Time Histories

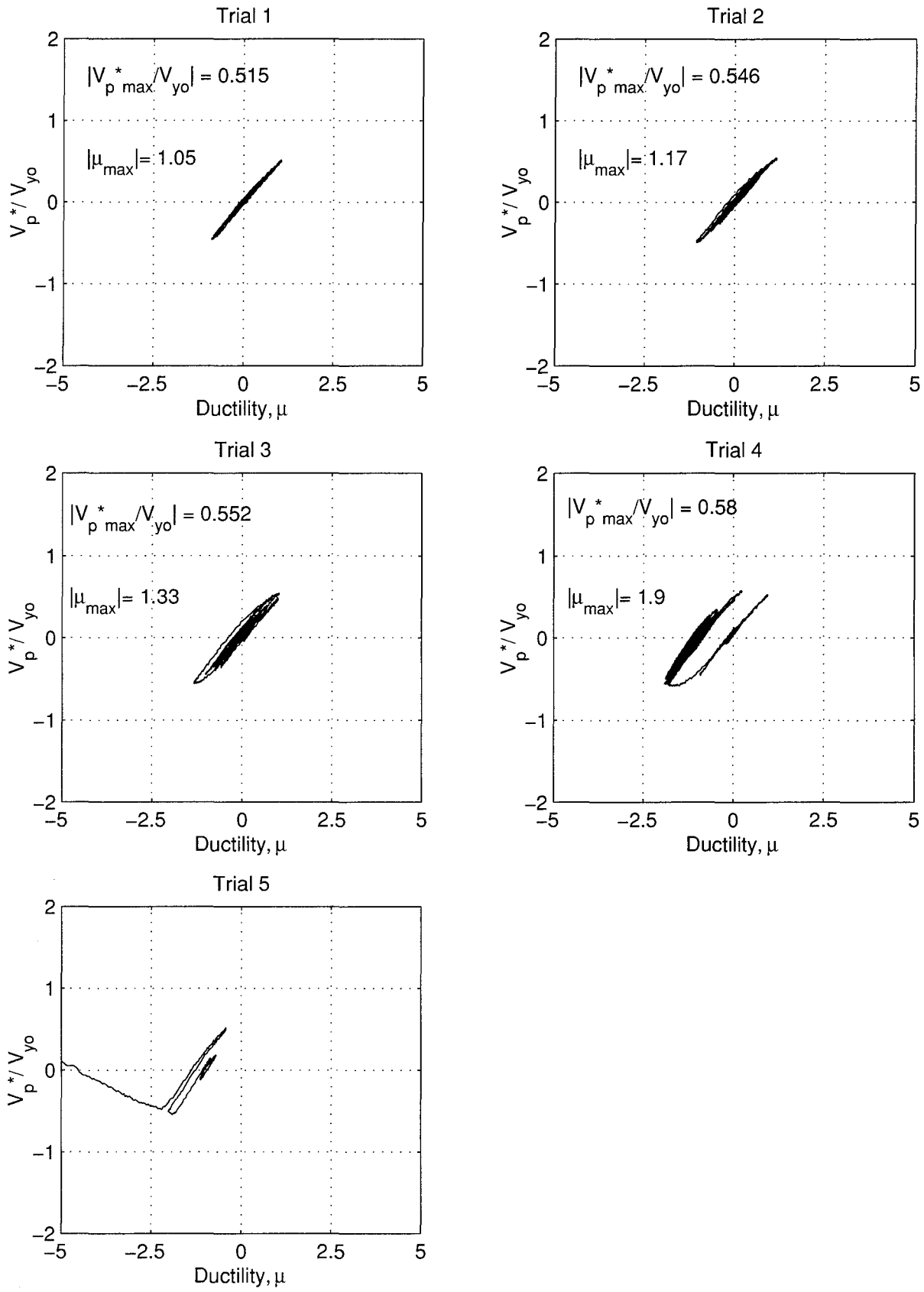

FIGURE 4–89 Specimen 13 – Normalized Base Shear vs. Ductility

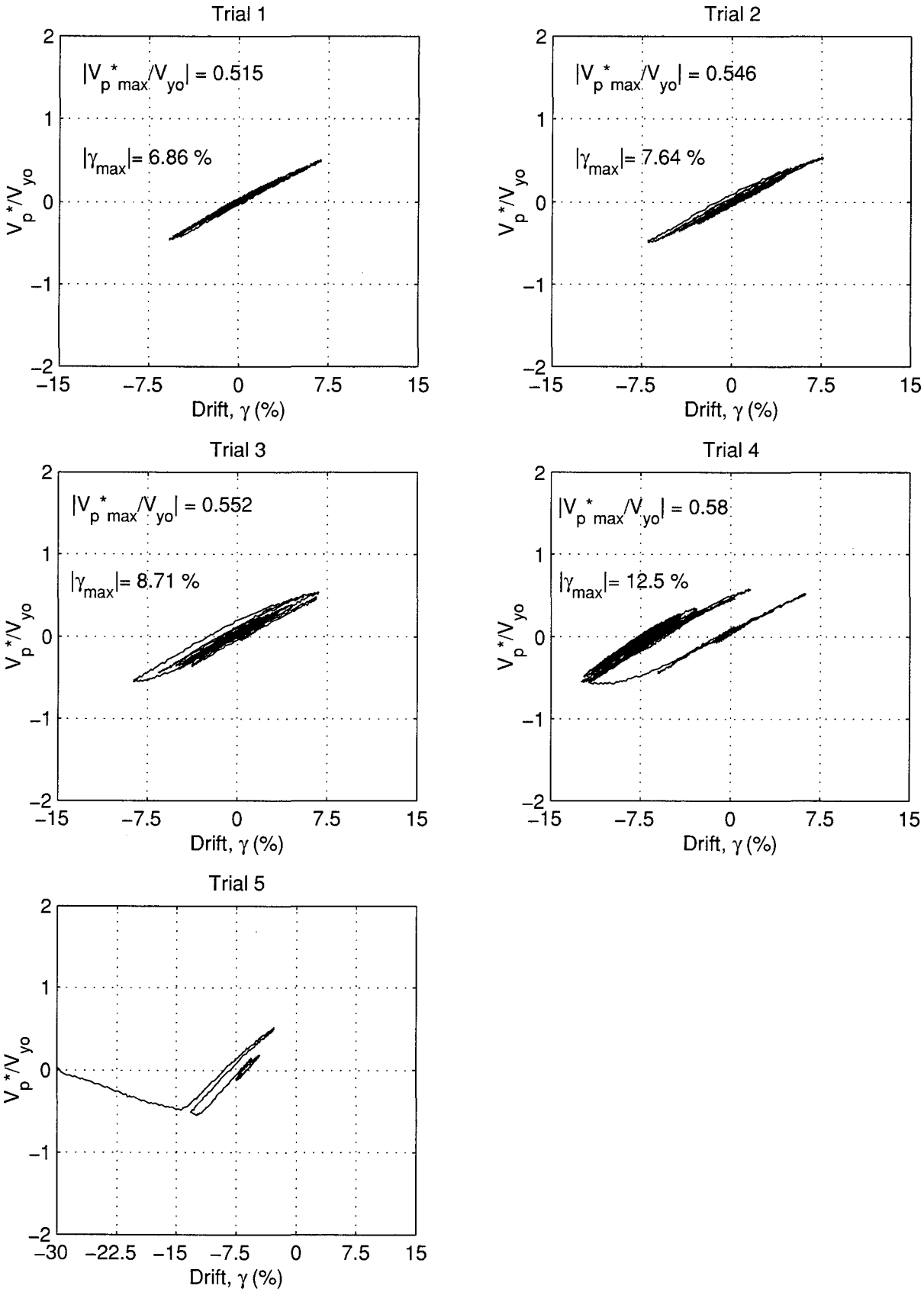

FIGURE 4–90 Specimen 13 – Normalized Base Shear vs. Drift

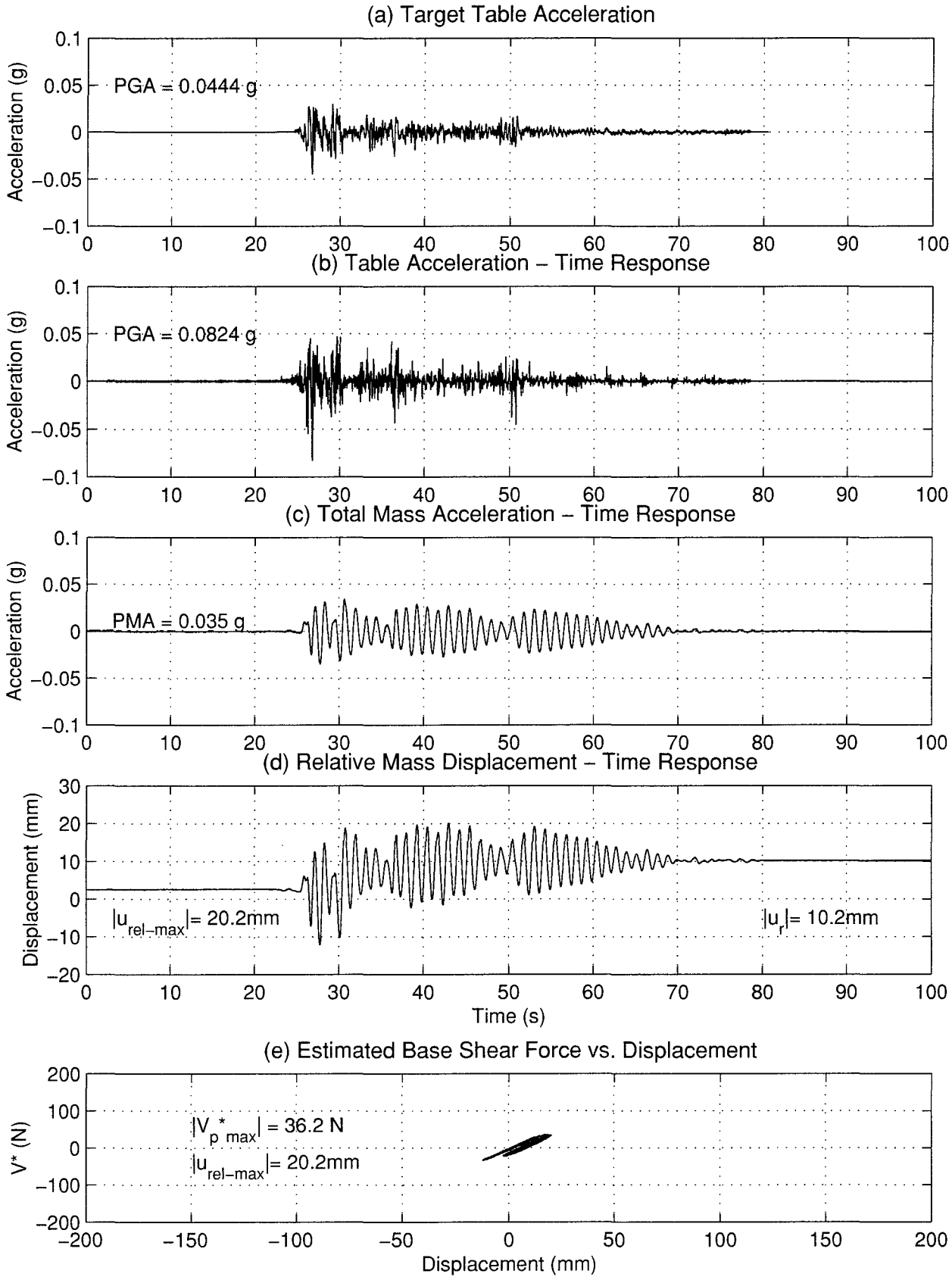

FIGURE 4–91 Seismic Response of Specimen 14 – Trial 4

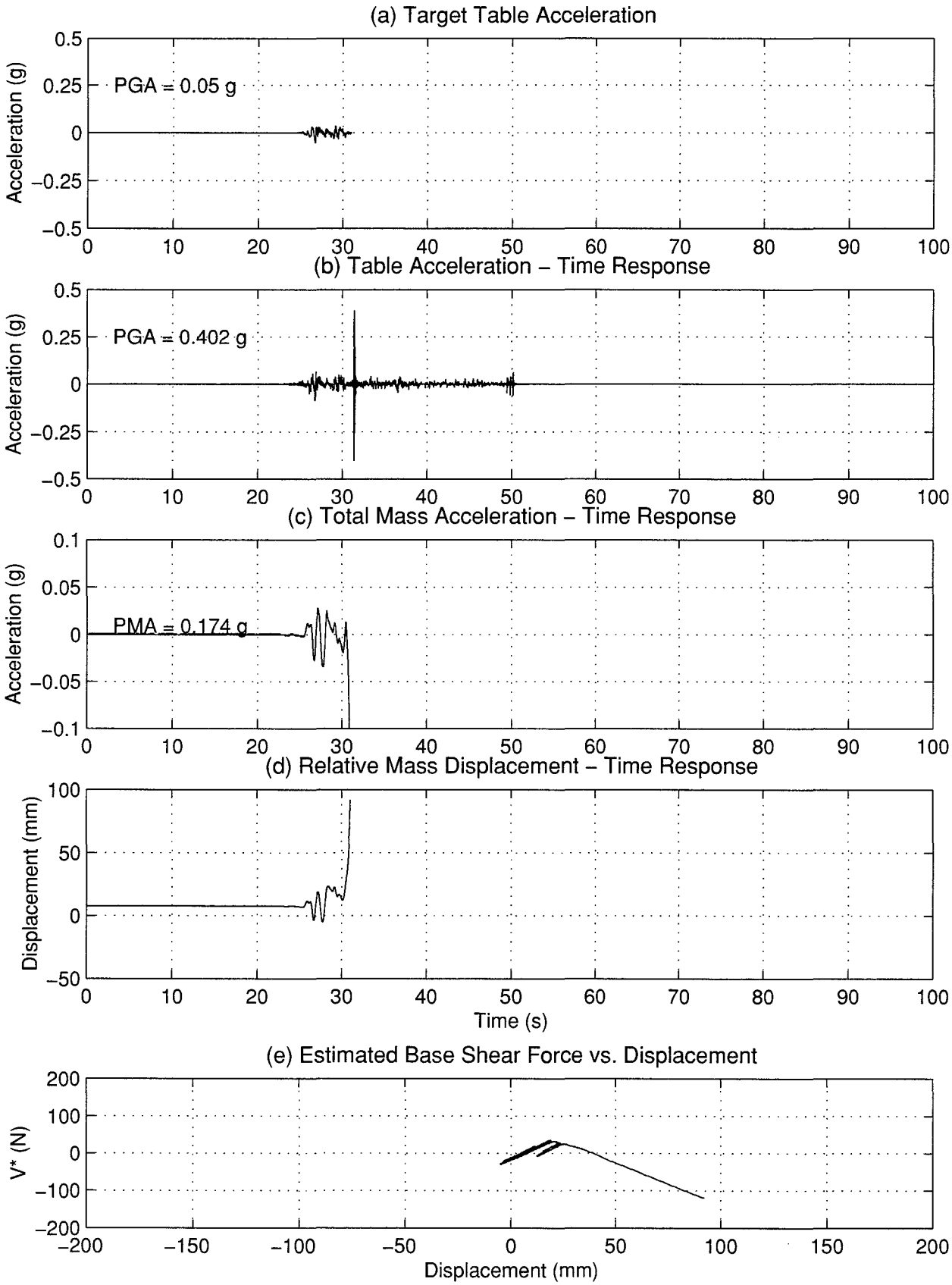

FIGURE 4–92 Seismic Response of Specimen 14 – Trial 5

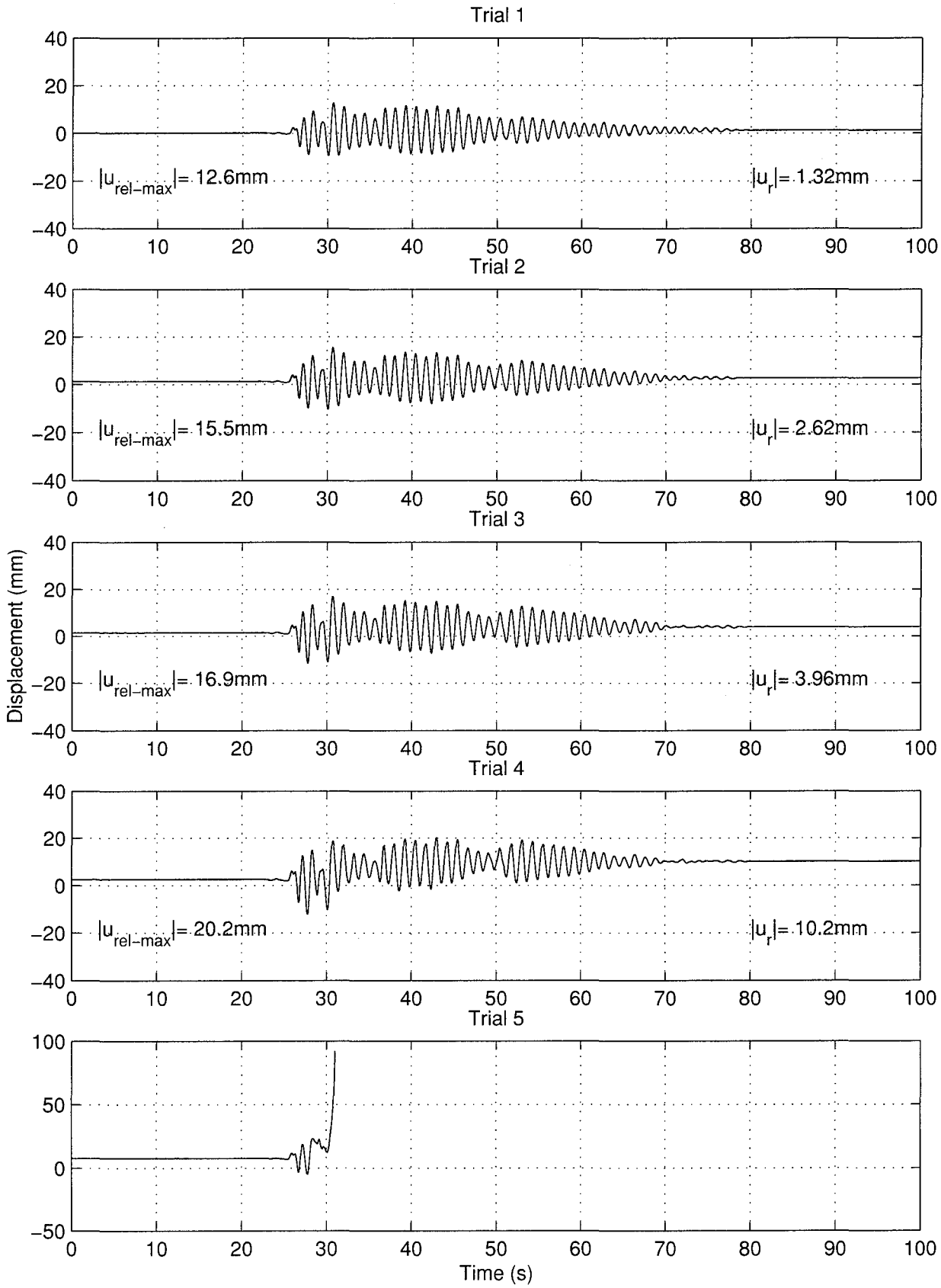

FIGURE 4–93 Specimen 14 – Progressive Displacement Time Histories

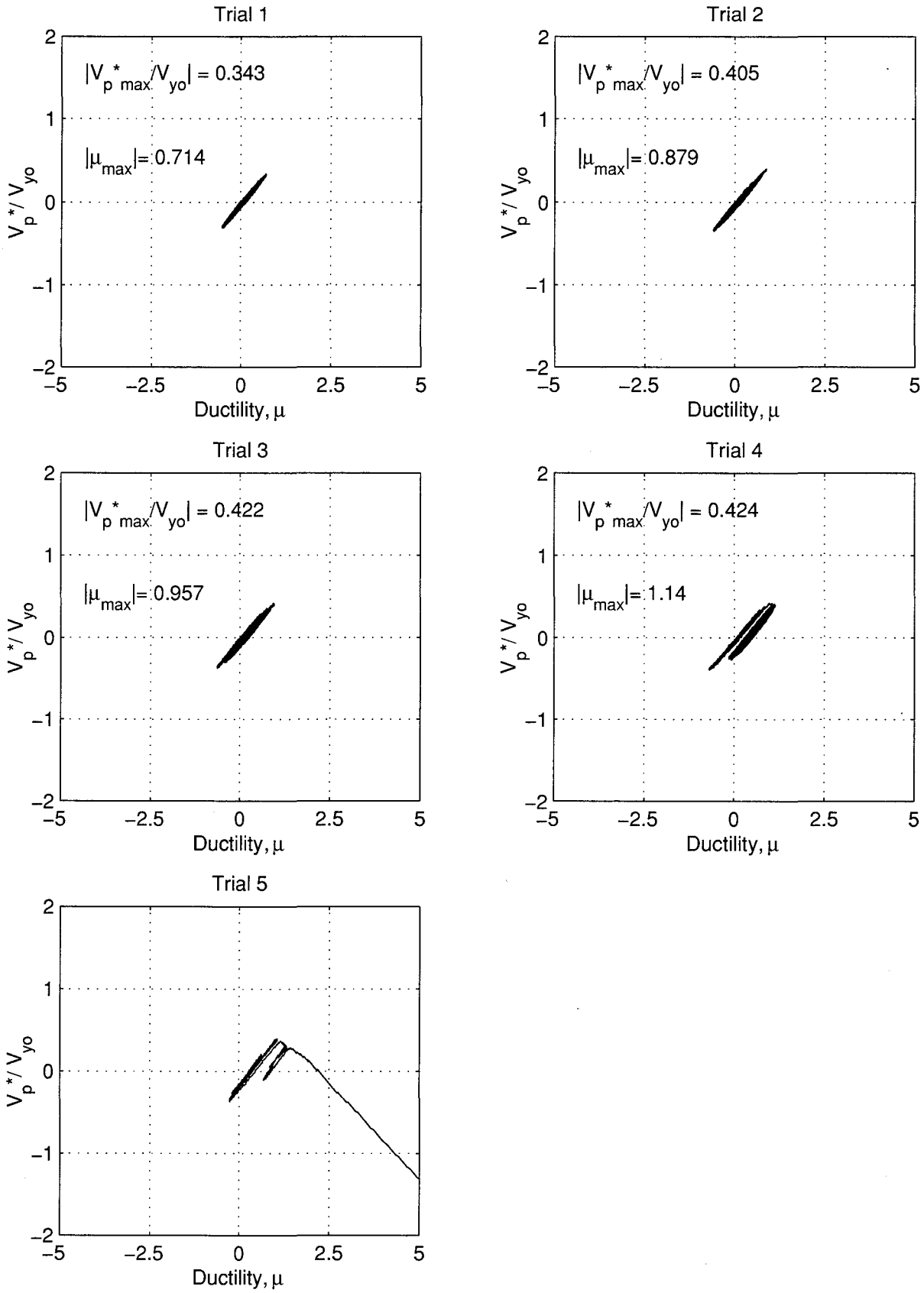

FIGURE 4–94 Specimen 14 – Normalized Base Shear vs. Ductility

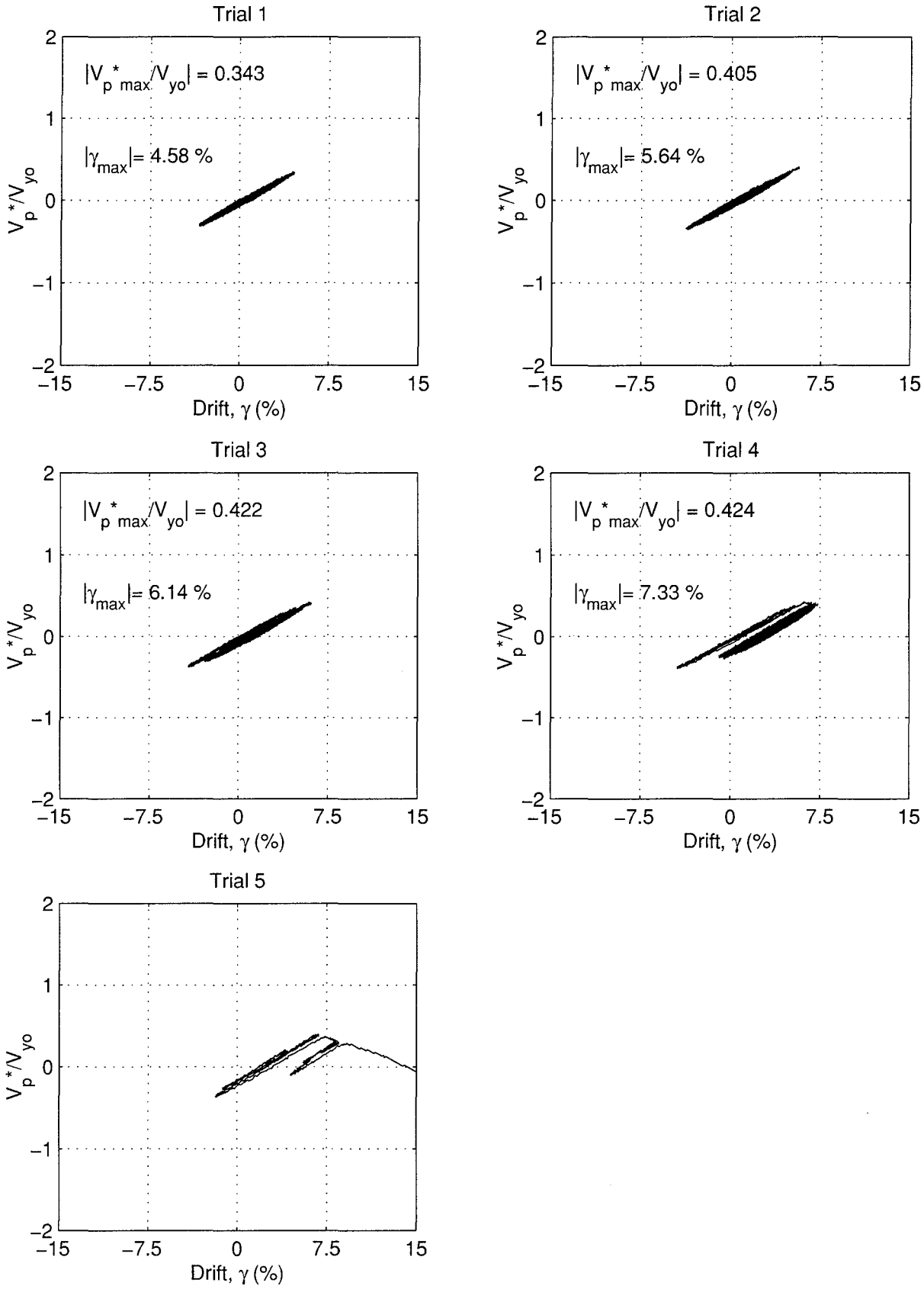

FIGURE 4–95 Specimen 14 – Normalized Base Shear vs. Drift

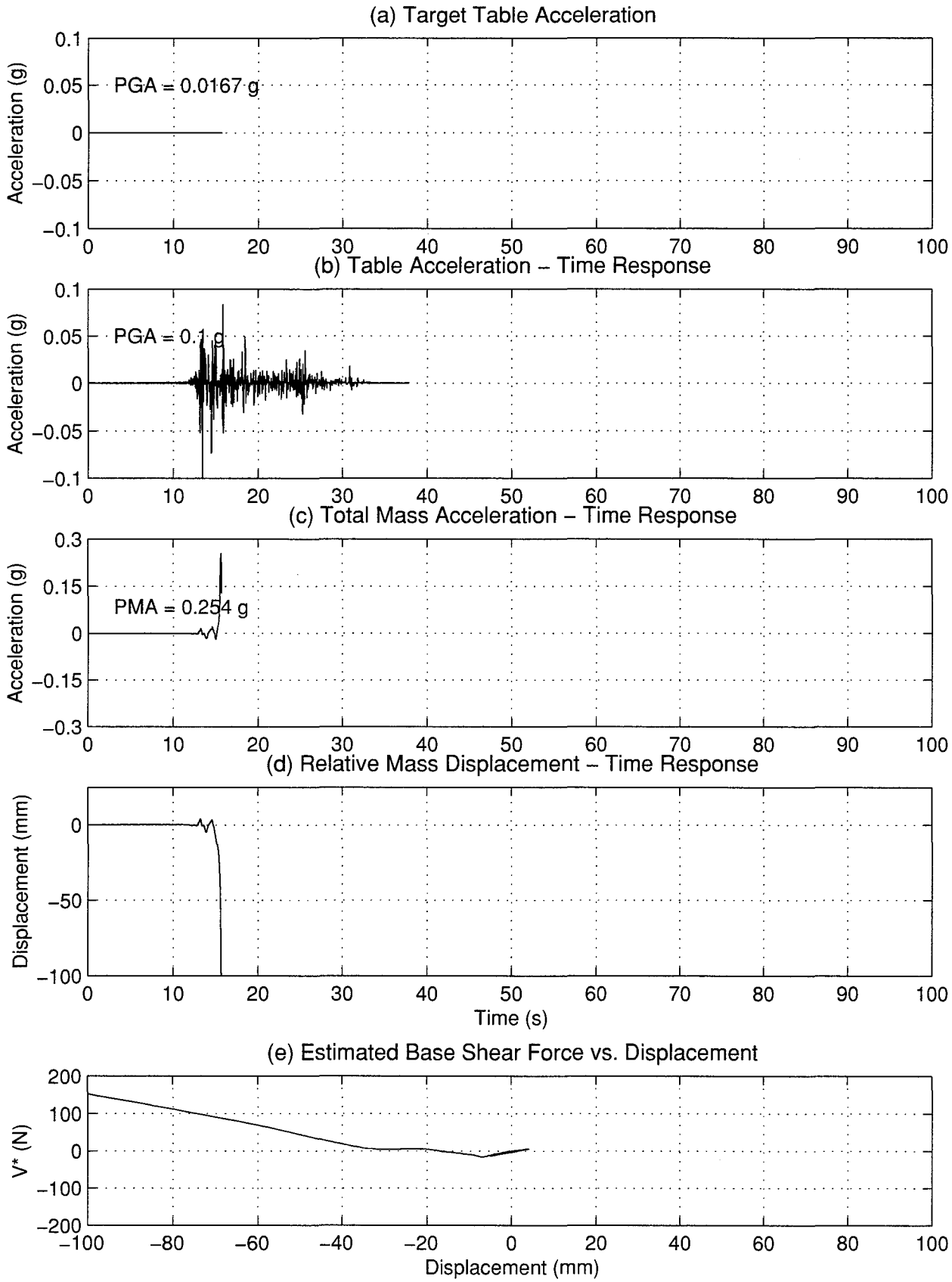

FIGURE 4–96 Seismic Response of Specimen 15 – Trial 1

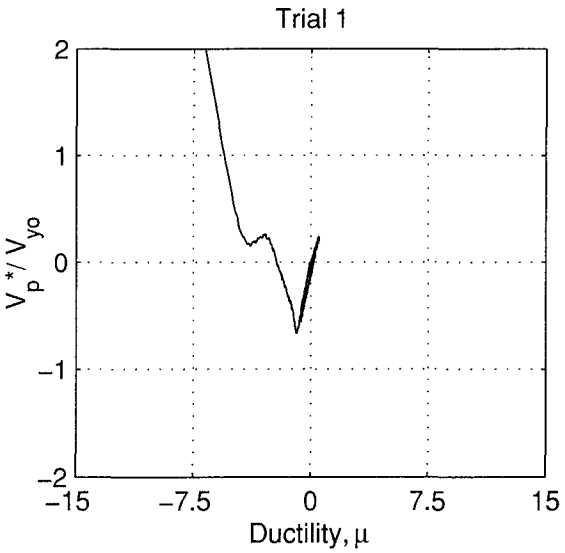

FIGURE 4–97 Specimen 15 – Normalized Base Shear vs. Ductility

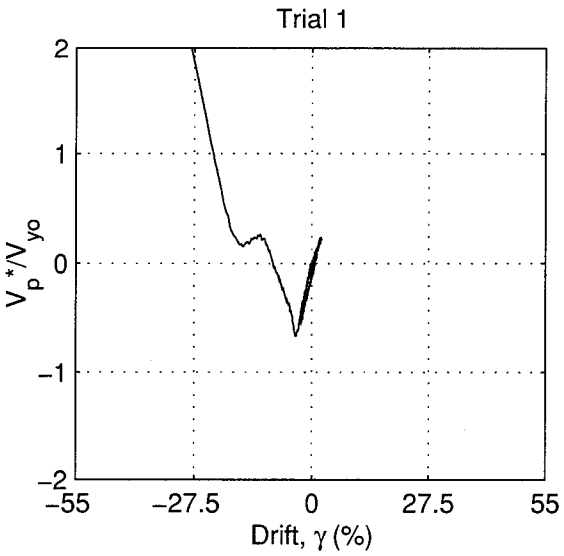

FIGURE 4–98 Specimen 15 – Normalized Base Shear vs. Drift

SECTION 5
DISCUSSION OF RESULTS

5.1 General

This section discusses the experimental shake table tests results presented earlier. An example of how to use of the test data for model calibration/verification is presented, using a simple inelastic program for illustration purposes, for one of the tested specimens. The location of the specimen physical data and test results is summarized for this purpose. The effect of various damping ratios on the analysis results is shown through comparison with a shake table test. A progressive bilinear dynamic analysis is performed in two ways to compare with the shake table test results.

All of the specimens are investigated with respect to the behavior over the entire test schedule. Peak response parameters are normalized and investigated for behavioral trends as a function of some of the key parameters defined in section 2. The progressive test results are compared to proposed limits to minimize P-Δ effects on highway bridge piers, as well as with axial-moment strength interaction considering both first and second order effects.

5.2 How to Use Experimental Data for Analytical Model Verification

Data from the experiments performed in this research can be used to assess the ability of SDOF time history analysis programs to model inelastic structural behavior up to collapse. To illustrate how the experimental data can be accessed and used for this purpose, an example follows using the simple freeware program NONLIN (Charney 1998), used in the preliminary analyses conducted to design the specimens.

5.2.1 Where to Find the Data

Specimen data necessary for model verification was presented in the description of the experimental setup in section 3. The dimensions of each column comprising the specimen are listed in table 3-4 and the average of those dimensions is listed in table 3-5. The orientation of the columns as tested is found in table 3-6. Finally, the average mass applied to each column is found in table 3-1. The average properties from those tables are summarized in table 3-2 along with the average bilinear properties, K_1, K_2, and θ, according to the equations in section 2.

Measured yield stresses discussed in section 4.2.1 are used to calculate the plastic moment of the section, and subsequently the plastic base shear, V_{yo}, and the yield displacement, Δ_y. These geometric and physical properties of the specimens can be used to construct the bilinear analytical model.

Filenames for test results are found in table 3-11. These files are in ASCII text in tabular form with data organized according to the convention described in section 3.6.3. Each file contains displacement and acceleration time histories of the table and specimens, for each of the data channels described in section 3.5 and illustrated in figure 3-12, and strain gage results for one column as identified in table 3-10.

Analysis of a test specimen was carried out using the average data described above from section 3 as model input, and results are presented in the following section. Note that the analyses are carried out on one column of the four making up the specimen, with one quarter of the total specimen mass acting on it. Also note that the recorded shake table acceleration, listed in g's in the sixth column of the above-mentioned data file, is processed by the 20 Hz lowpass filter, previously described in section 4.2.3, prior to its use as the input ground motion.

5.2.2 Effect of Damping on Analytical Results

The damping of the specimens tested is highly nonlinear, as shown by the free vibration tests in the previous section. Consider Specimen 11, which has a measured fundamental period of 0.597 seconds, only 0.32% more than the predicted value (table 4-2). The minimum, average, and maximum of the three damping estimates made for all data channels are 0.640, 1.804, and 3.497%, respectively. That range of values produces varying analytical results as expected. The response history of displacement calculated by NONLIN for each of the three damping ratio values is shown in figure 5-1 for the first test of the schedule, with the relative displacement measured by the HorEast channel, and corrected by the measured vertical displacement as described previously in section 3.8.2.

Considering the first case (a) using the minimum HorEast estimated damping ratio of 0.640%, there appears to be marginally good agreement between experimental and analytical results until approximately 29 seconds. Following that time, there is an unexplainable phase shift between

the experimental and analytical results, which is corrected at approximately 36.5 seconds, and a mismatch of the displacement amplitudes in the two time histories for the remaining duration of the response.

A subsequent analysis was performed using the average damping ratio of 1.804%. The results of this analysis, plotted in figure 5-1(b), show good agreement in displacement amplitudes until approximately 36.5 seconds, except for the phase shift once again starting at 29 seconds, followed by the same underestimate of experimental response observed in case (a).

A third and final analysis was performed using 3.497% - the maximum estimate from the AccWest free vibration history. The results are displayed in figure 5-1(c). The agreement between the measured and predicted time histories is similar to that obtained using the average damping ratio, but the analysis results underestimate the response before the 36 seconds mark, as is expected by the increase in damping.

Note that NONLIN utilizes a constant damping ratio for the duration of the analysis. This may account for the discrepancies in various parts of the time history, as the free vibration tests showed that the damping ratio varies with the amplitude of vibration. For that reason, none of the three values of damping seem to give better results. It appears that a program able to consider non-linear damping (i.e. varying as a function of displacement amplitude) might provide some improvement, but such an investigation is beyond the current scope of work.

Figure 5-2 shows the specimen total acceleration response history results for the same test again compared with results from the same three NONLIN analyses. Note that the qualitative differences between measured and analytical response histories are identical to that of the displacement histories.

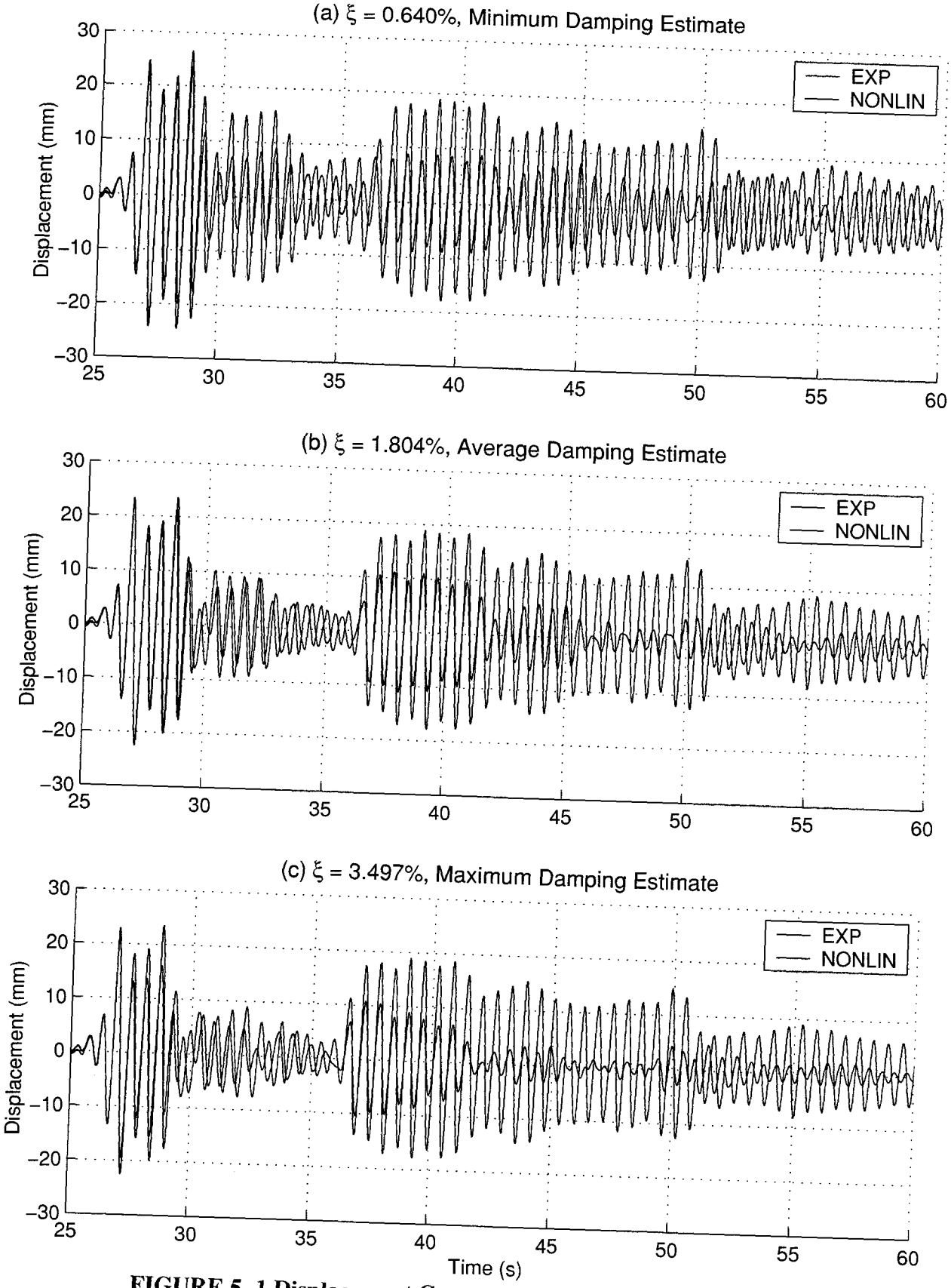

FIGURE 5-1 Displacement Comparison of Specimen 11 – Trial 1

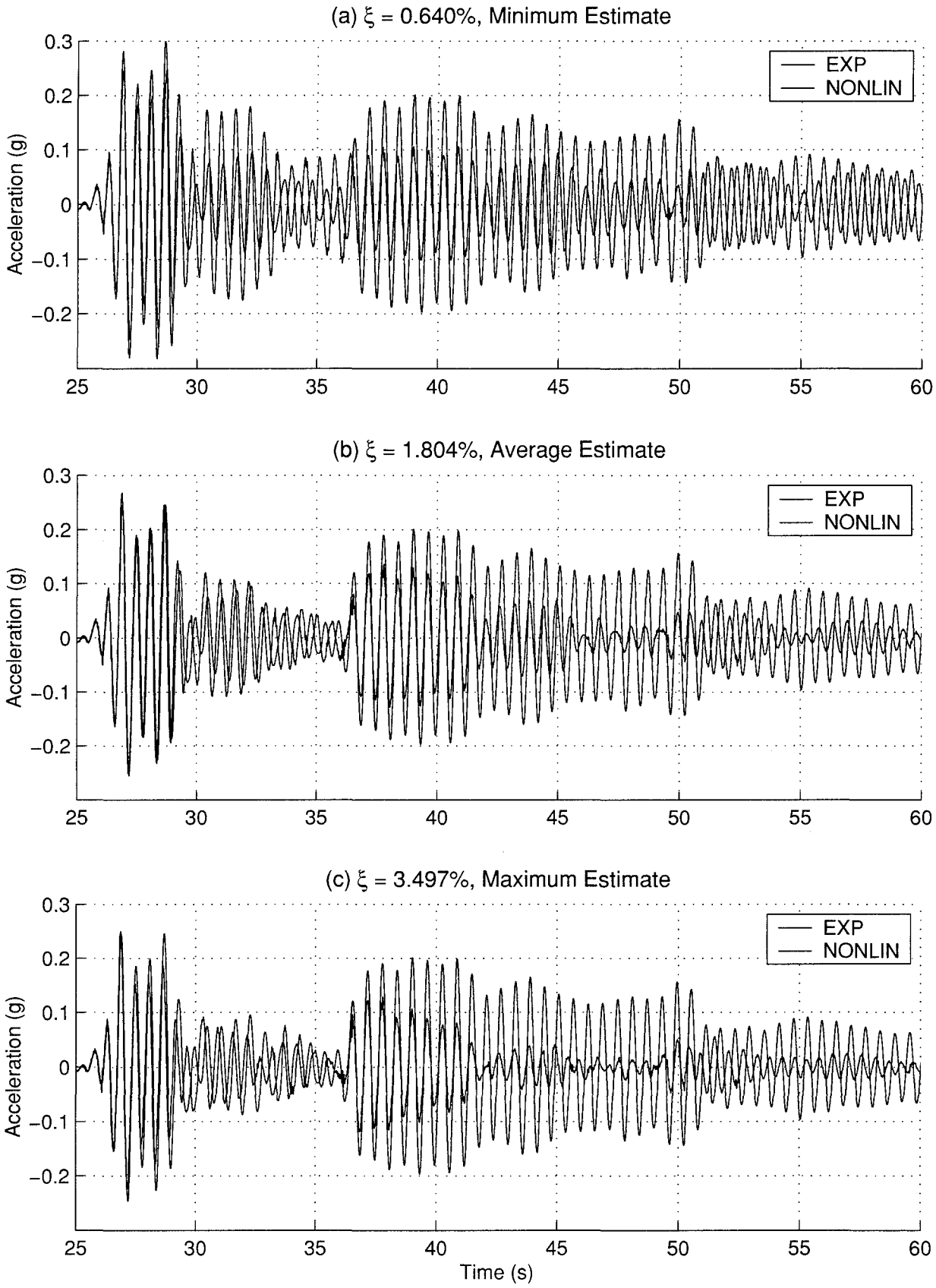

FIGURE 5–2 Acceleration Comparison of Specimen 11 – Trial 1

5.2.3 Force-Displacement Comparison

Analytically and experimentally obtained lateral force versus displacement results were compared for the same shake table test, and subsequent tests in the schedule, by performing a series of non-linear dynamic analyses using a bilinear elastic-perfectly plastic model. The average damping ratio estimate of 1.804% was used for each analysis. The bilinear parameters of the virgin specimen were obtained from the data presented in section 3 as described above, and used for the NONLIN model. However, when the specimen experienced a residual displacement at the conclusion of a test, the model was modified for the subsequent test to account for the lower yield stress upon reloading due to P-Δ effects and bias in the cumulative drifts.

Figure 5-3 shows, for the assumed bilinear force-displacement model, the reduced yield level, V_{yp}', following a residual displacement, u_r. From the geometry, an expression can be written, in terms of u_r, the elastic stiffness including P-Δ, k_1, the stability factor, θ, and yield displacement, Δ_y, using the various relations from section 2.2:

$$V_{yp}' = V_{yp} - \Delta F_y = k_1 \cdot \left[\Delta_y - \theta \cdot u_r\right] \tag{5-1}$$

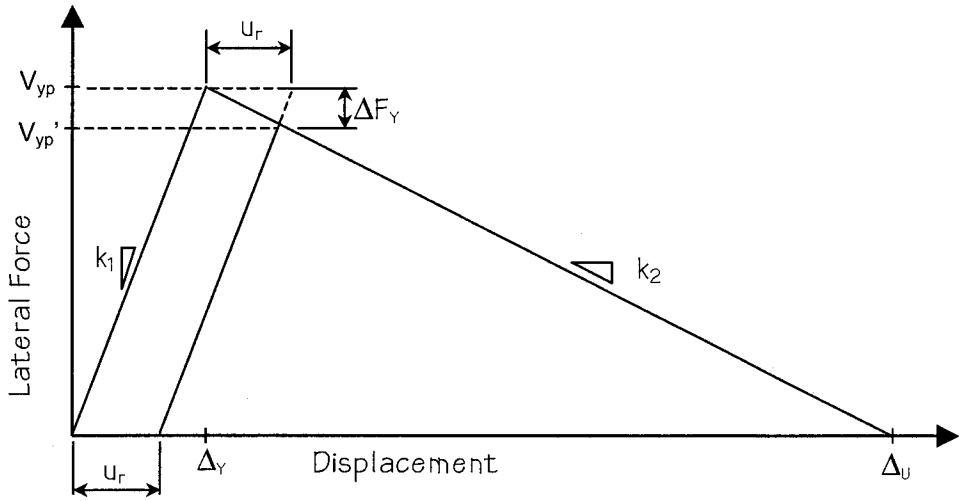

FIGURE 5-3 Bilinear Lateral Force versus Displacement model for SDOF structure

The series of bilinear dynamic analyses was performed accordingly: First, the experimentally obtained residual displacement from each test was used to calculate the reduced yield force for the subsequent analysis (referred to as Method 1 hereafter). Second, the residual displacement

obtained analytically was used to calculate the reduced yield force (Method 2). Note that Method 2 is a purely analytical approach, whereas Method 1 is a hybrid in that the experimental results are used to "adjust" each successive analysis.

Table 5-1 summarizes the residual displacement and reduced yield force values for each of these methods. The analytical results are plotted next to the experimental results for each of the two methods in figures 5-4 and 5-5, respectively. The experimental results are displayed in the left column of these figures, using the estimated base shear corrected for P-Δ, V_p* (defined in section 3.8.4), and relative horizontal displacement (measured by the HorEast transducer and corrected by the vertical measurements as described in section 3.8.2). The analytical results are in the right column of the figures, displaying the analytical base shear force, f_s, versus relative displacement. Note that neither method provides a good match with experimental data, and that the second method predicted collapse before the final test.

As observed previously for the elastic analyses in figure 5-1, the damping is underestimated for part of the analyses, resulting in the higher displacements and premature collapse obtained analytically. Note that these analyses are used for illustration purposes only. It is expected that more accurate and refined analytical models will be used, calibrated and developed to match, until collapse, the data from these benchmark experiments.

TABLE 5-1 Yield Force Reductions – Specimen 11

Test	V_{yp}' (N)	u_r (mm)	ΔF_y (N)	V_{yp}' (N)	u_r (mm)	ΔF_y (N)
	Experimental			Analytical		
1	255.0	0.7	-0.8	255.0	0.0	0.0
2	254.2	3.1	-3.4	255.0	0.0	0.0
3	251.6	12.8	-14.2	255.0	17.0	-18.9
4	240.8	24.3	-27.0	236.1	60.7	-67.4
5	228.0	35.7	-39.7	187.6	91.5	-101.6
6	215.3	63.2	-70.2	153.4	Q	-
7	184.8	Q	-	-	-	-
	V_{yp} =	255	N, k_1 =	8.05	N/mm	
	θ =	0.138	Δ_y =	31.67	mm	

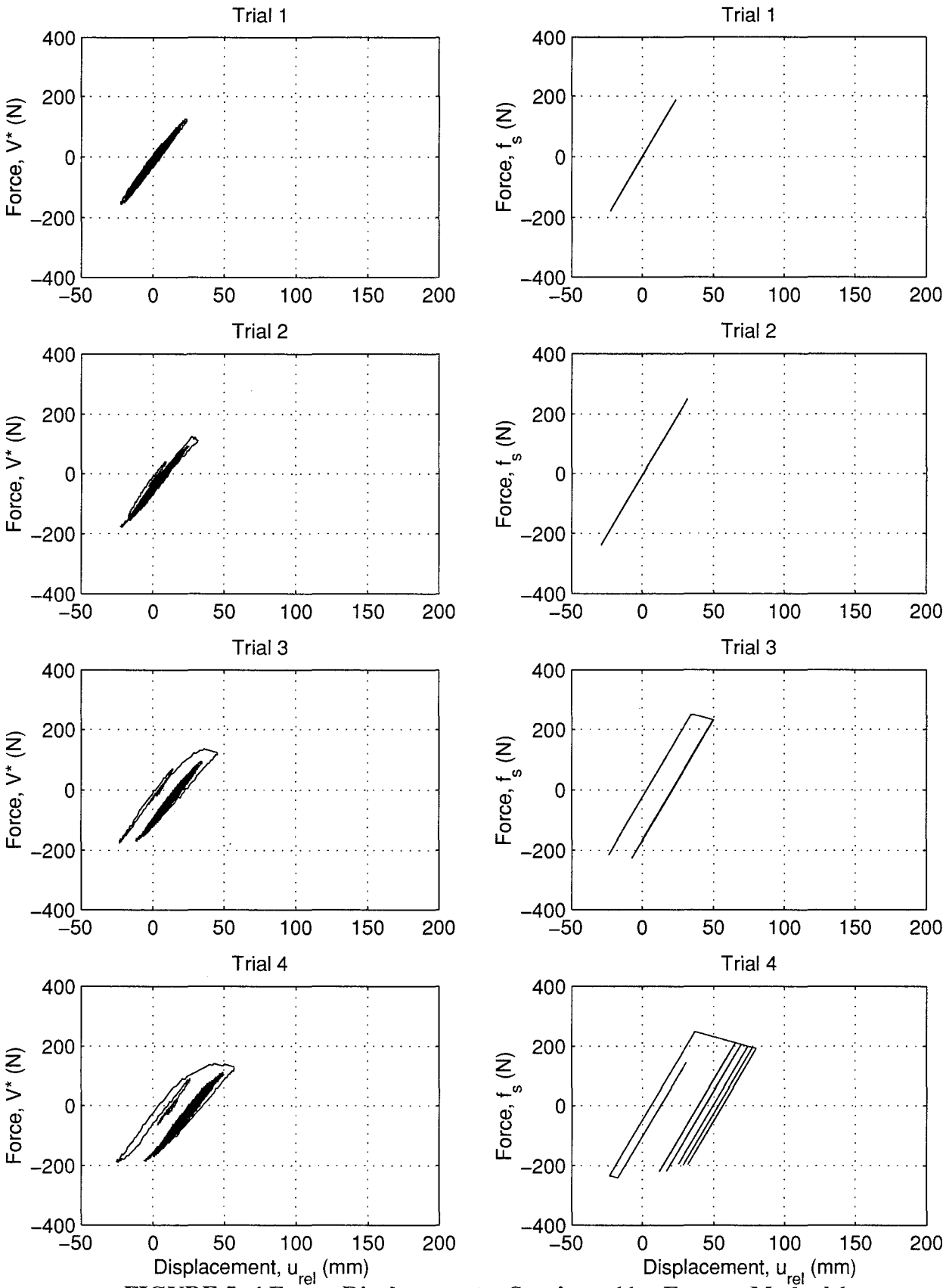

FIGURE 5–4 Force–Displacement – Specimen 11 – Exp. vs. Method 1

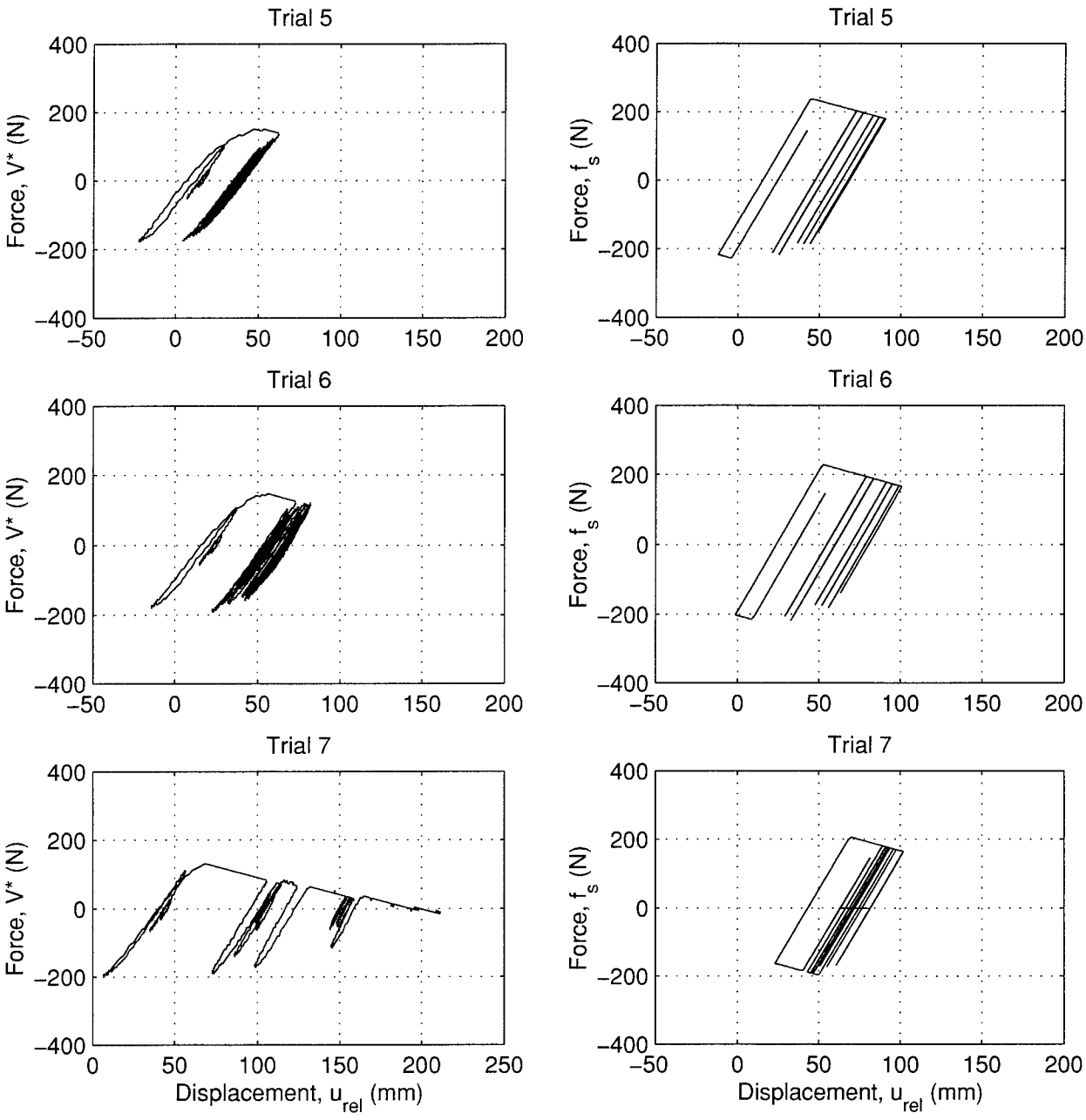

FIGURE 5–4 (cont'd) Force–Displacement – Specimen 11 – Exp. vs. Method 1

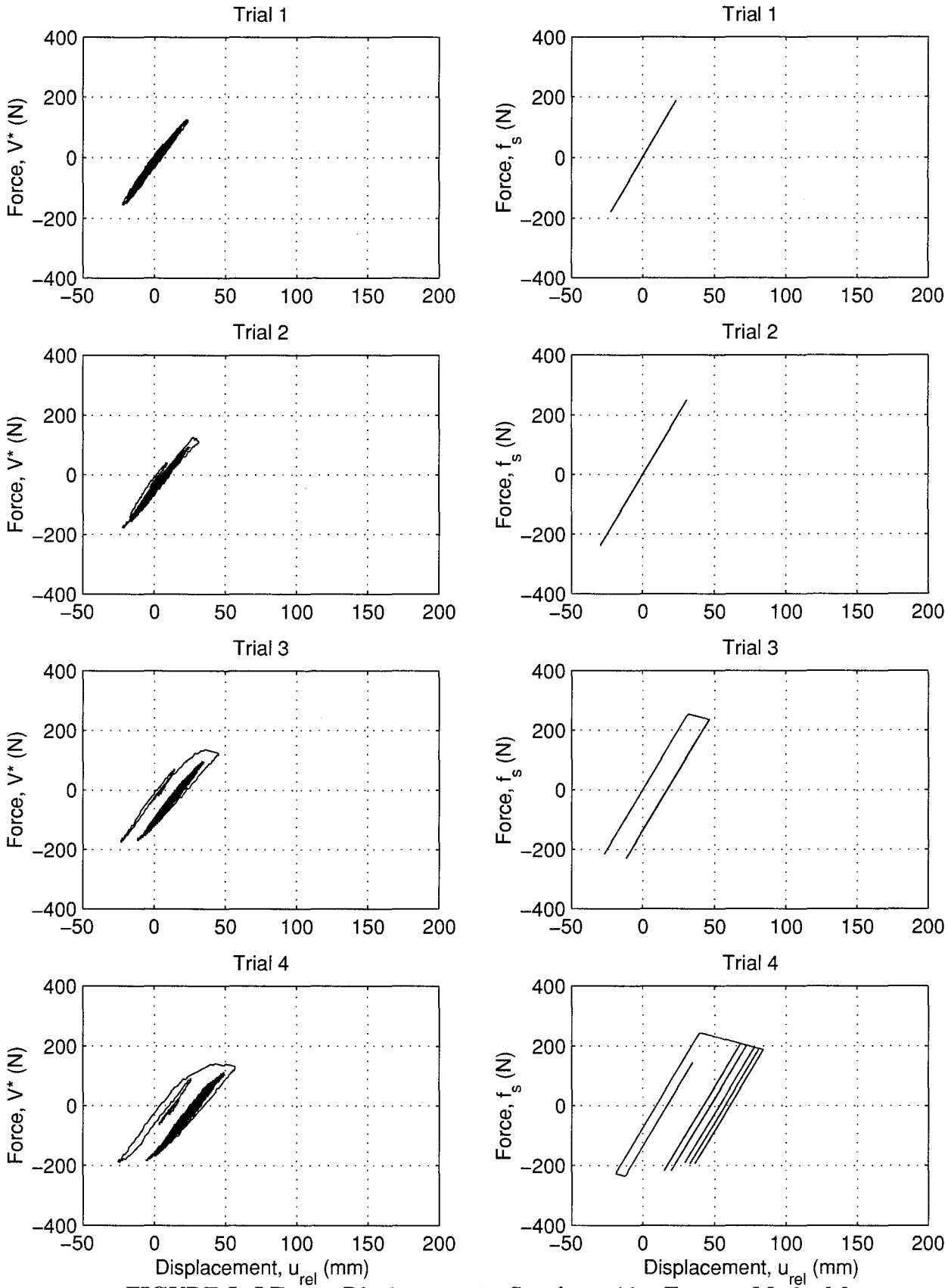

FIGURE 5–5 Force–Displacement – Specimen 11 – Exp. vs. Method 2

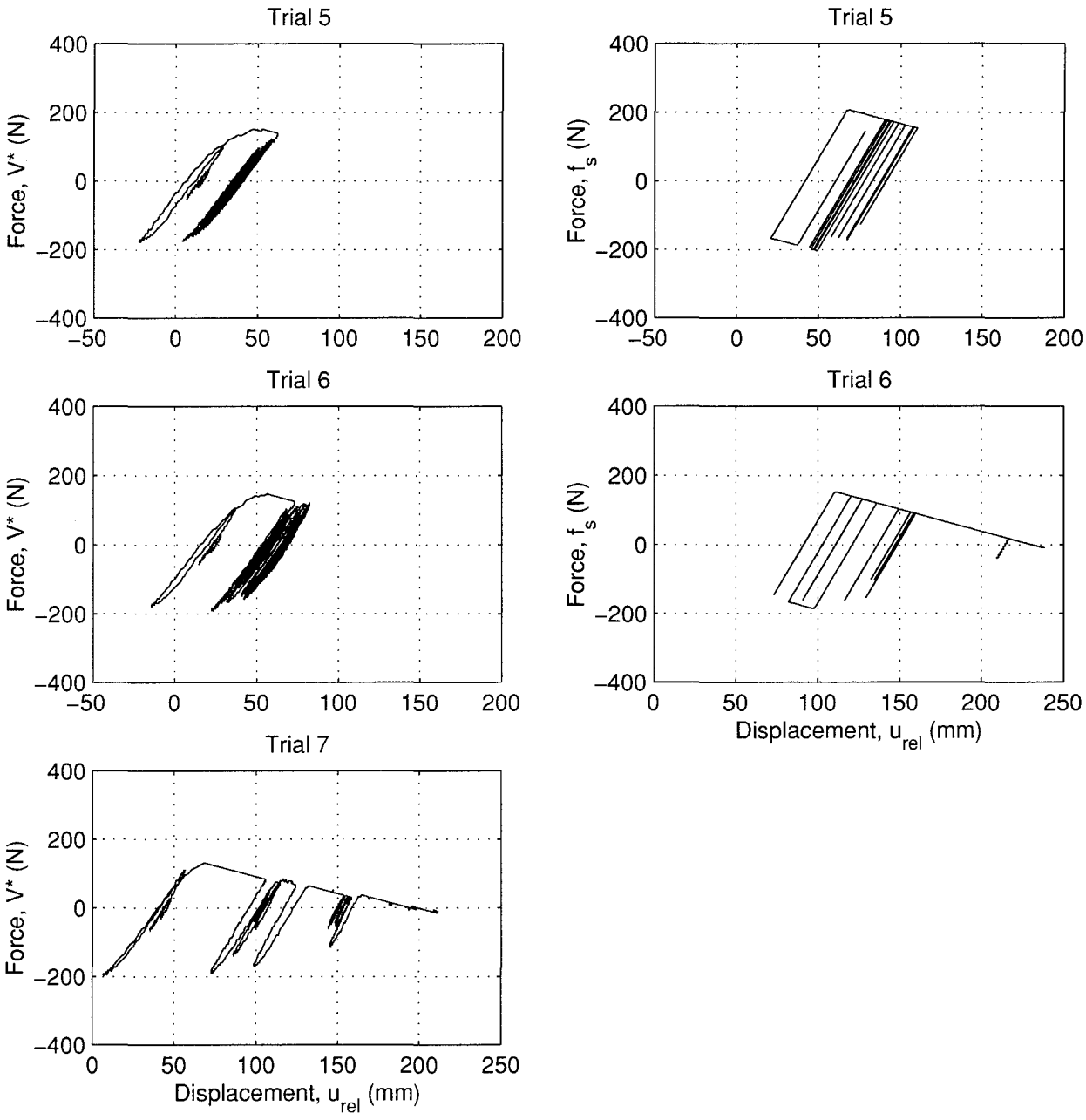

FIGURE 5–5 (cont'd) Force–Displacement – Specimen 11 – Exp. vs. Method 2

5.3 Behavioral Trends

The value of the stability factor, θ , has a significant effect on the response of the structure. In practical bridge and building structures, θ is unlikely to be greater than 0.10, and is generally less than 0.060 (Priestley, MacRae and Tao 1993). Specimen 1 is found to be the only one here that has a θ value near that suggested practical range for the stability factor, with a value of 0.065. Specimens 2,6, and 11 have stability factors slightly larger than the likely upper limit, at 0.123, 0.101, and 0.138, respectively. All other specimens have a value of $\theta \geq 0.155$.

A graphical study of peak response parameters is located in Appendix C. Three dimensionless acceleration parameters, V_o^*/V_{yo}, $S_a/(V_{yo}/W)$, and $\ddot{u}_T/(V_{yo}/W)$, were compared with five dimensionless displacement parameters, μ, u_r/Δ_{coll}, μ/μ_s, $u_r/ u_{rel\text{-}max}$, and $u_{rel\text{-}max}/L$. The results from all specimens considered together, as well as by grouping of the data over four ranges of the stability factor, namely: $\theta \leq 0.1$, $0.1 < \theta \leq 0.3$, $0.3 < \theta \leq 0.5$, and $\theta > 0.5$. The following general observations can be made:

- The elastic spectral acceleration, S_a, ductility, μ, and percent drift, γ, were observed to have inverse relationships with θ. In support of this observation, these variables are plotted in figures 5-6, 5-7, and 5-8, respectively, versus the stability factor for the next to last test (given subscript "final"). This suggests that the structures may be less able to undergo large inelastic excursions before imminent instability as the stability factor increases. Specimens 1 and 6, which have the lowest values of θ tested, were the only specimens able to withstand spectral accelerations greater than 0.75 g.
- Specimen 1 was the only specimen that underwent both a ductility greater than five (20.35), and a drift larger than 20% of the specimen height (64%), prior to collapse, as shown in figures 5-7 and 5-8, respectively. Recall that this is the only specimen that has a value of θ less than 0.1.

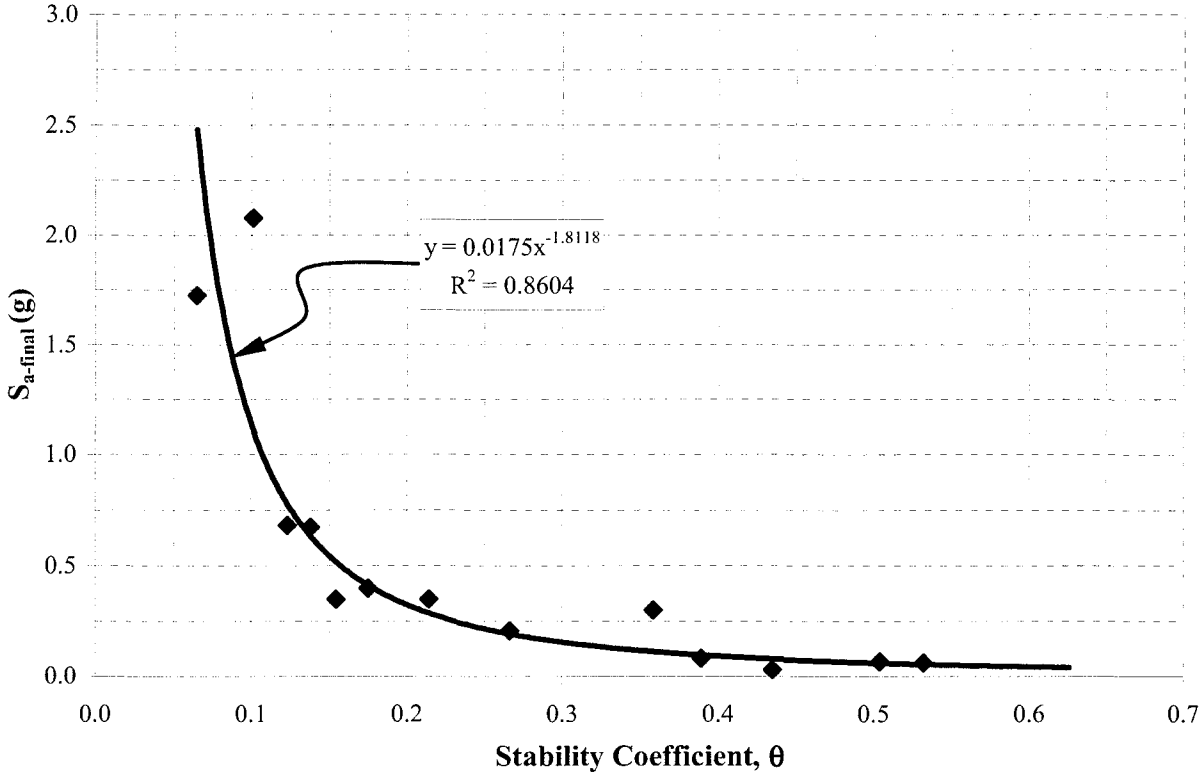

FIGURE 5-6 Spectral Acceleration versus Stability Coefficient

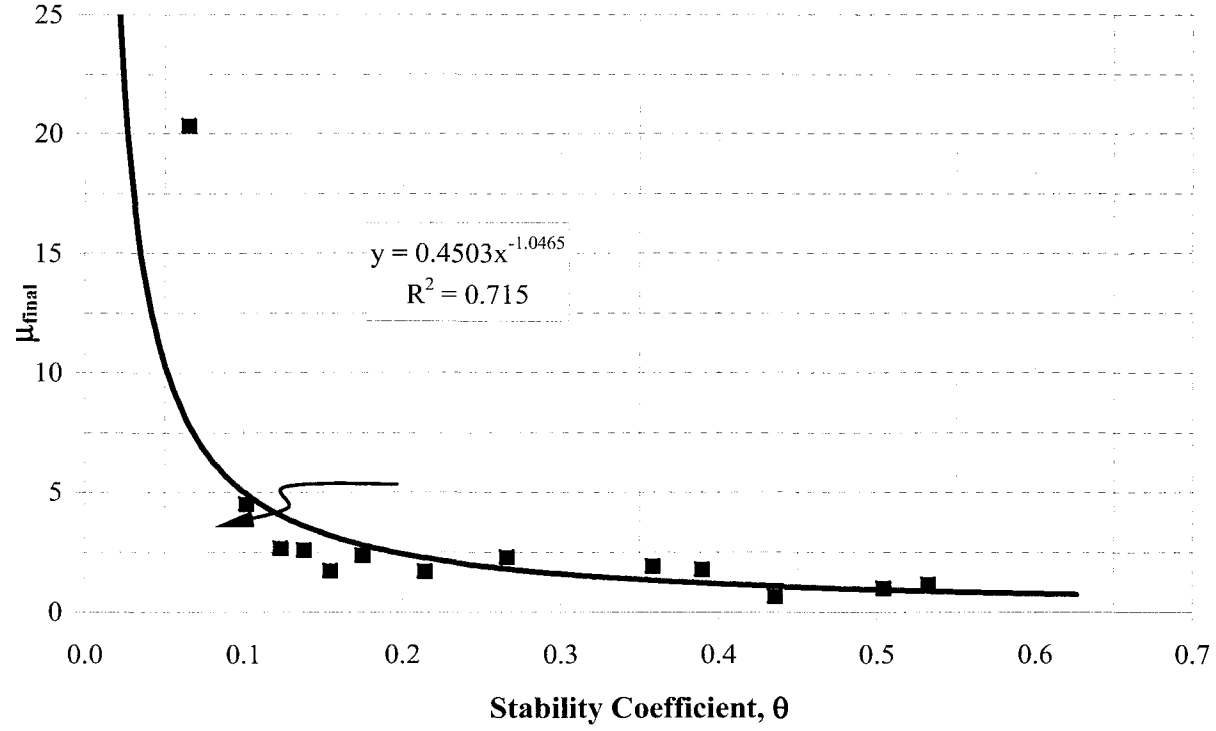

FIGURE 5-7 Displacement Ductility versus Stability Coefficient

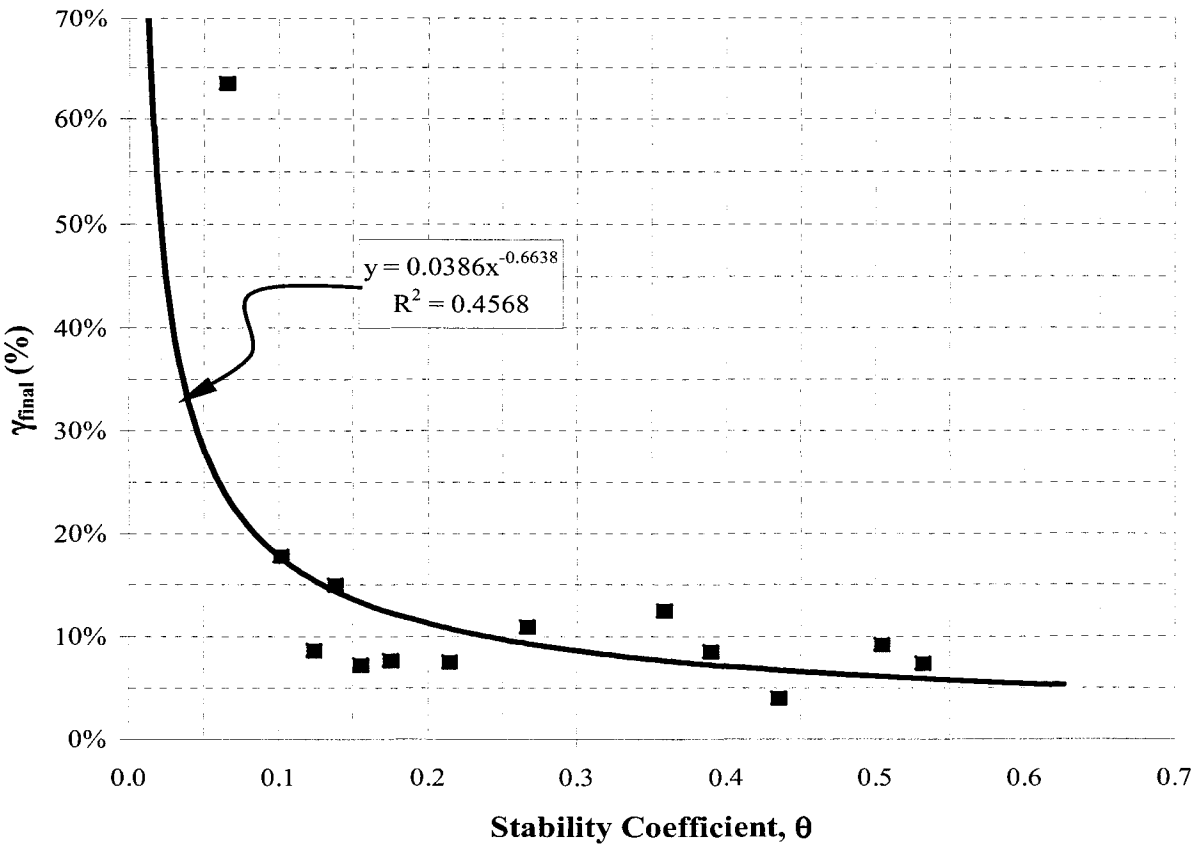

FIGURE 5-8 Drift versus Stability Coefficient

The static stability limit, μ_s, can be expressed as the inverse of the stability factor, as derived in section 2. The same set of ordinate parameters previously discussed is plotted versus μ_s in figure 5-9 through 5-11. A reverse trend than shown in figure 5-6 to 5-8 is observed, as expected. In figure 5-10, the line $\mu_{final} = \mu_s$ is shown for clarity. Only Specimen 1 was able to achieve ductility greater than the static stability limit on the next to last test.

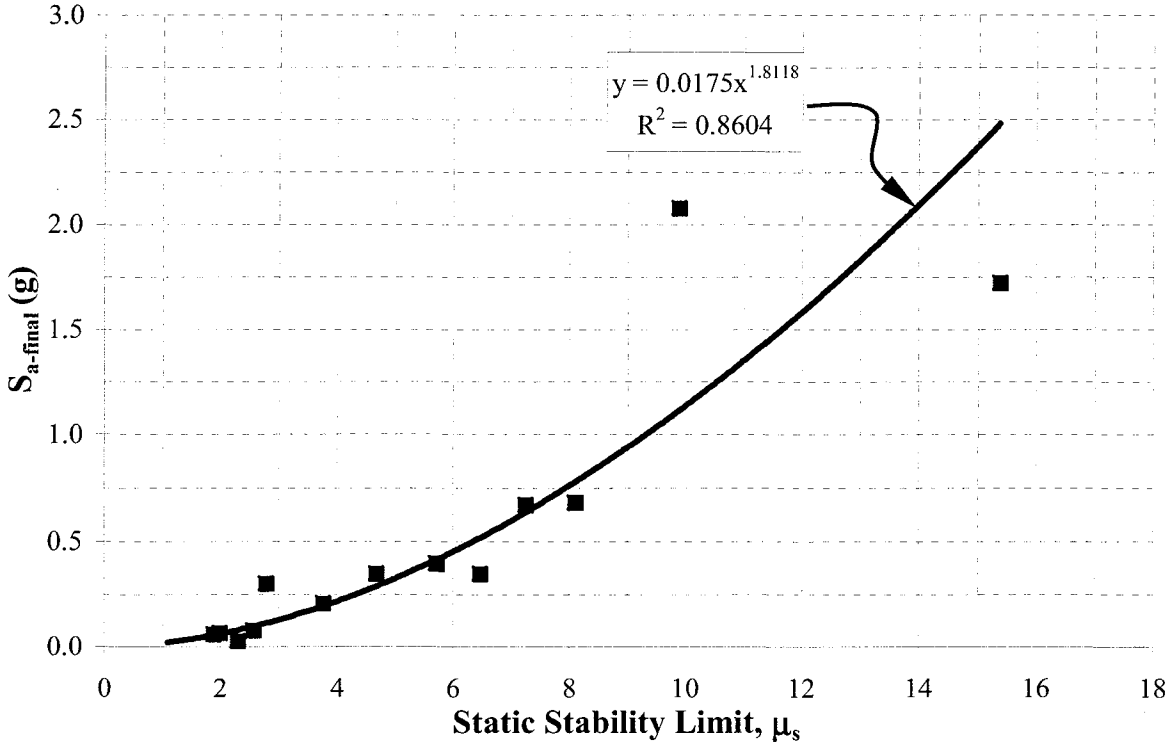

FIGURE 5-9 Spectral Acceleration versus Static Stability Limit

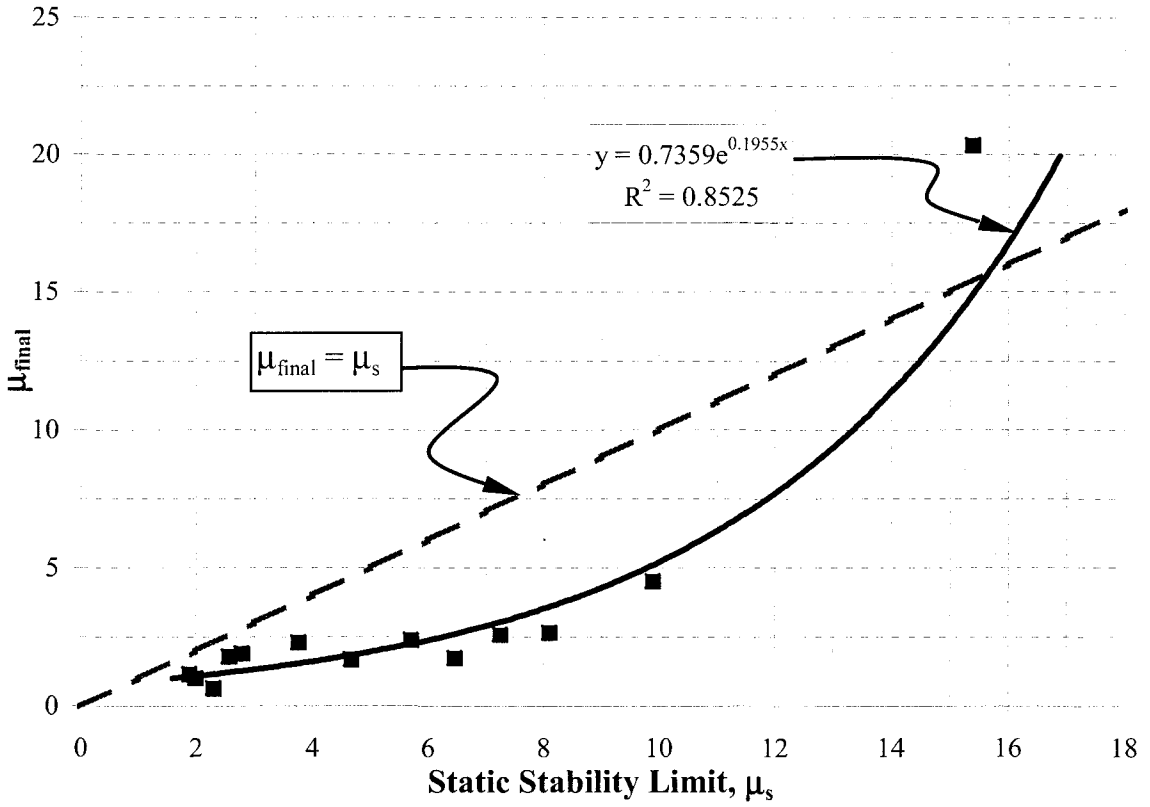

FIGURE 5-10 Displacement Ductility versus Static Stability Limit

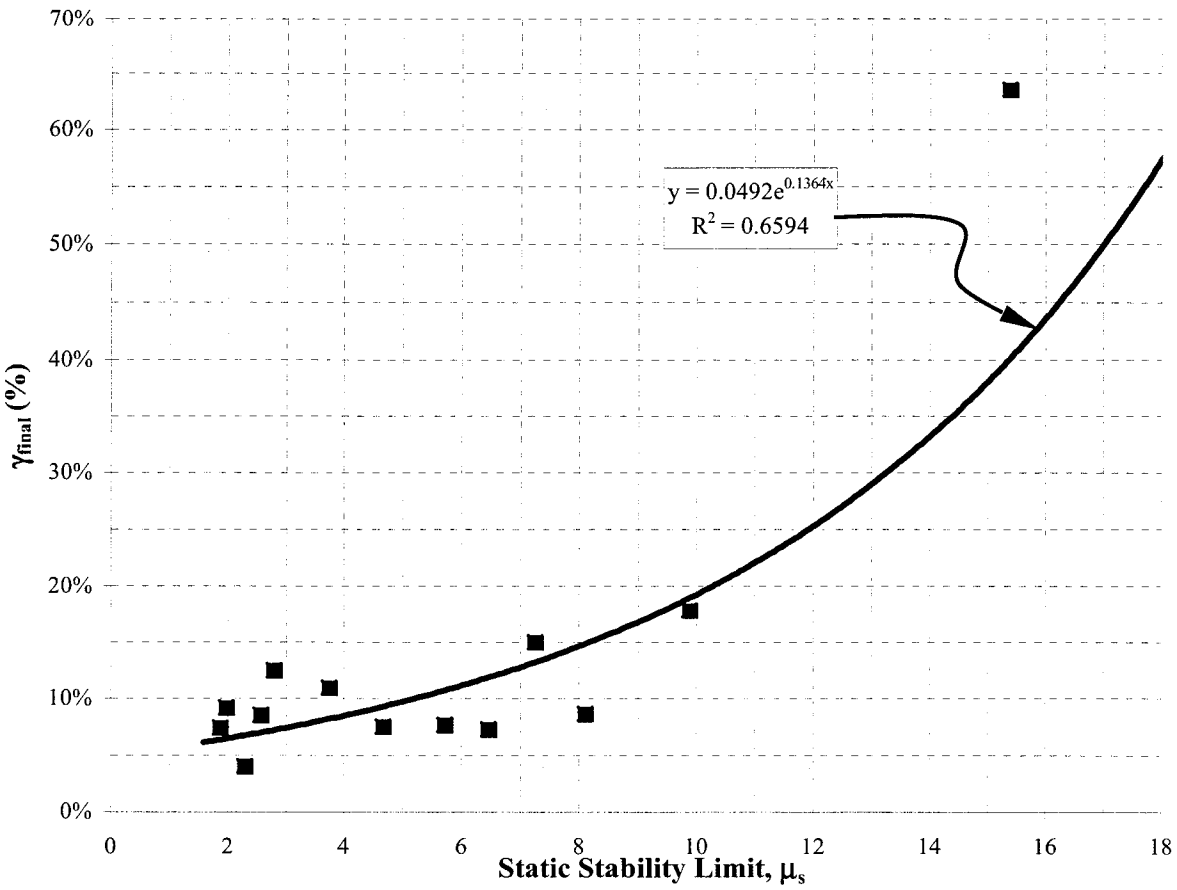

FIGURE 5-11 Drift versus Static Stability Limit

Overall, figures 5-6 to 5-11 show a high dependence of ultimate inelastic behavior upon the stability factor for a P-Δ affected structure. For the specimens tested in this research, those that had a value of θ equal to or greater than 0.1, tended to have a relatively low level of inelastic behavior before collapse of the structure. Structures with θ <0.1 were able to withstand ground motions with higher spectral accelerations, experience larger values of ductility, and accumulate larger drifts, than those with θ >0.1. The more slender structures, characterized by a larger θ value, will undergo relatively small inelastic excursions prior to collapse.

5.4 Comparison with NCHRP 12-49 Proposed P-Δ Limits

The National Cooperative Highway Research Program (NCHRP), Project 12-49, under the auspices of the Transportation Research Board, is investigating seismic design of bridges from all relevant aspects. At the conclusion of this project, proposed revisions to the current LRFD specifications for highway bridges will be presented to the American Association of State

Highway Transportation Organizations (AASHTO) for review and possible implementation. Included in the proposed revisions, are how additional demands from P-Δ affect structural performance. The most recent proposed provision, as of this writing, states:

The displacement of a pier or bent in the longitudinal and transverse direction must satisfy proposed AASHTO LRFD Equation 3.10.3.9.4-1:

$$\Delta m \leq 0.25 \cdot C \cdot \left(\frac{W}{P}\right) \cdot H \qquad (5\text{-}2)$$

where:

Δ_m = R_d x Δ

R_d = Factor related to response modification factor and fundamental period

Δ = Displacement demand from the seismic analysis

C = Seismic base shear coefficient based on lateral strength

W = Weight of the mass participating in the response of the pier

P = Vertical load on the pier from non-seismic loads

H = Height of the pier

For analysis of the specimens in this research, the W/P ratio is equal to unity, and the measured experimental displacements, u_{rel}, and estimated base shear coefficient, C_s*, can substitute for Δ_m and C, respectively.

In figure 5-12 the proposed limit is compared with the peak experimental responses. The estimated base shear coefficient, C_s*, is plotted as a function of the maximum drift, γ. In figure 5-12(a), the specimens with $\theta < 0.25$ (1, 2, 4, 6, 7, 11, and 12) are shown. During the initial tests, when the proposed limit was satisfied, none of these specimens failed. Due to repeated inelastic action, the cumulative drifts of the structure increased, eventually causing progressive collapse and violating the proposed limit. Collapse always occurred only after the limit was exceeded in a prior test, thus validating the proposed criterion. As shown in figure 5-12(b), the remaining specimens, for which $\theta \geq 0.25$, never satisfied the drift criteria, even for those tests that remained in the elastic range. The stability factor for these specimens, however, is well above the practical range discussed previously in section 5.3; therefore, the limit violation is of no consequence.

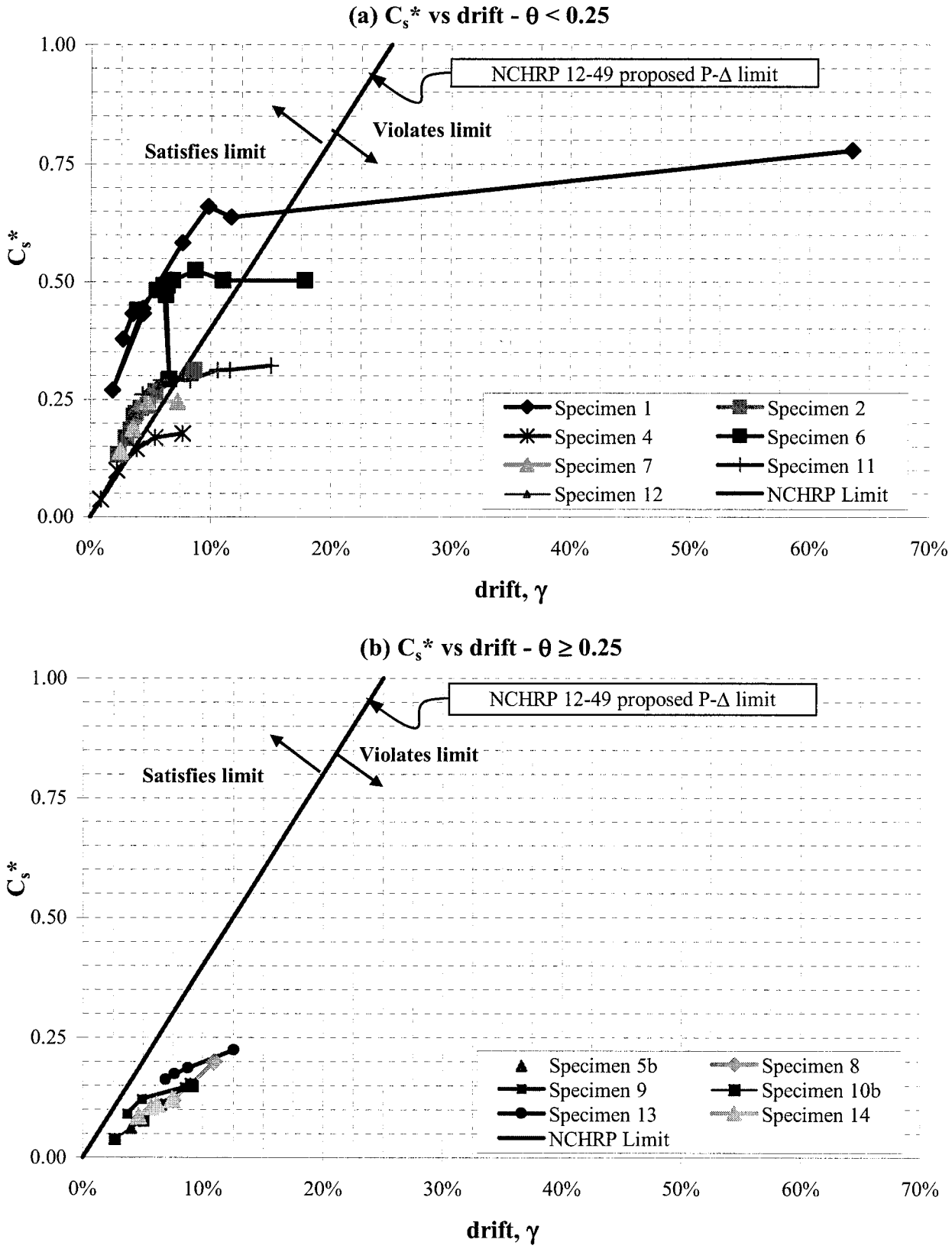

FIGURE 5-12 Test Results Comparison with NCHRP 12-49 Limits

5.5 Specimen Stability Analysis

The shake table test data is compared with various axial-moment interaction curves. The axial load on the specimen is constant, while the moment demand varies with the relative displacement. Axial-moment capacity of the specimen is calculated through first order equations that only consider the cross section strength, while the second order equations consider geometric effects in the overall stability of the specimen.

Both of the following equations can represent first order strength of the specimen:

$$\frac{M_{pr}}{M_p} + \left(\frac{P_u}{P_y}\right)^2 = 1 \qquad (5\text{-}3a)$$

$$\frac{8}{9} \cdot \frac{M_{pr}}{M_p} + \frac{P_u}{P_y} = 1 \qquad for: \frac{P_u}{P_y} \geq 0.2$$

$$\frac{M_{pr}}{M_p} + \frac{P_u}{2 \cdot P_y} = 1 \qquad for: \frac{P_u}{P_y} < 0.2 \qquad (5\text{-}3b)$$

where:

M_p = Plastic moment capacity of section

M_{pr} = Reduced plastic moment capacity due to presence of axial load

P_u = Axial load on column

P_y = Axial yield strength of column

The former, (5-3a), is the parabolic strength interaction equation for a rectangular cross section (Bruneau et. al 1998), while the latter, (5-3b), is a bilinear form of the interaction equation similar to that used by AISC (1994). Note that both of these equations address neither column axial stability, nor additional moment demand due to P-Δ effects.

Axial stability can be accounted for through the substitution of AISC-LRFD calculated axial compressive strength, P_n, for axial yield strength, P_y. Moment magnification due to P-Δ effects can be accounted for by the use of the AISC moment magnification factor, B_2, which is often used for the amplification of static loads:

$$B_2 = \frac{1}{1 - \frac{\Sigma P_u \cdot \Delta}{\Sigma V \cdot L}}$$

$$= \frac{1}{1 - \frac{P_u}{K \cdot L}} \qquad (5\text{-}4)$$

$$= \frac{1}{1 - \theta}$$

The reduced moment capacity, M_{pr}, in (5-3) is multiplied by B_2 to account for secondary moment effects during the elastic range of behavior. Inelastic systems must be analyzed in a slightly different manner. Typically, assuming equivalent inelastic and elastic maximum displacement (Newmark and Hall 1982), and a ductility demand of 4 for actual building structures consisting of ordinary moment frames, the design shear force will be reduced by this amount, which is designated the Response Modification Factor, R. The resulting modified (5-4) is:

$$B_2 = \frac{1}{1 - R \cdot \theta} \qquad (5\text{-}5)$$

Note that, for a R value of 4, as the stability factor approaches 0.25, the denominator of the expression approaches zero, and therefore, B_2 approaches infinity. When $\theta > 0.25$, this moment magnification factor is negative. Note that the inelastic amplification factor, α, presented in section 2.4 (Bernal 1987), is conceptually similar to (5-5), but does not suffer from this mathematical singularity. Recall that this factor which accounts for inelastic behavior is:

$$\alpha = \frac{1 + \beta \cdot \theta}{1 - \theta} \qquad (5\text{-}6)$$

where:

$$\beta = 1.87 \cdot (\mu - 1) \qquad (5\text{-}7)$$

where μ is the target ductility ratio.

Reduced moment capacity and resulting shear force are calculated as shown previously in Appendix A. The resulting spectral acceleration capacities are calculated by removing the response modification factor from the equations. In the perspective to compare with interaction curves, this is equivalent to the spectral acceleration producing first yield by assessing elastic

behavior up to M_{pr}. These quantities are listed for the specimens tested in tables 5-2 and 5-3 for first order and second order analyses, respectively.

Table 5-4 compares the maximum and minimum calculated spectral accelerations with the maximum measured mass acceleration, $\ddot{u}_{Tmax}$, and the maximum estimated base shear coefficient, C_{so}* and C_s*, respectively calculated by neglecting and including P-Δ effects. Each of the specimens reached values of these factors which exceed the minimum calculated spectral acceleration, which was dictated by the inelastic moment amplification factor, α .

The maximum calculated spectral acceleration was dictated by the section strength limit equation for all instances. Only Specimen 1, the only one with θ <0.1, reached a value of üTmax exceeding its corresponding $S_{a\text{-}max}$. Considering the base shear coefficient without P-Δ effects, C_{so}*, all of the specimens for which this value exceeds $S_{a\text{-}max}$ have θ <0.4, though not all specimens in this range of the stability factor reached this state. Specimens 1, 6, and 12 all reached values of the base shear coefficient with P-Δ effects, C_s*, larger than that of maximum calculated spectral acceleration.

TABLE 5-2 First Order Strength and Stability Analysis

Spec.	W (N)	L (mm)	P_y (N)	P_n (N)	P_u/P_y	P_u/P_n	M_p (N-mm)	First Order Limit Equation- P_y				First Order AISC- P_n			
								M_{lim} (N-mm)	*% of* M_p	V (N)	S_a (g)	$M_{u.1}$ (N-mm)	*% of* M_p	V (N)	S_a (g)
1	359.2	137.2	9918	3978	0.036	0.09	11,835	11,820	99.9	172.3	0.48	11,301	95.5	164.7	0.459
2	708.3	137.4	10696	4141	0.066	0.171	12,791	12,735	99.6	185.4	0.26	11,697	91.4	170.3	0.240
4	941.8	137.5	10080	3880	0.093	0.243	11,911	11,808	99.1	171.7	0.18	10,148	85.2	147.6	0.157
5b	941.8	91.7	8448	1157	0.111	0.814	6,070	5,994	98.8	130.7	0.14	1,268	20.9	27.7	0.029
6	941.8	412.4	32045	6711	0.029	0.14	75,735	75,669	99.9	367	0.39	70,420	93.0	341.5	0.363
7	941.8	343.7	22649	4388	0.042	0.215	43,820	43,745	99.8	254.6	0.27	38,718	88.4	225.3	0.239
8	941.8	274.5	15324	2549	0.061	0.369	23,153	23,065	99.6	168.1	0.18	16,424	70.9	119.7	0.127
9	941.8	205.8	9993	1744	0.094	0.54	11,879	11,774	99.1	114.4	0.12	6,146	51.7	59.7	0.063
10	476.4	137	2889	745	0.165	0.64	2,265	2,204	97.3	32.2	0.07	919	40.6	13.4	0.028
10b	476.4	137.4	8258	505	0.058	0.943	5,904	5,884	99.7	85.6	0.18	378	6.4	5.5	0.012
11	708.3	549.5	34691	3703	0.02	0.191	81,279	81,246	100	295.7	0.42	73,505	90.4	267.5	0.378
12	708.3	458.2	17569	2384	0.04	0.297	33,414	33,360	99.8	145.6	0.21	26,421	79.1	115.3	0.163
13	708.3	366.1	15613	1425	0.045	0.497	23,531	23,482	99.8	128.3	0.18	13,313	56.6	72.7	0.103
14	708.3	275.2	9875	960	0.072	0.738	11,675	11,615	99.5	84.4	0.12	3,445	29.5	25.0	0.035
15	359.2	182.8	2772	414	0.13	0.869	2,166	2,130	98.3	23.3	0.06	320	14.8	3.5	0.010

TABLE 5-3 Second Order Strength and Stability Analysis (LANDSCAPE PAGE)

Spec.	M_p (N-mm)	θ	Amplification Factors			α (μ=R=4)				B_2 (R=4)			
			B_2 (R=4)	α (μ=4)	α or B_2 (μ=R=1)	$M_{u.2}$ (N-mm)	*% of* M_p	V_2 (N)	$S_{a.2}$ (g)	$M_{u.2\alpha}$ (N-mm)	*% of* M_p	$V_{2\alpha}$ (N)	$S_{a.2\alpha}$ (g)
1	11,835	0.065	1.35	1.46	1.07	7,742	65.4	89.6	0.249	10,566	89.3	144.6	0.403
2	12,791	0.123	1.97	1.93	1.14	6,060	47.4	59.1	0.083	10,254	80.2	132.9	0.188
4	11,911	0.175	3.34	2.4	1.21	4,224	35.5	36.1	0.038	8,372	70.3	103.6	0.110
5b	6,070	0.435	-1.35	6.09	1.77	208	3.4	1.7	0.002	716	11.8	10.9	0.012
6	75,735	0.101	1.68	1.74	1.11	40,368	53.3	139.4	0.148	63,292	83.6	278.8	0.296
7	43,820	0.155	2.63	2.21	1.18	17,514	40.0	62.9	0.067	32,724	74.7	164.9	0.175
8	23,153	0.266	-15.17	3.4	1.36	4,829	20.9	17.0	0.018	12,048	52.0	69.3	0.074
9	11,879	0.39	-1.79	5.22	1.64	1,178	9.9	4.5	0.005	3,752	31.6	26.2	0.028
10	2,265	0.461	-1.18	6.66	1.86	138	6.1	0.7	0.001	495	21.8	4.9	0.010
10b	5,904	0.504	-0.98	7.72	2.02	49	0.8	0.2	0.000	188	3.2	1.8	0.004
11	81,279	0.138	2.23	2.06	1.16	35,714	43.9	83.8	0.118	63,362	78.0	202.7	0.286
12	33,414	0.214	7.01	2.8	1.27	9,426	28.2	22.2	0.031	20,759	62.1	74.6	0.105
13	23,531	0.359	-2.3	4.69	1.56	2,836	12.1	6.4	0.009	8,540	36.3	34.3	0.048
14	11,675	0.532	-0.89	8.52	2.14	404	3.5	0.9	0.001	1,612	13.8	7.6	0.011
15	2,166	0.627	-0.66	12.09	2.68	26	1.2	0.1	0.000	120	5.5	0.8	0.002

TABLE 5-4 Comparisons of Measured Acceleration and Base Shear Coefficients with Analytical Values

Spec.	* $S_{a\text{-}min}$ (g)	** $S_{a\text{-}max}$ (g)	$\ddot{u}_{Tmax}$ (g)	$\frac{\ddot{u}_{Tmax} - S_{a\text{-}min}}{S_{a\text{-}min}}$ (%)	$\frac{\ddot{u}_{Tmax} - S_{a\text{-}max}}{S_{a\text{-}max}}$ (%)	C_{so}* (g)	$\frac{C_{so}* - S_{a\text{-}min}}{S_{a\text{-}min}}$ (%)	$\frac{C_{so}* - S_{a\text{-}max}}{S_{a\text{-}max}}$ (%)	C_{so}* (g)	$\frac{C_s* - S_{a\text{-}min}}{S_{a\text{-}min}}$ (%)	$\frac{C_s* - S_{a\text{-}max}}{S_{a\text{-}max}}$ (%)
1	0.249	0.480	0.607	143.4%	26.5%	0.778	212.0%	62.2%	0.561	125.0%	16.9%
2	0.083	0.262	0.253	203.4%	-3.3%	0.312	274.1%	19.2%	0.226	170.5%	-13.8%
4	0.038	0.182	0.173	351.0%	-5.1%	0.177	361.4%	-2.9%	0.115	199.4%	-37.0%
5b	0.002	0.139	0.017	866.8%	-87.8%	0.061	3369.1%	-56.1%	0.021	1068.0%	-85.2%
6	0.148	0.390	0.381	157.5%	-2.2%	0.524	254.1%	34.5%	0.436	194.7%	11.9%
7	0.067	0.270	0.222	232.2%	-17.9%	0.245	266.6%	-9.4%	0.198	196.5%	-26.7%
8	0.018	0.178	0.110	508.2%	-38.4%	0.199	1000.3%	11.5%	0.090	396.4%	-49.7%
9	0.005	0.121	0.058	1121.0%	-52.3%	0.147	2994.6%	21.0%	0.073	1442.8%	-39.7%
10	0.001	--	--	--	--	--	--	--	--	--	--
10b	0.000	0.180	0.052	10382.5%	-71.1%	0.153	30742.8%	-14.9%	0.063	12596.5%	-65.0%
11	0.118	0.417	0.352	197.7%	-15.7%	0.322	172.3%	-22.9%	0.233	96.7%	-44.3%
12	0.031	0.206	0.184	488.3%	-10.5%	0.300	859.3%	45.9%	0.225	619.7%	9.5%
13	0.009	0.181	0.103	1046.3%	-43.1%	0.224	2393.0%	23.7%	0.099	996.5%	-45.6%
14	0.001	0.119	0.035	2539.0%	-70.6%	0.121	9023.3%	1.6%	0.048	3542.1%	-59.5%
15	0.000	--	--	--	--	--	--	--	--	--	--

*: Minimum value of Spectral Acceleration, S_a, from tables 5-2 and 5-3
**: Maximum value of Spectral Acceleration, S_a, from tables 5-2 and 5-3

SECTION 6
CONCLUSION

6.1 General

The experimental data generated by this project provides a well-documented base of shake table tests of a SDOF system subjected to earthquakes of progressively increasing intensity up to collapse due to instability. This data will be useful for, and shared with, other researchers who may wish to validate or develop algorithms capable of modeling inelastic behavior of steel frame structures up to and including collapse. The data presented here will also be located on the world-wide-web (with all intermediate data files) for immediate access by those other researchers.

The sizes of the specimens were chosen to allow testing to full collapse on a small-scale shake table. The size made the fabrication and erection of each of the test structures a delicate procedure. Once these procedures were standardized, tests could be performed in rapid succession while ensuring the safety of those performing the tests, as well as of the instruments recording data. Unscaled ground motions were used as the specimens were designed to fit actual parameters of interest, and not intended to be scaled models of actual structures.

Fabrication quality, as in every structure, varied for the various columns tested here, even among those making up the same specimen. Imperfections were therefore measured in a number of ways to allow for their proper consideration in subsequent analytical modeling. A procedure was also developed to correct the displacement time histories accounting for angle changes at large displacements.

Note that the damping of the specimens tested was measured to be non-linear. As a general trend, during free vibration testing, the damping ratio was observed to increase as the free vibration response amplitude decreased. This caused some modeling difficulties, when a simplified SDOF analysis program that only accounts for constant damping was used in an attempt to replicate the test results, even though this program was only used to illustrate how data generated by this research can be used.

The research presented here demonstrated a number of important points that must be considered in the design of slender steel structures. The stability coefficient, θ, has the most significant effect on the behavior of the structure. As θ increases, the maximum attainable ductility, sustainable drift, and spectral acceleration, which can be resisted before collapse, all decrease. When this factor is larger than 0.1, the ultimate values of the maximum spectral acceleration, displacement ductility, and drift reached before collapse are all grouped below values of 0.75 g, 5, and 20%, respectively. Stability coefficient values less than 0.1 tend to increase each of those response values significantly.

All specimens exceeded the strength dictated by inelastic moment amplification factors. In addition, some specimens actually exceeded the calculated strength based on first order effects. Specimen 1, having the lowest value of the stability factor of all specimens, exceeded all calculated strengths. Considering the base shear coefficient without P-Δ effects, C_{so}*, all of the specimens for which this value exceeds $S_{a\text{-}max}$ have $\theta<0.4$, though not all specimens in this range of the stability factor reached this state. In addition, Specimens 6 and 12 each reached a value of the base shear coefficient with P-Δ effects, C_s*, larger than that of maximum calculated spectral acceleration.

6.2 Recommendations for Further Research

A larger range of specimens should be tested under various conditions to further quantify the nonlinear inelastic behavior of columns under dynamic P-Δ effects. Parameters that should be considered are:

1. The stability coefficient, θ: This appears to be the most significant parameter affecting behavior, as illustrated in this study. However, more tests should be performed to more accurately quantify the impact of this factor over various ranges, and in combination with other parameters.
2. The frequency content of the ground motion with respect to the specimen being tested. The 1940 El Centro ground motion was utilized for all specimens in this study. A ground motion, measured or synthesized, with a more uniform response spectrum over the entire frequency range may be more desirable in removing the impact of ground motion as a

variable affecting the behavior of the specimens. Alternatively, the effects of large pulses (near-fault effects) versus more regular cyclical excitations could be considered.

3. The specimen setup: The specimens were fabricated in a way that made minimization of imperfections difficult. The size at which the specimens were fabricated increases the likelihood of them being affected by the heat imparted when welding the pieces together. A different method of fabrication, possibly one in which the specimen is clamped into the base plate rather that welded to it, may be a more effective solution.
4. The characterization of inherent damping in a highly non-linear system. This remains an important problem that deserves further investigation.

SECTION 7
REFERENCES

1. AISC, (1994) "Manual of Steel Construction, Load & Resistance Factor Design," 2nd Edition, American Institute of Steel Construction, Chicago, Ill.

2. Bernal, Dionisio, (1987), "Amplification Factors for Inelastic Dynamic p-Delta Effects in Earthquake Analysis," Earthquake Engineering and Structural Dynamics, Vol. 15, No. 5.

3. Bruneau, M., Uang, C-M, Whittaker, A.S., (1998) "Ductile Design of Steel Structures", The McGraw-Hill Companies, Inc, New York.

4. Charney, F. A., (1998), "NONLIN: Nonlinear Dynamic Time History Analysis of Single Degree of Freedom Systems," Federal Emergency Management Agency.

5. Chopra, A. K., (1995),"Dynamics of Structures: Theory and Applications to Earthquake Engineering," Prentice-Hall, New Jersey.

6. Constantinou, M.C., Pitman, M., Percassi, S., Boyle, T. A., Reinhorn, A.M., (1999) "Structural Engineering & Earthquake Simulation Laboratory Laboratory Manual," University at Buffalo, Department of Civil, Structural and Environmental Engineering, http://www.civil.buffalo.edu/cie/facilities/seesl/Cover.html

7. Kawashima, K., MacRae, G. A., Hoshikuma, J., and Nagaya, K., (1996) "Residual Displacement Response Spectrum and its Application to Reinforced Concrete Bridge Piers," Wind and Seismic Effects: Proceedings of the 28th Joint Meeting of the US-Japan, August 1996.

8. MacRae, G. A., Kawashima, K., (1993) "The seismic response of bilinear oscillators using Japanese earthquake records," Journal of Research, 30, Public Works Research Institute, Tsukuba, Japan.

9. MacRae, G. A., Priestley, M.J.N., Tao, J., (1993) "P-Δ Effects in Seismic Design," Report No. SSRP-93/05, Department of Applied Mechanics and Engineering Sciences, University of California, San Diego.

10. MacRae, G. A., (1994) "P-Δ Effects on Single-Degree-of-Freedom Structures in Earthquakes," Earthquake Spectra, Vol. 10, No. 3.

11. Naeim, Farzad, (Ed.) (1989) "The Seismic Design Handbook", Van Nostrand Reinhold, New York.

12. Newmark, N.M., and Hall, W.J., (1982), "Earthquake Spectra and Design," Earthquake Engineering Research Institute, Berkeley, CA.

13. Reinhorn, A. M., (1997), "Inelastic analysis techniques in seismic evaluations," Seismic Design Methodologies for the Next Generation of Codes, A. A. Balkema Publishers.

APPENDIX A
PRELIMINARY DESIGN CALCULATIONS

Specimen sizes were determined in the preliminary stages of this research based on the hand calculations summarized in the following pages.

Relations were derived such that a range of column dimensions over each of the values of slenderness (i.e. 100, 150, 200) produced a wide range of values of axial demand versus plastic axial capacity so that possible trends could be observed more easily. Expressions for the limit behavior of a specimen were developed. Weight on the specimen and the displacements at formation of plastic collapse mechanism are presented in terms of the dimensions, the yield stress, and the spectral acceleration needed for plastic collapse. The ratio of axial demand to the axial force at yield is written in terms of the plastic spectral acceleration and the slenderness ratio of the columns. These calculations appear on the following three pages.

Following those calculations are tables of the final selected nominal sizes and various other parameters as described below:

- Table A-1 lists nominal dimensions of each specimen, followed by calculated mechanical properties: moment of inertia, I, plastic modulus, Z, plastic axial capacity, P_y, plastic moment capacity, M_p, lateral shear force at first yield, V_y, and the lateral shear force at full plastic moment formation, V_p. The spectral acceleration, S_a, required to develop V_p in the specimen, and obtained using the procedures described in pages A-3 to A-6, is also listed.
- Table A-2 lists the nominal specimens dimensions, resulting stiffness, and applied mass. All these quantities are needed to calculate the fundamental frequencies and periods listed. Also listed is the "design" base shear for elastic response, V_e, to find the level of table excitation needed to produce a target ductility ratio of $\mu \cong 4$, and defined as equal to $R \cdot V_p$ where R is taken as 4 in this case. The base shear coefficient (or spectral acceleration) is calculated for this value of the base shear and compared with the preliminary value listed in table A-1. Note that the definition of V_e is for convenience in obtaining useful predictions of table accelerations required to achieve target ductilities and ensure that the table excitation capabilities are not exceeded. While this was done assuming a bilinear model yielding at M_p

(i.e. V_p), for the more sophisticated analyses expected to follow this study, one must recognize that rectangular sections have a shape factor of 1.5, and that consequently, $V_p = 1.5 \cdot V_y$

- Table A-3 lists the results of dynamic analyses conducted to find the peak displacement response of each specimen. Both a linear-elastic model and an elastic-perfectly-plastic bilinear model were considered in these analyses, completed using the program NONLIN. The elastic-perfectly-plastic bilinear model with the P-Δ effect included was used to calculate the minimum PGA that could theoretically be applied to the model so the model would progressively collapse under a single application of the ground motion history. This critical PGA was used to calculate the peak displacement response with an elastic response spectrum and also in the construction of an inelastic spectrum to compare with the NONLIN inelastic analyses. "N/A" is listed in the displacement column of the inelastic spectra results when no result could be read from the capacity-demand spectra plot. The minimum displacement response of all of these techniques is extracted for each specimen. A sample inelastic capacity-demand spectrum plot is shown for Specimen 2 in Figure A.1.
- Table A-4 lists the results of dynamic analyses to find the peak acceleration response of each specimen. Results are taken from the same analyses used in finding the displacement responses in Table A-3. Results are compared with the design spectral acceleration values for full plastic behavior.
- Tables A-5 and A-6 list the results of strength and stability analyses using first and second order methods, respectively. Parabolic limit equations for section strength are used, as well as bilinear equations as per AISC (1994) using first order strength, and magnified using the AISC moment magnification factor, and the inelastic P-Δ amplification factor presented in Chapter 2 (Bernal 1987). Four pages of sample calculations precede these tables, displaying the formulae used for the strength and stability check and results for Specimen 1, R=4.

Preliminary Calculations to find Specimen sizes

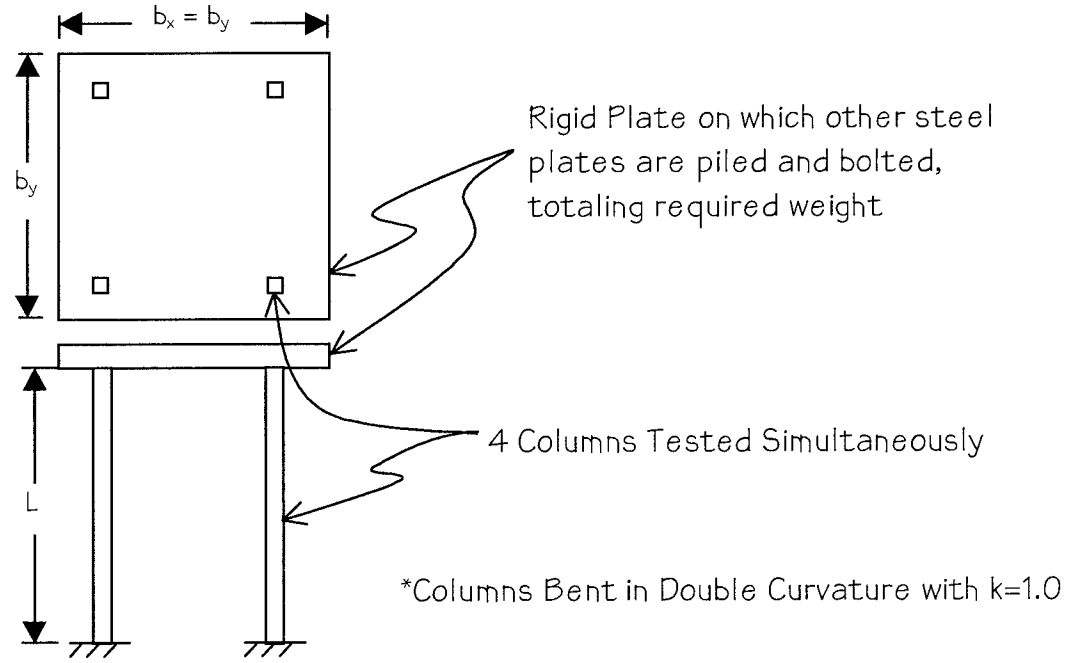

Assumptions: $F_y := 50 \cdot ksi$ $k := 1.0$ (Double Curvature)

$R := 4.0$ (Response Modification Factor)

Seismic Base Shear is given by: $V = C_s \cdot W$

$$V = \frac{V_e}{R} = \frac{S_a}{R} \cdot W \qquad (1)$$

where: S_a: Design Spectral Response Acceleration

W: Weight on structure (Full Slab=4W)

Base Shear or Lateral Force on single column:

$$H = V = \frac{S_a \cdot W}{4} \qquad (2)$$

Plastic Moment at Base due to this Force:

$$M_P = \frac{h^3}{4} \cdot F_y = \frac{H \cdot L}{2} = \frac{S_a}{4} \cdot \frac{W \cdot L}{2} \qquad (3)$$

Plastic Axial Capacity of Section:

$$P_y = h^2 \cdot F_y \qquad P = W \tag{4a, b}$$

$$\frac{P}{P_y} = \frac{W}{h^2 \cdot F_y} = \frac{\left[\frac{2 \cdot h^3 \cdot F_y}{S_a \cdot L}\right]}{h^2 \cdot F_y} = \frac{2 \cdot h}{S_a \cdot L} \tag{5}$$

For a given slenderness: $\frac{k \cdot L}{r} = \text{Given} = \frac{L}{h} \cdot \sqrt{12}$

where: $r = \frac{h}{\sqrt{12}}$ for square sections, and k=1.0 as stated previously

Solving for h/L:

$$\frac{h}{L} = \frac{\sqrt{12}}{\frac{k \cdot L}{r}} \tag{6}$$

Rewriting (5) in terms of Slenderness using (6):

$$\frac{P}{P_y} = \frac{4 \cdot \sqrt{3}}{S_a \cdot \frac{k \cdot L}{r}} \tag{7}$$

Deformation due to reduced elastic Base Shear: V_e/R:

$$\Delta_R = \frac{H}{K_s} = \frac{0.25 \cdot S_a \cdot W}{\frac{12 \cdot E \cdot I}{L^3}} = \frac{0.25 \cdot S_a \cdot W \cdot L^3}{E \cdot h^4}$$

$$\Delta_R = \frac{S_a \cdot W}{4 \cdot E \cdot h} \cdot \left(\frac{L}{h}\right)^3 = \frac{S_a \cdot W}{4 \cdot E \cdot h} \cdot \left(\frac{k \cdot L}{r}\right)^3 \cdot \frac{1}{\sqrt{12}^3} \tag{8}$$

Substitute expression for W in (3) into (8):

$$\Delta_R = \frac{S_a}{4 \cdot E \cdot h} \cdot \frac{2 \cdot h^3 \cdot F_y}{S_a \cdot L} \cdot \left(\frac{L}{h}\right)^3 = \frac{F_y \cdot L^2}{2 \cdot E \cdot h} \qquad (9)$$

Preliminary Charts for square section of h =3/8" and h=1/8":

S_a (g)	W (kip)	m (kg)	P/P_y	Δ_R (in)	Δ_R/L(%)
kL/r = 200		L = 21.65		h = 3/8	
1.00	0.244	110	0.009	1.0776	4.98%
0.50	0.487	221	0.017	1.0776	4.98%
0.25	0.974	442	0.035	1.0776	4.98%
kL/r = 150		L = 16.24		h = 3/8	
1.00	0.325	147	0.012	0.6061	3.73%
0.50	0.650	295	0.023	0.6061	3.73%
0.25	1.299	589	0.046	0.6061	3.73%
kL/r = 100		L = 10.83		h = 3/8	
1.00	0.487	221	0.017	0.2694	2.49%
0.50	0.974	442	0.035	0.2694	2.49%
0.25	1.949	884	0.069	0.2694	2.49%

S_a (g)	W (kip)	m (kg)	P/P_y	Δ_R (in)	Δ_R/L(%)
kL/r = 200		L = 7.22		h = 1/8	
1.00	0.027	12.3	0.009	0.3592	4.98%
0.50	0.054	24.5	0.017	0.3592	4.98%
0.25	0.108	49.1	0.035	0.3592	4.98%
kL/r = 150		L = 5.41		h = 1/8	
1.00	0.036	16.4	0.012	0.2020	3.73%
0.50	0.072	32.7	0.023	0.2020	3.73%
0.25	0.144	65.5	0.046	0.2020	3.73%
0.13	0.144	65.5	0.092	0.2020	3.73%
kL/r = 100		L = 3.61		h = 1/8	
1.00	0.054	24.5	0.017	0.0898	2.49%
0.50	0.108	49.1	0.035	0.0898	2.49%
0.25	0.217	98.2	0.069	0.0898	2.49%
0.13	0.433	196.4	0.139	0.0898	2.49%

TABLE A-1 Nominal Specimen Properties

Specimen	L (in)	b (in)	h (in)	A (in2)	Z (in3)	I (in4)	r (in)	Actual kL/r	W / Col. (kip)	S_{DS} (g)	P_y (kip)	M_p (kip-in)	V_p (kip)	V_y (kip)
1	5.41	0.1875	0.1875	0.0352	0.0016	0.00010	0.054	100.0	0.0771	0.790	1.758	0.082	0.030	0.020
2	5.41	0.1875	0.1875	0.0352	0.0016	0.00010	0.054	100.0	0.1542	0.395	1.758	0.082	0.030	0.020
3	3.61	0.1250	0.1250	0.0156	0.0005	0.00002	0.036	100.0	0.1542	0.175	0.781	0.024	0.014	0.009
4	5.41	0.1875	0.1875	0.0352	0.0016	0.00010	0.054	100.0	0.2056	0.296	1.758	0.082	0.030	0.020
5	3.61	0.1250	0.1250	0.0156	0.0005	0.00002	0.036	100.0	0.2056	0.316	1.875	0.059	0.032	0.022
6	16.24	0.3750	0.3750	0.1406	0.0132	0.00165	0.108	150.0	0.2056	0.790	7.031	0.659	0.081	0.054
7	13.51	0.3125	0.3125	0.0977	0.0076	0.00079	0.090	149.8	0.2056	0.549	4.883	0.381	0.056	0.038
8	10.81	0.2500	0.2500	0.0625	0.0039	0.00033	0.072	149.8	0.2056	0.351	3.125	0.195	0.036	0.024
9	8.12	0.1875	0.1875	0.0352	0.0016	0.00010	0.054	150.0	0.2056	0.197	1.758	0.082	0.020	0.014
10	5.41	0.1250	0.1250	0.0156	0.0005	0.00002	0.036	149.9	0.1028	0.421	1.875	0.024	0.009	0.006
11	21.65	0.3750	0.3750	0.1406	0.0132	0.00165	0.108	200.0	0.1542	0.790	7.031	0.659	0.061	0.041
12	18.02	0.3125	0.3125	0.0977	0.0076	0.00079	0.090	199.8	0.1542	0.549	4.883	0.381	0.042	0.028
13	14.43	0.2500	0.2500	0.0625	0.0039	0.00033	0.072	199.9	0.1542	0.351	3.125	0.195	0.027	0.018
14	10.83	0.1875	0.1875	0.0352	0.0016	0.00010	0.054	200.1	0.1542	0.197	1.758	0.082	0.015	0.010
15	7.22	0.1250	0.1250	0.0156	0.0005	0.00002	0.036	200.1	0.0771	0.175	0.781	0.024	0.007	0.005

TABLE A-2 Computation of Required Spectral Acceleration

Specimen	M ass (kg)	M ass (slugs)	L (in)	b (in)	h (in)	k (lbf/in)	ω_n (rad/s)	T_n (sec.)	$V_e=RV_p$ (kip)	Prev. S_a (g)	Req'd S_a (g)	Sa diff.
1	34.98	0.1996	5.41	0.1875	0.1875	226.37	33.68	0.187	0.122	0.790	1.580	-0.790
2	69.96	0.3992	5.41	0.1875	0.1875	226.37	23.81	0.264	0.122	0.395	0.790	-0.395
3	69.96	0.3992	3.61	0.1250	0.1250	150.49	19.42	0.324	0.054	0.175	0.351	-0.175
4	93.28	0.5322	5.41	0.1875	0.1875	226.37	20.62	0.305	0.122	0.296	0.592	-0.296
5	93.28	0.5322	3.61	0.1250	0.1250	150.49	16.82	0.374	0.130	0.132	0.631	-0.500
6	93.28	0.5322	16.24	0.3750	0.3750	133.90	15.86	0.396	0.325	0.790	1.579	-0.790
7	93.28	0.5322	13.51	0.3125	0.3125	112.16	14.52	0.433	0.226	0.549	1.098	-0.549
8	93.28	0.5322	10.81	0.2500	0.2500	89.68	12.98	0.484	0.145	0.351	0.703	-0.351
9	93.28	0.5322	8.12	0.1875	0.1875	66.95	11.22	0.560	0.081	0.197	0.395	-0.197
10	46.64	0.2661	5.41	0.1250	0.1250	44.71	12.96	0.485	0.036	0.176	0.351	-0.176
11	69.96	0.3992	21.65	0.3750	0.3750	56.51	11.90	0.528	0.244	0.790	1.579	-0.790
12	69.96	0.3992	18.02	0.3125	0.3125	47.26	10.88	0.577	0.169	0.549	1.098	-0.549
13	69.96	0.3992	14.43	0.2500	0.2500	37.70	9.72	0.647	0.108	0.351	0.702	-0.351
14	69.96	0.3992	10.83	0.1875	0.1875	28.22	8.41	0.747	0.061	0.197	0.395	-0.197
15	34.98	0.1996	7.22	0.1250	0.1250	18.81	9.71	0.647	0.027	0.175	0.351	-0.175

TABLE A-3 Computation of Maximum Displacement Response

Specimen	Δ_R @Mp (in)	$\Delta_{max} = R\Delta_R$ (in)	Δ_R/L	Peak Response in Nonlin					Elastic Spectra		Inelastic Spectra w/ P-Δ			OverallMin Displ. (in)
				T (s)	Linear (in)	NL-EPP (in)	NL-PΔ (in)	PGA_{crit} (g)	Linear (in)	Scaled (in)	V_e/W	r	Displ. (in)	
1	0.135	0.538	0.025	0.187	0.285	0.554	1.954	0.313	0.519	0.467	0.774	2.125	1.640	0.285
2	0.135	0.538	0.025	0.264	0.853	1.193	1.005	0.143	0.914	0.376	0.350	2.050	0.819	0.376
3	0.090	0.360	0.025	0.324	1.304	2.604	0.273	0.034	1.253	0.121	0.093	1.500	0.261	0.121
4	0.135	0.538	0.025	0.305	0.987	2.308	0.754	0.090	0.894	0.232	0.212	1.791	0.625	0.232
5	0.216	0.863	0.060	0.374	1.620	2.600	0.220	0.020	1.693	0.095	0.062	1.521	0.210	0.095
6	0.606	2.425	0.037	0.396	1.630	1.781	6.396	0.342	1.860	1.827	0.737	2.077	4.726	1.630
7	0.504	2.014	0.037	0.433	1.650	1.660	3.521	0.203	1.998	1.164	0.745	3.162	N/A	1.164
8	0.403	1.612	0.037	0.484	2.370	1.469	1.874	0.090	3.307	0.855	0.331	2.402	N/A	0.855
9	0.303	1.213	0.037	0.560	4.390	2.400	0.717	0.039	4.784	0.535	0.082	1.338	0.650	0.535
10	0.202	0.807	0.037	0.686	6.310	5.970	0.225	0.010	3.897	0.117	0.007	1.110	0.206	0.117
11	1.078	4.310	0.050	0.528	3.758	2.338	8.188	0.325	3.269	3.045	1.013	2.955	N/A	2.338
12	0.896	3.583	0.050	0.578	3.501	2.019	4.054	0.221	4.409	2.794	0.543	2.430	4.000	2.019
13	0.718	2.872	0.050	0.647	3.815	4.413	2.408	0.105	3.794	1.141	0.201	1.600	1.934	1.141
14	0.539	2.157	0.050	0.748	3.944	3.341	0.938	0.044	4.142	0.520	0.074	1.510	0.862	0.520
15	0.360	1.438	0.050	0.916	6.986	8.004	0.562	0.024	7.026	0.493	0.048	1.268	0.546	0.493

FIGURE A-1 Spectral Capacity of Specimen # 2

Spectral Demand from NONLIN (with P- Δ)

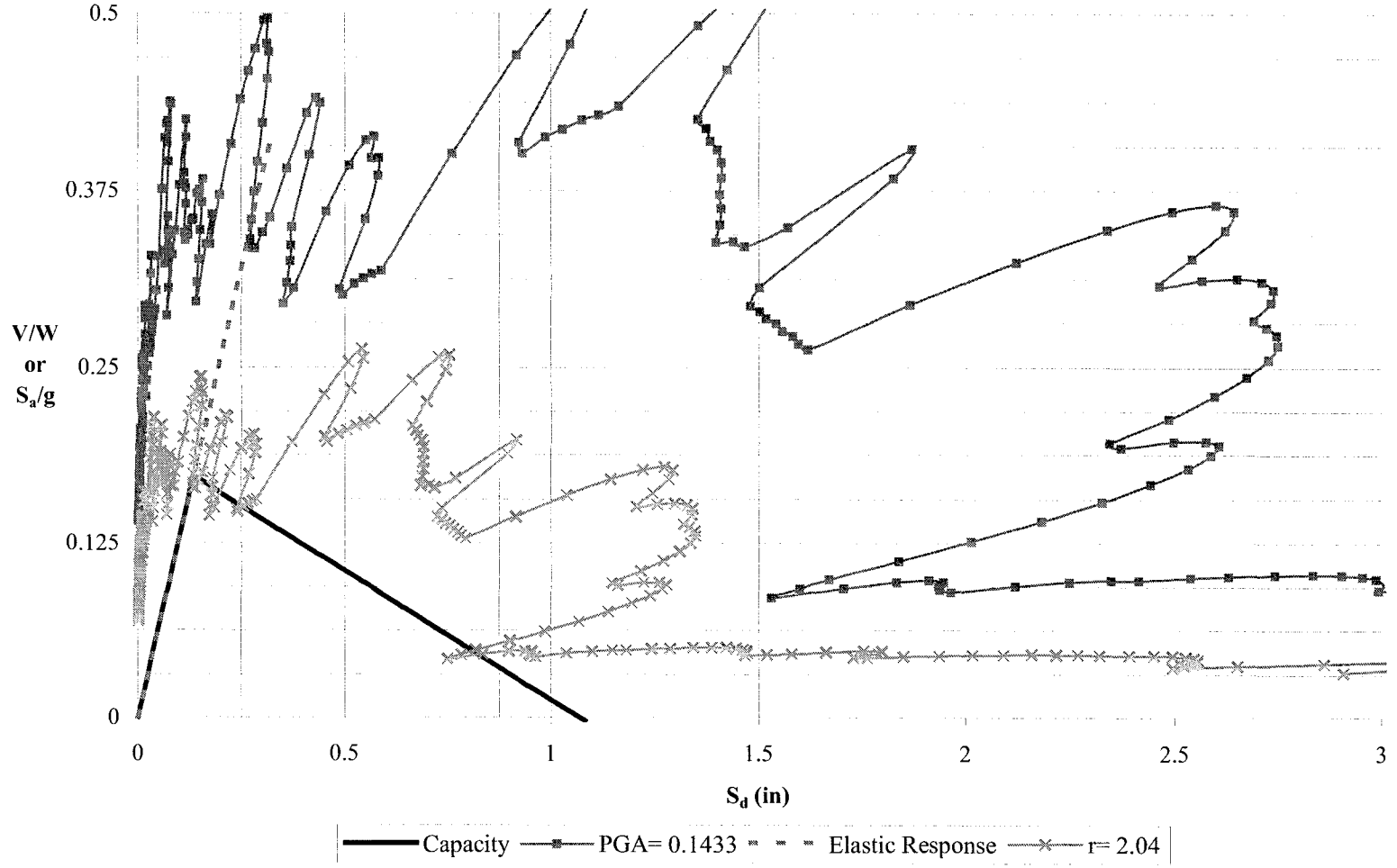

TABLE A-4 Computation of Maximum Acceleration Response

Specimen	Peak Response in Nonlin					Elastic Spectra		Overall Min. Resp. Accel. (g)	Required Resp. Accel. (g)
	T (s)	PGA (g)	Linear (g)	NL-EPP (g)	NL-PΔ (g)	Linear (in)	Scaled (in)		
1	0.187	0.313	0.908	0.473	0.484	1.762	1.732	0.473	1.580
2	0.264	0.143	0.590	0.436	0.296	1.330	0.598	0.436	0.790
3	0.324	0.034	0.133	0.342	0.095	1.213	0.128	0.342	0.351
4	0.305	0.090	0.297	0.376	0.915	0.982	0.278	0.376	0.592
5	0.374	0.020	0.068	0.325	0.043	1.231	0.076	0.325	0.631
6	0.396	0.342	1.090	0.565	0.522	1.219	1.308	0.565	1.579
7	0.433	0.203	0.581	0.478	0.325	1.079	0.687	0.478	1.098
8	0.484	0.090	0.322	0.396	0.225	1.437	0.406	0.396	0.703
9	0.560	0.039	0.177	0.351	0.095	1.559	0.190	0.351	0.395
10	0.485	0.010	0.046	0.341	0.012	0.849	0.028	0.341	0.351
11	0.528	0.325	1.344	0.577	0.593	1.189	1.211	0.577	1.579
12	0.577	0.221	0.909	0.478	0.415	1.340	0.927	0.478	1.098
13	0.647	0.105	0.346	0.402	0.236	0.918	0.302	0.402	0.702
14	0.747	0.044	0.098	0.379	0.070	0.753	0.103	0.379	0.395
15	0.647	0.024	0.076	0.359	0.060	0.858	0.066	0.359	0.351

Strength & Stability Calculations

(Check of Table values using Specimen #1 & R=4)

Specimen #1 Properties(single column): $E = 199948 \cdot MPa$

$h = 4.8 \cdot mm$ $L := 137.2 \cdot mm$ $mass := 34.98 \cdot kg$ $W := mass \cdot g$ $W = 343 \cdot N$

Cross-Sectional Area:

$A_g := h^2$ $A_g = 0.035 \cdot in^2$

Moment of Inertia:

$I := \frac{h^4}{12}$ $I = 42.9 \cdot mm^4$

Plastic Section Modulus:

$Z := \frac{h^3}{4}$ $Z = 1.648 \cdot 10^{-3} \cdot in^3$

Radius of Gyration:

$r := \sqrt{\frac{h^2}{12}}$ $r = 1.4 \cdot mm$

Assumptions: $F_y := 50\ ksi$ $k := 1.0$ $R := 4$ use $\phi := 1.0$ for experiment

Critical compressive stress
from Table 3-50 in AISC LRFD Manual: $\phi F_{cr} := 20.46\ ksi$ for $\frac{k \cdot L}{r} = 100$

$\phi_c := 0.85$

Axial Capacity of Specimen #1: $P_n := \frac{\phi F_{cr}}{\phi_c} \cdot A_g$ $P_n = 3764 \cdot N$

Plastic Moment: $M_p := Z \cdot F_y$ $M_p = 9309 \cdot N \cdot mm$

Plastic Axial Capacity: $P_y := A_g \cdot F_y$ $P_y = 7819 \cdot N$

$P_u := W$

Limit Analysis on Section:

Ultimate moment that can be applied on column based on limit analysis of cross section strength interaction (Bruneau et al. 1998):

$$M_{pr} := \left[1 - \left(\frac{P_u}{P_y}\right)^2\right] \cdot M_p \qquad M_{pr} = 9292 \cdot N \cdot mm \qquad \frac{M_{pr}}{M_p} = 99.81 \cdot \%$$

Corresponding Base Shear: $V_{Lim} := \frac{2 \cdot M_{pr}}{L}$ $\qquad V_{Lim} = 135.2 \cdot N$

Corresponding Spectral Acceleration: $S_{a.Lim} := \frac{V_{Lim} \cdot R}{W} \cdot g$ $\qquad S_{a.Lim} = 1.577 \cdot g$

1st Order Analysis (AISC 1994):

$$\begin{cases} \frac{P_u}{\phi \cdot P_n} + \frac{8}{9} \cdot \frac{M_u}{\phi \cdot M_n} \le 1.0 & \text{if } \frac{P_u}{\phi \cdot P_n} \ge 0.2 \\ \frac{P_u}{2 \cdot \phi \cdot P_n} + \frac{M_u}{\phi \cdot M_n} \le 1.0 & \text{if } \frac{P_u}{\phi \cdot P_n} < 0.2 \end{cases} \qquad \text{(AISC H1-1a)}$$

$$\frac{P_u}{\phi \cdot P_n} = 0.091 \quad < 0.2$$

Ultimate moment that can be applied on column based on 1st order strength interaction:

$$M_{u.1} := \left(1 - \frac{P_u}{2 \cdot \phi \cdot P_n}\right) \cdot M_p \qquad M_{u.1} = 8885 \cdot N \cdot mm \qquad \frac{M_{u.1}}{M_p} = 95.44 \cdot \%$$

Corresponding Base Shear: $V_1 := \frac{2 \cdot M_{u.1}}{L}$ $\qquad V_1 = 129.321 \cdot N$

Corresponding Spectral Acceleration: $S_{a.1} := \frac{V_1 \cdot R}{W} \cdot g$ $\qquad S_{a.1} = 1.508 \cdot g$

2nd Order Analysis (AISC 1994): $M_u = B_1 \cdot M_{nt} + B_2 \cdot M_{lt}$ (AISC C1-1)

$M_{nt} := 0$ $\quad B_2 = \dfrac{1}{1 - \dfrac{\Sigma P_u \cdot \Delta_{oh}}{\Sigma V \cdot L}}$ (C1-4)

B_2 can be rewritten as: $B_2 = \dfrac{1}{1 - \dfrac{P_u}{K \cdot L}}$

where $K := \dfrac{12 \cdot E \cdot I}{L^3}$ is the lateral column stiffness

$K = 39.6 \cdot \dfrac{N}{mm}$

Noting that the stability factor is given by: $\theta := \dfrac{P_u}{K \cdot L}$ $\quad \theta = 0.063$

B_2 can be again rewritten as: $B_2 := \dfrac{1}{1 - \theta}$

$B_2 = 1.067$

Ultimate moment on column based on 2nd order analysis and strength interaction:

$M_{u.2} := \left(1 - \dfrac{P_u}{2 \cdot \phi \cdot P_n}\right) \cdot \dfrac{M_p}{B_2}$ $\quad M_{u.2} = 8326 \cdot N \cdot mm$ $\quad \dfrac{M_{u.2}}{M_p} = 89.43 \cdot \%$

Given:

$2 \cdot M = P_u \cdot R \cdot \Delta_e + V \cdot L$ or $\dfrac{2 \cdot M}{V} = \dfrac{P_u \cdot \Delta_{oh}}{V} + L = \dfrac{P_u}{K} + L = L \cdot (\theta + 1)$

Corresponding Base Shear: $V_2 := \dfrac{2 \cdot M_{u.2}}{L \cdot (\theta + 1)}$ $\quad V_2 = 113.999 \cdot N$

Corresponding Spectral Acceleration: $S_{a.2} := \dfrac{V_2 \cdot R}{W} \cdot g$ $\quad S_{a.2} = 1.329 \cdot g$

2nd Order Analysis, using inelastic amplification factor:

Inelastic P-Δ Amplification Factor (Bernal 1987):

$$\alpha = \frac{1 + \beta \cdot \theta}{1 - \theta} \qquad \text{where:} \qquad \beta = 1.87 \cdot (\mu - 1)$$

taking a target ductility of 4: $\beta := 1.87 \cdot (4 - 1)$ $\beta = 5.61$

$$\alpha := \frac{1 + \beta \cdot \theta}{1 - \theta} \qquad \alpha = 1.444$$

Ultimate moment on column based on 2nd order analysis and strength interaction:

$$M_{u.2\alpha} := \left(1 - \frac{P_u}{2 \cdot \phi \cdot P_n}\right) \cdot \frac{M_p}{\alpha} \qquad M_{u.2\alpha} = 6152 \cdot N \cdot mm \qquad \frac{M_{u.2\alpha}}{M_p} = 66.09 \cdot \%$$

Given:

Corresponding Base Shear: $V_{2\alpha} := \frac{2 \cdot M_{u.2\alpha}}{L \cdot (\theta + 1)}$ $V_{2\alpha} = 84.239 \cdot N$

Corresponding Spectral Acceleration: $S_{a.2\alpha} := \frac{V_{2\alpha} \cdot R}{W} \cdot g$ $S_{a.2\alpha} = 0.982 \cdot g$

TABLE A-5 First Order Strength and Stability Analysis

Spec.	W (N)	L (mm)	P_y (N)	P_n (N)	P_u/P_y	P_u/P_n	M_p (N-mm)	First Order Limit Equation-P_y				First Order AISC-P_n			
								M_{lim} (N-mm)	*% of* M_p	V (N)	S_a *(g)*	$M_{u.l}$ (N-mm)	*% of* M_p	V (N)	S_a *(g)*
1	343.0	137.4	7825	3767	0.044	0.091	9,317	9,299	99.8	135.3	1.58	8,893	95.4	129.4	1.509
2	686.1	137.4	7825	3767	0.088	0.182	9,317	9,245	99.2	134.6	0.78	8,468	90.9	123.3	0.719
3	695.9	91.7	3478	1672	0.200	0.416	2,761	2,650	96.0	57.8	0.33	1,813	65.7	39.5	0.227
4	914.8	137.4	7825	3767	0.117	0.243	9,317	9,189	98.6	133.7	0.58	7,936	85.2	115.5	0.505
5	914.8	91.7	3478	1672	0.263	0.547	2,761	2,570	93.1	56.0	0.25	1,406	50.9	30.7	0.134
6	914.8	412.5	31300	6977	0.029	0.131	74,534	74,470	99.9	361.1	1.58	69,647	93.4	337.7	1.477
7	914.8	343.2	21736	4862	0.042	0.188	43,133	43,057	99.8	250.9	1.10	39,075	90.6	227.7	0.996
8	914.8	274.6	13911	3110	0.066	0.294	22,084	21,989	99.6	160.2	0.70	17,538	79.4	127.7	0.559
9	914.8	206.2	7825	1744	0.117	0.524	9,317	9,189	98.6	89.1	0.39	4,984	53.5	48.3	0.211
10	457.4	137.4	3478	776	0.132	0.589	2,761	2,713	98.3	39.5	0.35	1,275	46.2	18.6	0.162
11	686.1	549.9	31300	3926	0.022	0.175	74,534	74,498	100.0	270.9	1.58	68,021	91.3	247.4	1.442
12	686.1	457.7	21736	2733	0.032	0.251	43,133	43,090	99.9	188.3	1.10	36,342	84.3	158.8	0.926
13	686.1	366.5	13911	1746	0.049	0.393	22,084	22,030	99.8	120.2	0.70	15,079	68.3	82.3	0.480
14	686.1	275.1	7825	981	0.088	0.700	9,317	9,245	99.2	67.2	0.39	3,147	33.8	22.9	0.133
15	343.0	183.4	3478	436	0.099	0.787	2,761	2,734	99.0	29.8	0.35	661	23.9	7.2	0.084

TABLE A-6 Second Order Strength and Stability Analysis

Spec.	M_p (N-mm)	θ	Amplification Factors			α (μ=R=4)				B_2 (R=4)			
			B_2 (R=4)	α (μ=4)	α or B_2 (μ=R=1)	$M_{ult.2}$ (N-mm)	*% of* M_p	V (N)	S_a *(g)*	$M_{ult.2}$ (N-mm)	*% of* M_p	V (N)	S_a *(g)*
1	9,317	0.063	1.34	1.44	1.07	6,157	66.1	84.3	0.983	8,333	89.4	114.1	0.333
2	9,317	0.126	2.02	1.95	1.14	4,337	46.6	56.1	0.327	7,402	79.4	95.7	0.139
3	2,761	0.288	-6.59	3.67	1.40	494	17.9	8.4	0.048	1,291	46.8	21.9	0.031
4	9,317	0.168	3.05	2.33	1.20	3,400	36.5	42.4	0.185	6,603	70.9	82.3	0.090
5	2,761	0.281	-8.19	3.58	1.39	393	14.2	6.7	0.029	1,012	36.7	17.2	0.019
6	74,534	0.095	1.61	1.69	1.10	41,200	55.3	182.5	0.798	63,060	84.6	279.3	0.305
7	43,133	0.136	2.19	2.04	1.16	19,173	44.5	98.4	0.430	33,772	78.3	173.3	0.189
8	22,084	0.212	6.60	2.78	1.27	6,309	28.6	37.9	0.166	13,817	62.6	83.0	0.091
9	9,317	0.378	-1.95	5.02	1.61	992	10.7	7.0	0.031	3,099	33.3	21.8	0.024
10	2,761	0.425	-1.43	5.89	1.74	217	7.8	2.2	0.019	733	26.6	7.5	0.016
11	74,534	0.126	2.02	1.95	1.14	34,820	46.7	112.5	0.656	59,446	79.8	192.0	0.280
12	43,133	0.181	3.63	2.46	1.22	14,762	34.2	54.6	0.318	29,760	69.0	110.1	0.160
13	22,084	0.284	-7.46	3.62	1.40	4,171	18.9	17.7	0.103	10,804	48.9	45.9	0.067
14	9,317	0.505	-0.98	7.74	2.02	407	4.4	2.0	0.011	1,559	16.7	7.5	0.011
15	2,761	0.568	-0.79	9.68	2.31	68	2.5	0.5	0.006	286	10.3	2.0	0.006

APPENDIX B
EFFECTS OF TRANSVERSE BRACING ON BEHAVIOR OF TEST STRUCTURE

B.1 Introduction

The effect of adding members for the lateral bracing of the test structure was investigated. The following three pages of hand calculations show the negligible contribution of the braces to the stiffness of the test structure in the direction of shaking. Following that is a description of simple tests performed to approximate the mechanical properties of the polyurethane material used at the connection points of the bracing to the specimen mass and the base plate.

Finally, two separate free vibration tests were performed (one without any cross bracing, and one with the metal bracing attached) to investigate the impact of the bracing on behavior. This was done using an extra specimen described in this section.

Check of Steel Strips for use as Lateral Support of Frame

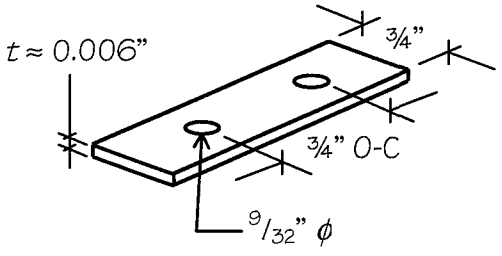

Neglect holes for conservatism

Assume $t := 0.02 \cdot in$ for conservatism

$width := \frac{3}{4} \cdot in$

$A := width \cdot t \qquad A = 0.015 \cdot in^2$

$I_{xx} := \frac{1}{12} \cdot width \cdot t^3 \qquad I_{xx} = 5.00 \cdot 10^{-7} \cdot in^4$

$I_{yy} := \frac{1}{12} \cdot width^3 \cdot t \qquad I_{yy} = 7.03 \cdot 10^{-4} \cdot in^4$

Length Across Frame

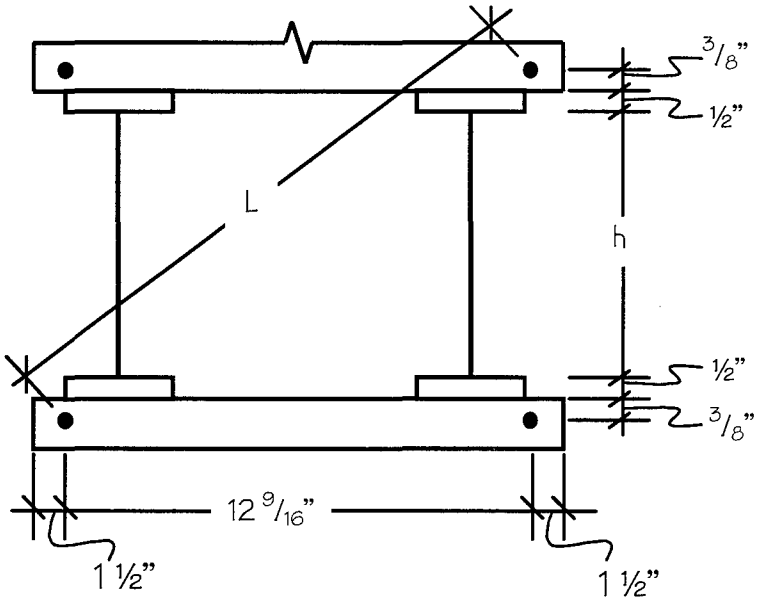

Specimen Indices	h (in)	L (in)
3, 5	3.61	13.658
1, 2, 4, 10	5.41	14.460
15	7.22	15.436
9	8.12	15.976
8	10.81	17.764
14	10.83	17.778
7	13.51	19.766
13	14.43	20.484
6	16.24	21.942
12	18.02	23.424
11	21.65	26.559

Shortest, & Therefore Stiffest Braces

∴ Check if additional buckling strength is added to structure

Gauge Length, L, varies with specimen Height, h, according to:

$$L(h) := \sqrt{(h + 1.75 \cdot in)^2 + (12.5625 \cdot in)^2}$$

$A = 0.015 \cdot in^2$ $I_{xx} = 5.00 \cdot 10^{-7} \cdot in^4$ $I_{yy} = 7.03 \cdot 10^{-4} \cdot in^4$

$h := 3.61 \cdot in$ $L(h) = 13.658 \cdot in$

$r_x := \sqrt{\frac{I_{xx}}{A}}$ $r_x = 5.7735 \cdot 10^{-3} \cdot in$ $r_y := \sqrt{\frac{I_{yy}}{A}}$ $r_y = 0.2165 \cdot in$

For Fixed Ends: $k := 0.5$

$$\frac{k \cdot L(h)}{r_x} = 1182.8$$

Assume: $E := 29000 \cdot ksi$ & $F_y := 36 \cdot ksi$

AISC-LRFD Compressive Strength:

$$\lambda_c := \frac{k \cdot L(h)}{r_x \cdot \pi} \cdot \sqrt{\frac{F_y}{E}} \qquad \lambda_c = 13.266 \qquad \text{(E2-4)}$$

$\lambda_c > 1.5 = 1$

$$F_{cr} := \frac{0.877}{\lambda_c^2} \cdot F_y \qquad F_{cr} = 0.179 \cdot ksi \qquad \text{(E2-3)}$$

$$P_{n.band} := A \cdot F_{cr} \qquad P_{n.band} = 2.691 \cdot lbf \qquad \text{(E2-1)}$$

Nominal Compressive Strength of Specimen 3 & 5: $P_{n.spec} := 0.3761 \cdot kip$ $P_{n.spec} = 1673 \cdot N$ (Table A-5 Strength & Stability Calcs)

$$\frac{P_{n.band}}{P_{n.spec}} = 0.716 \cdot \% \qquad \text{(E2-4)}$$

(Note: Both sets of compressive strength calcs (braces & specimen) are for single member, --> same ratio for entire structure (4 of each))

Lateral Stiffness of Brace

Assume fixed top & bottom, double curvature configuration:

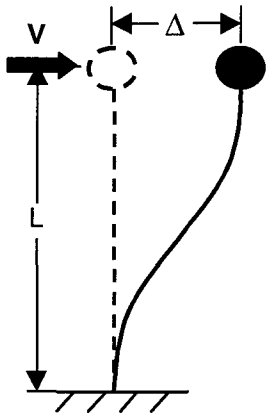

$V = K \cdot \Delta$ $\qquad K_{brace} := \dfrac{12 \cdot E \cdot I_{xx}}{L(h)^3}$

$$K_{brace} = 6.829 \cdot 10^{-5} \cdot \frac{kip}{in}$$

$$K_{col} := 0.1505 \cdot \frac{kip}{in}$$

$$\frac{K_{brace}}{K_{col}} = 0.045 \cdot \%$$

With extremely low axial compressive strength and lateral stiffness, steel strip appears to be good option for use as cross-bracing element.

B.2 Polyurethane Mechanical Properties

Prior to machining into the ends for the cross bracing the polyurethane material was tested to calculate a value for an approximate modulus of elasticity. Mechanical properties of the polyurethane material were investigated using a simply supported single point beam load as illustrated below:

Width, w=2.724"

Thickness, t=0.5665"

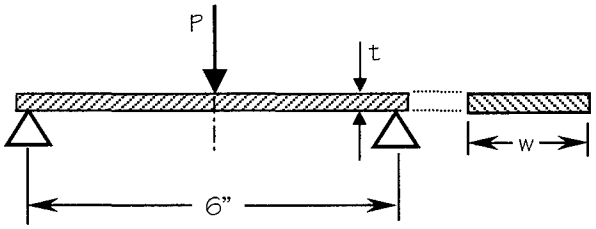

The beam was loaded incrementally with weights that were nominally 2 and 5 Newton and listed in the table below:

2N Weights		5N Weights	
mass (g)	Weight (N)	mass (g)	Weight (N)
203.8	1.999	507.0	4.972
203.1	1.992	502.6	4.929
204.3	2.004	508.7	4.989
203.3	1.994	504.9	4.952
205.1	2.011		
204.2	2.003		
205.1	2.011		
205.5	2.015		
w_{ave} =	2.004	w_{ave} =	4.960

Deflections at the centerline of the beam were measured with a dial gauge. For a simply supported beam loaded by a concentrated point load at mid-span, the deflection at the centerline is given by: $\Delta = \frac{P \cdot l^3}{48 \cdot E \cdot I}$, which can be solved for the elastic modulus, E, since all other quantities are either known, or measured over the course of the test.

Five trials were performed with various increments of weights. Results for all trials are presented below, where the average value is the average of E calculated for each loading step for each trial, and the "trendline" is the E calculated by taking the linear best-fit generated by Excel, and dividing it by $\frac{48 \cdot I}{l^3}$. Individual trial results are presented on the subsequent pages.

Modulus of Elasticity Calculation Summary			
Trial	Average (ksi)	Trendline (ksi)	
1	5.703	5.416	
2	5.933	5.575	
3	5.646	5.550	
4	5.840	5.652	
5	5.520	5.415	
Average of all trials:	5.728	5.522	ksi
	39.494	38.071	MPa

L =	6	in
t =	0.5665	in
w =	2.724	in
I =	0.04127	in^4

Average Value of Weights:	2N	5N
	2.00357	4.96038

Δ (in)	P (N)	P (lbf)	E (ksi)
0	0	0	0
0.016	4.0071	0.9009	6.1396
0.034	8.0143	1.8018	5.7784
0.055	12.0214	2.7027	5.3582
0.071	16.0286	3.6035	5.5342

E_{ave} = 5.7026 ksi

Slope = 49.671 lbf/in

E = 5.4161 ksi

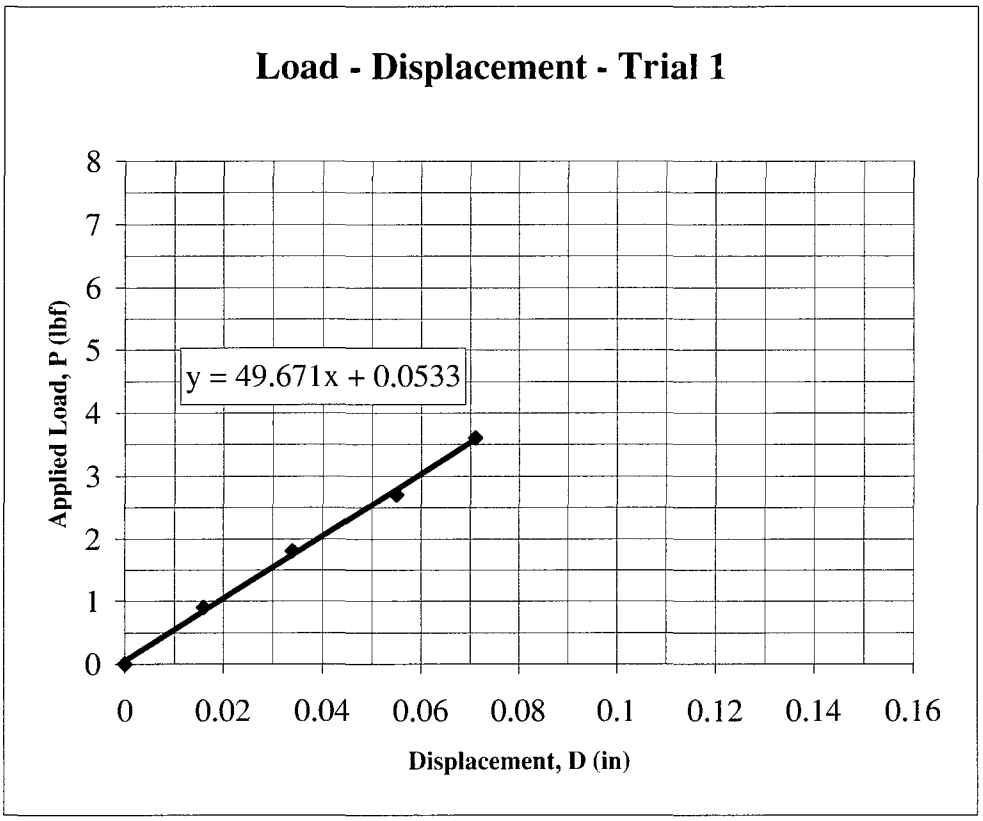

L =	6	in
t =	0.5665	in
w =	2.724	in
I =	0.04127	in^4

Average Value of Weights:	2N	5N
	2.0036	4.9604

Δ (in)	P (N)	P (lbf)	E (ksi)
0	0	0	0
0.015	4.0071	0.9009	6.5489
0.057	13.9279	3.1313	5.9901
0.075	17.9350	4.0322	5.8622
0.121	27.8558	6.2625	5.6436
0.139	31.8629	7.1634	5.6194

E_{ave} = 5.9328 ksi

Slope = 51.1320 lbf/in

E= 5.5754 ksi

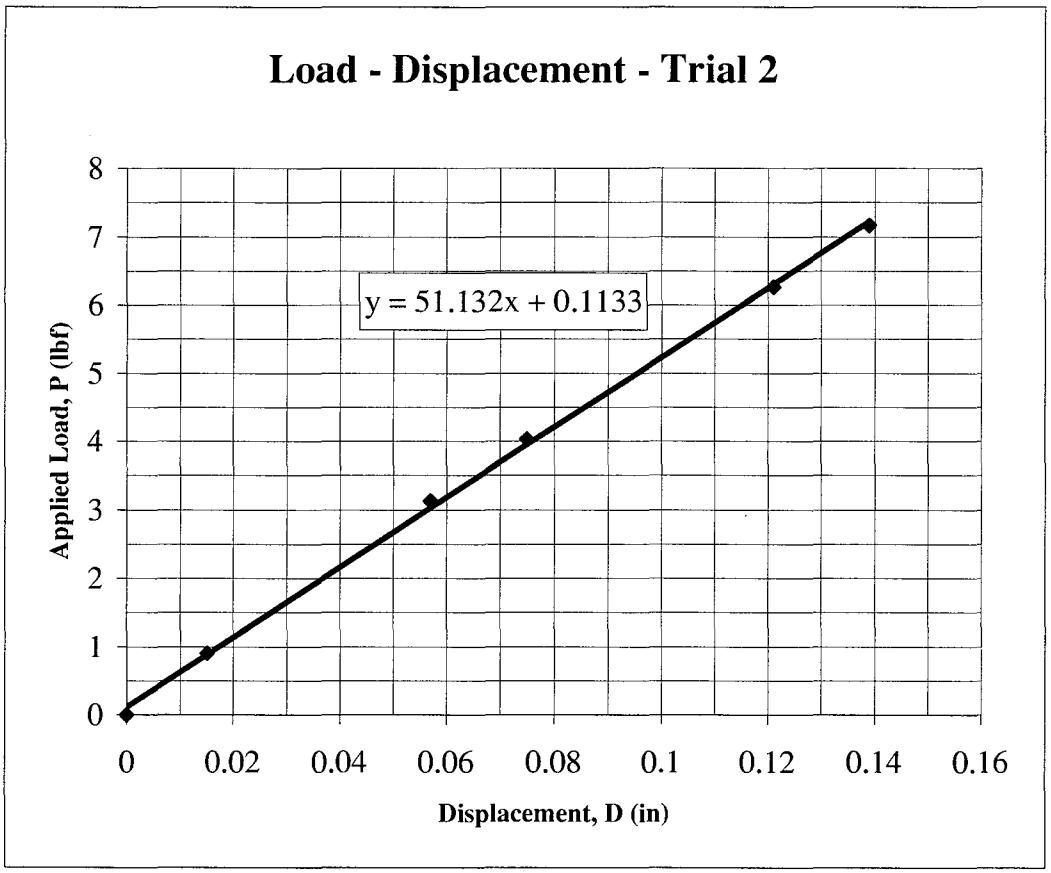

L =	6	in
t =	0.5665	in
w =	2.724	in
I =	0.04127	in^4

Average Value of Weights:	2N	5N
	2.0036	4.9604

Δ (in)	P (N)	P (lbf)	E (ksi)
0	0	0	0
0.0415	9.9208	2.2304	5.8603
0.0865	19.8415	4.4608	5.6232
0.105	23.8487	5.3617	5.5680
0.122	27.8558	6.2625	5.5973
0.14	31.8629	7.1634	5.5793

E_{ave} = 5.6456 ksi

Slope = 50.9010 lbf/in

E= 5.5503 ksi

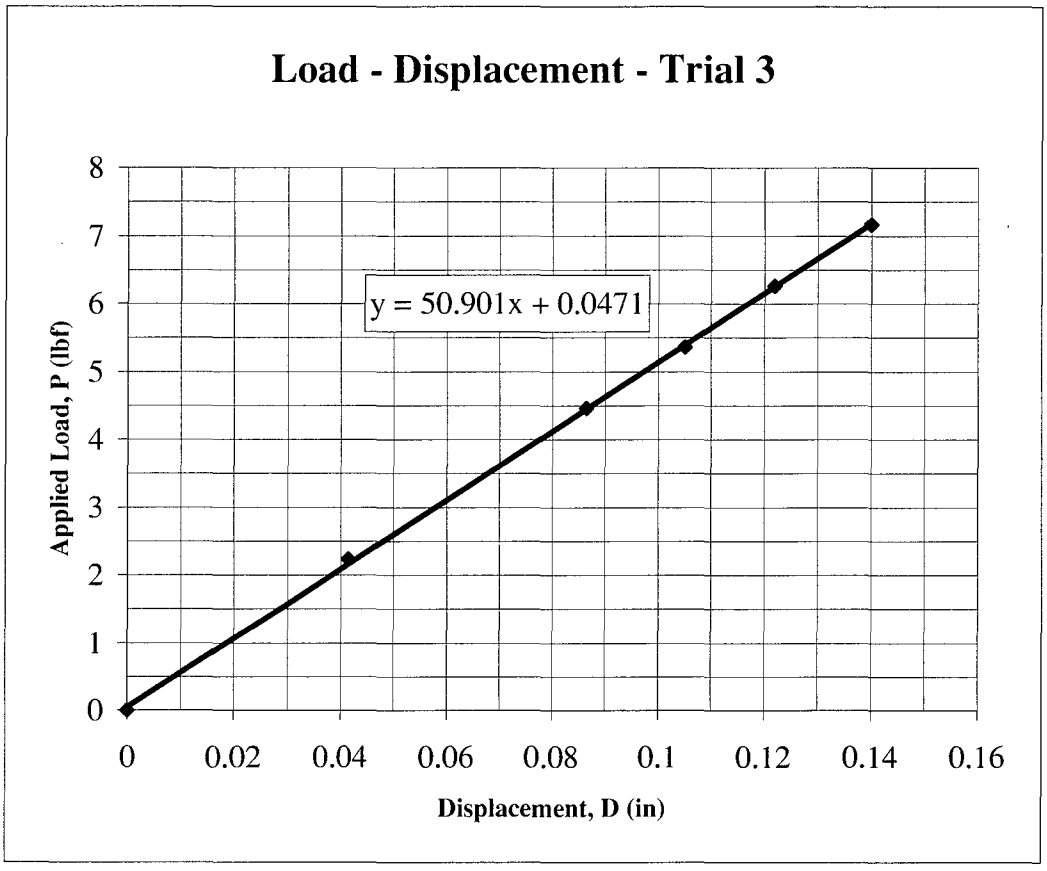

L =	6	in
t =	0.5665	in
w =	2.724	in
I =	0.04127	in^4

Average Value of Weights:	2N	5N
	2.0036	4.9604

Δ (in)	P (N)	P (lbf)	E (ksi)
0	0	0	0
0.0405	9.9208	2.2304	6.0050
0.058	13.9279	3.1313	5.8868
0.075	17.9350	4.0322	5.8622
0.093	21.9422	4.9330	5.7839
0.138	31.8629	7.1634	5.6602

E_{ave} = 5.8396 ksi

Slope = 51.8340 lbf/in

E= 5.6520 ksi

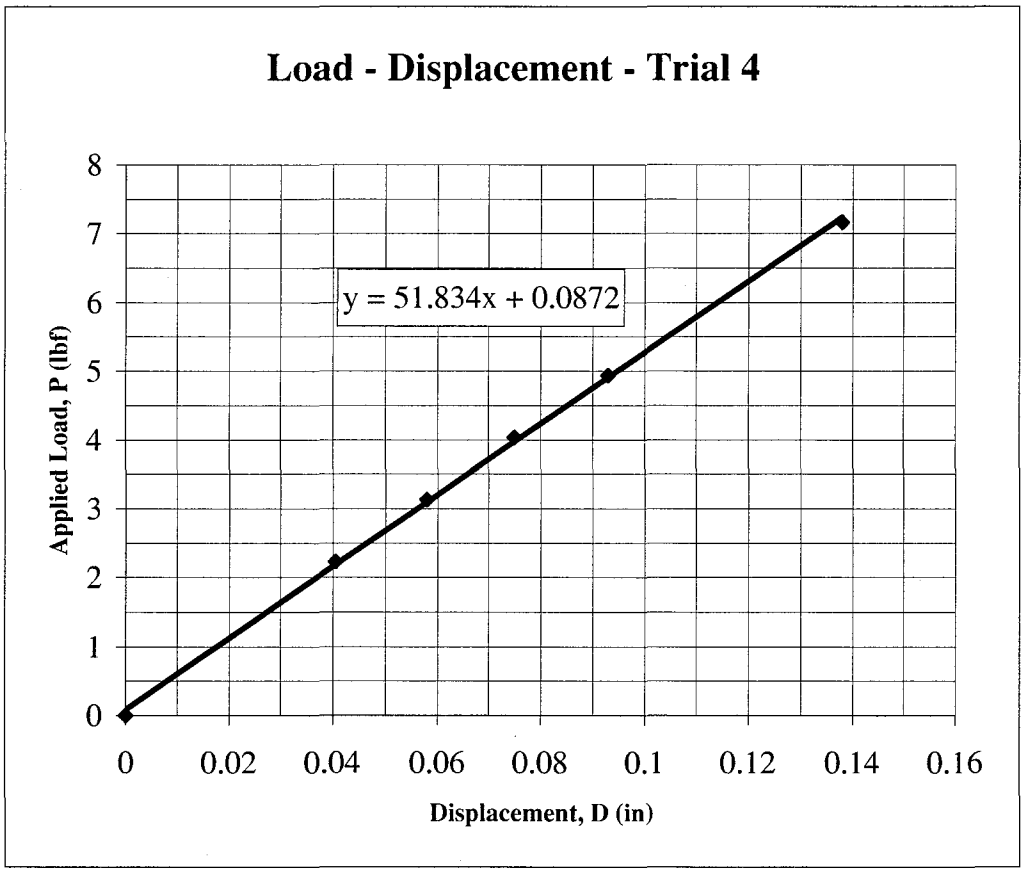

L =	6	in
t =	0.5665	in
w =	2.724	in
I =	0.04127	in^4

Average Value of Weights:	2N	5N
	2.0036	4.9604

Δ (in)	P (N)	P (lbf)	E (ksi)
0	0	0	0
0.043	9.9208	2.2304	5.6559
0.061	13.9279	3.1313	5.5973
0.107	23.8487	5.3617	5.4639
0.126	27.8558	6.2625	5.4196
0.143	31.8629	7.1634	5.4623

E_{ave} = 5.5198 ksi

Slope = 49.6600 lbf/in

E= 5.4149 ksi

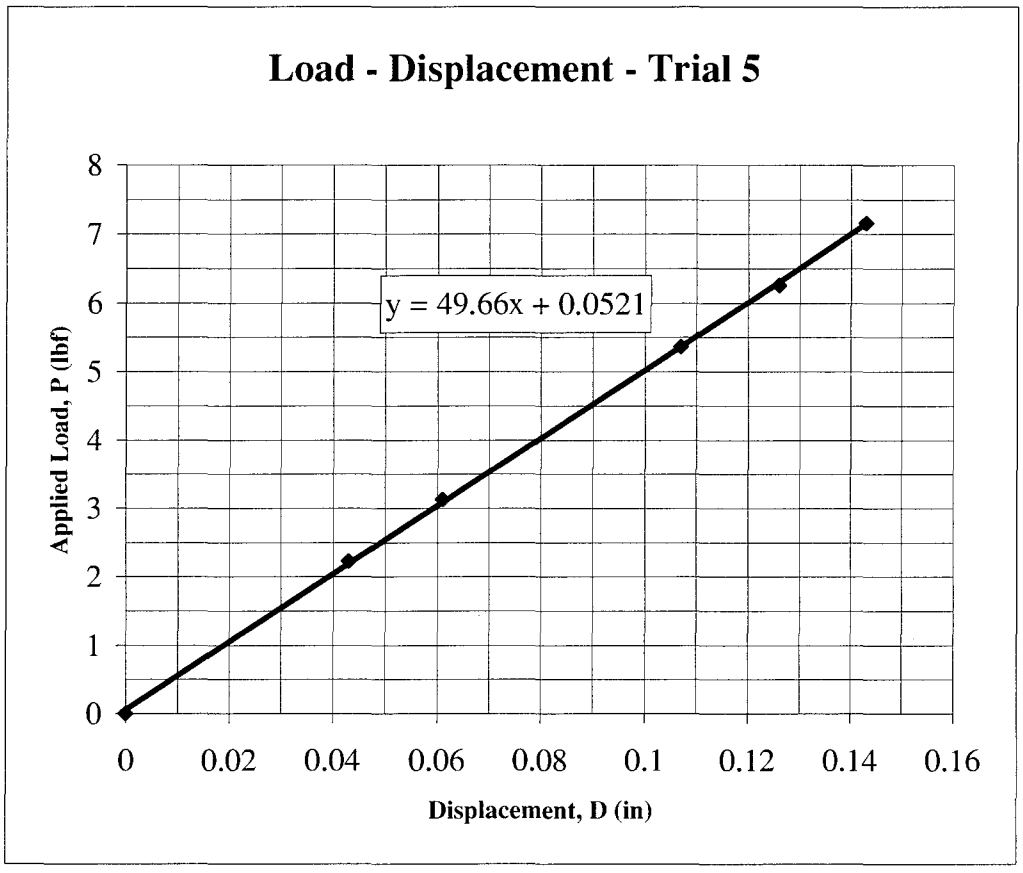

B.3 Specimen 9* Free Vibration Tests

An extra set of columns nominally identical to Specimen 9 was used to assess the effect of transverse bracing on the specimen. Fewer mass plates were used (compared to Specimen 9) in order to avoid collapse at this stage. The column dimensions, measured and calculated, as well as column orientations, are given in Tables B-1, B-2, and B-3, respectively. These tables follow the same format as those presented in Chap 3.

Table B-4, as well as Figures B-1 and B-2 summarize the results of the two free vibration tests performed, in the same manner as Chap 4. Inherent damping of the specimen appears to be little affected by the addition of bracing in the transverse direction.

TABLE B-1 Measured Specimen Dimensions (mm)

Orientation	w_1	w_2	w_3	$Base_1$	$Base_2$	L_1	L_2	v_1	v_2
Specimen 9*									
U-D_1	4.98	4.95	5.04	50.8	50.8	207.2	205.6	-2.13	1.66
L-R_1	4.86	4.86	4.89	50.8	50.8	206.5	206.4	-0.93	0.00
U-D_2	4.9	4.9	4.9	50.8	50.8	206.4	205.8	1.6	5.0
L-R_2	4.8	4.9	4.8	50.8	50.8	205.5	206.9	-0.3	-3.2
U-D_3	5.0	4.9	5.0	50.8	50.8	207.0	206.1	-2.1	-2.1
L-R_3	4.9	4.8	4.9	50.8	50.8	206.9	206.3	-2.0	-1.8
U-D_4	4.9	4.9	4.9	50.8	50.8	206.0	205.4	0.0	2.0
L-R_4	5.0	5.0	4.9	50.8	50.8	205.5	205.9	2.0	0.0

TABLE B-2 Calculated Specimen Dimensions

Orientation	w_{avg} (mm)	L_{avg} (mm)	θ (deg)	V_{unif} (mm)	ϕ (deg)
Specimen 9*					
U-D_1	4.99	206.4	1.730	-0.23	-4.287
L-R_1	4.87	206.4	0.143	-0.46	-1.046
U-D_2	4.9	206.1	0.645	3.29	-3.870
L-R_2	4.8	206.2	-1.576	-1.73	3.253
U-D_3	4.9	206.6	1.117	-2.11	0.057
L-R_3	4.9	206.6	0.731	-1.92	-0.258
U-D_4	4.9	205.7	0.573	0.98	-2.221
L-R_4	5.0	205.7	-0.530	0.98	2.221

TABLE B-3 Column Locations and Orientations

Column Index	Location	Orientation
Specimen 9*		
1	NW	1
2	NE	4
3	SW	2
4	SE	3

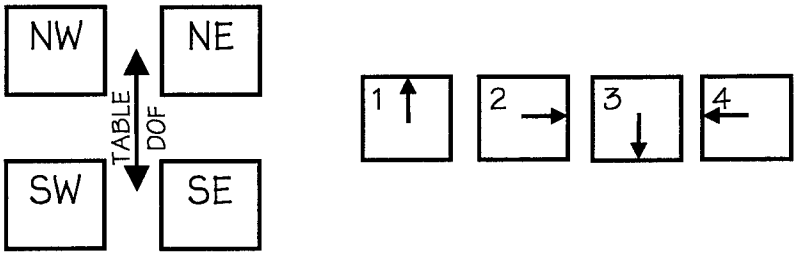

TABLE B-4 Free Vibration Damping Estimates

i	k_i	u_{ki}	k_i+j	u_{ki+j}	ξ_i (%)	Remarks
mass = 18.315 kg/col, no cross bracing						
HorWest Channel, u_o = 3.023 mm						
1	1	2.997	14	1.702	0.69	--
2	14	1.702	28	0.686	1.03	--
3	28	0.686	42	0.076	2.50	--
AccEast Channel, u_o = 0.053 g						
1	1	0.191	14	0.116	0.61	--
2	14	0.116	28	0.061	0.73	--
3	28	0.061	42	0.006	2.64	--
AccWest Channel, u_o = 0.050 g						
1	1	0.125	14	0.118	0.07	--
2	14	0.118	28	0.045	1.10	--
3	28	0.045	42	0.005	2.50	--
mass = 18.315 kg/col, with metal strip cross bracing						
HorEast Channel, u_o = 0.508 mm						
1	2	2.464	13	1.55	0.67	--
2	13	1.549	27	0.58	1.11	--
3	27	0.584	35	0.20	2.10	--
HorWest Channel, u_o = 0.483 mm						
1	2	2.337	13	1.58	0.57	--
2	13	1.575	27	0.53	1.23	--
3	27	0.533	35	0.08	3.87	--
AccEast Channel, u_o = 0.015 g						
1	2	0.169	13	0.106	0.68	--
2	13	0.106	27	0.041	1.08	--
3	27	0.041	35	0.013	2.29	--
AccWest Channel, u_o = 0.014 g						
1	2	0.162	13	0.105	0.63	--
2	13	0.105	27	0.042	1.04	--
3	27	0.042	35	0.011	2.67	--

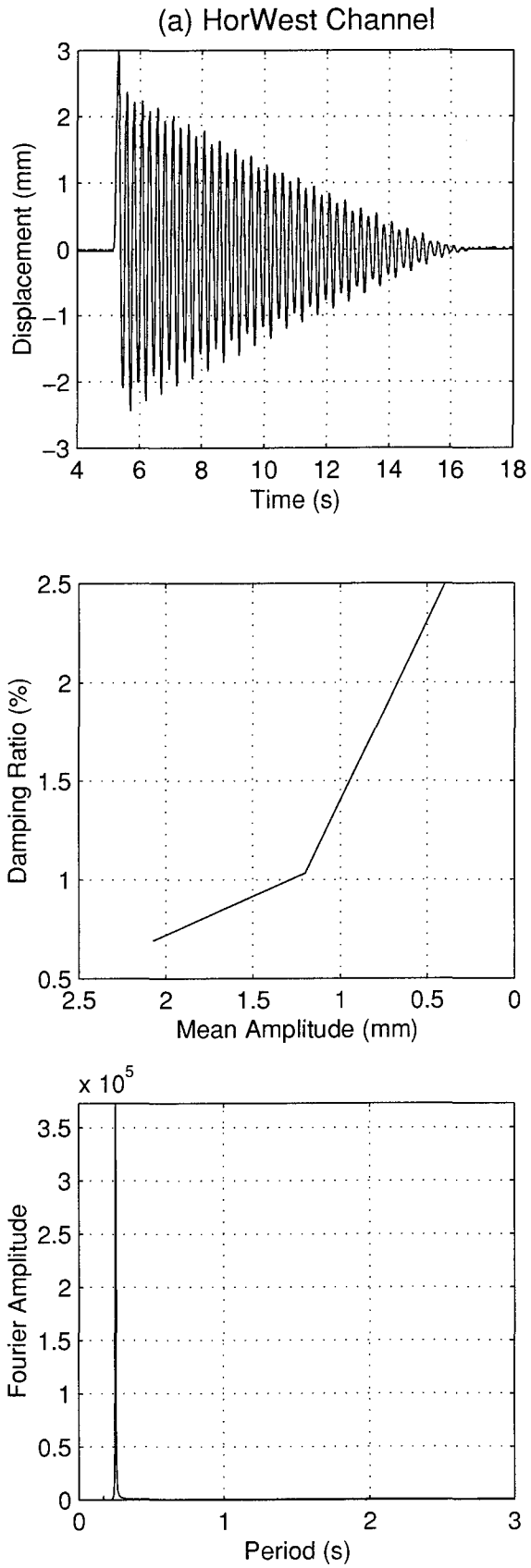

FIGURE B–1 Free Vibration Test of Specimen 9* – no Bracing

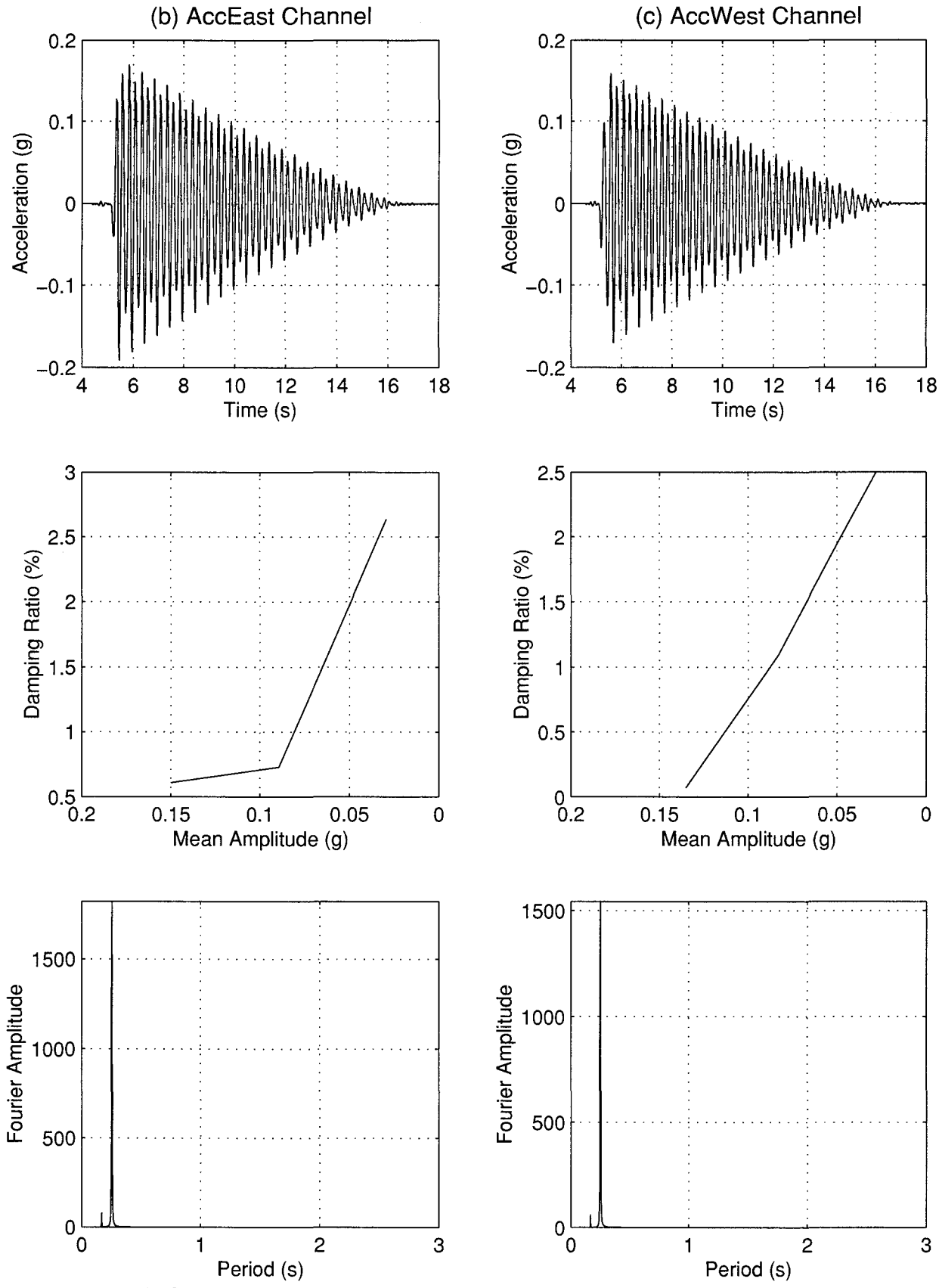

FIGURE B–1 (cont'd) Free Vibration Test of Specimen 9* – no Bracing

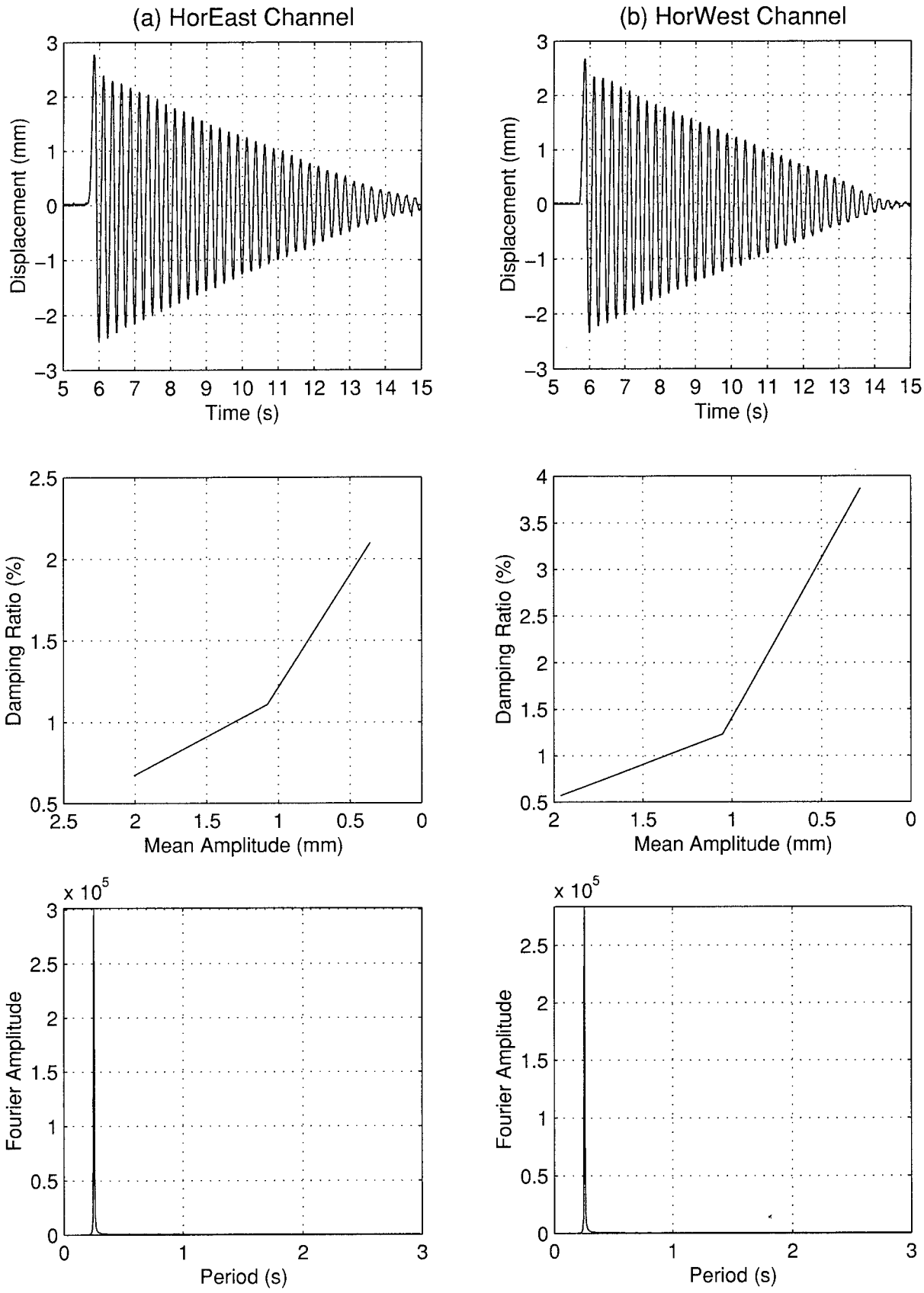

FIGURE B–2 Free Vibration Test of Specimen 9* – with Bracing

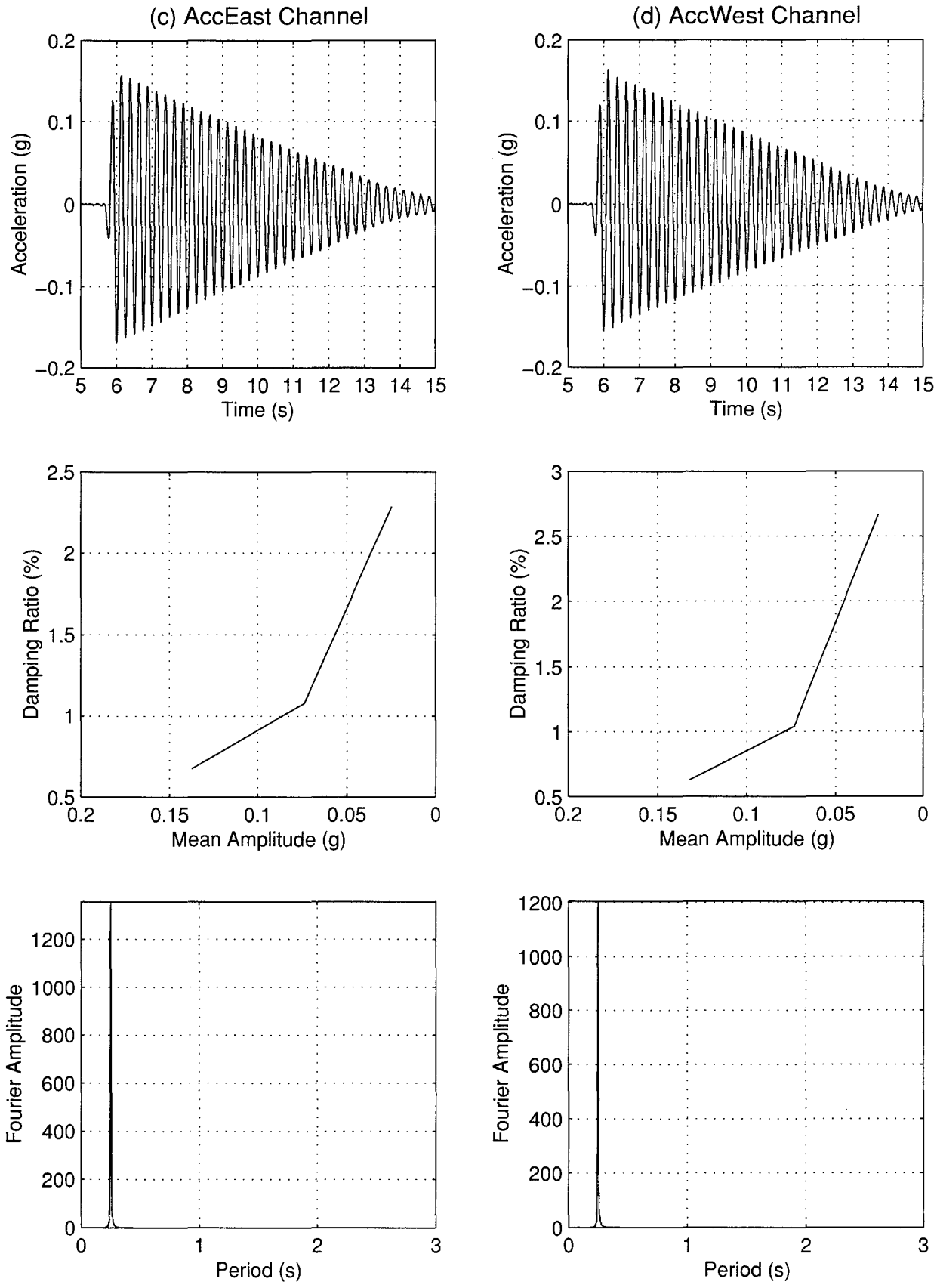

FIGURE B–2 (cont'd) Free Vibration Test of Specimen 9* – with Bracing

APPENDIX C
ANALYSIS OF RESULTS

Additional and more detailed results in support of the observations made in section 5.3 are presented in this appendix. In search of trends in the test data, data for all specimens are considered and grouped as a function of the stability factor for four ranges of that parameter, namely: $\theta \leq 0.1$, $0.1 < \theta \leq 0.3$, $0.3 < \theta \leq 0.5$, and $\theta > 0.5$.

Various peak response parameters for the specimens are considered for this purpose. The plastic base shear, V_{yo}, yield displacement, Δ_y, and ductility at the static stability limit, μ_s, each defined in section 2, are tabulated in table C-1 for specimens that did not collapse during the first trial of the testing schedule. The residual displacement at which plastic collapse mechanism is formed, is also tabulated and given by:

$$\Delta_{coll} = {}^{2 \cdot M_p}\!/_{W} \qquad \text{(C.1)}$$

Each of these parameters is calculated with average specimen dimensions using the relationships presented in section 2. Material properties (elastic modulus and yield stress) are utilized as described in the section on tension testing from section 4. These critical values are used to normalize the recorded values of force and displacement as described below. The data used for the plot presented in this section is contained in table C-2.

First, the maximum estimated base shear (ignoring P-Δ effects) from each test, V_o*, was normalized by the plastic base shear, V_{yo}, and plotted separately versus various normalized displacements: μ, u_r/Δ_{coll}, μ/μ_s, $u_r/u_{rel\text{-}max}$, and $u_{rel\text{-}max}/h$. Figures C-1 to C-5 show the results of that ratio, V_o^*/V_{yo}, versus: μ, u_r/Δ_{coll}, μ/μ_s, $u_r/u_{rel\text{-}max}$, and percent drift, respectively. The following general observations can be made regarding pattern of behavior: In figure C-1, the test data generally increase linearly towards $V_o^*/V_{yo}=1$ and $\mu=1$, followed by a decrease in slope as the specimen moves further into the inelastic range of behavior. Displacement ductility developed prior to collapse seems to decrease as θ increases. In figure C-2, all but two specimens (1 and 9) are observed to have a residual displacement of less than 50% of Δ_{coll} prior

to the final test that resulted in collapse. Figure C-3 shows that all but Specimen 1 have a maximum displacement ductility less than 75% of μ_s prior to the final test that resulted in collapse. No distinct pattern of behavior can be seen in figure C-4. Figure C-5 indicates that Specimen 1 is the only one with a maximum drift greater than 20% of its height prior to the final test.

Second, the same dimensionless displacement parameters were plotted against the elastic response spectral acceleration of the measured table acceleration, S_a, normalized by the spectral acceleration at plastic base shear, V_{yo}/W. These results are shown in figures C-6 to C-10. Similar to figure C-1, previously described, the data tends to a common trend and increases towards coordinate (1,1) of the plot before the slope gently decreases in the inelastic range. Since S_a is the elastic response to the ground motion and it is being normalized by the plastic spectral acceleration, this ratio should increase as the earthquake intensity progressively increases in the inelastic range. In fact, this ratio reflects the ability of the structure to dissipate energy, and should be conceptually related to the response modification factor. This factor should be at least equal to 4 for ordinary moment frames in actual buildings. Here, only Specimens 1 and 6 develop this amount of ductility, by reaching $S_a/(V_{yo}/W)$ values of 3.6 and 5.33, respectively. Note that where μ/μ_s was plotted versus V_o^*/V_{yo} (figure C-1), the grouping of data points suggested a comparable behavior amongst the specimens, but when the same μ/μ_s ratio is plotted versus $S_a/(V_{yo}/W)$ (figure C-5), no discernible pattern of behavior is observed.

Third, figures C-11 to C-15 provide a comparison of the maximum measured total acceleration of the specimen mass, $\ddot{u}_{T\text{-}max}$, normalized by the spectral acceleration at plastic base shear, V_{yo}/W, versus μ, u_r/Δ_{coll}, μ/μ_s, $u_r/u_{rel\text{-}max}$, and percent drift, respectively. In figure C-11, the test data generally increases linearly towards coordinate (1,0.75) of the graph followed by a decrease in slope as the specimens move further into the inelastic range of behavior. This emphasizes the trend displayed in figures C-1 and C-6. Figure C-15 shows eight of the twelve specimens behaving in a similar manner, with linear behavior until approximately $\ddot{u}_{T\text{-}max}/(V_{yo}/W)$ of 0.85 and a drift of 5.0%.

TABLE C-1 Shake Table Tests-Critical Parameters

Specimen	V_{yo} (N)	Δ_y (mm)	Δ_{coll} (mm)	μ_s
1	172.5	4.3	65.9	15.4
2	186.2	4.5	36.1	8.1
4	173.2	4.4	25.3	5.7
5b[1]	132.4	5.6	12.9	2.3
6	367.3	16.3	160.8	9.9
7	255.0	14.4	93.1	6.5
8	168.7	13.1	49.2	3.8
9	115.4	9.8	25.2	2.6
10	33.1	4.4	9.5	2.2
10b[1]	85.9	12.5	24.8	2.0
11	295.8	31.7	229.5	7.2
12	145.9	20.2	94.3	4.7
13	128.6	23.8	66.4	2.8
14	84.8	17.5	33.0	1.9
15	23.7	7.6	12.1	1.6

TABLE C-2 Shake Table Tests-Normalized Peak Responses

Test	C_s*	$\frac{V_o^*}{V_{yo}}$	$\frac{S_a}{(V_{yo}/W)}$	$\frac{\ddot{u}_T}{(V_{yo}/W)}$	μ	$\frac{u_r}{\Delta_{coll}}$	$\frac{\mu}{\mu_s}$	$\frac{u_r}{u_{relmax}}$	Drift (%)
Specimen 1									
1	0.378	0.787	0.702	0.691	0.872	0.000	0.057	0.000	0.027
2	0.432	0.899	1.017	0.806	1.126	0.003	0.073	0.037	0.035
3	0.432	0.899	1.017	0.874	1.364	0.006	0.089	0.065	0.043
4	0.432	0.899	1.328	0.893	1.399	0.003	0.091	0.034	0.044
5	0.270	0.562	0.392	0.481	0.581	0.001	0.038	0.031	0.018
6	0.443	0.922	1.516	0.897	1.387	0.004	0.090	0.043	0.043
7	0.583	1.214	2.296	1.031	2.454	0.025	0.160	0.157	0.077
8	0.659	1.372	2.784	1.097	3.142	0.012	0.204	0.060	0.098
9	0.637	1.326	3.183	1.135	3.741	0.047	0.243	0.195	0.117
10	0.778	1.620	3.589	1.264	20.346	1.307	1.323	0.988	0.635
11	0.897	1.868	3.341	--	∞	∞	∞	—	—
Specimen 2									
1	0.133	0.506	0.640	0.521	0.724	0.014	0.089	0.157	0.023
2	0.168	0.639	0.866	0.643	0.918	0.026	0.113	0.230	0.030
3	0.185	0.704	1.153	0.708	1.043	0.025	0.129	0.197	0.034
4	0.214	0.814	1.444	0.772	1.117	0.025	0.138	0.184	0.036
5	0.220	0.837	1.719	0.825	1.169	0.019	0.144	0.132	0.038
6	0.231	0.879	1.876	0.863	1.294	0.020	0.160	0.123	0.042
7	0.237	0.902	2.092	0.886	1.477	0.028	0.182	0.154	0.048
8	0.266	1.012	2.503	0.936	1.670	0.075	0.206	0.365	0.054
9	0.312	1.187	2.588	0.962	2.673	0.224	0.330	0.680	0.087
10	0.497	1.891	2.567	--	∞	∞	∞	—	—
Specimen 4									
1	0.037	0.201	0.350	0.190	0.270	0.005	0.047	0.106	0.009
2	0.099	0.538	0.848	0.527	0.688	0.010	0.120	0.083	0.022
3	0.144	0.783	1.212	0.734	1.193	0.025	0.209	0.120	0.038
4	0.169	0.919	1.678	0.859	1.675	0.059	0.293	0.202	0.054
5	0.177	0.962	2.162	0.941	2.392	0.211	0.419	0.504	0.077
6	0.510	2.773	2.575	--	∞	∞	∞	—	—
Specimen 5b									
1	0.061	0.434	0.197	0.121	0.656	0.154	0.286	0.538	0.040
2	2.703	19.228	0.479	--	∞	∞	∞	—	—

TABLE C-2 (cont'd) Shake Table Tests-Displacement Comparison

Test	C_s*	$\frac{V_o^*}{V_{yo}}$	$\frac{S_a}{(V_{yo}/W)}$	$\frac{\ddot{u}_T}{(V_{yo}/W)}$	μ	$\frac{u_r}{\Delta_{coll}}$	$\frac{\mu}{\mu_s}$	$\frac{u_r}{u_{relmax}}$	Drift (%)
Specimen 6									
1	0.440	1.128	0.782	0.813	0.986	0.001	0.100	0.008	0.039
2	0.482	1.236	1.096	0.923	1.390	0.015	0.141	0.104	0.055
3	0.492	1.261	1.468	0.928	1.624	0.029	0.164	0.174	0.064
4	0.492	1.261	1.447	0.918	1.546	0.024	0.157	0.153	0.061
5	0.293	0.751	0.621	0.577	1.666	0.007	0.169	0.041	0.066
6	0.471	1.208	2.179	0.900	1.589	0.008	0.161	0.048	0.063
7	0.503	1.290	3.267	0.936	1.746	0.001	0.177	0.004	0.069
8	0.524	1.343	3.939	0.913	2.214	0.028	0.224	0.124	0.087
9	0.503	1.290	4.569	0.920	2.785	0.088	0.282	0.312	0.110
10	0.503	1.290	5.328	0.977	4.516	0.372	0.457	0.813	0.178
11	11.329	29.046	4.658	--	∞	∞	∞	--	--
Specimen 7									
1	0.140	0.517	0.498	0.543	0.599	0.002	0.093	0.027	0.025
2	0.189	0.698	0.775	0.728	0.850	0.002	0.132	0.019	0.036
3	0.245	0.905	1.029	0.820	1.125	0.031	0.174	0.176	0.047
4	0.245	0.905	1.293	0.768	1.740	0.144	0.269	0.534	0.073
5	0.400	1.477	1.556	--	∞	∞	∞	-	-
Specimen 8									
1	0.079	0.441	0.408	0.402	0.989	0.002	0.263	0.006	0.047
2	0.120	0.670	0.845	0.586	1.588	0.040	0.423	0.094	0.076
3	0.199	1.111	1.160	0.614	2.295	0.405	0.612	0.662	0.110
4	0.365	2.037	1.529	--	∞	∞	∞	--	--
Specimen 9									
1	0.092	1.326	0.812	0.692	0.773	0.032	0.301	0.107	0.037
2	0.122	1.758	0.981	0.792	1.023	0.096	0.399	0.240	0.049
3	0.147	2.118	1.172	0.836	1.788	0.531	0.697	0.762	0.085
4	0.415	5.980	1.336	--	∞	∞	∞	-	-
Specimen 10									
1	0.206	2.968	0.574	--	∞	∞	∞	--	--
Specimen 10b									
1	0.039	0.216	0.112	0.122	0.289	0.045	0.146	0.310	0.026
2	0.077	0.427	0.184	0.216	0.551	0.085	0.278	0.306	0.050
3	0.110	0.610	0.247	0.283	0.716	0.115	0.361	0.318	0.065
4	0.153	0.848	0.321	0.288	0.988	0.275	0.498	0.551	0.090
5	0.149	0.826	0.372	0.266	1.008	0.326	0.508	0.641	0.092
6	0.173	0.959	0.439	--	∞	∞	∞	-	-

TABLE C-2 (cont'd) Shake Table Tests-Displacement Comparison

Test	C_s*	$\frac{V_o^*}{V_{yo}}$	$\frac{S_a}{(V_{yo}/W)}$	$\frac{\ddot{u}_T}{(V_{yo}/W)}$	μ	$\frac{u_r}{\Delta_{coll}}$	$\frac{\mu}{\mu_s}$	$\frac{u_r}{u_{relmax}}$	Drift (%)
Specimen 11									
1	0.260	0.623	0.638	0.649	0.750	0.003	0.103	0.031	0.043
2	0.291	0.697	0.849	0.776	1.016	0.014	0.140	0.096	0.059
3	0.291	0.697	1.208	0.843	1.443	0.056	0.199	0.280	0.083
4	0.312	0.747	1.602	0.828	1.833	0.106	0.253	0.419	0.106
5	0.312	0.747	1.611	0.757	2.011	0.156	0.278	0.561	0.116
6	0.322	0.771	1.608	0.726	2.602	0.276	0.359	0.768	0.150
7	0.749	1.793	1.608	--	∞	∞	∞	-	-
Specimen 12									
1	0.279	1.355	1.163	0.889	1.300	0.050	0.279	0.180	0.057
2	0.300	1.457	1.698	0.894	1.706	0.150	0.366	0.410	0.075
3	0.845	4.104	2.466	--	∞	∞	∞	-	-
Specimen 13									
1	0.162	0.893	0.737	0.551	1.062	0.011	0.381	0.030	0.069
2	0.174	0.959	1.047	0.545	1.174	0.039	0.421	0.094	0.076
3	0.186	1.025	1.330	0.568	1.349	0.015	0.484	0.031	0.088
4	0.224	1.234	1.650	0.562	1.924	0.426	0.690	0.617	0.125
5	0.327	1.802	1.937	--	∞	∞	∞	-	-
Specimen 14									
1	0.086	0.718	0.326	0.250	0.728	0.044	0.388	0.113	0.046
2	0.105	0.877	0.382	0.276	0.892	0.081	0.475	0.170	0.057
3	0.110	0.918	0.456	0.284	0.967	0.120	0.515	0.234	0.062
4	0.121	1.010	0.510	0.292	1.164	0.311	0.620	0.501	0.074
5	0.239	1.996	0.576	--	∞	∞	∞	-	-
Specimen 15									
1	0.169	2.561	0.711	--	∞	∞	∞	-	-

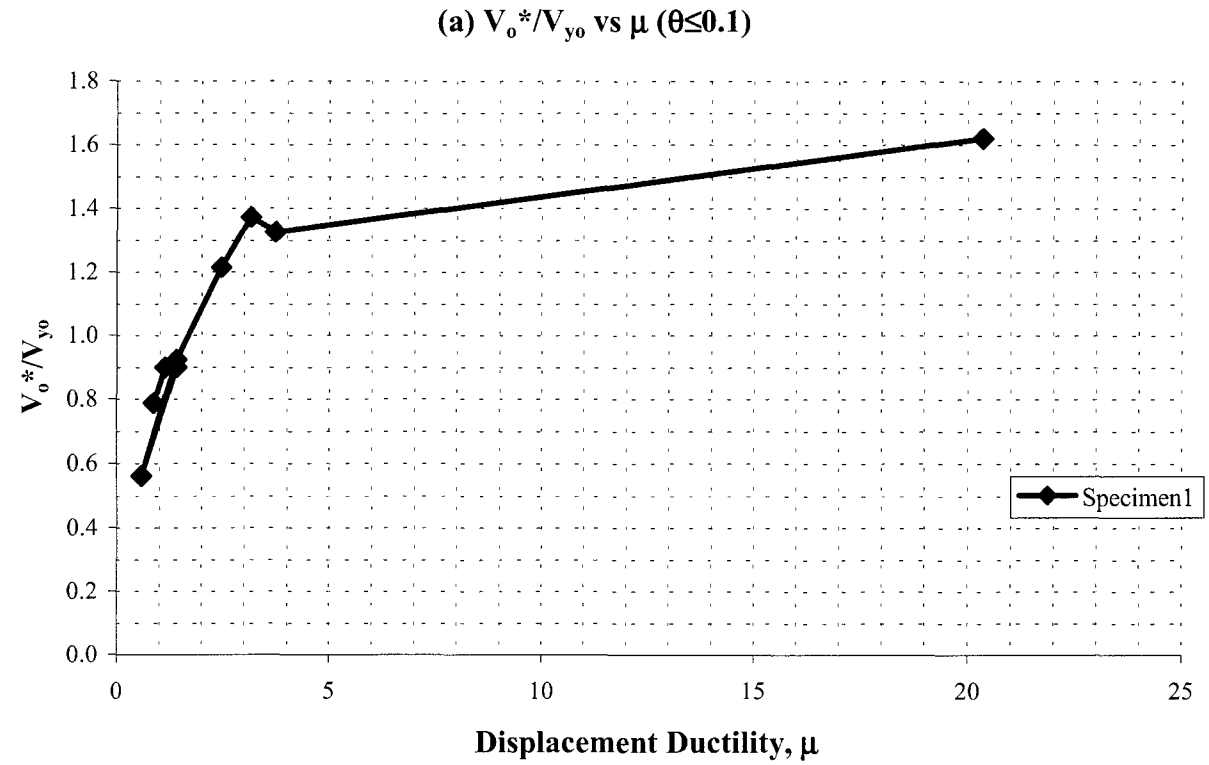

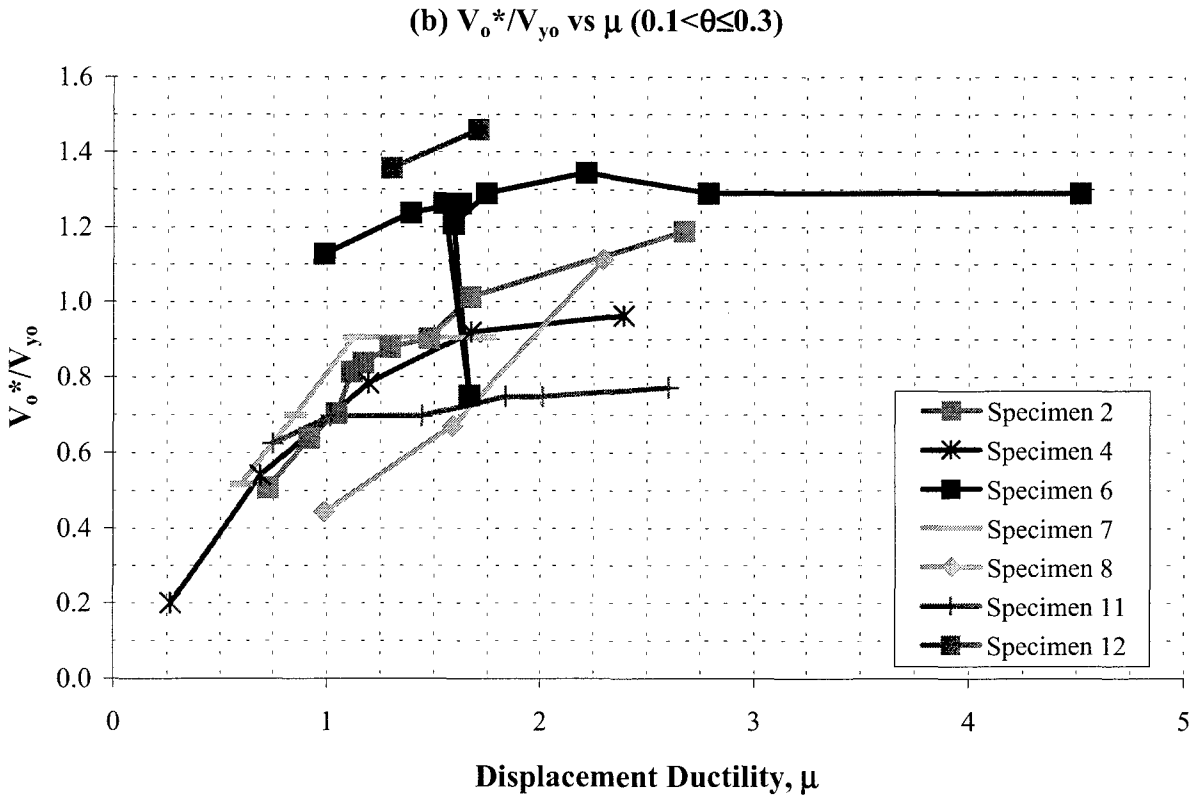

FIGURE C-1 Normalized Base Shear vs Displacement Ductility

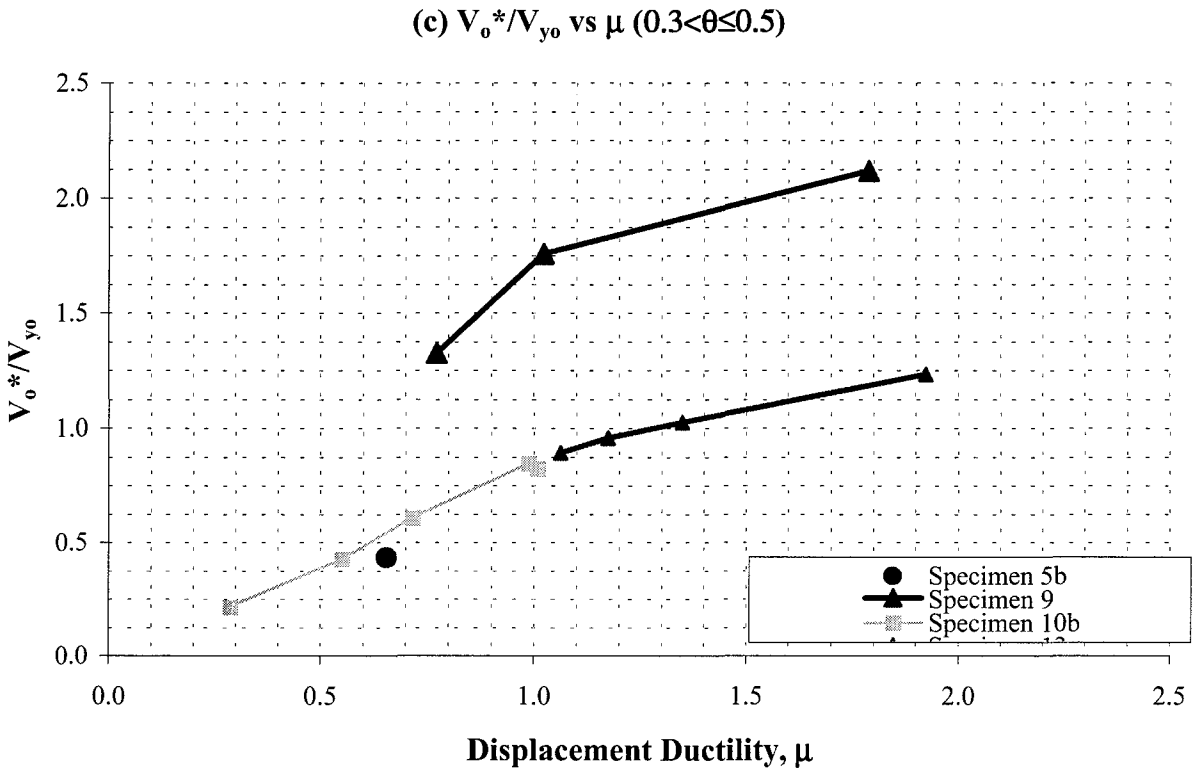

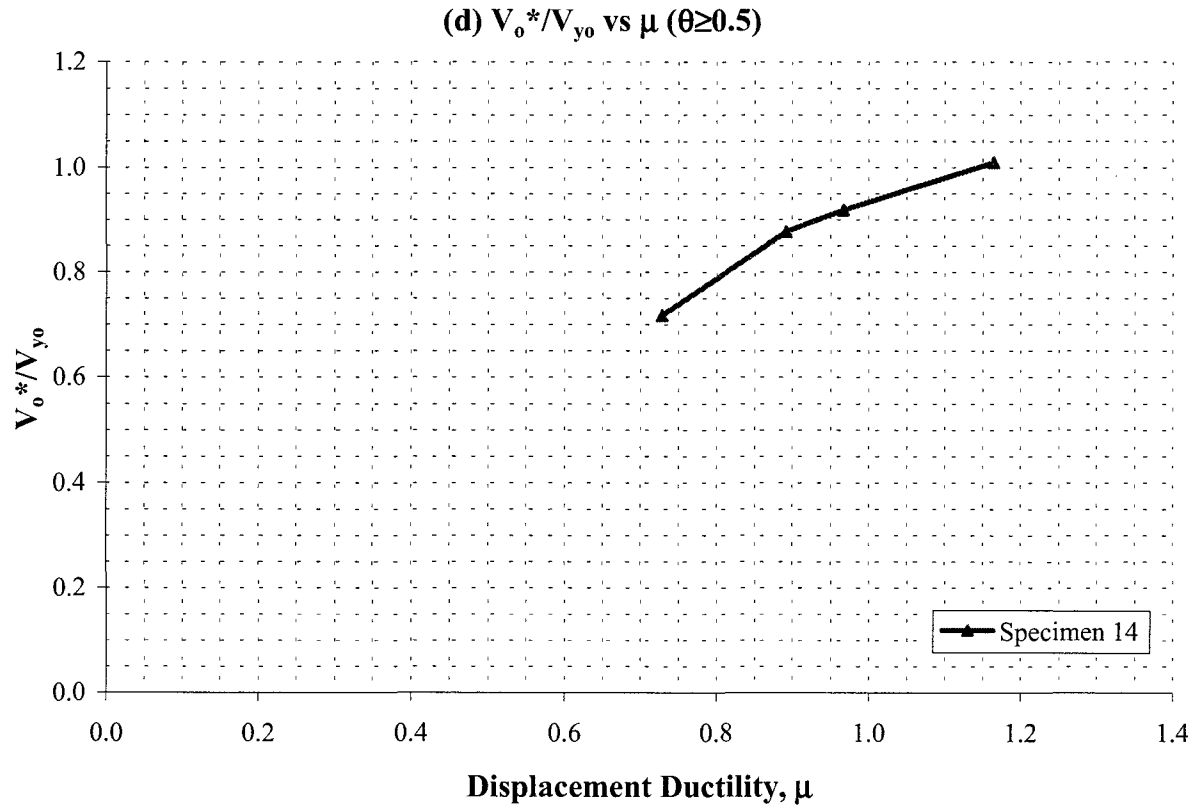

FIGURE C-1 (cont'd) Normalized Base Shear vs Displacement Ductility

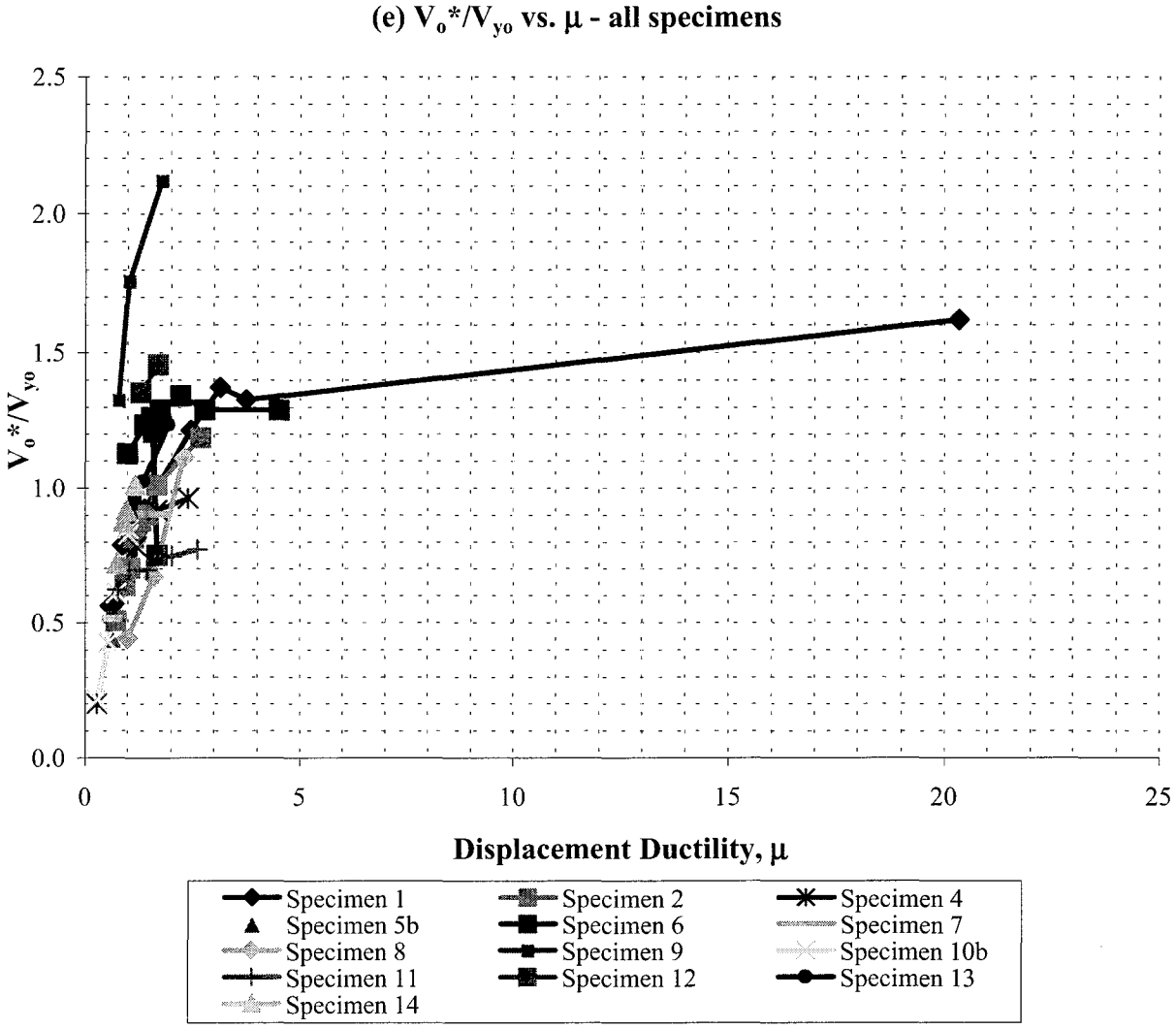

FIGURE C-1 (cont'd) Normalized Base Shear vs Displacement Ductility

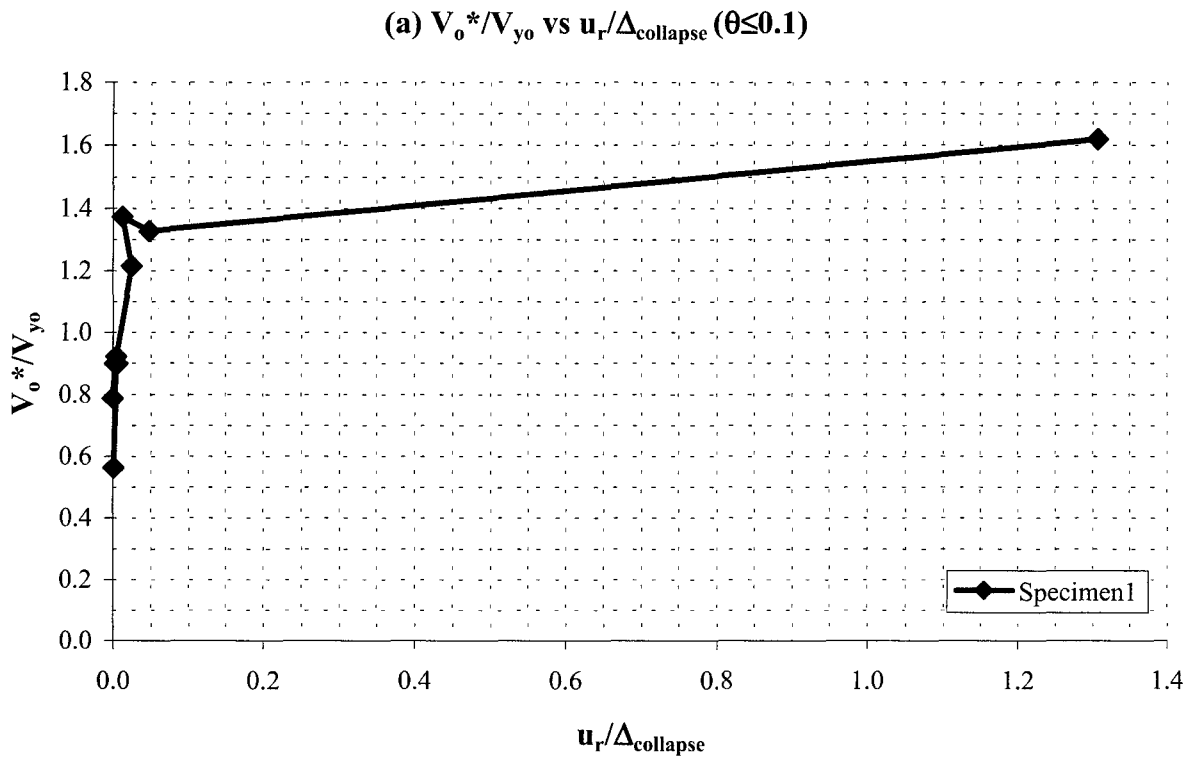

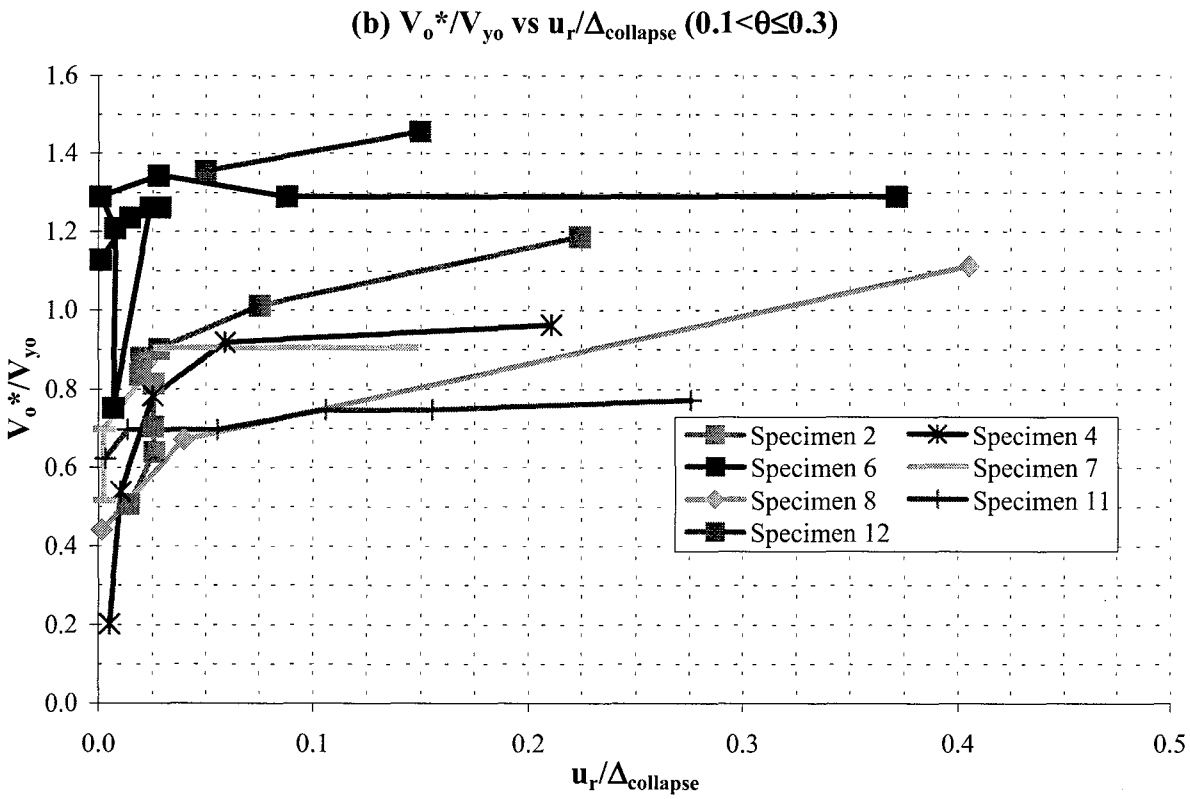

FIGURE C-2 Normalized Base Shear vs Normalized Residual Displacement

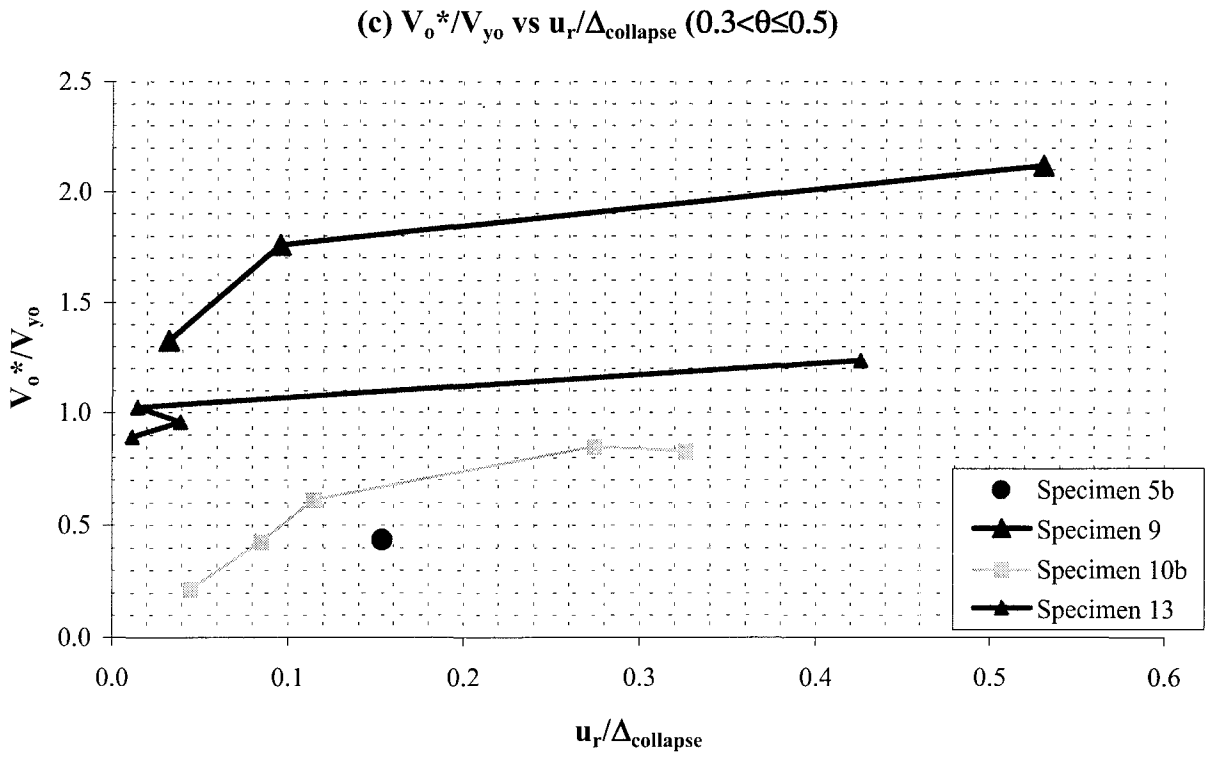

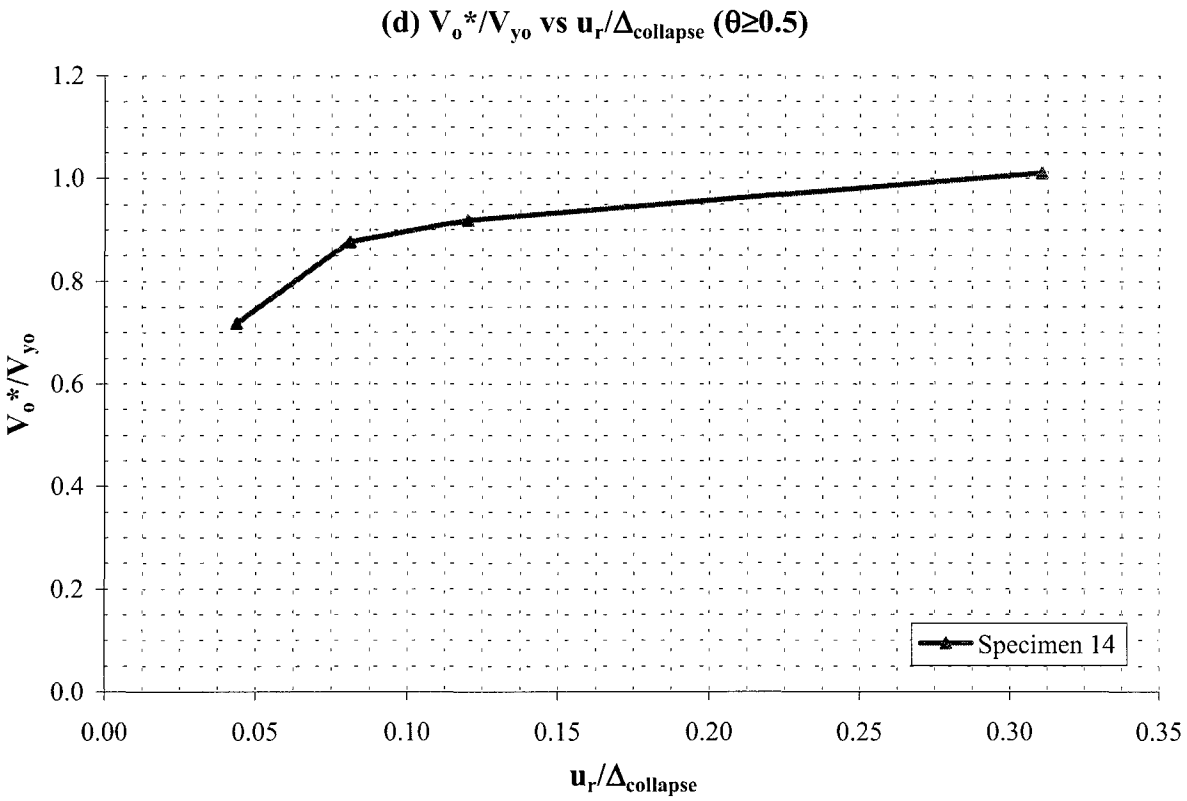

FIGURE C-2 (cont'd) Normalized Base Shear vs Normalized Residual Displacement

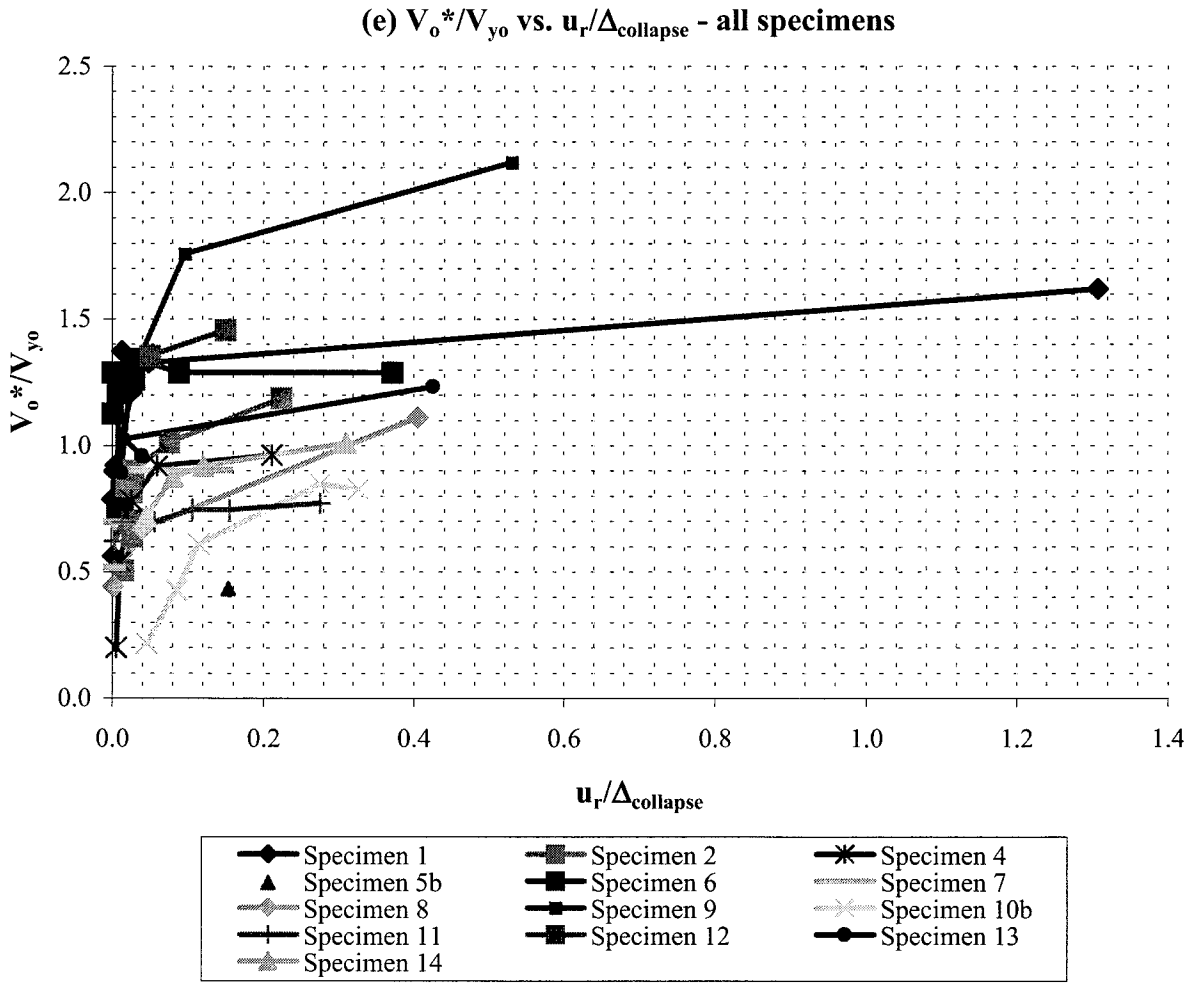

FIGURE C-2 (cont'd) Normalized Base Shear vs Normalized Residual Displacement

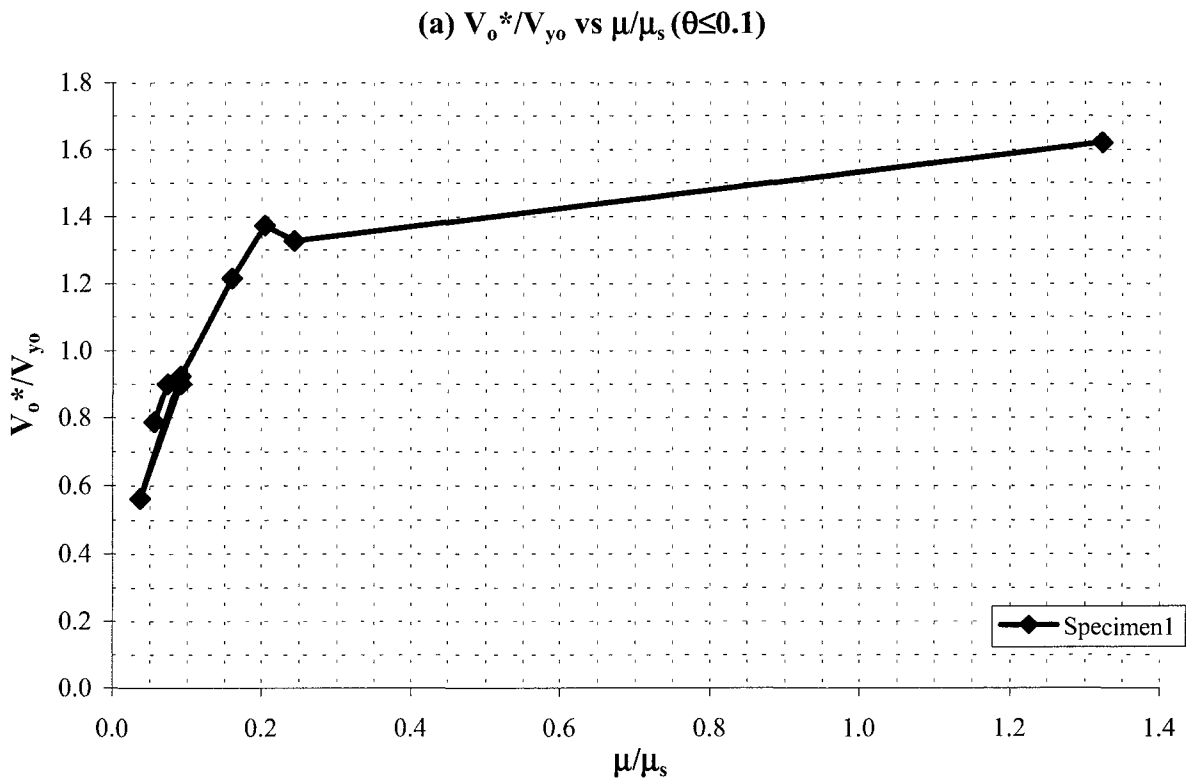

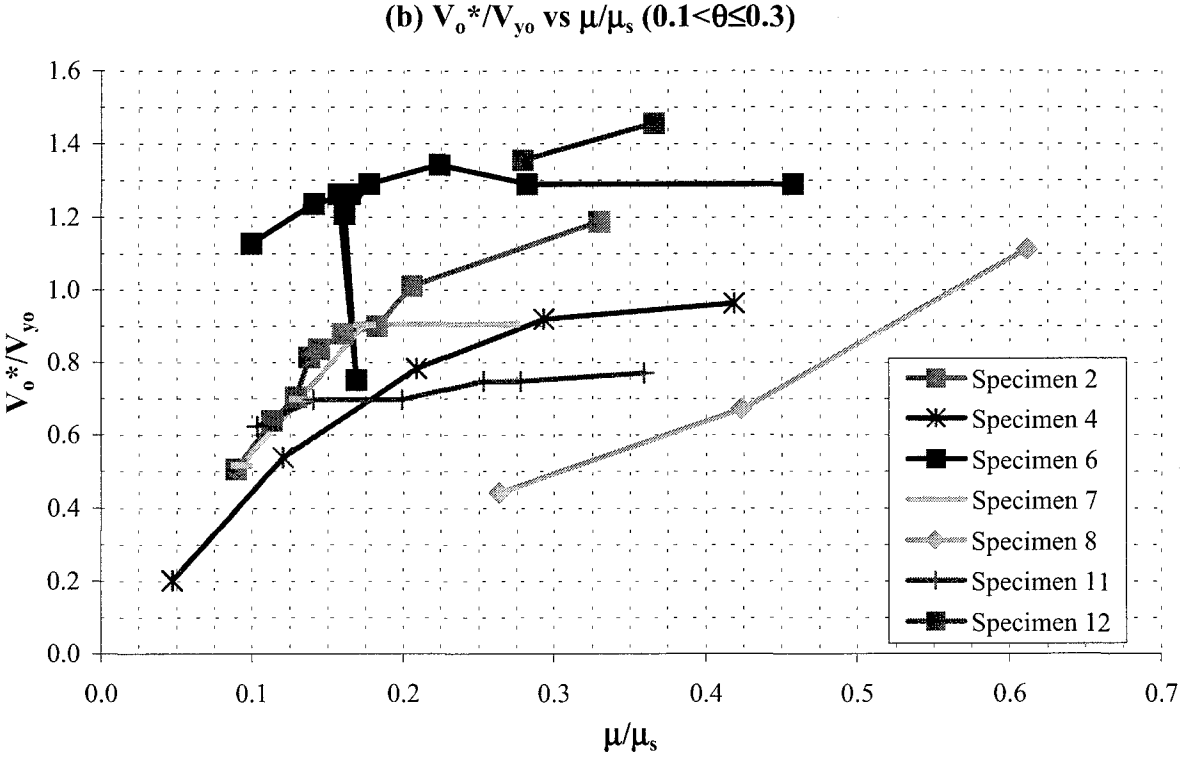

FIGURE C-3 Normalized Base Shear vs Normalized Ductility

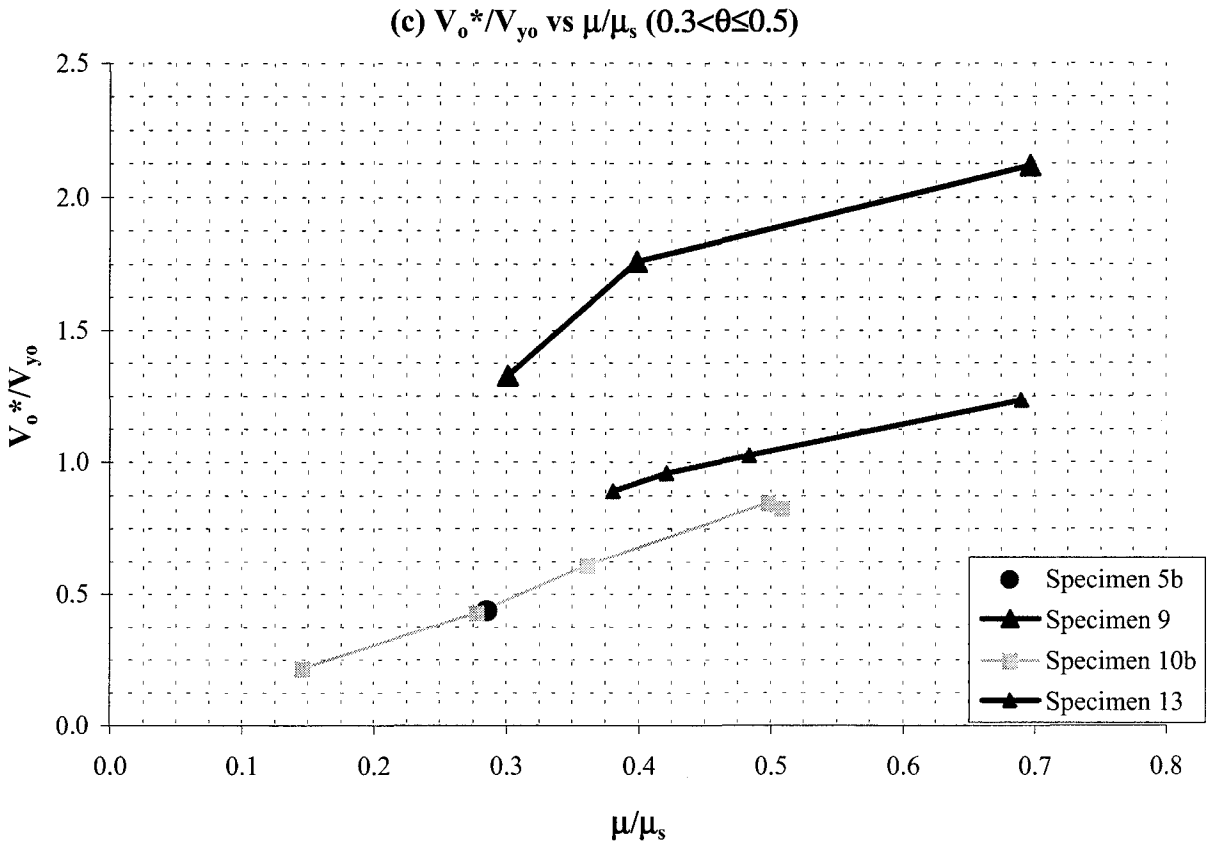

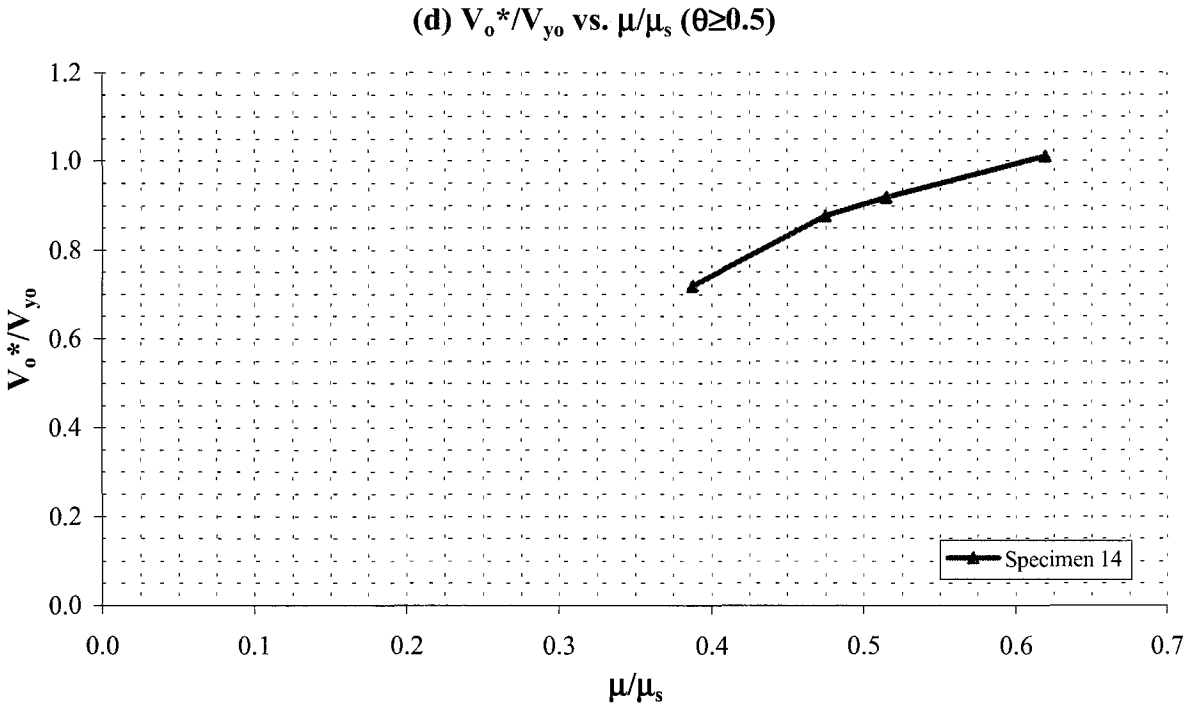

FIGURE C-3 (cont'd) Normalized Base Shear vs Normalized Ductility

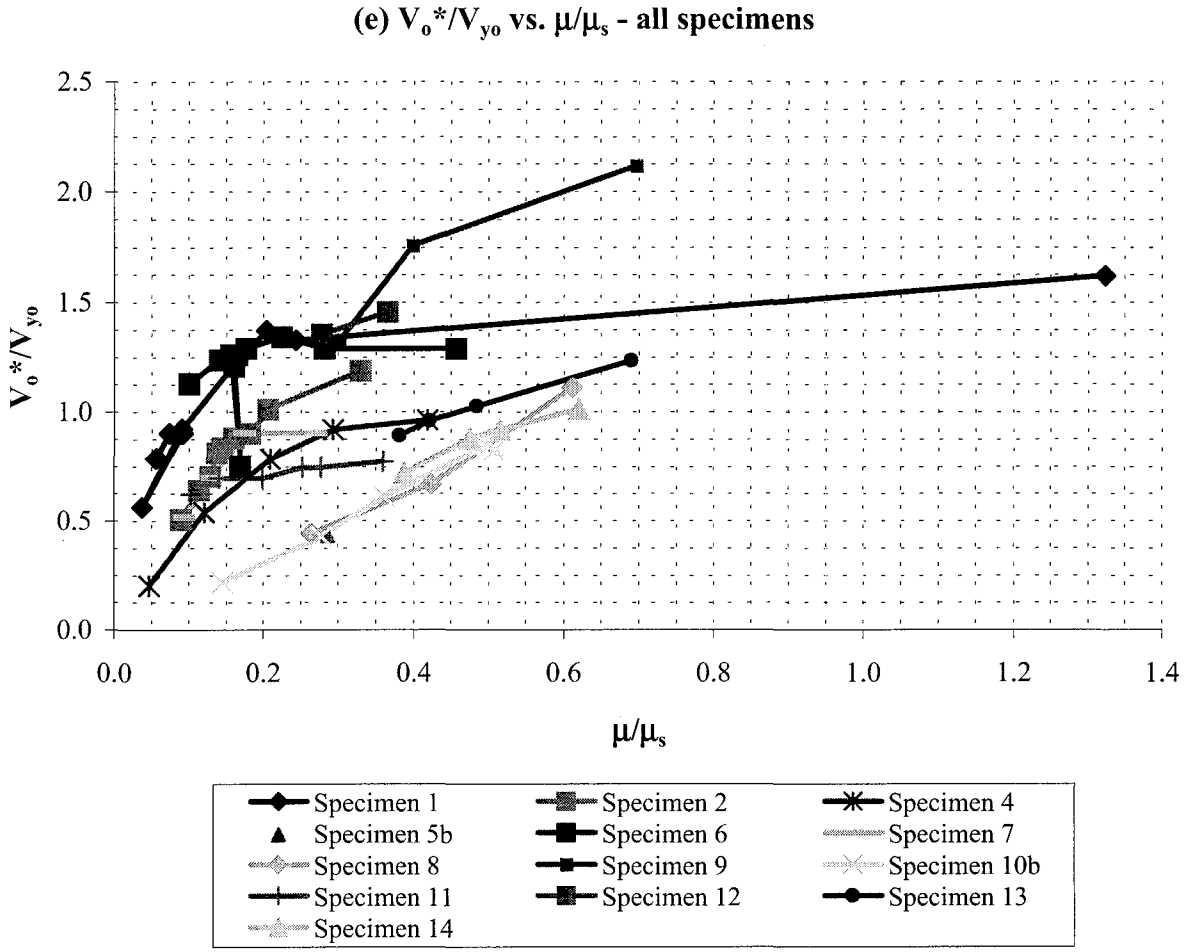

FIGURE C-3 (cont'd) Normalized Base Shear vs Normalized Ductility

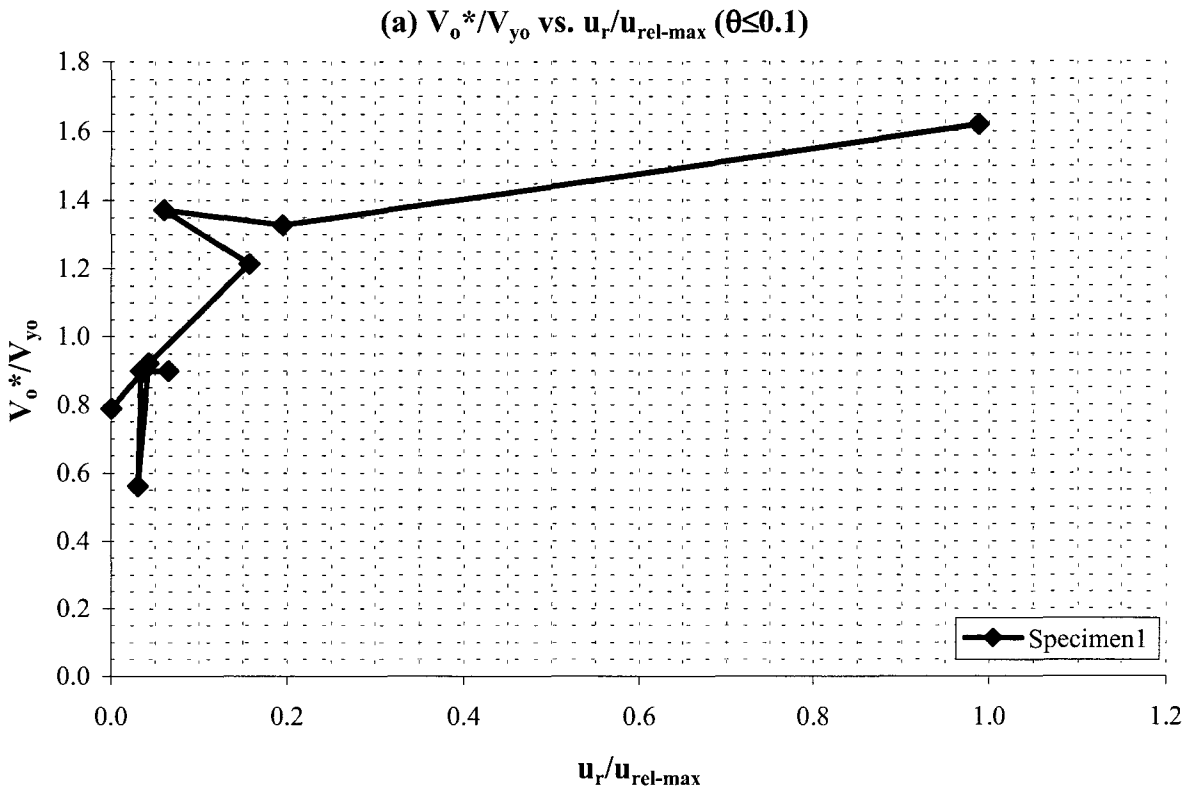

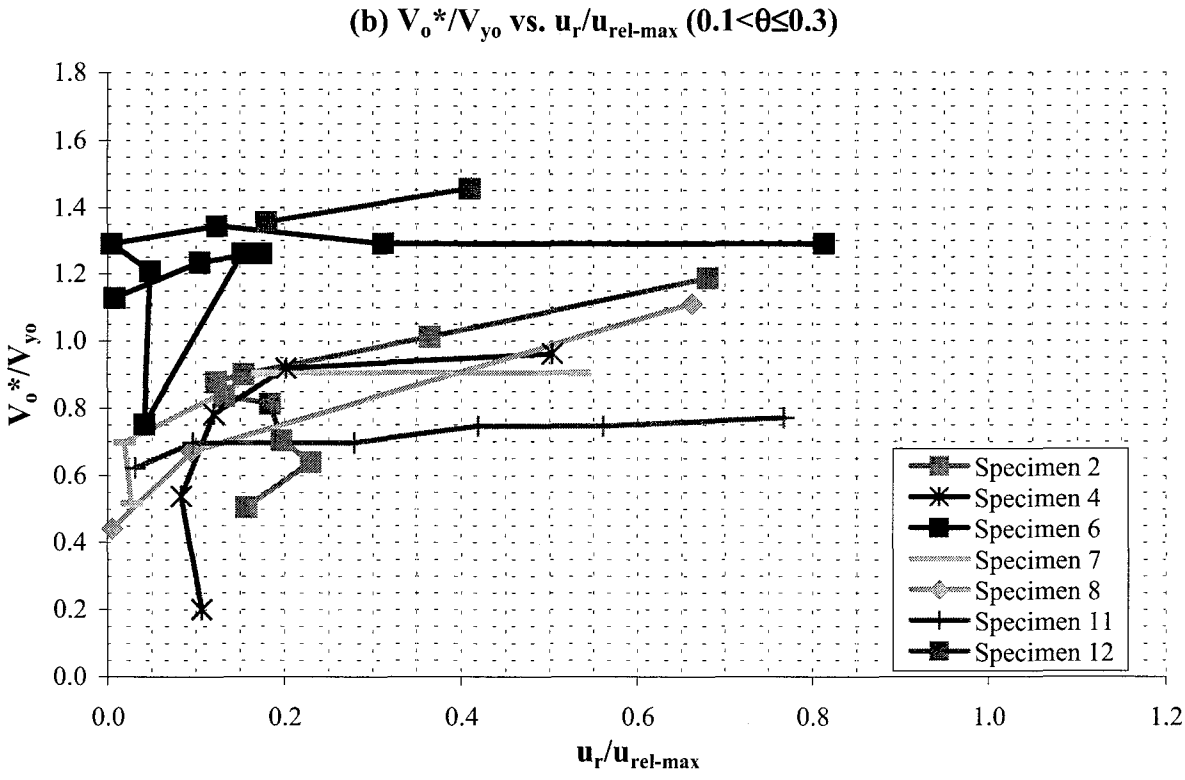

FIGURE C-4 Normalized Base Shear vs Displacement Ratio

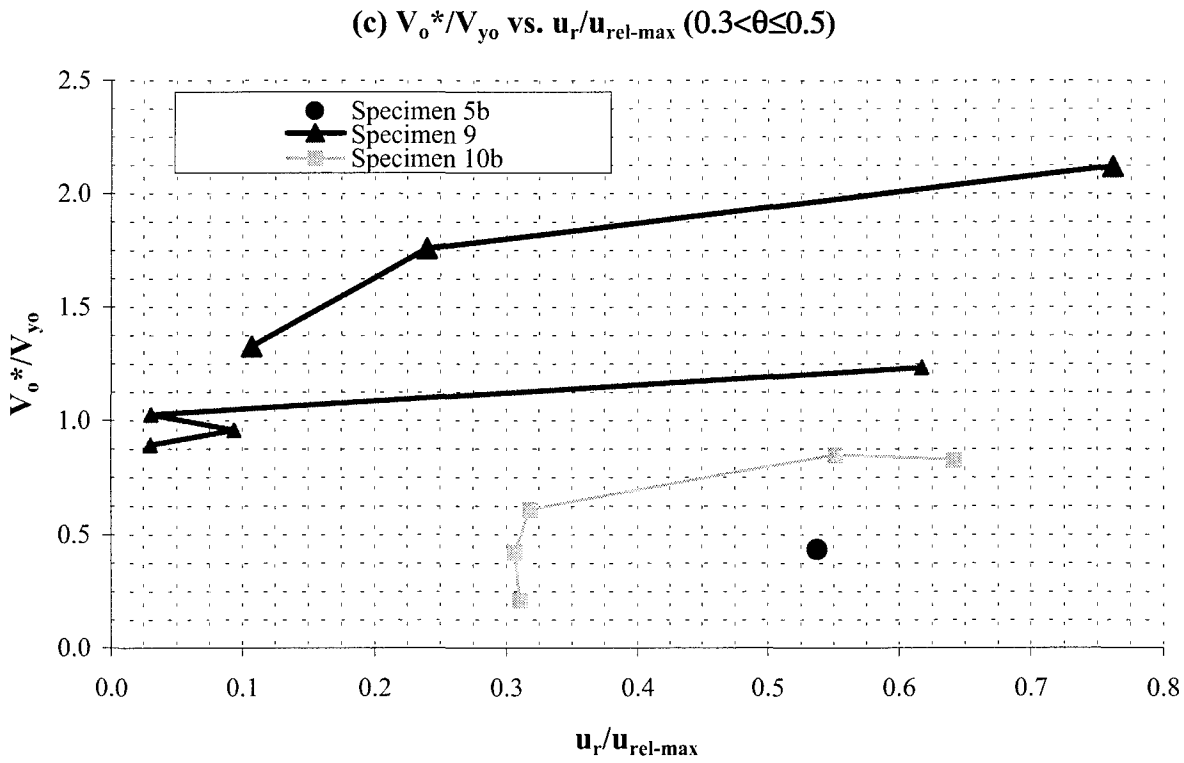

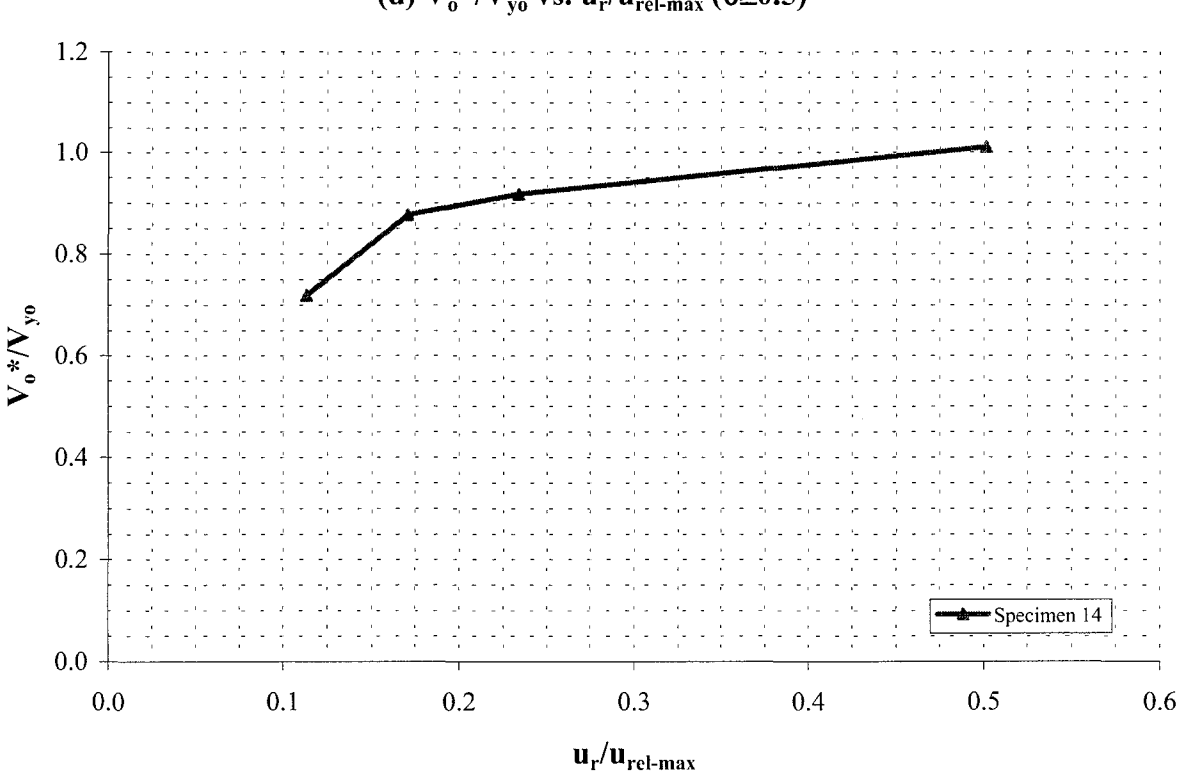

FIGURE C-4 (cont'd) Normalized Base Shear vs Displacement Ratio

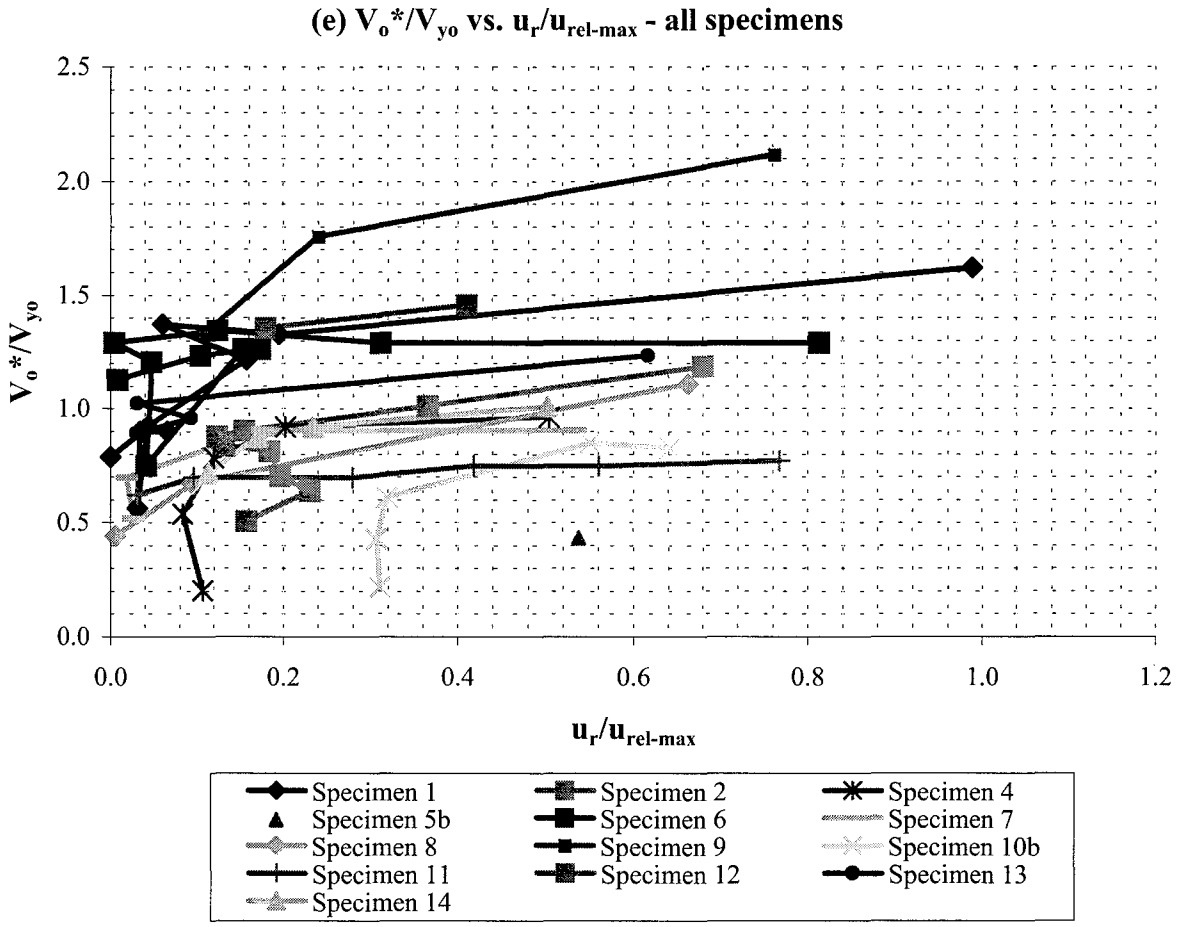

FIGURE C-4 (cont'd) Normalized Base Shear vs Displacement Ratio

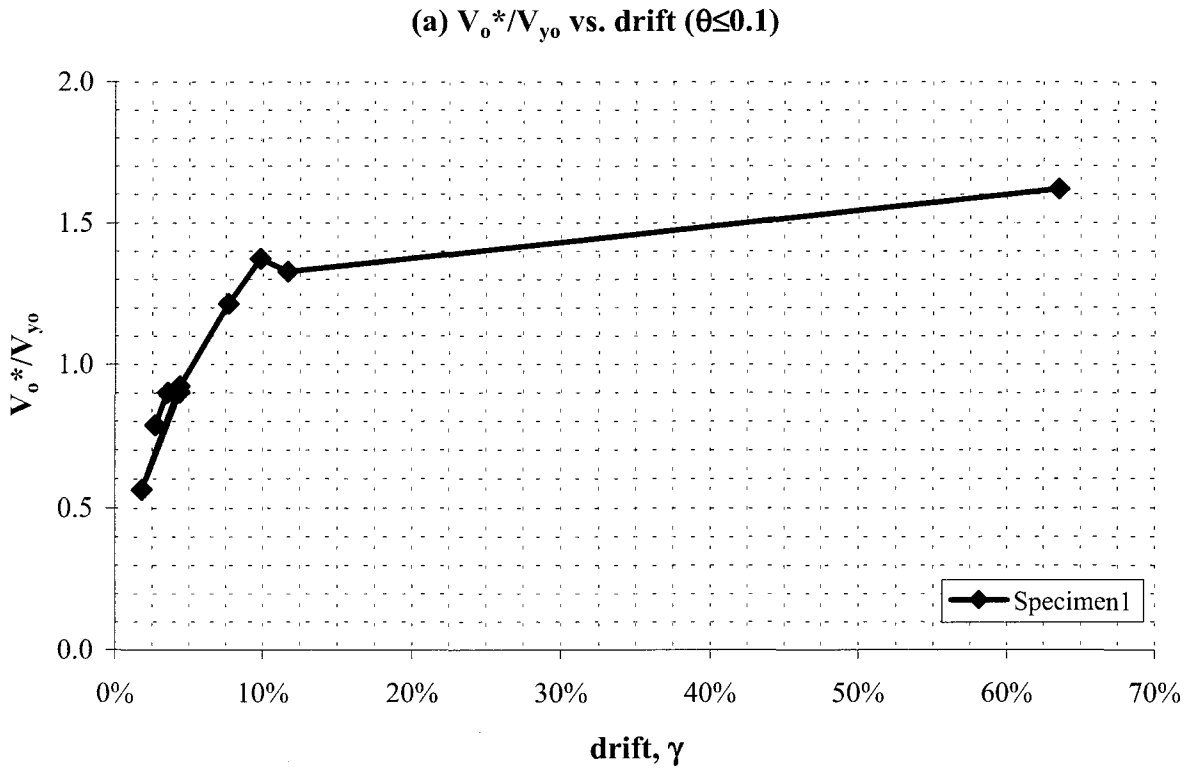

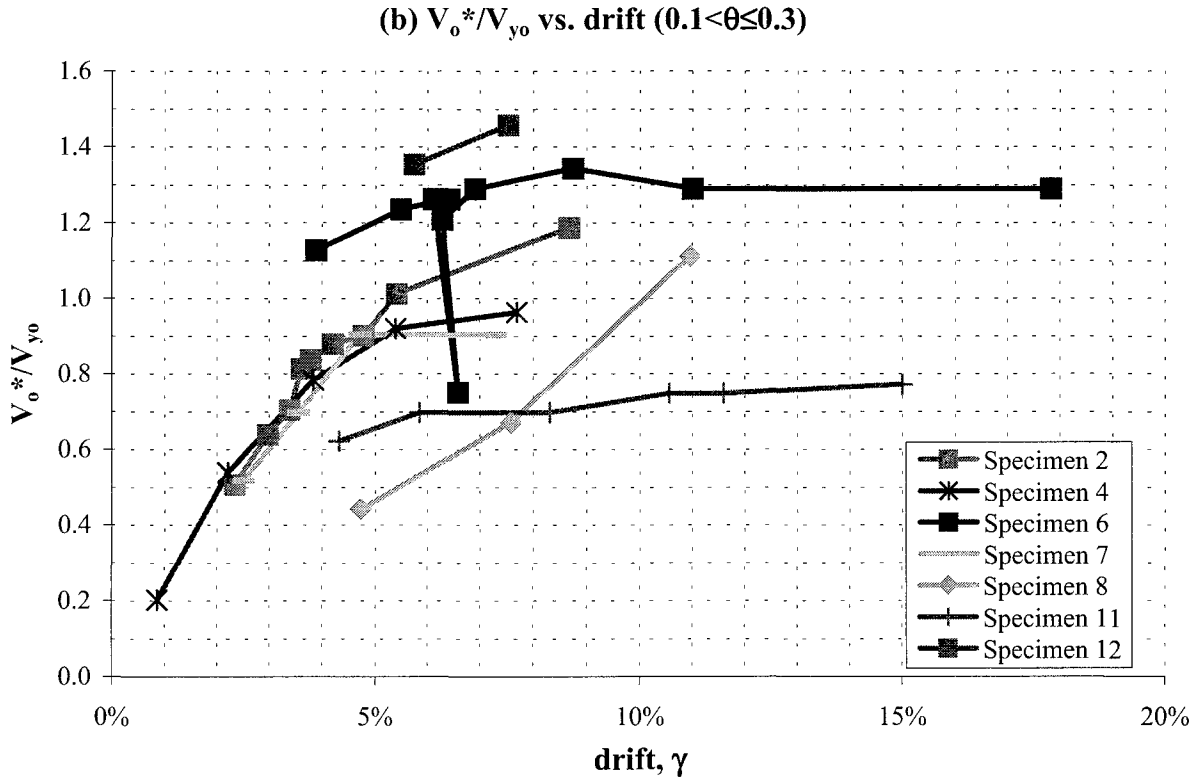

FIGURE C-5 Normalized Base Shear vs Drift

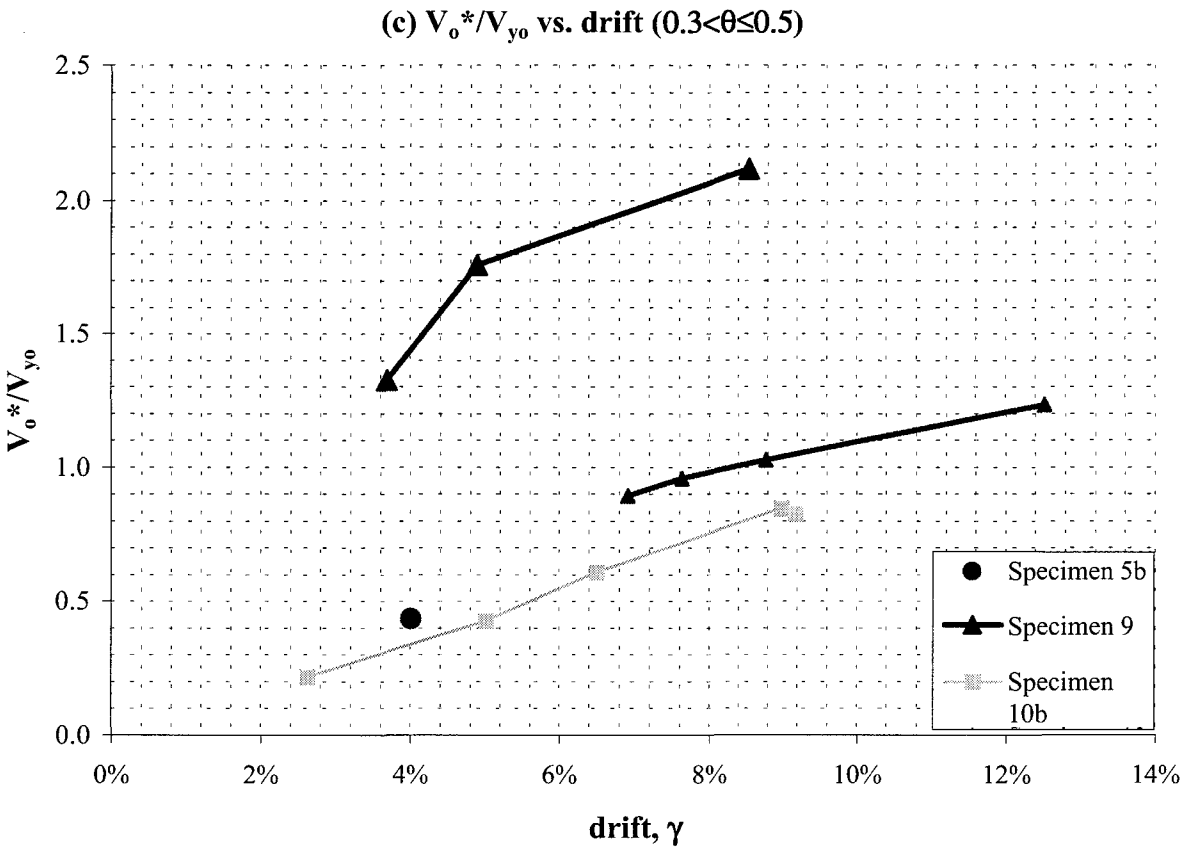

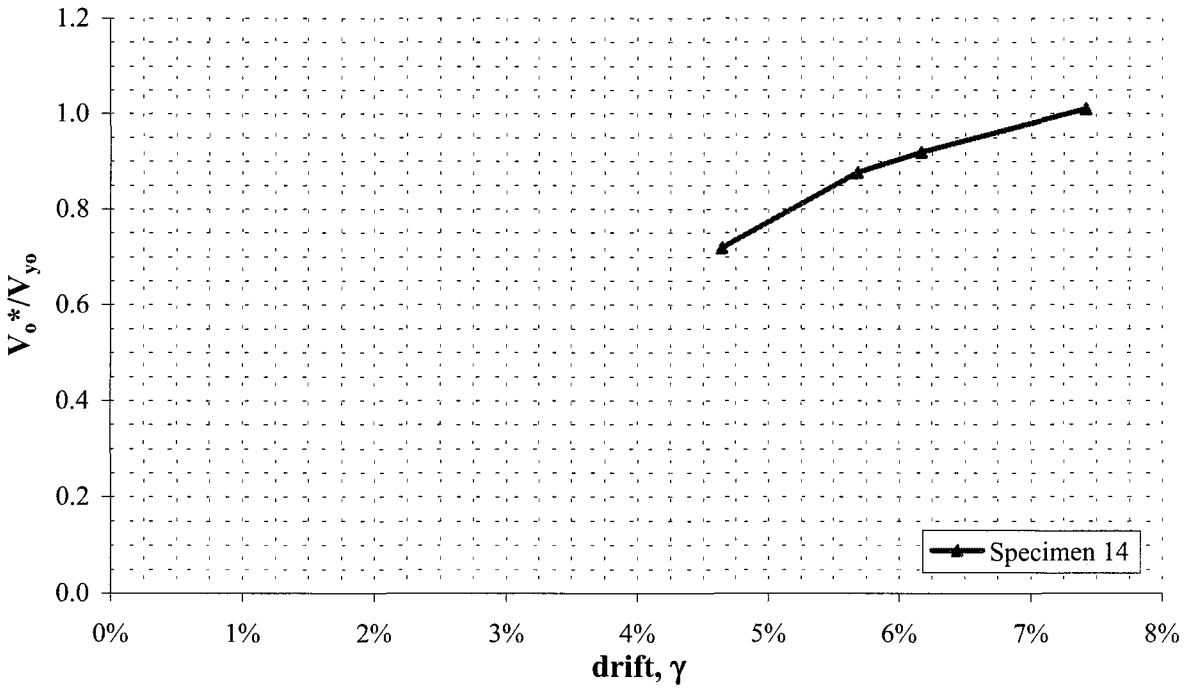

FIGURE C-5 (cont'd) Normalized Base Shear vs Drift

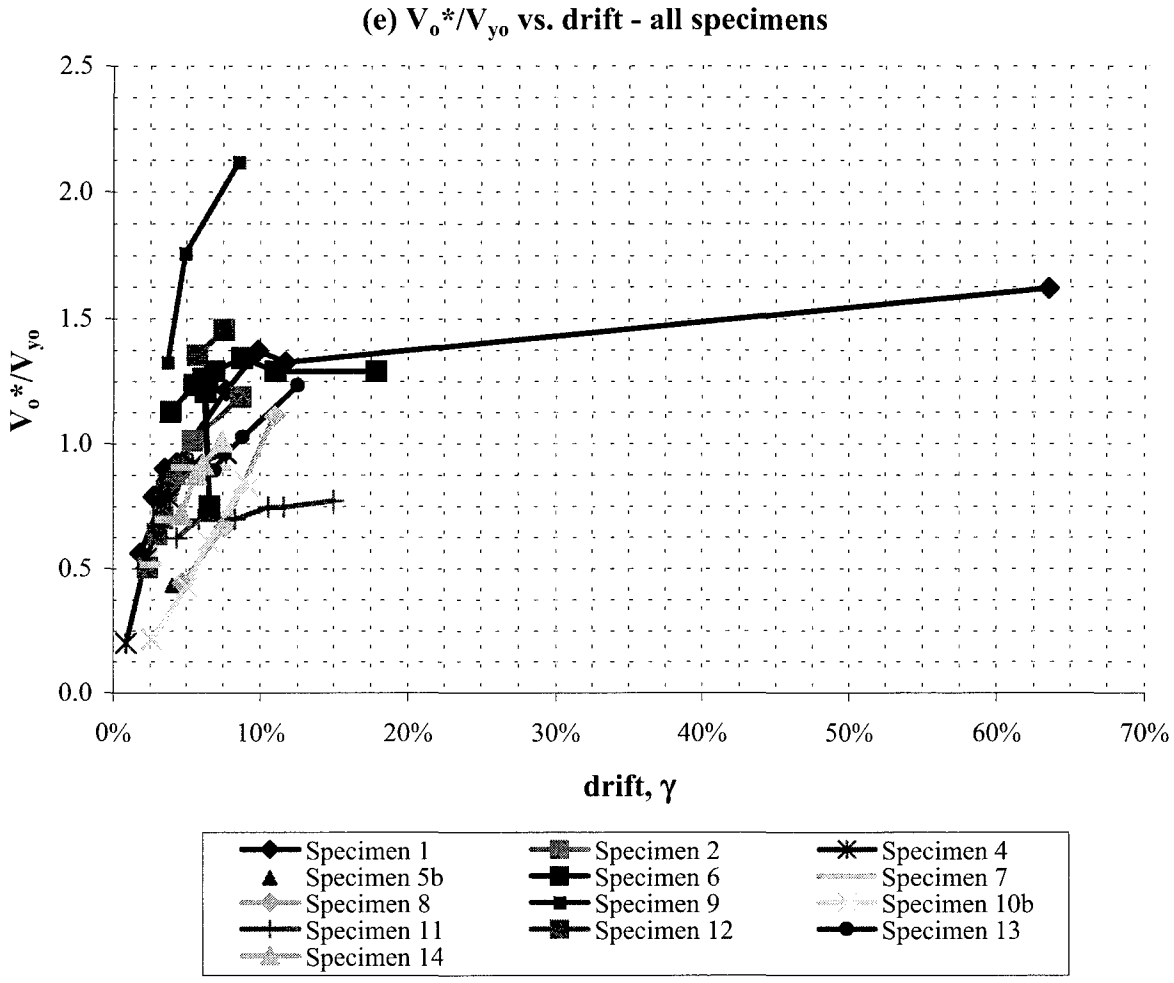

FIGURE C-5 (cont'd) Normalized Base Shear vs Drift

(a) $S_a/(V_{yo}/W)$ vs μ ($\theta \leq 0.1$)

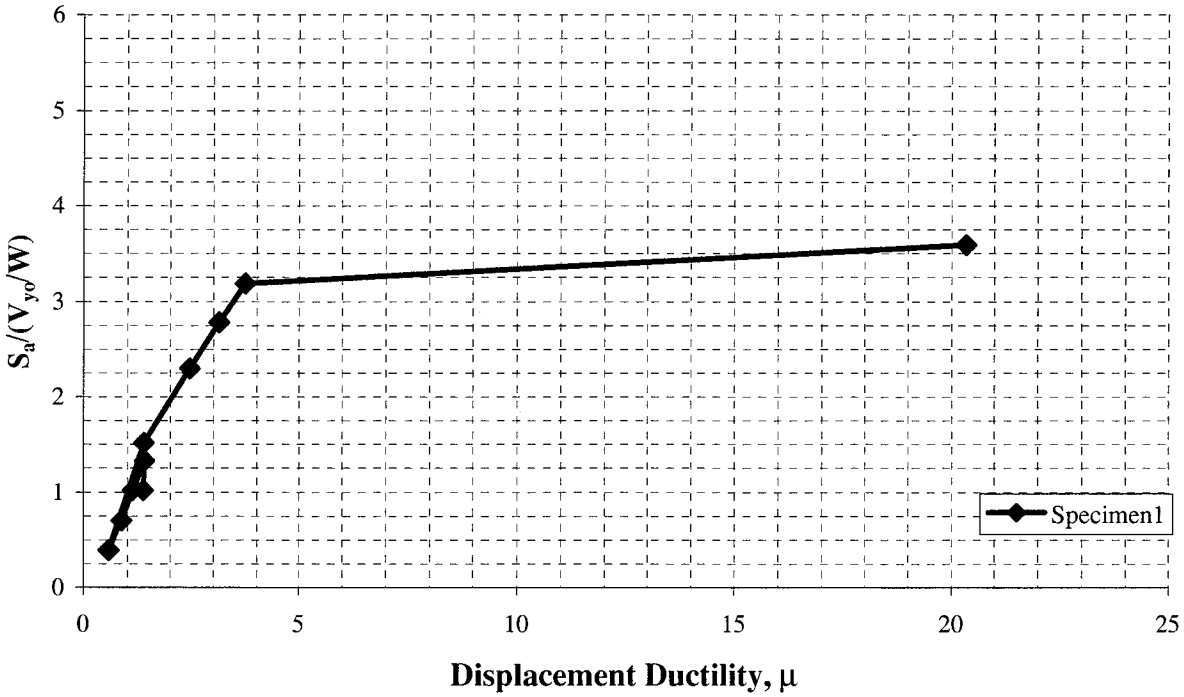

(b) $S_a/(V_{yo}/W)$ vs μ ($0.1 < \theta \leq 0.3$)

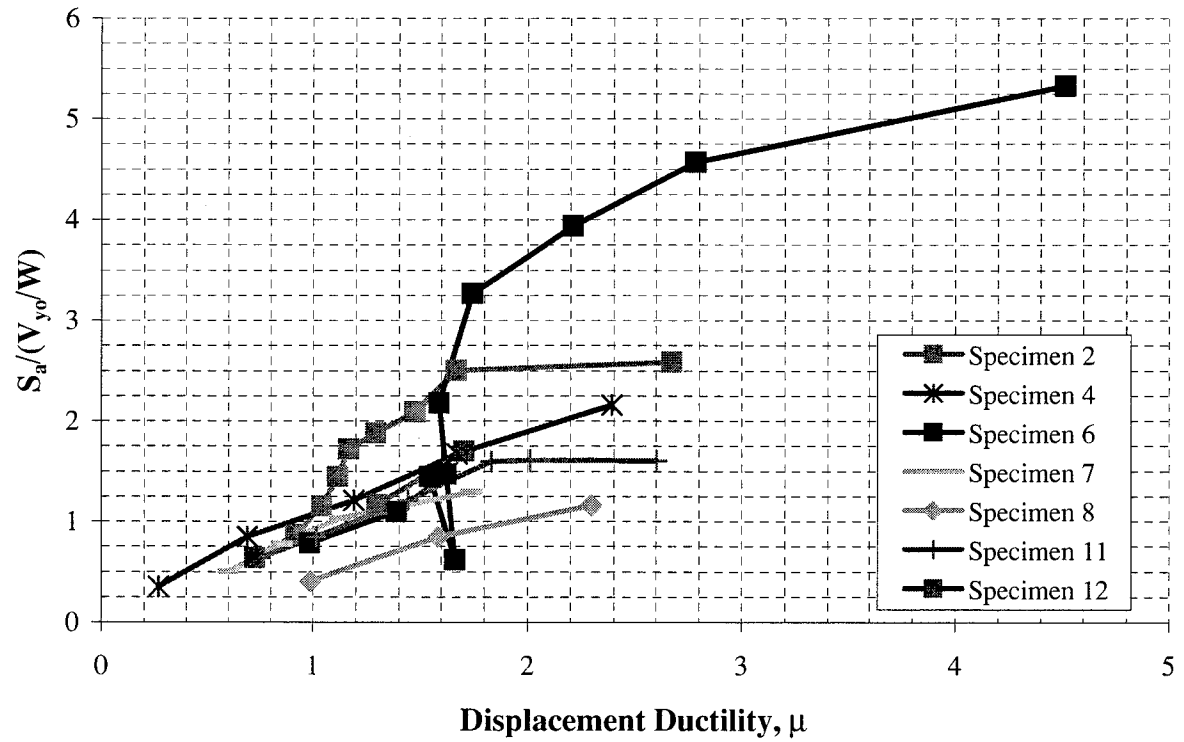

FIGURE C-6 Normalized Spectral Acceleration vs. Displacement Ductility

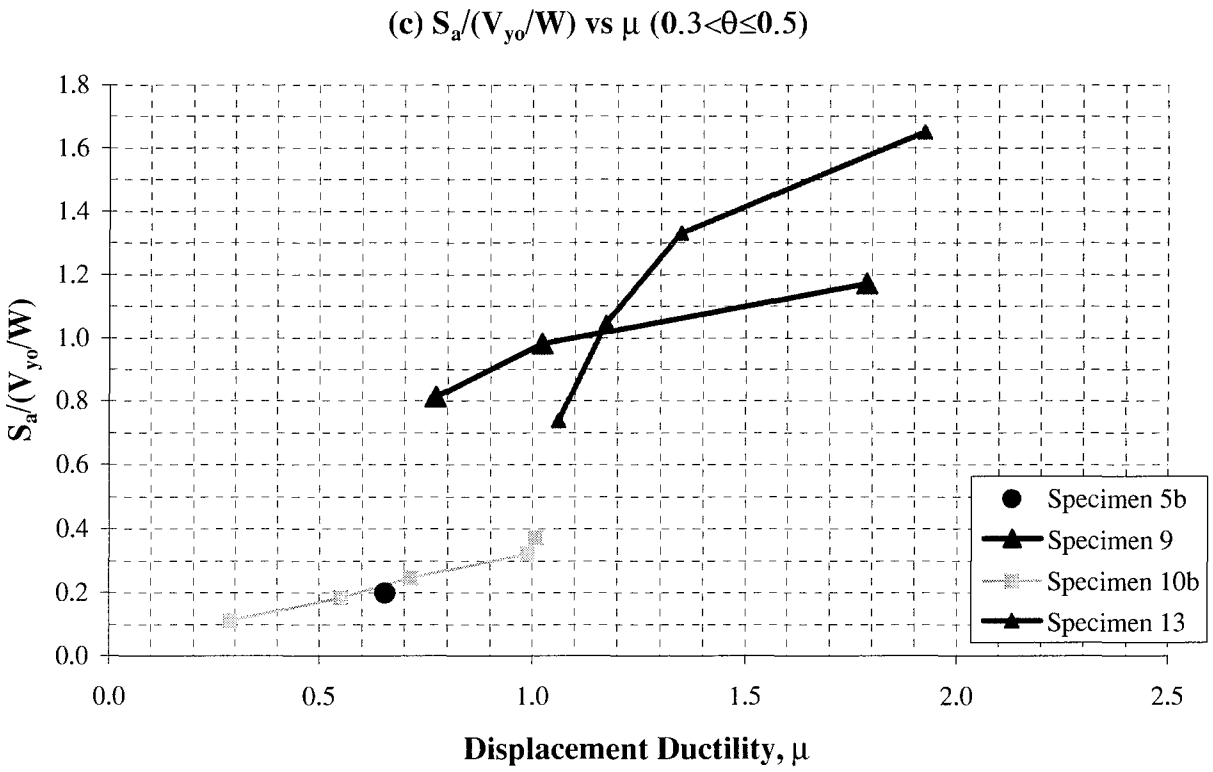

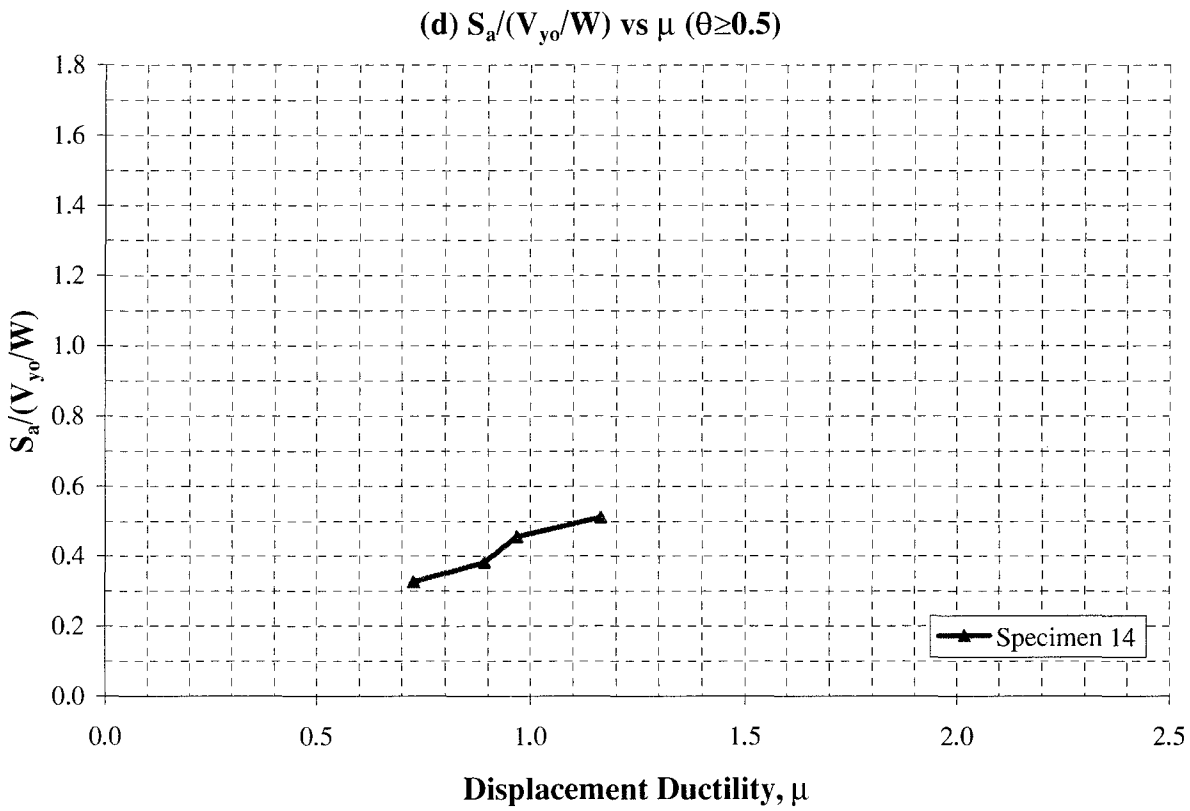

FIGURE C-6 (cont'd) Normalized Spectral Acceleration vs. Displacement Ductility

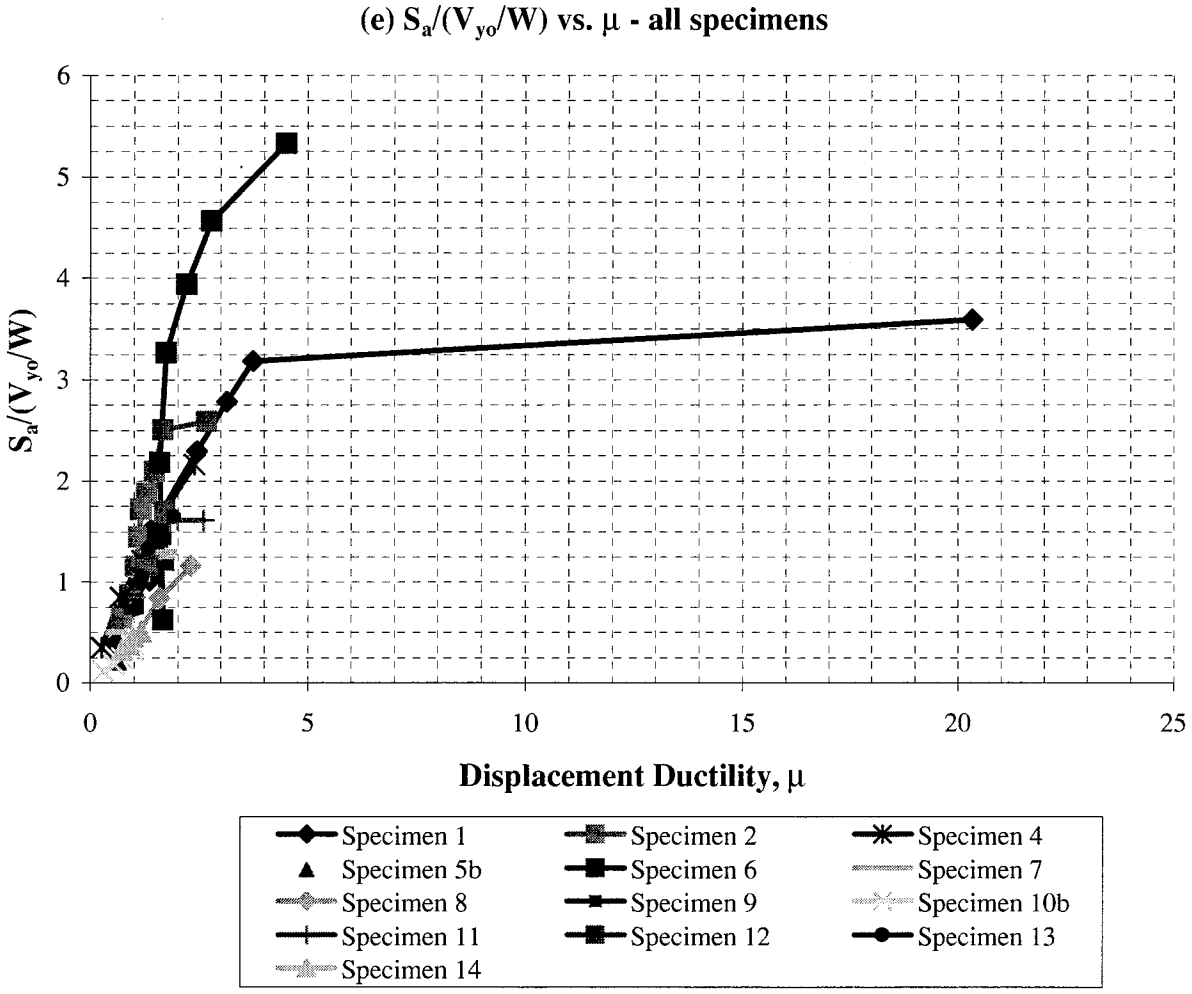

FIGURE C-6 (cont'd) Normalized Spectral Acceleration vs. Displacement Ductility

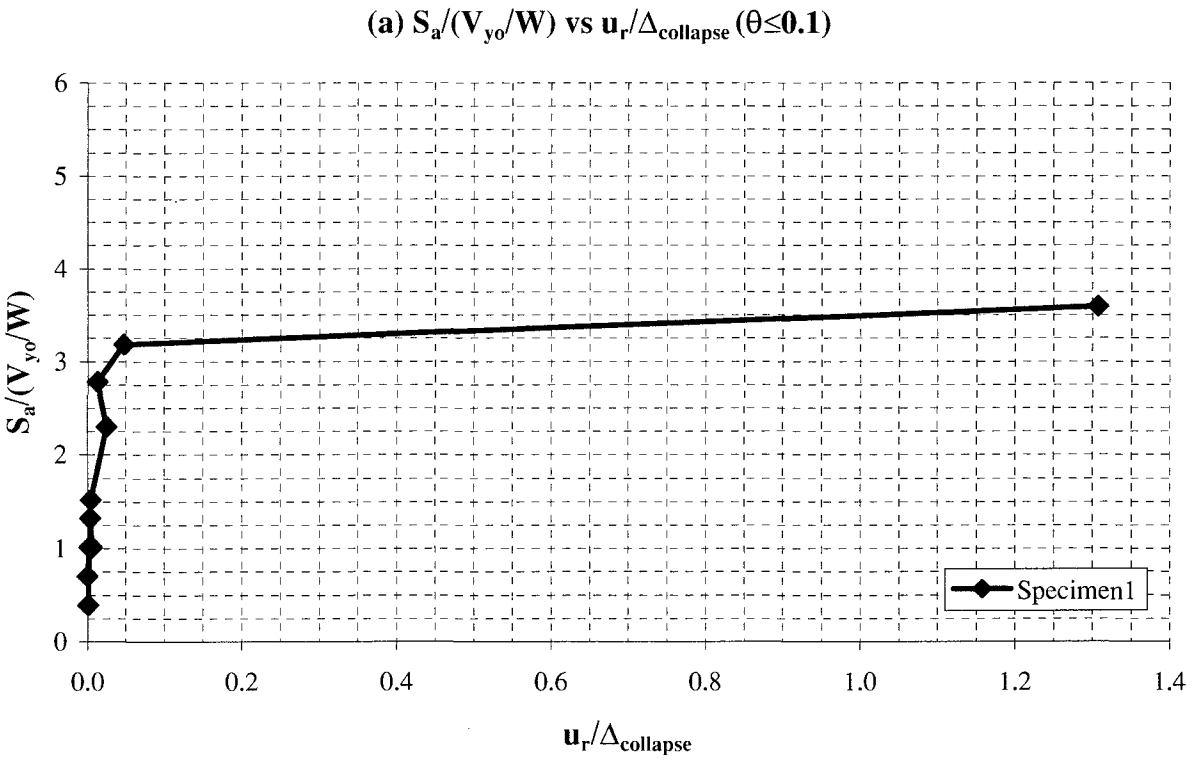

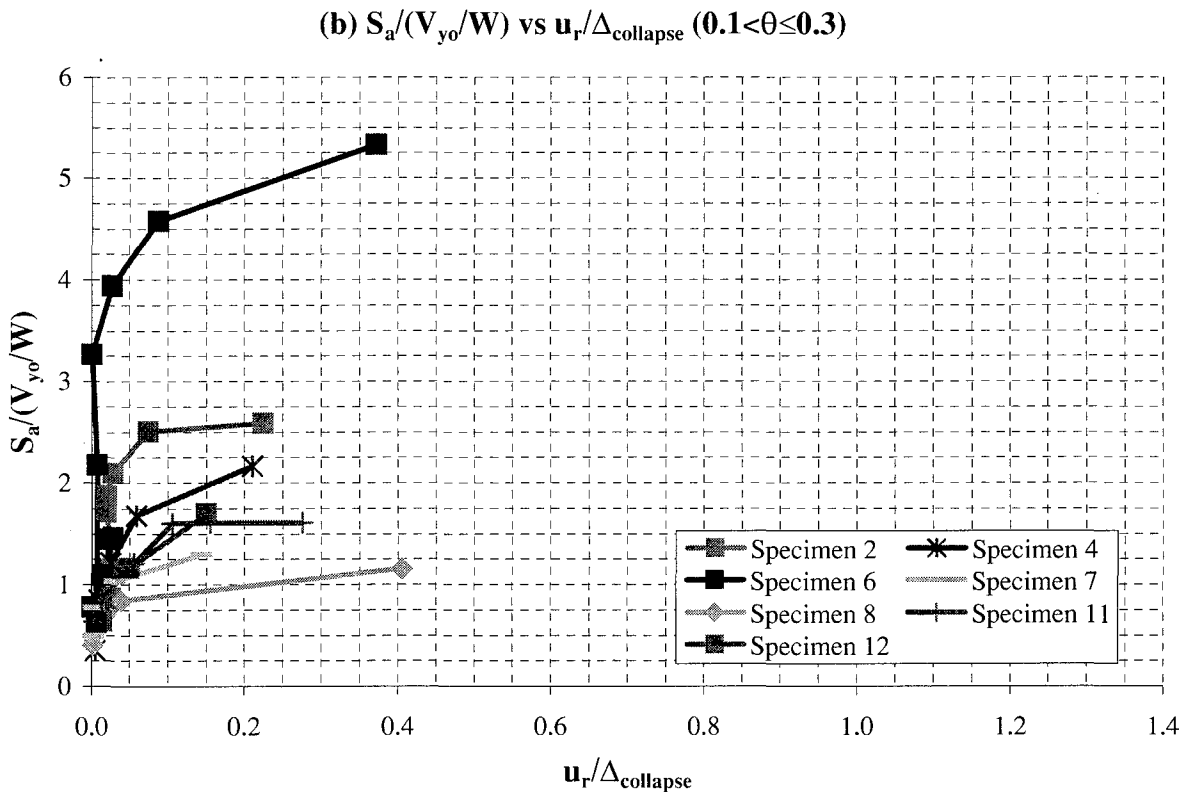

FIGURE C-7 Normalized Spectral Acceleration vs. Residual Displacement

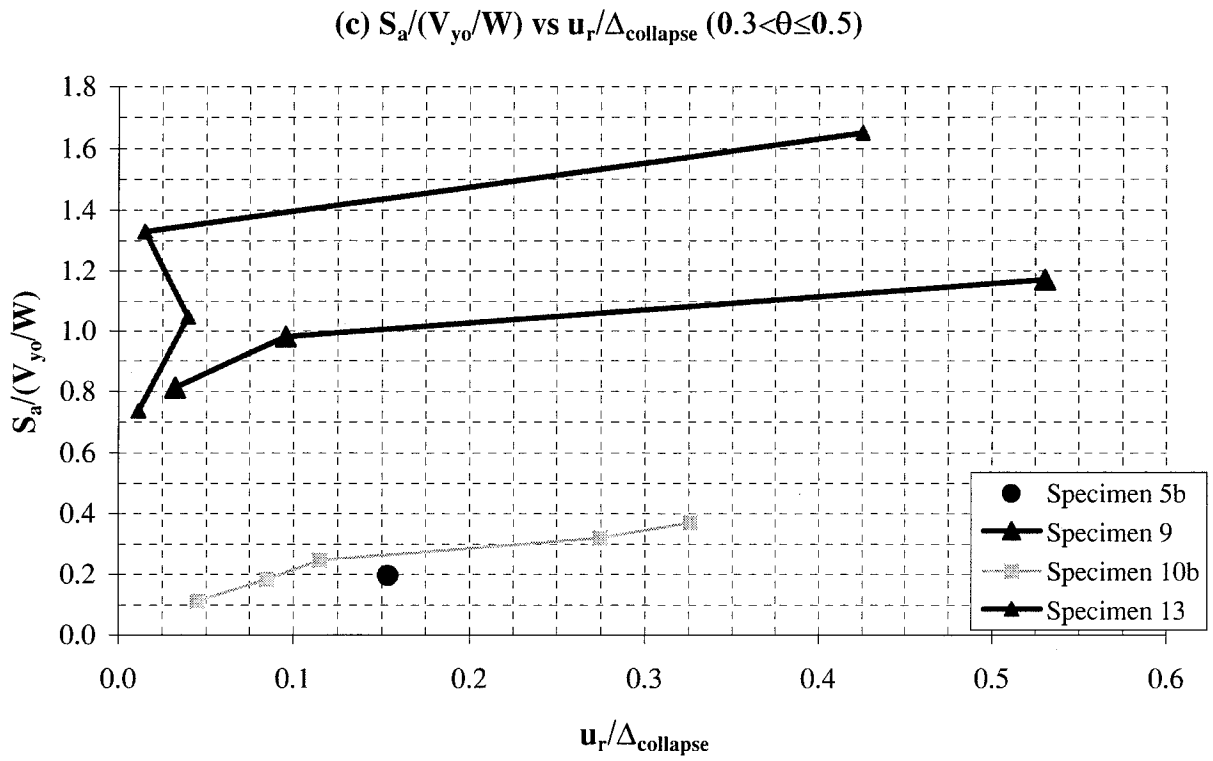

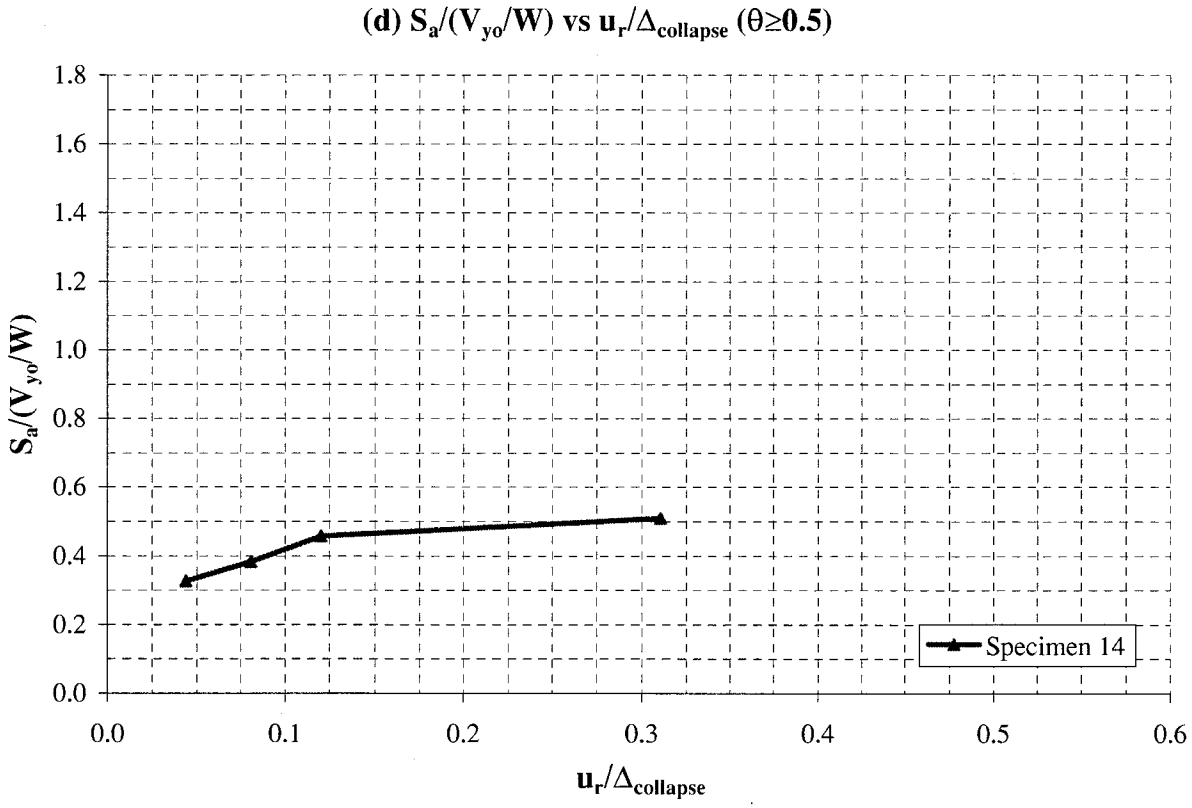

FIGURE C-7 (cont'd) Normalized Spectral Acceleration vs. Residual Displacement

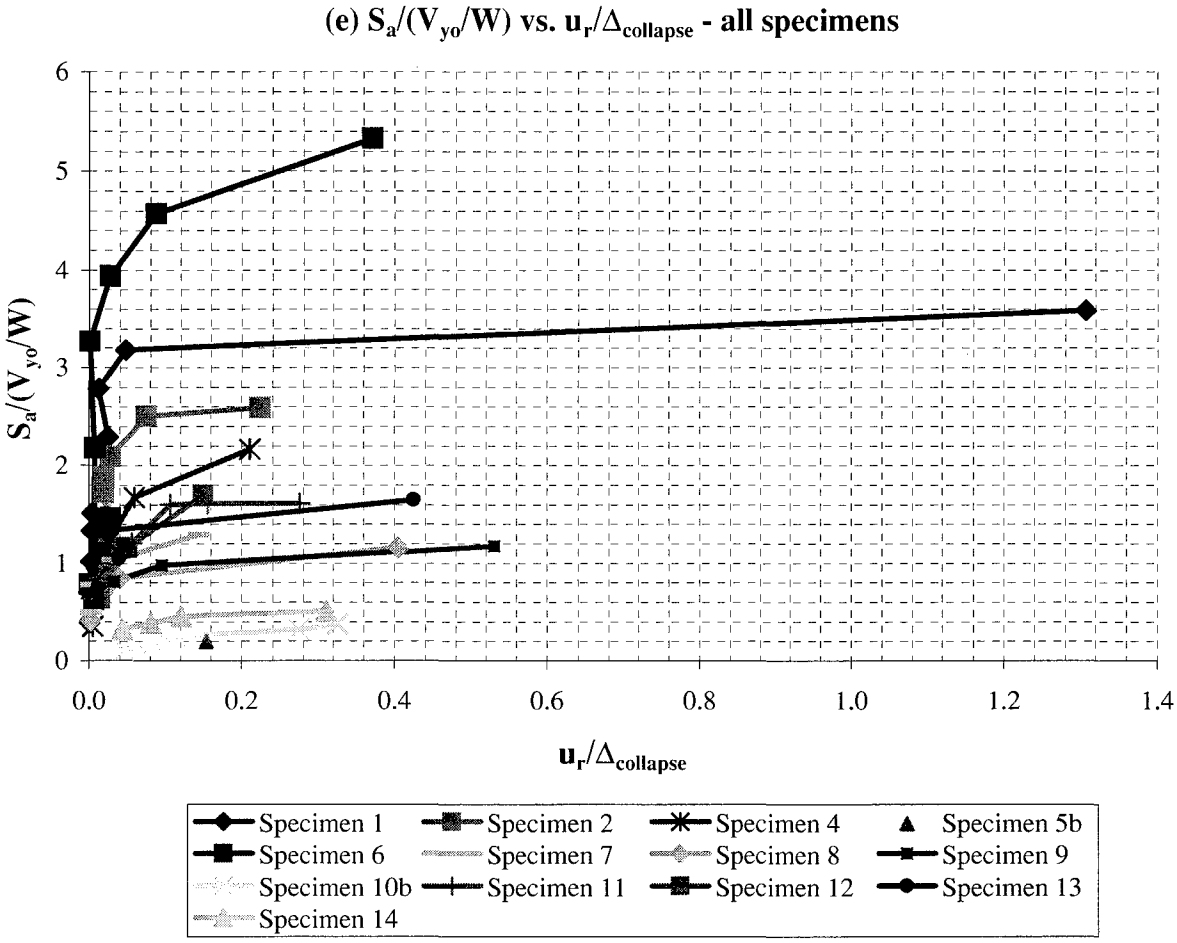

FIGURE C-7 (cont'd) Normalized Spectral Acceleration vs. Residual Displacement

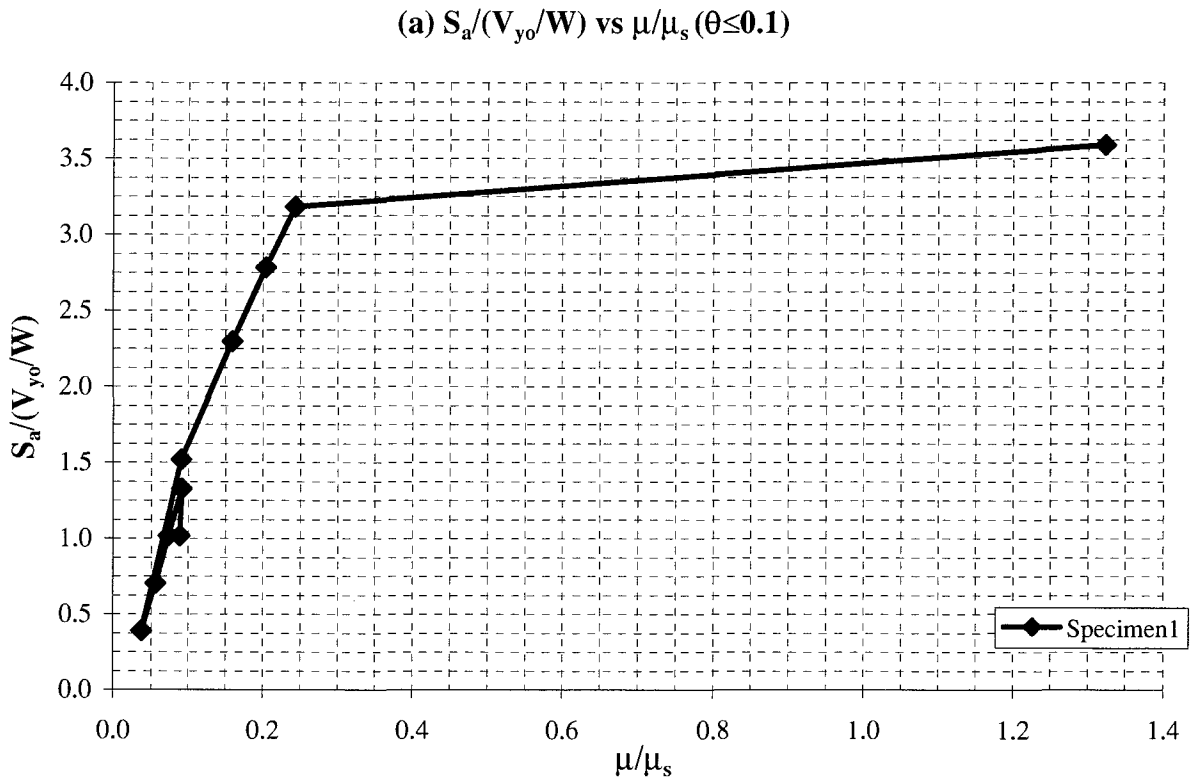

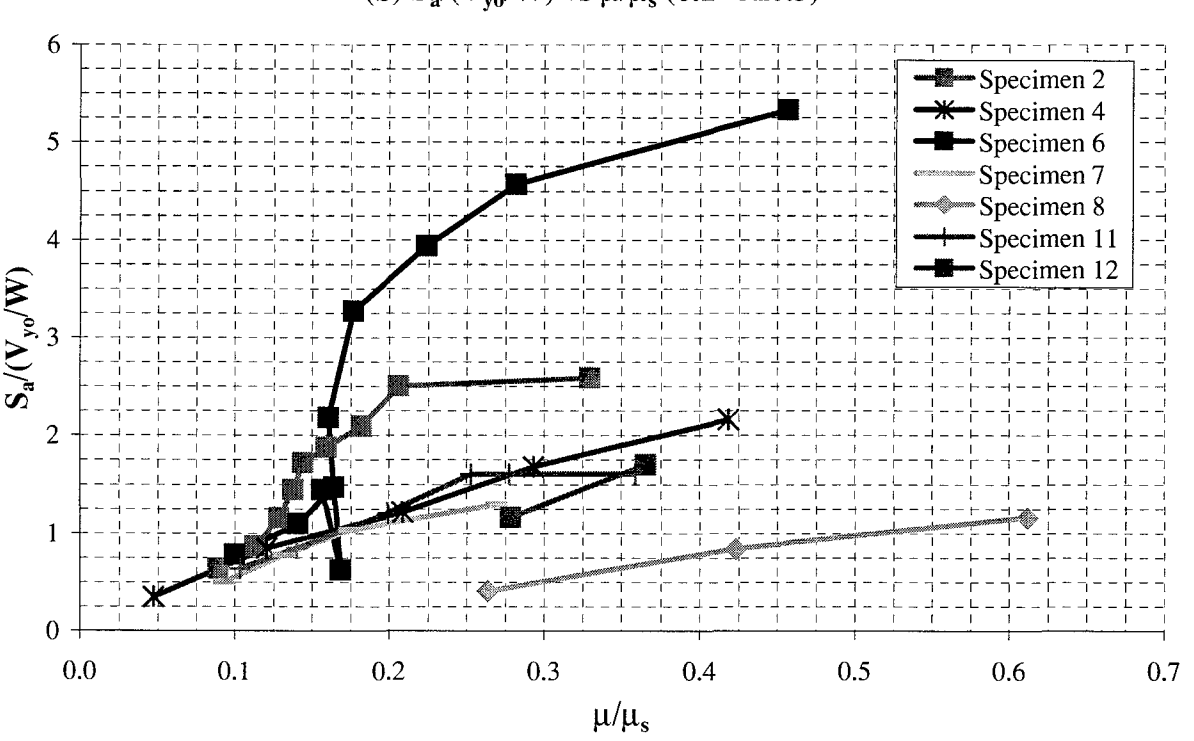

FIGURE C-8 Normalized Spectral Acceleration vs. Normalized Ductility

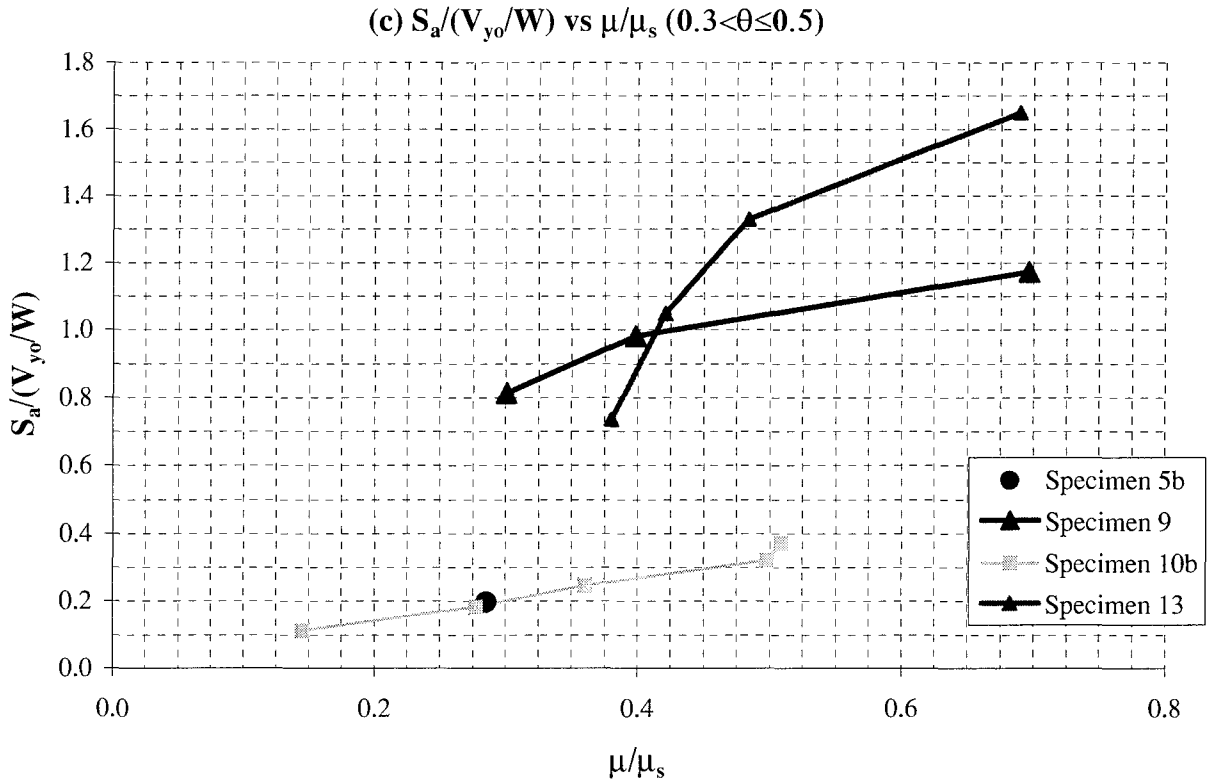

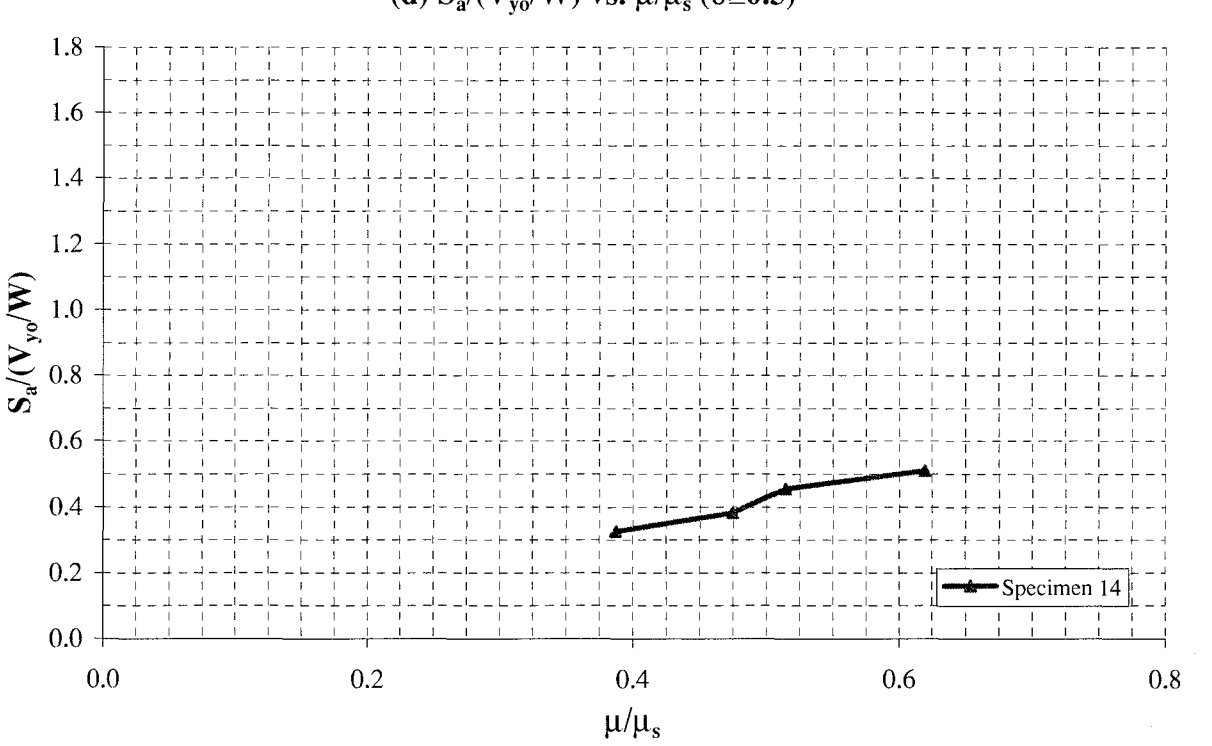

FIGURE C-8 (cont'd) Normalized Spectral Acceleration vs. Normalized Ductility

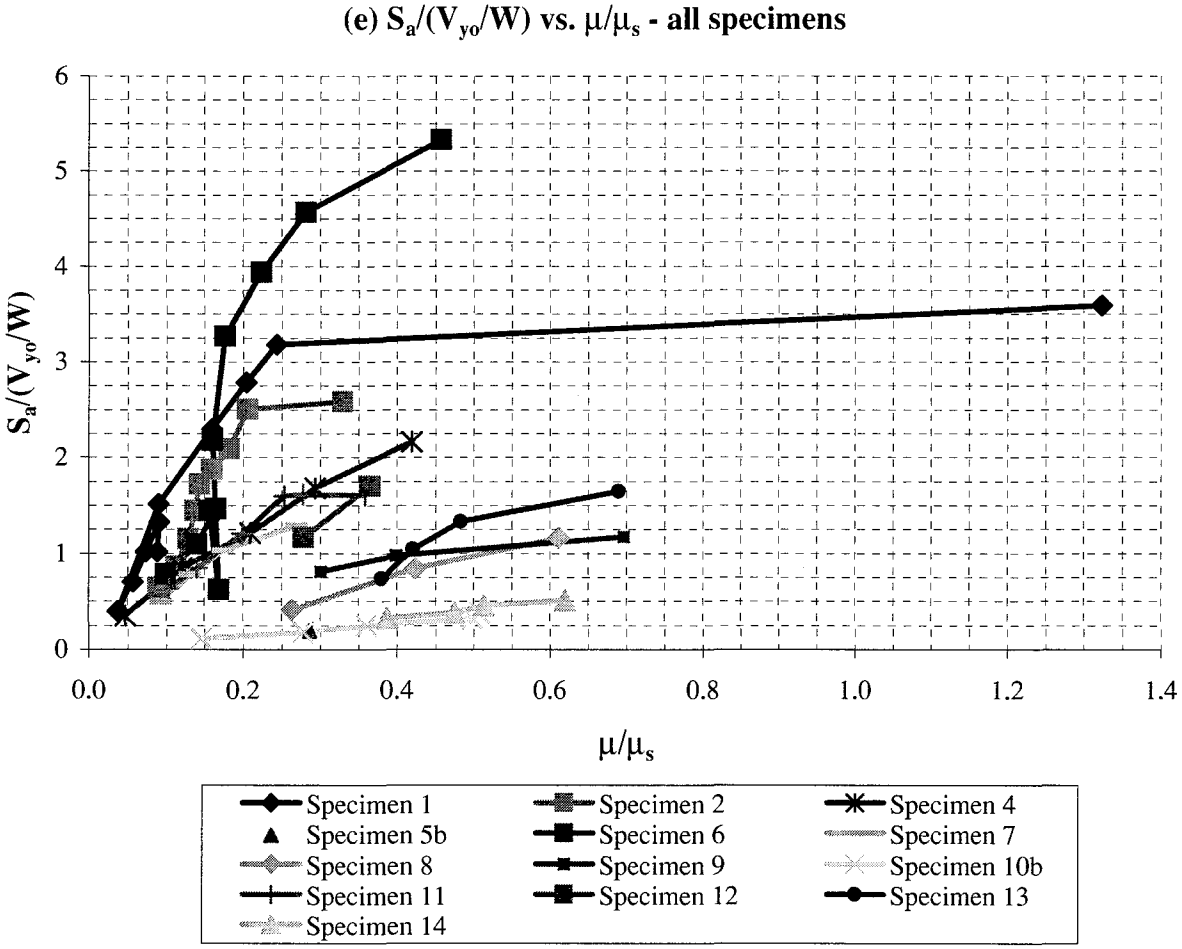

FIGURE C-8 (cont'd) Normalized Spectral Acceleration vs. Normalized Ductility

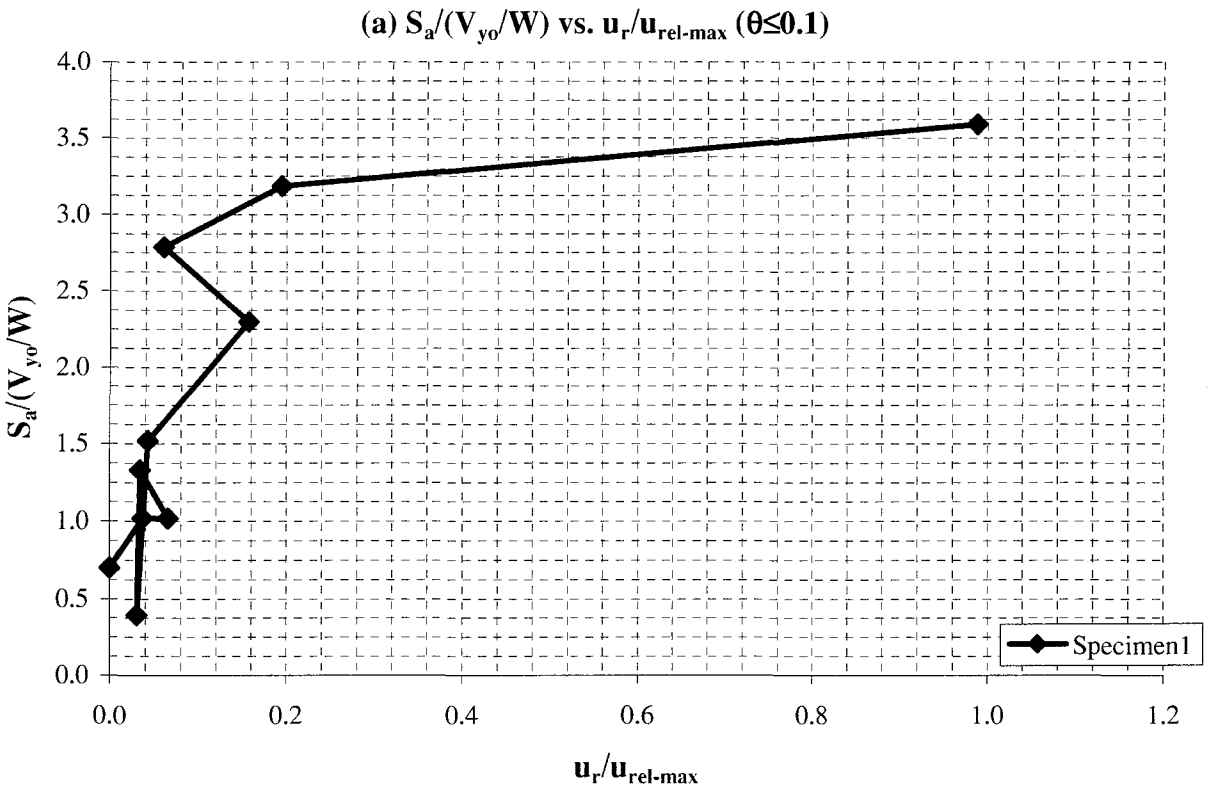

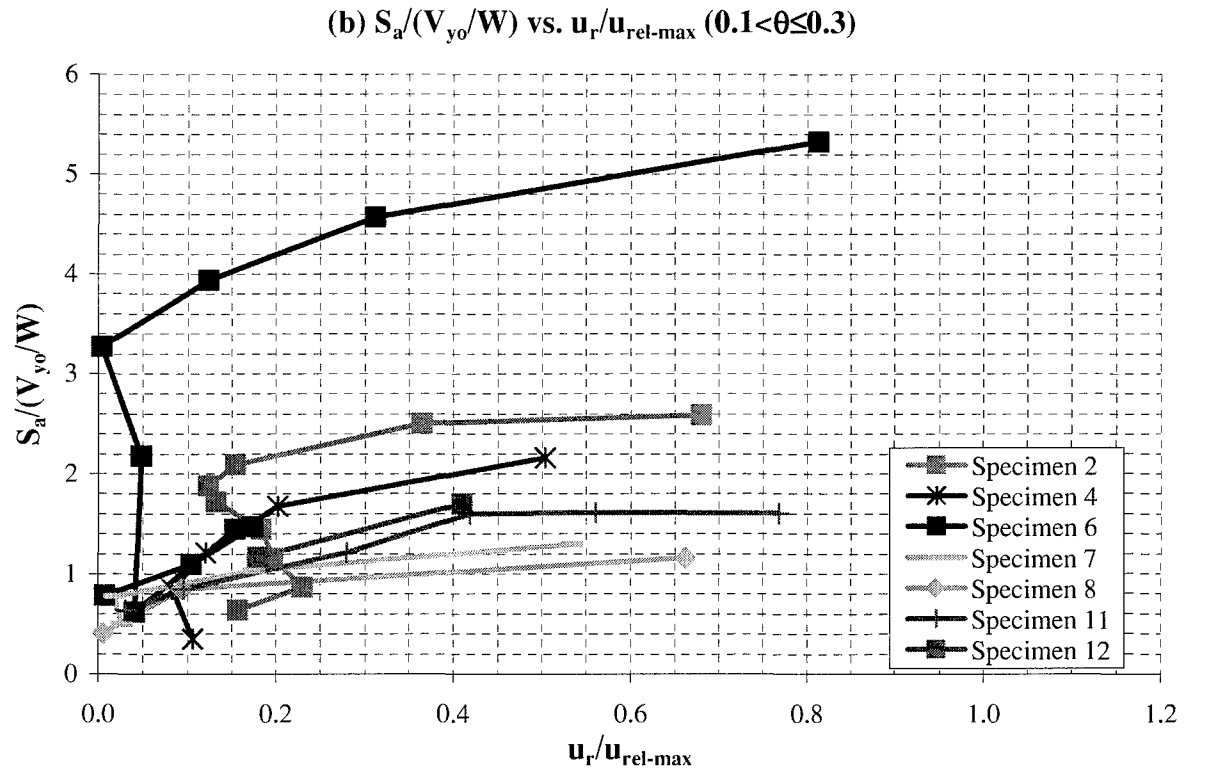

FIGURE C-9 Normalized Spectral Acceleration vs. Displacement Ratio

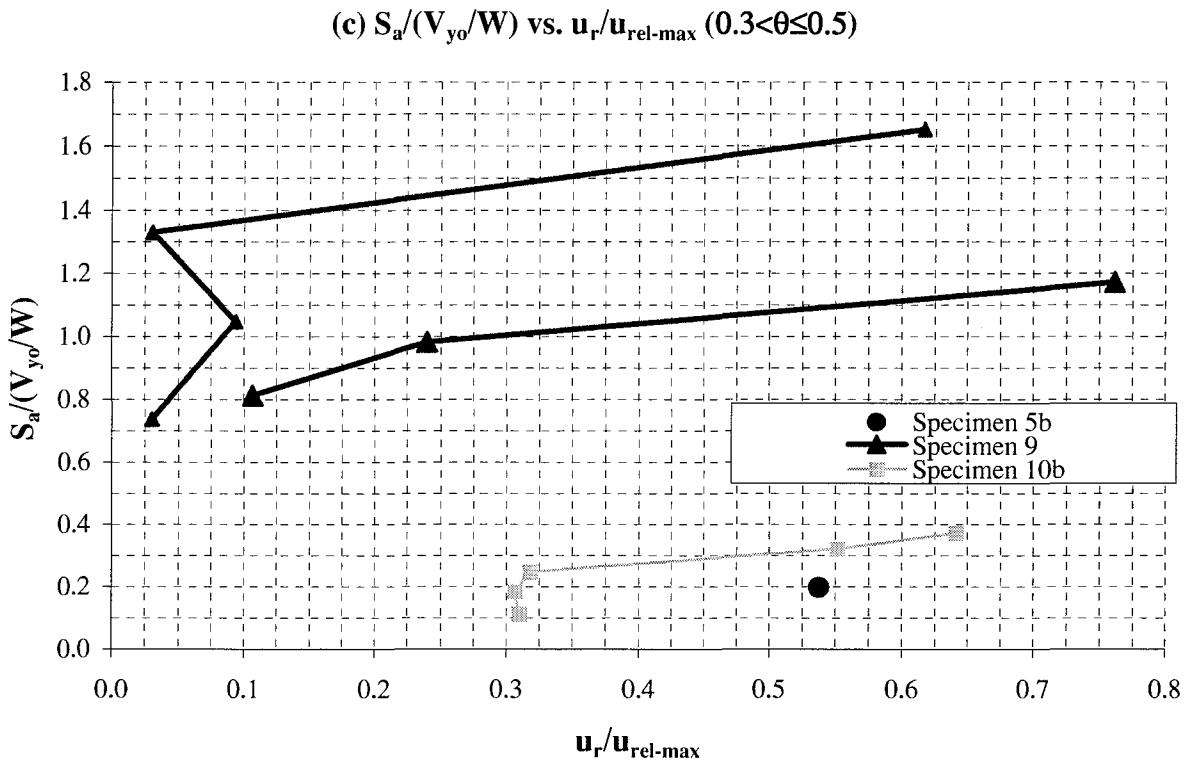

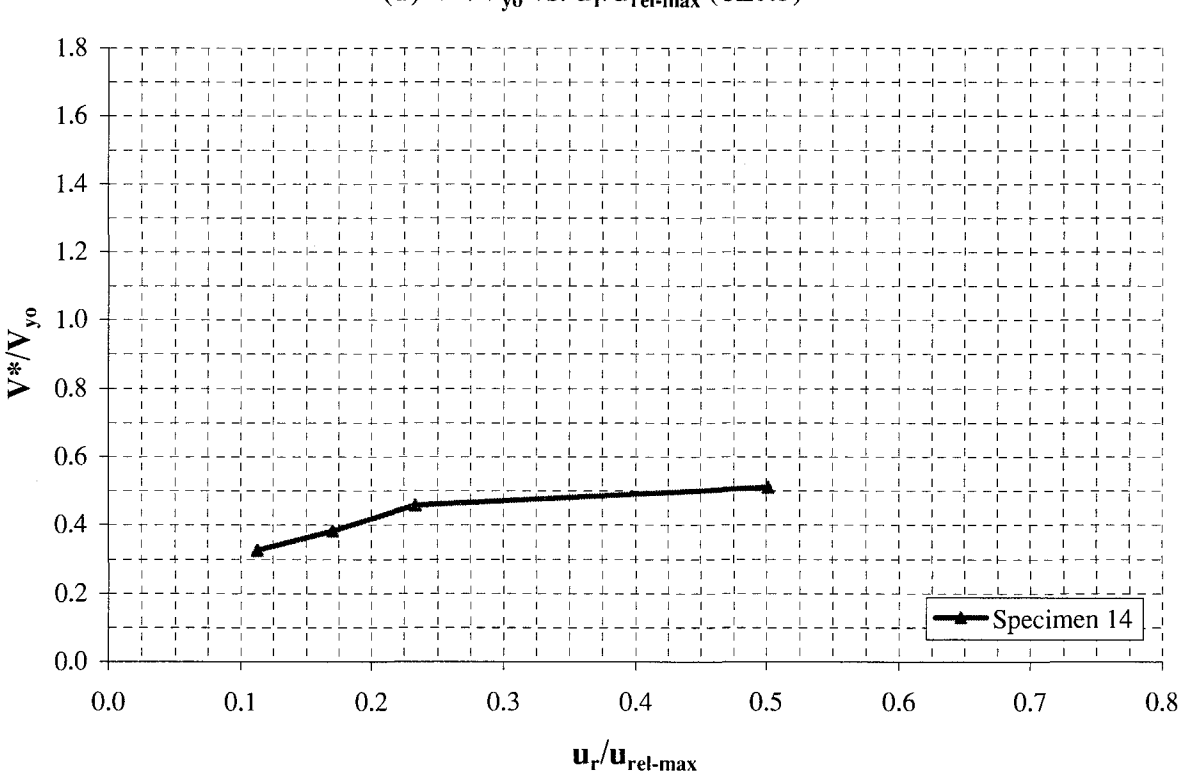

FIGURE C-9 (cont'd) Normalized Spectral Acceleration vs. Displacement Ratio

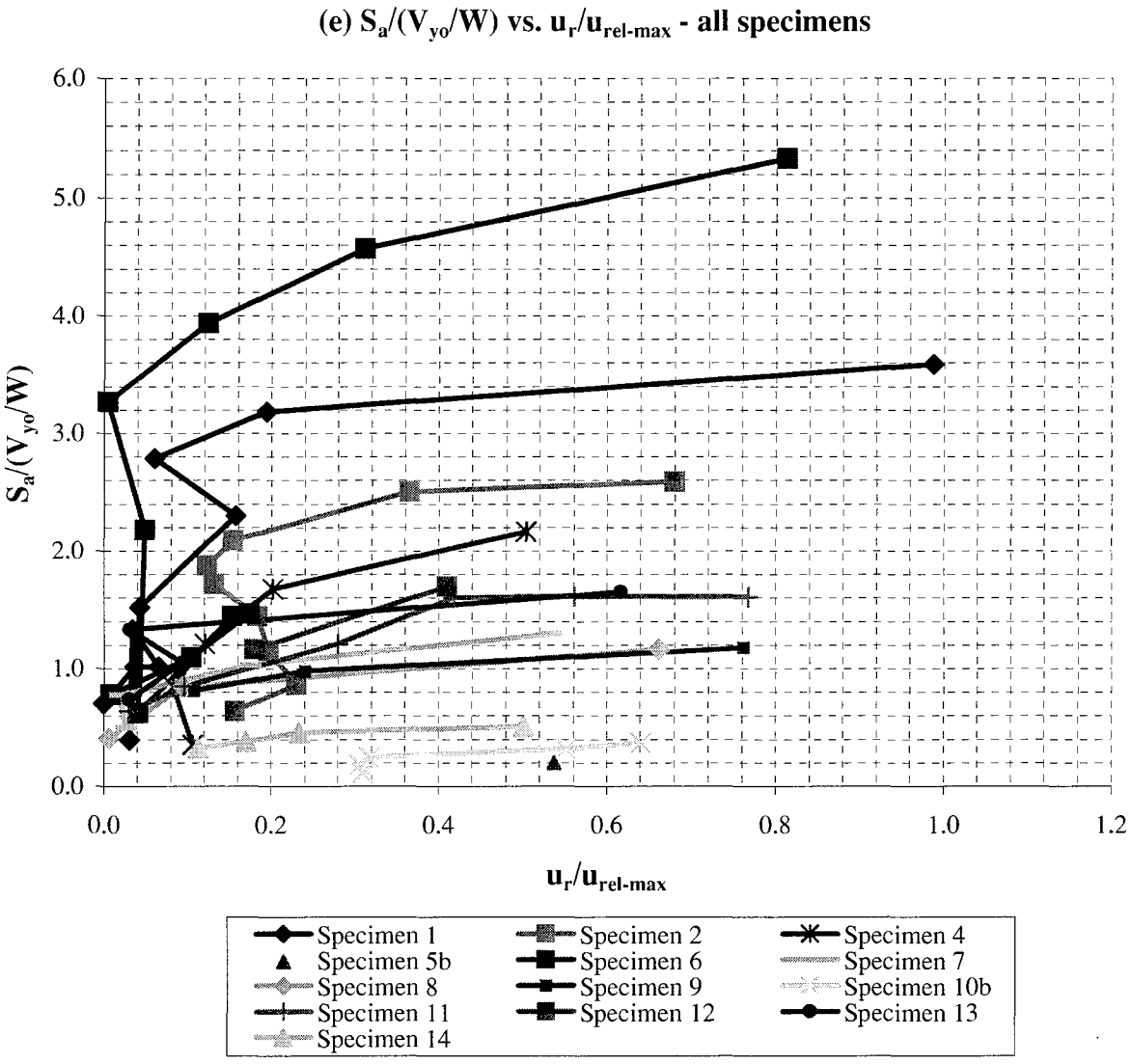

FIGURE C-9 (cont'd) Normalized Spectral Acceleration vs. Displacement Ratio

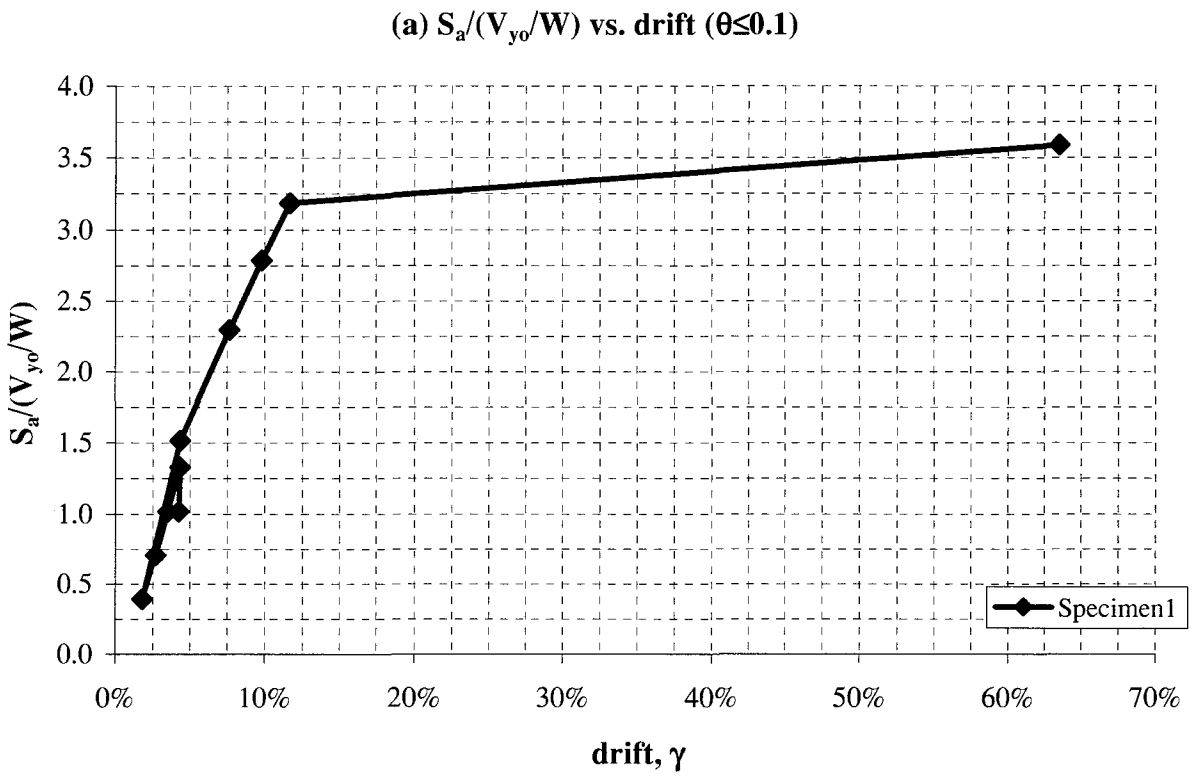

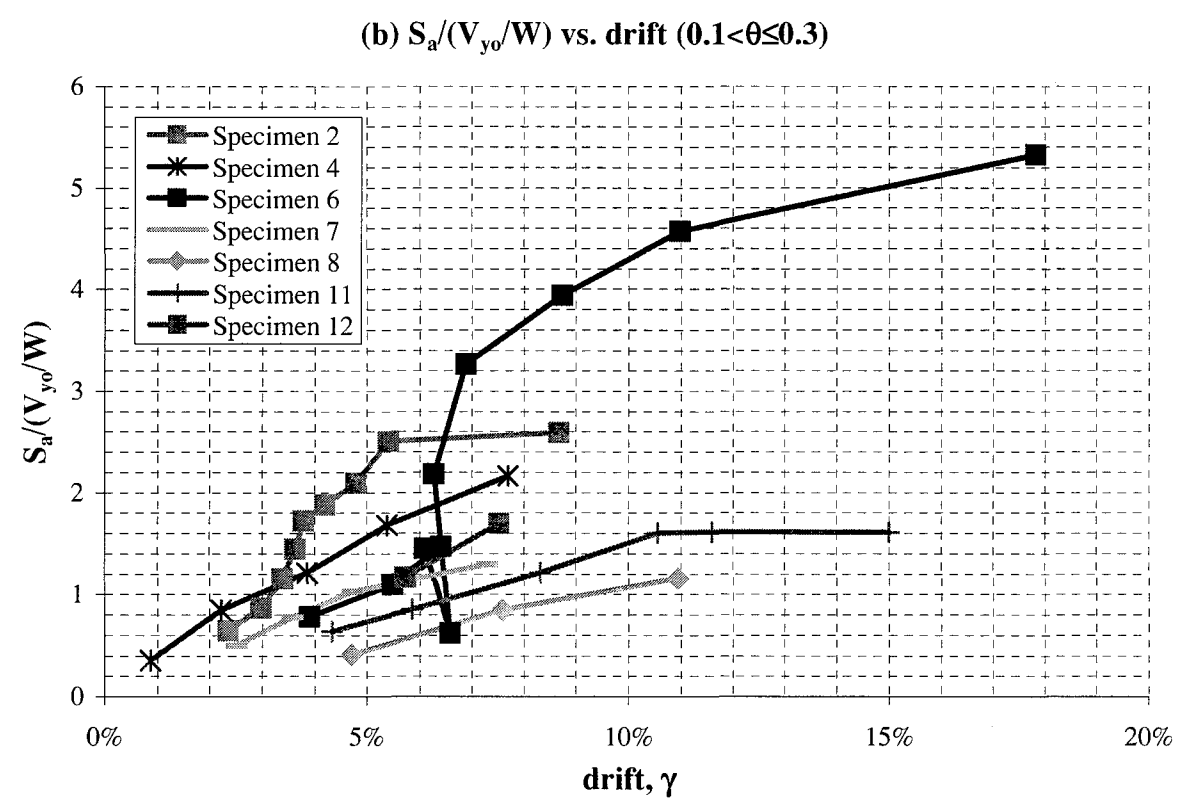

FIGURE C-10 Normalized Spectral Acceleration vs. Drift

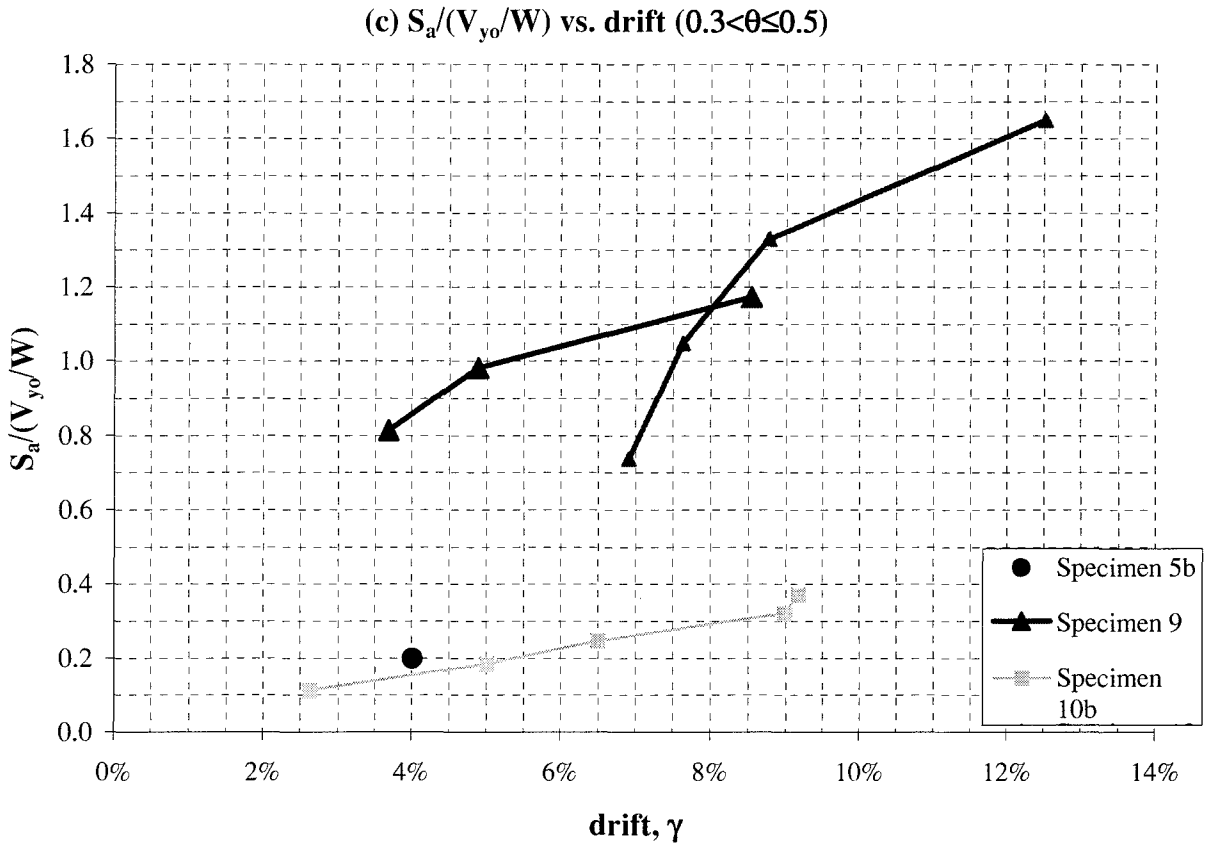

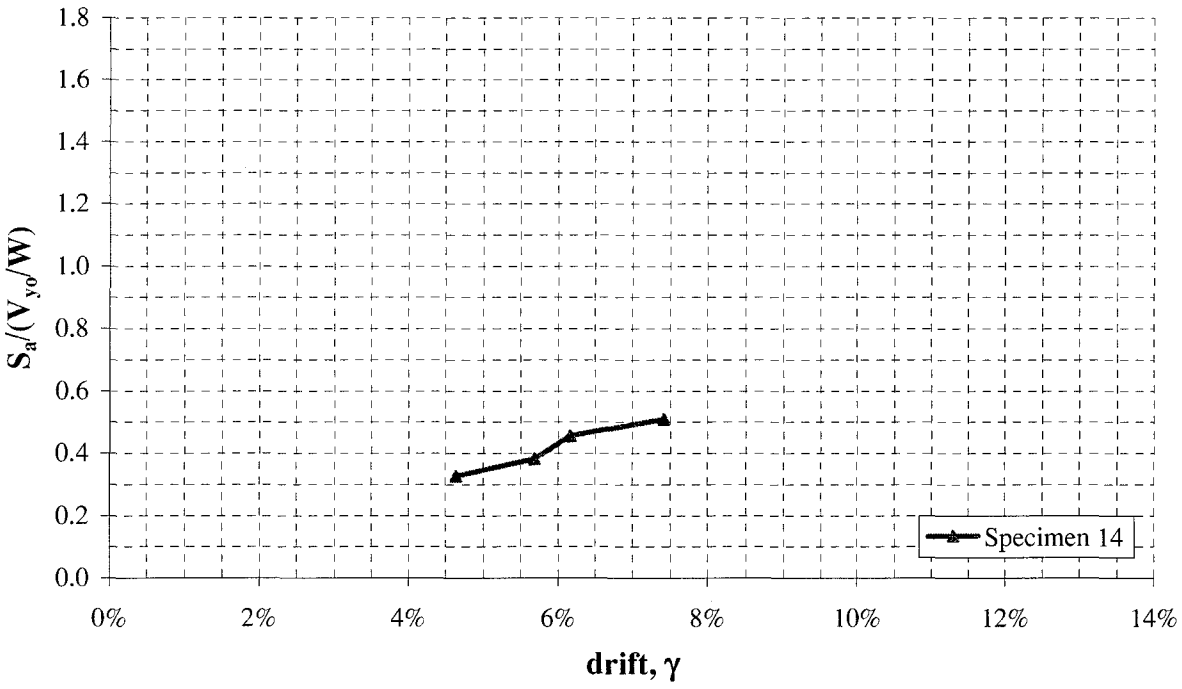

FIGURE C-10 (cont'd) Normalized Spectral Acceleration vs. Drift

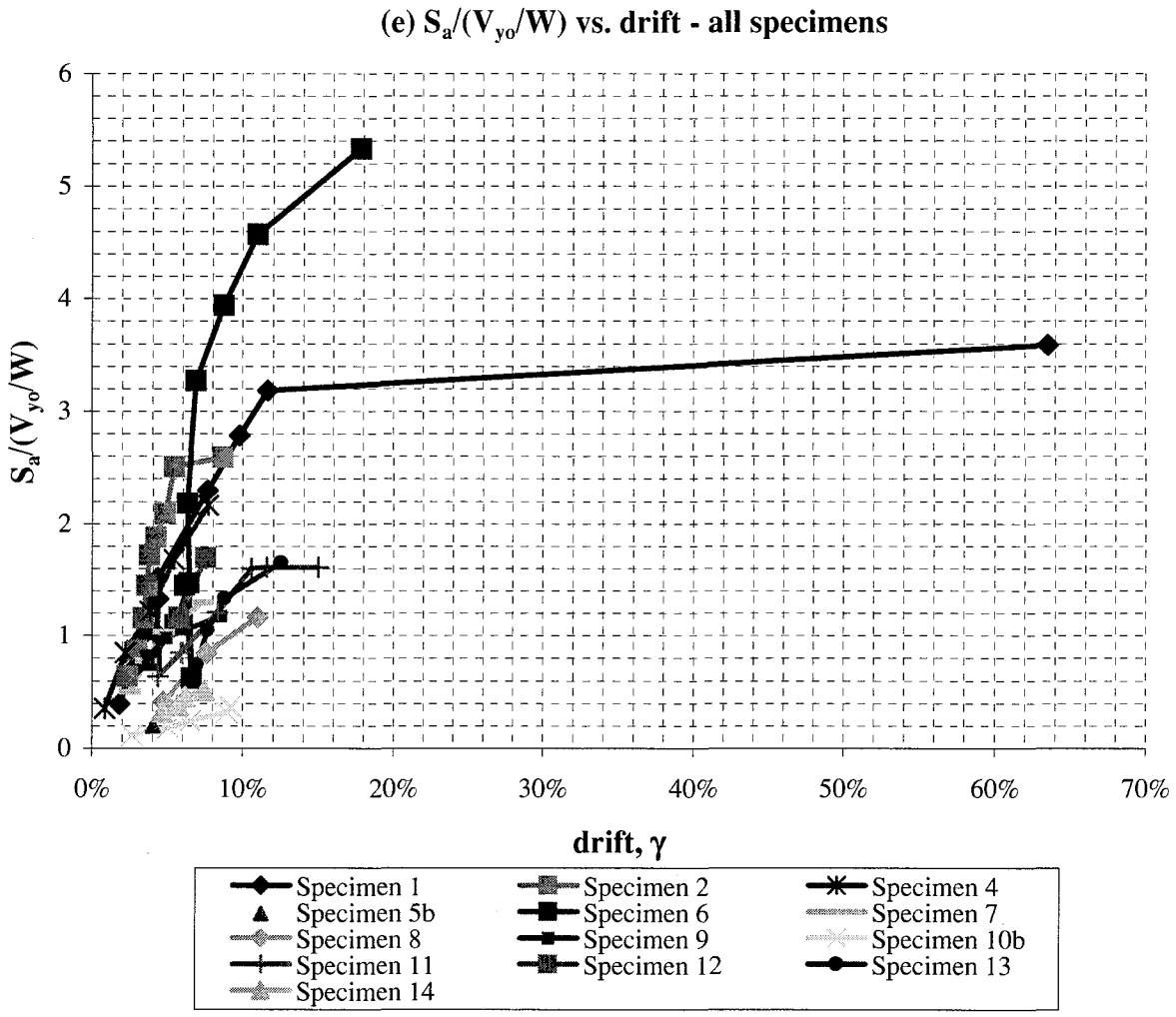

FIGURE C-10 (cont'd) Normalized Spectral Acceleration vs. Drift

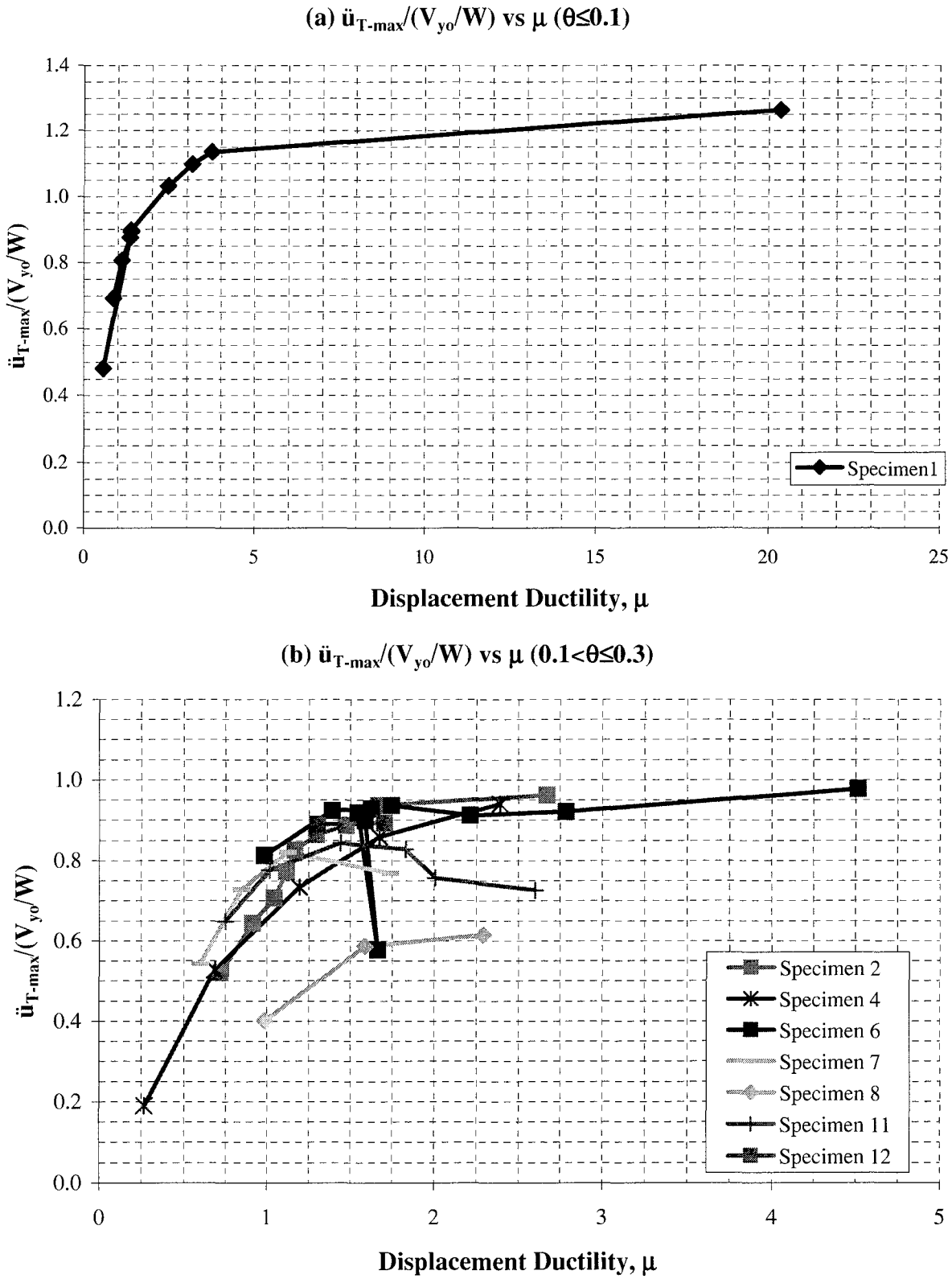

FIGURE C-11 Normalized Absolute Acceleration vs. Displacement Ductility

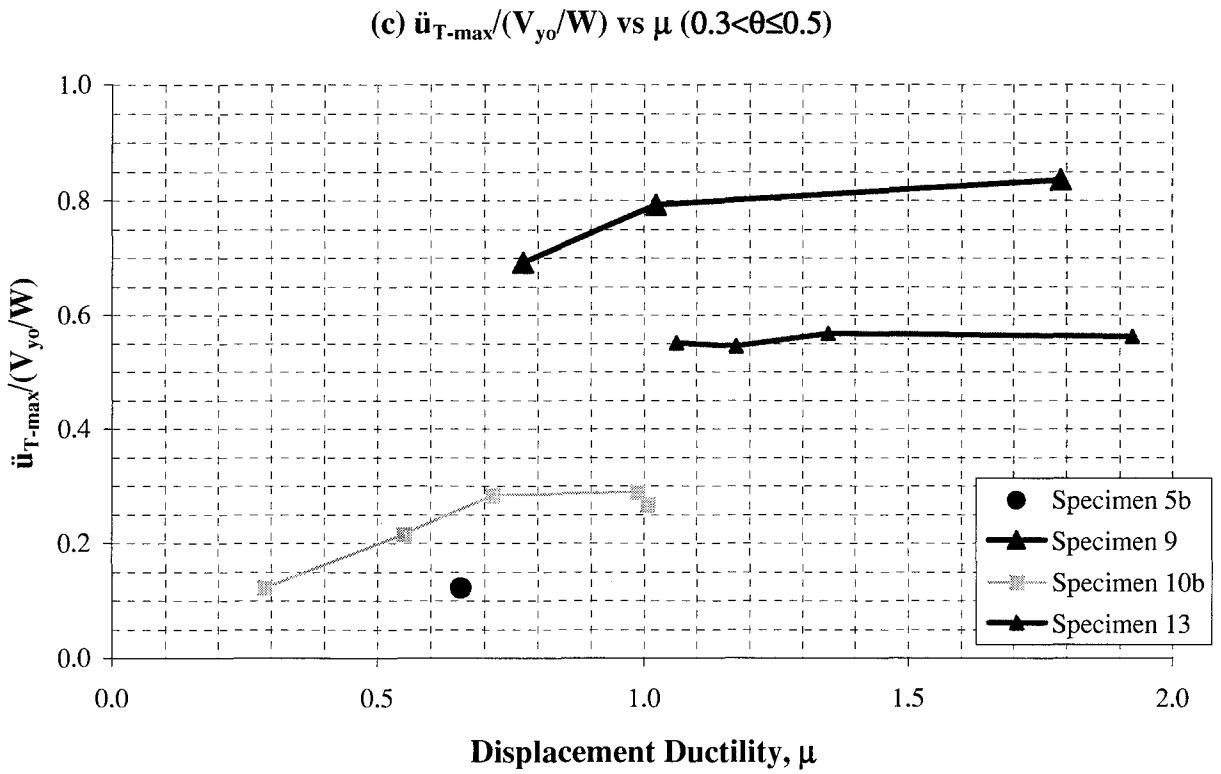

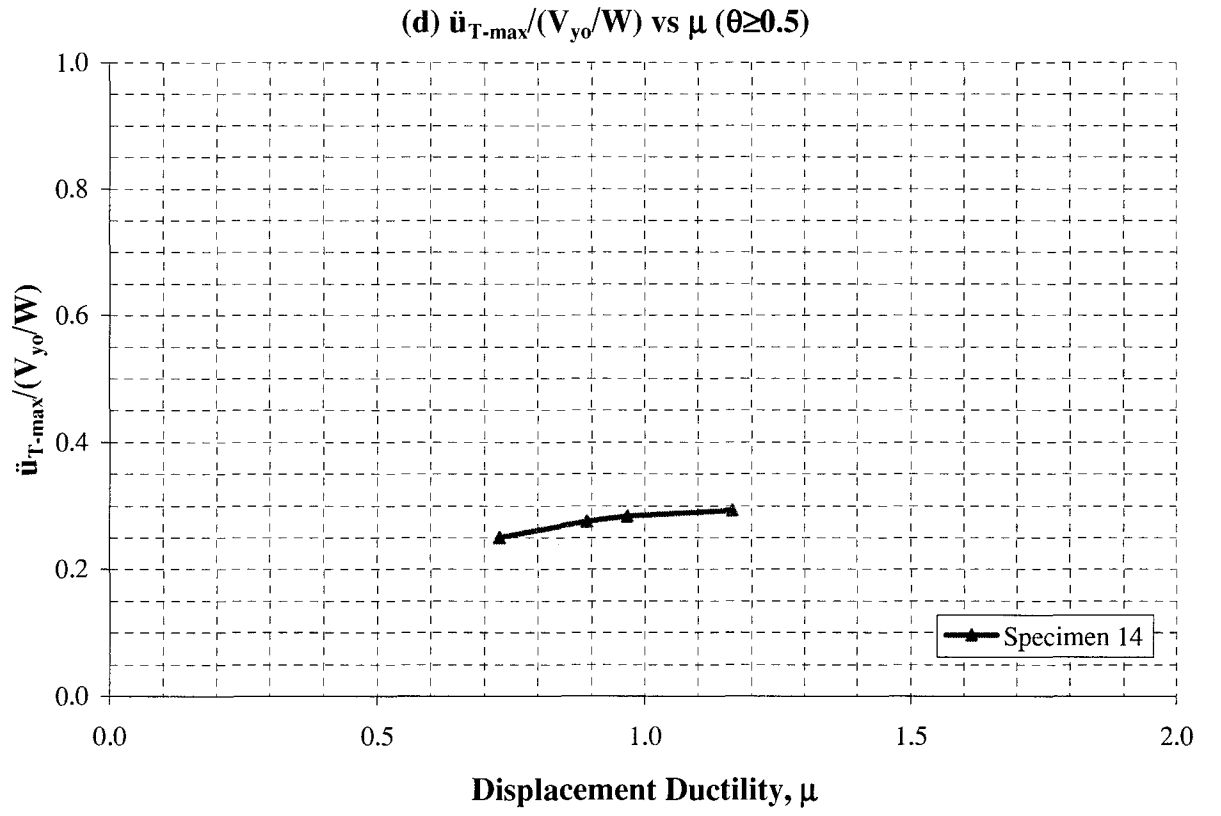

FIGURE C-11 (cont'd) Normalized Absolute Acceleration vs. Displacement Ductility

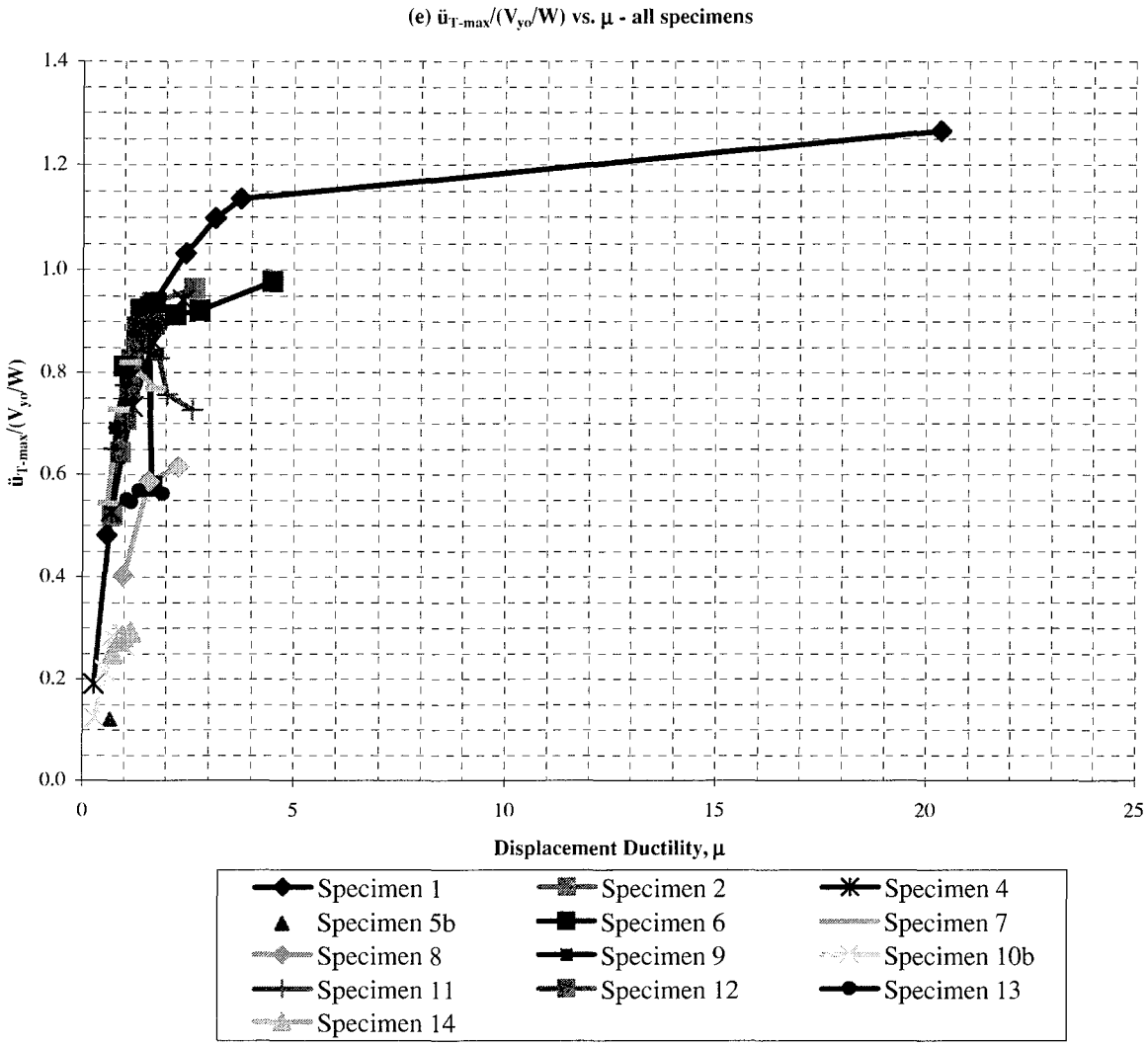

FIGURE C-11 (cont'd) Normalized Absolute Acceleration vs. Displacement Ductility

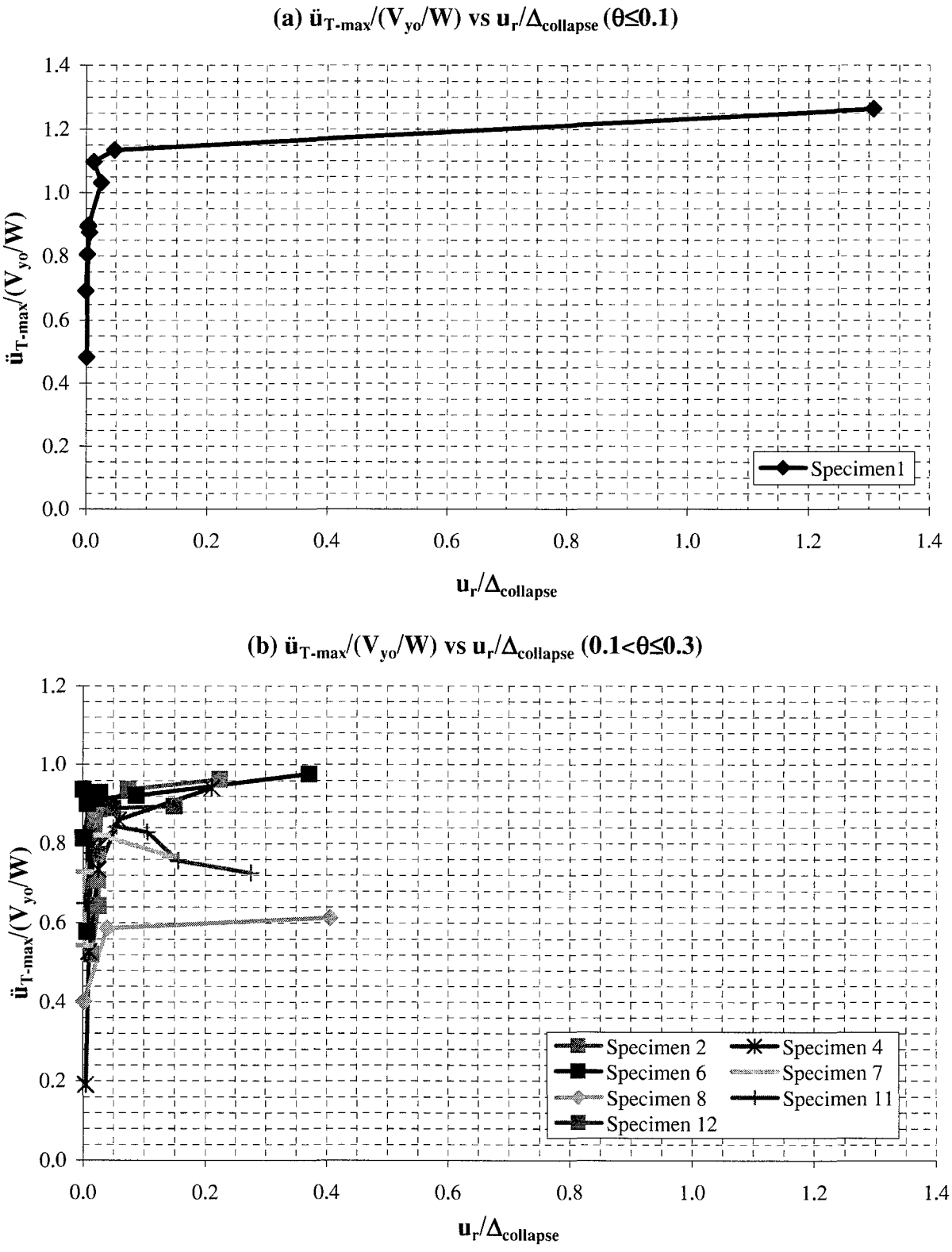

FIGURE C-12 Normalized Absolute Acceleration vs. Normalized Residual Displacement

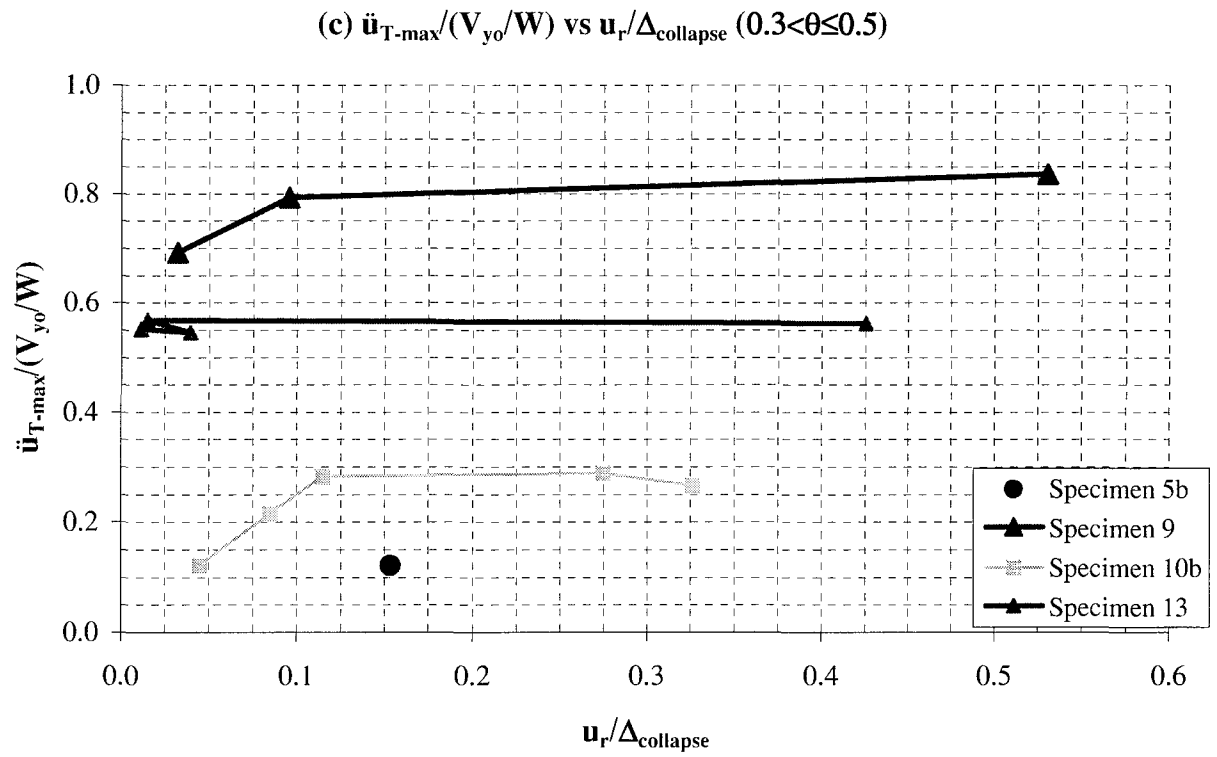

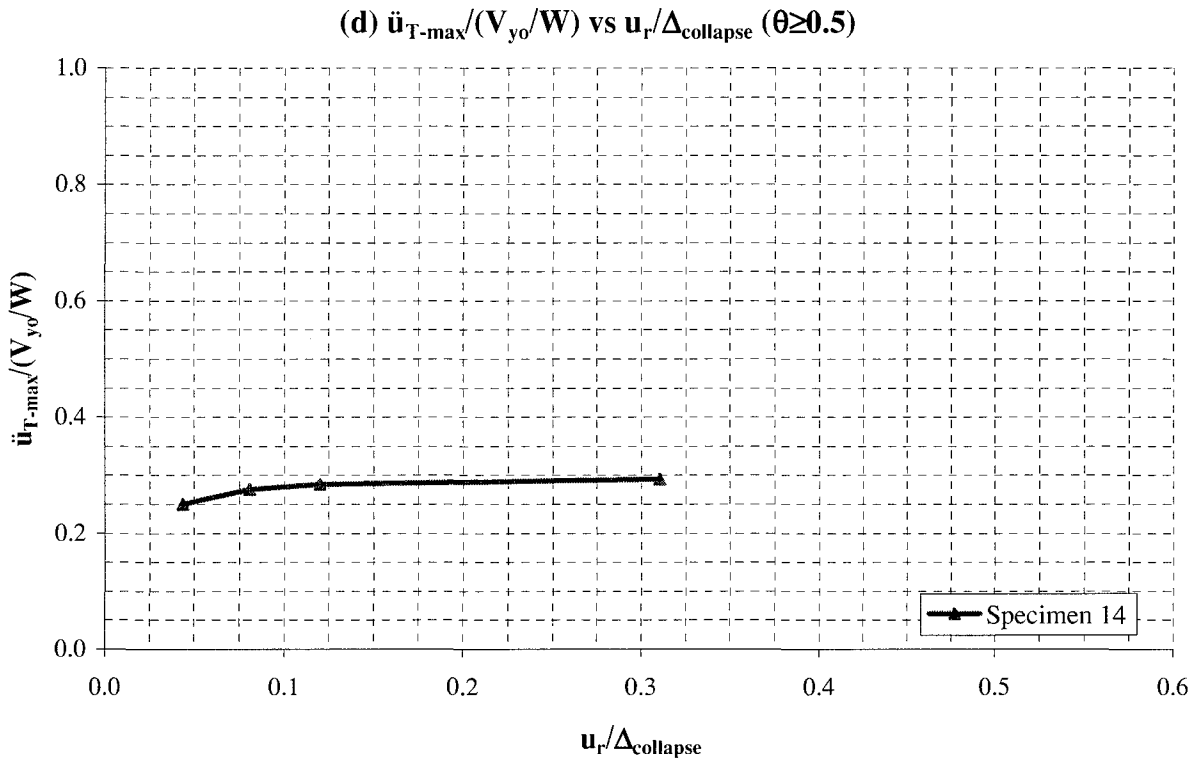

FIGURE C-12 (cont'd) Normalized Absolute Acceleration vs. Normalized Residual Displacement

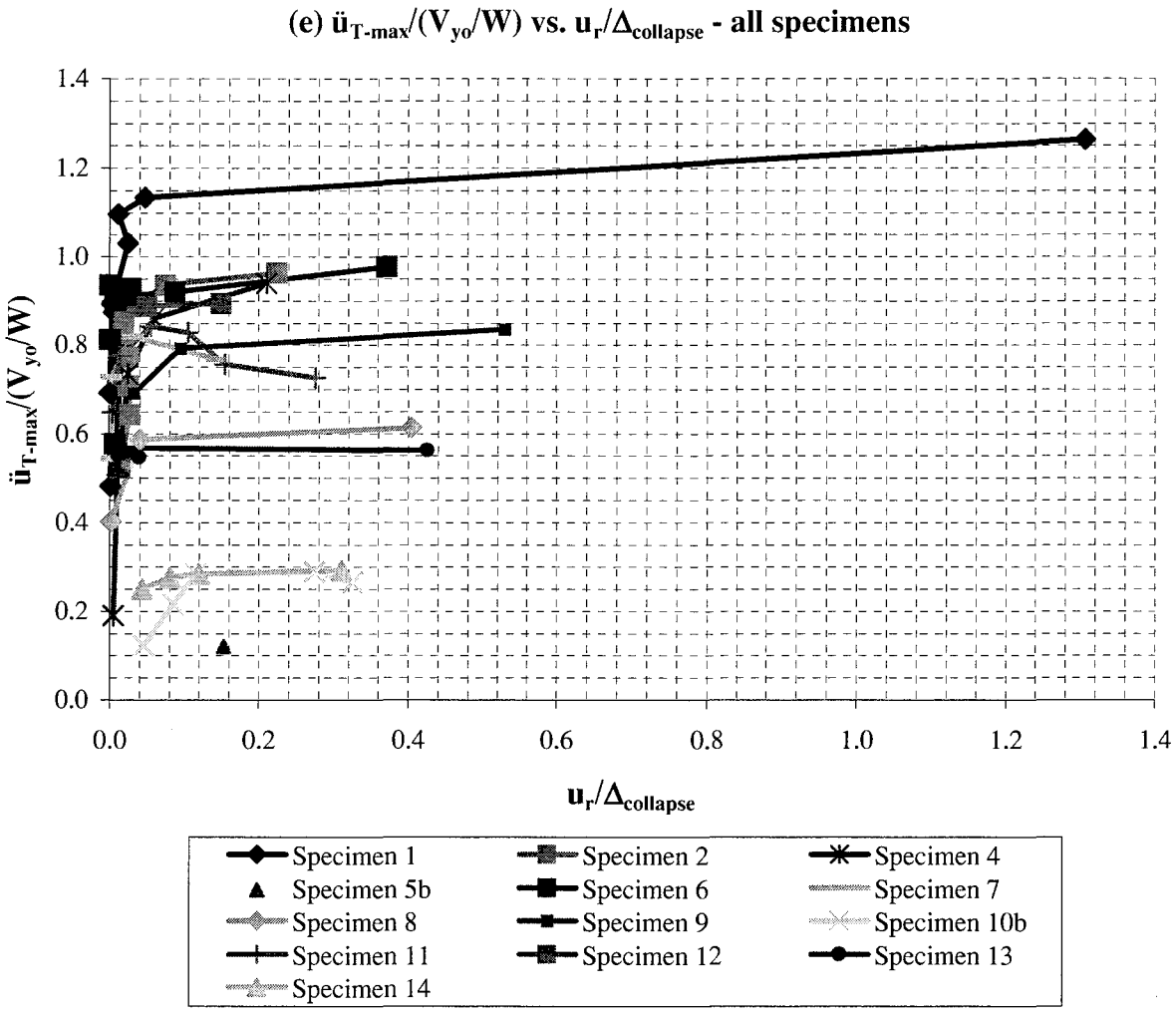

FIGURE C-12 (cont'd) Normalized Absolute Acceleration vs. Normalized Residual Displacement

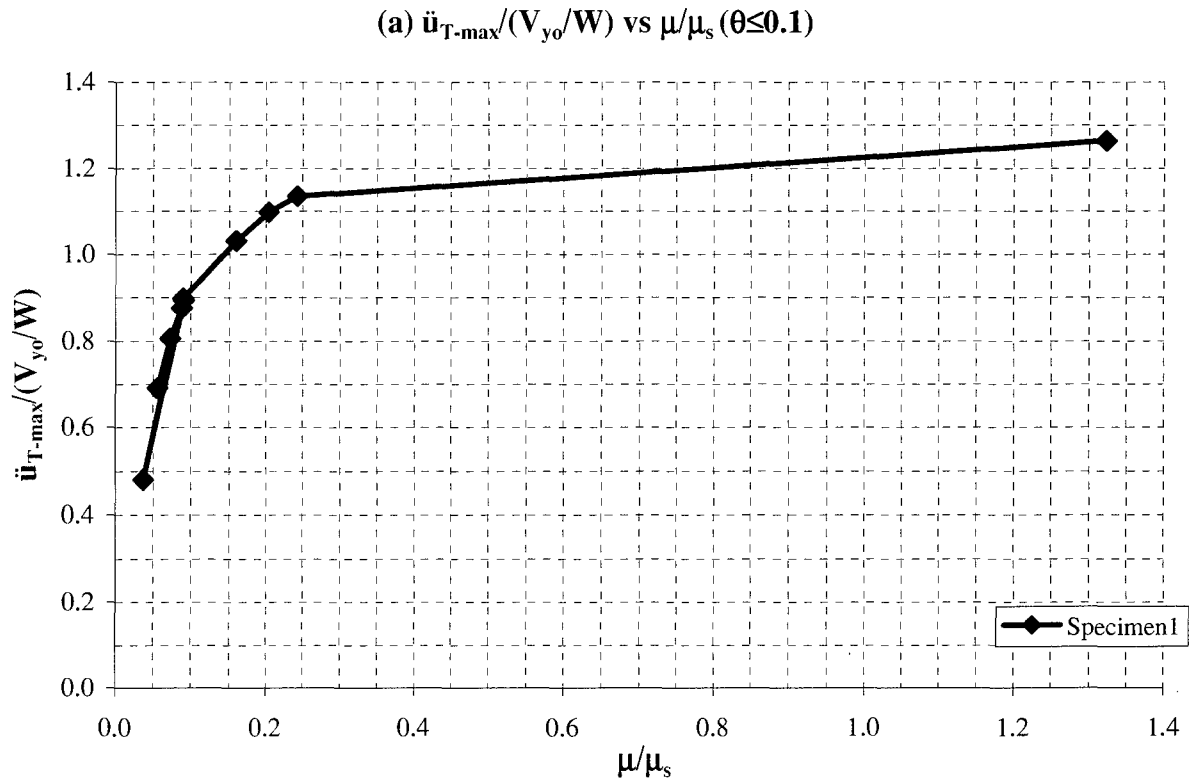

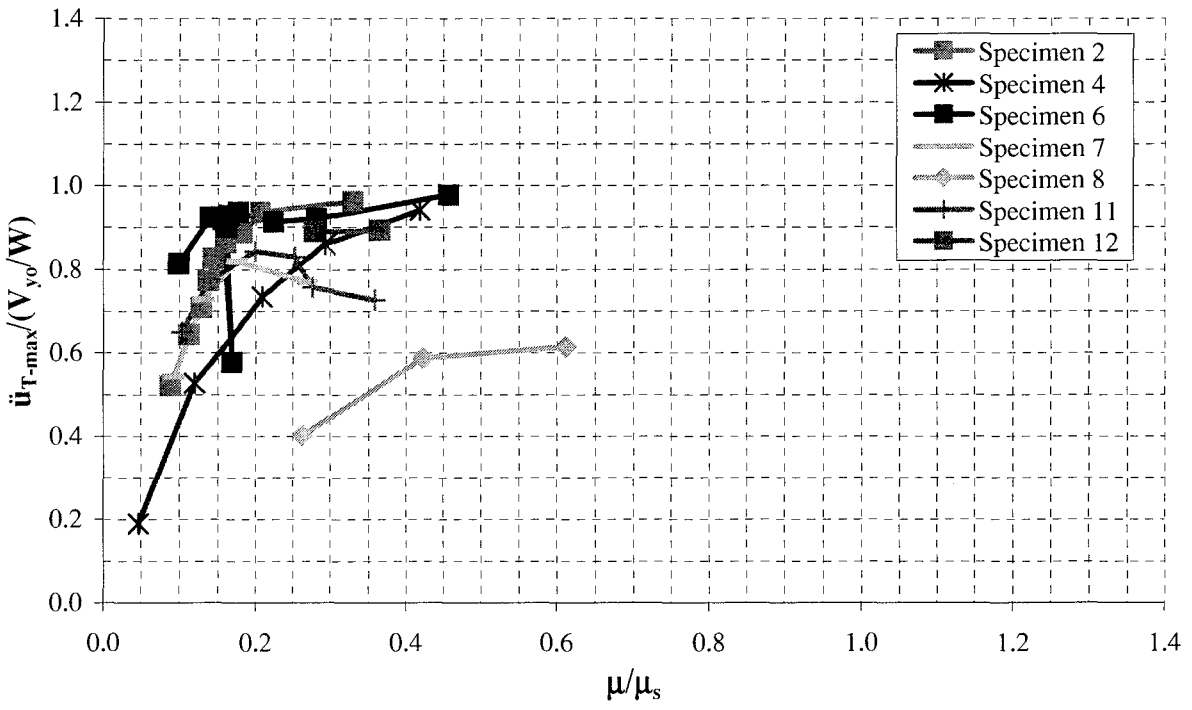

FIGURE C-13 Normalized Absolute Acceleration vs. Normalized Ductility

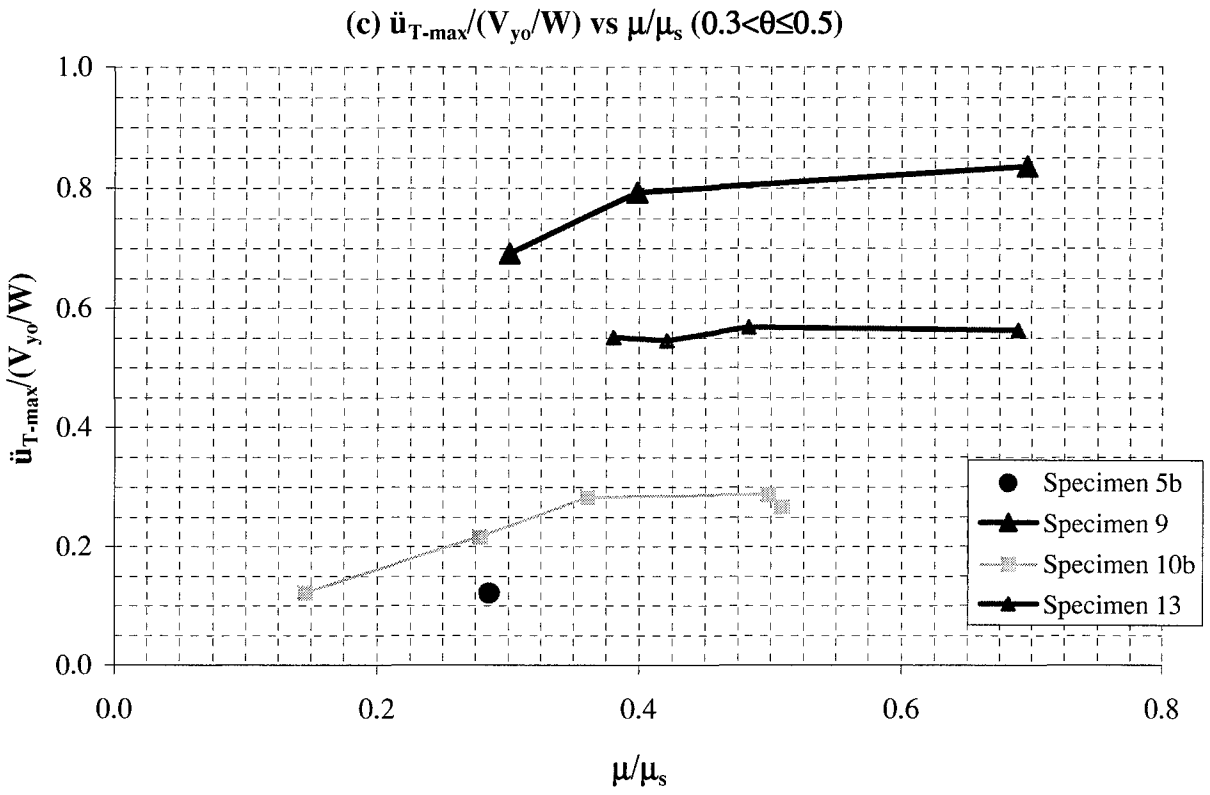

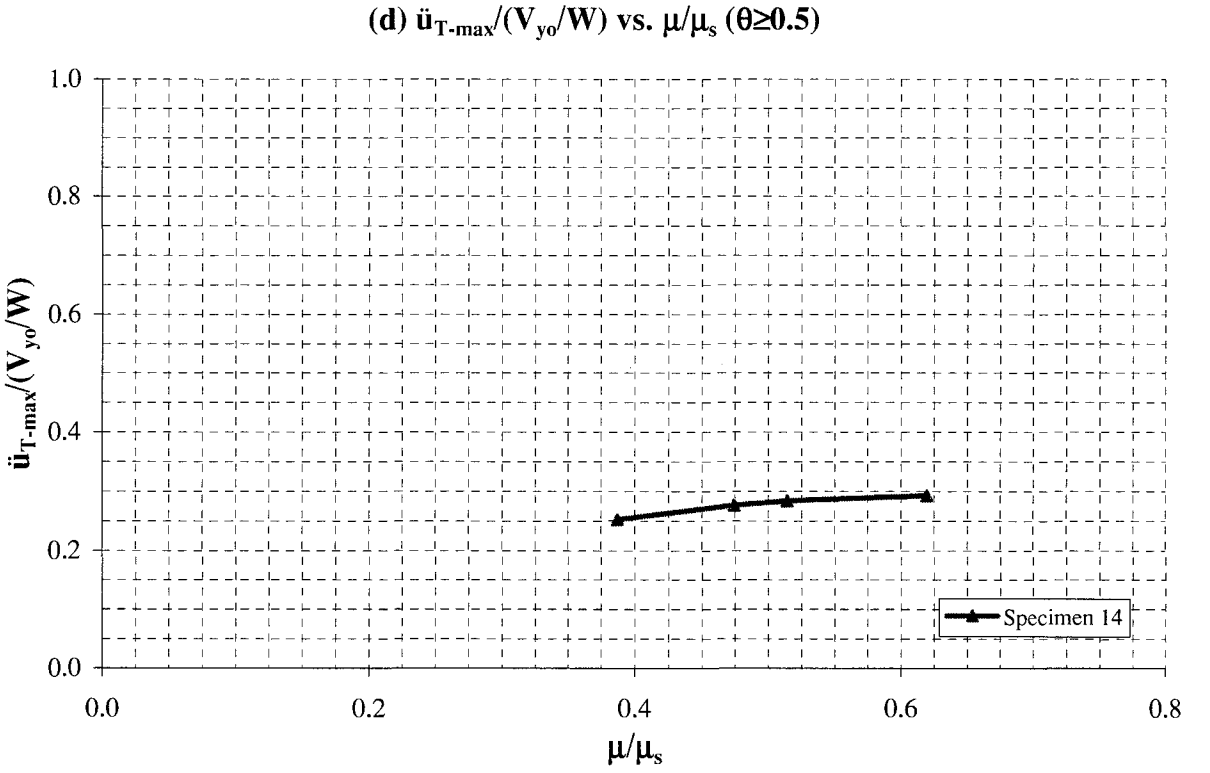

FIGURE C-13 (cont'd) Normalized Absolute Acceleration vs. Normalized Ductility

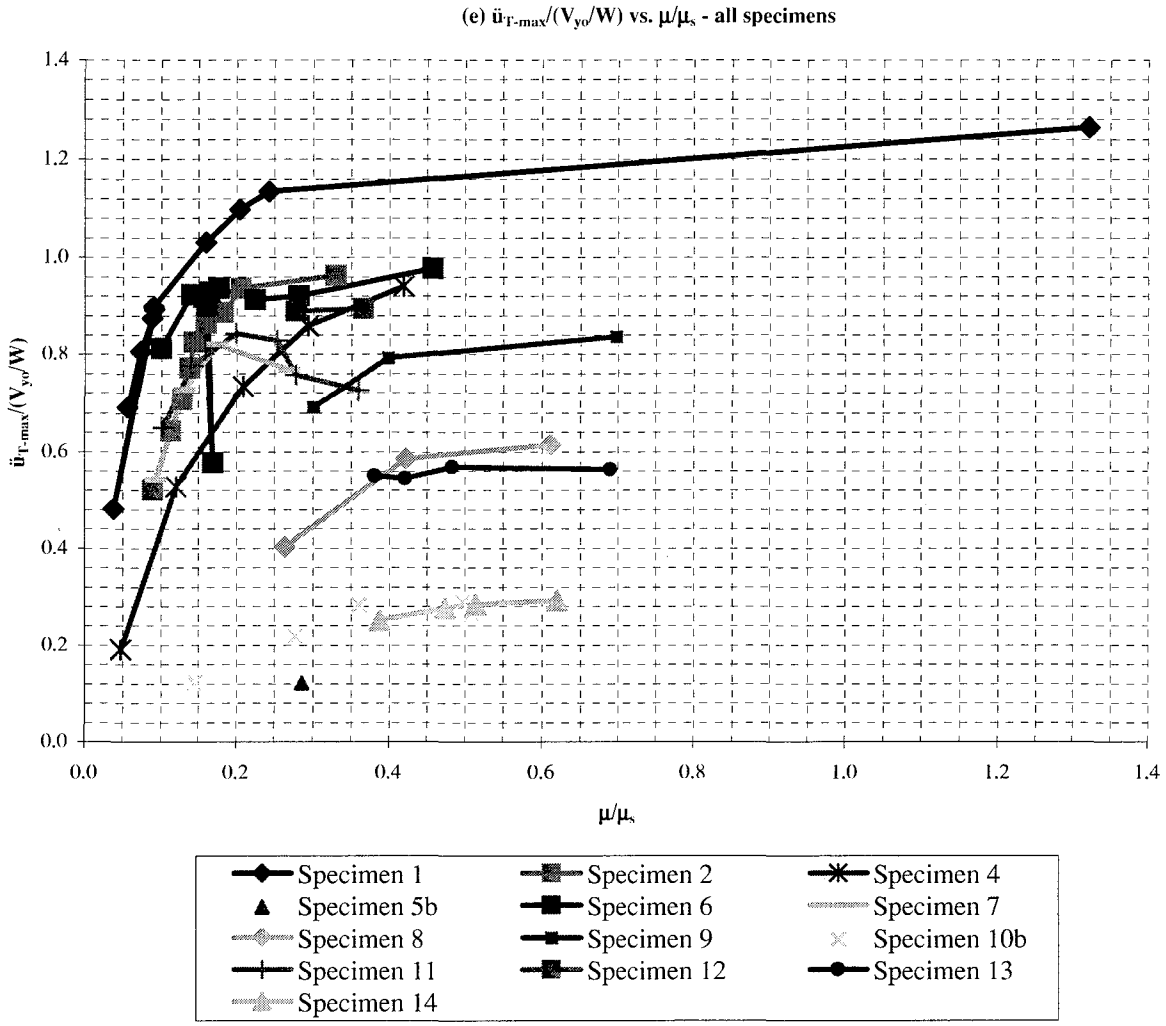

FIGURE C-13 (cont'd) Normalized Absolute Acceleration vs. Normalized Ductility

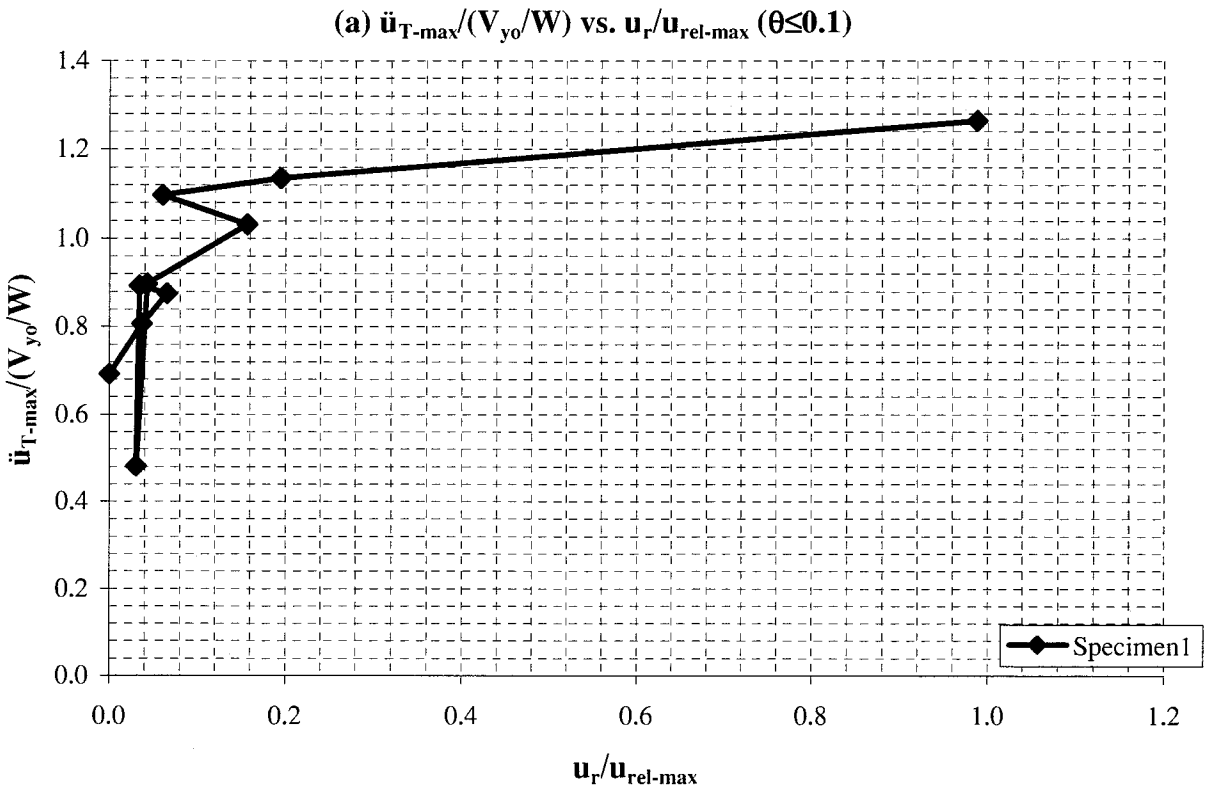

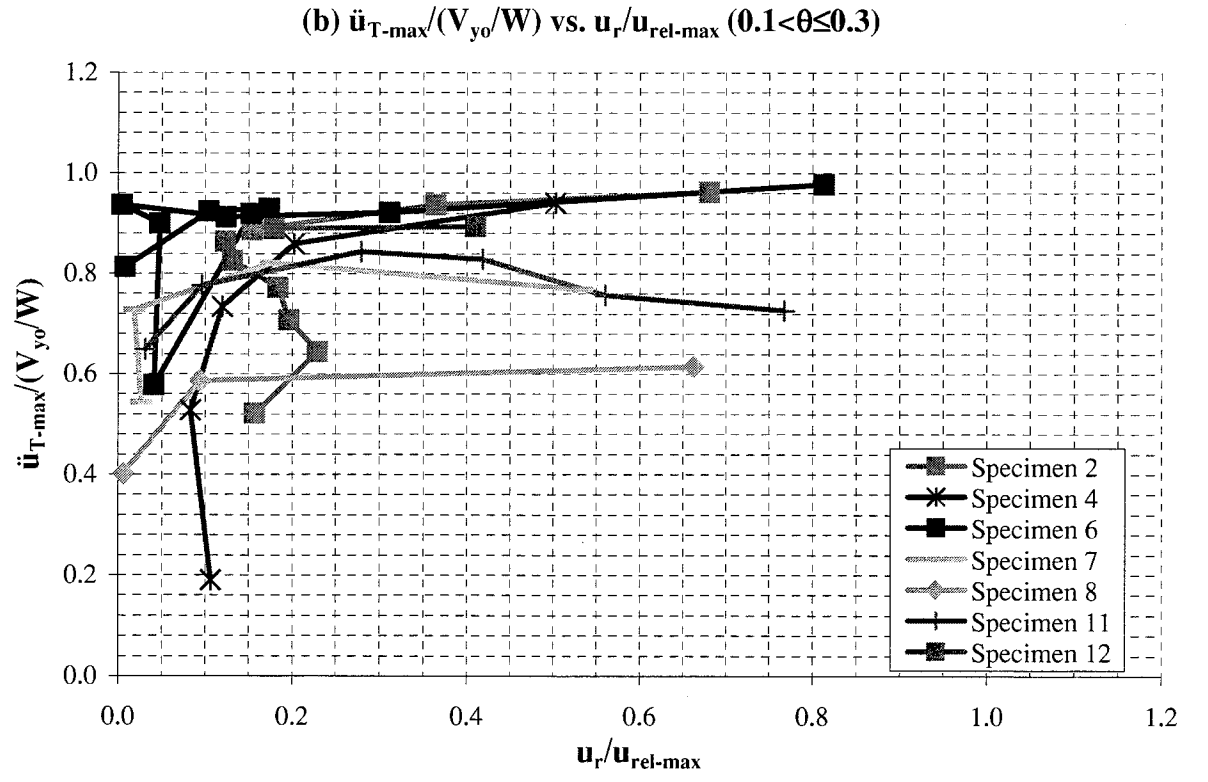

FIGURE C-14 Normalized Absolute Acceleration vs. Displacement Ratio

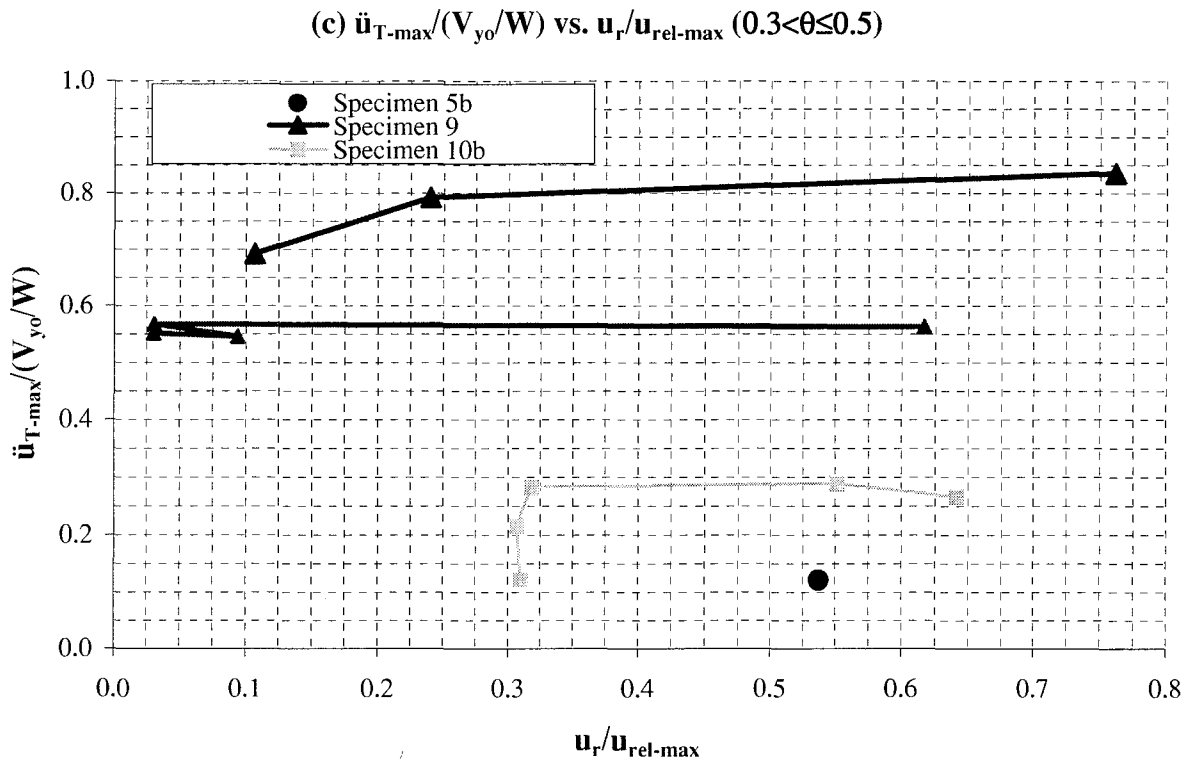

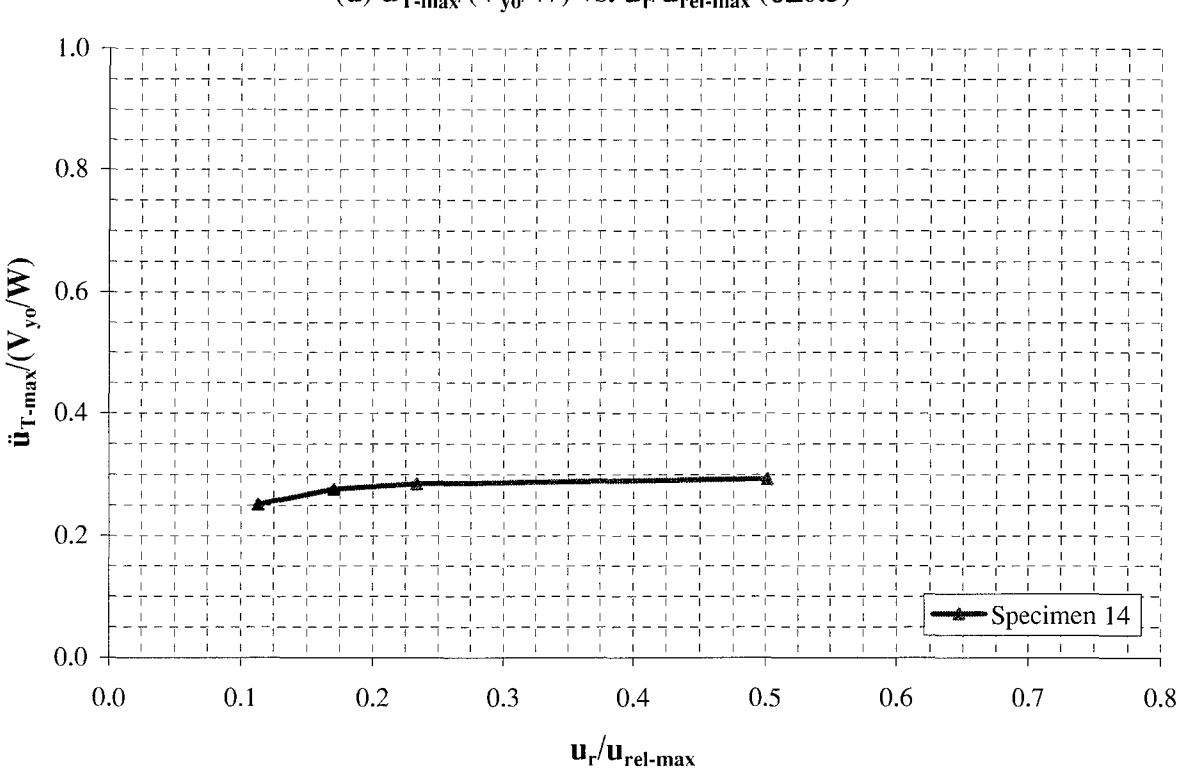

FIGURE C-14 (cont'd) Normalized Absolute Acceleration vs. Displacement Ratio

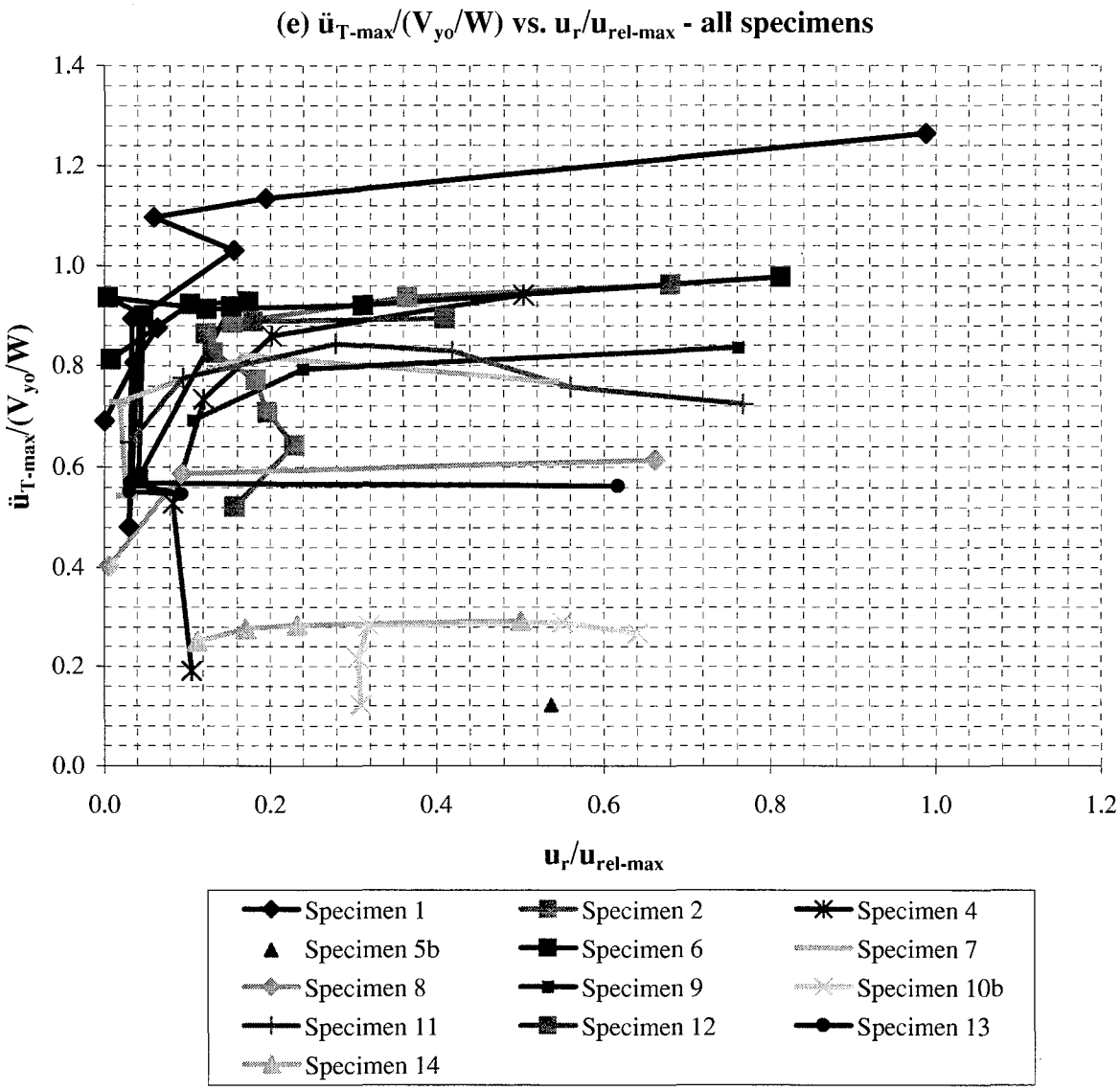

FIGURE C-14 (cont'd) Normalized Absolute Acceleration vs. Displacement Ratio

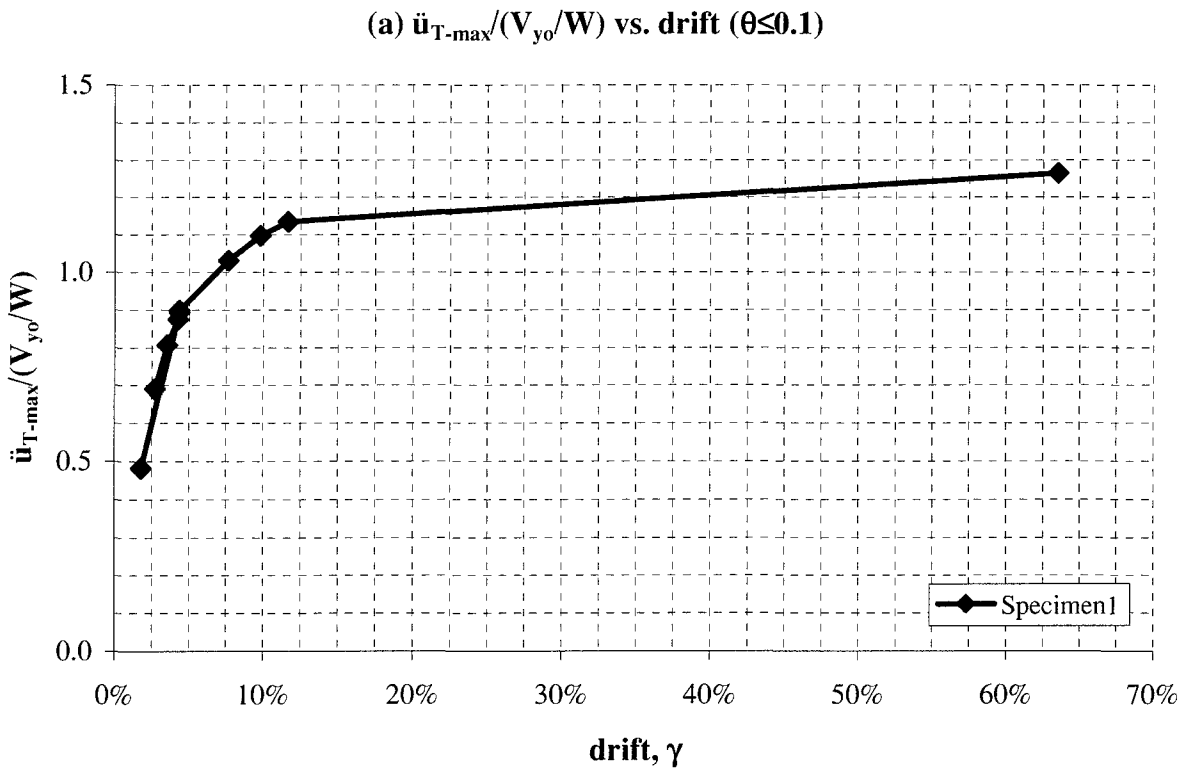

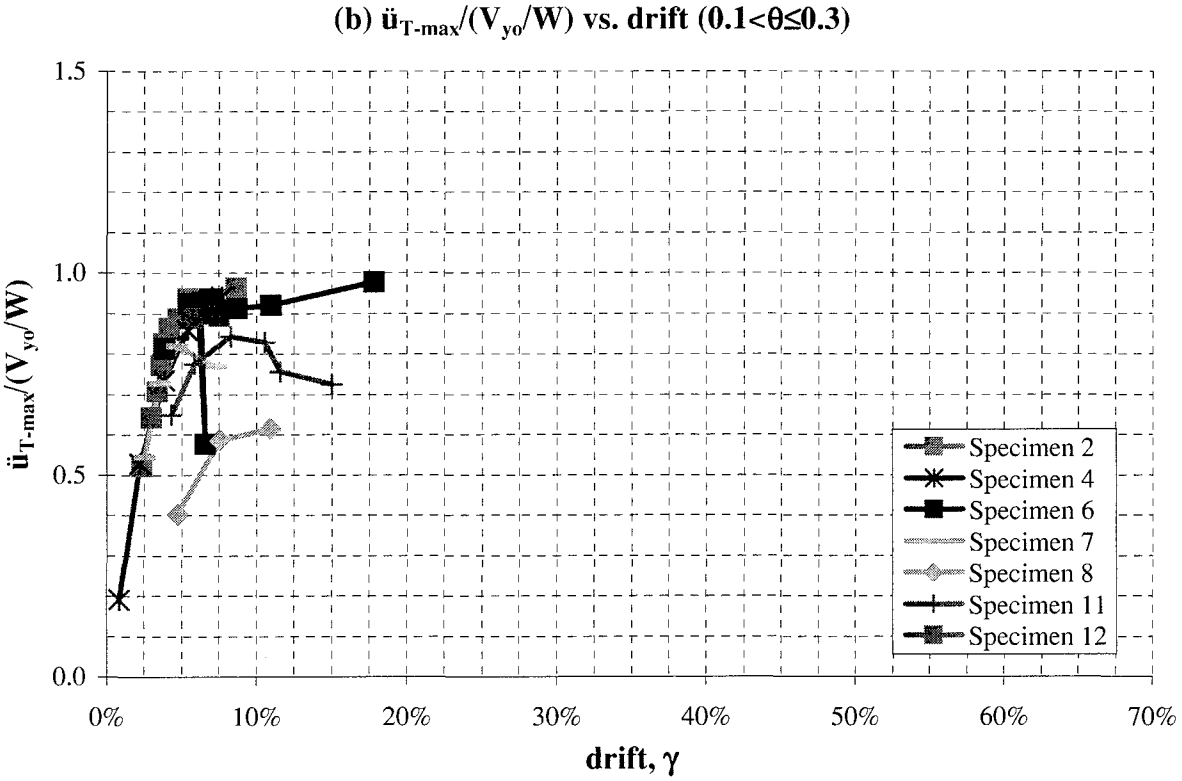

FIGURE C-15 Normalized Absolute Acceleration vs. Drift

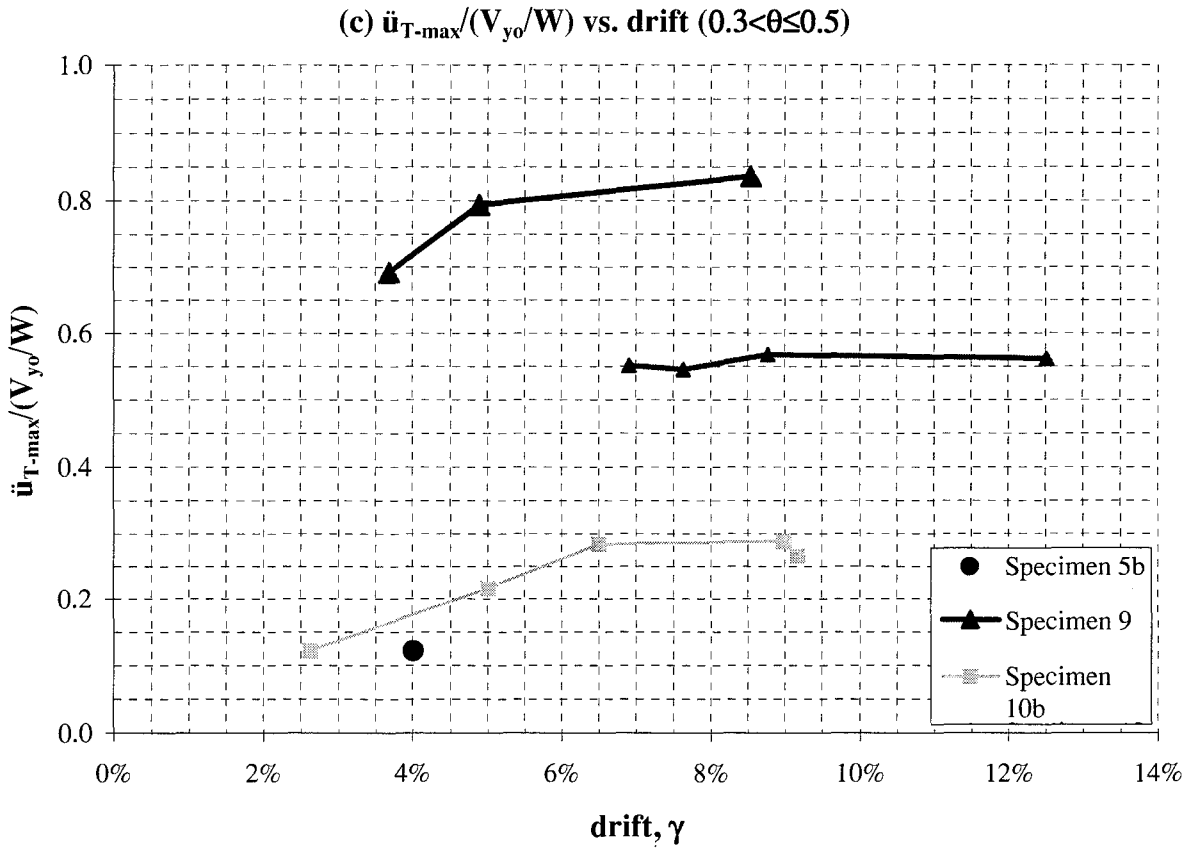

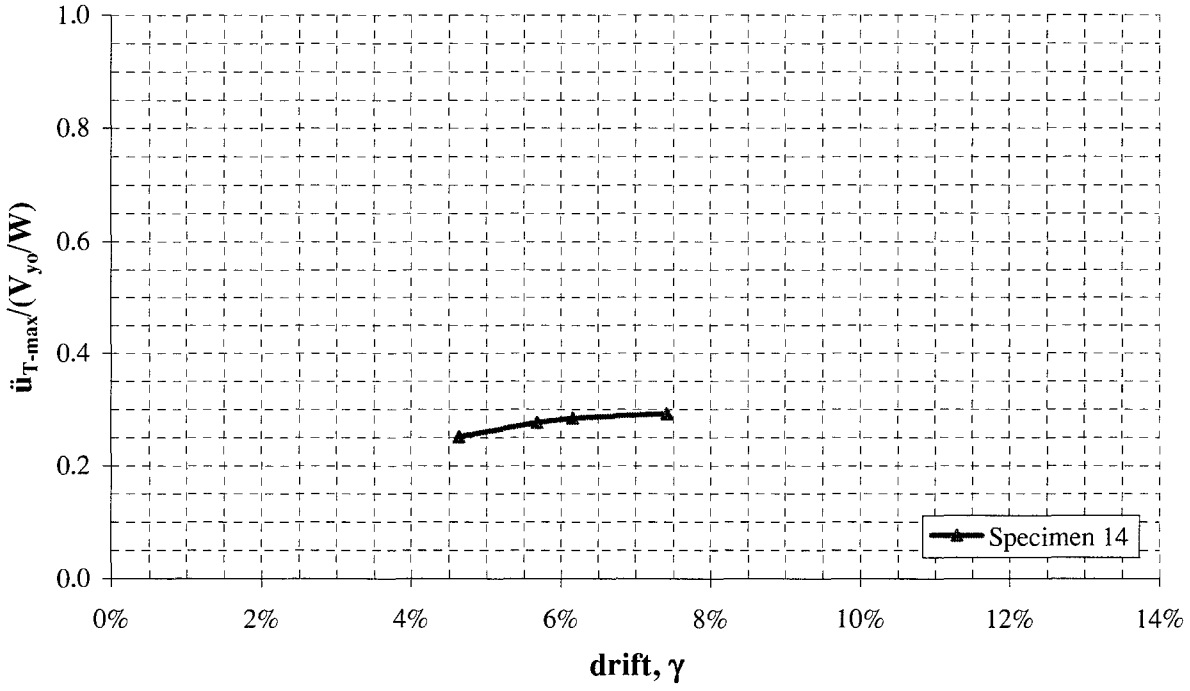

FIGURE C-15 (cont'd) Normalized Absolute Acceleration vs. Drift

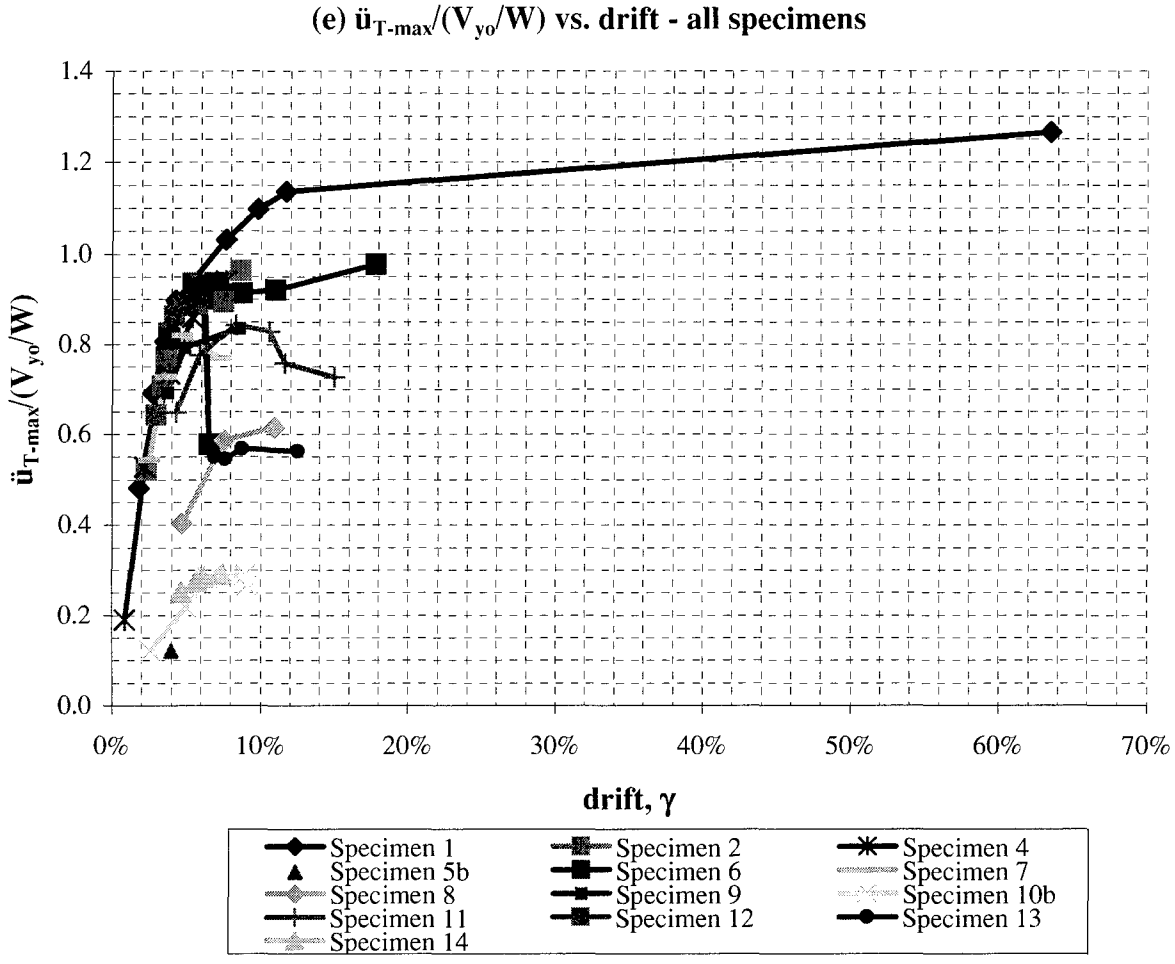

FIGURE C-15 (cont'd) Normalized Absolute Acceleration vs. Drift

Multidisciplinary Center for Earthquake Engineering Research
List of Technical Reports

The Multidisciplinary Center for Earthquake Engineering Research (MCEER) publishes technical reports on a variety of subjects related to earthquake engineering written by authors funded through MCEER. These reports are available from both MCEER Publications and the National Technical Information Service (NTIS). Requests for reports should be directed to MCEER Publications, Multidisciplinary Center for Earthquake Engineering Research, State University of New York at Buffalo, Red Jacket Quadrangle, Buffalo, New York 14261. Reports can also be requested through NTIS, 5285 Port Royal Road, Springfield, Virginia 22161. NTIS accession numbers are shown in parenthesis, if available.

NCEER-87-0001 "First-Year Program in Research, Education and Technology Transfer," 3/5/87, (PB88-134275, A04, MF-A01).

NCEER-87-0002 "Experimental Evaluation of Instantaneous Optimal Algorithms for Structural Control," by R.C. Lin, T.T. Soong and A.M. Reinhorn, 4/20/87, (PB88-134341, A04, MF-A01).

NCEER-87-0003 "Experimentation Using the Earthquake Simulation Facilities at University at Buffalo," by A.M. Reinhorn and R.L. Ketter, to be published.

NCEER-87-0004 "The System Characteristics and Performance of a Shaking Table," by J.S. Hwang, K.C. Chang and G.C. Lee, 6/1/87, (PB88-134259, A03, MF-A01). This report is available only through NTIS (see address given above).

NCEER-87-0005 "A Finite Element Formulation for Nonlinear Viscoplastic Material Using a Q Model," by O. Gyebi and G. Dasgupta, 11/2/87, (PB88-213764, A08, MF-A01).

NCEER-87-0006 "Symbolic Manipulation Program (SMP) - Algebraic Codes for Two and Three Dimensional Finite Element Formulations," by X. Lee and G. Dasgupta, 11/9/87, (PB88-218522, A05, MF-A01).

NCEER-87-0007 "Instantaneous Optimal Control Laws for Tall Buildings Under Seismic Excitations," by J.N. Yang, A. Akbarpour and P. Ghaemmaghami, 6/10/87, (PB88-134333, A06, MF-A01). This report is only available through NTIS (see address given above).

NCEER-87-0008 "IDARC: Inelastic Damage Analysis of Reinforced Concrete Frame - Shear-Wall Structures," by Y.J. Park, A.M. Reinhorn and S.K. Kunnath, 7/20/87, (PB88-134325, A09, MF-A01). This report is only available through NTIS (see address given above).

NCEER-87-0009 "Liquefaction Potential for New York State: A Preliminary Report on Sites in Manhattan and Buffalo," by M. Budhu, V. Vijayakumar, R.F. Giese and L. Baumgras, 8/31/87, (PB88-163704, A03, MF-A01). This report is available only through NTIS (see address given above).

NCEER-87-0010 "Vertical and Torsional Vibration of Foundations in Inhomogeneous Media," by A.S. Veletsos and K.W. Dotson, 6/1/87, (PB88-134291, A03, MF-A01). This report is only available through NTIS (see address given above).

NCEER-87-0011 "Seismic Probabilistic Risk Assessment and Seismic Margins Studies for Nuclear Power Plants," by Howard H.M. Hwang, 6/15/87, (PB88-134267, A03, MF-A01). This report is only available through NTIS (see address given above).

NCEER-87-0012 "Parametric Studies of Frequency Response of Secondary Systems Under Ground-Acceleration Excitations," by Y. Yong and Y.K. Lin, 6/10/87, (PB88-134309, A03, MF-A01). This report is only available through NTIS (see address given above).

NCEER-87-0013 "Frequency Response of Secondary Systems Under Seismic Excitation," by J.A. HoLung, J. Cai and Y.K. Lin, 7/31/87, (PB88-134317, A05, MF-A01). This report is only available through NTIS (see address given above).

NCEER-87-0014 "Modelling Earthquake Ground Motions in Seismically Active Regions Using Parametric Time Series Methods," by G.W. Ellis and A.S. Cakmak, 8/25/87, (PB88-134283, A08, MF-A01). This report is only available through NTIS (see address given above).

NCEER-87-0015 "Detection and Assessment of Seismic Structural Damage," by E. DiPasquale and A.S. Cakmak, 8/25/87, (PB88-163712, A05, MF-A01). This report is only available through NTIS (see address given above).

NCEER-87-0016 "Pipeline Experiment at Parkfield, California," by J. Isenberg and E. Richardson, 9/15/87, (PB88-163720, A03, MF-A01). This report is available only through NTIS (see address given above).

NCEER-87-0017 "Digital Simulation of Seismic Ground Motion," by M. Shinozuka, G. Deodatis and T. Harada, 8/31/87, (PB88-155197, A04, MF-A01). This report is available only through NTIS (see address given above).

NCEER-87-0018 "Practical Considerations for Structural Control: System Uncertainty, System Time Delay and Truncation of Small Control Forces," J.N. Yang and A. Akbarpour, 8/10/87, (PB88-163738, A08, MF-A01). This report is only available through NTIS (see address given above).

NCEER-87-0019 "Modal Analysis of Nonclassically Damped Structural Systems Using Canonical Transformation," by J.N. Yang, S. Sarkani and F.X. Long, 9/27/87, (PB88-187851, A04, MF-A01).

NCEER-87-0020 "A Nonstationary Solution in Random Vibration Theory," by J.R. Red-Horse and P.D. Spanos, 11/3/87, (PB88-163746, A03, MF-A01).

NCEER-87-0021 "Horizontal Impedances for Radially Inhomogeneous Viscoelastic Soil Layers," by A.S. Veletsos and K.W. Dotson, 10/15/87, (PB88-150859, A04, MF-A01).

NCEER-87-0022 "Seismic Damage Assessment of Reinforced Concrete Members," by Y.S. Chung, C. Meyer and M. Shinozuka, 10/9/87, (PB88-150867, A05, MF-A01). This report is available only through NTIS (see address given above).

NCEER-87-0023 "Active Structural Control in Civil Engineering," by T.T. Soong, 11/11/87, (PB88-187778, A03, MF-A01).

NCEER-87-0024 "Vertical and Torsional Impedances for Radially Inhomogeneous Viscoelastic Soil Layers," by K.W. Dotson and A.S. Veletsos, 12/87, (PB88-187786, A03, MF-A01).

NCEER-87-0025 "Proceedings from the Symposium on Seismic Hazards, Ground Motions, Soil-Liquefaction and Engineering Practice in Eastern North America," October 20-22, 1987, edited by K.H. Jacob, 12/87, (PB88-188115, A23, MF-A01). This report is available only through NTIS (see address given above).

NCEER-87-0026 "Report on the Whittier-Narrows, California, Earthquake of October 1, 1987," by J. Pantelic and A. Reinhorn, 11/87, (PB88-187752, A03, MF-A01). This report is available only through NTIS (see address given above).

NCEER-87-0027 "Design of a Modular Program for Transient Nonlinear Analysis of Large 3-D Building Structures," by S. Srivastav and J.F. Abel, 12/30/87, (PB88-187950, A05, MF-A01). This report is only available through NTIS (see address given above).

NCEER-87-0028 "Second-Year Program in Research, Education and Technology Transfer," 3/8/88, (PB88-219480, A04, MF-A01).

NCEER-88-0001 "Workshop on Seismic Computer Analysis and Design of Buildings With Interactive Graphics," by W. McGuire, J.F. Abel and C.H. Conley, 1/18/88, (PB88-187760, A03, MF-A01). This report is only available through NTIS (see address given above).

NCEER-88-0002 "Optimal Control of Nonlinear Flexible Structures," by J.N. Yang, F.X. Long and D. Wong, 1/22/88, (PB88-213772, A06, MF-A01).

NCEER-88-0003 "Substructuring Techniques in the Time Domain for Primary-Secondary Structural Systems," by G.D. Manolis and G. Juhn, 2/10/88, (PB88-213780, A04, MF-A01).

NCEER-88-0004 "Iterative Seismic Analysis of Primary-Secondary Systems," by A. Singhal, L.D. Lutes and P.D. Spanos, 2/23/88, (PB88-213798, A04, MF-A01).

NCEER-88-0005 "Stochastic Finite Element Expansion for Random Media," by P.D. Spanos and R. Ghanem, 3/14/88, (PB88-213806, A03, MF-A01).

NCEER-88-0006 "Combining Structural Optimization and Structural Control," by F.Y. Cheng and C.P. Pantelides, 1/10/88, (PB88-213814, A05, MF-A01).

NCEER-88-0007 "Seismic Performance Assessment of Code-Designed Structures," by H.H-M. Hwang, J-W. Jaw and H-J. Shau, 3/20/88, (PB88-219423, A04, MF-A01). This report is only available through NTIS (see address given above).

NCEER-88-0008 "Reliability Analysis of Code-Designed Structures Under Natural Hazards," by H.H-M. Hwang, H. Ushiba and M. Shinozuka, 2/29/88, (PB88-229471, A07, MF-A01). This report is only available through NTIS (see address given above).

NCEER-88-0009 "Seismic Fragility Analysis of Shear Wall Structures," by J-W Jaw and H.H-M. Hwang, 4/30/88, (PB89-102867, A04, MF-A01).

NCEER-88-0010 "Base Isolation of a Multi-Story Building Under a Harmonic Ground Motion - A Comparison of Performances of Various Systems," by F-G Fan, G. Ahmadi and I.G. Tadjbakhsh, 5/18/88, (PB89-122238, A06, MF-A01). This report is only available through NTIS (see address given above).

NCEER-88-0011 "Seismic Floor Response Spectra for a Combined System by Green's Functions," by F.M. Lavelle, L.A. Bergman and P.D. Spanos, 5/1/88, (PB89-102875, A03, MF-A01).

NCEER-88-0012 "A New Solution Technique for Randomly Excited Hysteretic Structures," by G.Q. Cai and Y.K. Lin, 5/16/88, (PB89-102883, A03, MF-A01).

NCEER-88-0013 "A Study of Radiation Damping and Soil-Structure Interaction Effects in the Centrifuge," by K. Weissman, supervised by J.H. Prevost, 5/24/88, (PB89-144703, A06, MF-A01).

NCEER-88-0014 "Parameter Identification and Implementation of a Kinematic Plasticity Model for Frictional Soils," by J.H. Prevost and D.V. Griffiths, to be published.

NCEER-88-0015 "Two- and Three- Dimensional Dynamic Finite Element Analyses of the Long Valley Dam," by D.V. Griffiths and J.H. Prevost, 6/17/88, (PB89-144711, A04, MF-A01).

NCEER-88-0016 "Damage Assessment of Reinforced Concrete Structures in Eastern United States," by A.M. Reinhorn, M.J. Seidel, S.K. Kunnath and Y.J. Park, 6/15/88, (PB89-122220, A04, MF-A01). This report is only available through NTIS (see address given above).

NCEER-88-0017 "Dynamic Compliance of Vertically Loaded Strip Foundations in Multilayered Viscoelastic Soils," by S. Ahmad and A.S.M. Israil, 6/17/88, (PB89-102891, A04, MF-A01).

NCEER-88-0018 "An Experimental Study of Seismic Structural Response With Added Viscoelastic Dampers," by R.C. Lin, Z. Liang, T.T. Soong and R.H. Zhang, 6/30/88, (PB89-122212, A05, MF-A01). This report is available only through NTIS (see address given above).

NCEER-88-0019 "Experimental Investigation of Primary - Secondary System Interaction," by G.D. Manolis, G. Juhn and A.M. Reinhorn, 5/27/88, (PB89-122204, A04, MF-A01).

NCEER-88-0020 "A Response Spectrum Approach For Analysis of Nonclassically Damped Structures," by J.N. Yang, S. Sarkani and F.X. Long, 4/22/88, (PB89-102909, A04, MF-A01).

NCEER-88-0021 "Seismic Interaction of Structures and Soils: Stochastic Approach," by A.S. Veletsos and A.M. Prasad, 7/21/88, (PB89-122196, A04, MF-A01). This report is only available through NTIS (see address given above).

NCEER-88-0022 "Identification of the Serviceability Limit State and Detection of Seismic Structural Damage," by E. DiPasquale and A.S. Cakmak, 6/15/88, (PB89-122188, A05, MF-A01). This report is available only through NTIS (see address given above).

NCEER-88-0023 "Multi-Hazard Risk Analysis: Case of a Simple Offshore Structure," by B.K. Bhartia and E.H. Vanmarcke, 7/21/88, (PB89-145213, A05, MF-A01).

NCEER-88-0024 "Automated Seismic Design of Reinforced Concrete Buildings," by Y.S. Chung, C. Meyer and M. Shinozuka, 7/5/88, (PB89-122170, A06, MF-A01). This report is available only through NTIS (see address given above).

NCEER-88-0025 "Experimental Study of Active Control of MDOF Structures Under Seismic Excitations," by L.L. Chung, R.C. Lin, T.T. Soong and A.M. Reinhorn, 7/10/88, (PB89-122600, A04, MF-A01).

NCEER-88-0026 "Earthquake Simulation Tests of a Low-Rise Metal Structure," by J.S. Hwang, K.C. Chang, G.C. Lee and R.L. Ketter, 8/1/88, (PB89-102917, A04, MF-A01).

NCEER-88-0027 "Systems Study of Urban Response and Reconstruction Due to Catastrophic Earthquakes," by F. Kozin and H.K. Zhou, 9/22/88, (PB90-162348, A04, MF-A01).

NCEER-88-0028 "Seismic Fragility Analysis of Plane Frame Structures," by H.H-M. Hwang and Y.K. Low, 7/31/88, (PB89-131445, A06, MF-A01).

NCEER-88-0029 "Response Analysis of Stochastic Structures," by A. Kardara, C. Bucher and M. Shinozuka, 9/22/88, (PB89-174429, A04, MF-A01).

NCEER-88-0030 "Nonnormal Accelerations Due to Yielding in a Primary Structure," by D.C.K. Chen and L.D. Lutes, 9/19/88, (PB89-131437, A04, MF-A01).

NCEER-88-0031 "Design Approaches for Soil-Structure Interaction," by A.S. Veletsos, A.M. Prasad and Y. Tang, 12/30/88, (PB89-174437, A03, MF-A01). This report is available only through NTIS (see address given above).

NCEER-88-0032 "A Re-evaluation of Design Spectra for Seismic Damage Control," by C.J. Turkstra and A.G. Tallin, 11/7/88, (PB89-145221, A05, MF-A01).

NCEER-88-0033 "The Behavior and Design of Noncontact Lap Splices Subjected to Repeated Inelastic Tensile Loading," by V.E. Sagan, P. Gergely and R.N. White, 12/8/88, (PB89-163737, A08, MF-A01).

NCEER-88-0034 "Seismic Response of Pile Foundations," by S.M. Mamoon, P.K. Banerjee and S. Ahmad, 11/1/88, (PB89-145239, A04, MF-A01).

NCEER-88-0035 "Modeling of R/C Building Structures With Flexible Floor Diaphragms (IDARC2)," by A.M. Reinhorn, S.K. Kunnath and N. Panahshahi, 9/7/88, (PB89-207153, A07, MF-A01).

NCEER-88-0036 "Solution of the Dam-Reservoir Interaction Problem Using a Combination of FEM, BEM with Particular Integrals, Modal Analysis, and Substructuring," by C-S. Tsai, G.C. Lee and R.L. Ketter, 12/31/88, (PB89-207146, A04, MF-A01).

NCEER-88-0037 "Optimal Placement of Actuators for Structural Control," by F.Y. Cheng and C.P. Pantelides, 8/15/88, (PB89-162846, A05, MF-A01).

NCEER-88-0038 "Teflon Bearings in Aseismic Base Isolation: Experimental Studies and Mathematical Modeling," by A. Mokha, M.C. Constantinou and A.M. Reinhorn, 12/5/88, (PB89-218457, A10, MF-A01). This report is available only through NTIS (see address given above).

NCEER-88-0039 "Seismic Behavior of Flat Slab High-Rise Buildings in the New York City Area," by P. Weidlinger and M. Ettouney, 10/15/88, (PB90-145681, A04, MF-A01).

NCEER-88-0040 "Evaluation of the Earthquake Resistance of Existing Buildings in New York City," by P. Weidlinger and M. Ettouney, 10/15/88, to be published.

NCEER-88-0041 "Small-Scale Modeling Techniques for Reinforced Concrete Structures Subjected to Seismic Loads," by W. Kim, A. El-Attar and R.N. White, 11/22/88, (PB89-189625, A05, MF-A01).

NCEER-88-0042 "Modeling Strong Ground Motion from Multiple Event Earthquakes," by G.W. Ellis and A.S. Cakmak, 10/15/88, (PB89-174445, A03, MF-A01).

NCEER-88-0043 "Nonstationary Models of Seismic Ground Acceleration," by M. Grigoriu, S.E. Ruiz and E. Rosenblueth, 7/15/88, (PB89-189617, A04, MF-A01).

NCEER-88-0044 "SARCF User's Guide: Seismic Analysis of Reinforced Concrete Frames," by Y.S. Chung, C. Meyer and M. Shinozuka, 11/9/88, (PB89-174452, A08, MF-A01).

NCEER-88-0045 "First Expert Panel Meeting on Disaster Research and Planning," edited by J. Pantelic and J. Stoyle, 9/15/88, (PB89-174460, A05, MF-A01).

NCEER-88-0046 "Preliminary Studies of the Effect of Degrading Infill Walls on the Nonlinear Seismic Response of Steel Frames," by C.Z. Chrysostomou, P. Gergely and J.F. Abel, 12/19/88, (PB89-208383, A05, MF-A01).

NCEER-88-0047 "Reinforced Concrete Frame Component Testing Facility - Design, Construction, Instrumentation and Operation," by S.P. Pessiki, C. Conley, T. Bond, P. Gergely and R.N. White, 12/16/88, (PB89-174478, A04, MF-A01).

NCEER-89-0001 "Effects of Protective Cushion and Soil Compliancy on the Response of Equipment Within a Seismically Excited Building," by J.A. HoLung, 2/16/89, (PB89-207179, A04, MF-A01).

NCEER-89-0002 "Statistical Evaluation of Response Modification Factors for Reinforced Concrete Structures," by H.H-M. Hwang and J-W. Jaw, 2/17/89, (PB89-207187, A05, MF-A01).

NCEER-89-0003 "Hysteretic Columns Under Random Excitation," by G-Q. Cai and Y.K. Lin, 1/9/89, (PB89-196513, A03, MF-A01).

NCEER-89-0004 "Experimental Study of `Elephant Foot Bulge' Instability of Thin-Walled Metal Tanks," by Z-H. Jia and R.L. Ketter, 2/22/89, (PB89-207195, A03, MF-A01).

NCEER-89-0005 "Experiment on Performance of Buried Pipelines Across San Andreas Fault," by J. Isenberg, E. Richardson and T.D. O'Rourke, 3/10/89, (PB89-218440, A04, MF-A01). This report is available only through NTIS (see address given above).

NCEER-89-0006 "A Knowledge-Based Approach to Structural Design of Earthquake-Resistant Buildings," by M. Subramani, P. Gergely, C.H. Conley, J.F. Abel and A.H. Zaghw, 1/15/89, (PB89-218465, A06, MF-A01).

NCEER-89-0007 "Liquefaction Hazards and Their Effects on Buried Pipelines," by T.D. O'Rourke and P.A. Lane, 2/1/89, (PB89-218481, A09, MF-A01).

NCEER-89-0008 "Fundamentals of System Identification in Structural Dynamics," by H. Imai, C-B. Yun, O. Maruyama and M. Shinozuka, 1/26/89, (PB89-207211, A04, MF-A01).

NCEER-89-0009 "Effects of the 1985 Michoacan Earthquake on Water Systems and Other Buried Lifelines in Mexico," by A.G. Ayala and M.J. O'Rourke, 3/8/89, (PB89-207229, A06, MF-A01).

NCEER-89-R010 "NCEER Bibliography of Earthquake Education Materials," by K.E.K. Ross, Second Revision, 9/1/89, (PB90-125352, A05, MF-A01). This report is replaced by NCEER-92-0018.

NCEER-89-0011 "Inelastic Three-Dimensional Response Analysis of Reinforced Concrete Building Structures (IDARC-3D), Part I - Modeling," by S.K. Kunnath and A.M. Reinhorn, 4/17/89, (PB90-114612, A07, MF-A01). This report is available only through NTIS (see address given above).

NCEER-89-0012 "Recommended Modifications to ATC-14," by C.D. Poland and J.O. Malley, 4/12/89, (PB90-108648, A15, MF-A01).

NCEER-89-0013 "Repair and Strengthening of Beam-to-Column Connections Subjected to Earthquake Loading," by M. Corazao and A.J. Durrani, 2/28/89, (PB90-109885, A06, MF-A01).

NCEER-89-0014 "Program EXKAL2 for Identification of Structural Dynamic Systems," by O. Maruyama, C-B. Yun, M. Hoshiya and M. Shinozuka, 5/19/89, (PB90-109877, A09, MF-A01).

NCEER-89-0015 "Response of Frames With Bolted Semi-Rigid Connections, Part I - Experimental Study and Analytical Predictions," by P.J. DiCorso, A.M. Reinhorn, J.R. Dickerson, J.B. Radziminski and W.L. Harper, 6/1/89, to be published.

NCEER-89-0016 "ARMA Monte Carlo Simulation in Probabilistic Structural Analysis," by P.D. Spanos and M.P. Mignolet, 7/10/89, (PB90-109893, A03, MF-A01).

NCEER-89-P017 "Preliminary Proceedings from the Conference on Disaster Preparedness - The Place of Earthquake Education in Our Schools," Edited by K.E.K. Ross, 6/23/89, (PB90-108606, A03, MF-A01).

NCEER-89-0017 "Proceedings from the Conference on Disaster Preparedness - The Place of Earthquake Education in Our Schools," Edited by K.E.K. Ross, 12/31/89, (PB90-207895, A012, MF-A02). This report is available only through NTIS (see address given above).

NCEER-89-0018 "Multidimensional Models of Hysteretic Material Behavior for Vibration Analysis of Shape Memory Energy Absorbing Devices, by E.J. Graesser and F.A. Cozzarelli, 6/7/89, (PB90-164146, A04, MF-A01).

NCEER-89-0019 "Nonlinear Dynamic Analysis of Three-Dimensional Base Isolated Structures (3D-BASIS)," by S. Nagarajaiah, A.M. Reinhorn and M.C. Constantinou, 8/3/89, (PB90-161936, A06, MF-A01). This report has been replaced by NCEER-93-0011.

NCEER-89-0020 "Structural Control Considering Time-Rate of Control Forces and Control Rate Constraints," by F.Y. Cheng and C.P. Pantelides, 8/3/89, (PB90-120445, A04, MF-A01).

NCEER-89-0021 "Subsurface Conditions of Memphis and Shelby County," by K.W. Ng, T-S. Chang and H-H.M. Hwang, 7/26/89, (PB90-120437, A03, MF-A01).

NCEER-89-0022 "Seismic Wave Propagation Effects on Straight Jointed Buried Pipelines," by K. Elhmadi and M.J. O'Rourke, 8/24/89, (PB90-162322, A10, MF-A02).

NCEER-89-0023 "Workshop on Serviceability Analysis of Water Delivery Systems," edited by M. Grigoriu, 3/6/89, (PB90-127424, A03, MF-A01).

NCEER-89-0024 "Shaking Table Study of a 1/5 Scale Steel Frame Composed of Tapered Members," by K.C. Chang, J.S. Hwang and G.C. Lee, 9/18/89, (PB90-160169, A04, MF-A01).

NCEER-89-0025 "DYNA1D: A Computer Program for Nonlinear Seismic Site Response Analysis - Technical Documentation," by Jean H. Prevost, 9/14/89, (PB90-161944, A07, MF-A01). This report is available only through NTIS (see address given above).

NCEER-89-0026 "1:4 Scale Model Studies of Active Tendon Systems and Active Mass Dampers for Aseismic Protection," by A.M. Reinhorn, T.T. Soong, R.C. Lin, Y.P. Yang, Y. Fukao, H. Abe and M. Nakai, 9/15/89, (PB90-173246, A10, MF-A02). This report is available only through NTIS (see address given above).

NCEER-89-0027 "Scattering of Waves by Inclusions in a Nonhomogeneous Elastic Half Space Solved by Boundary Element Methods," by P.K. Hadley, A. Askar and A.S. Cakmak, 6/15/89, (PB90-145699, A07, MF-A01).

NCEER-89-0028 "Statistical Evaluation of Deflection Amplification Factors for Reinforced Concrete Structures," by H.H.M. Hwang, J-W. Jaw and A.L. Ch'ng, 8/31/89, (PB90-164633, A05, MF-A01).

NCEER-89-0029 "Bedrock Accelerations in Memphis Area Due to Large New Madrid Earthquakes," by H.H.M. Hwang, C.H.S. Chen and G. Yu, 11/7/89, (PB90-162330, A04, MF-A01).

NCEER-89-0030 "Seismic Behavior and Response Sensitivity of Secondary Structural Systems," by Y.Q. Chen and T.T. Soong, 10/23/89, (PB90-164658, A08, MF-A01).

NCEER-89-0031 "Random Vibration and Reliability Analysis of Primary-Secondary Structural Systems," by Y. Ibrahim, M. Grigoriu and T.T. Soong, 11/10/89, (PB90-161951, A04, MF-A01).

NCEER-89-0032 "Proceedings from the Second U.S. - Japan Workshop on Liquefaction, Large Ground Deformation and Their Effects on Lifelines, September 26-29, 1989," Edited by T.D. O'Rourke and M. Hamada, 12/1/89, (PB90-209388, A22, MF-A03).

NCEER-89-0033 "Deterministic Model for Seismic Damage Evaluation of Reinforced Concrete Structures," by J.M. Bracci, A.M. Reinhorn, J.B. Mander and S.K. Kunnath, 9/27/89, (PB91-108803, A06, MF-A01).

NCEER-89-0034 "On the Relation Between Local and Global Damage Indices," by E. DiPasquale and A.S. Cakmak, 8/15/89, (PB90-173865, A05, MF-A01).

NCEER-89-0035 "Cyclic Undrained Behavior of Nonplastic and Low Plasticity Silts," by A.J. Walker and H.E. Stewart, 7/26/89, (PB90-183518, A10, MF-A01).

NCEER-89-0036 "Liquefaction Potential of Surficial Deposits in the City of Buffalo, New York," by M. Budhu, R. Giese and L. Baumgrass, 1/17/89, (PB90-208455, A04, MF-A01).

NCEER-89-0037 "A Deterministic Assessment of Effects of Ground Motion Incoherence," by A.S. Veletsos and Y. Tang, 7/15/89, (PB90-164294, A03, MF-A01).

NCEER-89-0038 "Workshop on Ground Motion Parameters for Seismic Hazard Mapping," July 17-18, 1989, edited by R.V. Whitman, 12/1/89, (PB90-173923, A04, MF-A01).

NCEER-89-0039 "Seismic Effects on Elevated Transit Lines of the New York City Transit Authority," by C.J. Costantino, C.A. Miller and E. Heymsfield, 12/26/89, (PB90-207887, A06, MF-A01).

NCEER-89-0040 "Centrifugal Modeling of Dynamic Soil-Structure Interaction," by K. Weissman, Supervised by J.H. Prevost, 5/10/89, (PB90-207879, A07, MF-A01).

NCEER-89-0041 "Linearized Identification of Buildings With Cores for Seismic Vulnerability Assessment," by I-K. Ho and A.E. Aktan, 11/1/89, (PB90-251943, A07, MF-A01).

NCEER-90-0001 "Geotechnical and Lifeline Aspects of the October 17, 1989 Loma Prieta Earthquake in San Francisco," by T.D. O'Rourke, H.E. Stewart, F.T. Blackburn and T.S. Dickerman, 1/90, (PB90-208596, A05, MF-A01).

NCEER-90-0002 "Nonnormal Secondary Response Due to Yielding in a Primary Structure," by D.C.K. Chen and L.D. Lutes, 2/28/90, (PB90-251976, A07, MF-A01).

NCEER-90-0003 "Earthquake Education Materials for Grades K-12," by K.E.K. Ross, 4/16/90, (PB91-251984, A05, MF-A05). This report has been replaced by NCEER-92-0018.

NCEER-90-0004 "Catalog of Strong Motion Stations in Eastern North America," by R.W. Busby, 4/3/90, (PB90-251984, A05, MF-A01).

NCEER-90-0005 "NCEER Strong-Motion Data Base: A User Manual for the GeoBase Release (Version 1.0 for the Sun3)," by P. Friberg and K. Jacob, 3/31/90 (PB90-258062, A04, MF-A01).

NCEER-90-0006 "Seismic Hazard Along a Crude Oil Pipeline in the Event of an 1811-1812 Type New Madrid Earthquake," by H.H.M. Hwang and C-H.S. Chen, 4/16/90, (PB90-258054, A04, MF-A01).

NCEER-90-0007 "Site-Specific Response Spectra for Memphis Sheahan Pumping Station," by H.H.M. Hwang and C.S. Lee, 5/15/90, (PB91-108811, A05, MF-A01).

NCEER-90-0008 "Pilot Study on Seismic Vulnerability of Crude Oil Transmission Systems," by T. Ariman, R. Dobry, M. Grigoriu, F. Kozin, M. O'Rourke, T. O'Rourke and M. Shinozuka, 5/25/90, (PB91-108837, A06, MF-A01).

NCEER-90-0009 "A Program to Generate Site Dependent Time Histories: EQGEN," by G.W. Ellis, M. Srinivasan and A.S. Cakmak, 1/30/90, (PB91-108829, A04, MF-A01).

NCEER-90-0010 "Active Isolation for Seismic Protection of Operating Rooms," by M.E. Talbott, Supervised by M. Shinozuka, 6/8/9, (PB91-110205, A05, MF-A01).

NCEER-90-0011 "Program LINEARID for Identification of Linear Structural Dynamic Systems," by C-B. Yun and M. Shinozuka, 6/25/90, (PB91-110312, A08, MF-A01).

NCEER-90-0012 "Two-Dimensional Two-Phase Elasto-Plastic Seismic Response of Earth Dams," by A.N. Yiagos, Supervised by J.H. Prevost, 6/20/90, (PB91-110197, A13, MF-A02).

NCEER-90-0013 "Secondary Systems in Base-Isolated Structures: Experimental Investigation, Stochastic Response and Stochastic Sensitivity," by G.D. Manolis, G. Juhn, M.C. Constantinou and A.M. Reinhorn, 7/1/90, (PB91-110320, A08, MF-A01).

NCEER-90-0014 "Seismic Behavior of Lightly-Reinforced Concrete Column and Beam-Column Joint Details," by S.P. Pessiki, C.H. Conley, P. Gergely and R.N. White, 8/22/90, (PB91-108795, A11, MF-A02).

NCEER-90-0015 "Two Hybrid Control Systems for Building Structures Under Strong Earthquakes," by J.N. Yang and A. Danielians, 6/29/90, (PB91-125393, A04, MF-A01).

NCEER-90-0016 "Instantaneous Optimal Control with Acceleration and Velocity Feedback," by J.N. Yang and Z. Li, 6/29/90, (PB91-125401, A03, MF-A01).

NCEER-90-0017 "Reconnaissance Report on the Northern Iran Earthquake of June 21, 1990," by M. Mehrain, 10/4/90, (PB91-125377, A03, MF-A01).

NCEER-90-0018 "Evaluation of Liquefaction Potential in Memphis and Shelby County," by T.S. Chang, P.S. Tang, C.S. Lee and H. Hwang, 8/10/90, (PB91-125427, A09, MF-A01).

NCEER-90-0019 "Experimental and Analytical Study of a Combined Sliding Disc Bearing and Helical Steel Spring Isolation System," by M.C. Constantinou, A.S. Mokha and A.M. Reinhorn, 10/4/90, (PB91-125385, A06, MF-A01). This report is available only through NTIS (see address given above).

NCEER-90-0020 "Experimental Study and Analytical Prediction of Earthquake Response of a Sliding Isolation System with a Spherical Surface," by A.S. Mokha, M.C. Constantinou and A.M. Reinhorn, 10/11/90, (PB91-125419, A05, MF-A01).

NCEER-90-0021 "Dynamic Interaction Factors for Floating Pile Groups," by G. Gazetas, K. Fan, A. Kaynia and E. Kausel, 9/10/90, (PB91-170381, A05, MF-A01).

NCEER-90-0022 "Evaluation of Seismic Damage Indices for Reinforced Concrete Structures," by S. Rodriguez-Gomez and A.S. Cakmak, 9/30/90, PB91-171322, A06, MF-A01).

NCEER-90-0023 "Study of Site Response at a Selected Memphis Site," by H. Desai, S. Ahmad, E.S. Gazetas and M.R. Oh, 10/11/90, (PB91-196857, A03, MF-A01).

NCEER-90-0024 "A User's Guide to Strongmo: Version 1.0 of NCEER's Strong-Motion Data Access Tool for PCs and Terminals," by P.A. Friberg and C.A.T. Susch, 11/15/90, (PB91-171272, A03, MF-A01).

NCEER-90-0025 "A Three-Dimensional Analytical Study of Spatial Variability of Seismic Ground Motions," by L-L. Hong and A.H.-S. Ang, 10/30/90, (PB91-170399, A09, MF-A01).

NCEER-90-0026 "MUMOID User's Guide - A Program for the Identification of Modal Parameters," by S. Rodriguez-Gomez and E. DiPasquale, 9/30/90, (PB91-171298, A04, MF-A01).

NCEER-90-0027 "SARCF-II User's Guide - Seismic Analysis of Reinforced Concrete Frames," by S. Rodriguez-Gomez, Y.S. Chung and C. Meyer, 9/30/90, (PB91-171280, A05, MF-A01).

NCEER-90-0028 "Viscous Dampers: Testing, Modeling and Application in Vibration and Seismic Isolation," by N. Makris and M.C. Constantinou, 12/20/90 (PB91-190561, A06, MF-A01).

NCEER-90-0029 "Soil Effects on Earthquake Ground Motions in the Memphis Area," by H. Hwang, C.S. Lee, K.W. Ng and T.S. Chang, 8/2/90, (PB91-190751, A05, MF-A01).

NCEER-91-0001 "Proceedings from the Third Japan-U.S. Workshop on Earthquake Resistant Design of Lifeline Facilities and Countermeasures for Soil Liquefaction, December 17-19, 1990," edited by T.D. O'Rourke and M. Hamada, 2/1/91, (PB91-179259, A99, MF-A04).

NCEER-91-0002 "Physical Space Solutions of Non-Proportionally Damped Systems," by M. Tong, Z. Liang and G.C. Lee, 1/15/91, (PB91-179242, A04, MF-A01).

NCEER-91-0003 "Seismic Response of Single Piles and Pile Groups," by K. Fan and G. Gazetas, 1/10/91, (PB92-174994, A04, MF-A01).

NCEER-91-0004 "Damping of Structures: Part 1 - Theory of Complex Damping," by Z. Liang and G. Lee, 10/10/91, (PB92-197235, A12, MF-A03).

NCEER-91-0005 "3D-BASIS - Nonlinear Dynamic Analysis of Three Dimensional Base Isolated Structures: Part II," by S. Nagarajaiah, A.M. Reinhorn and M.C. Constantinou, 2/28/91, (PB91-190553, A07, MF-A01). This report has been replaced by NCEER-93-0011.

NCEER-91-0006 "A Multidimensional Hysteretic Model for Plasticity Deforming Metals in Energy Absorbing Devices," by E.J. Graesser and F.A. Cozzarelli, 4/9/91, (PB92-108364, A04, MF-A01).

NCEER-91-0007 "A Framework for Customizable Knowledge-Based Expert Systems with an Application to a KBES for Evaluating the Seismic Resistance of Existing Buildings," by E.G. Ibarra-Anaya and S.J. Fenves, 4/9/91, (PB91-210930, A08, MF-A01).

NCEER-91-0008 "Nonlinear Analysis of Steel Frames with Semi-Rigid Connections Using the Capacity Spectrum Method," by G.G. Deierlein, S-H. Hsieh, Y-J. Shen and J.F. Abel, 7/2/91, (PB92-113828, A05, MF-A01).

NCEER-91-0009 "Earthquake Education Materials for Grades K-12," by K.E.K. Ross, 4/30/91, (PB91-212142, A06, MF-A01). This report has been replaced by NCEER-92-0018.

NCEER-91-0010 "Phase Wave Velocities and Displacement Phase Differences in a Harmonically Oscillating Pile," by N. Makris and G. Gazetas, 7/8/91, (PB92-108356, A04, MF-A01).

NCEER-91-0011 "Dynamic Characteristics of a Full-Size Five-Story Steel Structure and a 2/5 Scale Model," by K.C. Chang, G.C. Yao, G.C. Lee, D.S. Hao and Y.C. Yeh," 7/2/91, (PB93-116648, A06, MF-A02).

NCEER-91-0012 "Seismic Response of a 2/5 Scale Steel Structure with Added Viscoelastic Dampers," by K.C. Chang, T.T. Soong, S-T. Oh and M.L. Lai, 5/17/91, (PB92-110816, A05, MF-A01).

NCEER-91-0013 "Earthquake Response of Retaining Walls; Full-Scale Testing and Computational Modeling," by S. Alampalli and A-W.M. Elgamal, 6/20/91, to be published.

NCEER-91-0014 "3D-BASIS-M: Nonlinear Dynamic Analysis of Multiple Building Base Isolated Structures," by P.C. Tsopelas, S. Nagarajaiah, M.C. Constantinou and A.M. Reinhorn, 5/28/91, (PB92-113885, A09, MF-A02).

NCEER-91-0015 "Evaluation of SEAOC Design Requirements for Sliding Isolated Structures," by D. Theodossiou and M.C. Constantinou, 6/10/91, (PB92-114602, A11, MF-A03).

NCEER-91-0016 "Closed-Loop Modal Testing of a 27-Story Reinforced Concrete Flat Plate-Core Building," by H.R. Somaprasad, T. Toksoy, H. Yoshiyuki and A.E. Aktan, 7/15/91, (PB92-129980, A07, MF-A02).

NCEER-91-0017 "Shake Table Test of a 1/6 Scale Two-Story Lightly Reinforced Concrete Building," by A.G. El-Attar, R.N. White and P. Gergely, 2/28/91, (PB92-222447, A06, MF-A02).

NCEER-91-0018 "Shake Table Test of a 1/8 Scale Three-Story Lightly Reinforced Concrete Building," by A.G. El-Attar, R.N. White and P. Gergely, 2/28/91, (PB93-116630, A08, MF-A02).

NCEER-91-0019 "Transfer Functions for Rigid Rectangular Foundations," by A.S. Veletsos, A.M. Prasad and W.H. Wu, 7/31/91, to be published.

NCEER-91-0020 "Hybrid Control of Seismic-Excited Nonlinear and Inelastic Structural Systems," by J.N. Yang, Z. Li and A. Danielians, 8/1/91, (PB92-143171, A06, MF-A02).

NCEER-91-0021 "The NCEER-91 Earthquake Catalog: Improved Intensity-Based Magnitudes and Recurrence Relations for U.S. Earthquakes East of New Madrid," by L. Seeber and J.G. Armbruster, 8/28/91, (PB92-176742, A06, MF-A02).

NCEER-91-0022 "Proceedings from the Implementation of Earthquake Planning and Education in Schools: The Need for Change - The Roles of the Changemakers," by K.E.K. Ross and F. Winslow, 7/23/91, (PB92-129998, A12, MF-A03).

NCEER-91-0023 "A Study of Reliability-Based Criteria for Seismic Design of Reinforced Concrete Frame Buildings," by H.H.M. Hwang and H-M. Hsu, 8/10/91, (PB92-140235, A09, MF-A02).

NCEER-91-0024 "Experimental Verification of a Number of Structural System Identification Algorithms," by R.G. Ghanem, H. Gavin and M. Shinozuka, 9/18/91, (PB92-176577, A18, MF-A04).

NCEER-91-0025 "Probabilistic Evaluation of Liquefaction Potential," by H.H.M. Hwang and C.S. Lee," 11/25/91, (PB92-143429, A05, MF-A01).

NCEER-91-0026 "Instantaneous Optimal Control for Linear, Nonlinear and Hysteretic Structures - Stable Controllers," by J.N. Yang and Z. Li, 11/15/91, (PB92-163807, A04, MF-A01).

NCEER-91-0027 "Experimental and Theoretical Study of a Sliding Isolation System for Bridges," by M.C. Constantinou, A. Kartoum, A.M. Reinhorn and P. Bradford, 11/15/91, (PB92-176973, A10, MF-A03).

NCEER-92-0001 "Case Studies of Liquefaction and Lifeline Performance During Past Earthquakes, Volume 1: Japanese Case Studies," Edited by M. Hamada and T. O'Rourke, 2/17/92, (PB92-197243, A18, MF-A04).

NCEER-92-0002 "Case Studies of Liquefaction and Lifeline Performance During Past Earthquakes, Volume 2: United States Case Studies," Edited by T. O'Rourke and M. Hamada, 2/17/92, (PB92-197250, A20, MF-A04).

NCEER-92-0003 "Issues in Earthquake Education," Edited by K. Ross, 2/3/92, (PB92-222389, A07, MF-A02).

NCEER-92-0004 "Proceedings from the First U.S. - Japan Workshop on Earthquake Protective Systems for Bridges," Edited by I.G. Buckle, 2/4/92, (PB94-142239, A99, MF-A06).

NCEER-92-0005 "Seismic Ground Motion from a Haskell-Type Source in a Multiple-Layered Half-Space," A.P. Theoharis, G. Deodatis and M. Shinozuka, 1/2/92, to be published.

NCEER-92-0006 "Proceedings from the Site Effects Workshop," Edited by R. Whitman, 2/29/92, (PB92-197201, A04, MF-A01).

NCEER-92-0007 "Engineering Evaluation of Permanent Ground Deformations Due to Seismically-Induced Liquefaction," by M.H. Baziar, R. Dobry and A-W.M. Elgamal, 3/24/92, (PB92-222421, A13, MF-A03).

NCEER-92-0008 "A Procedure for the Seismic Evaluation of Buildings in the Central and Eastern United States," by C.D. Poland and J.O. Malley, 4/2/92, (PB92-222439, A20, MF-A04).

NCEER-92-0009 "Experimental and Analytical Study of a Hybrid Isolation System Using Friction Controllable Sliding Bearings," by M.Q. Feng, S. Fujii and M. Shinozuka, 5/15/92, (PB93-150282, A06, MF-A02).

NCEER-92-0010 "Seismic Resistance of Slab-Column Connections in Existing Non-Ductile Flat-Plate Buildings," by A.J. Durrani and Y. Du, 5/18/92, (PB93-116812, A06, MF-A02).

NCEER-92-0011 "The Hysteretic and Dynamic Behavior of Brick Masonry Walls Upgraded by Ferrocement Coatings Under Cyclic Loading and Strong Simulated Ground Motion," by H. Lee and S.P. Prawel, 5/11/92, to be published.

NCEER-92-0012 "Study of Wire Rope Systems for Seismic Protection of Equipment in Buildings," by G.F. Demetriades, M.C. Constantinou and A.M. Reinhorn, 5/20/92, (PB93-116655, A08, MF-A02).

NCEER-92-0013 "Shape Memory Structural Dampers: Material Properties, Design and Seismic Testing," by P.R. Witting and F.A. Cozzarelli, 5/26/92, (PB93-116663, A05, MF-A01).

NCEER-92-0014 "Longitudinal Permanent Ground Deformation Effects on Buried Continuous Pipelines," by M.J. O'Rourke, and C. Nordberg, 6/15/92, (PB93-116671, A08, MF-A02).

NCEER-92-0015 "A Simulation Method for Stationary Gaussian Random Functions Based on the Sampling Theorem," by M. Grigoriu and S. Balopoulou, 6/11/92, (PB93-127496, A05, MF-A01).

NCEER-92-0016 "Gravity-Load-Designed Reinforced Concrete Buildings: Seismic Evaluation of Existing Construction and Detailing Strategies for Improved Seismic Resistance," by G.W. Hoffmann, S.K. Kunnath, A.M. Reinhorn and J.B. Mander, 7/15/92, (PB94-142007, A08, MF-A02).

NCEER-92-0017 "Observations on Water System and Pipeline Performance in the Limón Area of Costa Rica Due to the April 22, 1991 Earthquake," by M. O'Rourke and D. Ballantyne, 6/30/92, (PB93-126811, A06, MF-A02).

NCEER-92-0018 "Fourth Edition of Earthquake Education Materials for Grades K-12," Edited by K.E.K. Ross, 8/10/92, (PB93-114023, A07, MF-A02).

NCEER-92-0019 "Proceedings from the Fourth Japan-U.S. Workshop on Earthquake Resistant Design of Lifeline Facilities and Countermeasures for Soil Liquefaction," Edited by M. Hamada and T.D. O'Rourke, 8/12/92, (PB93-163939, A99, MF-E11).

NCEER-92-0020 "Active Bracing System: A Full Scale Implementation of Active Control," by A.M. Reinhorn, T.T. Soong, R.C. Lin, M.A. Riley, Y.P. Wang, S. Aizawa and M. Higashino, 8/14/92, (PB93-127512, A06, MF-A02).

NCEER-92-0021 "Empirical Analysis of Horizontal Ground Displacement Generated by Liquefaction-Induced Lateral Spreads," by S.F. Bartlett and T.L. Youd, 8/17/92, (PB93-188241, A06, MF-A02).

NCEER-92-0022 "IDARC Version 3.0: Inelastic Damage Analysis of Reinforced Concrete Structures," by S.K. Kunnath, A.M. Reinhorn and R.F. Lobo, 8/31/92, (PB93-227502, A07, MF-A02).

NCEER-92-0023 "A Semi-Empirical Analysis of Strong-Motion Peaks in Terms of Seismic Source, Propagation Path and Local Site Conditions, by M. Kamiyama, M.J. O'Rourke and R. Flores-Berrones, 9/9/92, (PB93-150266, A08, MF-A02).

NCEER-92-0024 "Seismic Behavior of Reinforced Concrete Frame Structures with Nonductile Details, Part I: Summary of Experimental Findings of Full Scale Beam-Column Joint Tests," by A. Beres, R.N. White and P. Gergely, 9/30/92, (PB93-227783, A05, MF-A01).

NCEER-92-0025 "Experimental Results of Repaired and Retrofitted Beam-Column Joint Tests in Lightly Reinforced Concrete Frame Buildings," by A. Beres, S. El-Borgi, R.N. White and P. Gergely, 10/29/92, (PB93-227791, A05, MF-A01).

NCEER-92-0026 "A Generalization of Optimal Control Theory: Linear and Nonlinear Structures," by J.N. Yang, Z. Li and S. Vongchavalitkul, 11/2/92, (PB93-188621, A05, MF-A01).

NCEER-92-0027 "Seismic Resistance of Reinforced Concrete Frame Structures Designed Only for Gravity Loads: Part I - Design and Properties of a One-Third Scale Model Structure," by J.M. Bracci, A.M. Reinhorn and J.B. Mander, 12/1/92, (PB94-104502, A08, MF-A02).

NCEER-92-0028 "Seismic Resistance of Reinforced Concrete Frame Structures Designed Only for Gravity Loads: Part II - Experimental Performance of Subassemblages," by L.E. Aycardi, J.B. Mander and A.M. Reinhorn, 12/1/92, (PB94-104510, A08, MF-A02).

NCEER-92-0029 "Seismic Resistance of Reinforced Concrete Frame Structures Designed Only for Gravity Loads: Part III - Experimental Performance and Analytical Study of a Structural Model," by J.M. Bracci, A.M. Reinhorn and J.B. Mander, 12/1/92, (PB93-227528, A09, MF-A01).

NCEER-92-0030 "Evaluation of Seismic Retrofit of Reinforced Concrete Frame Structures: Part I - Experimental Performance of Retrofitted Subassemblages," by D. Choudhuri, J.B. Mander and A.M. Reinhorn, 12/8/92, (PB93-198307, A07, MF-A02).

NCEER-92-0031 "Evaluation of Seismic Retrofit of Reinforced Concrete Frame Structures: Part II - Experimental Performance and Analytical Study of a Retrofitted Structural Model," by J.M. Bracci, A.M. Reinhorn and J.B. Mander, 12/8/92, (PB93-198315, A09, MF-A03).

NCEER-92-0032 "Experimental and Analytical Investigation of Seismic Response of Structures with Supplemental Fluid Viscous Dampers," by M.C. Constantinou and M.D. Symans, 12/21/92, (PB93-191435, A10, MF-A03). This report is available only through NTIS (see address given above).

NCEER-92-0033 "Reconnaissance Report on the Cairo, Egypt Earthquake of October 12, 1992," by M. Khater, 12/23/92, (PB93-188621, A03, MF-A01).

NCEER-92-0034 "Low-Level Dynamic Characteristics of Four Tall Flat-Plate Buildings in New York City," by H. Gavin, S. Yuan, J. Grossman, E. Pekelis and K. Jacob, 12/28/92, (PB93-188217, A07, MF-A02).

NCEER-93-0001 "An Experimental Study on the Seismic Performance of Brick-Infilled Steel Frames With and Without Retrofit," by J.B. Mander, B. Nair, K. Wojtkowski and J. Ma, 1/29/93, (PB93-227510, A07, MF-A02).

NCEER-93-0002 "Social Accounting for Disaster Preparedness and Recovery Planning," by S. Cole, E. Pantoja and V. Razak, 2/22/93, (PB94-142114, A12, MF-A03).

NCEER-93-0003 "Assessment of 1991 NEHRP Provisions for Nonstructural Components and Recommended Revisions," by T.T. Soong, G. Chen, Z. Wu, R-H. Zhang and M. Grigoriu, 3/1/93, (PB93-188639, A06, MF-A02).

NCEER-93-0004 "Evaluation of Static and Response Spectrum Analysis Procedures of SEAOC/UBC for Seismic Isolated Structures," by C.W. Winters and M.C. Constantinou, 3/23/93, (PB93-198299, A10, MF-A03).

NCEER-93-0005 "Earthquakes in the Northeast - Are We Ignoring the Hazard? A Workshop on Earthquake Science and Safety for Educators," edited by K.E.K. Ross, 4/2/93, (PB94-103066, A09, MF-A02).

NCEER-93-0006 "Inelastic Response of Reinforced Concrete Structures with Viscoelastic Braces," by R.F. Lobo, J.M. Bracci, K.L. Shen, A.M. Reinhorn and T.T. Soong, 4/5/93, (PB93-227486, A05, MF-A02).

NCEER-93-0007 "Seismic Testing of Installation Methods for Computers and Data Processing Equipment," by K. Kosar, T.T. Soong, K.L. Shen, J.A. HoLung and Y.K. Lin, 4/12/93, (PB93-198299, A07, MF-A02).

NCEER-93-0008 "Retrofit of Reinforced Concrete Frames Using Added Dampers," by A. Reinhorn, M. Constantinou and C. Li, to be published.

NCEER-93-0009 "Seismic Behavior and Design Guidelines for Steel Frame Structures with Added Viscoelastic Dampers," by K.C. Chang, M.L. Lai, T.T. Soong, D.S. Hao and Y.C. Yeh, 5/1/93, (PB94-141959, A07, MF-A02).

NCEER-93-0010 "Seismic Performance of Shear-Critical Reinforced Concrete Bridge Piers," by J.B. Mander, S.M. Waheed, M.T.A. Chaudhary and S.S. Chen, 5/12/93, (PB93-227494, A08, MF-A02).

NCEER-93-0011 "3D-BASIS-TABS: Computer Program for Nonlinear Dynamic Analysis of Three Dimensional Base Isolated Structures," by S. Nagarajaiah, C. Li, A.M. Reinhorn and M.C. Constantinou, 8/2/93, (PB94-141819, A09, MF-A02).

NCEER-93-0012 "Effects of Hydrocarbon Spills from an Oil Pipeline Break on Ground Water," by O.J. Helweg and H.H.M. Hwang, 8/3/93, (PB94-141942, A06, MF-A02).

NCEER-93-0013 "Simplified Procedures for Seismic Design of Nonstructural Components and Assessment of Current Code Provisions," by M.P. Singh, L.E. Suarez, E.E. Matheu and G.O. Maldonado, 8/4/93, (PB94-141827, A09, MF-A02).

NCEER-93-0014 "An Energy Approach to Seismic Analysis and Design of Secondary Systems," by G. Chen and T.T. Soong, 8/6/93, (PB94-142767, A11, MF-A03).

NCEER-93-0015 "Proceedings from School Sites: Becoming Prepared for Earthquakes - Commemorating the Third Anniversary of the Loma Prieta Earthquake," Edited by F.E. Winslow and K.E.K. Ross, 8/16/93, (PB94-154275, A16, MF-A02).

NCEER-93-0016 "Reconnaissance Report of Damage to Historic Monuments in Cairo, Egypt Following the October 12, 1992 Dahshur Earthquake," by D. Sykora, D. Look, G. Croci, E. Karaesmen and E. Karaesmen, 8/19/93, (PB94-142221, A08, MF-A02).

NCEER-93-0017 "The Island of Guam Earthquake of August 8, 1993," by S.W. Swan and S.K. Harris, 9/30/93, (PB94-141843, A04, MF-A01).

NCEER-93-0018 "Engineering Aspects of the October 12, 1992 Egyptian Earthquake," by A.W. Elgamal, M. Amer, K. Adalier and A. Abul-Fadl, 10/7/93, (PB94-141983, A05, MF-A01).

NCEER-93-0019 "Development of an Earthquake Motion Simulator and its Application in Dynamic Centrifuge Testing," by I. Krstelj, Supervised by J.H. Prevost, 10/23/93, (PB94-181773, A-10, MF-A03).

NCEER-93-0020 "NCEER-Taisei Corporation Research Program on Sliding Seismic Isolation Systems for Bridges: Experimental and Analytical Study of a Friction Pendulum System (FPS)," by M.C. Constantinou, P. Tsopelas, Y-S. Kim and S. Okamoto, 11/1/93, (PB94-142775, A08, MF-A02).

NCEER-93-0021 "Finite Element Modeling of Elastomeric Seismic Isolation Bearings," by L.J. Billings, Supervised by R. Shepherd, 11/8/93, to be published.

NCEER-93-0022 "Seismic Vulnerability of Equipment in Critical Facilities: Life-Safety and Operational Consequences," by K. Porter, G.S. Johnson, M.M. Zadeh, C. Scawthorn and S. Eder, 11/24/93, (PB94-181765, A16, MF-A03).

NCEER-93-0023 "Hokkaido Nansei-oki, Japan Earthquake of July 12, 1993, by P.I. Yanev and C.R. Scawthorn, 12/23/93, (PB94-181500, A07, MF-A01).

NCEER-94-0001 "An Evaluation of Seismic Serviceability of Water Supply Networks with Application to the San Francisco Auxiliary Water Supply System," by I. Markov, Supervised by M. Grigoriu and T. O'Rourke, 1/21/94, (PB94-204013, A07, MF-A02).

NCEER-94-0002 "NCEER-Taisei Corporation Research Program on Sliding Seismic Isolation Systems for Bridges: Experimental and Analytical Study of Systems Consisting of Sliding Bearings, Rubber Restoring Force Devices and Fluid Dampers," Volumes I and II, by P. Tsopelas, S. Okamoto, M.C. Constantinou, D. Ozaki and S. Fujii, 2/4/94, (PB94-181740, A09, MF-A02 and PB94-181757, A12, MF-A03).

NCEER-94-0003 "A Markov Model for Local and Global Damage Indices in Seismic Analysis," by S. Rahman and M. Grigoriu, 2/18/94, (PB94-206000, A12, MF-A03).

NCEER-94-0004 "Proceedings from the NCEER Workshop on Seismic Response of Masonry Infills," edited by D.P. Abrams, 3/1/94, (PB94-180783, A07, MF-A02).

NCEER-94-0005 "The Northridge, California Earthquake of January 17, 1994: General Reconnaissance Report," edited by J.D. Goltz, 3/11/94, (PB193943, A10, MF-A03).

NCEER-94-0006 "Seismic Energy Based Fatigue Damage Analysis of Bridge Columns: Part I - Evaluation of Seismic Capacity," by G.A. Chang and J.B. Mander, 3/14/94, (PB94-219185, A11, MF-A03).

NCEER-94-0007 "Seismic Isolation of Multi-Story Frame Structures Using Spherical Sliding Isolation Systems," by T.M. Al-Hussaini, V.A. Zayas and M.C. Constantinou, 3/17/94, (PB193745, A09, MF-A02).

NCEER-94-0008 "The Northridge, California Earthquake of January 17, 1994: Performance of Highway Bridges," edited by I.G. Buckle, 3/24/94, (PB94-193851, A06, MF-A02).

NCEER-94-0009 "Proceedings of the Third U.S.-Japan Workshop on Earthquake Protective Systems for Bridges," edited by I.G. Buckle and I. Friedland, 3/31/94, (PB94-195815, A99, MF-A06).

NCEER-94-0010 "3D-BASIS-ME: Computer Program for Nonlinear Dynamic Analysis of Seismically Isolated Single and Multiple Structures and Liquid Storage Tanks," by P.C. Tsopelas, M.C. Constantinou and A.M. Reinhorn, 4/12/94, (PB94-204922, A09, MF-A02).

NCEER-94-0011 "The Northridge, California Earthquake of January 17, 1994: Performance of Gas Transmission Pipelines," by T.D. O'Rourke and M.C. Palmer, 5/16/94, (PB94-204989, A05, MF-A01).

NCEER-94-0012 "Feasibility Study of Replacement Procedures and Earthquake Performance Related to Gas Transmission Pipelines," by T.D. O'Rourke and M.C. Palmer, 5/25/94, (PB94-206638, A09, MF-A02).

NCEER-94-0013 "Seismic Energy Based Fatigue Damage Analysis of Bridge Columns: Part II - Evaluation of Seismic Demand," by G.A. Chang and J.B. Mander, 6/1/94, (PB95-18106, A08, MF-A02).

NCEER-94-0014 "NCEER-Taisei Corporation Research Program on Sliding Seismic Isolation Systems for Bridges: Experimental and Analytical Study of a System Consisting of Sliding Bearings and Fluid Restoring Force/Damping Devices," by P. Tsopelas and M.C. Constantinou, 6/13/94, (PB94-219144, A10, MF-A03).

NCEER-94-0015 "Generation of Hazard-Consistent Fragility Curves for Seismic Loss Estimation Studies," by H. Hwang and J-R. Huo, 6/14/94, (PB95-181996, A09, MF-A02).

NCEER-94-0016 "Seismic Study of Building Frames with Added Energy-Absorbing Devices," by W.S. Pong, C.S. Tsai and G.C. Lee, 6/20/94, (PB94-219136, A10, A03).

NCEER-94-0017 "Sliding Mode Control for Seismic-Excited Linear and Nonlinear Civil Engineering Structures," by J. Yang, J. Wu, A. Agrawal and Z. Li, 6/21/94, (PB95-138483, A06, MF-A02).

NCEER-94-0018 "3D-BASIS-TABS Version 2.0: Computer Program for Nonlinear Dynamic Analysis of Three Dimensional Base Isolated Structures," by A.M. Reinhorn, S. Nagarajaiah, M.C. Constantinou, P. Tsopelas and R. Li, 6/22/94, (PB95-182176, A08, MF-A02).

NCEER-94-0019 "Proceedings of the International Workshop on Civil Infrastructure Systems: Application of Intelligent Systems and Advanced Materials on Bridge Systems," Edited by G.C. Lee and K.C. Chang, 7/18/94, (PB95-252474, A20, MF-A04).

NCEER-94-0020 "Study of Seismic Isolation Systems for Computer Floors," by V. Lambrou and M.C. Constantinou, 7/19/94, (PB95-138533, A10, MF-A03).

NCEER-94-0021 "Proceedings of the U.S.-Italian Workshop on Guidelines for Seismic Evaluation and Rehabilitation of Unreinforced Masonry Buildings," Edited by D.P. Abrams and G.M. Calvi, 7/20/94, (PB95-138749, A13, MF-A03).

NCEER-94-0022 "NCEER-Taisei Corporation Research Program on Sliding Seismic Isolation Systems for Bridges: Experimental and Analytical Study of a System Consisting of Lubricated PTFE Sliding Bearings and Mild Steel Dampers," by P. Tsopelas and M.C. Constantinou, 7/22/94, (PB95-182184, A08, MF-A02).

NCEER-94-0023 "Development of Reliability-Based Design Criteria for Buildings Under Seismic Load," by Y.K. Wen, H. Hwang and M. Shinozuka, 8/1/94, (PB95-211934, A08, MF-A02).

NCEER-94-0024 "Experimental Verification of Acceleration Feedback Control Strategies for an Active Tendon System," by S.J. Dyke, B.F. Spencer, Jr., P. Quast, M.K. Sain, D.C. Kaspari, Jr. and T.T. Soong, 8/29/94, (PB95-212320, A05, MF-A01).

NCEER-94-0025 "Seismic Retrofitting Manual for Highway Bridges," Edited by I.G. Buckle and I.F. Friedland, published by the Federal Highway Administration (PB95-212676, A15, MF-A03).

NCEER-94-0026 "Proceedings from the Fifth U.S.-Japan Workshop on Earthquake Resistant Design of Lifeline Facilities and Countermeasures Against Soil Liquefaction," Edited by T.D. O'Rourke and M. Hamada, 11/7/94, (PB95-220802, A99, MF-E08).

NCEER-95-0001 "Experimental and Analytical Investigation of Seismic Retrofit of Structures with Supplemental Damping: Part I - Fluid Viscous Damping Devices," by A.M. Reinhorn, C. Li and M.C. Constantinou, 1/3/95, (PB95-266599, A09, MF-A02).

NCEER-95-0002 "Experimental and Analytical Study of Low-Cycle Fatigue Behavior of Semi-Rigid Top-And-Seat Angle Connections," by G. Pekcan, J.B. Mander and S.S. Chen, 1/5/95, (PB95-220042, A07, MF-A02).

NCEER-95-0003 "NCEER-ATC Joint Study on Fragility of Buildings," by T. Anagnos, C. Rojahn and A.S. Kiremidjian, 1/20/95, (PB95-220026, A06, MF-A02).

NCEER-95-0004 "Nonlinear Control Algorithms for Peak Response Reduction," by Z. Wu, T.T. Soong, V. Gattulli and R.C. Lin, 2/16/95, (PB95-220349, A05, MF-A01).

NCEER-95-0005 "Pipeline Replacement Feasibility Study: A Methodology for Minimizing Seismic and Corrosion Risks to Underground Natural Gas Pipelines," by R.T. Eguchi, H.A. Seligson and D.G. Honegger, 3/2/95, (PB95-252326, A06, MF-A02).

NCEER-95-0006 "Evaluation of Seismic Performance of an 11-Story Frame Building During the 1994 Northridge Earthquake," by F. Naeim, R. DiSulio, K. Benuska, A. Reinhorn and C. Li, to be published.

NCEER-95-0007 "Prioritization of Bridges for Seismic Retrofitting," by N. Basöz and A.S. Kiremidjian, 4/24/95, (PB95-252300, A08, MF-A02).

NCEER-95-0008 "Method for Developing Motion Damage Relationships for Reinforced Concrete Frames," by A. Singhal and A.S. Kiremidjian, 5/11/95, (PB95-266607, A06, MF-A02).

NCEER-95-0009 "Experimental and Analytical Investigation of Seismic Retrofit of Structures with Supplemental Damping: Part II - Friction Devices," by C. Li and A.M. Reinhorn, 7/6/95, (PB96-128087, A11, MF-A03).

NCEER-95-0010 "Experimental Performance and Analytical Study of a Non-Ductile Reinforced Concrete Frame Structure Retrofitted with Elastomeric Spring Dampers," by G. Pekcan, J.B. Mander and S.S. Chen, 7/14/95, (PB96-137161, A08, MF-A02).

NCEER-95-0011 "Development and Experimental Study of Semi-Active Fluid Damping Devices for Seismic Protection of Structures," by M.D. Symans and M.C. Constantinou, 8/3/95, (PB96-136940, A23, MF-A04).

NCEER-95-0012 "Real-Time Structural Parameter Modification (RSPM): Development of Innervated Structures," by Z. Liang, M. Tong and G.C. Lee, 4/11/95, (PB96-137153, A06, MF-A01).

NCEER-95-0013 "Experimental and Analytical Investigation of Seismic Retrofit of Structures with Supplemental Damping: Part III - Viscous Damping Walls," by A.M. Reinhorn and C. Li, 10/1/95, (PB96-176409, A11, MF-A03).

NCEER-95-0014 "Seismic Fragility Analysis of Equipment and Structures in a Memphis Electric Substation," by J-R. Huo and H.H.M. Hwang, (PB96-128087, A09, MF-A02), 8/10/95.

NCEER-95-0015 "The Hanshin-Awaji Earthquake of January 17, 1995: Performance of Lifelines," Edited by M. Shinozuka, 11/3/95, (PB96-176383, A15, MF-A03).

NCEER-95-0016 "Highway Culvert Performance During Earthquakes," by T.L. Youd and C.J. Beckman, available as NCEER-96-0015.

NCEER-95-0017 "The Hanshin-Awaji Earthquake of January 17, 1995: Performance of Highway Bridges," Edited by I.G. Buckle, 12/1/95, to be published.

NCEER-95-0018 "Modeling of Masonry Infill Panels for Structural Analysis," by A.M. Reinhorn, A. Madan, R.E. Valles, Y. Reichmann and J.B. Mander, 12/8/95, (PB97-110886, MF-A01, A06).

NCEER-95-0019 "Optimal Polynomial Control for Linear and Nonlinear Structures," by A.K. Agrawal and J.N. Yang, 12/11/95, (PB96-168737, A07, MF-A02).

NCEER-95-0020 "Retrofit of Non-Ductile Reinforced Concrete Frames Using Friction Dampers," by R.S. Rao, P. Gergely and R.N. White, 12/22/95, (PB97-133508, A10, MF-A02).

NCEER-95-0021 "Parametric Results for Seismic Response of Pile-Supported Bridge Bents," by G. Mylonakis, A. Nikolaou and G. Gazetas, 12/22/95, (PB97-100242, A12, MF-A03).

NCEER-95-0022 "Kinematic Bending Moments in Seismically Stressed Piles," by A. Nikolaou, G. Mylonakis and G. Gazetas, 12/23/95, (PB97-113914, MF-A03, A13).

NCEER-96-0001 "Dynamic Response of Unreinforced Masonry Buildings with Flexible Diaphragms," by A.C. Costley and D.P. Abrams," 10/10/96, (PB97-133573, MF-A03, A15).

NCEER-96-0002 "State of the Art Review: Foundations and Retaining Structures," by I. Po Lam, to be published.

NCEER-96-0003 "Ductility of Rectangular Reinforced Concrete Bridge Columns with Moderate Confinement," by N. Wehbe, M. Saiidi, D. Sanders and B. Douglas, 11/7/96, (PB97-133557, A06, MF-A02).

NCEER-96-0004 "Proceedings of the Long-Span Bridge Seismic Research Workshop," edited by I.G. Buckle and I.M. Friedland, to be published.

NCEER-96-0005 "Establish Representative Pier Types for Comprehensive Study: Eastern United States," by J. Kulicki and Z. Prucz, 5/28/96, (PB98-119217, A07, MF-A02).

NCEER-96-0006 "Establish Representative Pier Types for Comprehensive Study: Western United States," by R. Imbsen, R.A. Schamber and T.A. Osterkamp, 5/28/96, (PB98-118607, A07, MF-A02).

NCEER-96-0007 "Nonlinear Control Techniques for Dynamical Systems with Uncertain Parameters," by R.G. Ghanem and M.I. Bujakov, 5/27/96, (PB97-100259, A17, MF-A03).

NCEER-96-0008 "Seismic Evaluation of a 30-Year Old Non-Ductile Highway Bridge Pier and Its Retrofit," by J.B. Mander, B. Mahmoodzadegan, S. Bhadra and S.S. Chen, 5/31/96, (PB97-110902, MF-A03, A10).

NCEER-96-0009 "Seismic Performance of a Model Reinforced Concrete Bridge Pier Before and After Retrofit," by J.B. Mander, J.H. Kim and C.A. Ligozio, 5/31/96, (PB97-110910, MF-A02, A10).

NCEER-96-0010 "IDARC2D Version 4.0: A Computer Program for the Inelastic Damage Analysis of Buildings," by R.E. Valles, A.M. Reinhorn, S.K. Kunnath, C. Li and A. Madan, 6/3/96, (PB97-100234, A17, MF-A03).

NCEER-96-0011 "Estimation of the Economic Impact of Multiple Lifeline Disruption: Memphis Light, Gas and Water Division Case Study," by S.E. Chang, H.A. Seligson and R.T. Eguchi, 8/16/96, (PB97-133490, A11, MF-A03).

NCEER-96-0012 "Proceedings from the Sixth Japan-U.S. Workshop on Earthquake Resistant Design of Lifeline Facilities and Countermeasures Against Soil Liquefaction, Edited by M. Hamada and T. O'Rourke, 9/11/96, (PB97-133581, A99, MF-A06).

NCEER-96-0013 "Chemical Hazards, Mitigation and Preparedness in Areas of High Seismic Risk: A Methodology for Estimating the Risk of Post-Earthquake Hazardous Materials Release," by H.A. Seligson, R.T. Eguchi, K.J. Tierney and K. Richmond, 11/7/96, (PB97-133565, MF-A02, A08).

NCEER-96-0014 "Response of Steel Bridge Bearings to Reversed Cyclic Loading," by J.B. Mander, D-K. Kim, S.S. Chen and G.J. Premus, 11/13/96, (PB97-140735, A12, MF-A03).

NCEER-96-0015 "Highway Culvert Performance During Past Earthquakes," by T.L. Youd and C.J. Beckman, 11/25/96, (PB97-133532, A06, MF-A01).

NCEER-97-0001 "Evaluation, Prevention and Mitigation of Pounding Effects in Building Structures," by R.E. Valles and A.M. Reinhorn, 2/20/97, (PB97-159552, A14, MF-A03).

NCEER-97-0002 "Seismic Design Criteria for Bridges and Other Highway Structures," by C. Rojahn, R. Mayes, D.G. Anderson, J. Clark, J.H. Hom, R.V. Nutt and M.J. O'Rourke, 4/30/97, (PB97-194658, A06, MF-A03).

NCEER-97-0003 "Proceedings of the U.S.-Italian Workshop on Seismic Evaluation and Retrofit," Edited by D.P. Abrams and G.M. Calvi, 3/19/97, (PB97-194666, A13, MF-A03).

NCEER-97-0004 "Investigation of Seismic Response of Buildings with Linear and Nonlinear Fluid Viscous Dampers," by A.A. Seleemah and M.C. Constantinou, 5/21/97, (PB98-109002, A15, MF-A03).

NCEER-97-0005 "Proceedings of the Workshop on Earthquake Engineering Frontiers in Transportation Facilities," edited by G.C. Lee and I.M. Friedland, 8/29/97, (PB98-128911, A25, MR-A04).

NCEER-97-0006 "Cumulative Seismic Damage of Reinforced Concrete Bridge Piers," by S.K. Kunnath, A. El-Bahy, A. Taylor and W. Stone, 9/2/97, (PB98-108814, A11, MF-A03).

NCEER-97-0007 "Structural Details to Accommodate Seismic Movements of Highway Bridges and Retaining Walls," by R.A. Imbsen, R.A. Schamber, E. Thorkildsen, A. Kartoum, B.T. Martin, T.N. Rosser and J.M. Kulicki, 9/3/97, (PB98-108996, A09, MF-A02).

NCEER-97-0008 "A Method for Earthquake Motion-Damage Relationships with Application to Reinforced Concrete Frames," by A. Singhal and A.S. Kiremidjian, 9/10/97, (PB98-108988, A13, MF-A03).

NCEER-97-0009 "Seismic Analysis and Design of Bridge Abutments Considering Sliding and Rotation," by K. Fishman and R. Richards, Jr., 9/15/97, (PB98-108897, A06, MF-A02).

NCEER-97-0010 "Proceedings of the FHWA/NCEER Workshop on the National Representation of Seismic Ground Motion for New and Existing Highway Facilities," edited by I.M. Friedland, M.S. Power and R.L. Mayes, 9/22/97, (PB98-128903, A21, MF-A04).

NCEER-97-0011 "Seismic Analysis for Design or Retrofit of Gravity Bridge Abutments," by K.L. Fishman, R. Richards, Jr. and R.C. Divito, 10/2/97, (PB98-128937, A08, MF-A02).

NCEER-97-0012 "Evaluation of Simplified Methods of Analysis for Yielding Structures," by P. Tsopelas, M.C. Constantinou, C.A. Kircher and A.S. Whittaker, 10/31/97, (PB98-128929, A10, MF-A03).

NCEER-97-0013 "Seismic Design of Bridge Columns Based on Control and Repairability of Damage," by C-T. Cheng and J.B. Mander, 12/8/97, (PB98-144249, A11, MF-A03).

NCEER-97-0014 "Seismic Resistance of Bridge Piers Based on Damage Avoidance Design," by J.B. Mander and C-T. Cheng, 12/10/97, (PB98-144223, A09, MF-A02).

NCEER-97-0015 "Seismic Response of Nominally Symmetric Systems with Strength Uncertainty," by S. Balopoulou and M. Grigoriu, 12/23/97, (PB98-153422, A11, MF-A03).

NCEER-97-0016 "Evaluation of Seismic Retrofit Methods for Reinforced Concrete Bridge Columns," by T.J. Wipf, F.W. Klaiber and F.M. Russo, 12/28/97, (PB98-144215, A12, MF-A03).

NCEER-97-0017 "Seismic Fragility of Existing Conventional Reinforced Concrete Highway Bridges," by C.L. Mullen and A.S. Cakmak, 12/30/97, (PB98-153406, A08, MF-A02).

NCEER-97-0018 "Loss Asssessment of Memphis Buildings," edited by D.P. Abrams and M. Shinozuka, 12/31/97, (PB98-144231, A13, MF-A03).

NCEER-97-0019 "Seismic Evaluation of Frames with Infill Walls Using Quasi-static Experiments," by K.M. Mosalam, R.N. White and P. Gergely, 12/31/97, (PB98-153455, A07, MF-A02).

NCEER-97-0020 "Seismic Evaluation of Frames with Infill Walls Using Pseudo-dynamic Experiments," by K.M. Mosalam, R.N. White and P. Gergely, 12/31/97, (PB98-153430, A07, MF-A02).

NCEER-97-0021 "Computational Strategies for Frames with Infill Walls: Discrete and Smeared Crack Analyses and Seismic Fragility," by K.M. Mosalam, R.N. White and P. Gergely, 12/31/97, (PB98-153414, A10, MF-A02).

NCEER-97-0022 "Proceedings of the NCEER Workshop on Evaluation of Liquefaction Resistance of Soils," edited by T.L. Youd and I.M. Idriss, 12/31/97, (PB98-155617, A15, MF-A03).

MCEER-98-0001 "Extraction of Nonlinear Hysteretic Properties of Seismically Isolated Bridges from Quick-Release Field Tests," by Q. Chen, B.M. Douglas, E.M. Maragakis and I.G. Buckle, 5/26/98, (PB99-118838, A06, MF-A01).

MCEER-98-0002 "Methodologies for Evaluating the Importance of Highway Bridges," by A. Thomas, S. Eshenaur and J. Kulicki, 5/29/98, (PB99-118846, A10, MF-A02).

MCEER-98-0003 "Capacity Design of Bridge Piers and the Analysis of Overstrength," by J.B. Mander, A. Dutta and P. Goel, 6/1/98, (PB99-118853, A09, MF-A02).

MCEER-98-0004 "Evaluation of Bridge Damage Data from the Loma Prieta and Northridge, California Earthquakes," by N. Basoz and A. Kiremidjian, 6/2/98, (PB99-118861, A15, MF-A03).

MCEER-98-0005 "Screening Guide for Rapid Assessment of Liquefaction Hazard at Highway Bridge Sites," by T. L. Youd, 6/16/98, (PB99-118879, A06, not available on microfiche).

MCEER-98-0006 "Structural Steel and Steel/Concrete Interface Details for Bridges," by P. Ritchie, N. Kauhl and J. Kulicki, 7/13/98, (PB99-118945, A06, MF-A01).

MCEER-98-0007 "Capacity Design and Fatigue Analysis of Confined Concrete Columns," by A. Dutta and J.B. Mander, 7/14/98, (PB99-118960, A14, MF-A03).

MCEER-98-0008 "Proceedings of the Workshop on Performance Criteria for Telecommunication Services Under Earthquake Conditions," edited by A.J. Schiff, 7/15/98, (PB99-118952, A08, MF-A02).

MCEER-98-0009 "Fatigue Analysis of Unconfined Concrete Columns," by J.B. Mander, A. Dutta and J.H. Kim, 9/12/98, (PB99-123655, A10, MF-A02).

MCEER-98-0010 "Centrifuge Modeling of Cyclic Lateral Response of Pile-Cap Systems and Seat-Type Abutments in Dry Sands," by A.D. Gadre and R. Dobry, 10/2/98, (PB99-123606, A13, MF-A03).

MCEER-98-0011 "IDARC-BRIDGE: A Computational Platform for Seismic Damage Assessment of Bridge Structures," by A.M. Reinhorn, V. Simeonov, G. Mylonakis and Y. Reichman, 10/2/98, (PB99-162919, A15, MF-A03).

MCEER-98-0012 "Experimental Investigation of the Dynamic Response of Two Bridges Before and After Retrofitting with Elastomeric Bearings," by D.A. Wendichansky, S.S. Chen and J.B. Mander, 10/2/98, (PB99-162927, A15, MF-A03).

MCEER-98-0013 "Design Procedures for Hinge Restrainers and Hinge Sear Width for Multiple-Frame Bridges," by R. Des Roches and G.L. Fenves, 11/3/98, (PB99-140477, A13, MF-A03).

MCEER-98-0014 "Response Modification Factors for Seismically Isolated Bridges," by M.C. Constantinou and J.K. Quarshie, 11/3/98, (PB99-140485, A14, MF-A03).

MCEER-98-0015 "Proceedings of the U.S.-Italy Workshop on Seismic Protective Systems for Bridges," edited by I.M. Friedland and M.C. Constantinou, 11/3/98, (PB2000-101711, A22, MF-A04).

MCEER-98-0016 "Appropriate Seismic Reliability for Critical Equipment Systems: Recommendations Based on Regional Analysis of Financial and Life Loss," by K. Porter, C. Scawthorn, C. Taylor and N. Blais, 11/10/98, (PB99-157265, A08, MF-A02).

MCEER-98-0017 "Proceedings of the U.S. Japan Joint Seminar on Civil Infrastructure Systems Research," edited by M. Shinozuka and A. Rose, 11/12/98, (PB99-156713, A16, MF-A03).

MCEER-98-0018 "Modeling of Pile Footings and Drilled Shafts for Seismic Design," by I. PoLam, M. Kapuskar and D. Chaudhuri, 12/21/98, (PB99-157257, A09, MF-A02).

MCEER-99-0001 "Seismic Evaluation of a Masonry Infilled Reinforced Concrete Frame by Pseudodynamic Testing," by S.G. Buonopane and R.N. White, 2/16/99, (PB99-162851, A09, MF-A02).

MCEER-99-0002 "Response History Analysis of Structures with Seismic Isolation and Energy Dissipation Systems: Verification Examples for Program SAP2000," by J. Scheller and M.C. Constantinou, 2/22/99, (PB99-162869, A08, MF-A02).

MCEER-99-0003 "Experimental Study on the Seismic Design and Retrofit of Bridge Columns Including Axial Load Effects," by A. Dutta, T. Kokorina and J.B. Mander, 2/22/99, (PB99-162877, A09, MF-A02).

MCEER-99-0004 "Experimental Study of Bridge Elastomeric and Other Isolation and Energy Dissipation Systems with Emphasis on Uplift Prevention and High Velocity Near-source Seismic Excitation," by A. Kasalanati and M. C. Constantinou, 2/26/99, (PB99-162885, A12, MF-A03).

MCEER-99-0005 "Truss Modeling of Reinforced Concrete Shear-flexure Behavior," by J.H. Kim and J.B. Mander, 3/8/99, (PB99-163693, A12, MF-A03).

MCEER-99-0006 "Experimental Investigation and Computational Modeling of Seismic Response of a 1:4 Scale Model Steel Structure with a Load Balancing Supplemental Damping System," by G. Pekcan, J.B. Mander and S.S. Chen, 4/2/99, (PB99-162893, A11, MF-A03).

MCEER-99-0007 "Effect of Vertical Ground Motions on the Structural Response of Highway Bridges," by M.R. Button, C.J. Cronin and R.L. Mayes, 4/10/99, (PB2000-101411, A10, MF-A03).

MCEER-99-0008 "Seismic Reliability Assessment of Critical Facilities: A Handbook, Supporting Documentation, and Model Code Provisions," by G.S. Johnson, R.E. Sheppard, M.D. Quilici, S.J. Eder and C.R. Scawthorn, 4/12/99, (PB2000-101701, A18, MF-A04).

MCEER-99-0009 "Impact Assessment of Selected MCEER Highway Project Research on the Seismic Design of Highway Structures," by C. Rojahn, R. Mayes, D.G. Anderson, J.H. Clark, D'Appolonia Engineering, S. Gloyd and R.V. Nutt, 4/14/99, (PB99-162901, A10, MF-A02).

MCEER-99-0010 "Site Factors and Site Categories in Seismic Codes," by R. Dobry, R. Ramos and M.S. Power, 7/19/99, (PB2000-101705, A08, MF-A02).

MCEER-99-0011 "Restrainer Design Procedures for Multi-Span Simply-Supported Bridges," by M.J. Randall, M. Saiidi, E. Maragakis and T. Isakovic, 7/20/99, (PB2000-101702, A10, MF-A02).

MCEER-99-0012 "Property Modification Factors for Seismic Isolation Bearings," by M.C. Constantinou, P. Tsopelas, A. Kasalanati and E. Wolff, 7/20/99, (PB2000-103387, A11, MF-A03).

MCEER-99-0013 "Critical Seismic Issues for Existing Steel Bridges," by P. Ritchie, N. Kauhl and J. Kulicki, 7/20/99, (PB2000-101697, A09, MF-A02).

MCEER-99-0014 "Nonstructural Damage Database," by A. Kao, T.T. Soong and A. Vender, 7/24/99, (PB2000-101407, A06, MF-A01).

MCEER-99-0015 "Guide to Remedial Measures for Liquefaction Mitigation at Existing Highway Bridge Sites," by H.G. Cooke and J. K. Mitchell, 7/26/99, (PB2000-101703, A11, MF-A03).

MCEER-99-0016 "Proceedings of the MCEER Workshop on Ground Motion Methodologies for the Eastern United States," edited by N. Abrahamson and A. Becker, 8/11/99, (PB2000-103385, A07, MF-A02).

MCEER-99-0017 "Quindío, Colombia Earthquake of January 25, 1999: Reconnaissance Report," by A.P. Asfura and P.J. Flores, 10/4/99, (PB2000-106893, A06, MF-A01).

MCEER-99-0018 "Hysteretic Models for Cyclic Behavior of Deteriorating Inelastic Structures," by M.V. Sivaselvan and A.M. Reinhorn, 11/5/99, (PB2000-103386, A08, MF-A02).

MCEER-99-0019 "Proceedings of the 7th U.S.- Japan Workshop on Earthquake Resistant Design of Lifeline Facilities and Countermeasures Against Soil Liquefaction," edited by T.D. O'Rourke, J.P. Bardet and M. Hamada, 11/19/99, (PB2000-103354, A99, MF-A06).

MCEER-99-0020 "Development of Measurement Capability for Micro-Vibration Evaluations with Application to Chip Fabrication Facilities," by G.C. Lee, Z. Liang, J.W. Song, J.D. Shen and W.C. Liu, 12/1/99, (PB2000-105993, A08, MF-A02).

MCEER-99-0021 "Design and Retrofit Methodology for Building Structures with Supplemental Energy Dissipating Systems," by G. Pekcan, J.B. Mander and S.S. Chen, 12/31/99, (PB2000-105994, A11, MF-A03).

MCEER-00-0001 "The Marmara, Turkey Earthquake of August 17, 1999: Reconnaissance Report," edited by C. Scawthorn; with major contributions by M. Bruneau, R. Eguchi, T. Holzer, G. Johnson, J. Mander, J. Mitchell, W. Mitchell, A. Papageorgiou, C. Scaethorn, and G. Webb, 3/23/00, (PB2000-106200, A11, MF-A03).

MCEER-00-0002 "Proceedings of the MCEER Workshop for Seismic Hazard Mitigation of Health Care Facilities," edited by G.C. Lee, M. Ettouney, M. Grigoriu, J. Hauer and J. Nigg, 3/29/00, (PB2000-106892, A08, MF-A02).

MCEER-00-0003 "The Chi-Chi, Taiwan Earthquake of September 21, 1999: Reconnaissance Report," edited by G.C. Lee and C.H. Loh, with major contributions by G.C. Lee, M. Bruneau, I.G. Buckle, S.E. Chang, P.J. Flores, T.D. O'Rourke, M. Shinozuka, T.T. Soong, C-H. Loh, K-C. Chang, Z-J. Chen, J-S. Hwang, M-L. Lin, G-Y. Liu, K-C. Tsai, G.C. Yao and C-L. Yen, 4/30/00.

MCEER-00-0004 "Seismic Retrofit of End-Sway Frames of Steel Deck-Truss Bridges with a Supplemental Tendon System: Experimental and Analytical Investigation," by G. Pekcan, J.B. Mander and S.S. Chen, 7/1/00.

MCEER-00-0005 "Sliding Fragility of Unrestrained Equipment in Critical Facilities," by W.H. Chong and T.T. Soong, 7/5/00.

MCEER-00-0006 "Seismic Response of Reinforced Concrete Bridge Pier Walls in the Weak Direction," by N. Abo-Shadi, M. Saiidi and D. Sanders, 7/17/00.

MCEER-00-0007 "Low-Cycle Fatigue Behavior of Longitudinal Reinforcement in Reinforced Concrete Bridge Columns," by J. Brown and S.K. Kunnath, 7/23/00.

MCEER-00-0008 "Soil Structure Interaction of Bridges for Seismic Analysis," I. PoLam and H. Law, 9/25/00.

MCEER-00-0009 "Proceedings of the First MCEER Workshop on Mitigation of Earthquake Disaster by Advanced Technologies (MEDAT-1), edited by M. Shinozuka, D.J. Inman and T.D. O'Rourke, 11/10/00.

MCEER-00-0010 "Development and Evaluation of Simplified Procedures for Analysis and Design of Buildings with Passive Energy Dissipation Systems," by O.M. Ramirez, M.C. Constantinou, C.A. Kircher, A.S. Whittaker, M.W. Johnson, and J.D. Gomez, 12/8/00.

MCEER-00-0011 "Dynamic Soil-Foundation-Structure Interaction Analyses of Large Caissons," by C-Y. Chang, C-M. Mok, Z-L. Wang, R. Settgast, F. Waggoner, M.A. Ketchum, H.M. Gonnermann and C-C. Chin, 12/30/00.

MCEER-00-0012 "Experimental Evaluation of Seismic Performance of Bridge Restrainers," by A.G. Vlassis, E.M. Maragakis and M. Saiid Saiidi, 12/30/00.

MCEER-00-0013 "Effect of Spatial Variation of Ground Motion on Highway Structures," by M. Shinozuka, V. Saxena and G. Deodatis, 12/31/00.

MCEER-00-0014 "A Risk-Based Methodology for Assessing the Seismic Performance of Highway Systems," by S.D. Werner, C.E. Taylor, J.E. Moore, II, J.S. Walton and S. Cho, 12/31/00.

MCEER-01-0001 "Experimental Investigation of P-Delta Effects to Collapse During Earthquakes," by D. Vian and M. Bruneau, 6/25/01.